CONF-9603171--

PROCEEDINGS OF THE INTERNATIONAL WORKSHOP ON THE TECHNOLOGY AND THERMAL HYDRAULICS OF HEAVY LIQUID METALS (Hg, Pb, Bi, AND THEIR EUTECTICS)

Compiled by
B. R. Appleton
and
G. S. Bauer

June 1996

MASTER

Prepared by
OAK RIDGE NATIONAL LABORATORY
Oak Ridge, Tennessee 37831
managed by
LOCKHEED MARTIN ENERGY RESEARCH CORP.
for the
U.S. DEPARTMENT OF ENERGY
under contract DE-AC05-96OR22464

DISTRIBUTION OF THIS DOCUMENT IS UNLIMITED

DISCLAIMER

Portions of this document may be illegible in electronic image products. Images are produced from the best available original document.

Table of Contents

Page

Acknowledgements vii

Introduction ix

Session 1: Opening Remarks and Presentation of Projects,
Chairman, M. Schuster
The European Scene Regarding Spallation Neutron Sources, G. Bauer 1-1
The Oak Ridge Spallation Neutron Source (ORSNS) Collaborative
Design Project, B. Appleton 1-21
High Power Neutron Production Targets, S. Wender 1-35

Session 2: Thermal Hydraulics, Heat Removal, and Circuit Design (1),
Chairman, O. Lielausis
Conceptual Studies for a Mercury Target Circuit, B. Sigg 2-1
Design, Components, Controls and Operational Experience of
Mercury Circuits, O. Lielausis 2-8

Session 3: Thermal Hydraulics, Heat Removal and Circuit Design (2),
Chairman, O. Lielausis
Theoretical Investigation of the Thermal Hydraulic Behavior of a
Slab-type Liquid Metal Target, T. Dury and B. Smith 3-1
Thermal-Hydraulic Simulation of Mercury Target Concepts for a
Pulsed Spallation Neutron Source, M. Siman-Tov, M. Wendel, and J. Haines 3-33

Session 4: Thermal Hydraulics, Heat Removal, and Circuit Design (3),
Chairman, S. Lesin
Thermohydraulic Behavior of the Liquid Metal Target of a Spallation
Neutron Source, Y. Takeda 4-1
Engineering Aspects of the Application of Structural Materials in the
5MW-ESS-Mercury-Target, B. Guttek 4-10
Oak Ridge Spallation Neutron Source (ORSNS) Target Station
Design Integration, T. McManamy, R. Booth, J. Cleaves, T. Gabriel
J. Galambos, G. McNutt 4-22

Session 5: Structural Materials: Corrosion and Radiation Damage (1),
Chairman, Y. Shubin
Compatibility of Structural Materials with Liquid Bismuth, Lead,
and Mercury, J. Weeks 5-1
Compatibility of Materials with Liquid Metal Targets for
SNS, J. DiStefano, S. Pawel, and J. DeVan 5-31

Session 6: Structure Materials: Corrosion and Radiation Damage (2),
Chairman, Y. Shubin
Spallation Radiation Effects in Materials, L. Mansur, K. Farrell, M. Wechsler 6-1
Martensitic/ferritic Steels as Container Materials for Liquid
Mercury Target of ESS, Y. Dai 6-27

Session 7: Pulsed Operation and Gas Admixture (1)
Chairman, E. Yefimov
Pressure Waves in Liquid Mercury Target from Pulsed Heat
Loads and the Possible Way Controlling Their Effects, L. Ni and K. Skala 7-1
Integrated Modeling/Analyses of Thermal-Shock Effects
in SNS Targets, R. Taleyarkhan and J. Haines 7-9

Session 8: Pulsed Operation and Gas Admixture (2),
Chairmanm, E. Yefimov
Generation and Characterization of Gas Bubbles in
Liquid Metals, S. Eckert, G. Gerbeth, H. Langenbrunner, W. Witke 8-1
Experimental Study of Two - Component Flow Structure
"Lead - Bismuth - Gas", B. Gromov, Y. Orlov, M. Sotov, G. Poletaev 8-15
Comments on the Possibility of Cavitation in Liquid
Metal Targets for Pulsed Spallation Neutron Sources, J. Carpenter 8-22

Session 9: Safety Issues,
Chairman, J. Carpenter
Energy Release, Beam Attenuation, Radiation Damage, Gas
Production and Accumulation of Long-lived Activity,
in Pb, Pb-Bi and Hg Targets, Y. Shubin 9-1
Polonium Problem in Lead-bismuth Flow Target, D. Pankratov,
E. Yefimov and M. Burgreev 9-23

Session 10: R&D Needs and Options (1),
Chairman, Y. Gelfgat
Needs and Opportunities for CFD-Code Validation, B. Smith 10-1
Assessment of the Neutron Cross Section Database for
Mercury for the ORNL Spallation Source, L. Leal, R. Spencer,
D. Ingersoll, and T. Gabriel 10-13
Mercury Target R&D for the Oak Ridge Spallation
Neutron Source, J. Haines, J. DiStefano, K. Farrell, T. Gabriel 10-32

Session 11: R&D Needs and Options (2),
Chairman, Y. Gelfgat
Heavy Liquid Metals: Research Programs at PSI, Y. Takeda 11-1
LM-Research Opportunities and Activities at Beer-Sheva, S. Lesin 11-9
LM-Research Opportunities and Activities at the Latvian
Academy of Sciences, O. Lielausis 11-38

Summary Session A: Different Target Materials: Corrosion and Corrosion Control
Coordinators: Y. Takeda, L. Mansur, Y. Dai, J. DiStefano
Workshop Session on the Pros and Cons for Different Target/Materials/Corrosion and Corrosion Control, Y. Takeda, L. Mansur, Y. Dai, J. DiStefano A-1

Summary Session B: Heat Removal
Coordinators: T. Dury and M. Siman-Tov
Heat Removal (Wetting, Heat Transfer, T/H, Secondary Circuit, Code Validation Etc.), T. Dury and M. Siman-Tov B-1

Summary Session C: Effects of Pulsed Operation
Coordinators: T. Gabriel and L. Ni
Working Group Summary Report on Effects of Pulsed Operation, T. Gabriel and L. Ni C-1

Summary Session D: Process Technology and Effects of Spallation Products, Circuit Components
Coordinators: B. Sigg, J. Haines, R. Dressler, T. McManamy D-1

Summary Session E: Discussion of R&D Needs and Opportunities to Broaden the Data Base on Materials and Technology for Liquid Metal Spallation Targets, G. Bauer E-1

APPENDIX A: Participants Ap-1

DISCLAIMER

This report was prepared as an account of work sponsored by an agency of the United States Government. Neither the United States Government nor any agency thereof, nor any of their employees, makes any warranty, express or implied, or assumes any legal liability or responsibility for the accuracy, completeness, or usefulness of any information, apparatus, product, or process disclosed, or represents that its use would not infringe privately owned rights. Reference herein to any specific commercial product, process, or service by trade name, trademark, manufacturer, or otherwise does not necessarily constitute or imply its endorsement, recommendation, or favoring by the United States Government or any agency thereof. The views and opinions of authors expressed herein do not necessarily state or reflect those of the United States Government or any agency thereof.

Acknowledgements

We wish to acknowledge the staff of the Oak Ridge National Laboratory and the Paul Scherrer Institut who worked to make this workshop a success. A special thanks goes to Ms. Karen Lee and Ms. Renate Bercher who served as Conference Secretaries, handled the mailings and announcements, arranged the travel and accommodations, handled on-site needs, and prepared the proceedings. Thanks also to Dr. Martin Schuster for assisting with arrangements to bring some of the participants to Austria. Finally, we wish to express our appreciation to the staff and management of the Hotel Löwen in Schruns, Austria, whose extraordinary efforts not only made it possible to keep to a difficult workshop schedule, but made it a most enjoyable experience for all the participants.

Introduction

The International Workshop on the Technology and Thermal Hydraulics of Heavy Liquid Metals (Schruns Workshop) was organized to assess the R&D and technology problems associated with designing and building a heavy liquid metal target for a spallation neutron source. The European scientific community is completing a feasibility study for a future, accelerator-based, pulsed spallation neutron source that would deliver a beam power of 5 megawatts (MW) to a target. They have concluded that a liquid metal target is preferable to conventional solid targets for handling the extreme radiation environments, high heat loads, and pulsed power. Similarly, the Oak Ridge National Laboratory has been funded by the Department of Energy to design a high-power, pulsed spallation neutron source that would begin operation at about 1 MW but that could be upgraded to significantly higher powers in the future. Again, the most feasible target design appears to be a liquid metal target. Since the expertise needed to consider these problems resides in a number of disparate disciplines not normally covered by existing conferences, this workshop was organized to bring a small number of scientists and engineers together to assess the opportunities for building such a target.

The objectives and goals of the Schruns Workshop were to:

- Review and share existing information on the science and technology of heavy liquid metal systems.
- Evaluate the opportunities and limitations of materials compatibility, thermal hydraulics and heat transfer, chemical reactions, corrosion, radiation effects, liquid-gas mixtures, systems designs, and circuit components for a heavy liquid metal target.
- Establish the critical R&D and technology that is necessary to construct a liquid metal target.
- Explore opportunities for cooperative R&D among members of the international community that could expedite results, and share expertise and resources.

The Schruns Workshop brought together scientists and engineers from a multiplicity of backgrounds and disciplines—accelerator physicists; neutron scientists; thermal, chemical, and mechanical engineers; materials and corrosion experts; teams who had constructed and operated MHD systems or liquid metal cooling systems for reactors; etc. The workshop was arranged with oral presentations and discussions on the mornings and evenings of the first three days. The afternoons were left unscheduled to allow for informal discussions. The oral sessions provided a forum to understand the relevance and connectivity of the presentations, and the possibilities for collaborative work at the various facilities that were described. The morning of the final day of the workshop was devoted to four working sessions considering target materials, process technology and the effects of spallation products, heat removal, the effects of pulsed operation, and target components, maintenance, and handling. The conclusions from these working groups were presented in the afternoon, and a plenary discussion was held to establish coordinated plans for international cooperative efforts.

These proceedings contain abstracts and viewgraphs from the oral presentations, the summaries and conclusions from the working groups, and a technology roadmap for initiating international cooperation. The workshop was very successful. It brought consensus that mercury was the preferable liquid metal for a pulsed spallation source target; it narrowed the construction materials to a few and identified the compatibility and corrosion problems; it established boundaries for considering the heat transfer and thermal shock problems arising from pulsed operation; it clearly identified the necessary R&D needed to answer remaining questions; and it identified facilities and participants for several future cooperative experiments that will accelerate completion of a mercury target.

Gunter S. Bauer
Paul Scherrer Institut

Bill R. Appleton
Oak Ridge National Laboratory

SESSION 1

Opening Remarks and Presentation of Related Projects

Chairman
M. Schuster

Workshop on the Technology and Thermal Hydraulics of Heavy Liquid Metals
Hotel Löwen, Schruns, Austria March 24-29,1996

The European Scene Regarding Spallation Neutron Sources

G.S. Bauer, Paul Scherrer Institut, CH-5232 Villigen-PSI

Abstract

In Europe, a short pulse spallation neutron source, ISIS, has been operating for over 10 years, working its way up to a beam power level of 200 kW. A continuous source, SINQ, designed for a beam power of up to 1 MW, is scheduled to start operating at the end of 1996, and a detailed feasibility study has been completed for a 410 kW short pulse source, AUSTRON. Each of these sources seems to have settled for a target concept which is at or near the limits of its feasibility: The ISIS depleted uranium plate targets, heavy water cooled and Zircaloy clad, have so far not shown satisfactory service time and operation is likely to continue with a Ta-plate target, which, in the past has been used successfully for the equivalent of one full-beam-year before it was taken out of service due to degrading thermal properties. SINQ will initially use a rod target, made of Zircaloy only, but plans exist to move on to clad lead rods as quickly as possible. Apart from the not yet explored effect of hydrogen and helium production, there are also concerns about the generation of 7-Be in the cooling water from the spallation of oxygen, which might result in undesirably high radioactivity in the cooling plant room. A Liquid metal target, also under investigation for SINQ, would not only reduce this problem to a level of about 10 %, but would also minimize the risk of radiolytic corrosion in the beam interaction zone. Base on similar arguments, AUSTRON has been designed for edge cooled targets, but thermal and stress analyses show, that this concept is not feasible at higher power levels.

For The ESS-Project, for which the goal has been set to study the feasibility and tradeoffs of a short pulse source at 5 MW beam power, parallel studies were started on plate and rod targets and on a liquid metal target system. One serious problem arising from the use of solid targets at high power is the concentration of decay heat in a small volume and the resulting need for emergency and decay heat removal, requiring a second and independent cooling system which is difficult to accommodate, given the restrictions of close target-moderator coupling one tries to achieve in a pulsed spallation neutron source. After an evaluation of various pros and cons, the ESS-project team settled for a liquid metal target as its first choice, selecting mercury as target material, because of its superior properties for a pulsed source target /1/ and because it does not require auxiliary heating to keep it molten. Monte Carlo studies /2/ confirmed the expectation that, due to the absence of neutron moderation in the target zone, a reflected mercury target shows better neutronic performance than a water cooled target of either Tantalum or Tungsten, both of which show significant resonance absorption. The high thermal neutron absorption of mercury, a disadvantage in the case of a continuous source, can probably be turned into an advantage on a pulsed source by making it unnecessary to decouple the moderator from the target. This not only eliminates the need to cool this decoupler but also allows to move the moderator in more closely. Even for otherwise non-decoupled moderators in a fast reflector, such as lead, a mercury target can be expected to show excellent performance.

The total power deposition in the ESS mercury target, including some allowance for neutron, pion and gamma absorption is estimated at 2.8 MW with a distribution following the (2-dimensionally parabolic) beam profile laterally and an essentially exponential decrease with an initial buildup zone axially. This results in very high local power density during the pulse and gives rise to some concern about the effect of pressure waves in the liquid metal. Initial scoping calculations /3/, /4/ have shown that this could indeed become a problem and that some method to midgigate the stress in the container wall must be found. One way, which still needs more theoretical and experimental verification, could be to inject about 3 vol% of Helium in the liquid metal.

Optimizing the flow and temperature distribution in the beam interaction zone is another important issue. Fluid dynamics calculations /5/ have shown that a satisfactory solution seems possible which, by directing part of the flow asymmetrically across the beam entrance window, allows to control also the temperature of this critical part in reasonable limits.

Finally, due to the large mass of the target, the concentration of spallation products generated during 10 years of operation remains well within the solubility limit /6/ with only a few exceptions, which happen to be Iron and Chromium, the main components of the steel foreseen as structural material /7/.

/1/ G.S. Bauer: "Mercury as a Target Material for Pulsed (Fast) Spallation Neutron Sources" Proc. ICANS-XIII, Paul Scherrer Insitut, PSI-Proceedings 95-02 (1995) T12, 547-558

/2/ D. Filges et alD. Filges, R.D. Neef and H. Schaal: "Nuclear Studies for Different Target Systems for the European Spallation Source (ESS) Proc. ICANS-XIII, PSI-Proc. 95-02 (1995) T11, 537-546

/3/ K. Skala and G.S. Bauer "On the Pressure Wave Problem in Liquid Metal Targets" Proc. ICANS-XIII, Paul Scherrer Insitut, PSI-Proceedings 95-02 (1995)

/4/ L. Ni, this workshop

/5/ T, Dury, this workshop

/6/ R. Dressler, this workshop

/7/ Y. Dai, this workshop

Workshop on the Technology and Thermal-Hydraulics of Heavy Liquid Metals

Hotel Löwen
Schruns, Austria
March 24-29, 1996

The European Scene regarding Spallation Neutron Sources

G.S. Bauer
Paul Scherrer Institut
CH-5232 Villigen-PSI, Switzerland

Design Features for European Spallation Neutron Source Projects

Parameter	ISIS	AUSTRON	SINQ	ESS
Proton beam energy	800 MeV	1600 MeV	570 MeV	1334 MeV
Proton beam current (av.)	200 μA	250 μA	>1mA	3.8 mA
Proton beam power	160 kW	410 kW	0.6 (1) MW	5 MW
Nominal max. current density	10 $\mu A/cm^2$	18 $\mu A/cm^2$	25 $\mu A/cm^2$	90 $\mu A/cm^2$
Mode of operation	50 Hz	50 Hz	continuous	50 (40+10) Hz
Proton pulse duration	0,4 μsec	0,44 μsec	-	1 μsec
Energy in one pulse	3.2 kJ	8 kJ	-	100 kJ
Accelerator system	Linac + RCS	Linac + RCS	2-stage cyclotron	Linac + 2 PCR
Target material	(238-U) Ta	W5%Re	Pb* (Zy-2)	Hg
Time av. of peak power density	(0,9) 0,5 MW/l	0.4 MW/l	0.4 (0.25) MW/l	3 MW/l
Target cooling	D_2O in volume	D_2O edge	Pb* (D_2O in vol.)	Hg

Pb* : Lead-based eutectic (PbBi, PbMg or Pb)

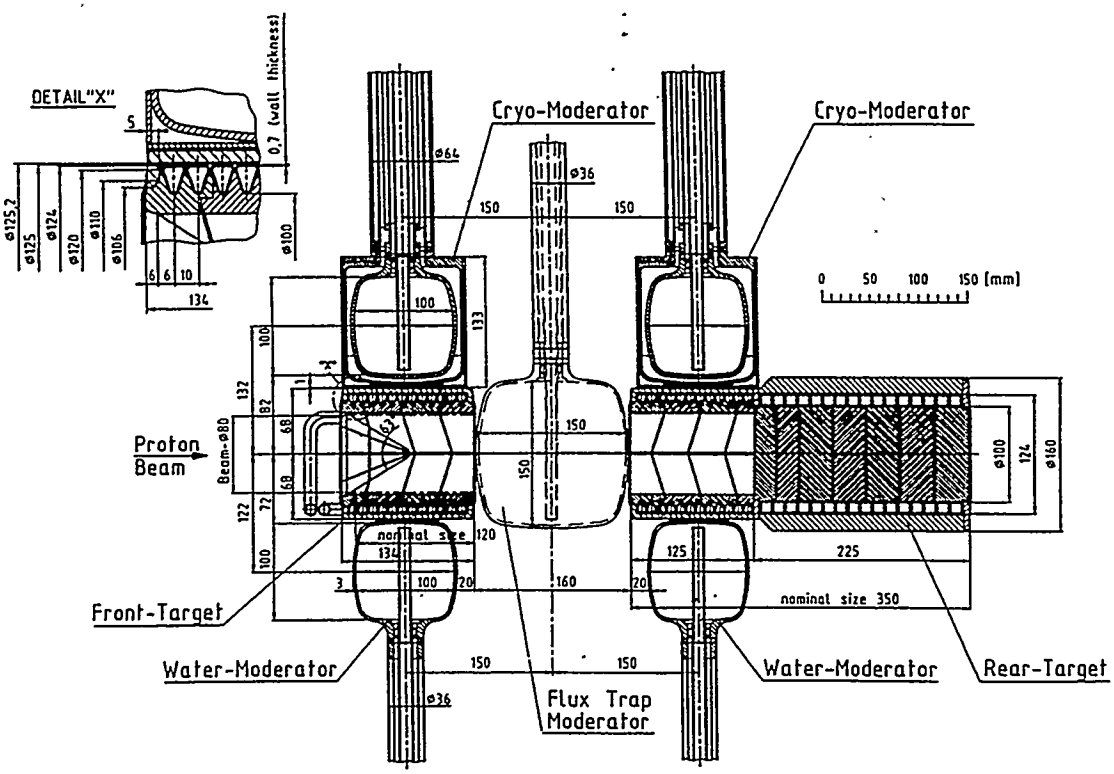

Split-Target with Moderators
(Cross-Section in front view - Reflector is not shown)

FZ Seibersdorf

"AUSTRON Target Group"
Schmeskal / Ritter
W824/93-Skizze 98
02-06-94

The AUSTRON Target

The AUSTRON-Target
Some characteristic Data (*)

Quantity	Target version cylindrical	flat
Beam power (kW)	205	205
Power in target (kW)	86	90
Gaussian profile σ_x^2, σ_y^2 (cm^2)	2.25,2.25	20,1.2
Av. power density (W/cm^3)	32	12
Peak temperature (°C)	928	563
Peak stress (MPa)$^{++}$	278	286

$^{++}$ Time average, not accounting for pulsed energy deposition within 0.4 μs.

(*)(From: AUSTRON-Feasibility Study, Ch. 5.5)
Numbers refer to the AUSTRON-II version (25 Hz, 205 kW in beam), which is now considered an initial stage, leading to the AUSTRON III version with 410 kW beam power by doubling of the repetition rate and adding a second target station.

SINQ Design Features

Accelerator

8 sector isochronous cyclotron, 590 MeV, 51 MHz
Injector: 4 sector isochronous cyclotron, 72 MeV
Proton beam current 1.5 mA
Beam behind pion target: 570 MeV, 1mA

Beam on Target

2-dim. gaussian distribution, SDx/y = 3.3/3.83 cm
→ 17 μA / cm² in maximum (30 μA/cm²/MW)

Target Station

Vertical beam injection from underneath
Zircaloy rod target => Liquid PbBi-eutectic
2 m diameter heavy water moderator
25 litre liquid deuterium cold moderator
5 twin beam ports (4 thermal, 1 cold)
7 cold neutron guides

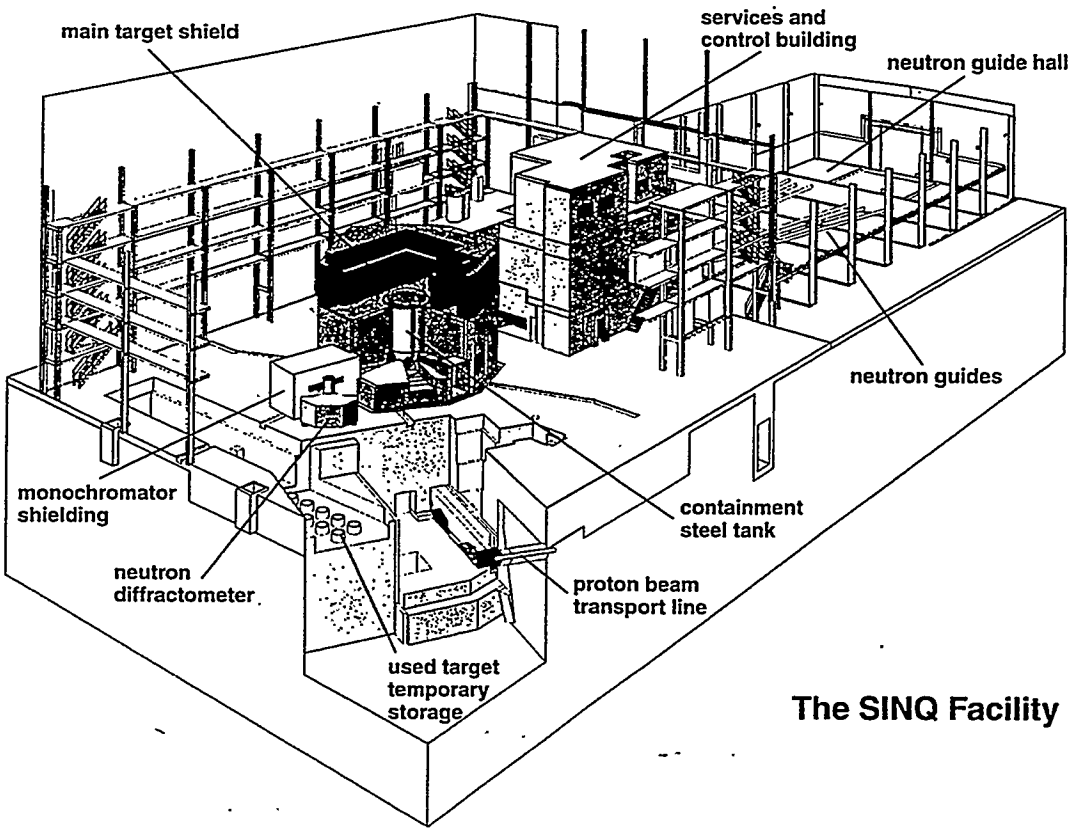

The SINQ Facility

The Inner Region of the SINQ Target Block

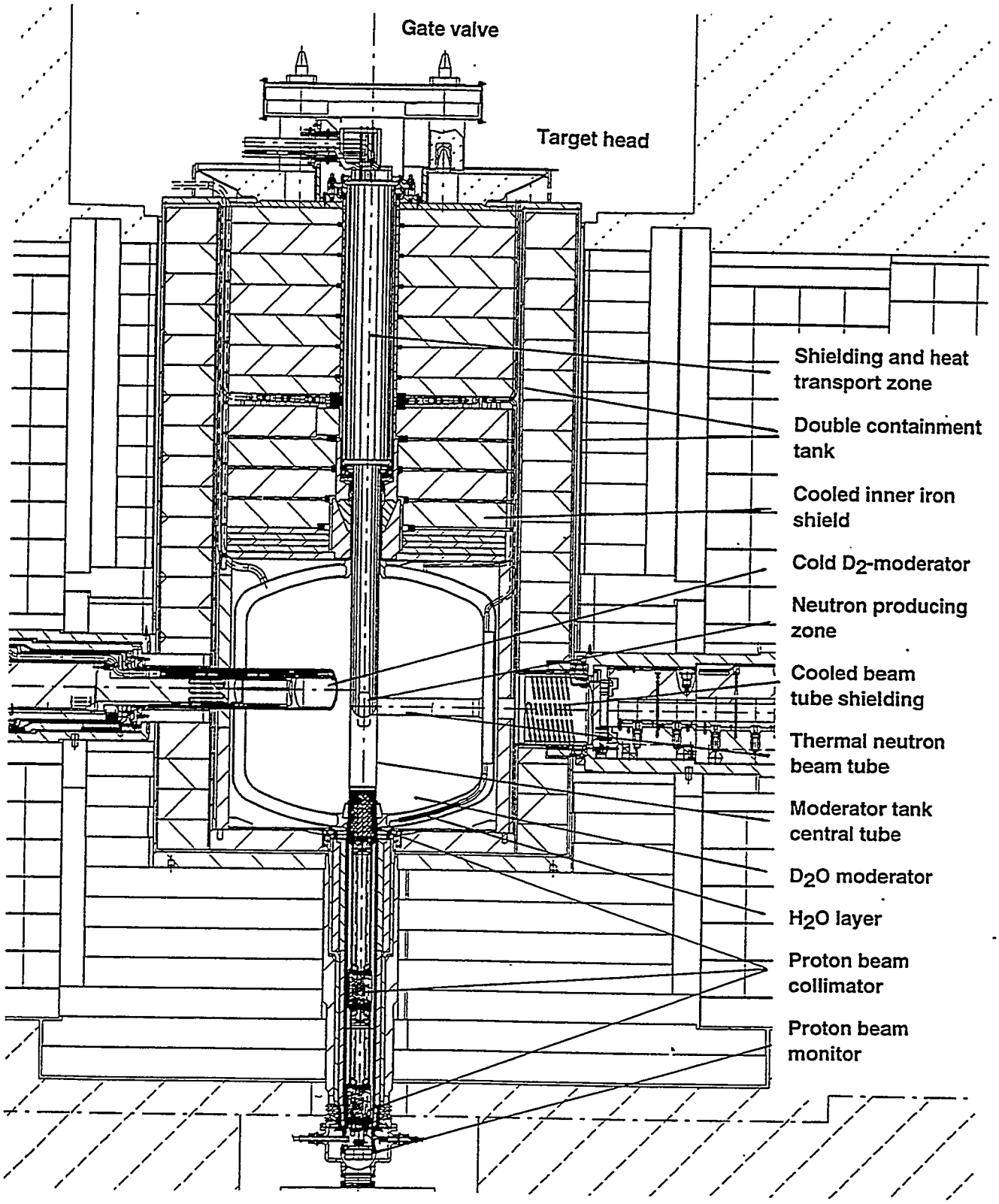

Calculated flux levels per mA of 570 MeV protons for different taret concepts for SINQ

Target system	Maximum thermal flux ($cm^{-2}s^{-1}$)	Useable flux at 25 cm ($cm^{-2}s^{-1}$)	Relative flux at 25 cm radius
Pb (or PbBi) with weakly absorbing container	2×10^{14}	1.3×10^{14}	1
Pb-Bi with steel container(4mm)	0.9×10^{14}	0.85×10^{14}	0.65
W-plates in Al-container	0.8×10^{14}	0.6×10^{14}	0.46
Ta-plates in Al container	0.55×10^{14}	0.45×10^{14}	0.35
Pb-rods in (zircaloy) tubes	1.5×10^{14}	1×10^{14}	0.70
Zircaloy rods	0.8×10^{14}	0.5×10^{14}	0.38

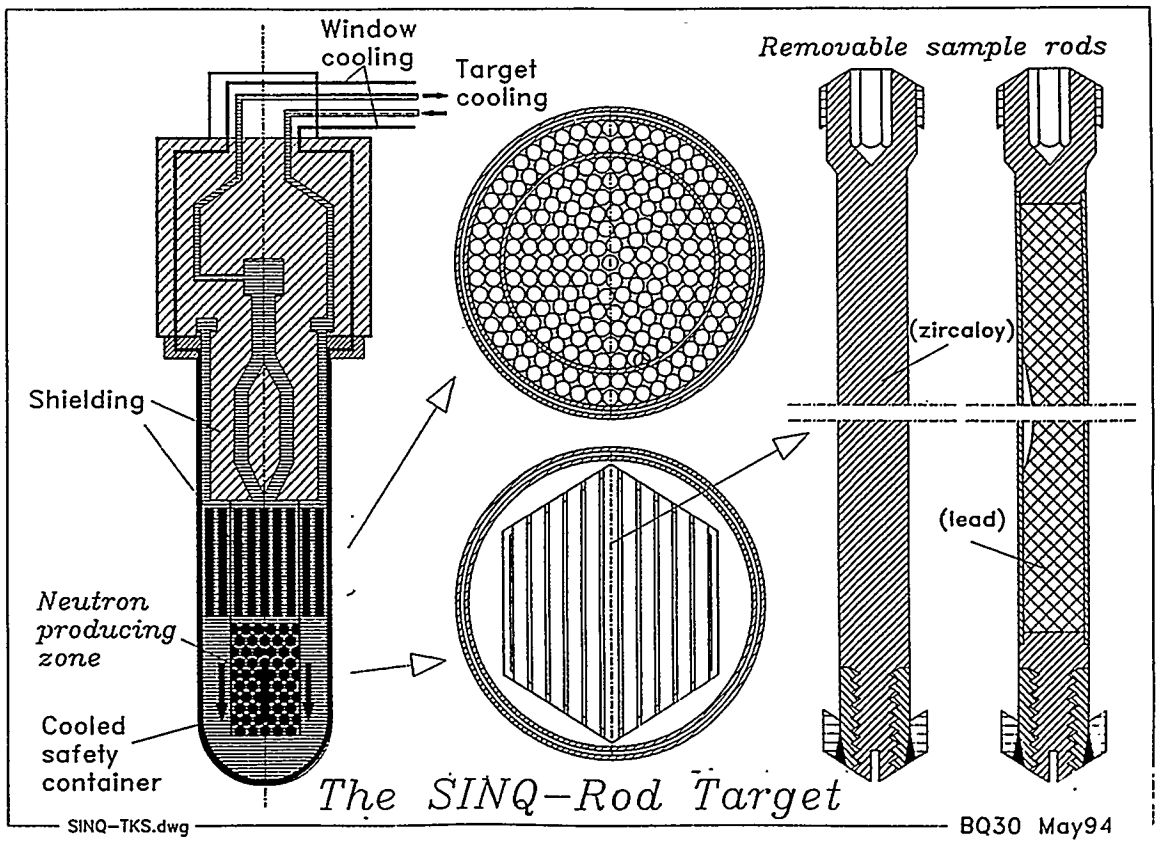

Radioactivity data for SINQ cooling circuits

Quantity	Safety hull	Target
direct energy deposition (kW)	3.6	94
coolant mass flow rate (kg/sec)	2.2	9
pipe inner diameter (cm)	2.8	6.6
dose rate at target exit per m of pipe		
- from gamma rays (mS/h)	37	410
- from delayed neutrons (mS/h)	20	178
tritium production		
- after 1 year (10^{12} Bq	0.5	7.4
- equilibrium (10^{12} Bq)	14	180
7-Be production (equil., 10^{12} Bq)	0.3	5.2
10-Be production (per year, 10^{6} Bq)	0.2	3
14-C production (per year, 10^{9} Bq)	6	15

Data do not include the effects of corrosion, erosion and direct injection of spallation products into the coolant. These effects increase with surface area!

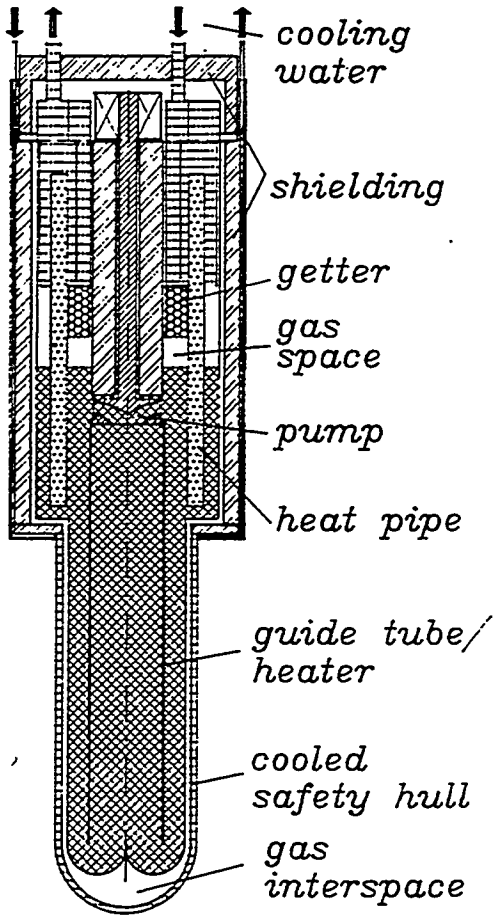

Pumped and heat pipe cooled liquid metal target

sinq-plt.dwg — BQ30 Jun94

Rationale for a Liquid Metal Target

- no "good" material for a solid target available (especially for cw-sources)
- no coolant (water) in the beam
- no LOCA problem
- "infinite" life time of target material

There exists no "good" material for a solid target

Candidate	Problems
Uranium	metallurgical (growth) cladding required (reacts with water) fission products (gaseous) absorption (7.7 barn)
Tantalum	absorption (21 barn) high decay heat and activity (hydride?)
Tungsten	absorption (19 barn) brittleness machinability (corrosion in machinable composites)
Lead	softness poor thermal conductivity corrosion with water high thermal expansion (cladding) low melting point
Bismuth	anisotropic recrystallization formation of 210-Po
Gold	absorption (9.3 barn) price
Zircaloy	low neutron yield hydride radiation growth

Radiation effects in materials for various ranges of reduced temperature

(H. Ullmeier, n. F. Carsughi, NIM B, 101 /1995)

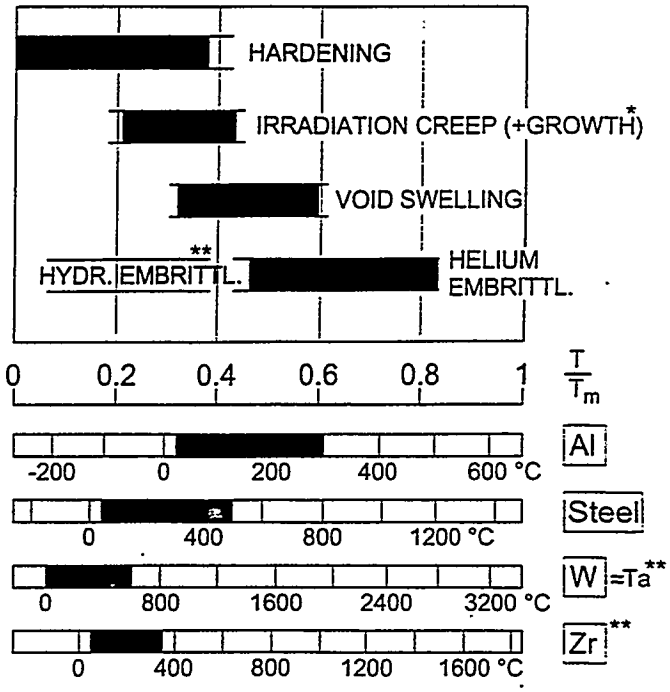

* in non-cubic metals ** in hydride-forming materials

BO30-14/KI82 22.03.95

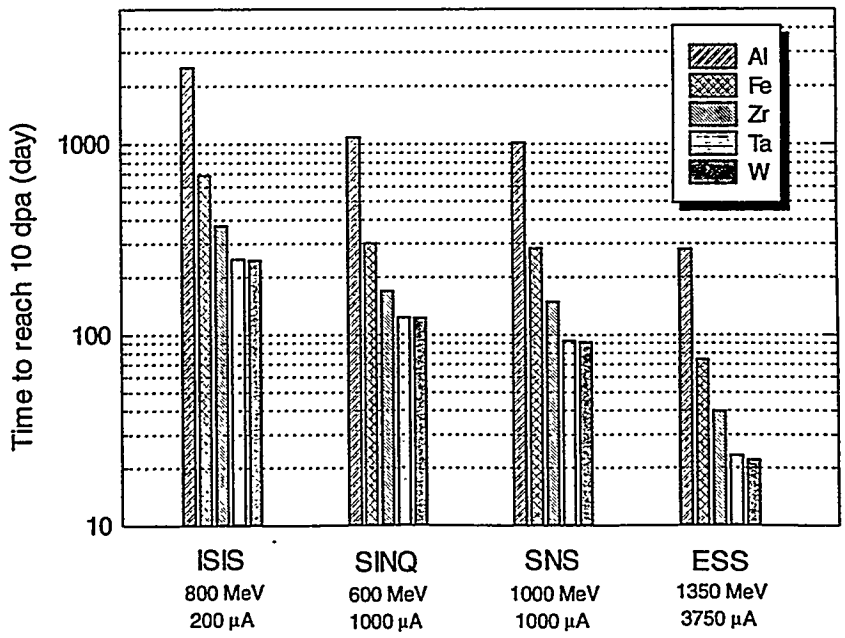

Relative damage for various target materials expected at several facilities.

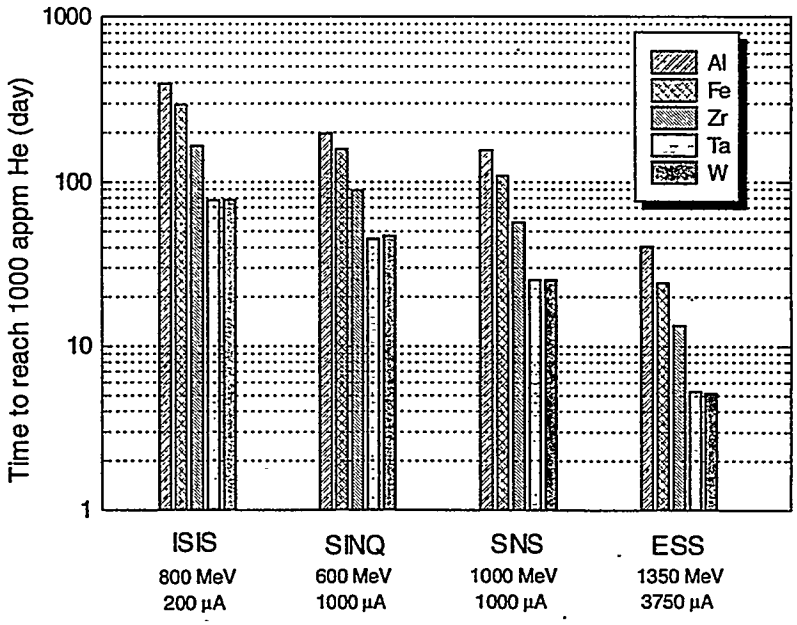

Relative He production expected in various target materials at several facilities.

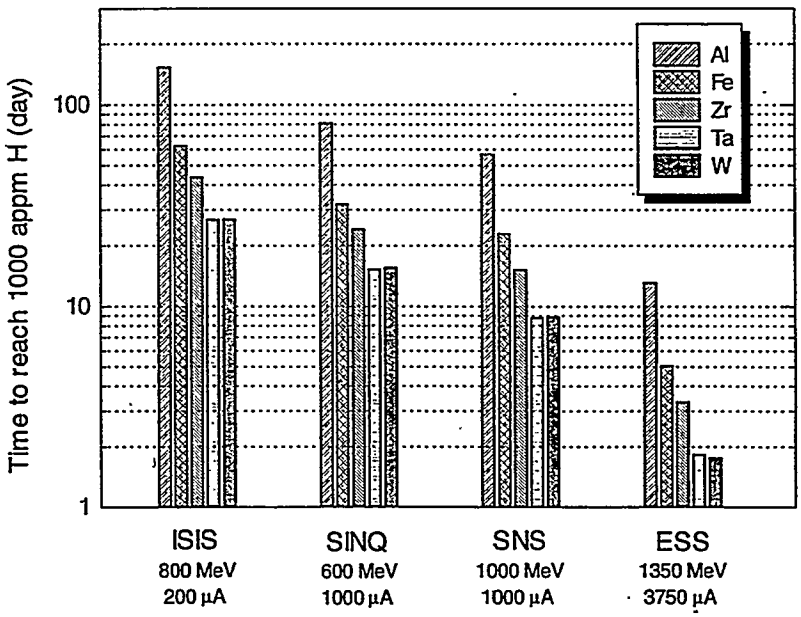

Relative H production in various target materials expected at several facilities.

Coolant (water) in the proton beam

Features	Potential problems
Large metal surface and coolant fraction for heat transfer	♦ average density low ("brightness")
	♦ contamination from recoils (~ 50μg/cm^2)
Radiolysis	♦ corrosion
	♦ growth of oxide layer (heat transfer)
Pressure level (flow, prevention of boiling)	♦ window thickness (coolability)
	♦ stress corrosion (radiation enhanced?)
Spallation in Oxygen	♦ enhanced production of Tritium
	♦ production of ^{7}Be (γ, 56 days)
	♦ complicated water circuit (contaminated)
LOCA	♦ high decay heat density (emergency cooling /risk of metal-steam reaction)
Damage recognition	♦ SINQ: 6 to 12 hours delay (γ's from β^+)

Liquid Metal Target Candidate Materials and Their Relevant Properties in Comparison

	Pb	Bi	LME	LBE	Hg
Composition	elemental	elemental	97.5%Pb +2.5%Mg	45% Pb +55%Bi	elemental
Atomic number Z	82	83			80
Atomic mass A (g/mole)	207.2	209			200.6
Density (g/cm^3) solid (20°C)	11.35	9.75			
liquid	10.7	10.07	10.6	10.5	13.55
Coeff. of thermal expansion (K^{-1})	$2.91 \cdot 10^{-5}$	$1.75 \cdot 10^{-5}$			$6.1 \cdot 10^{-5}$
Contraction on solidification (%)	3.32	-3.35	≈3.6	≈0	
Melting point (°C)	327.5	271.3	250	125	-38.87
Boiling point at 1 atm. (°C)	1740	1560			356.58
Specific heat capacity (J/g/K)	0.14	0.15	0.15	0.15	0.12
Thermal neutron absorption (barn)	0.17	0.034	0.17	0.11	389
Corrosivity	moderate	highest	moderate	high	low
Chemical activity	moderate	highest	moderate	high	low

Desirable properties of the target material

* High atomic number for neutron yield
* High density for brightness
* Low melting point
* Low corrosive activity (solubility of containment elements)
* Chemical inertness
* Low resonance integral (absorption of keV neutrons)
* High scattering cross section (reflector)
* (Low absorption cross section for thermal neutrons)

For pulsed neutron sources Mercury looks good

► Thermal neutron absorption not relevant due to decoupler
* Resonance integral lower than in solid competitors (Hg:73, Ta:710, W: 352 barns)
* Scattering cross section high (20 barns, Ta, W: 5 barns)
* Liquid at room temperature => no auxilliary heating
* 30 % higher density than PbBi (13.6 g/cm^3)
* Not corrosive (solubilities 1 to 2 OoM below Bi or Pb)
* Chemically inert (easy to purify)
* No very long lived isotopes (194-Hg, 367 y as spallation product)
* Can be converted to stable and insoluble amalgam

High toxicity of fumes, low vapor pressure

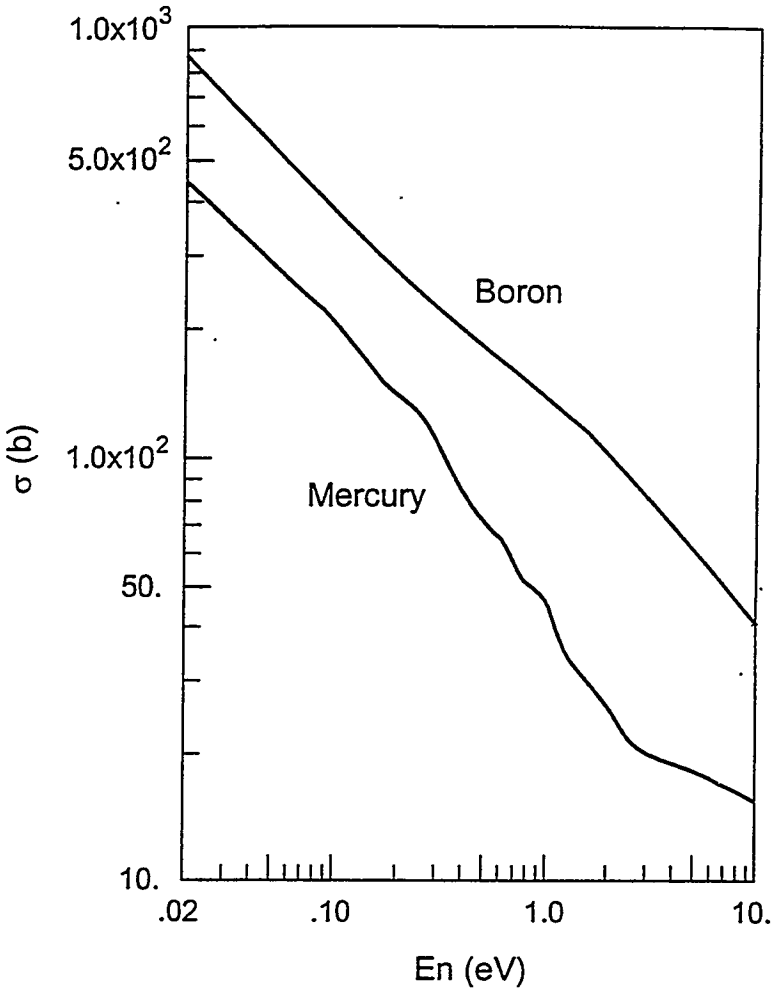

Thermal neutron total cross section

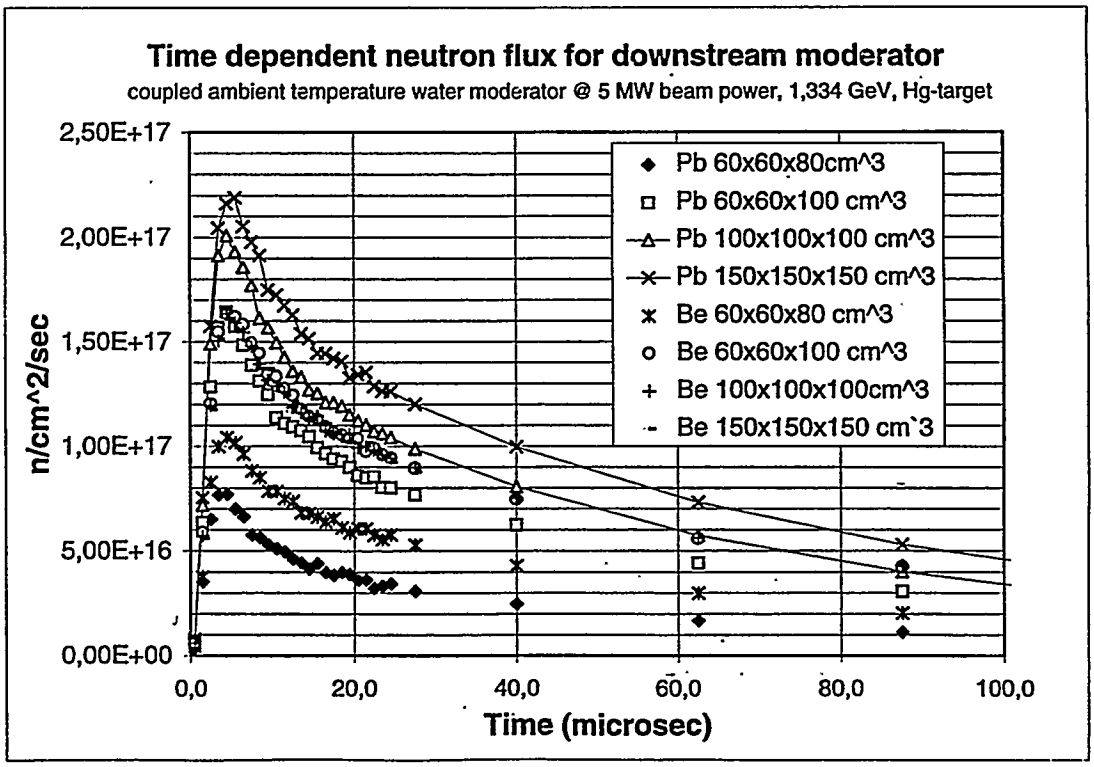

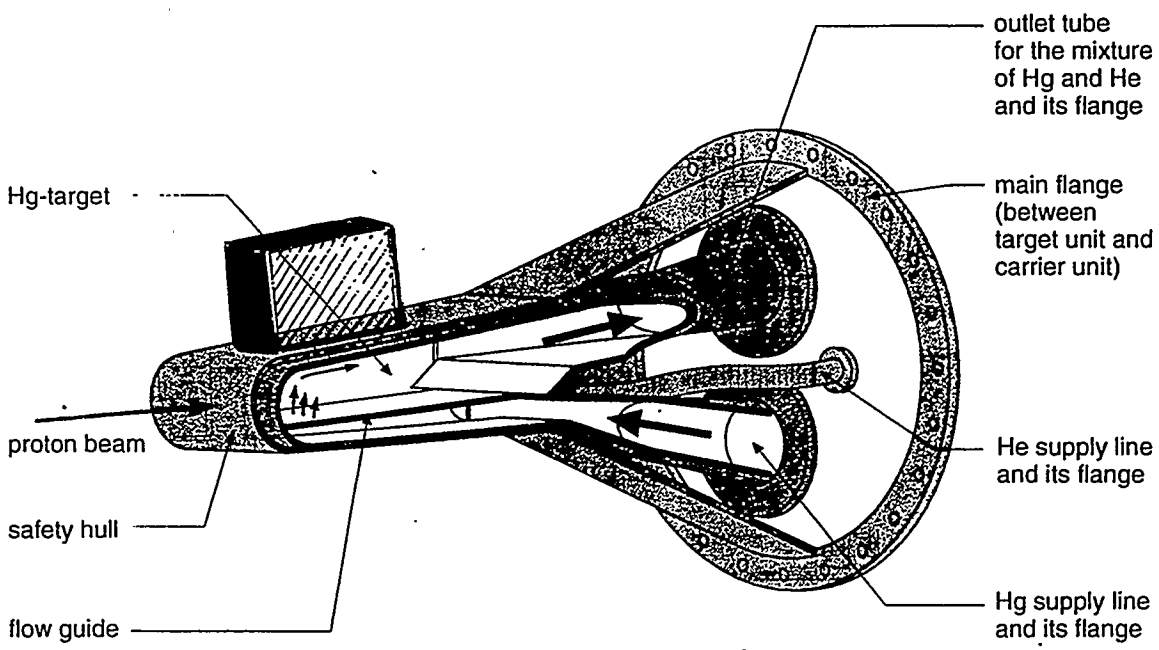

Design of target unit

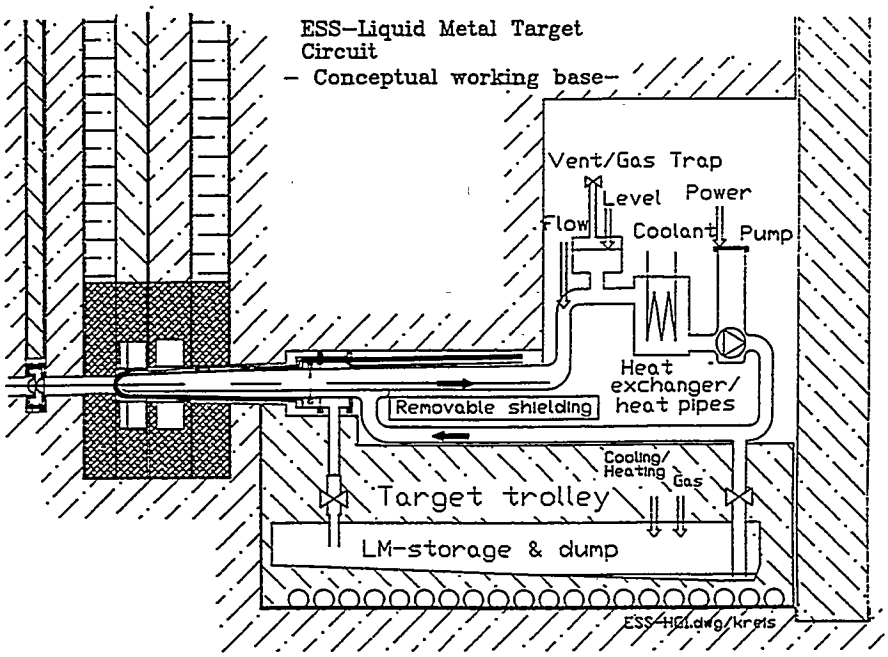

Schematic of the ESS-liquid metal target concept.
The liquid metal circuit is mounted on a trolley which also contains the storage tank. In the beam interaction region the target shell is surrounded by a double-walled, water cooled, safety hull which, in case of a failure of the target shell, guides the liquid metal back to the storage tank via a drain pipe equipped with a rupture disk.

ESS Mercury Circuit

Power in Target		3,30 MW
Design margin for components		20 %
Design flow rate (max)		250 kg/s
Mean temperarure in return flow		max. 300 °C
	Preferred temperature	200 °C
Max. difference in mean temperature		120 °C
Amount of Hg in circuit		1 m^3
	Volume of dump tank	2 m^3
Decay heat	at shutdown	10 kW
	after 100 years	1,60E-03 kW
Activity	at shutdown	1,20E+05 TBq
	after 100 years	13 TBq

FORSCHUNGSZENTRUM JÜLICH GmbH KFA IKP

HG – TARGET ESS 5 MW P BEAM

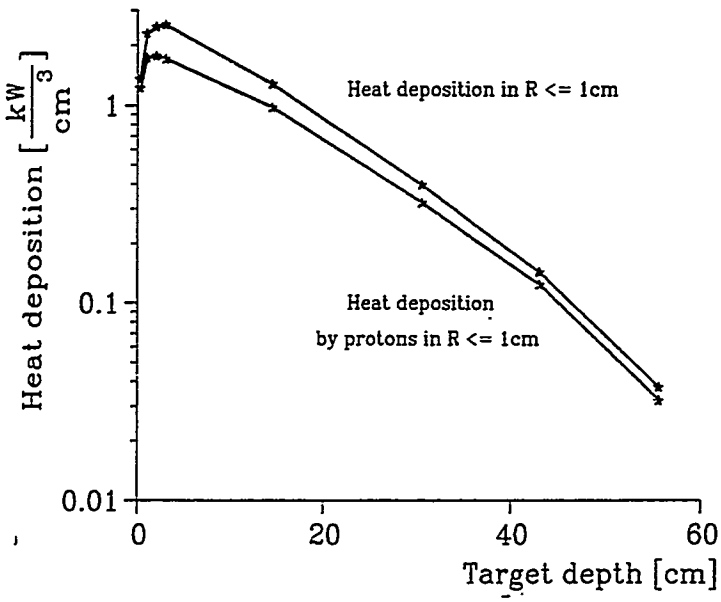

file: heat.gli Arbeitsgruppe Strahlungstransport

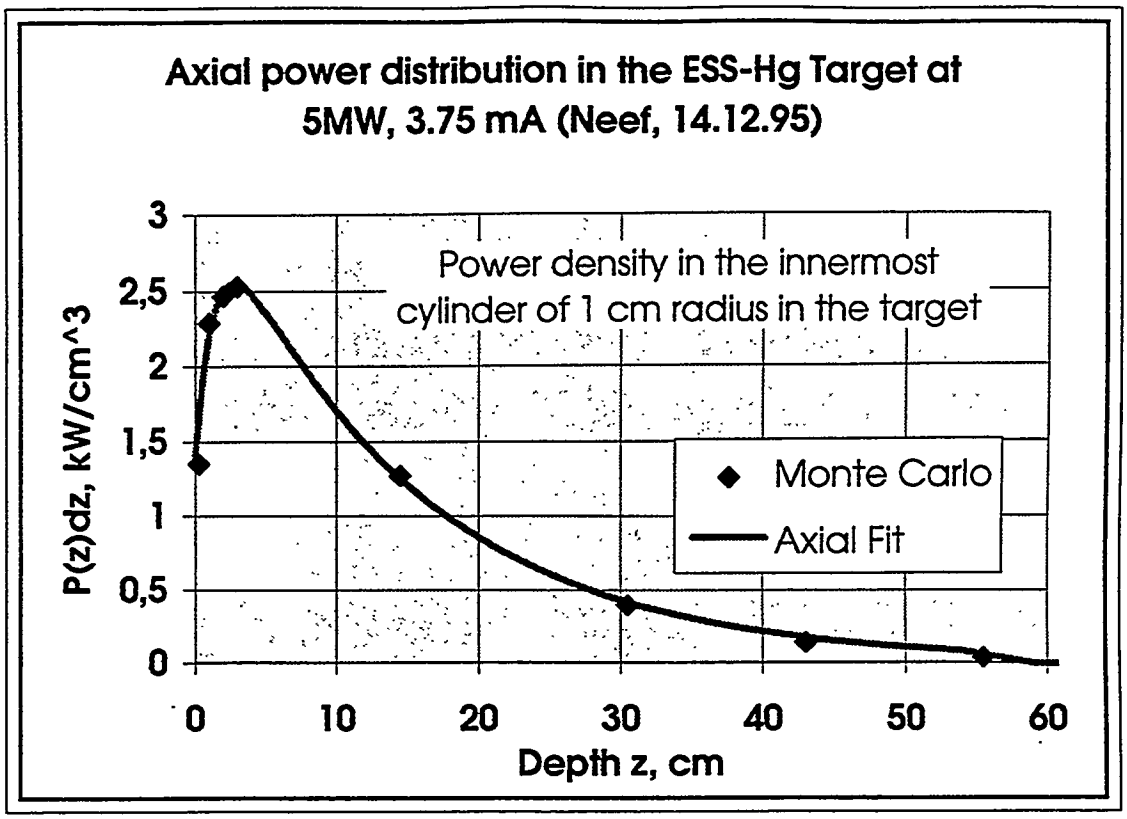
Axial power distribution in the ESS-Hg Target at
5MW, 3.75 mA (Neef, 14.12.95)
Power density in the innermost
cylinder of 1 cm radius in the target
Monte Carlo
Axial Fit
P(z)dz, kW/cm^3
Depth z, cm
0
0,5
1
1,5
2
2,5
3
0
10
20
30
40
50
60

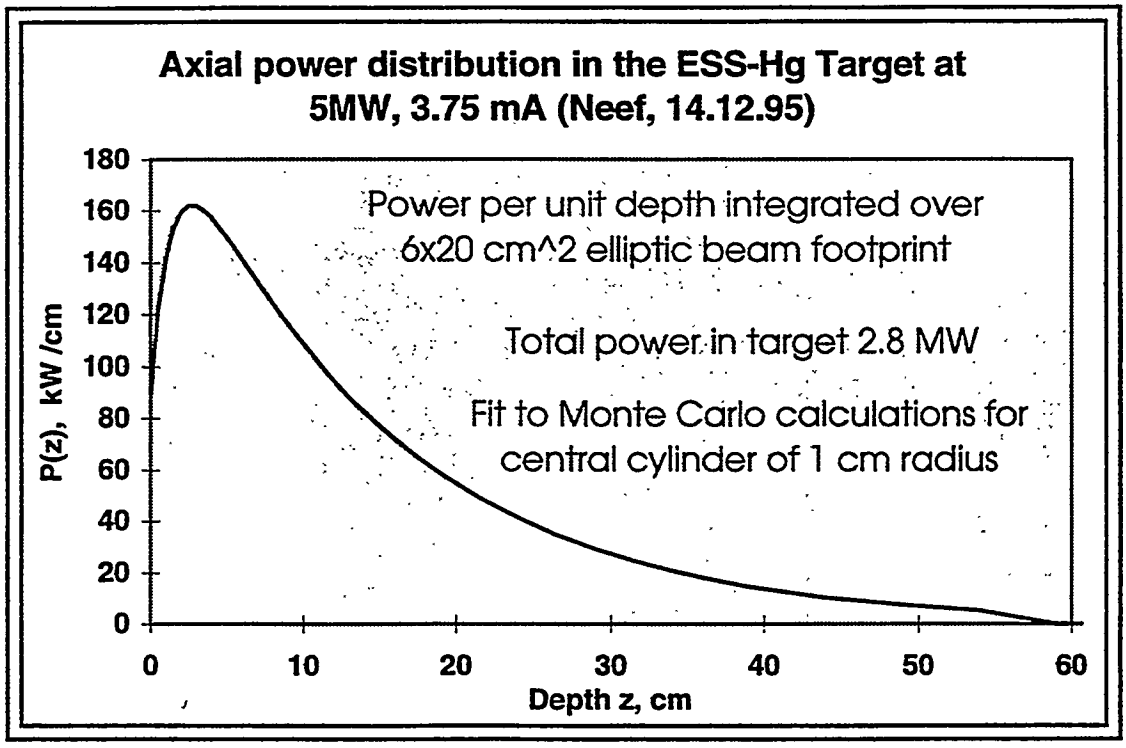
Axial power distribution in the ESS-Hg Target at
5MW, 3.75 mA (Neef, 14.12.95)
Power per unit depth integrated over
6x20 cm^2 elliptic beam footprint
Total power in target 2.8 MW
Fit to Monte Carlo calculations for
central cylinder of 1 cm radius
P(z), kW /cm
Depth z, cm
0
20
40
60
80
100
120
140
160
180
0
10
20
30
40
50
60

TARGET SURFACE NEUTRON FLUX

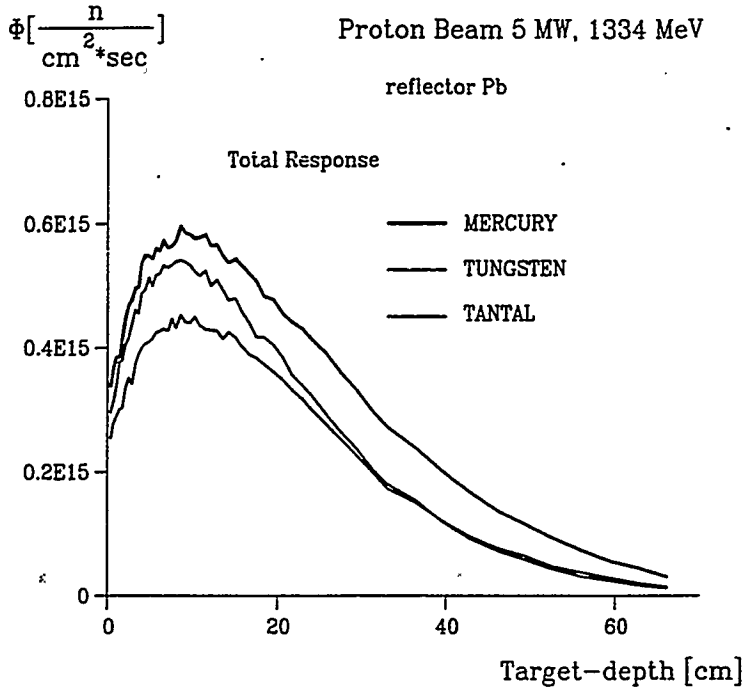

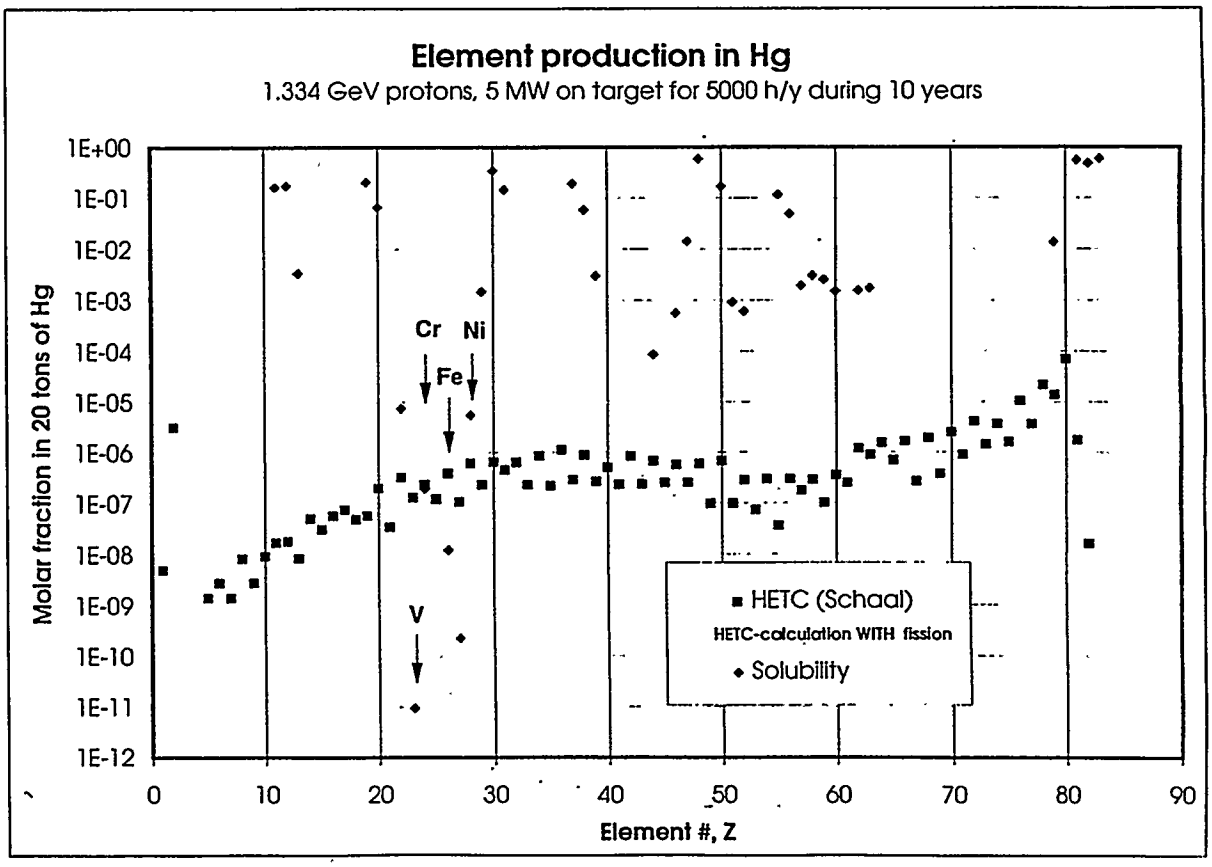

Summary of ESS-Liquid Metal Target Concept

Problem	Risk / Consequences	Proposed Solution	Added features
Radiation damage in target material (dpa, H and He)	Very short target life	Liquid metal target	Convective heat remval; Avoids radiolysis and corrosion in water circuit
Volume change upon solidification / melting / cooling	Damage to structural components	Mercury	Less corrosive than Pb and Bi; no 210-Po; Saves decoupler
Temperature quenches during beam trips	Transition into brittle regime; Thermal fatigue	Variable conductance double wall heat pipes	Minimizes risk of water ingress into LM
Pressure waves due to power pulses	50 Hz cyclic load beyond recommended design stress	3 vol% He in reaction volume	Supports removal of volatile species (safety feature)

Flow optimization in interaction zone
Highest temperature in liquid => pressure level
Adequate window cooling => mechanical strength and radiation damage
Maximum temperature of liquid in contact with wall => corrosion and thermal cycling

The Great Challenge: Check theory against experiments

Out-of beam:

Flow distribution	**Water** **Mercury** **(PbBi)**
Window cooling	**(Sodium)** **Mercury**
Bubble generation	**(Water)** **Mercury**
Corrosion (stagnant and flowing; ΔT; prestressed)	**Mercury** **PbBi** **(PbMg)**

In-beam:

"Shock absorption"	**ISOLDE (?)**
Rad.-enhancement of corrosion	**INR Troitsk(?)** **SINQ (?)**
IPPE-Prototype	**LANL (INR?)**
Radiation damage	**LANL** **ORNL triple beam** **PIREX**

ORNL DWG 96Z-3865

The Oak Ridge Spallation Neutron Source (ORSNS) Collaborative Design Project

Bill R. Appleton
Associate Director
Oak Ridge National Laboratory

International Workshop on the

Technology and Thermal Hydraulics of Heavy Liquid Metals

Schruns, Austria
March 25-28, 1996

Origins of the ORSNS Collaborative Design Project

ORSNS

- Since the early 1970s, numerous assessments by the National Research Council (i.e., Seitz-Eastman Report, Major Facilities for Materials Research and Related Disciplines, 1984) and the Department of Energy (i.e., Kohn BESAC Panel Report, Neutron Sources for America's Future, 1993) have firmly established the need for new neutron sources and instrumentation in the U.S.
- As a follow-on to the Seitz-Eastman study, the DOE/ER issued a memorandum titled Secretarial Site Selection Decisions on Specific Energy Research Projects proposing sites for four specific ER facilities "to maintain the technical viability among the DOE Laboratories"
  - Relativistic Heavy Ion Collider at BNL
  - 1 to 2 GeV Synchrotron Radiation Source at LBNL
  - 6 to 7 GeV Synchrotron Radiation Source at ANL
  - Advanced Research Reactor at ORNL

This long-range plan has been closely followed by DOE/ER since the mid-1980s.

- The Basic Energy Sciences Advisory Committee (BESAC) Panel on *Neutron Sources for America's Future* (Kohn Panel) recommended in 1993:

  "**Recommendation 1:** Complete the design and construction of the ANS according to the schedule proposed by the project.

  "**Recommendation 2:** Immediately authorize the development of competitive proposals for the cost-effective design and construction of a 1-MW PSS. Evaluation of these proposals should be done as soon as possible, leading to a construction timetable that does not interfere with rapid completion of the ANS."
- The Conceptual Design Report for the ANS was completed (1986-1993), ORNL was DOE's preferred site, and the project was in the 1994 and 1995 President's Budgets as a construction line item but was not approved by Congress either year.
- The DOE/ER asked LBNL to coordinate a study for design of a 1MW pulsed spallation neutron source complementary to ANS, and ANL, BNL, and LANL initiated studies of their own.

Origins of the ORSNS Collaborative Design Project

ORSNS

- Funds to continue ANS were not included in the FY 1996 budget due to the large project costs ($2.9 billion) and DOE proposed design of a new spallation source as an alternative
- The appropriation bill passed by Congress in FY 1996
  - Provided $8 million for conceptual design of a new spallation neutron source
  - Asked DOE to select the final site of the new spallation source in a fair and unbiased manner
  - Directed DOE to evaluate upgrades of existing reactors and spallation sources as a cost-effective means of providing neutrons to the scientific scientific community while the next generation source is developed
- The DOE/ER directed the $8 million to ORNL to initiate conceptual design on the new spallation source, and designated ORNL the preferred site.
- **The ORSNS collaborative design project is ORNL's response to this charge from DOE/ER.**

The ORSNS Is A Design-to-Cost Project

ORSNS

- As a follow-up to the 1993 Kohn Panel Report, the DOE/ER formed a new BESAC panel on Spallation Neutron Sources in 1996 to provide guidance on:

  "(1) source characteristics, including pulse length, power, and neutron energy spectrum; and

  "(2) trade-offs such as upgradable source, full performance but with limited instrumentation, and low performance source with full instrumentation"

  ... "The total cost of a new spallation source should be kept below $1 billion."

- In response to Congressional directives, two other BESAC panels considered upgrade scenarios to existing spallation and reactor sources to provide neutron capabilities while this new source is being designed and built.

- Beginning in FY 1995, ORNL developed a Design-to-Cost model to aid in selecting technologies for an accelerator-based, spallation neutron source

- The ORNL Design-to-Cost model included input from the ANL, BNL, LANL, and ESS feasibility studies, and was validated against the:
  - ANL IPNS Upgrade Feasibility Study
  - BNL 5 MW Pulsed Spallation Neutron Source Preconceptual Design Study
  - The Advanced Neutron Source Project

ORSNS Technology Approach

ORSNS

- The design approach proposed by ORSNS to meet the needs of the neutron scattering community is:
  - Design an accelerator-based, ~5 MW, pulsed (μs) spallation neutron source that can be constructed in stages
  - Align technology choices with performance criteria established by the neutron scattering users and the DOE
  - Utilize validated design-to-cost models to select the best technologies consistent with available funds
  - Design and construct the first stage at a power consistent with available technology and funds
  - Upgrade the facility to ~5 MW in the future as funds and technology allow

ORNL-DWG 96Z-2354

ORSNS Collaborative Design Project

ORSNS

- The ORSNS project is organized to take full advantage of previous studies and assessments, and of the technical expertise and experience that exists at the other DOE laboratories, industry, and universities in the U.S.
- Memorandums of Understanding (MOUs) have been initiated to share technical and scientific information with the European Spallation Source (ESS) project and several European laboratories.
- Workshops have been held to ensure that ORSNS takes full advantage of mutually beneficial R&D with the Accelerator Production of Tritium (APT) project.

ORNL-DWG 96Z-2355

ORSNS Collaborative Project Management

ORSNS

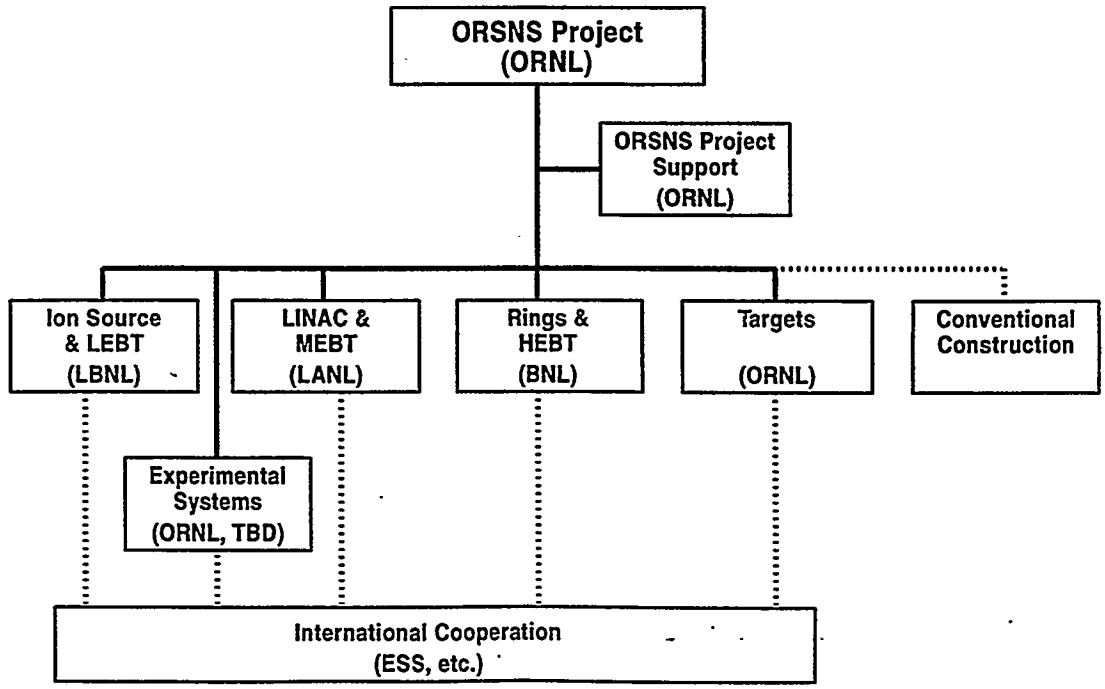

Status of ORSNS Project

ORSNS

- Design studies were initiated at ORNL in the fourth quarter of FY 1995
  - A target design group was formed
  - A materials qualification/evaluation group was started
  - A design-to-cost model was constructed and validated against existing spallation source and accelerator projects, and ANS
  - The site selection process at ORNL was initiated
  - Cooperative projects were initiated to:
    - Cost validate the BNL 5 MW PSS study
    - Evaluate accumulator ring options (BNL)
    - Study background effects during target bombardment (RAL)
  - The relevant ANS Project management and R&D was transferred to ORSNS

- In FY 1996, DOE provided $8 million to initiate the conceptual design study at ORNL
  - The project management structure was established.
  - Formal design collaborations were initiated with BNL, LANL, and LBNL. Other collaborations are pending.
  - Cooperative MOUs were established with several international laboratories and the ESS project.
  - A senior accelerator physicist and support group will be hired into ORNL.
  - ORNL will host an International Workshop on the Technology and Thermal Hydraulics of Heavy Liquid Metals in collaboration with the Paul Scherrer Institute (Switzerland) March 25-28, 1996, and an International Workshop on Spallation Materials Technology at ORNL April 23-25, 1996.
  - The ORSNS Project is on schedule for an FY 1998 construction line item request to the DOE.

Recommendations for a High Power (~ 5 MW) Spallation Neutron Source

ORSNS

- The U.S. should plan for a high power (~ 5 MW), short pulse, spallation source to become competitive in neutron scattering
- The ORSNS recommended reference design for an upgradable (~ 5 mw), source is:
  - 1-1.25 GeV conventional linac
  - Two accumulator rings
  - Mercury targets and appropriate moderator systems
  - Two experimental target stations/guide halls producing neutrons from microsecond pulses at 10 Hz and 50 Hz
- Options that should be evaluated are a lower energy linac with rapid cycling synchrotrons replacing accumulator rings, solid Ta targets, and superconducting linacs.
- The initial ~ 1 MW facility that could be built for ~ $1 billion invalues low risk technology, a single accumulator ring, one target station, and four instrumented beam lines.
- There are various upgrade scenarios to higher power that involve increased ion source performance and/or funneling, two accumulator rings, and additional target stations and instrumentation.
- Preliminary design-to-cost evaluations have shown that:
  - There is only a modest penalty to design a 5 MW facility and construct it in stages as funds allow. There is a significant cost to building two sequential facilities leading to 5 MW.
  - The choice between RCSs and accumulator ring options should be made on technical grounds since the costs are comparable.
  - A 1 MW facility can be built for about $1 billion and a 5 MW facility for about $1.5 billion TPC (30% contingency).

ORSNS Pulsed Spallation Neutron Source Performance

ORSNS

Reference Design Parameters:	Initial	Upgrade #1
Ion Source: Assume H^- pulsed current (mA) =	35.0	70.0
RFQ: Assume capture/bunching factor =	0.80	
Linac: Assume capture and accel. eff. =	1.00	
Assume final beam energy (GeV) =	1.00	$\beta = 0.8737$
Assume source/linac duty factor (%) =	6.11	6.11
Ring: Accumulator with circumference (m) =	208.6	
Assume ring filling fraction =	0.65	0.65
Insertion efficiency fraction =	0.90	
Assume ring pulse rate (Hz) =	60	
Orbit rotation time (μsec) =	0.80	0.80
Number of turns injected =	1279	1279
Time to fill ring (msec) =	1.02	1.02
Injected pulse charge (μA-sec) =	16.7	33.3
Particles per pulse =	1.04E+14	2.08E+14
Extracted pulse length (μsec) =	0.52	0.52
Beam kicker gap (μsec) =	0.28	0.28
Time-average particles per second =	6.3E+15	1.3E+16
Time-average beam current (mA) =	1.00	2.00
Average beam power (MW) =	**1.00**	**2.00**

National Spallation Neutron Source Reference Design

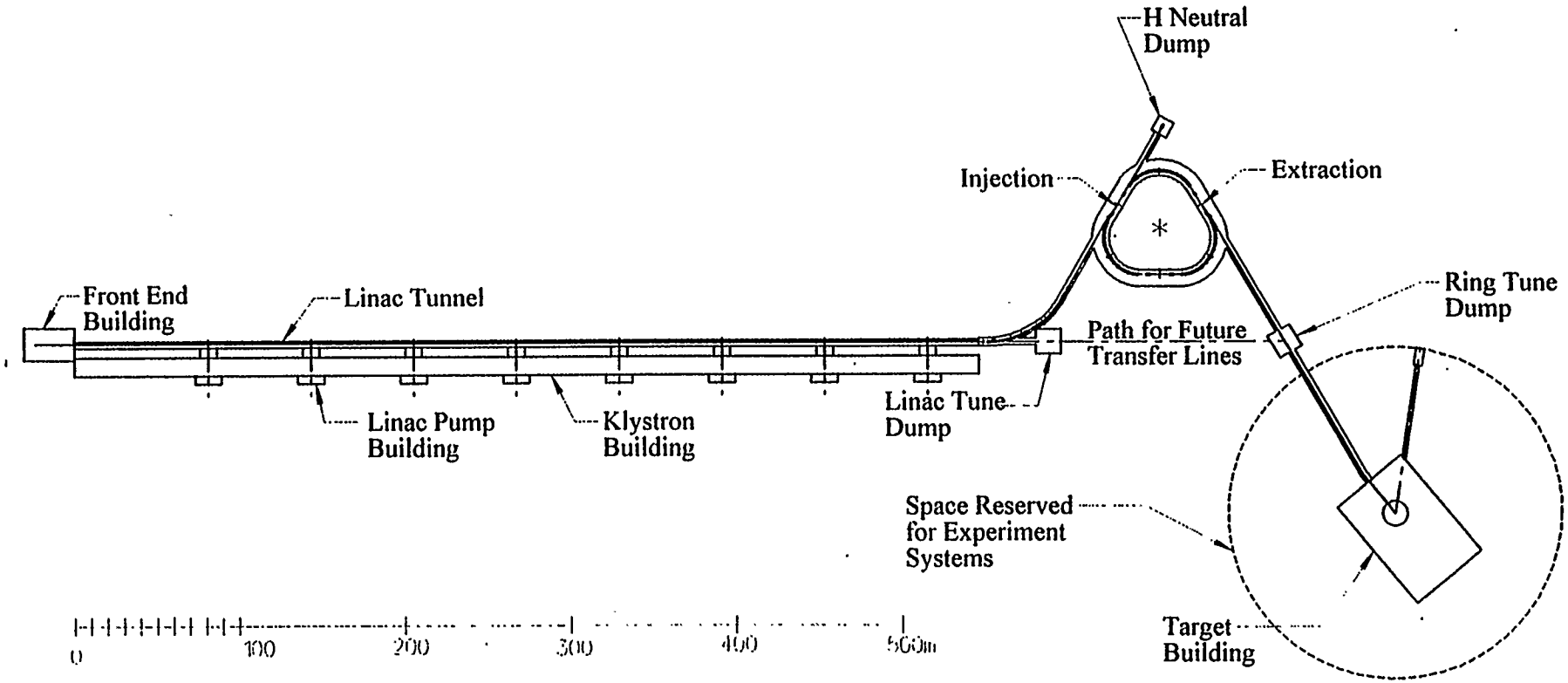

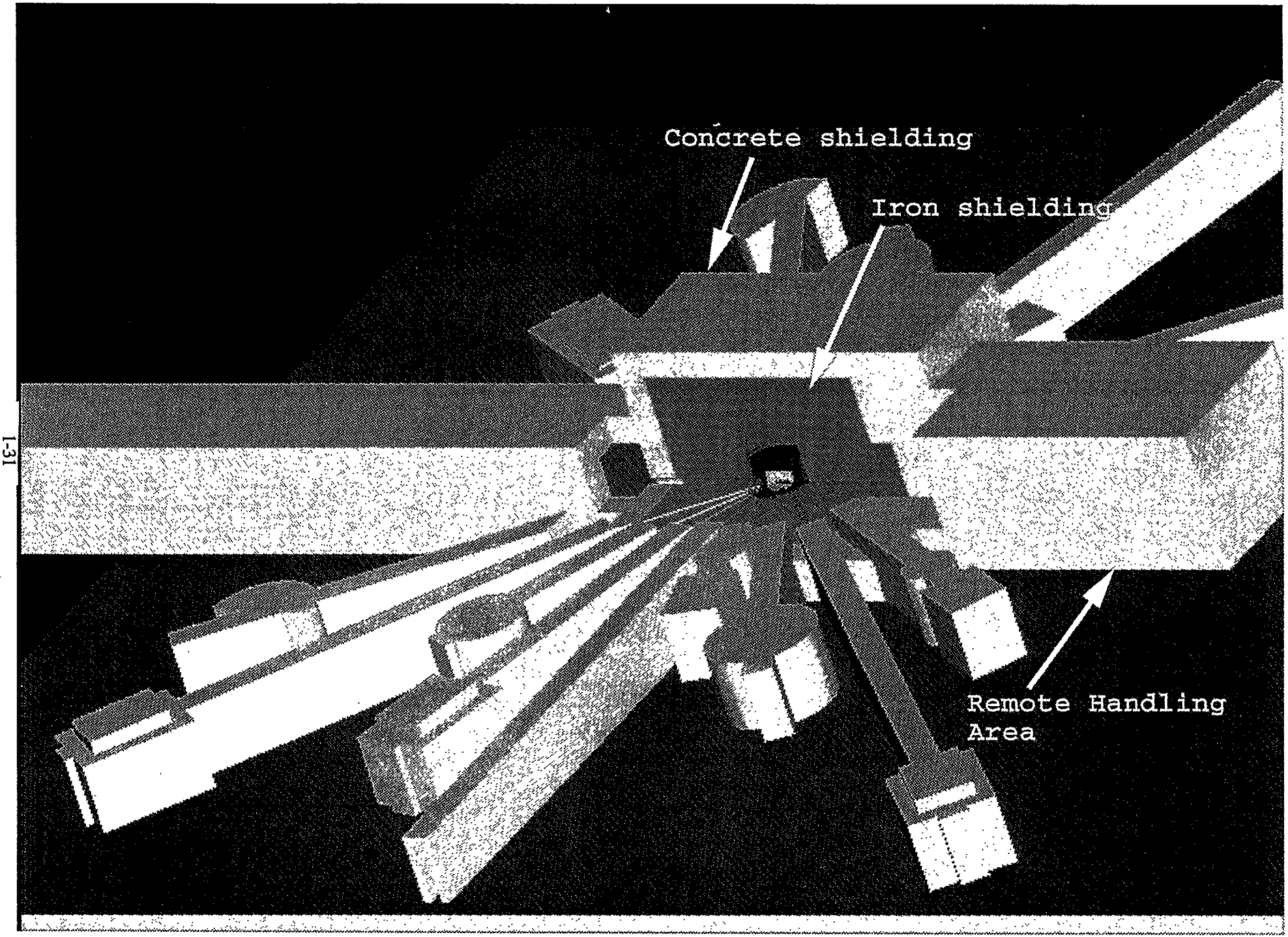
Concrete shielding
Iron shielding
Remote Handling
Area

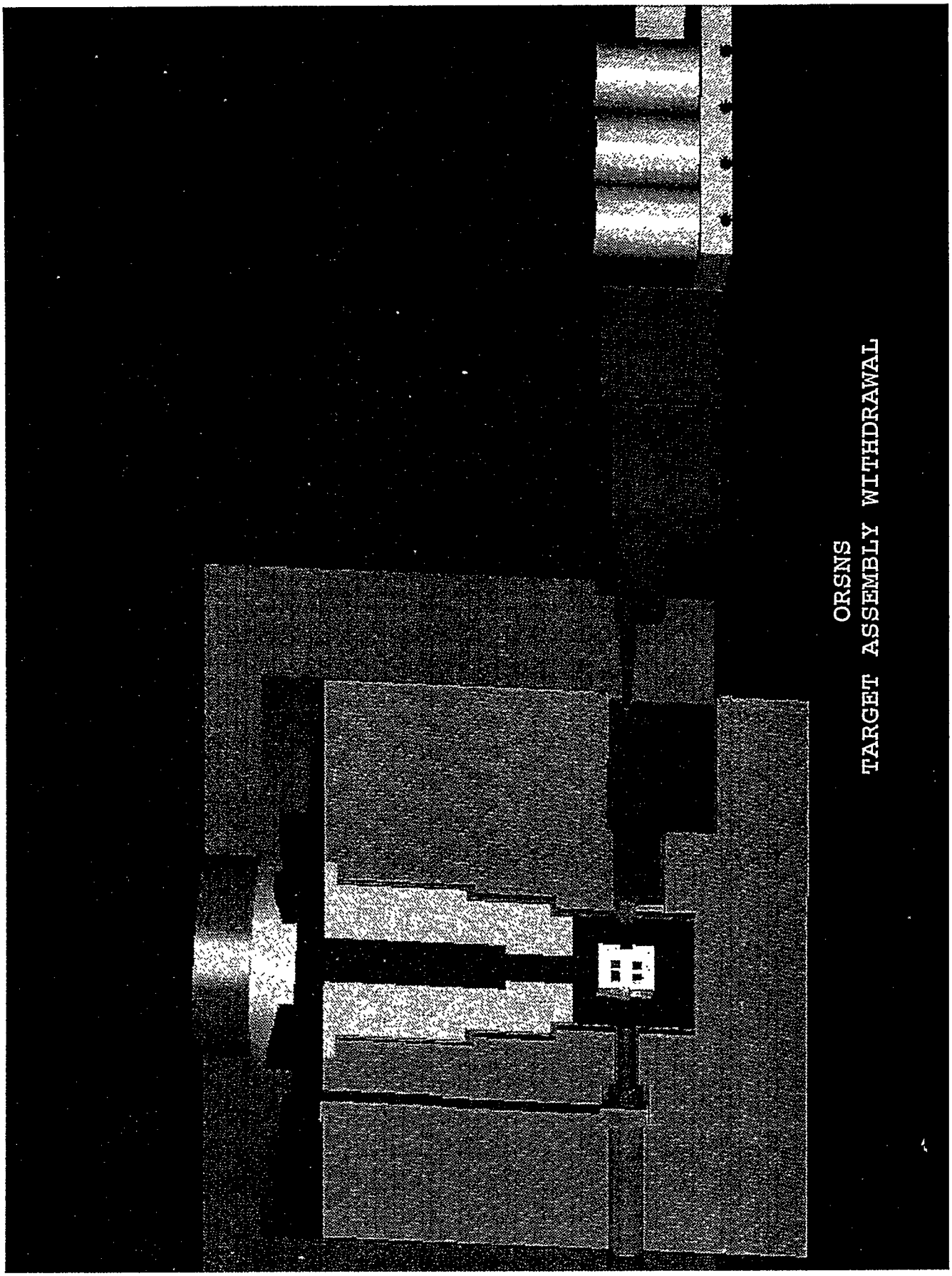
ORSNS
TARGET ASSEMBLY WITHDRAWAL

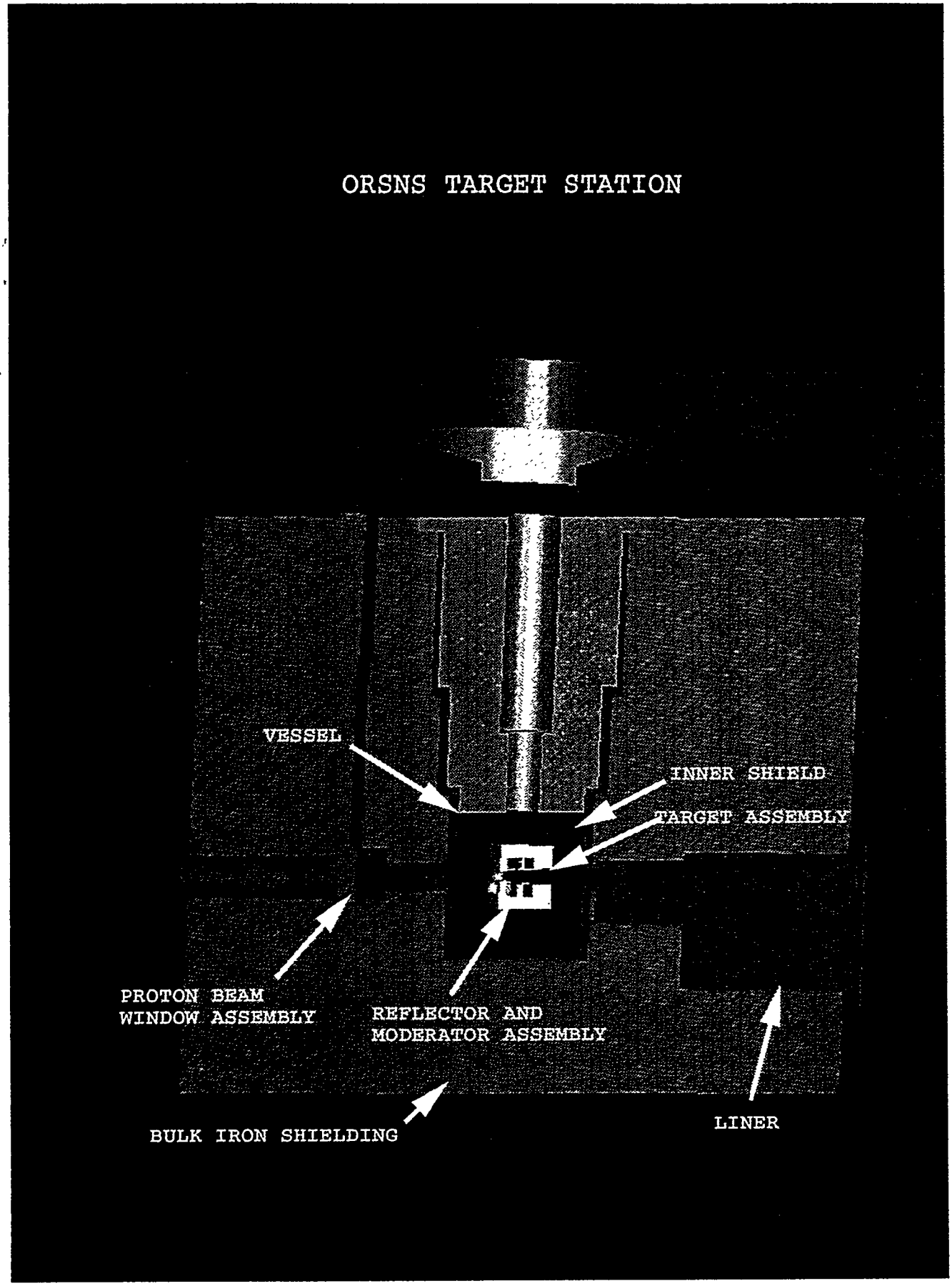
ORSNS TARGET STATION
VESSEL
INNER SHIELD
TARGET ASSEMBLY
PROTON BEAM
WINDOW ASSEMBLY
REFLECTOR AND
MODERATOR ASSEMBLY
BULK IRON SHIELDING
LINER

ORNL-DWG 98M-2479

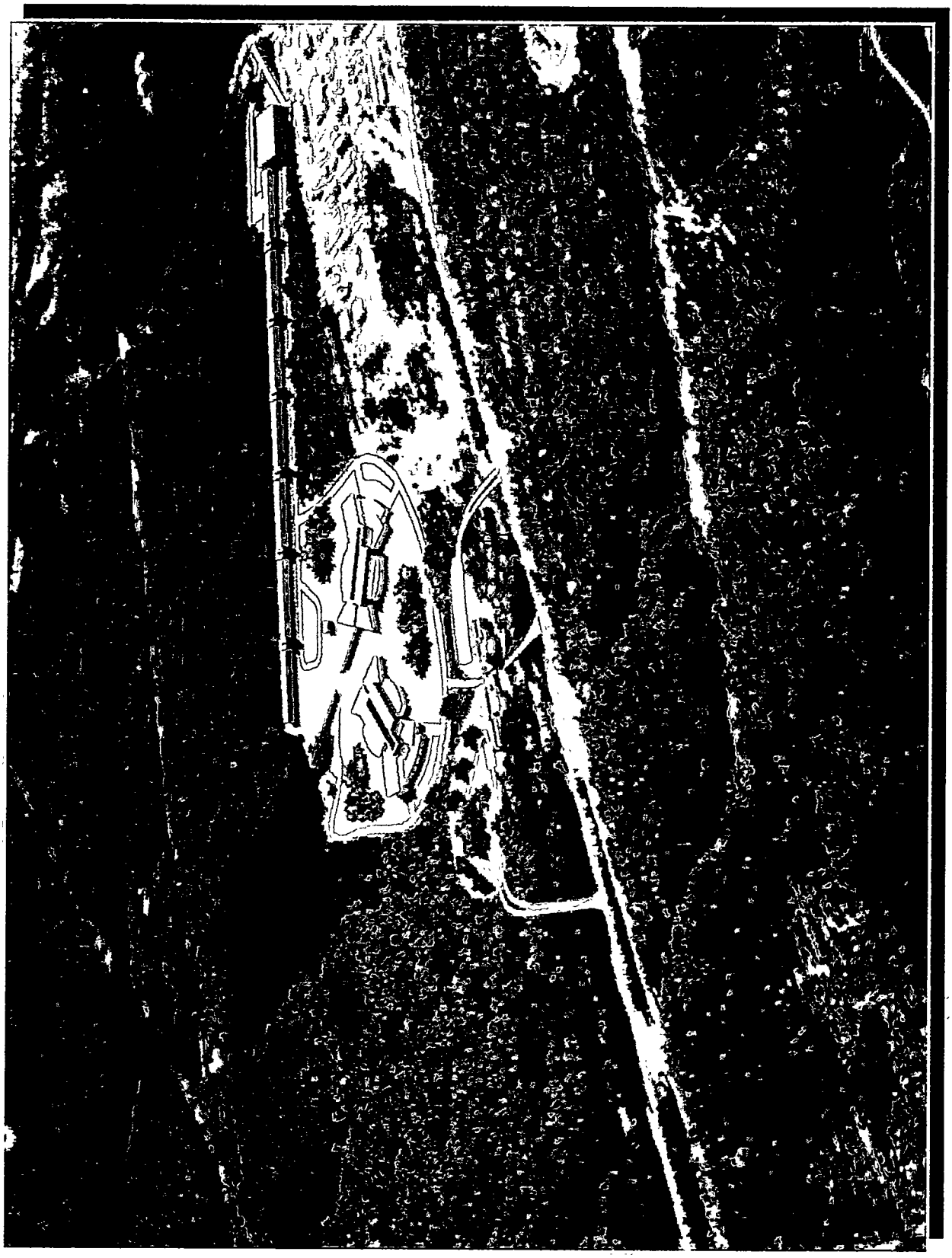

High Power Neutron Production Targets

International Workshop on the Technology and Thermal Hydraulics of Heavy Liquid Metals

Steve Wender
Los Alamos National Laboratory

March 25-28, 1996

High-Power Neutron Production Target Applications

- Neutron Scattering
  - Short pulse neutron sources
  - Long pulse neutron sources
- Accelerator-Driven Transmutation Technology
  - CW source ~ 10 MW beam power
- Accelerator Production of Tritium
  - Up to 200 MW beam power

Moderated Neutron Sources Neutron Scattering Experiments

- Short pulse spallation source
  - 250 ns wide, 20 Hz
  - Compact, high brightness
  - 1 to 5 MW power
  - Temporal response important
- Long pulse spallation source
  - 1 ms wide, 60 Hz
  - 1 MW
  - Compact, high brightness
  - Temporal response not crucial

LANSCE Target-Moderator Geometries

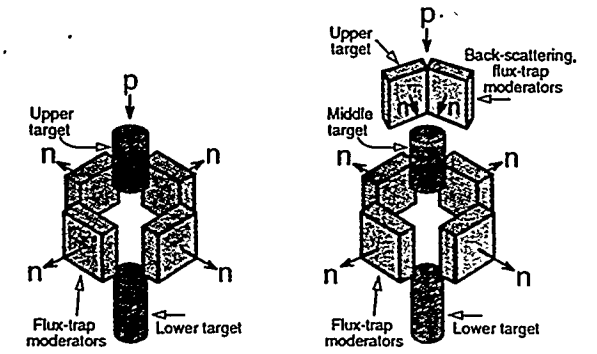

present LANSCE design LANSCE1.5 upgrade design

p=protons
n=neutrons

Upstream Rod Target Exploded View

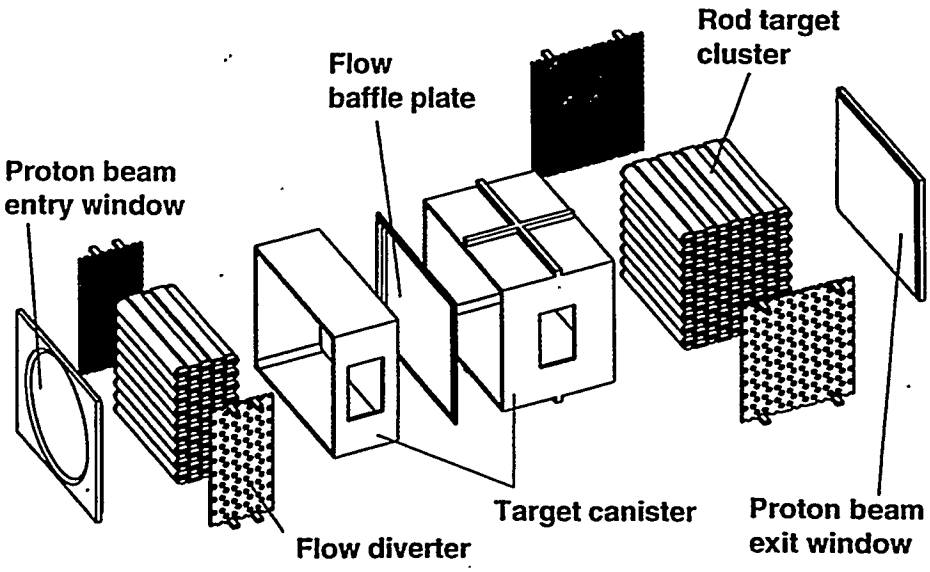

1-MW LPSS Target System and Shielding Monolith

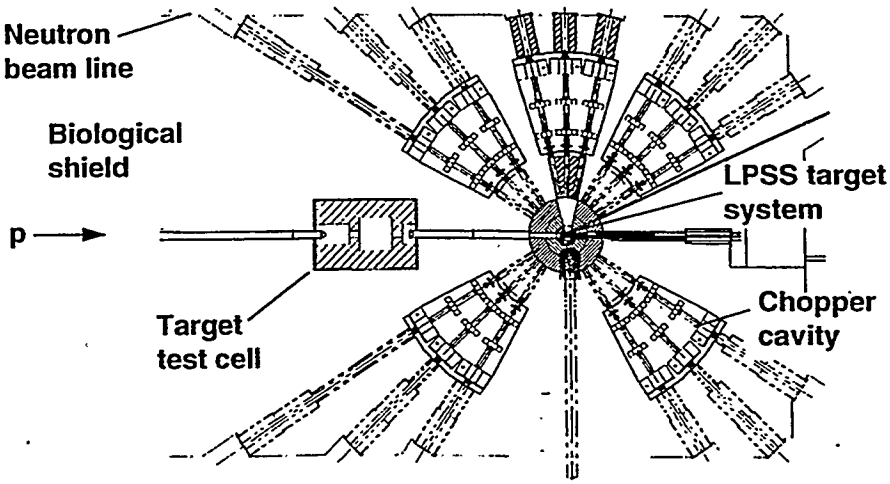

Accelerator Production of Tritium

- Very high power dissipation
  - Up to 200 MW designs
- Can be large volume target (low power density)
- CW beam
- No fissionable material

Upgradeable Room Temperature Linac for Tritium Production

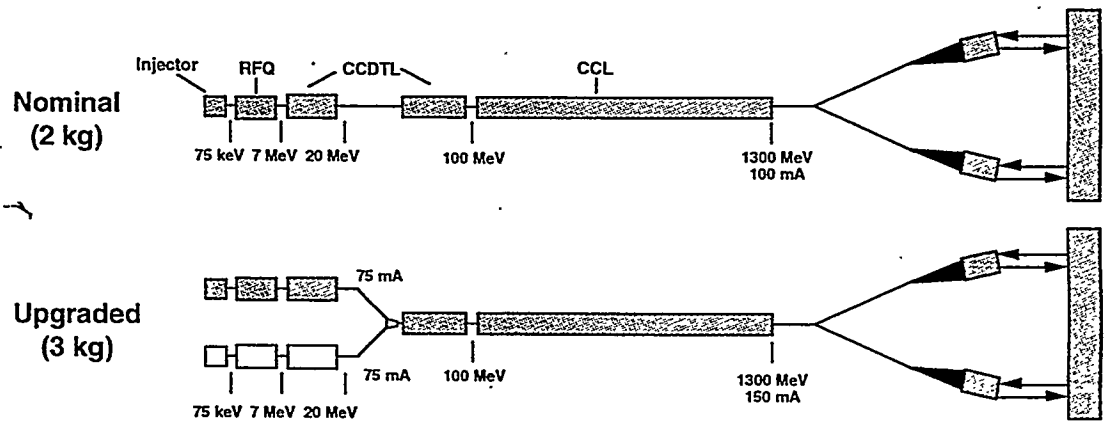

	Nominal	Upgraded
• Proton Energy	1300 MeV	1300 MeV
• CW beam current	100 mA	150 mA
• Beam Power	130 MW	195 MW
• Plant AC Power	438 MW	553 MW
• Linac length	1450 m	1450 m

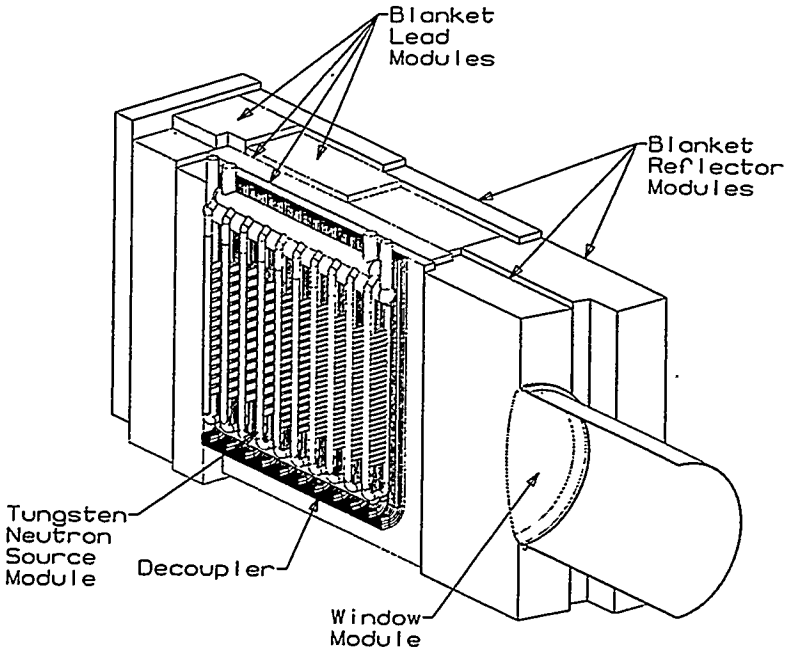

Outline

- Summary of ADTT
- System requirements for target
- Issues concerning molten lead technology
- Target/blanket demonstration experiment

High-Level Overview of ATW System

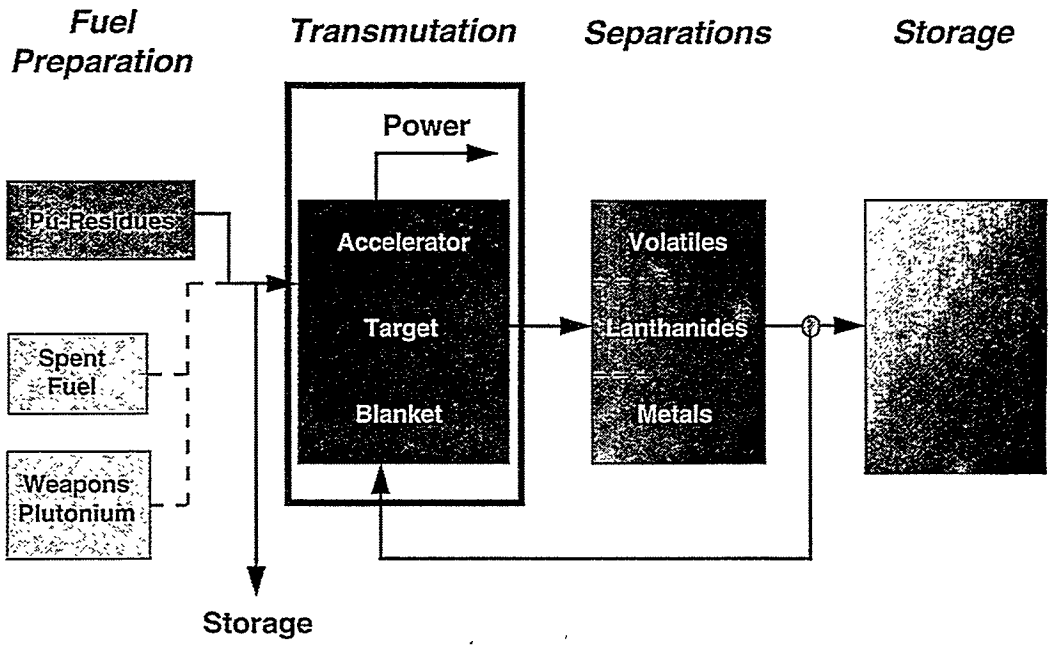

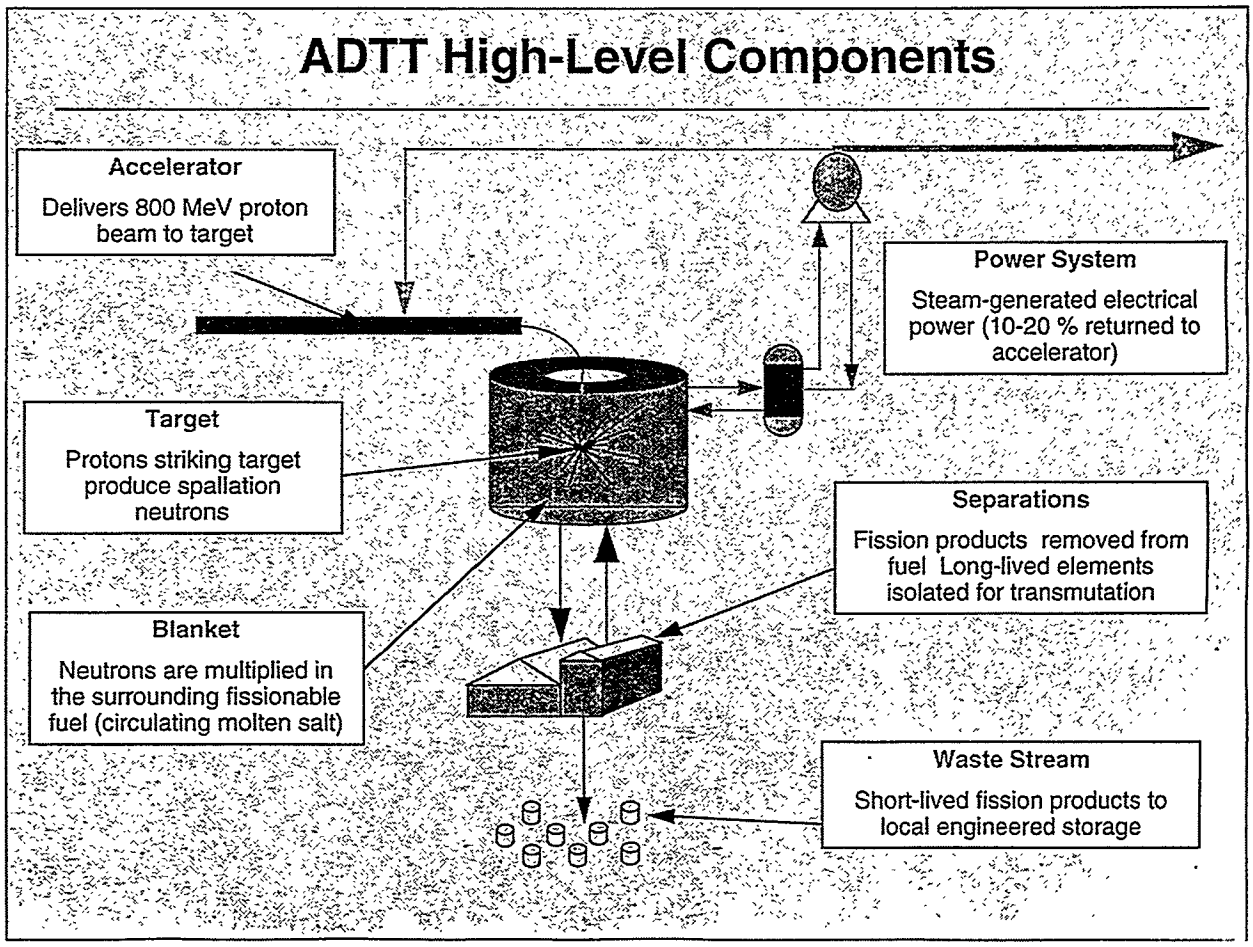

A design concept for the ATW molten salt blanket

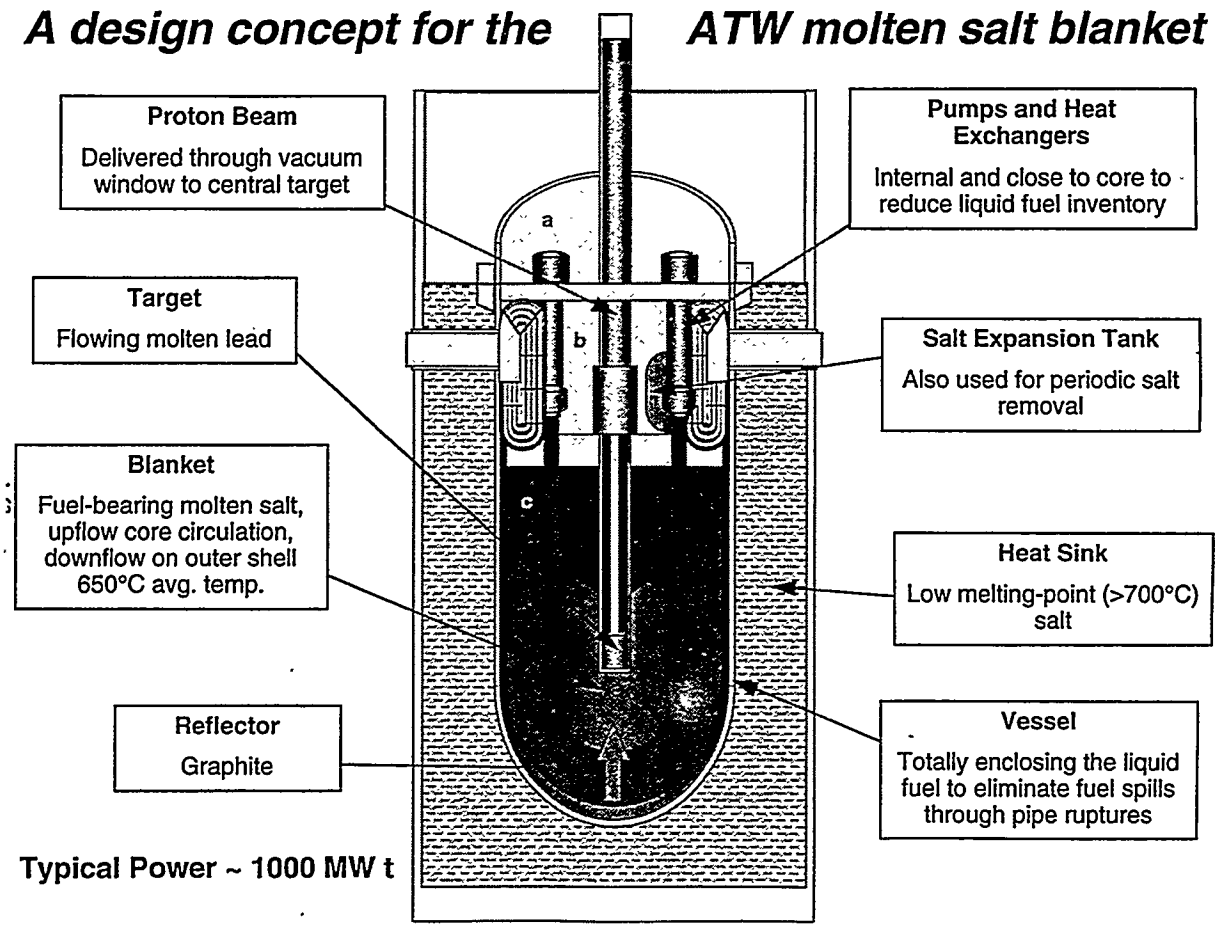

Typical Power ~ 1000 MW t

System Requirements for Target

- Compact size
  - Good coupling to blanket
- High power operation
  - Up to 40 MW operation
- High neutron output
  - High n/p
- Reliable, low maintenance operation
- Safe operation, minimize hazards and waste

Molten Lead Target

- Operates at high beam powers and power densities
- Good neutron/proton yield
- Fewer material radiation damage issues, longer lifetime
- Reduced radioactive waste, reuse lead
- Decouples cooling from blanket volume
  - Easy removal from blanket
- No beam window into blanket volume
  - Enhanced safety

Target Materials

Mat'l	Z/A	σ_A (b)	Thermal Conductivity (W/m°K)	Melting Point (°C)	Boiling Point (°C)	Density (g/cm³)	Range (800 MeV) (cm)	n/p
Ta	73/181	21.	54.	3,017.	5458.	16.7	26.	12
W	74/184	18.4	180.	3,422.	5555.	19.3	22.5	12
Pb	82/207	0.17	35.	327.	1749.	11.4	39.	20
Bi	83/209	0.03	8.5	271.	1564.	9.7	45.	20
Pb-Bi	82.5/208	0.09	9.3	125.	1670.	10.2	42.	20
Th	90/232	7.4	41.	1,750.	4788.	11.7	39.	17
U	92/238	2.7	25.	1,135.	4131.	19.0	24.	27
Hg	80/201	372.		-39.	357.	13.5		

Issues for Molten Lead Target

- Target material selection
  - Lead or LBE or other eutectic
- Materials : Target container and window
  - Radiation damage, structural, corrosion/compatibility
- Windows
- Lead control
  - Purity
  - Oxidation
- Interface and coupling to blanket
- Volatile material and polonium containment
- Heat removal and heat exchangers
- Instrumentation and control, sampling
- Safety and accident scenarios
- Radioactive isotope inventories- Decay heat

NEUTRON PRODUCTION TARGET

Experience Base

- ***Solid targets and windows at LAMPF accelerator***
- ***Flowing Pb-Bi technology in Russian reactors***

Development Areas

- ***Adaptation of domestic and Russian molten metal technologies***
- ***Optimal integration with blanket***

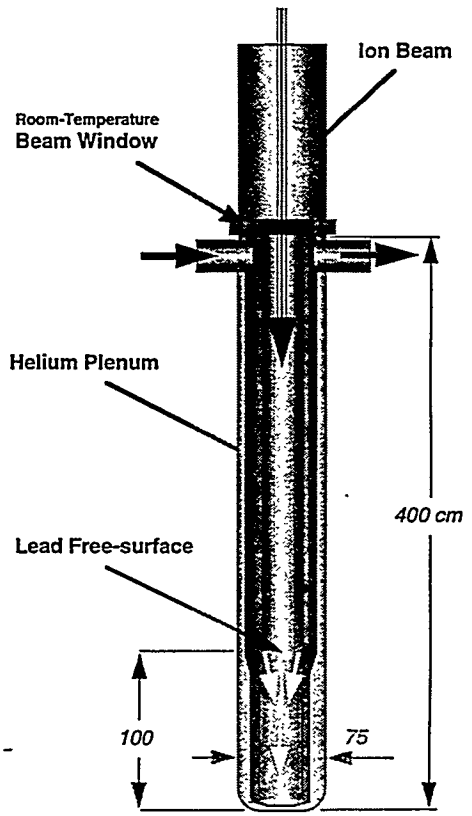

ADTT Experiments

- Microscopic measurements
  - Capture and fission cross section measurements on unstable nuclei
  - Proton and neutron reaction cross sections
- Macroscopic measurements
  - Neutron performance, transport, code verification
  - Radioactive nuclei production
- Demonstration experiment at LAMPF
  - Molten metal target
- Engineering experiments
  - Materials issues: structural, corrosion, radiation damage
  - Chemistry: separations, fuel preparation

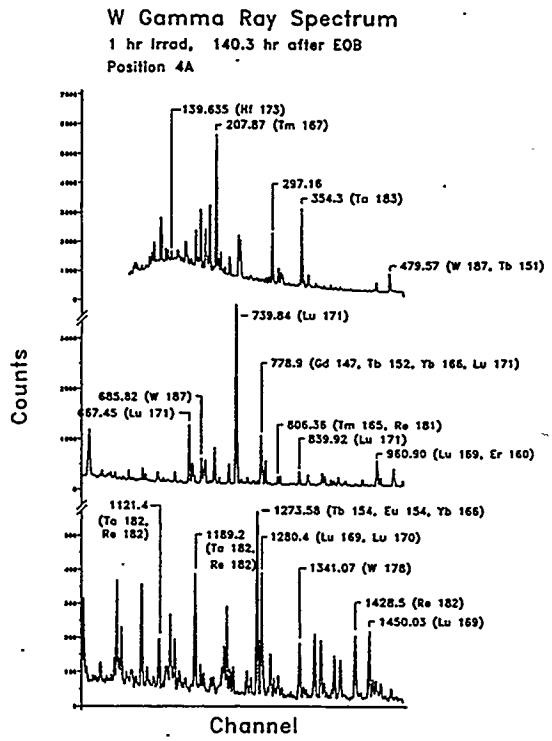

Fig 12. Tungsten gamma ray spectrum from on-axis position 4A (Foil 614) 140 hours after end of 1 hr bombardment.

from the samples and counted to determine activity. The measured activities were corrected for decay after and during irradiation and scaled to total volume of water in the moderator system to determine the total number of ^{56}Mn atoms produced. The aluminum activation foil was removed and counted at the same location to determine the total number of protons using the measured cross sections with appropriate corrections for the decay of the activation products.

RESULTS

Having the total number of ^{56}Mn atoms and the total number of protons, one can determine the number of ^{56}Mn atoms produced per incident proton. This number was the experimentally measured quantity which could be compared to that calculated by the LAHET / MCNP code and used to test the neutron yield per proton generated by the code.

The statistical uncertainties from the counting of the various activities were generally less than 2%. Additional systematic uncertainties arise from the calibration of the counters used to measure the ^{56}Mn and Al activation, the uncertainty in the total volume of water in the system, the concentration of $MnSO_4$, and the cross sections for proton activation of Al at 800 MeV [2]. The quadratic combination of all these systematic uncertainties is estimated to be 4.2%.

Table 1 gives the results of the yield determinations with their total uncertainties and compares them to the calculated values. Agreement is very good for all systems except the thorium-salt mock-up. This disagreement is probably attributable to problems with the fabrication of this target which caused its actual make-up to be poorly determined. With this exception, the experiment demonstrates the accuracy of LAHET / MCNP in predicting the total neutron production over a range of elements and proton energies.

Table 1. Neutron/Proton Measurements Compared to LAHET / MCNP

Target	Energy (Mev)	^{56}Mn/proton (Experiment)	Uncertainty (Absolute)	^{56}Mn/proton (Calculated)	Neutron/Proton (Calculated)	Neutrons/proton (Measured)
Lead	800	0.2046	0.0089	0.204	22.2	22.3
Lithium	397	0.0458	0.0022	0.0459	4.35	4.34
Tungsten	800	0.1255	0.0055	0.126	18.2	18.1
Th-Li-F	800	0.1094	0.0049	0.1243	12.6	11.1

A separate paper at this conference [3] will present results of the flux mapping done with a series of activation foils in the blanket and moderator. In addition, measurements of the neutron leakage spectra were obtained for the lead and lithium targets and are presently being analyzed. These data sets will provide test of a more differential nature.

Fig. 4 shows a schematic of Target 2 with the associated neutron flight paths. Calibrated plastic scintillators [4,5] were used to measure neutron time-of-flight spectra from 0.5 to 800 MeV at four angles with respect to the incident proton beam. The availability of additional beam time permitted the acquisition of data for the bare lead target and lead target/blanket combination without the water tank in place. ^{6}Li loaded glass scintillation counters were used along with the plastic scintillators and produced data over the energy region from 0.01 to 800 MeV.

ADTT Demonstration Experiment

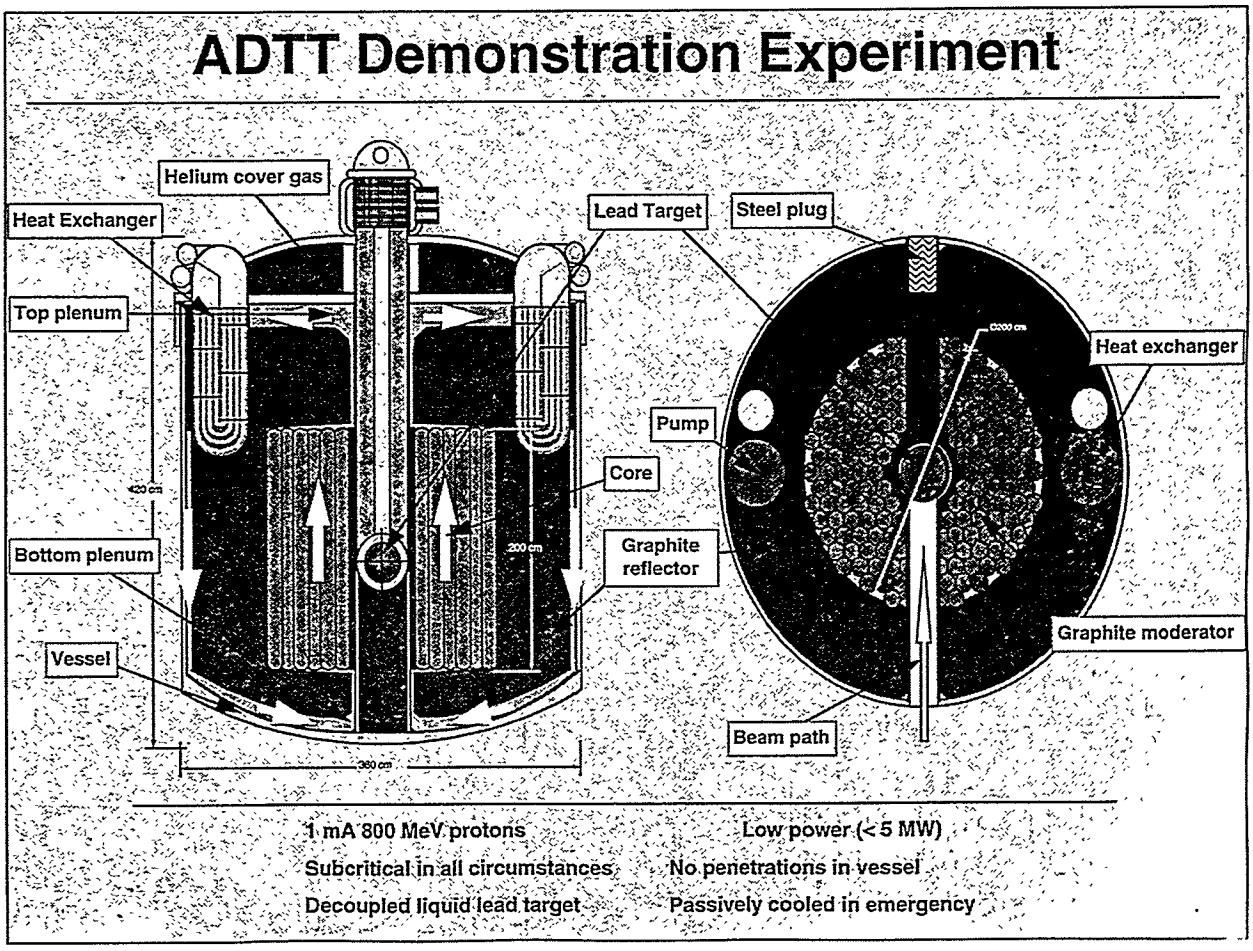

Liquid Lead Target for ADTT Experiment

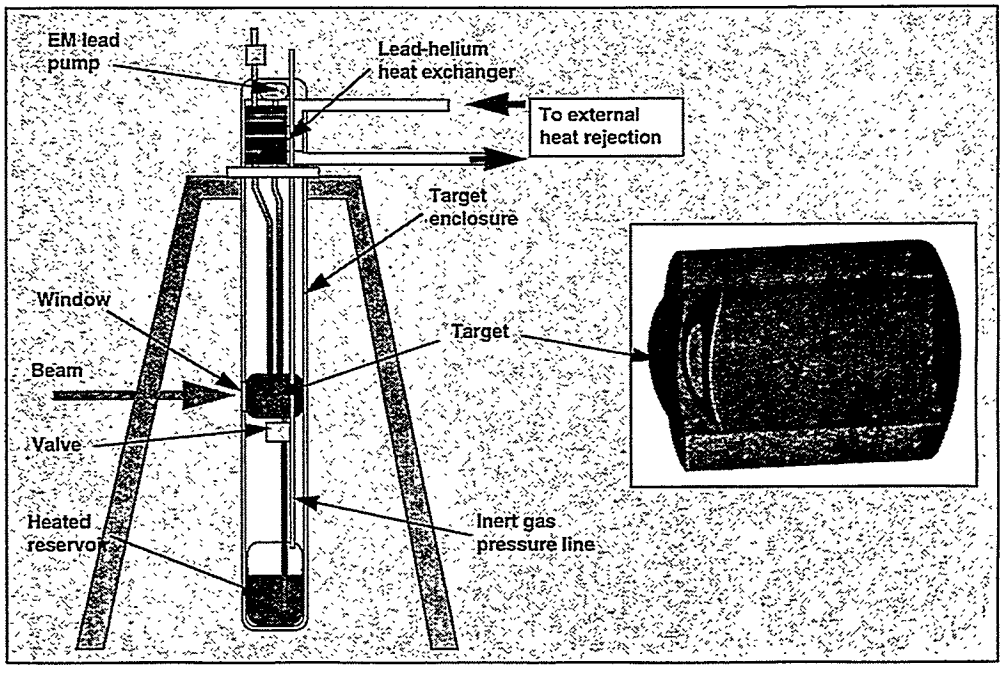

ADTT Experiment-Technical Details

- Target
  - Material — LBE
  - Temperature range — 150-300°C
  - Neutron flux — 10^{12} n/cm^2
  - Power dissipation — 1 MW beam
  - Volume of material — 60 liters
  - Container material — Cr-Mo alloy
- Blanket
  - Material — $LiF\text{-}BeF_2$
  - Temperature — 600°C
  - Power — 5 MW
  - Volume of salt — 1 m^3
  - Volume of graphite — 10 m^3
  - Container material — Modified Hastelloy

Molten Lead Target

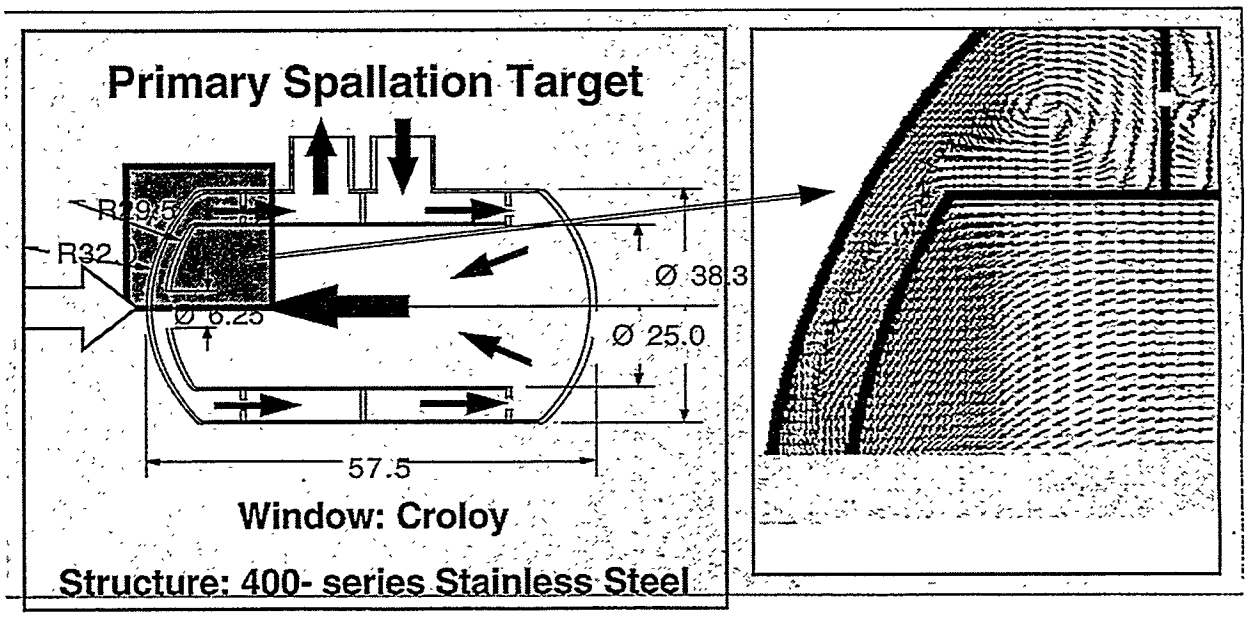

ADTT Flow Visualization Experiment

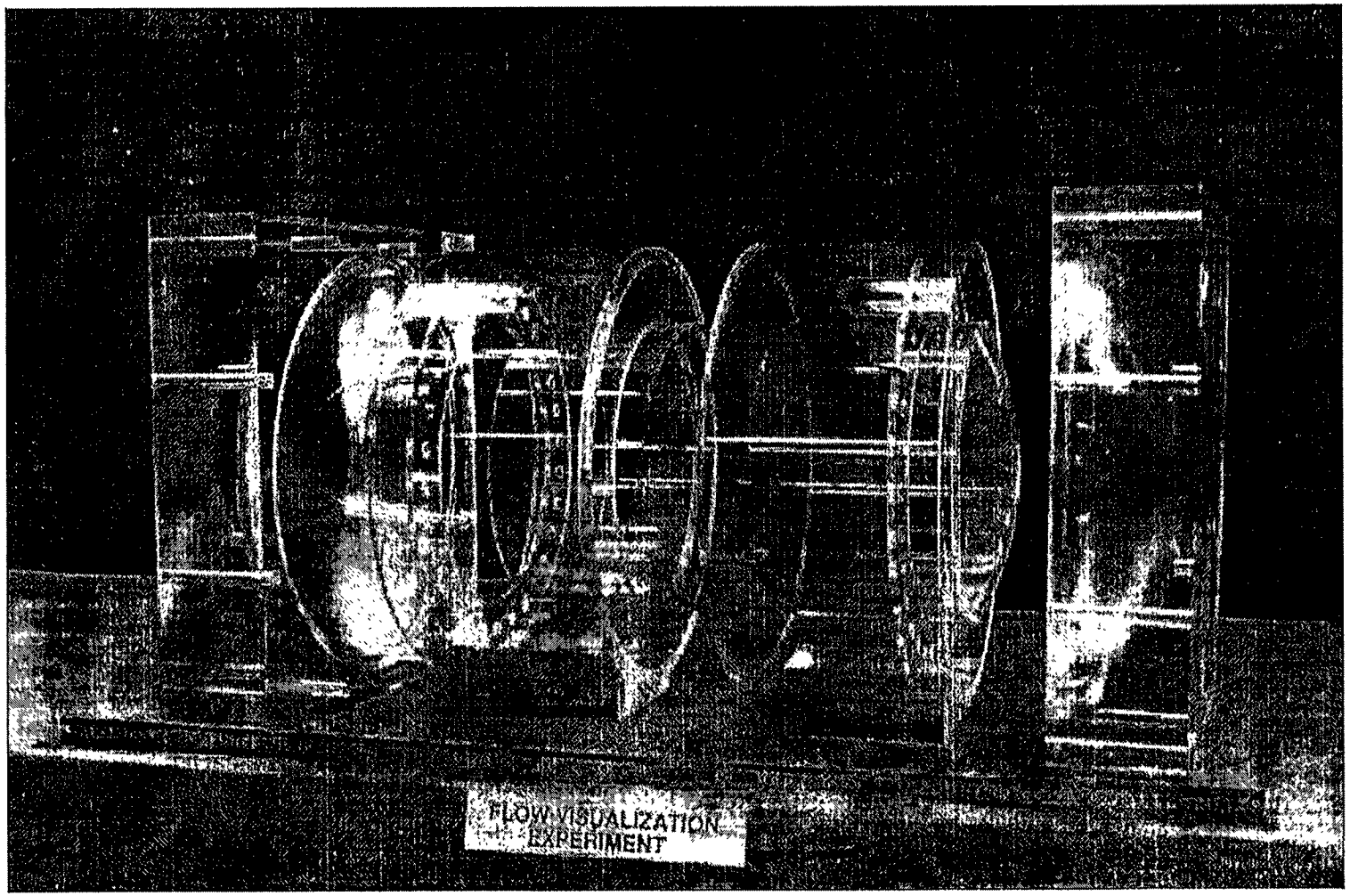

LBE Target

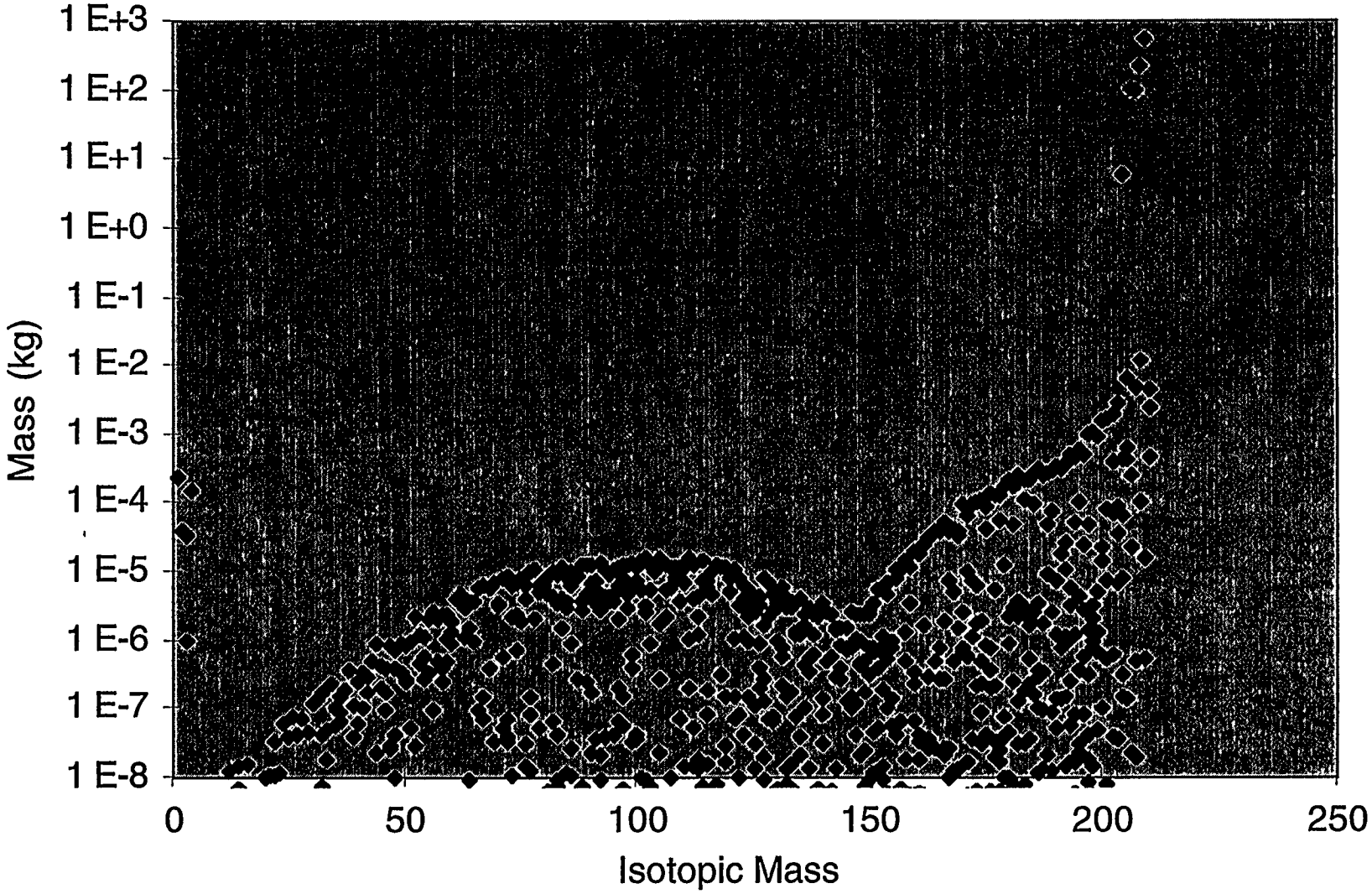
1 E+3
1 E+2
1 E+1
1 E+0
1 E-1
1 E-2
1 E-3
1 E-4
1 E-5
1 E-6
1 E-7
1 E-8
Mass (kg)
0
50
100
150
200
250
Isotopic Mass

Molten Lead Target Decay Heat

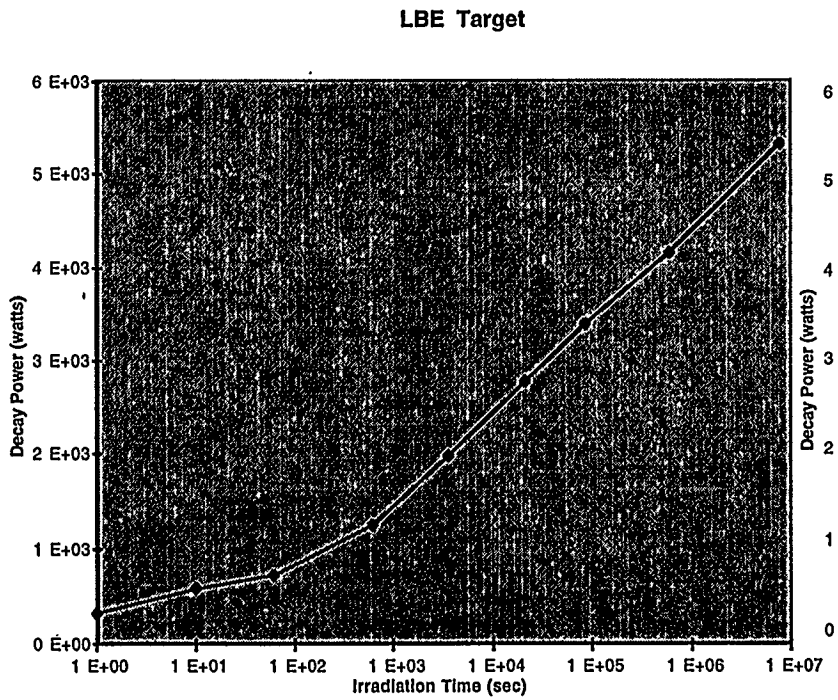

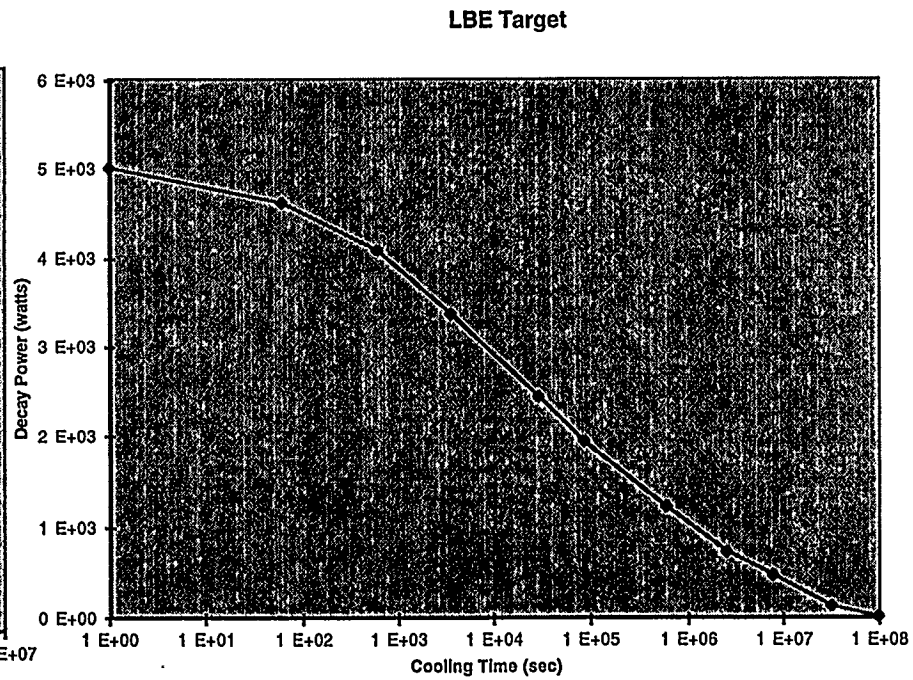

Molten Target Development Plan

- Evaluate most promising target fluids
- Address technical issues with molten lead test stand
- Test prototype of molten lead target in test stand
- Test prototype of molten lead target in proton beam at LAMPF beam stop at 1 MW level

Experiment Location

Site Selection:

- High-power beamline exits
- Easy access to beamline
- Relatively unactivated
- Good staging area available
- Good infrastructure:
  - Crane, Forklift access
  - Power, Cooling

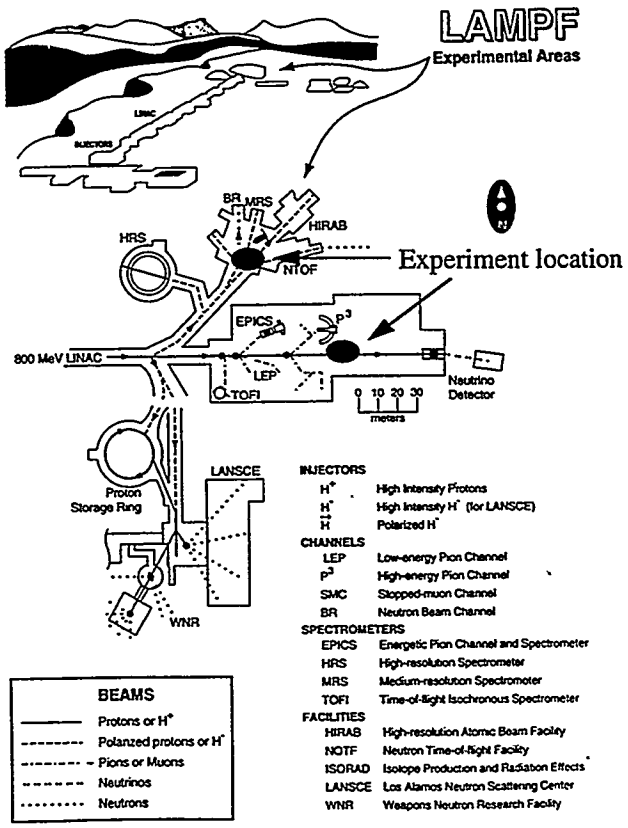

Summary

- High-power spallation targets are crucial technology for many applications
- Molten metal targets appear to be best choice for compact high power systems
- Design of target for each application will be different

SESSION 2

Thermal Hydraulics, Heat Removal, and Circuit Design (1)

Chairman
O. Lielausis

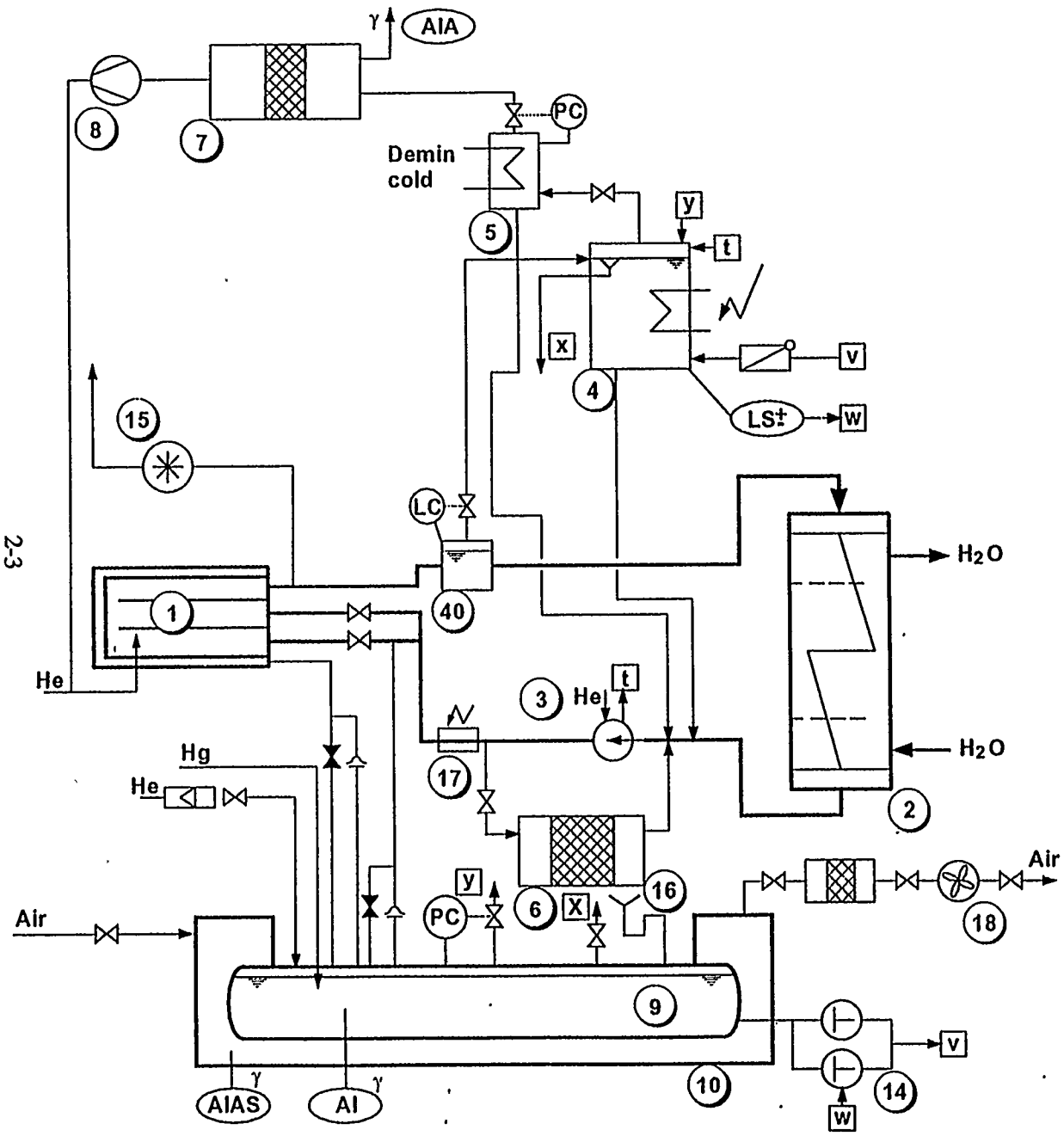

Schematic for Hg handling system.

P&ID Legend

1 Target
2 Primary Heat Exchanger
3 Hg Circulation Pump
4 Hg Expansion Vessel
5 Hg Condenser
6 Hg Purification
7 Gas Treatment
8 He Compressor
9 Hg Drain Tank
10 Residual Heat Removal Basin
14 Hg Filling Pumps
15 Startup Evacuation Pump
16 Floor Drain
17 Preheater
18 Fan

[...] (Letter in square box): connection to other location in P & ID

LS Level Switch
PC Pressure Control
A Analysis
I Indication
A Alarm
S Switch

Filter

Hg / ESS P & ID

Main Characteristics of Primary System

- Hg circuit on trolley, detachable intermediate cooling circuit.
- MHD induction or canned - motor pump
- Double-wall tube IHX with leak detection (Surveillance of interstitial gas). Straight-tube bundle, Hg on tube side, pressurised water on shell side.
- Hg temperature high enough to avoid brittle fracture of target structural materials (window).
- No boiling of Hg in target (cavitation)
- Closed loop for He gas (Hg condensation, gas separation.
- Separation of solid impurities in Hg system (erosion).
- Decay heat removal system for drain tank. Emergency cooling by radiation and natural convection.
- Safety containment for primary Hg and He systems with drainage for spilled Hg.
- Special drain pipe for Hg from target safety hull.
- Retention or possibly controlled release of volatile radioactive spallation products
- Complete draining of Hg and condensation of Hg vapour for maintenance.

Gas and Impurity Separation System (ESS)

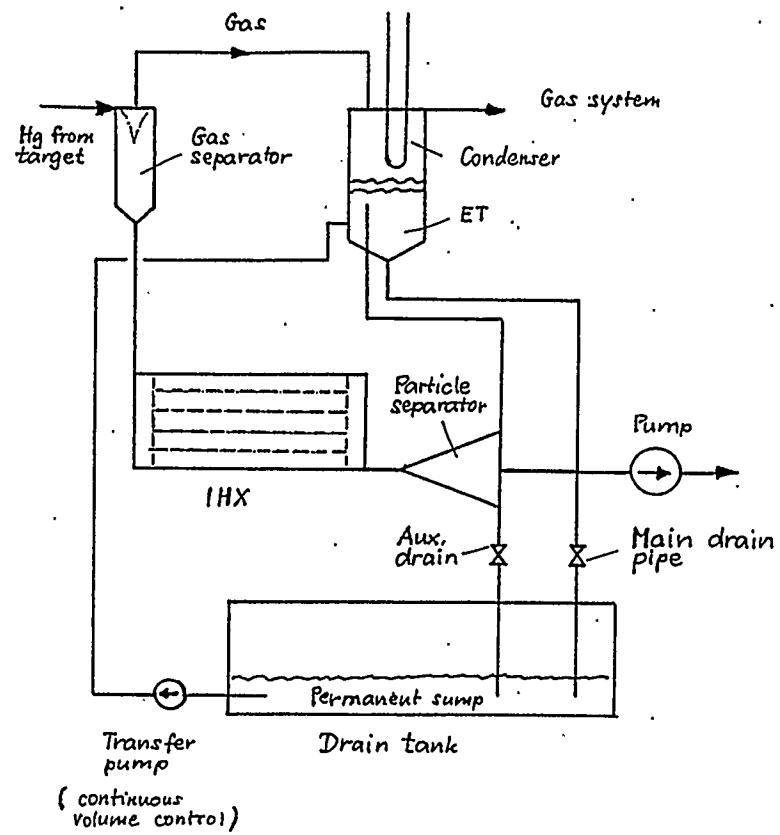

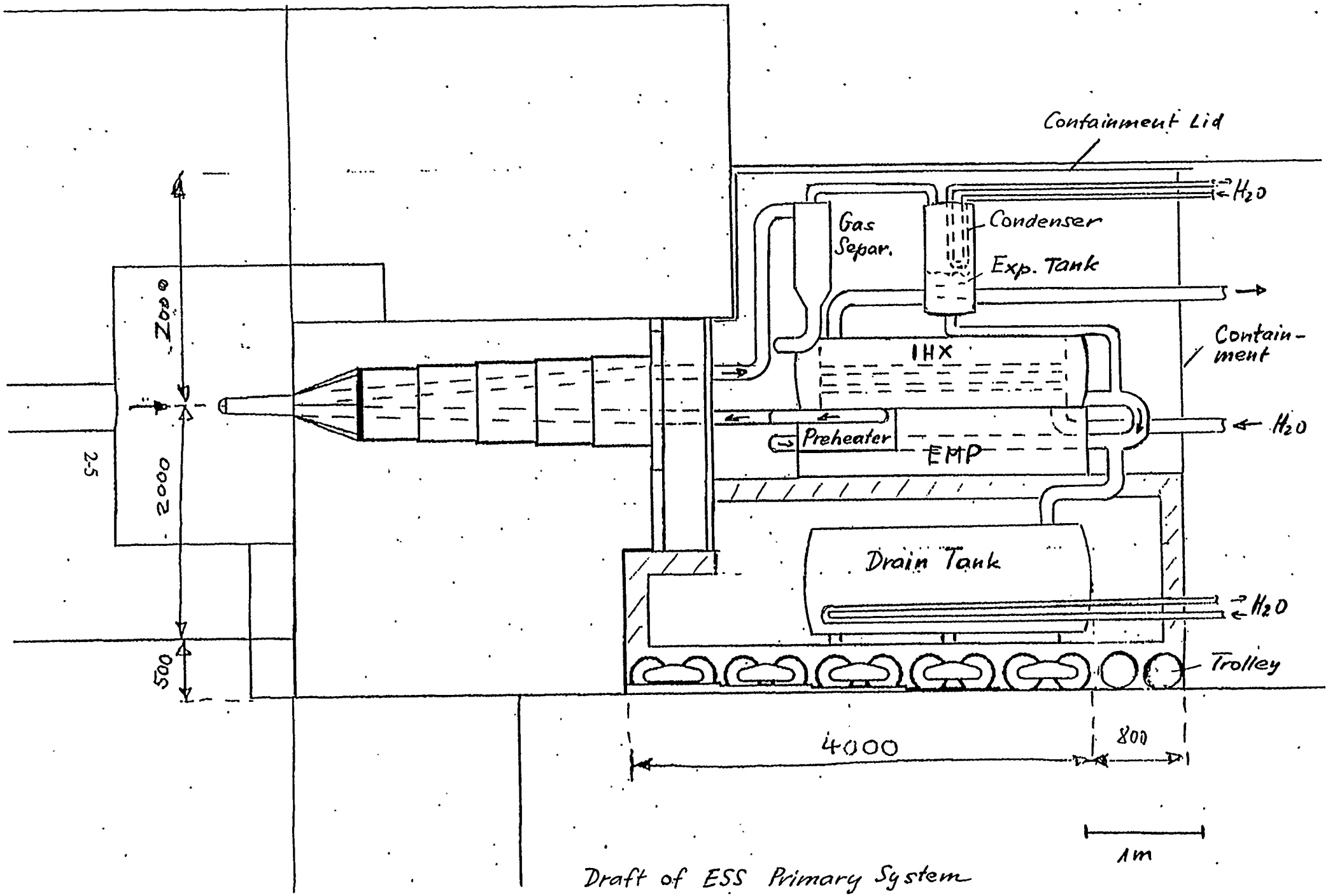

Draft of ESS Primary System

Estimated Thermal-Hydraulic Design Parameters

1. Primary mercury circuit:

Thermal power	3 MW
Hg flowrate	185 kg/s
Hg temperature at target inlet	180 °C
Hg temperature at target outlet	300 °C
Hg pressure at target inlet	6 bar
Hg frictional pressure drop	3 bar
Estimatet Hg inventory including permanent sump in drain tank	15 t

2. Intermediate water circuit

Flowrate	25 kg/s
Temperature cold leg	80 °C
Temperature hot leg	110 °C
Pressure at IHX inlet	4 bar

3. Characteristics of IHX

Length	2.5 m
Diameter	0.6 m
Tube outer diameter	21 mm
Tube wall thickness	4 mm
Number of tubes	150

Thermal-Hydraulic Design Alternatives

1. Intermediate cooling system:
   - Heat pipes in IHX as designed for SINQ (50 kW per unit, L = 2.7 m, D = 95 mm, pitch 142.5 mm)

     For ESS, bundle of 61 heat pipes in hexagonal array. Mercury flow in annuli along evaporator section or at 90° across bundle.

     → Resulting size of IHX H = 3 m, D = 1.3 m
   - Natural-circulation boiler-condenser system (IPPE proposal for LAMPF target test)
2. Pump
   - Canned - motor pump
   - Sump pump (Sump serves as expansion tank and segregates impurities)
3. Lower operating temperature in primary system

   → Lower vapour pressure of Hg in gas system

   → Larger IHX (and Hg inventory)

Safety Issues

- Mercury or gas leaks
- Water ingress into primary system
- Loss of heat sink
  (Loss of flow in intermediate cooling system)
- Hg pump failure

System Operation and Maintenance

- Start-up
- Transients
- Shut-down for maintenance

Needs for Further Research and Engineering Analysis

- Behaviour of spallation products in mercury and He circuits. Effects on materials.
- Specification of processing requirements and equipment (All circuits)
- Thermal-hydraulic and structural-mechanic analysis (Including abnormal events)
- Feasibility and effectiveness of gas injection into mercury
- Identification of safety problems and specification of safety measures
- Shielding and handling of radioactive components
- Detailed system design with evaluation of alternatives

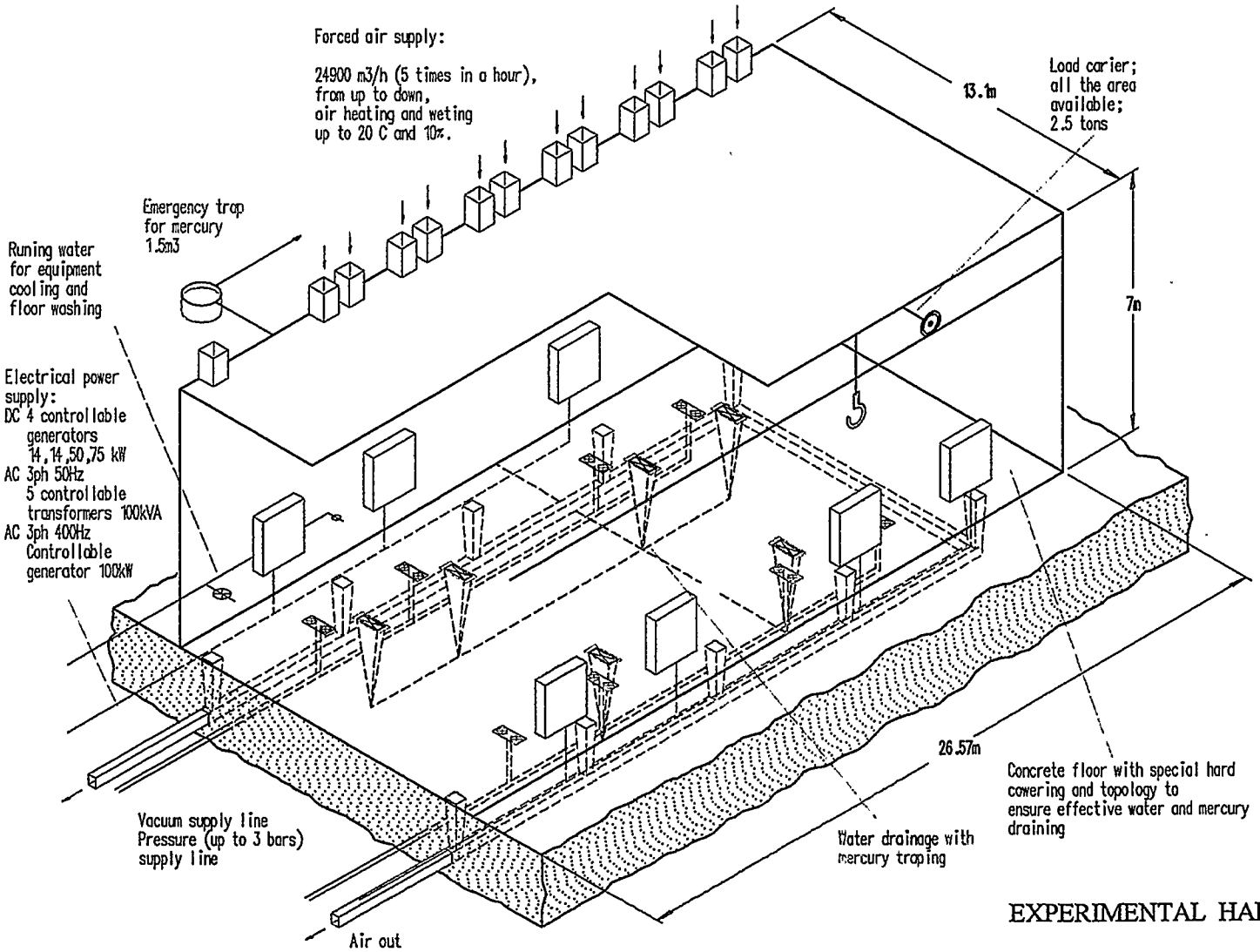

EXPERIMENTAL HALL

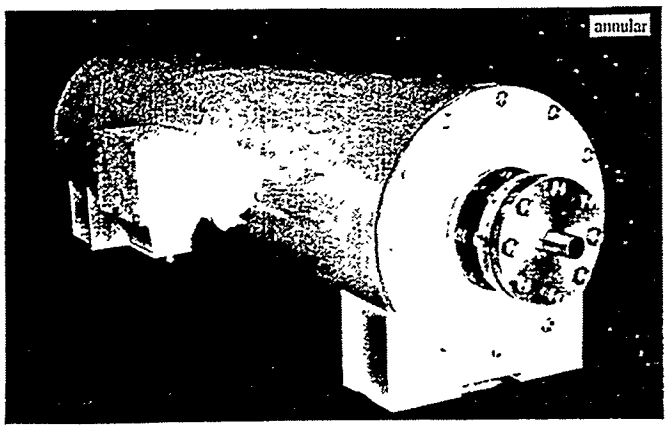

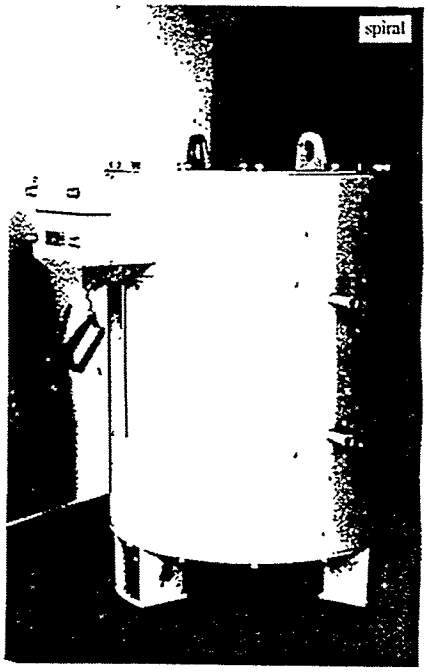

flat

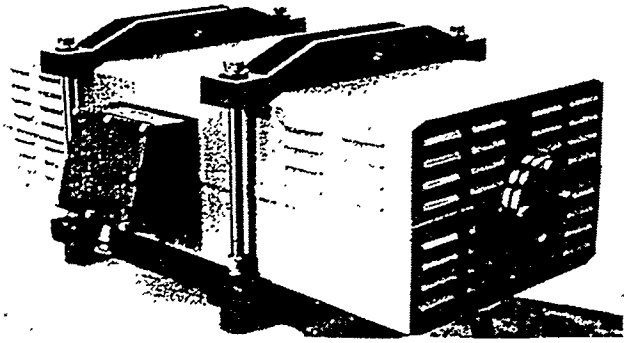

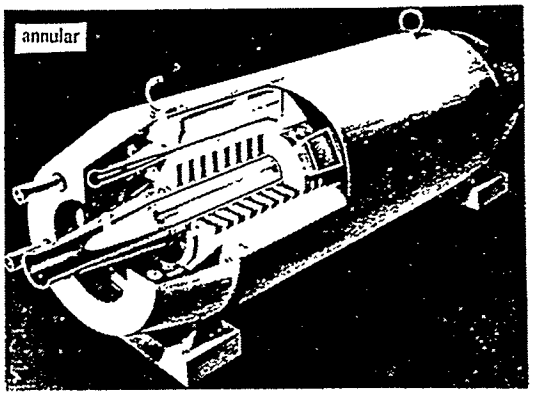

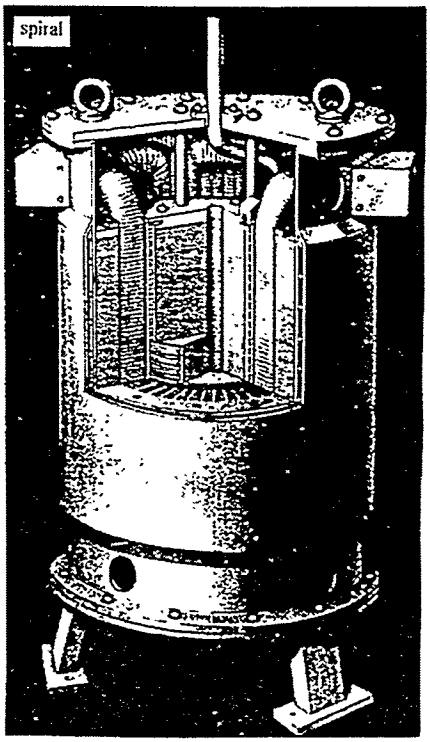

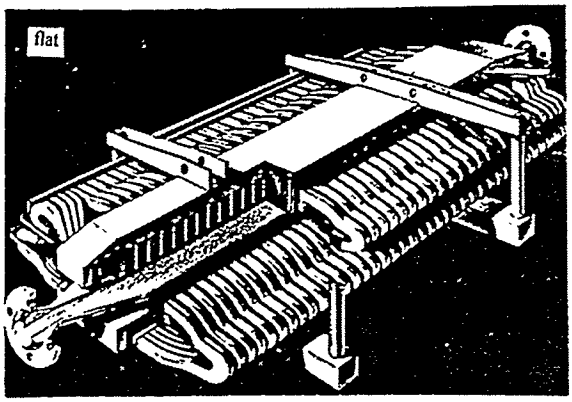

CHARACTERISTICS OF PUMPS FOR HEAVY METALS

Pump	Operating temperature, °C	Pressure, kg/cm^2	Productivity, m^3/s	Active power, kW
ENC-21		0.73		270.0
ENC-31 (Pb, Bi)	500	6.23	$8.34 \cdot 10^{-4}$	42.0
ENC-46 (Pb, Bi)	400	6.80	$0.97 \cdot 10^{-3}$	40.0
ENC-47 (Pb, Zn)	550	7.20	$0.80 \cdot 10^{-3}$	38.0
ENC-49 (Zn, Pb)	550	7.20	$0.90 \cdot 10^{-3}$	38.4
ENC-50 (steel)	1650	0.50	$0.765 \cdot 10^{-3}$	62.0
ENC-51 (steel)	1650	0.50	$0.765 \cdot 10^{-3}$	11.0
ENC-53 (Sn)	300	1.35	$0.603 \cdot 10^{-3}$	5.0
ENC-61 (In, Ga, Sn, Pb)	150	10.00	$2.50 \cdot 10^{-3}$	38.0
ENCS-68 (Pb, Bi)	400	0.52	$1.45 \cdot 10^{-3}$	2.8
ENCSP-69 (Pb, Bi)	400	1.20	$1.37 \cdot 10^{-3}$	12.1
ENC-81 (Pb, Bi)	180	3.50	$7.39 \cdot 10^{-3}$	54

CHARACTERISTICS OF PUMPS FOR MERCURY

Pump type	Operating temperature, °C	Pressure, kg/cm^2	Productivity, m^3/s	Active power, kW
flat	from 60 to 105	from 0.665 to 3	from $0.138 \cdot 10^{-5}$ to $1.04 \cdot 10^{-3}$	from 3.8 to 11.5
spiral	40	from 28.2 to 40	from $2.5 \cdot 10^{-5}$ to $4.13 \cdot 10^{-5}$	from 9 to 19
annular	from 20 to 200	from 0.785 to 12.2	from $0.28 \cdot 10^{-3}$ to $5 \cdot 10^{-3}$	from 4 to 58

Universal Electromagnetic Mercury Cleaning Plants

Description

The universal industrial plant is a set of technological MHD units for mercury purification. It was created as a result of application of the electromagnetic contactless method of mixing a mercury droplet flow with reagents in MHD equipment.

The plant has the following advantages:

— high productivity and metal purification efficiency;

— simple design (no moving parts and sealings);

— reliable and easy to use;

— sealed and ecologically clean.

The set of the units is successfully used in industrial plants

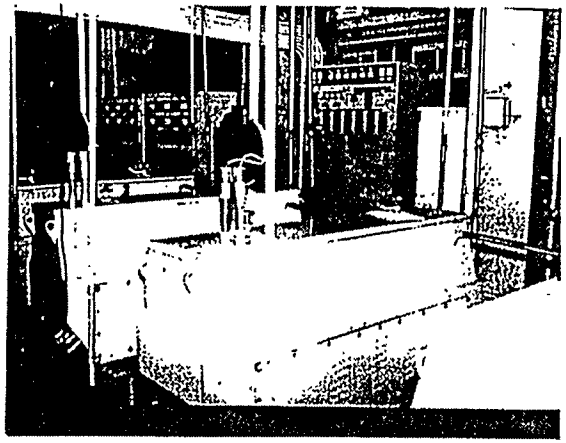

Main Technical Characteristics

— mercury purity, % - 99.9995

— productivity, t/h - 0.1-0.5

— consumed power, kW - 15.

Areas of Application

The equipment can be used at mercury producing or processing factories as well as in laboratories.

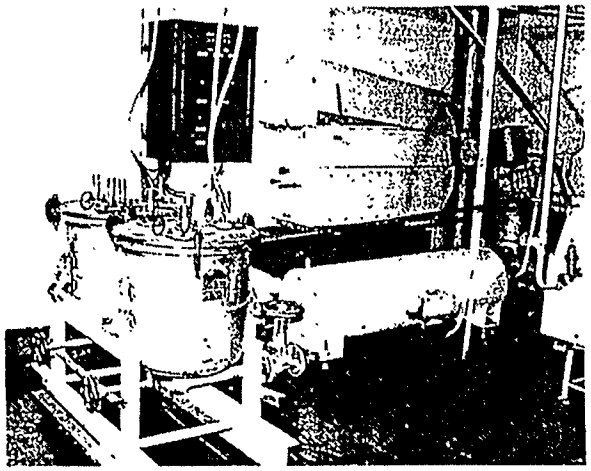

EQUIPMENT FOR PRODUCTION OF HIGH PURITY MERCURY

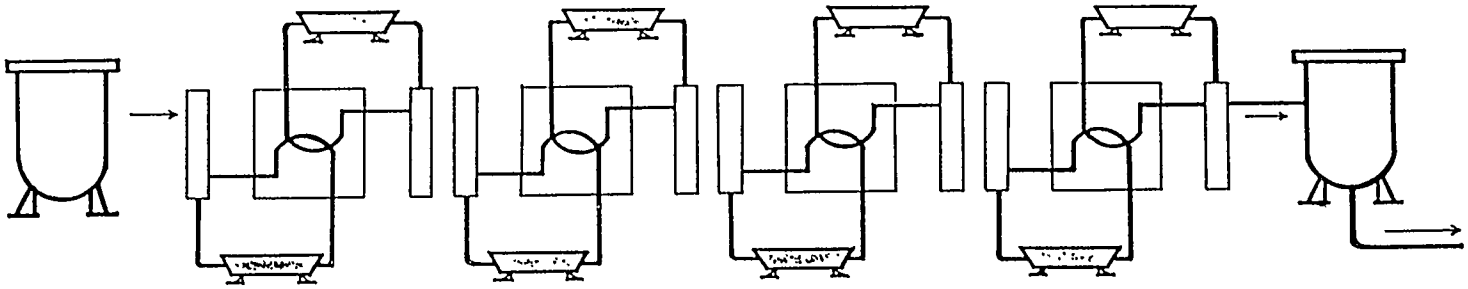

Initial Hg
99.999 %

High purity Hg
99.999999 %

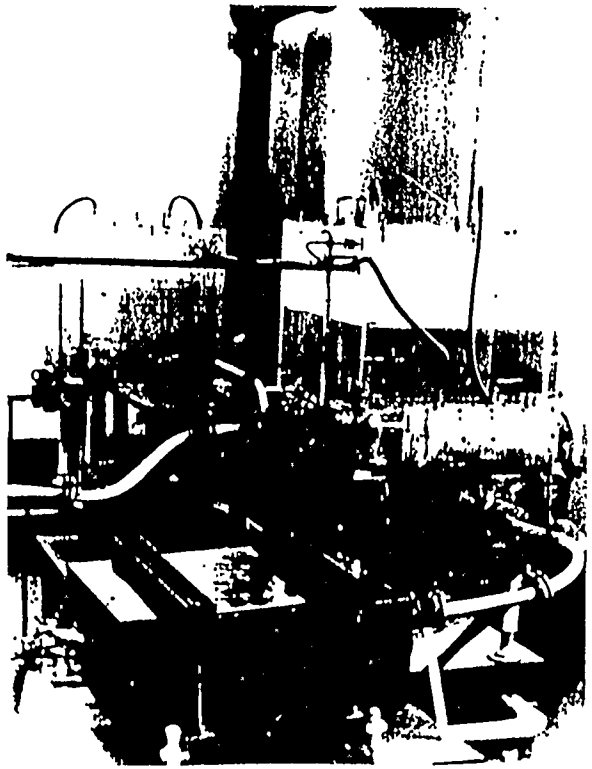

High purity Hg is produced by four-phase precipitation on bipolar Hg electrodes moving (running) in mercury salt solutions.

- used for production of alloys with unique properties.
- was used for alloy production on space station "Saljut-6".

EXPERIMENTAL MERCURY FACILITIES

SOLENOID FOR MHD-FLOW IN LONGITUDIONAL MAGNETIC FIELD

- the length of the field homogeneous , mm 2000
- operating tube diameter, mm 160
- flow rate of mercury, cm^3/s up to $5 \cdot 10^3$
- operating pressure of EMP, Pa $5 \cdot 10^5$
- operating volume (Hg), m^3 0.35

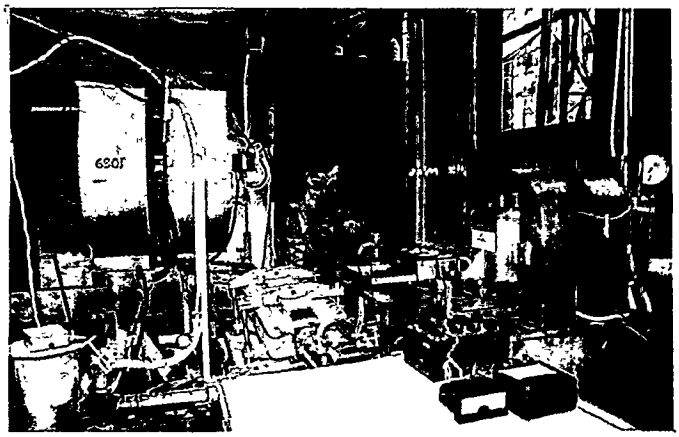

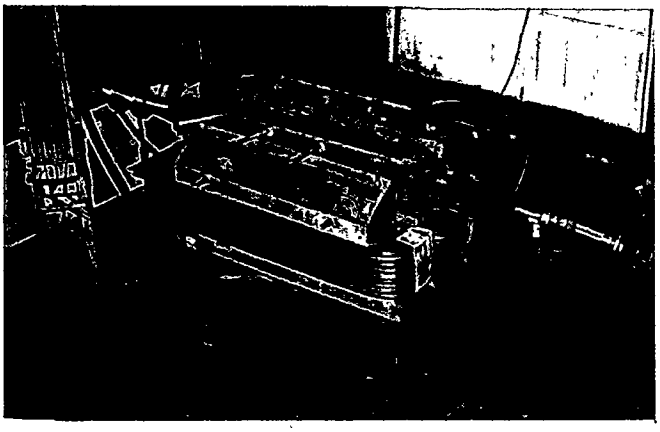

Hg -LOOP FOR MHD FLOW IN PERPENDICULAR MAGNETIC FIELD

- B_{max} at poles D=500 mm and small gap , T 2.0
- B at gap 200 mm, T 1 0

Hg -LOOP FOR MHD TURBULENCE INVESTIGATIONS

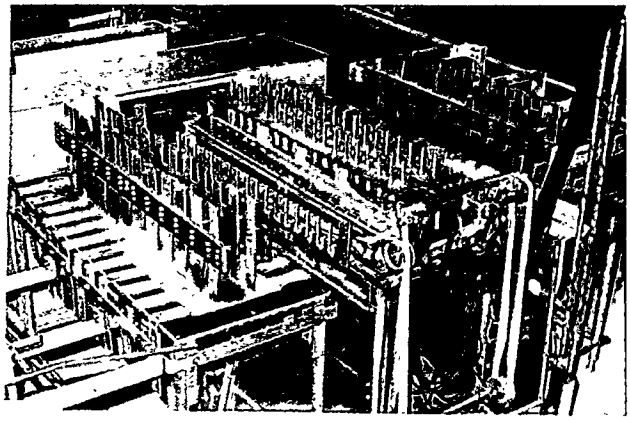

PHYSICAL MODEL OF ALUMINIUM ELECTROLYSER FOR 250 Ka

- scale of model 1:10

Velocity Field Studies in Channel Mercury Flows

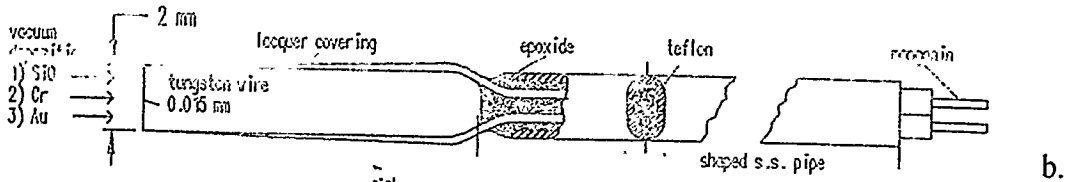

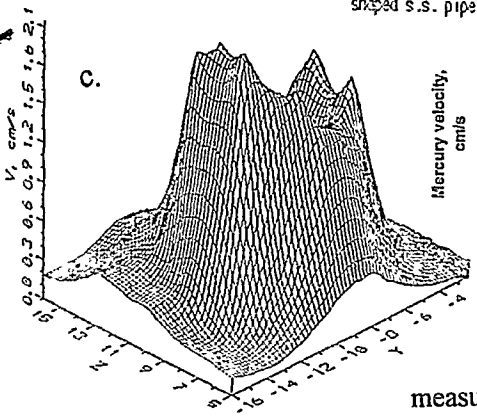

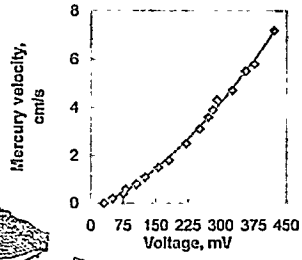

Hot wire probe for measurements of mercury velocity and temperature: a - the principal diagram; b - the characteristic calibration curve; c - an example of velocity distribution for a nozzle flow.

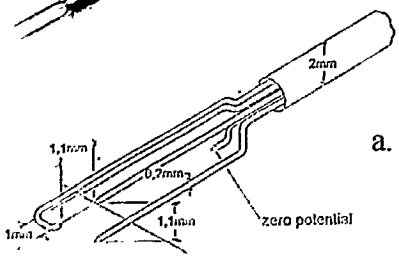

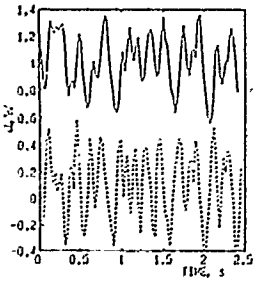

Three dimensional potential probe: a - the principal diagram; b and c - temporal signals and spectrum (u- and w-velocity components).

Typical test section: 1 - channel; 2 - magnet; 3 - elements of the mercury loop; 4 - mercury column manometers

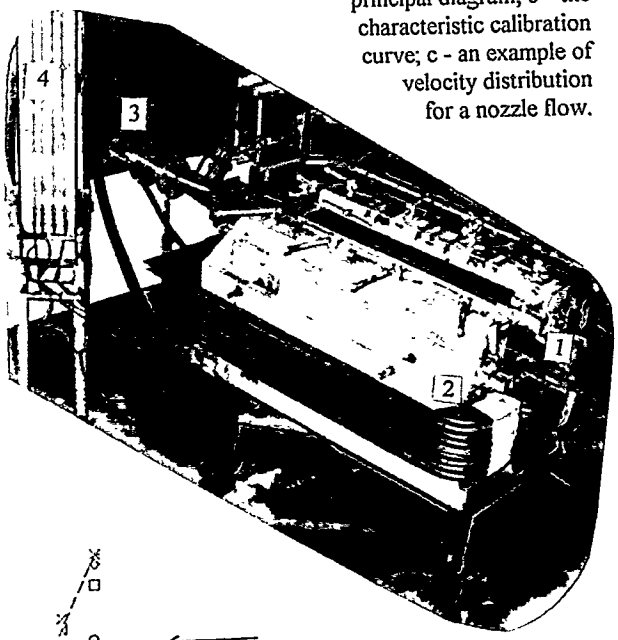

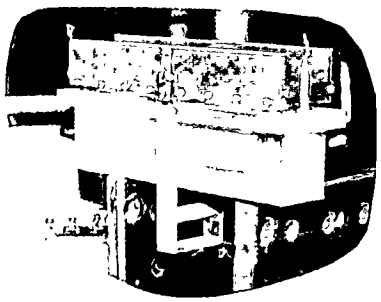

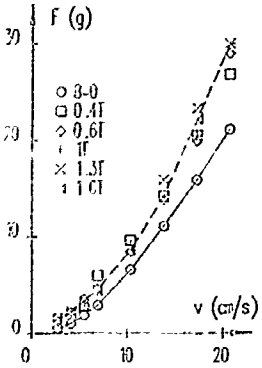

Special device for drag force measuring: a - the external view; b - an example of results obtained for cylinder with the axis parallel to magnetic field in the transverse mercury flow.

MERCURY FLOW VELOCITY STRUCTURE INVESTIGATION TECHNIQUES

1) Thermoanemometry with self-developed hot-wire sensor

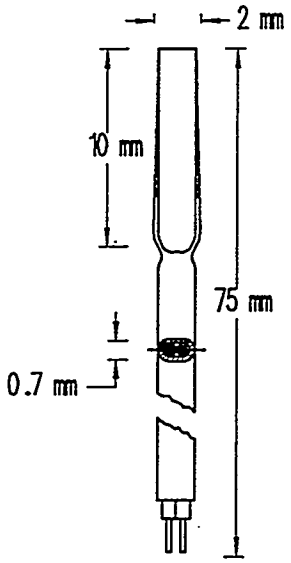

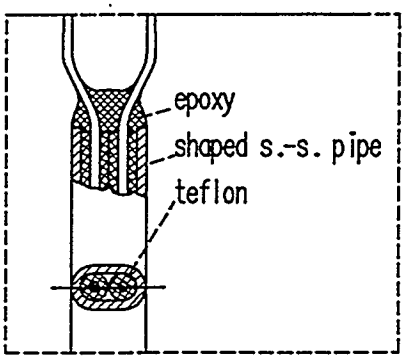

Configuration

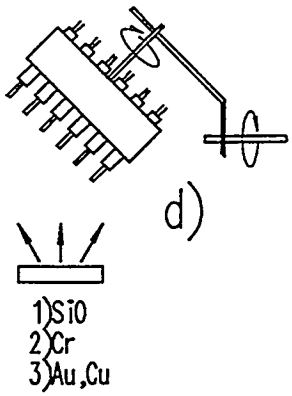

The insulation layer and other technological layers are obtined by deposition in vacuum

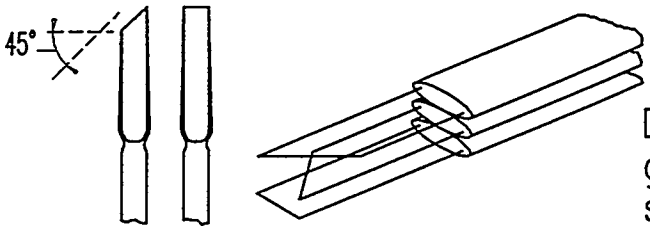

Different wire orentation gives possibility to collect sets for different velocity components measurements

2) Electrical anemometry

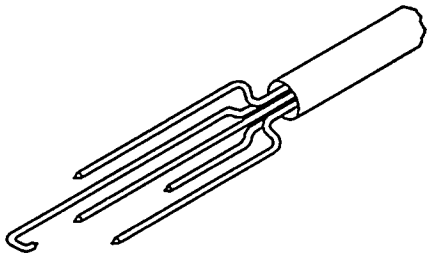

Presence of magnetic field creates measurable electrical potentials usable for velocity structure investigations

Physical Modelling of Electrometallurgical Processes.

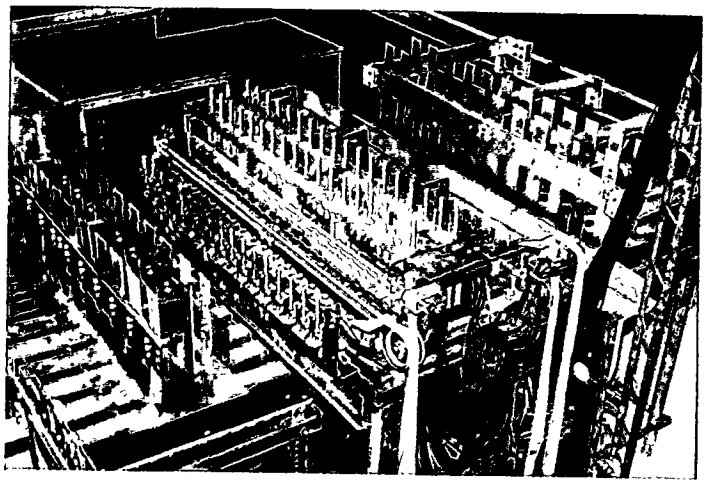

← Mercury model of the aluminium producing electrolysis cell
volume - 19 litters; supply current - 10 kA

↓ Mercury model of the induction channel furnac
volume - 10 litters; supply power - 2 kW; mercury velocity - 50 cm

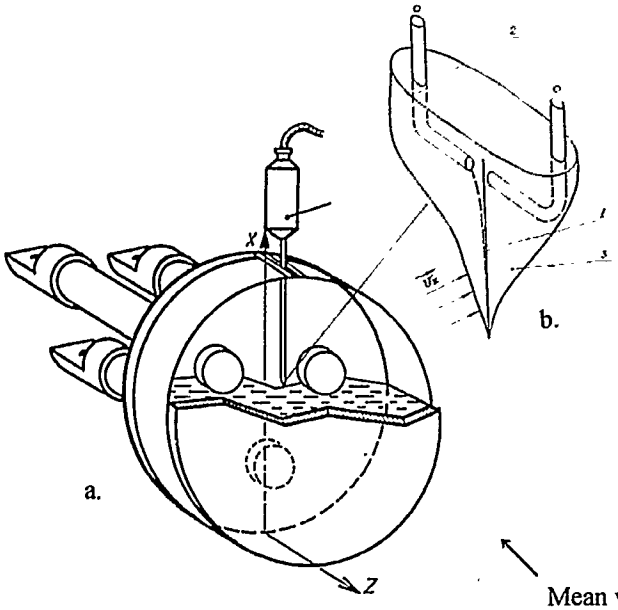

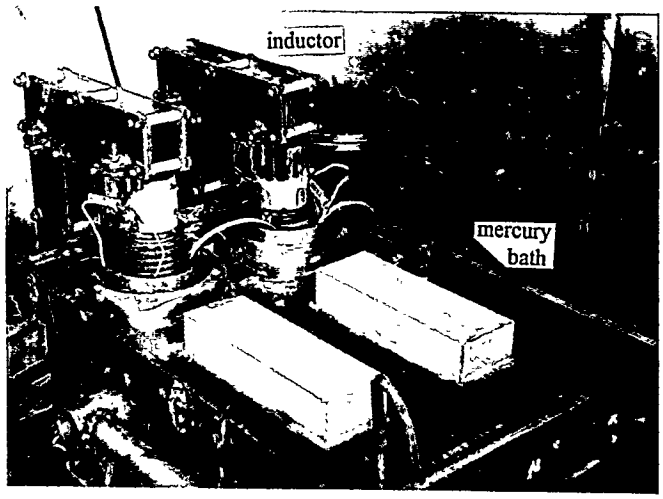

Mean velocity measurements in the mercury model of the electroslag furnace using the fiber optical probe: a - the experimental scheme; b - design of sensitive elements. (1 - deformable partition, 2 - lightguides; 3 - light source; 4 - light flux measure; 5 - glass body)

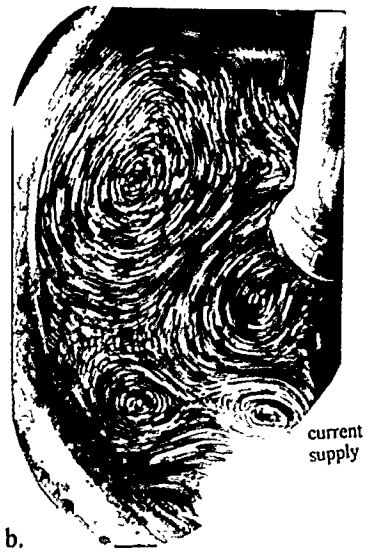

b.

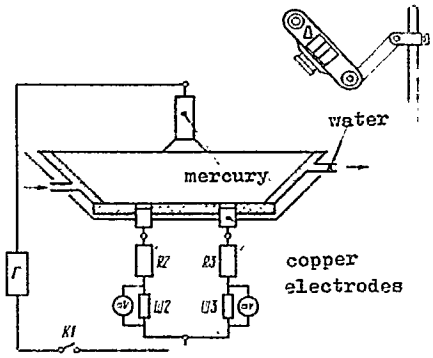

Model of the arc furnace for production of aluminium (3 litters; 3 kA): a - principal scheme; b - photograph of a characteristic flow structure on mercury free surface.

Experimental Mercury-loop

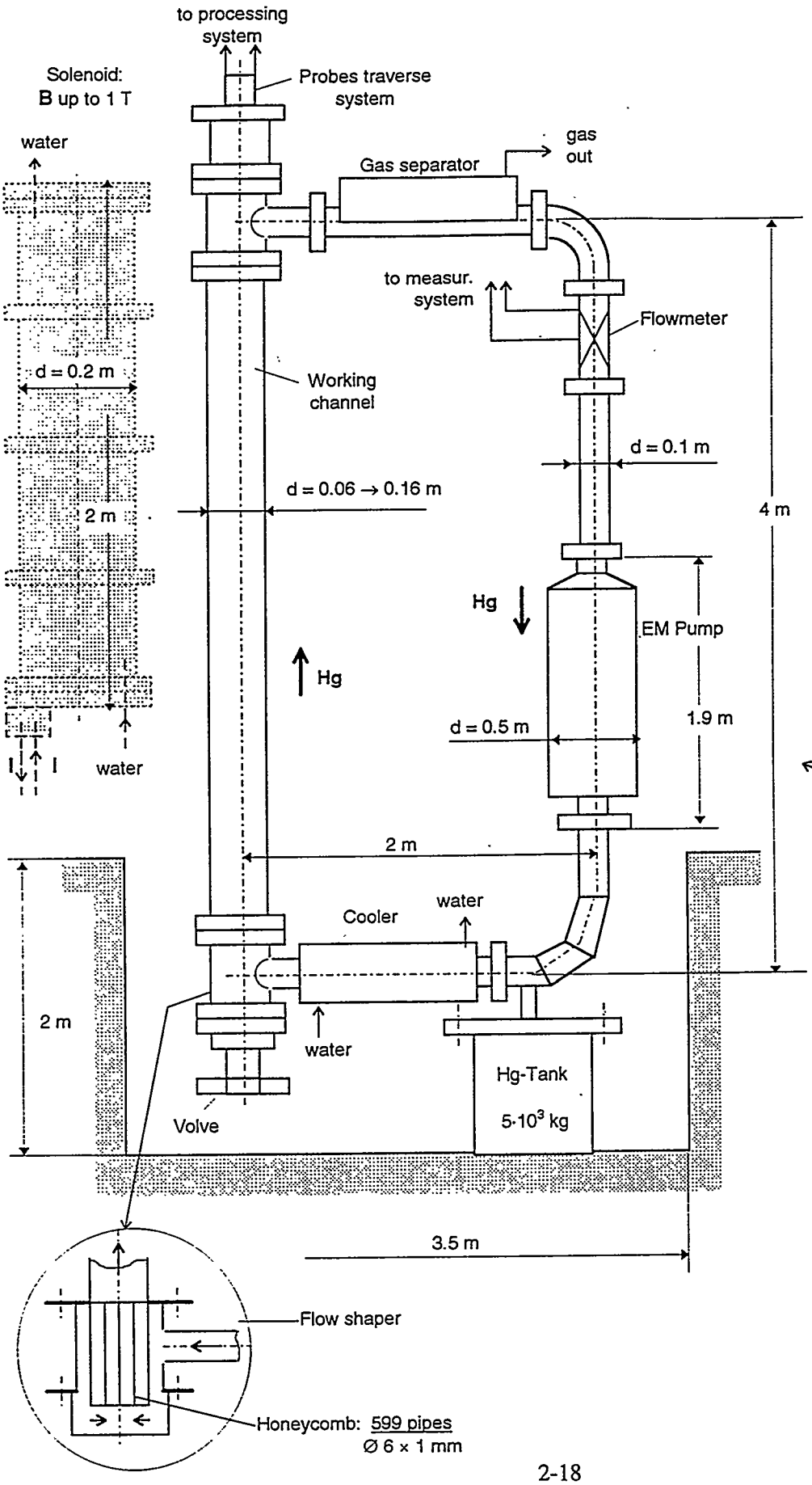

Loop parameters

Total volume $= 3.5 \cdot 10^5$ cm^3
Mercury weight $= 4.7 \cdot 10^3$ kg

EM Pump

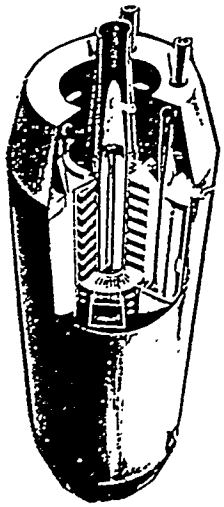

Outlet pressure $P = 5 \cdot 10^5$ N/m^2
Flow rate $Q = 5 \cdot 10^3$ cm^3/s
Active power $N = 59$ kW
Water cooling

SCHEMATICAL INSTALLATION OF
A HORIZONTAL TARGET IN THE LOOP

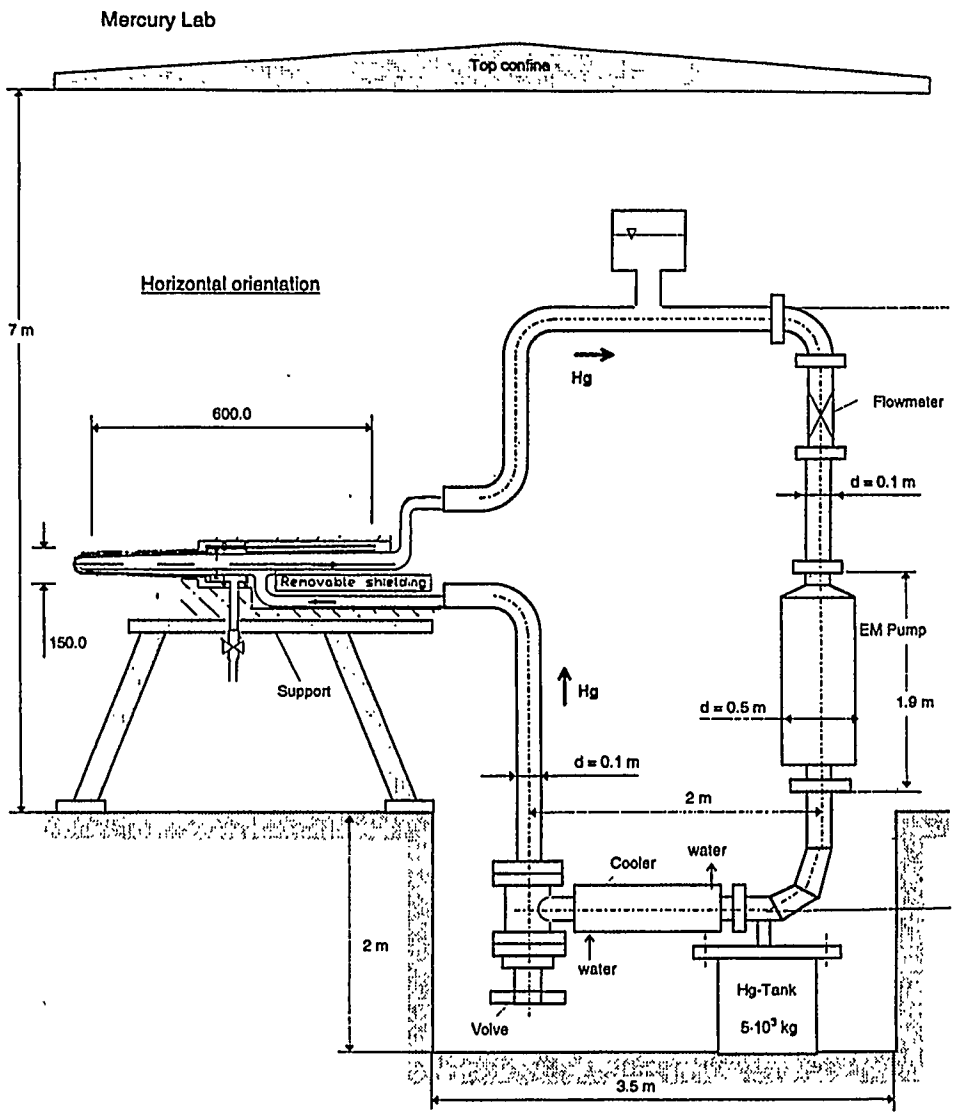

SCHEMATICAL INSTALLATION OF
A VERTICAL TARGET IN THE LOOP

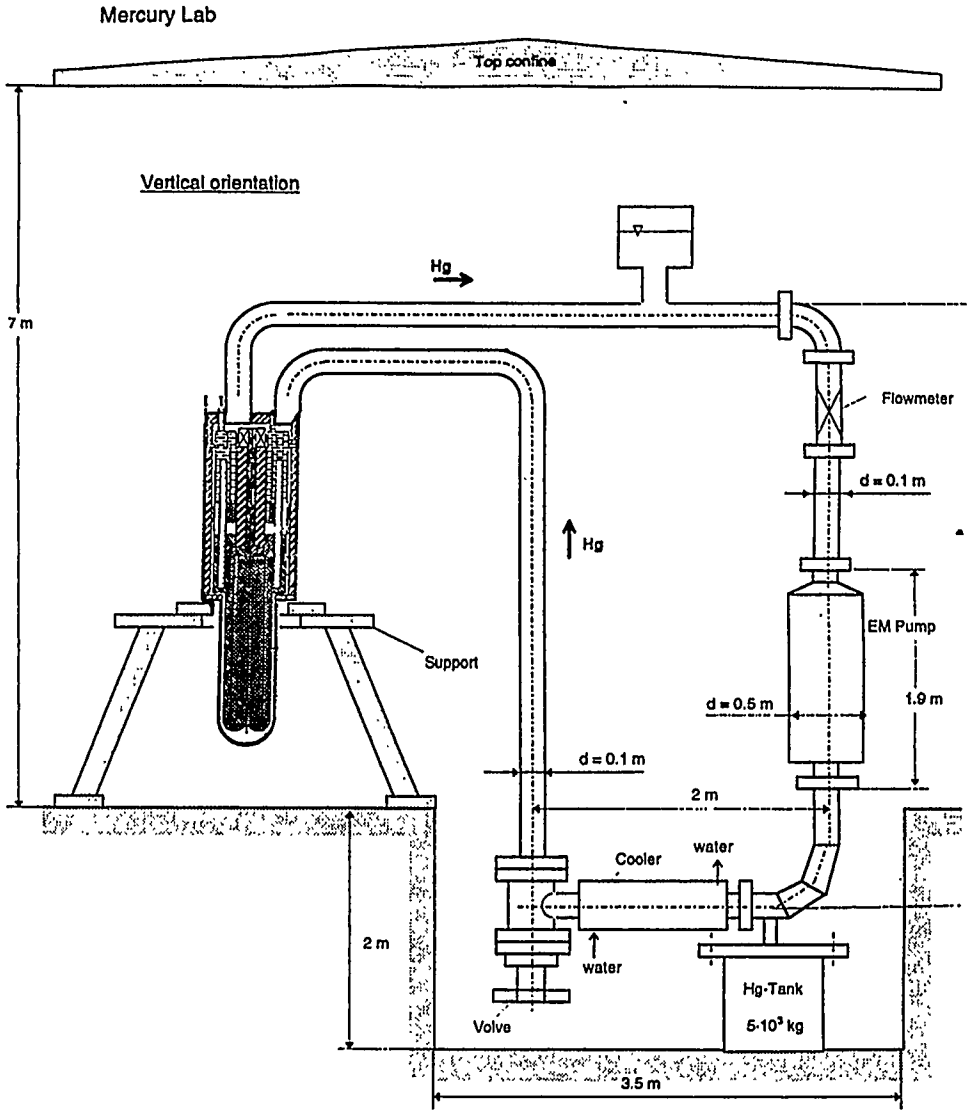

SIMILARITY OF PROCESSES IN A FUSION REACTOR BLANKET AND IN THE SPALLATION TARGET

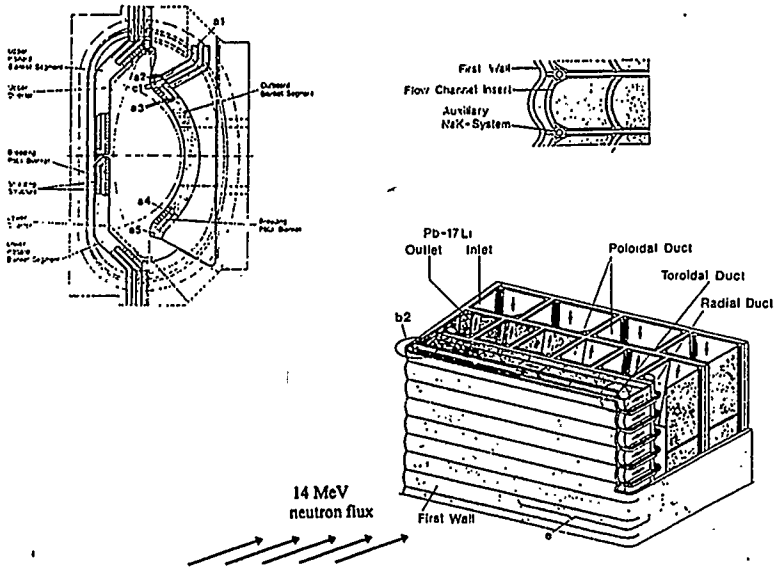

MHD issues of the Pb-17Li blanket

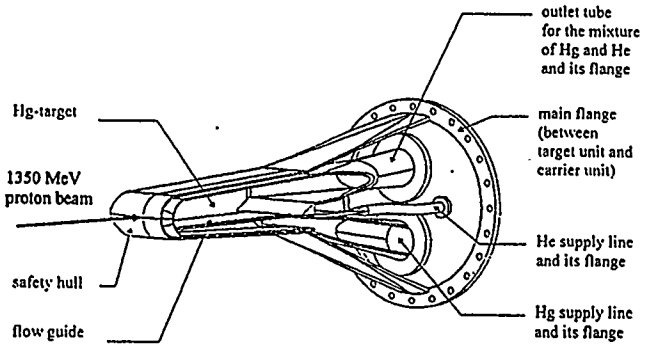

Design of the target unit

ENERGETICAL RELATIONS IN A LIQUID METAL BLANKET AND IN THE TARGET

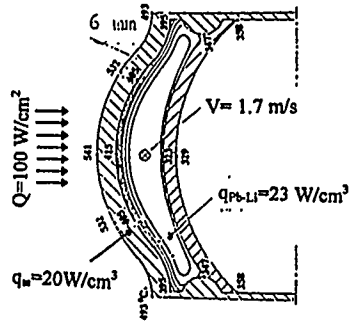

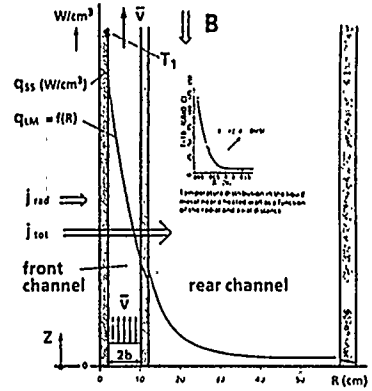

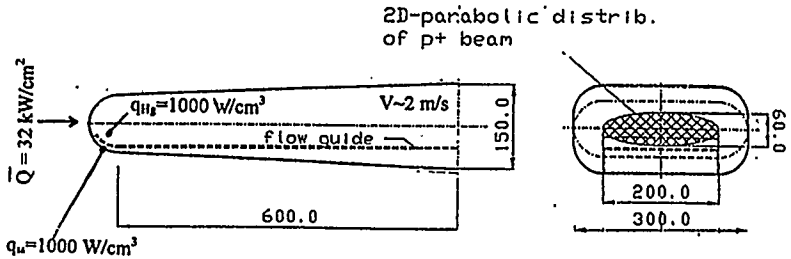

Proposed Target Geometry

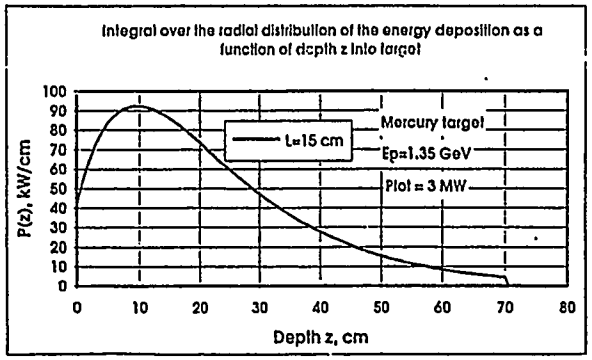

SESSION 3

Thermal Hydraulics, Heat Removal and Circuit Design (2)

Chairman
O. Lielausis

International Workshop on the Technology and
Thermal Hydraulics of Heavy Metals

Schruns, Austria, 25-28 March 1996

Theoretical investigation of the thermal hydraulic behaviour of a slab-type liquid metal target

T. V. Dury and B. L. Smith

Thermal Hydraulics Laboratory
Paul Scherrer Institut
Villigen
Switzerland

Introduction

The thermal hydraulics codes CFDS-FLOW3D and ASTEC have been used to simulate a slab-type design of ESS spallation target. This design is single-skinned, and of tapering form (in the beam direction), with rounded sides in a cross-section through a plane normal to the beam. The coolant fluid used is mercury, under forced circulation, with an inlet temperature of 180°C. The goal of these computer studies was to understand the behaviour of the coolant flow, and hence to arrive at a design which optimises the heat extraction for a given beam power — in the sense of:

- minimising the peak local fluid temperature within the target,
- maintaining an acceptable temperature level and distribution over and through the target outer wall,
- keeping the overall fluid pressure loss through the complete target to a minimum,
- staying within the physical limits of overall size required, particularly in the region of primary spallation.

Two- and three-dimensional models have been used, with different arrangements and design of internal baffles, and different coolant flow distributions at the target inlet. Nominal total inlet mass flow was 245 kg/s, and a heat deposition profile used which was based on the proton beam energy distribution. This gave a nominal total heat load of 3.23 MW — of which 8.2 kW were deposited in the window steel.

2D Model

This model was based on an early design concept in which the inlet and outlet streams are separated by a single flow guide. The inlet channel under this guide contracts to accelerate the flow over the window. The analysis is undertaken for a 2D vertical slice through the centre of the target, representing a worst-case situation with no lateral reduction in power, and no lateral heat transfer.

Detailed calculations revealed that, although the window cooling was acceptable, internal fluid temperatures were far too high, due to recirculation of the coolant in the outlet channel. The use of a perforated flow guide, to discourage the creation of the recirculation zone, actually exacerbated the problem, with coolant diverted from the main heating region. Peak fluid temperatures of over 900°C were always obtained. However, it was shown that the window itself could be adequately cooled with only 12% of the total flow directed over it. The remaining 88% clearly needs to be better utilized for the bulk fluid cooling. This leads to a multi-inlet design.

3D Half Model

A 3D model was then developed, with a side baffle introduced in order to direct fluid forceably into the body of the target, but with a slightly broader flow exit at the end of this guide than with the lower one. This would ensure flow penetration to the centre, but not at the expense of significantly disturbingthe flow over the window from below. Because of symmetry about a vertical plane down the centre of the target, parameter studies of relative inlet flowrates were initially carried out on a half-model only. These showed that the window temperature can be kept below about 330°C, with the fluid not exceeding 310°C. Pressures at the lower and side inlets could be made the same, at between 3 and 4 bar, with suitable adjustment of the respective inlet flow rates.

3D Full Model

A full 3D model was constructed to examine the consequences of unequal flow rates in the side channels. No assumptions regarding symmetry are then imposed. The same dimensions as for the previous 2D calculations were used.

The conclusions were that imbalance of up to ±10% had almost no effect on the window temperatures. However, because the asymmetry moved the location of maximum fluid velocity down the target, and away from the centre-line, fluid temperatures could rise significantly. Indeed, for a flow difference of only ±5%, peak fluid temperature rose by about 30°C. Thus it is important to ensure both that the side flows are similar, and that the beam remains central on the target.

Further Work

Further computer simulation remains to be done to:

- investigate the mesh-dependency of the results,
- investigate the distribution of helium bubbles injected in the system.

ESS Studies

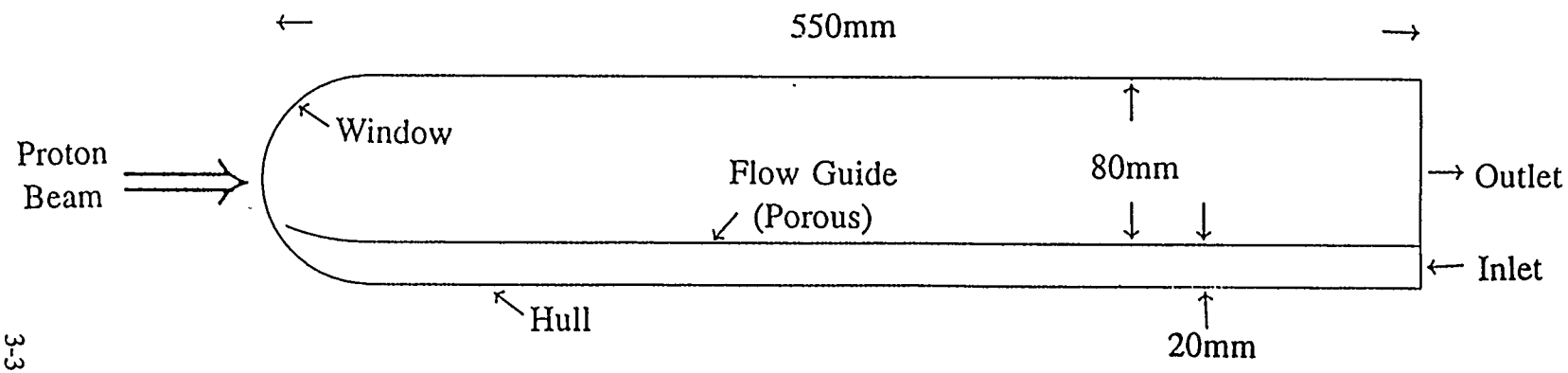
550mm
Proton
Beam
Window
Flow Guide
(Porous)
80mm
Outlet
Inlet
Hull
20mm

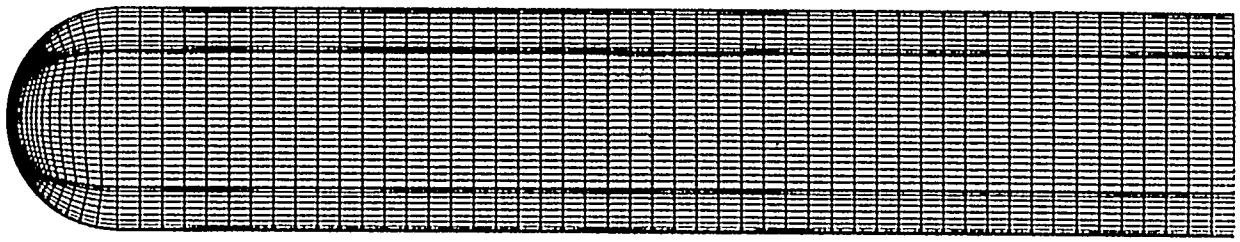

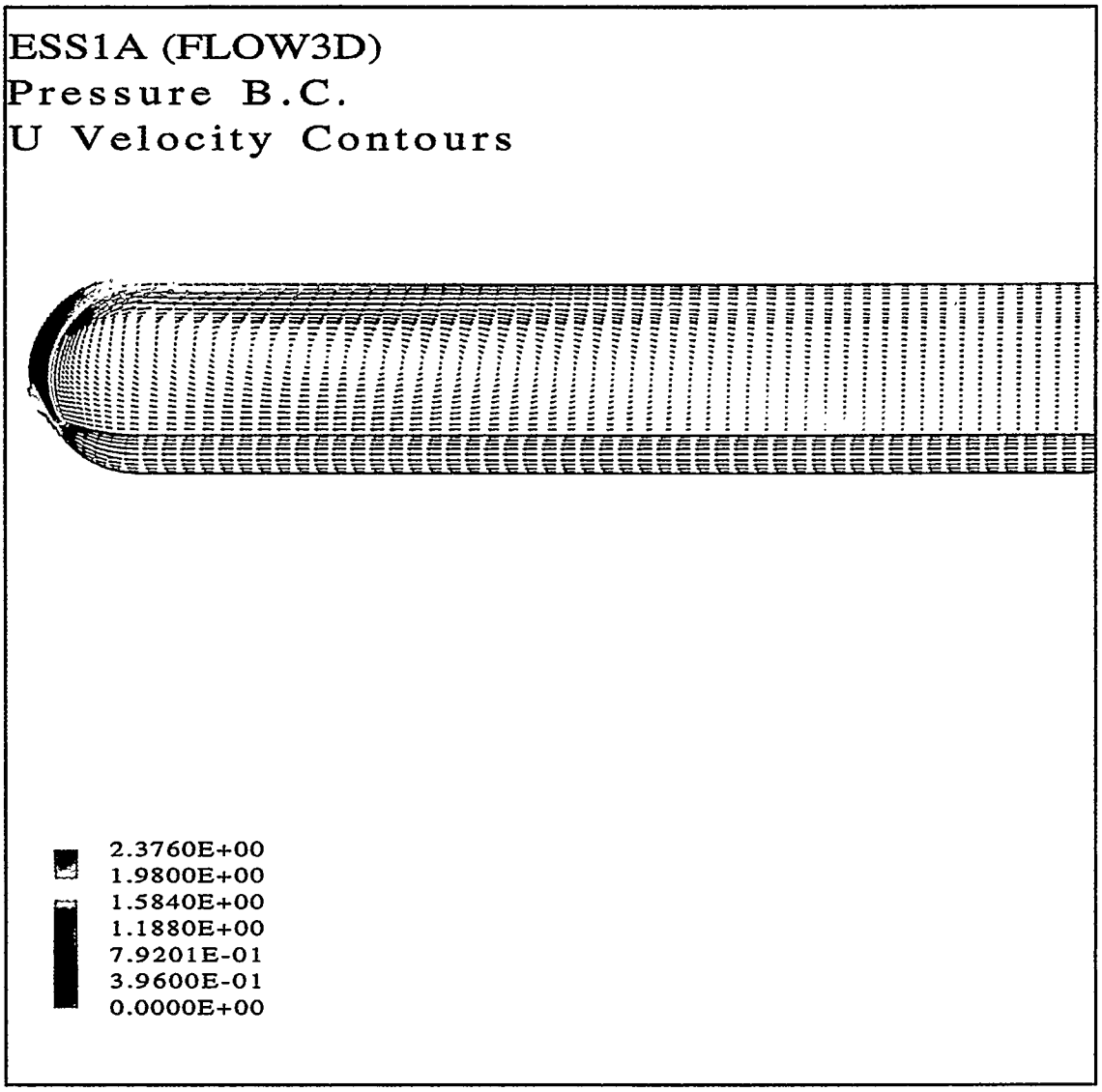
ESS1A (FLOW3D)
Pressure B.C.
U Velocity Contours
2.3760E+00
1.9800E+00
1.5840E+00
1.1880E+00
7.9201E-01
3.9600E-01
0.0000E+00

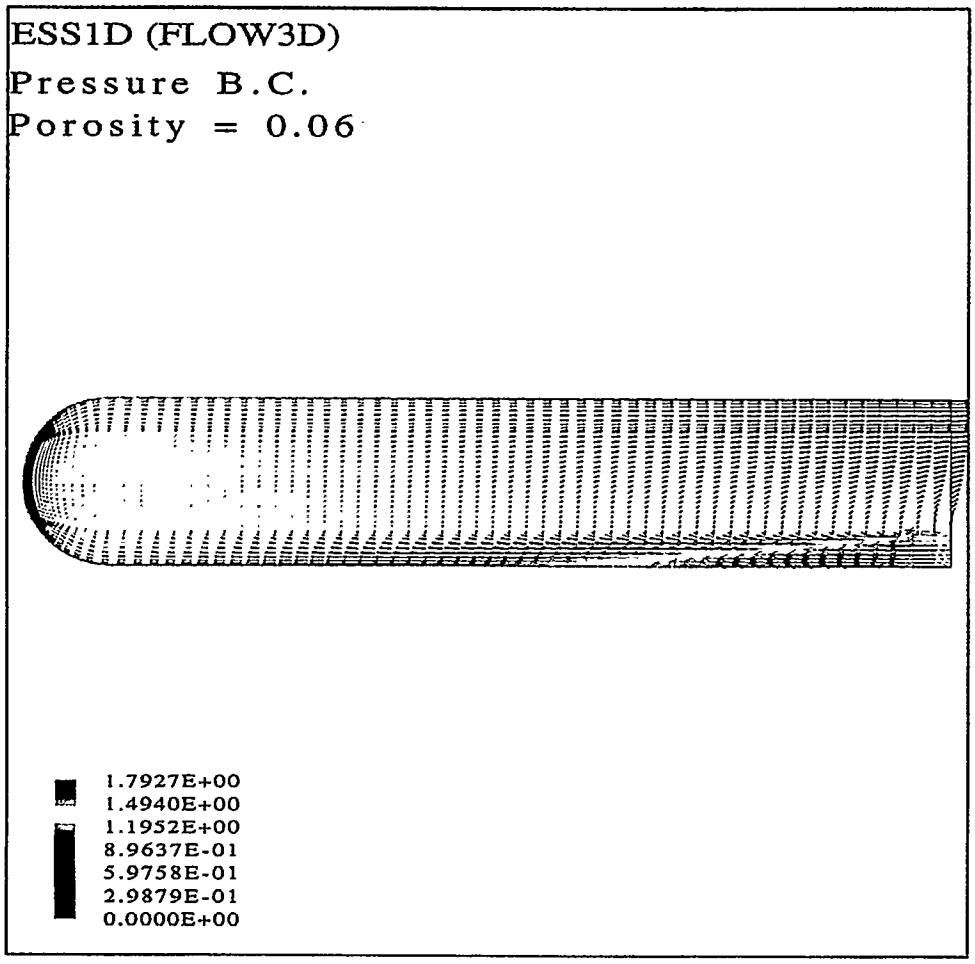
ESS1D (FLOW3D)
Pressure B.C.
Porosity = 0.06
1.7927E+00
1.4940E+00
1.1952E+00
8.9637E-01
5.9758E-01
2.9879E-01
0.0000E+00

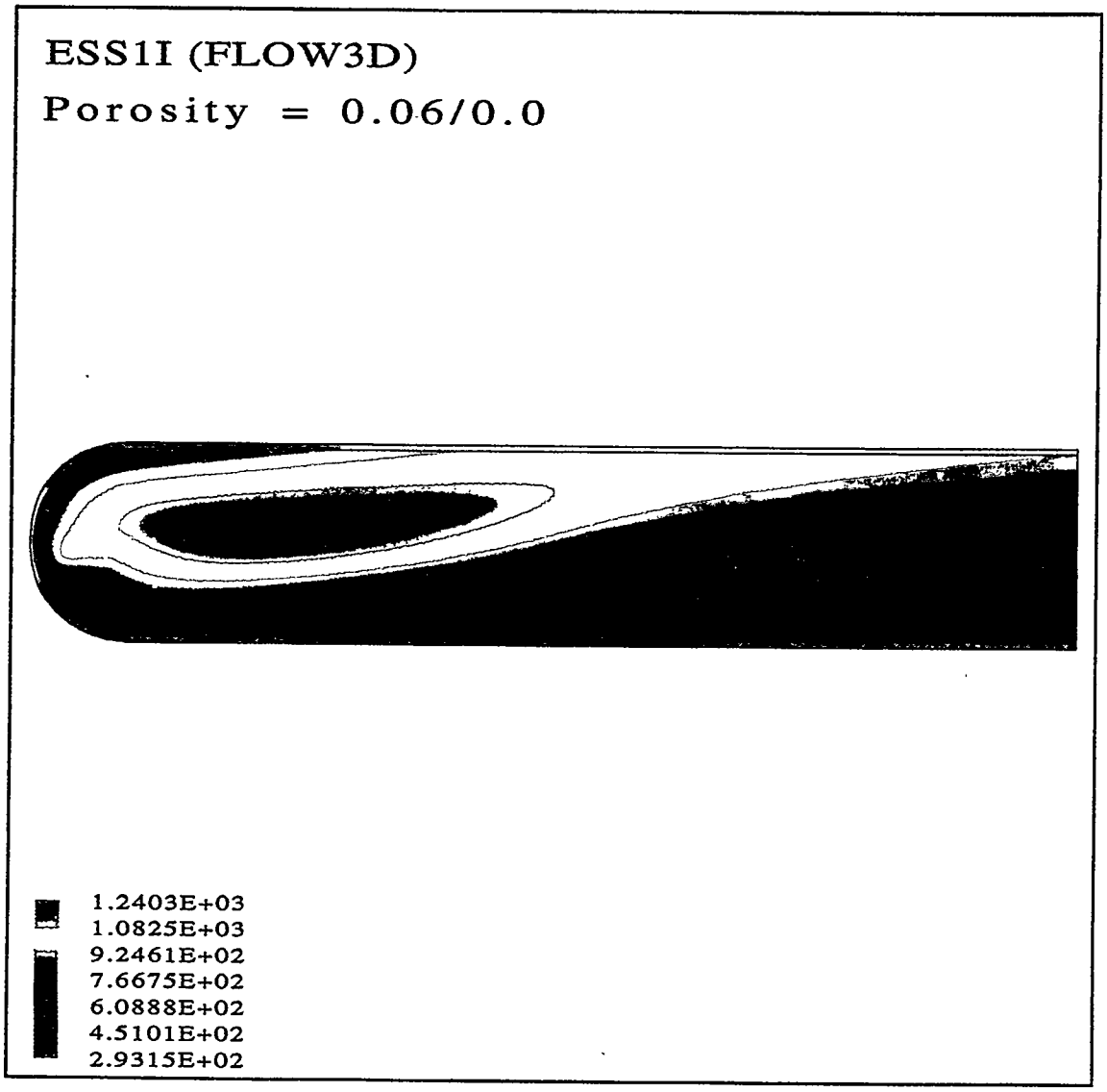
ESS1I (FLOW3D)
Porosity = 0.06/0.0
1.2403E+03
1.0825E+03
9.2461E+02
7.6675E+02
6.0888E+02
4.5101E+02
2.9315E+02

ESS Studies

Case No.	Target Length (mm)	Flow Guide Porosity	Recirculation Zone Length (mm)	Mass Flow over Window (%)
A	200	0.0	430	100
B	550	0.0	430	100
C	550	0.15 (z <550)	–	2
D	550	0.06 (z <550)	–	5
E	550	0.06 (z <50)	440	41
F	550	0.06 (z <300)	–	12
G	Case F above with hull structure			
H	Case F above with hull structure and heat			
I	Case E above with hull structure and heat			

ESS Studies

Conclusions

- Preliminary 2-D fluid-dynamic calculations have been performed for the single-inlet design of the ESS Liquid Metal Target.
- The principle of using a porous flow guide to discourage recirculation in the outlet channel is confirmed.
- Adequate window cooling is maintained as long as at least 12% of the total inlet mass flow is discharged to the window region.
- However, the design is fundamentally flawed because the bulk of the beam heating occurs in the region of least flow, leading to excessive local overheating.

Recommendations

- Maintain lower flow guide (non-porous) with flow restriction to induce strong cross-flow over the window. Only 10-15% of the total mass flow is required for this purpose.
- Need stronger downflow down the centre of the target to deal with bulk-heating effect. Move to multi-inlet design.

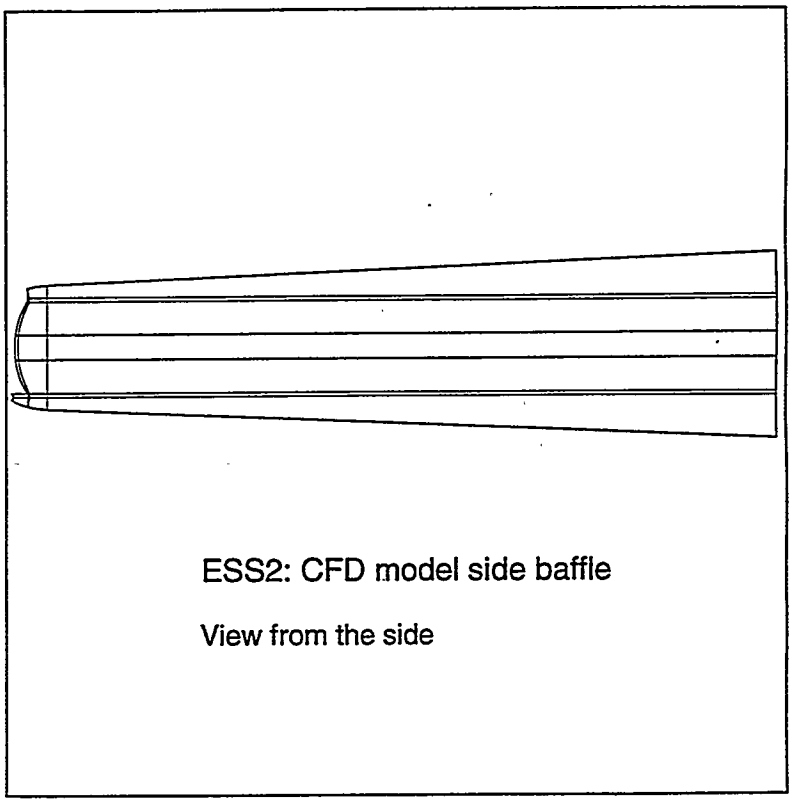
ESS2: CFD model side baffle
View from the side

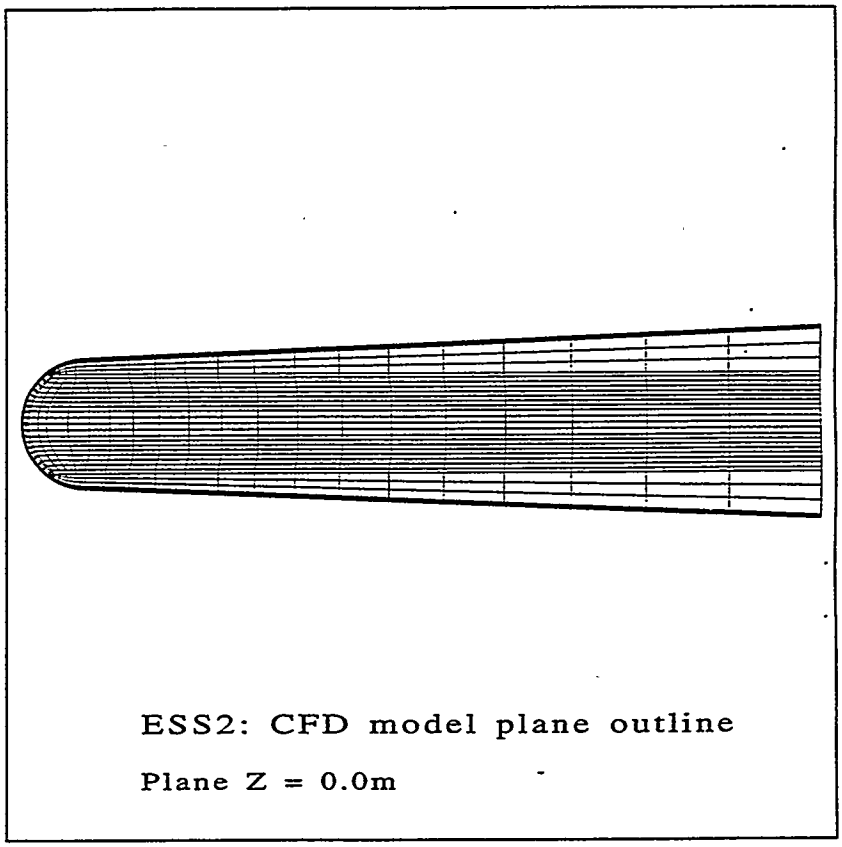
ESS2: CFD model plane outline
Plane Z = 0.0m

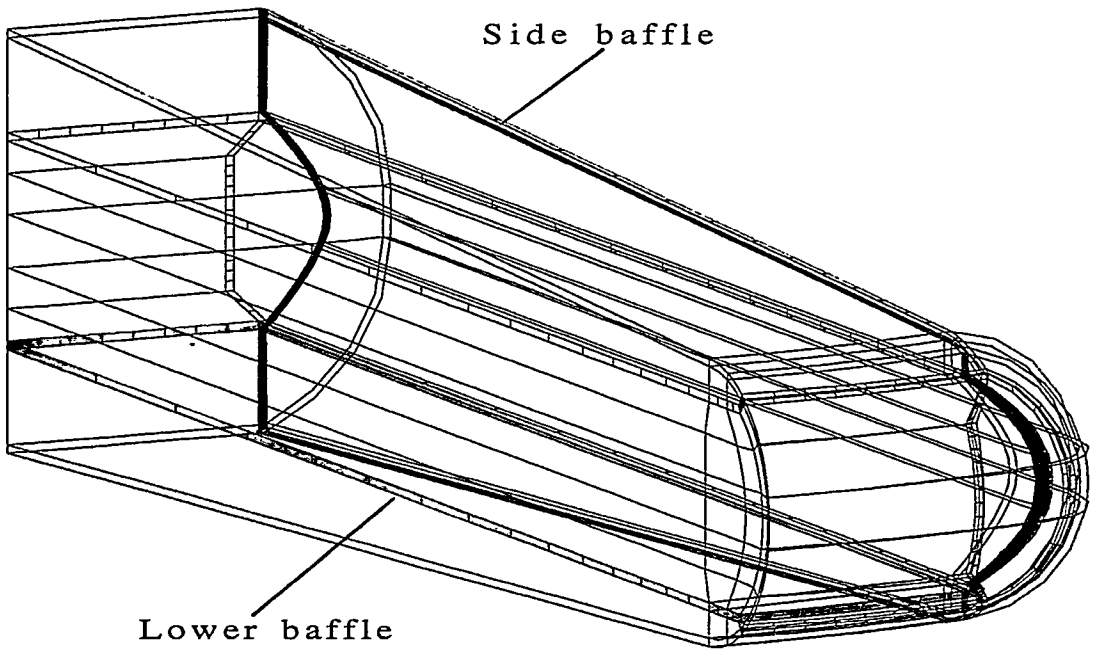

ESS2: CFD full model outline

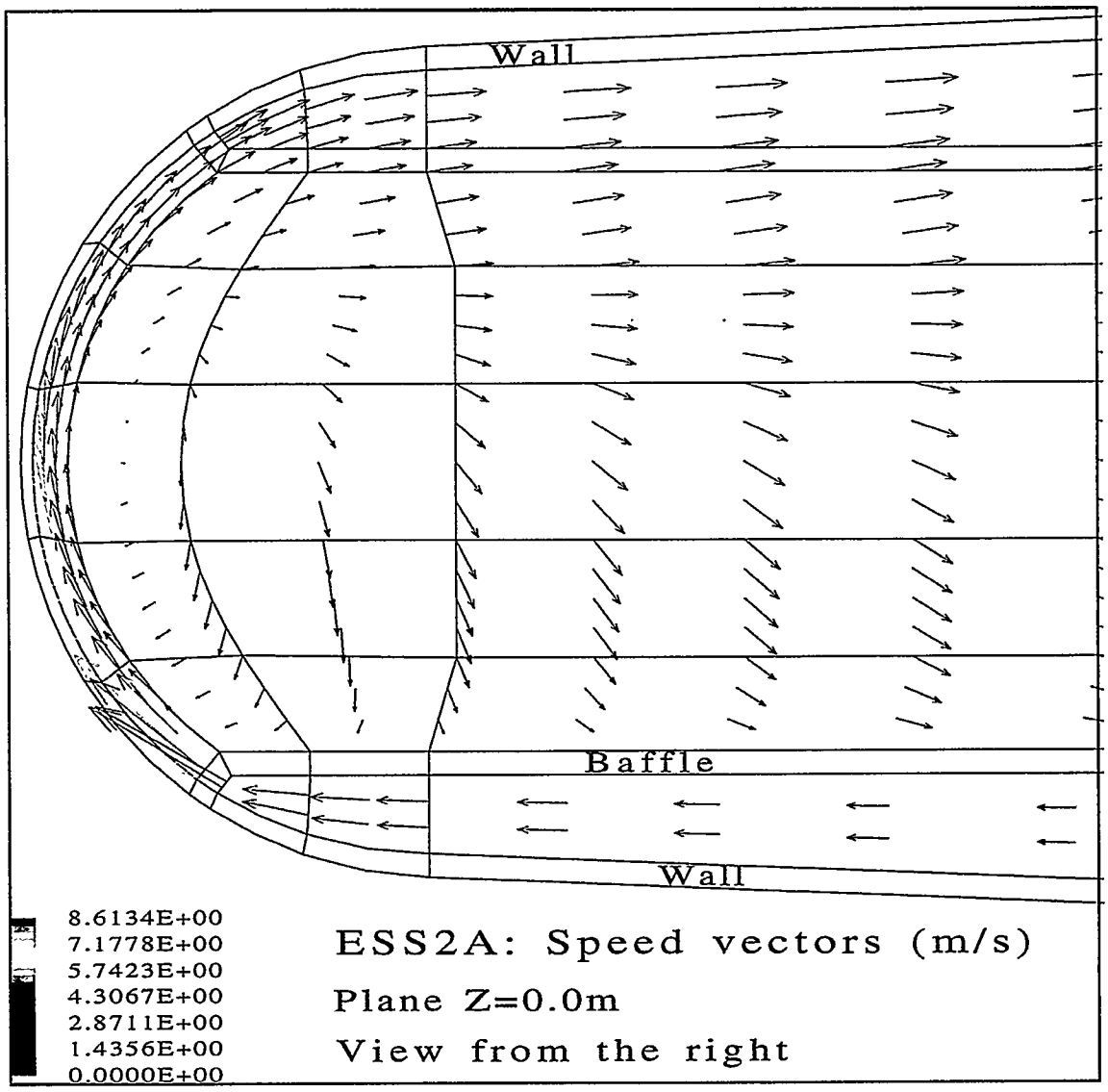
Wall
Baffle
Wall
8.6134E+00
7.1778E+00
5.7423E+00
4.3067E+00
2.8711E+00
1.4356E+00
0.0000E+00
ESS2A: Speed vectors (m/s)
Plane Z=0.0m
View from the right

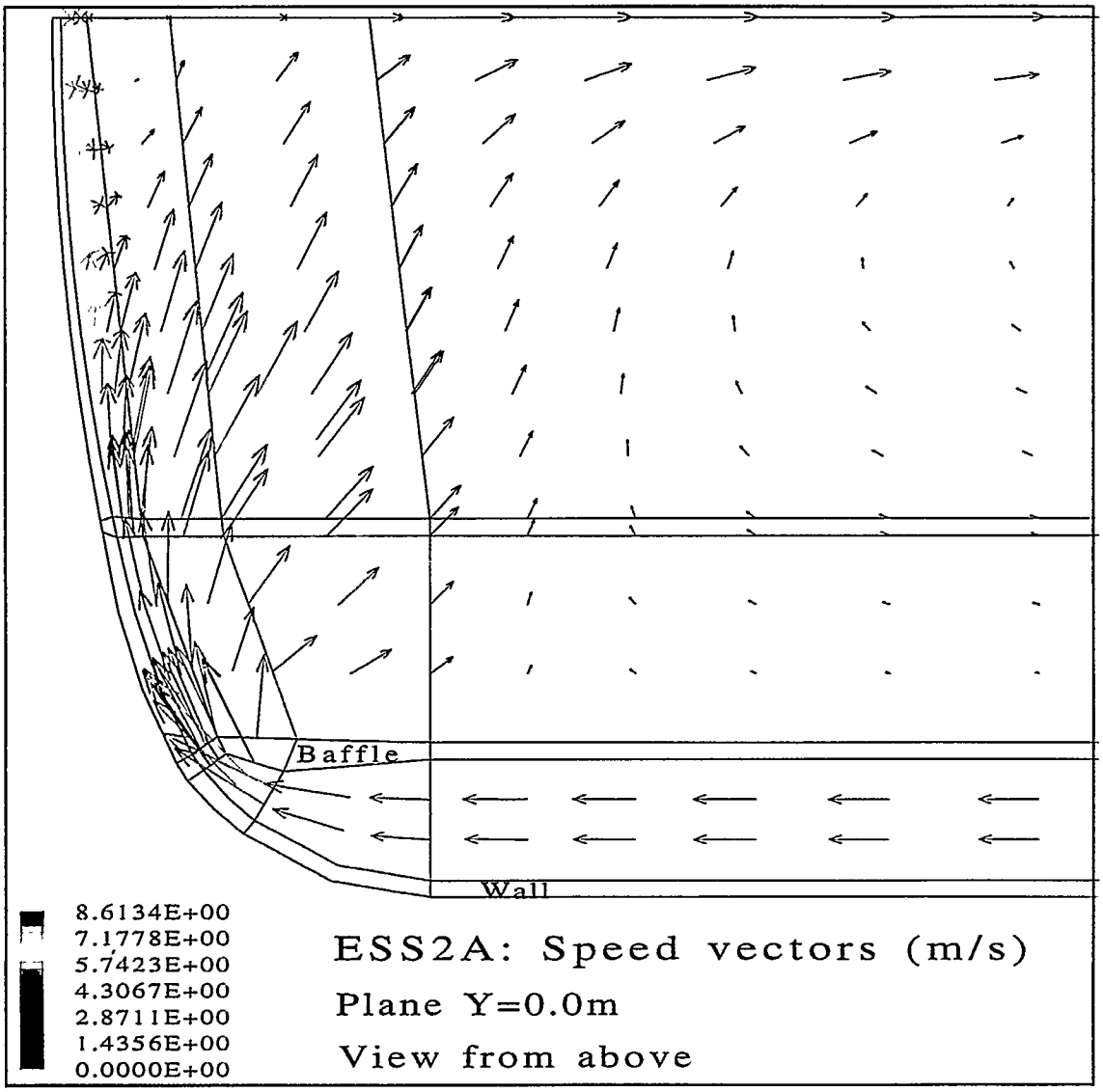
Baffle
Wall
8.6134E+00
7.1778E+00
5.7423E+00
4.3067E+00
2.8711E+00
1.4356E+00
0.0000E+00
ESS2A: Speed vectors (m/s)
Plane Y=0.0m
View from above

ESS2A: Planar temperatures (C)

Total heat = 3.235 MW (8.4 kW in walls)

Mass flow (whole target) = 244.6 kg/sec

Uinlet: Lower = 0.8 m/s: Side = 1.6 m/s

Maximum fluid temperature = 353 C

Maximum wall temperature = 279 C

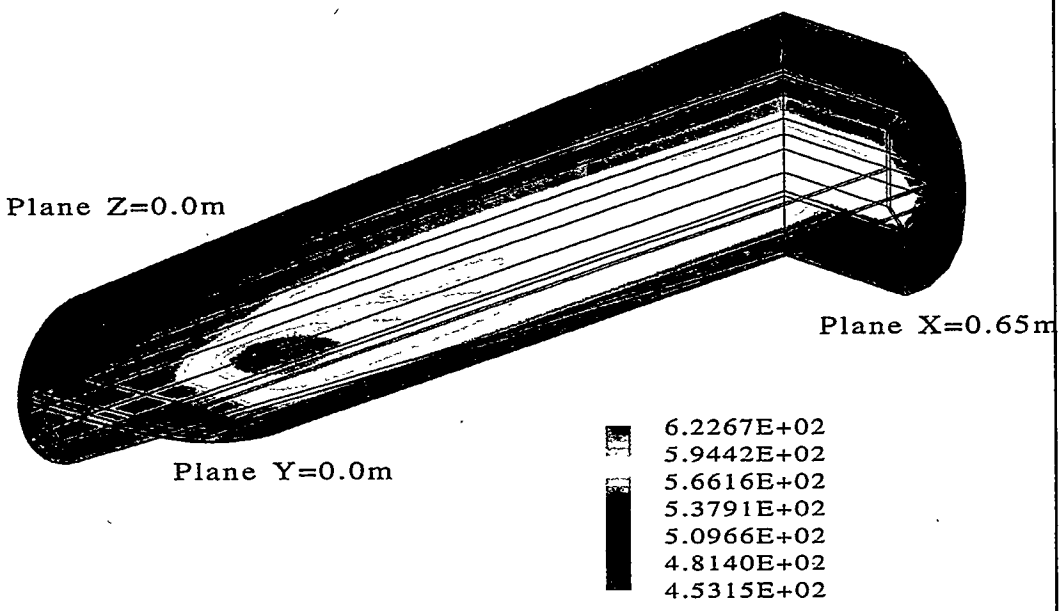

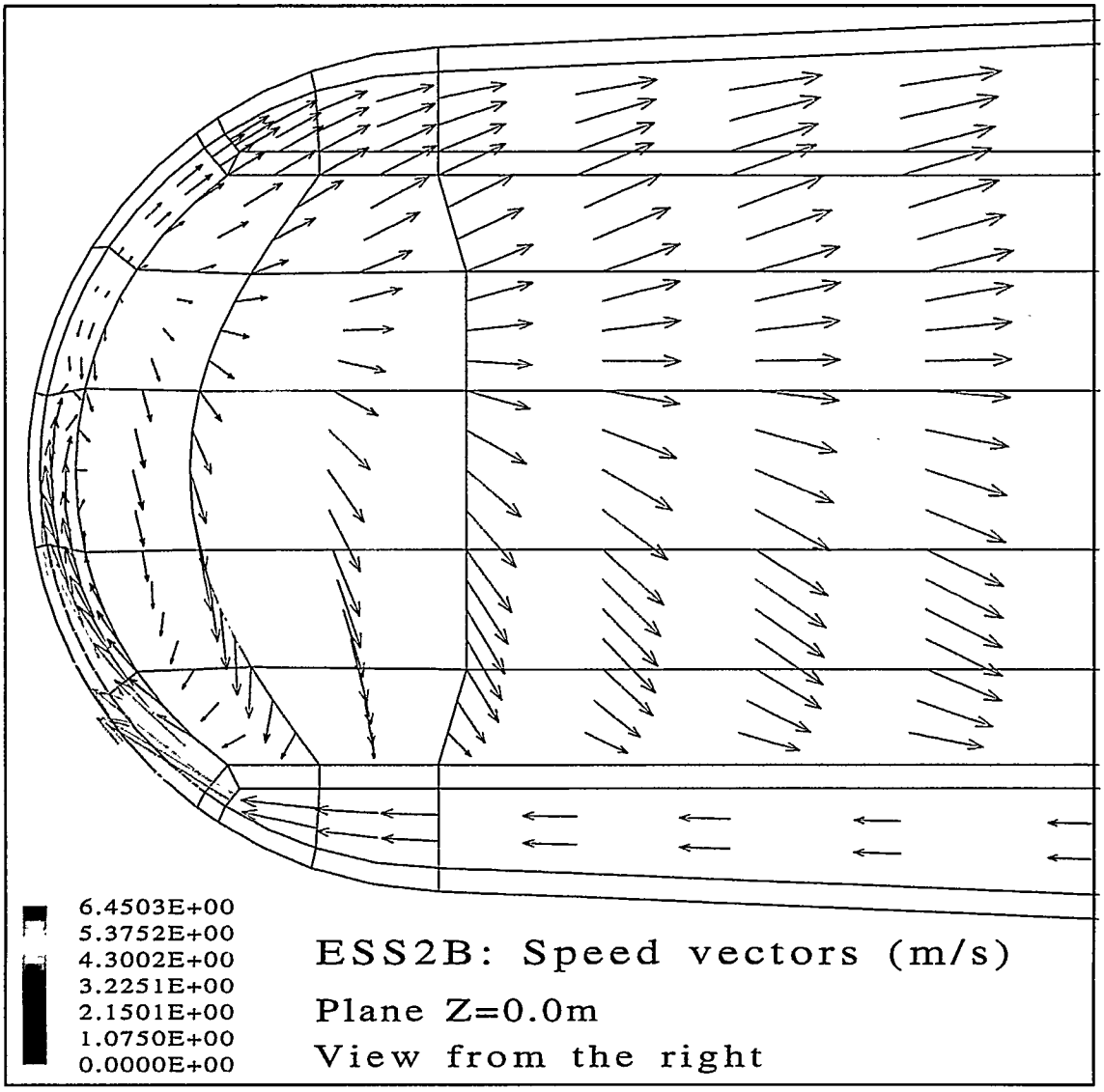
6.4503E+00
5.3752E+00
4.3002E+00
3.2251E+00
2.1501E+00
1.0750E+00
0.0000E+00
ESS2B: Speed vectors (m/s)
Plane Z=0.0m
View from the right

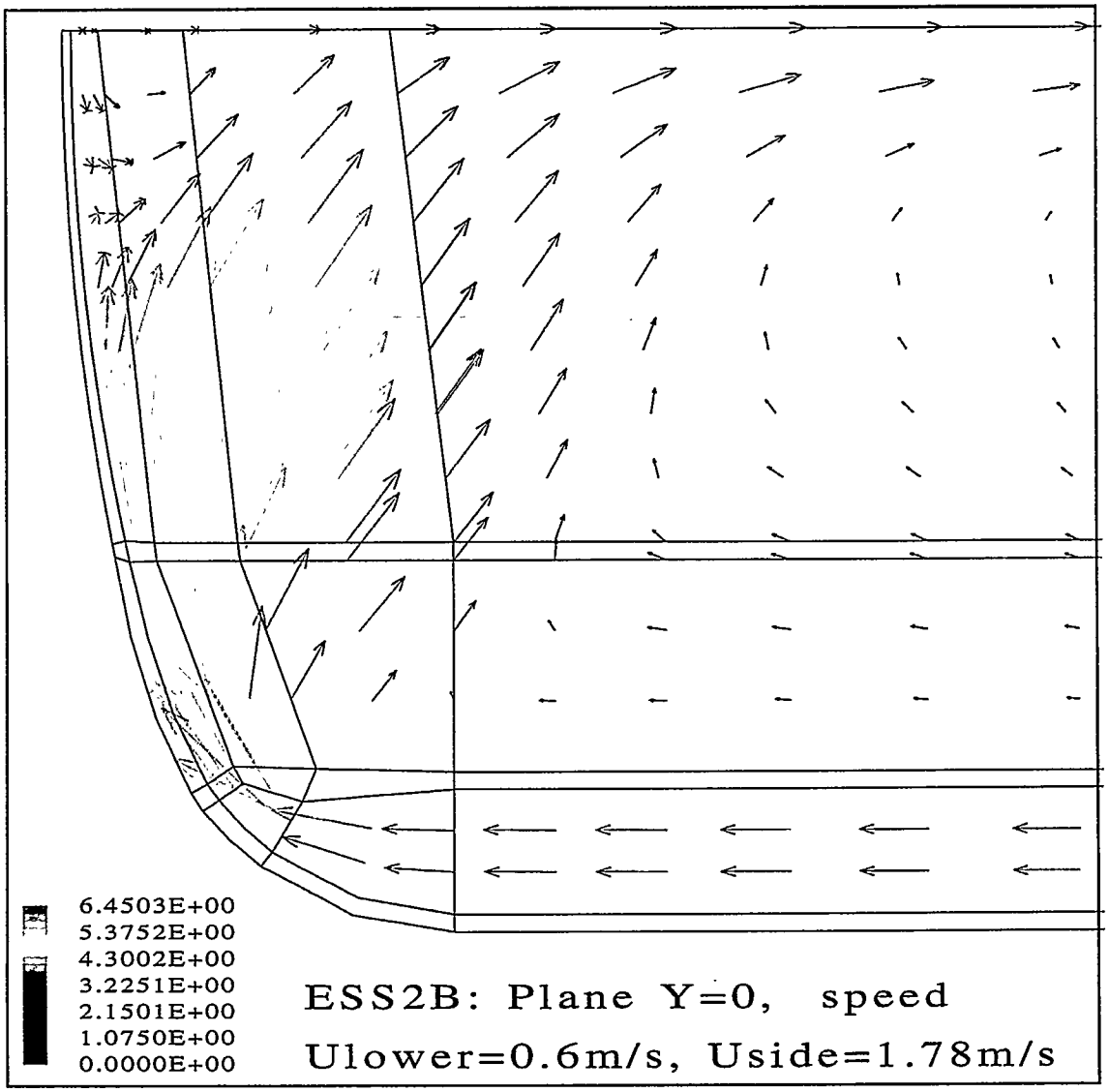
6.4503E+00
5.3752E+00
4.3002E+00
3.2251E+00
2.1501E+00
1.0750E+00
0.0000E+00
ESS2B: Plane Y=0, speed
Ulower=0.6m/s, Uside=1.78m/s

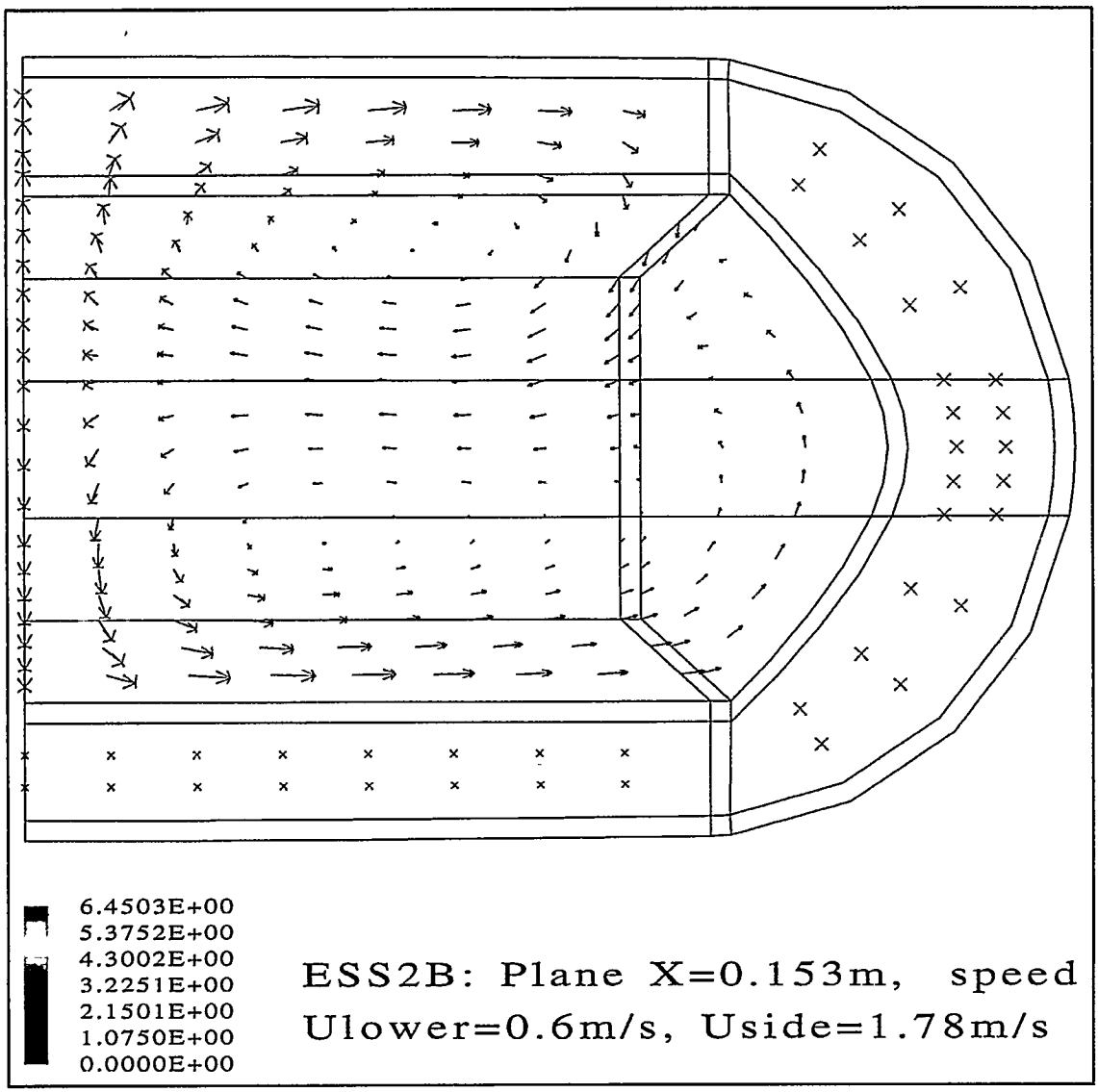
6.4503E+00
5.3752E+00
4.3002E+00
3.2251E+00
2.1501E+00
1.0750E+00
0.0000E+00
ESS2B: Plane X=0.153m, speed
Ulower=0.6m/s, Uside=1.78m/s

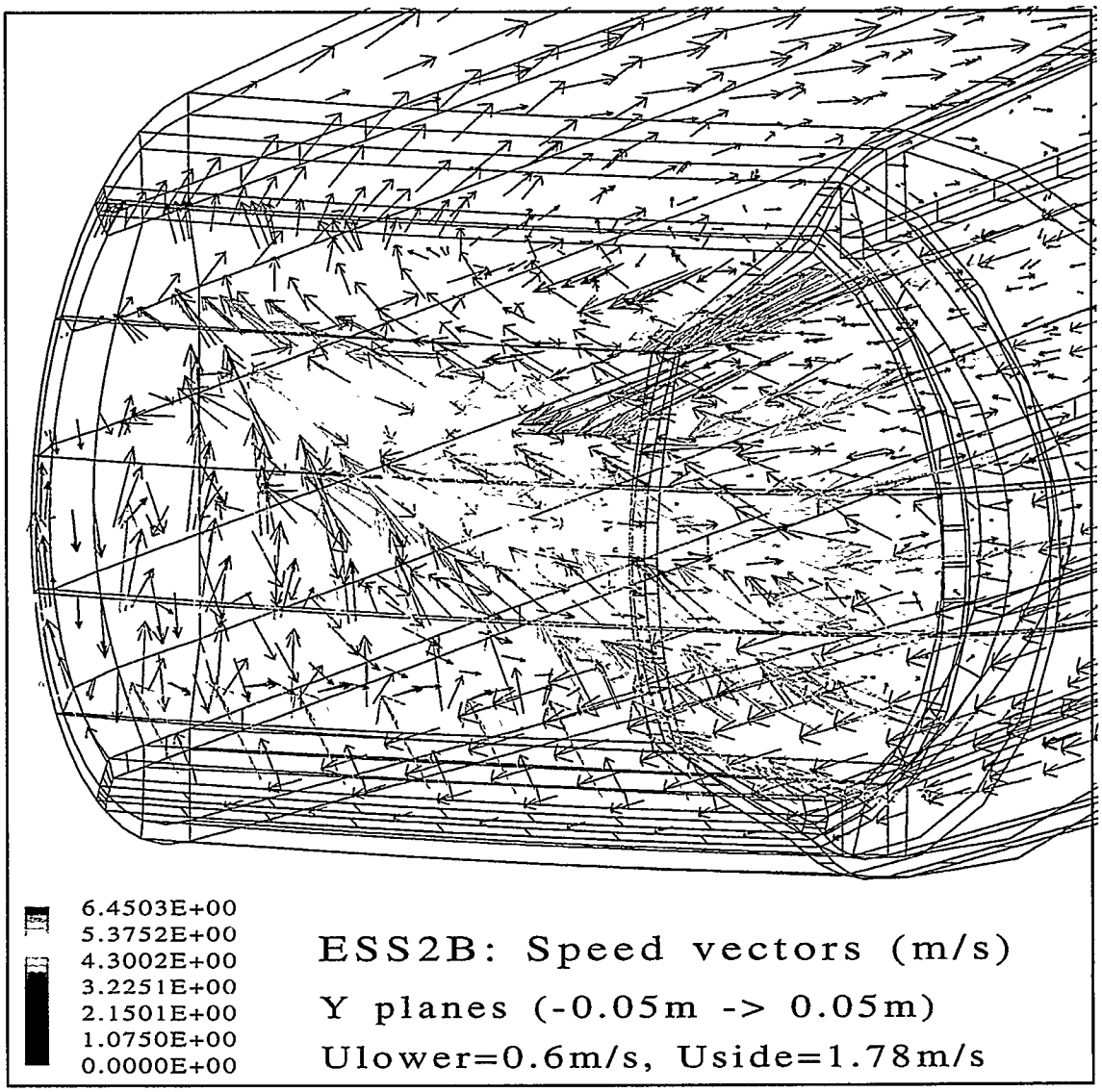
6.4503E+00
5.3752E+00
4.3002E+00
3.2251E+00
2.1501E+00
1.0750E+00
0.0000E+00
ESS2B: Speed vectors (m/s)
Y planes (-0.05m -> 0.05m)
Ulower=0.6m/s, Uside=1.78m/s

ESS2B: Planar temperatures (K)

Total heat = 3.235 MW (8.4 kW in wall)

Mass flow (whole target) = 244.6 kg/s

Uinlet: Lower=0.6 m/s; Side = 1.78 m/s

Max fluid temperature = 312 C

Max wall temperature = 331 C

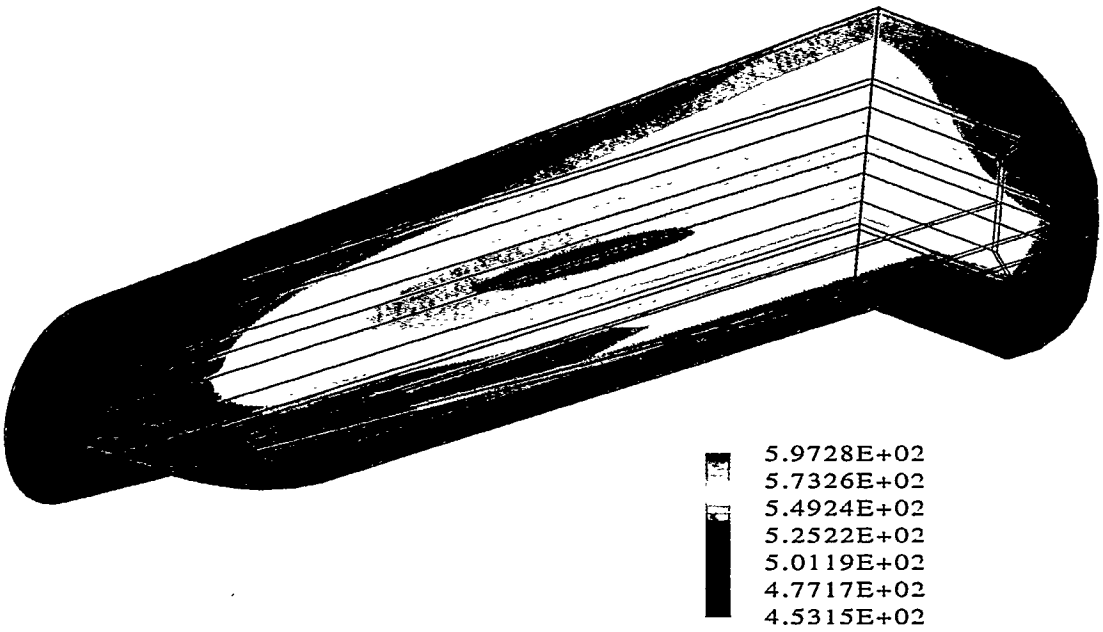

ESS2B: CENTRELINE TEMPERATURES

LOWER BAFFLE FLOW - 23.3%

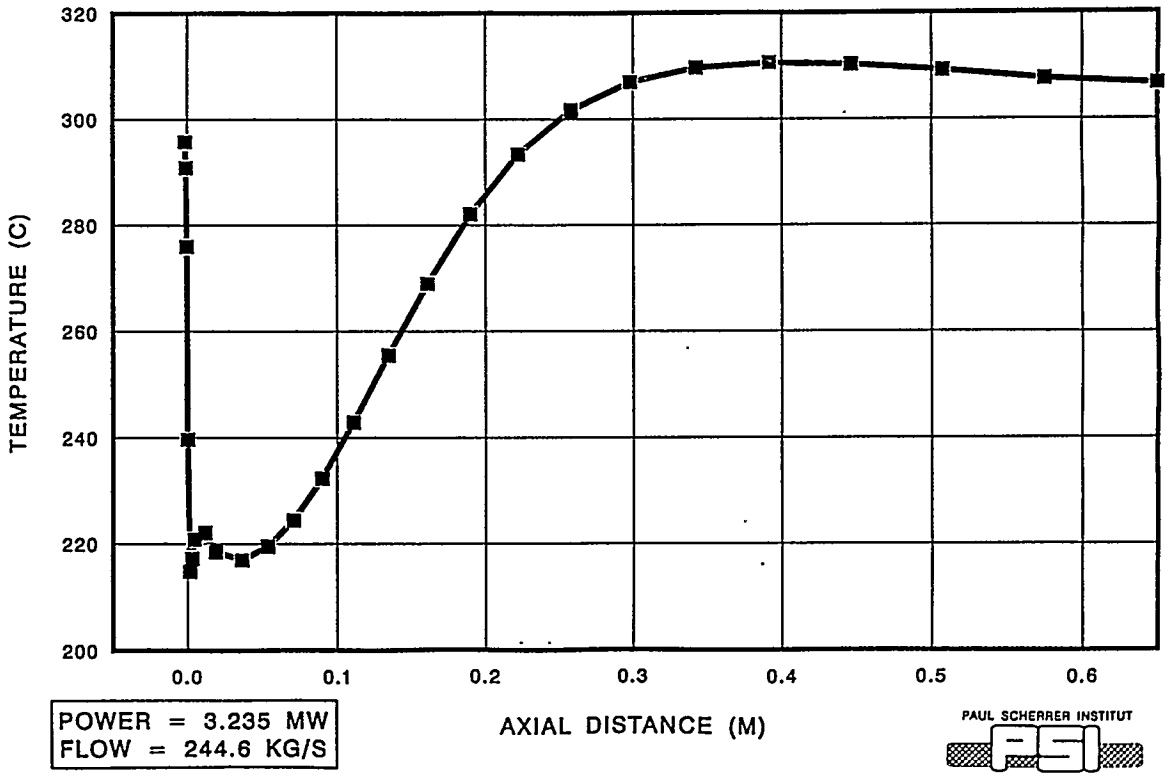

ESS2 - WINDOW AND FLUID PEAK TEMPERATURES

AS A FUNCTION OF INLET PRESSURE DROP RATIO

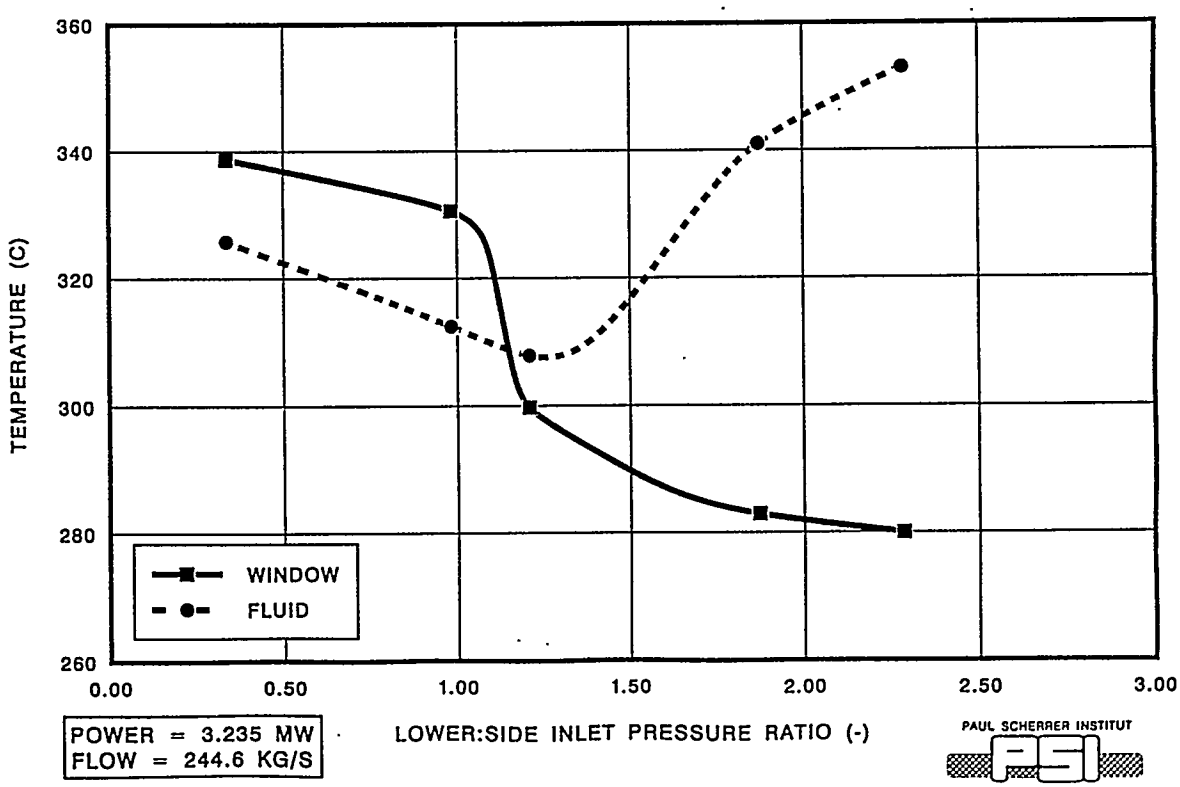

ESS4A: Full-mesh model of complete target

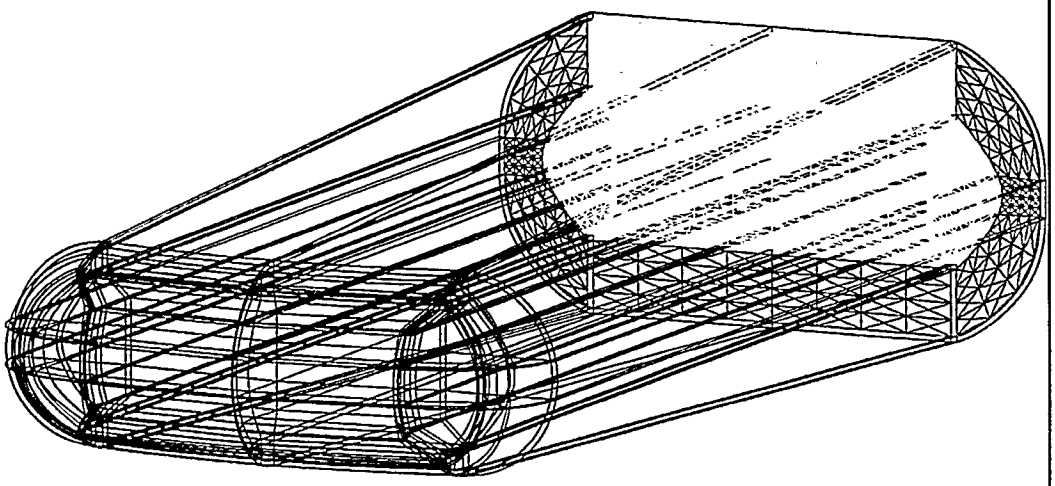

Green hatching: Side and bottom inlets

Yellow hatching: Outlet area

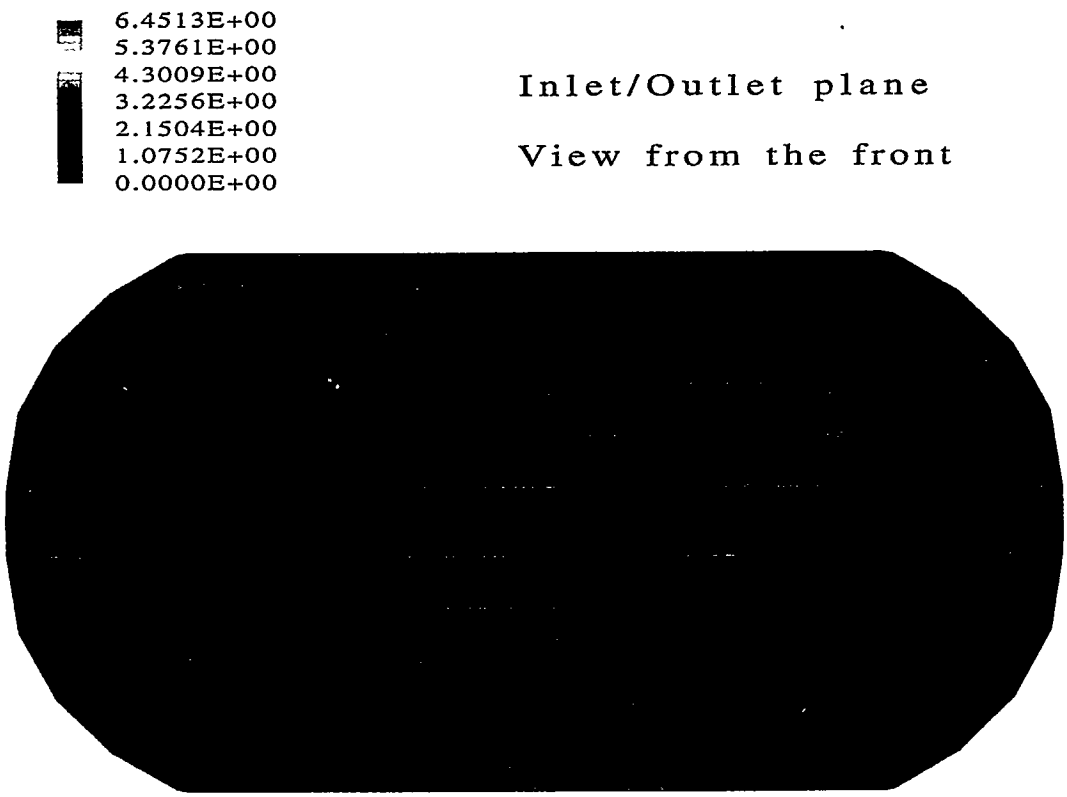

ESS4A: Speed contours (m/s)

23.3% flow from below

Side flows equal

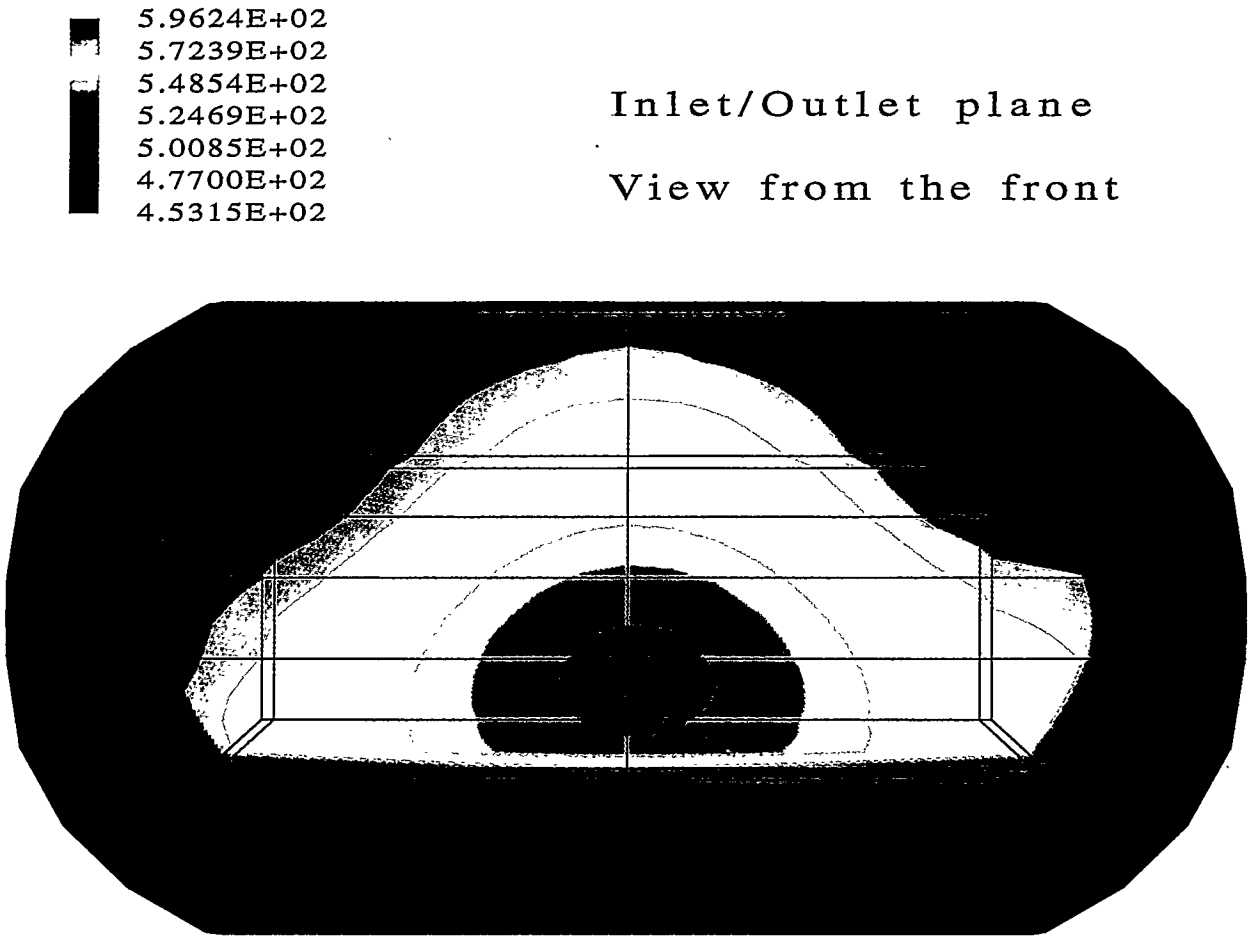

ESS4A: Temperatures (K)

23.3% flow from below

Side flows equal

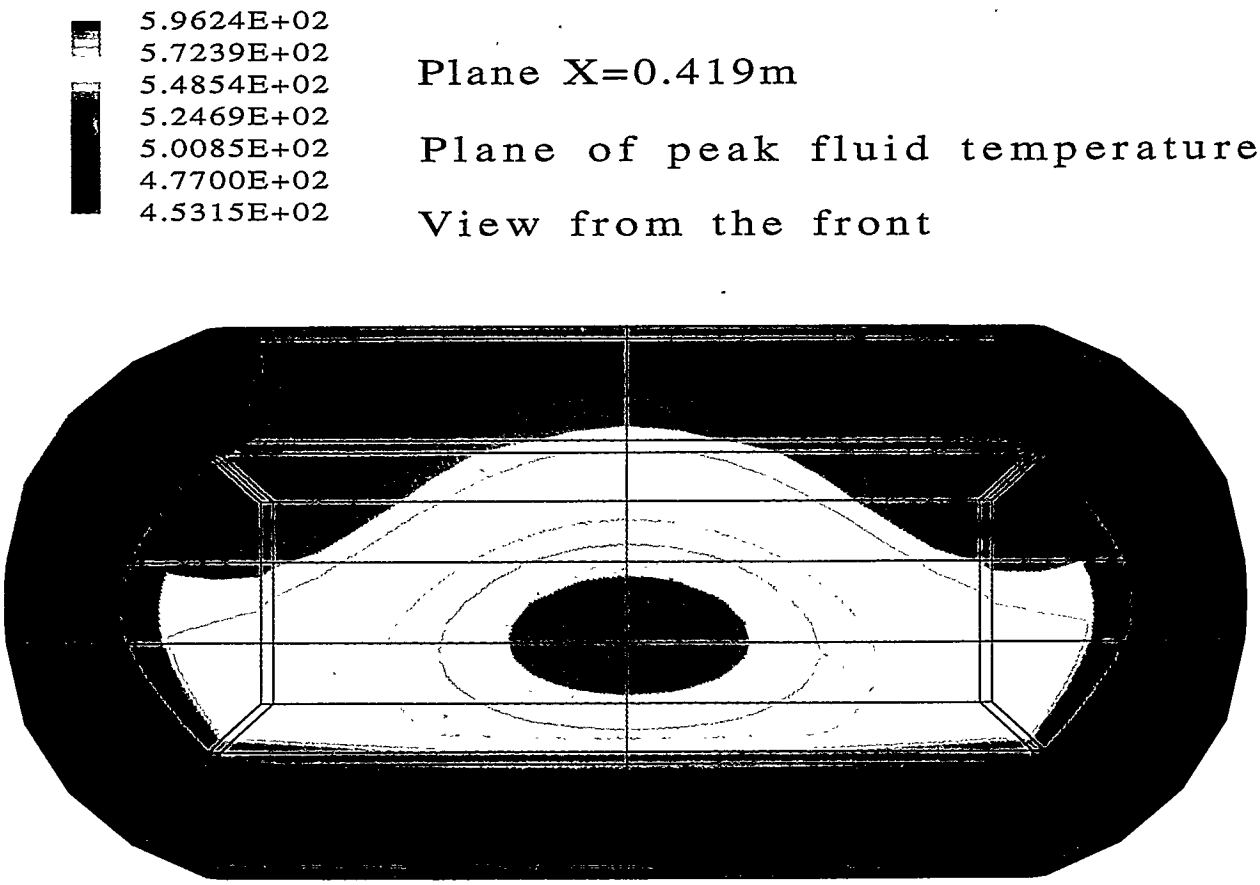

ESS4A: Temperatures (K)

23.3% flow from below

Side flows equal

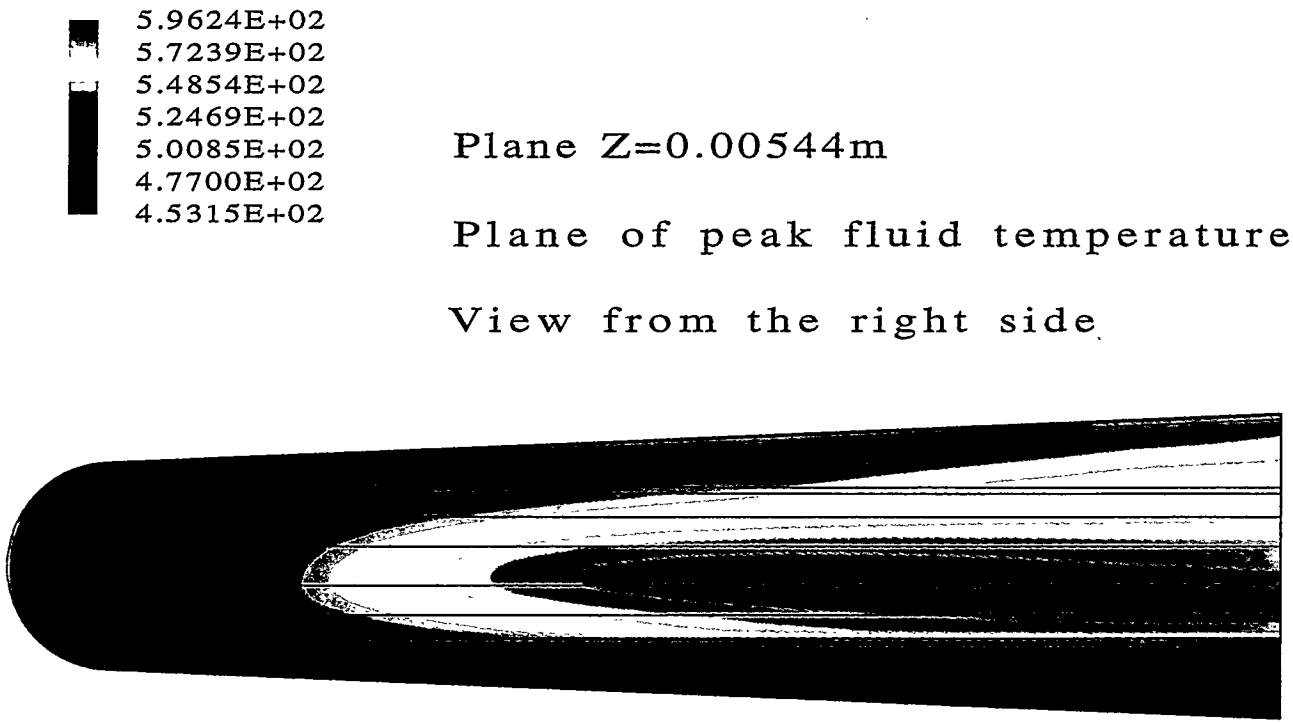

ESS4A: Temperatures (K)

23.3% flow from below

Side flows equal

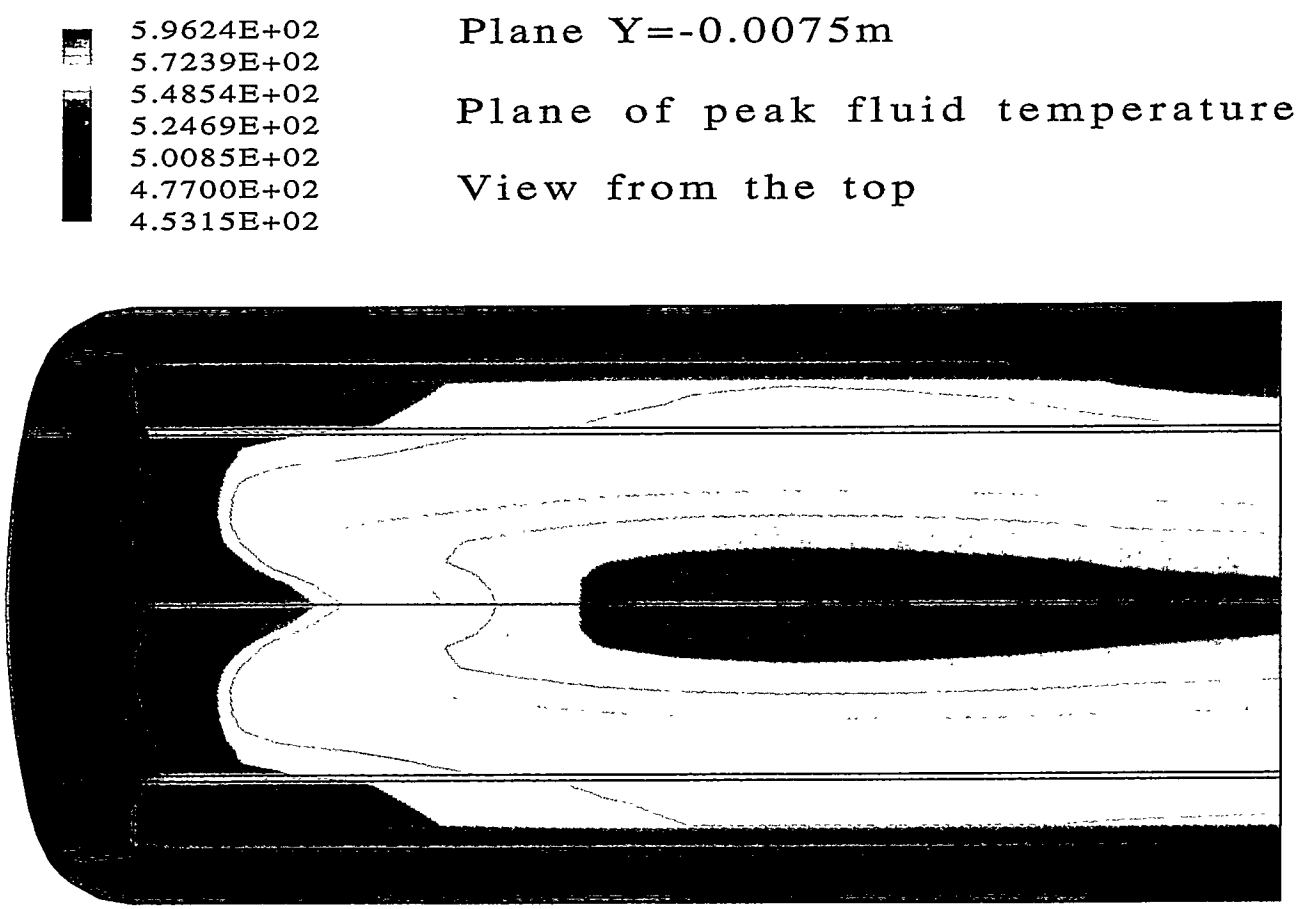

ESS4A: Temperatures (K)

23.3% flow from below

Side flows equal

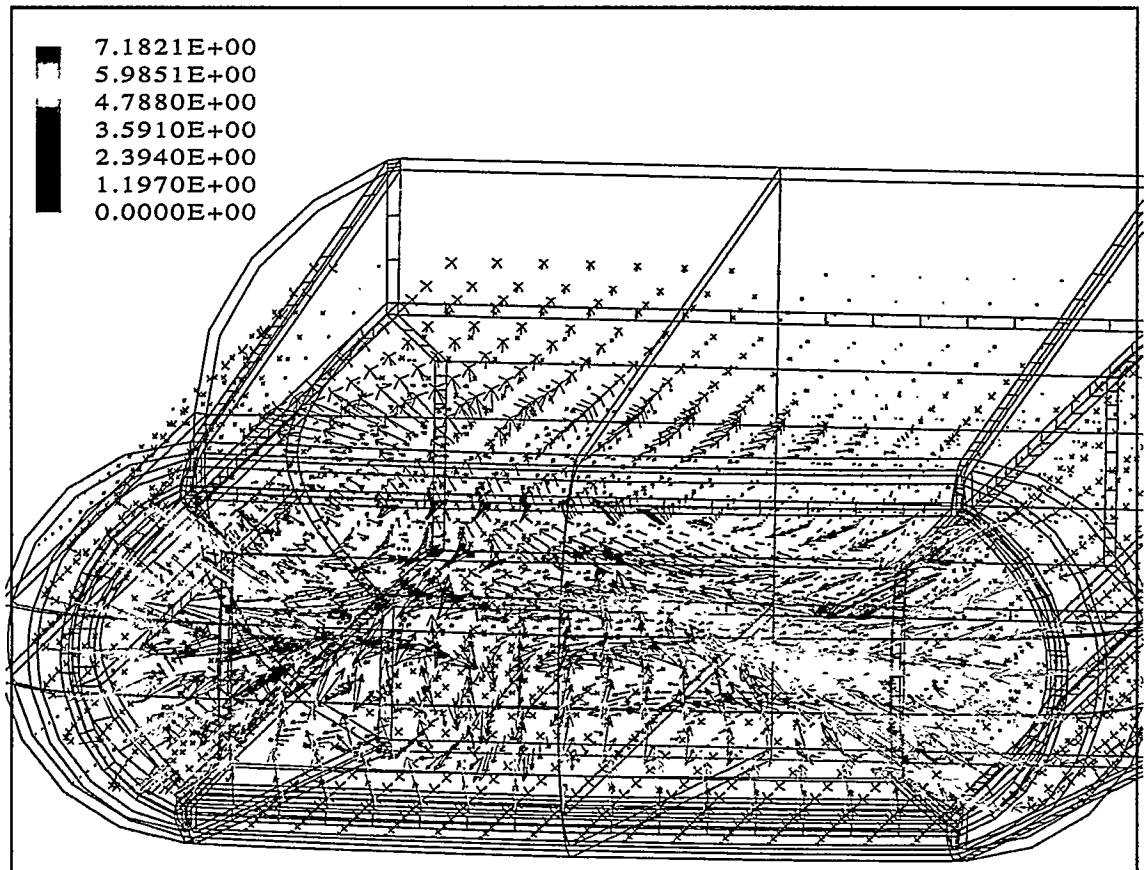

ESS4B: Velocity vectors

23.3% flow from below

Right:Left flow ratio = 1.22

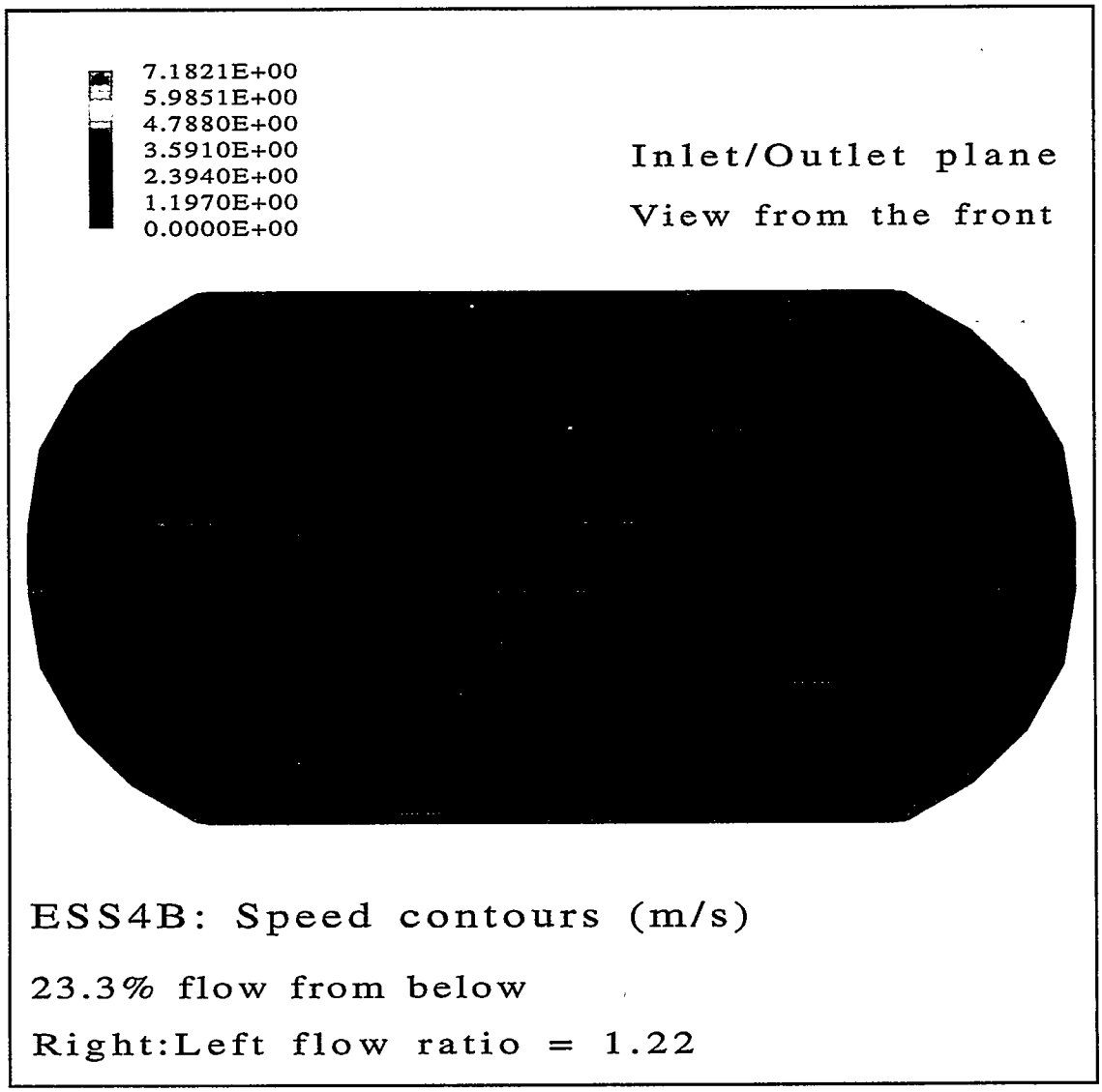
7.1821E+00
5.9851E+00
4.7880E+00
3.5910E+00
2.3940E+00
1.1970E+00
0.0000E+00
Inlet/Outlet plane
View from the front
ESS4B: Speed contours (m/s)
23.3% flow from below
Right:Left flow ratio = 1.22

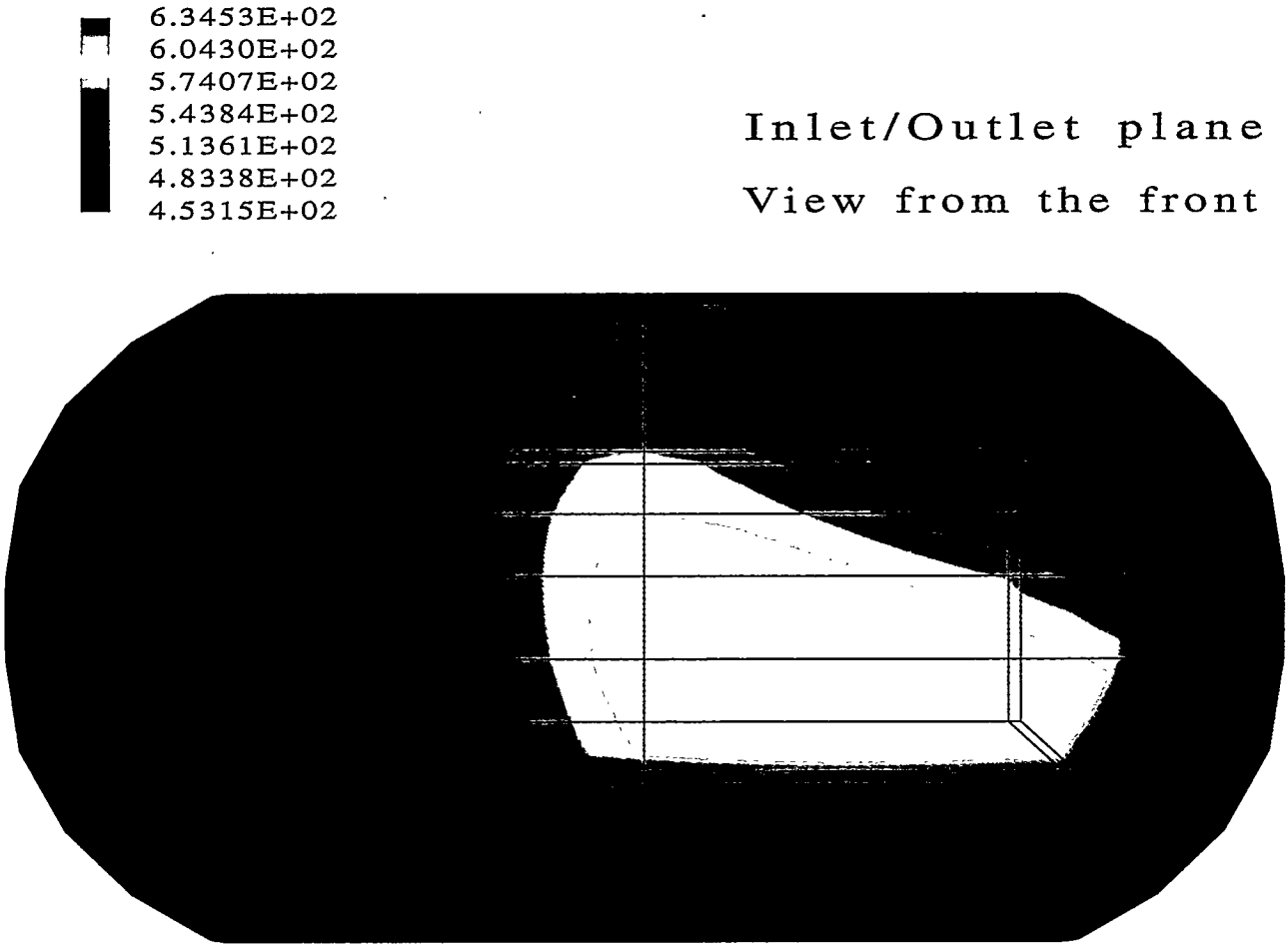

ESS4B: Temperature contours (K)

23.3% flow from below

Right:Left flow ratio = 1.22

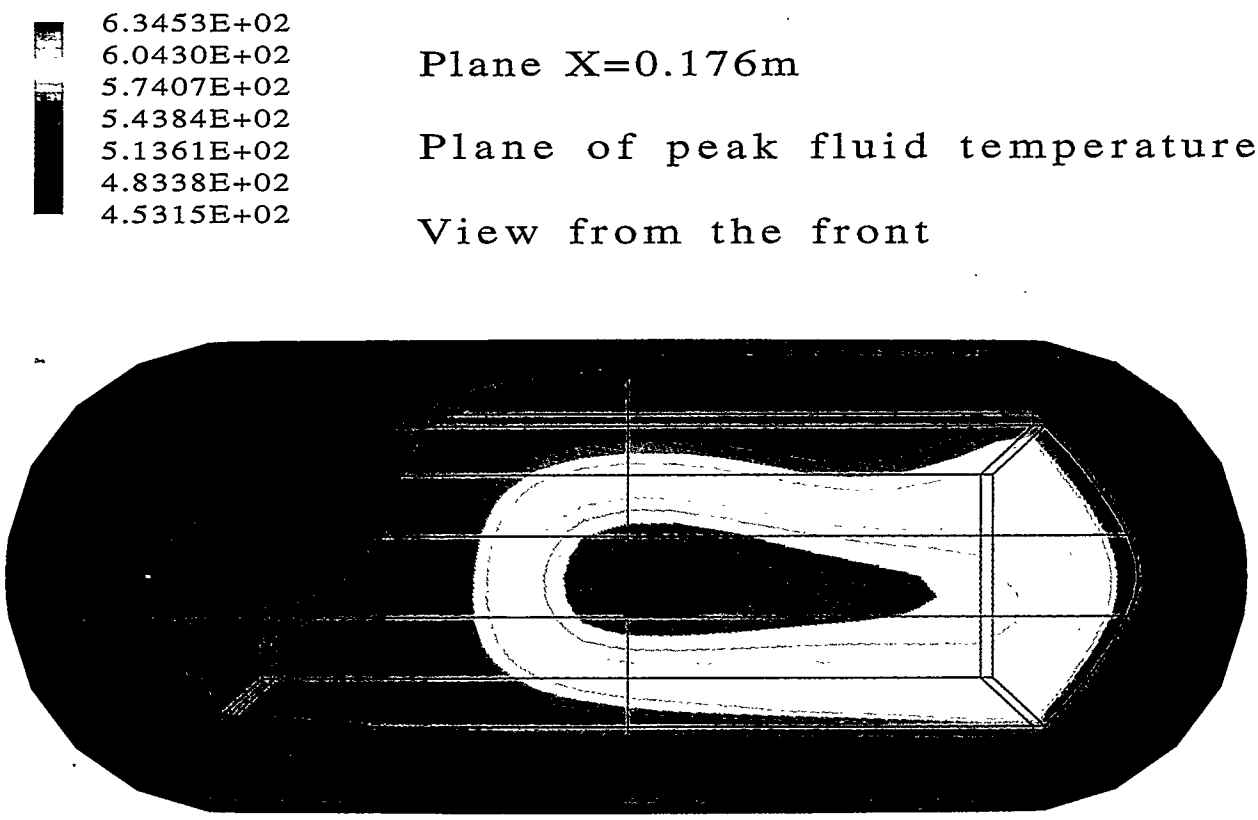

ESS4B: Temperature contours (K)

23.3% flow from below

Right:Left flow ratio = 1.22

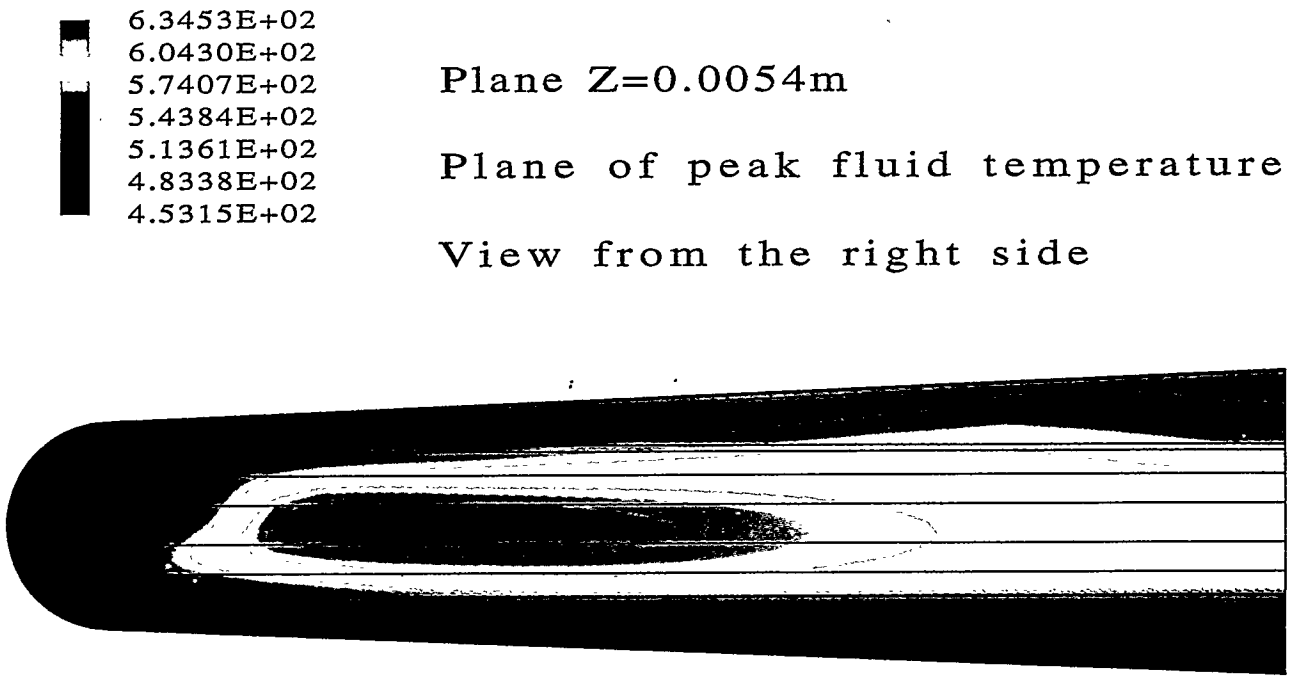

ESS4B: Temperature contours (K)

23.3% flow from below

Right:Left flow ratio = 1.22

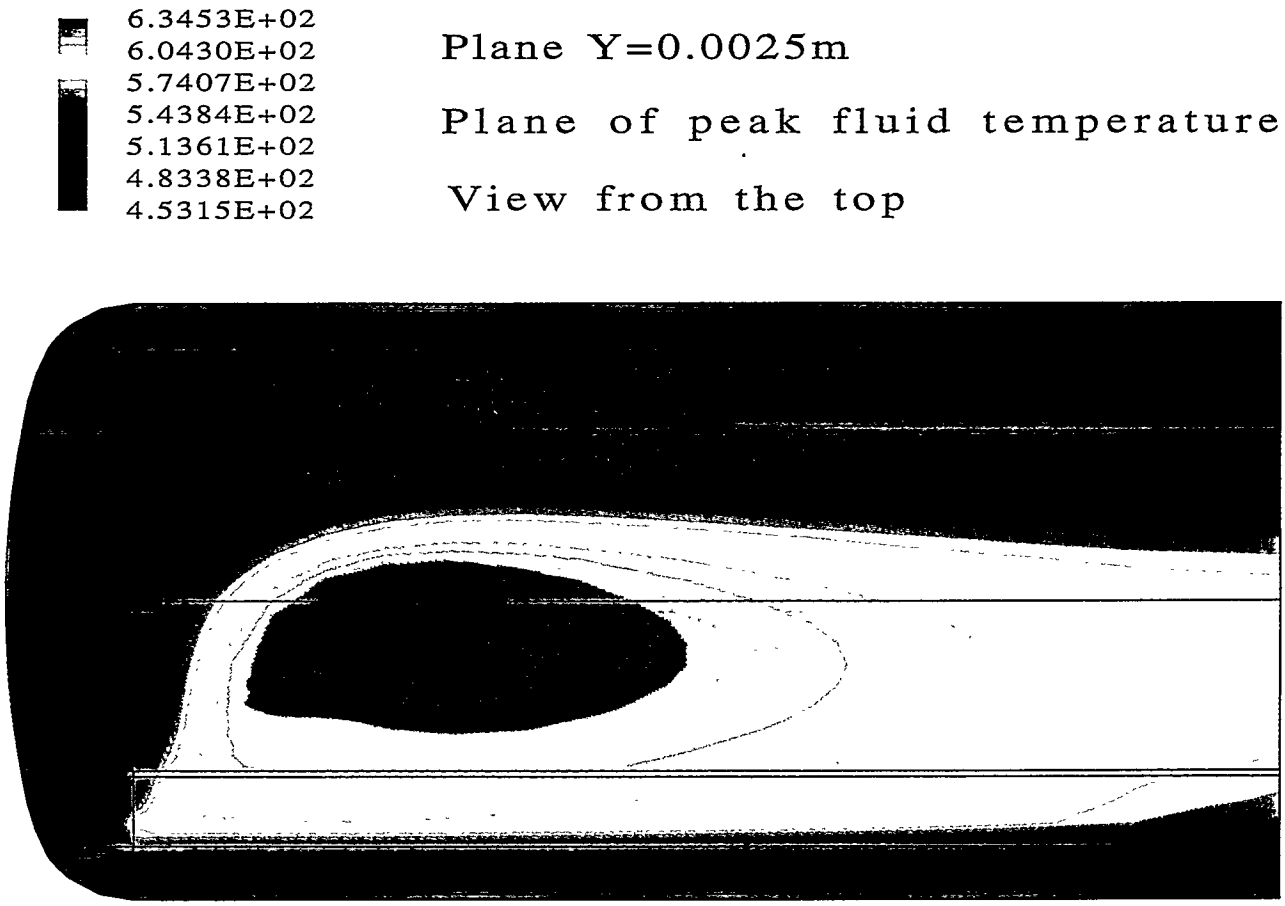

ESS4B: Temperature contours (K)

23.3% flow from below

Right:Left flow ratio = 1.22

ESS4 - WINDOW AND FLUID PEAK TEMPERATURES

AS A FUNCTION OF SIDE-INLET FLOW RATIO

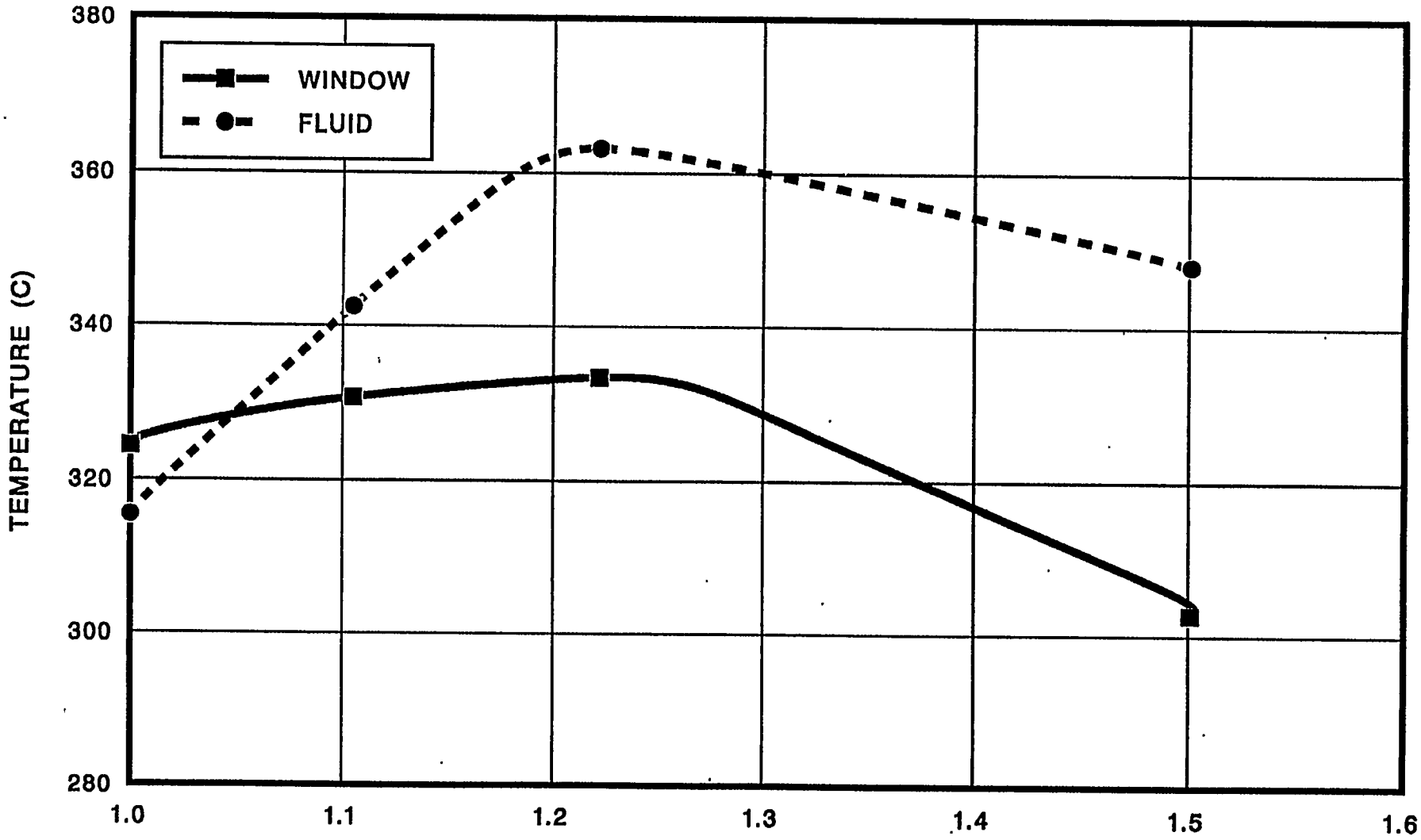

POWER = 3.235 MW
FLOW = 244.6 KG/S

PAUL SCHERRER INSTITUT

CONCLUSIONS

2D and 3D CFDS-FLOW3D Computer Models Studies

- Possible to remove 3.3MW from a mercury-cooled target
- Target has lower and side coolant inlets
- Equal inlet pressures $\approx 3 \rightarrow 4$ bar
- Inlet temperature = 180°C
- Mean outlet temperature $\approx$ 280°C
- Peak window temperature $\approx$ 330°C
- Peak fluid temperature $\approx$ 310°C

Future Work

- Investigate mesh-dependency of results
- Use thermal data for stress analysis
- Introduce helium bubbles
- Validate the code against experiment

International Workshop on the Technology and T/H of Heavy Liquid Metals
March 25-28, 1996, Schruns, Montafon, Austria

Thermal-Hydraulic Simulation of Mercury Target Concepts for A Pulsed Spallation Neutron Source

Moshe Siman-Tov
Mark Wendel
John Haines

Oak Ridge National Laboratory*, Oak Ridge TN
423-574-6515

EXTENDED ABSTRACT

The Oak Ridge Spallation Neutron Source (ORSNS) is a high-power, accelerator-based pulsed spallation neutron source being designed by a multi-laboratory team led by Oak Ridge National Laboratory to achieve very high fluxes of neutrons for scientific experiments. The ORSNS is projected to have a 1 MW proton beam upgradable to 5 MW. About 60% of the beam power (1-5 MW, 17-83 kJ/pulse in 0.5 microsec at 60 cps) is deposited in the liquid metal (mercury) target having the dimensions of 65x30x10 cm (about 19.5 liter). Peak steady state power density is about 150 and 785 MW/m^3 for 1 MW and 5 MW beam respectively, whereas peak pulsed power density is as high as 5.2 and 26.1 GW/m^3, respectively. The peak pulse temperature rise rate is 14 million C/s (for 5 MW beam) whereas the total pulse temperature rise is only 7 C. In addition to thermal shock and materials compatibility, key feasibility issues for the target are related to its thermal-hydraulic performance. This includes proper flow distribution, flow reversals, possible "hot spots" and the challenge of mitigating the effects of thermal shock through possible injection of helium bubbles throughout the mercury volume or other concepts.

The general computational fluid dynamics (CFD) code CFDS-FLOW3D was used to simulate the thermal and flow distribution in three preliminary concepts of the mercury target. Axial power density distribution and proportional internal heat generation in the target's stainless steel structure and baffles were include in the model. The exterior of the structure was assumed to be cooled by a water jacket. Inlet and outlet channels, external walls and their cooling jackets or channels, internal baffles, flow reversals and potential hot spots were investigated. The analysis for the base case shows flow recirculation at the tail end of the baffles. As a result, "hot spots" of 244 C and 163 C for the structure steel and the liquid mercury, respectively, appear at this location for the 5 MW beam power. The corresponding "hot spots" for 1 MW are 173 C and 161 C, respectively. Preliminary CFD (FLOW-3D) simulation of a proposed concept with flow coming in the middle shows some recirculation at the tail ends of the top and bottom baffles, but both are outside the beam "path". The stream lines are very smooth and the "hot spots" of 212 C and 160 C for the structure steel and the liquid mercury, respectively, are quite acceptable.

Very initial CFD simulation of He bubbles injection demonstrates some potential for simulating behavior of He bubbles in flowing mercury. Much study and development will be required to be able to "predict", even in a crude way, such a complex phenomena. Future directions in both design and R&D is outlined.

---

* The Oak Ridge National Laboratory is managed by Lockheed Martin Energy Research Corp. for the US Department of Energy under contract number DE-AC05-96OR22464.

OBJECTIVE

- Provide to other disciplines preliminary information on thermal-hydraulic parameteric values
- Perform preliminary thermal and flow distributions to design arround "hot spots" and "flow stagnation" zones
- Investigate the concept of injecting He bubbles into Mercury as a thermal-shock mitigation technique

Current Base Configuration for the ORSNS Liquid Mercury Target

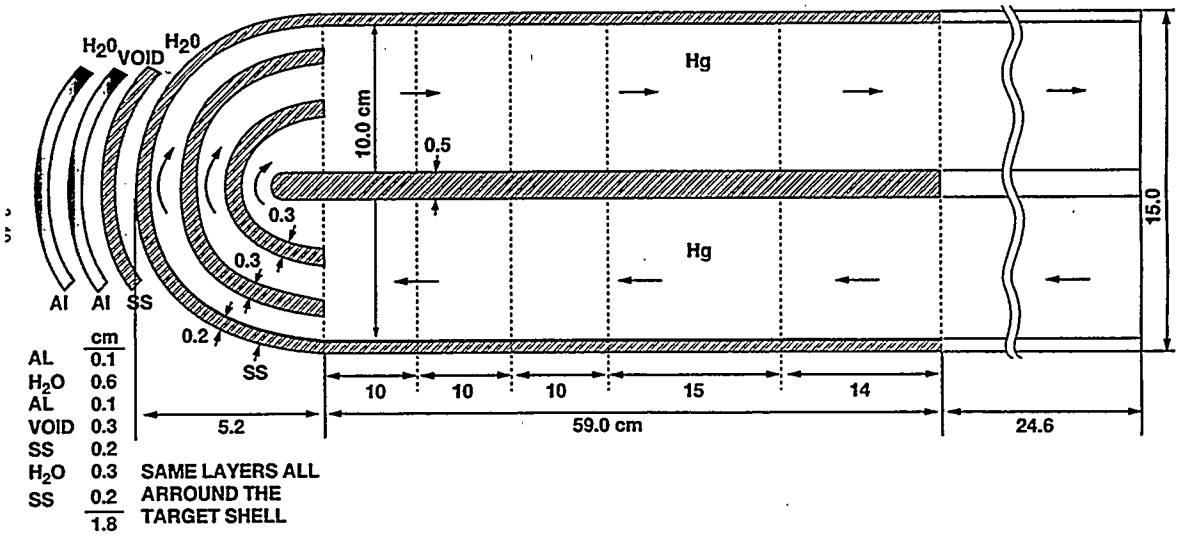

Scoping Calculations Have Been Performed to Examine the Thermal Behavior of a Liquid Mercury Target in a Pulse Spallation Source System

- Assumptions and input made:
  - Average power (60% in target): 1, 2.5, and 5 MW
  - Pulse duration of 0.5 microsec
  - Axial power distribution in the mercury
  - Proportional internal heat generation in the structure
  - Rectangular geometry: 65cm × 30cm × 10cm (19.5L)
  - Beam cross section at the window: 20cm × 7cm
  - Liquid Mercury convective cooling from inside
  - Water or Helium cooling from outside

Preliminary Results from Thermal Hydraulic Scoping Studies Indicate that a Liquid Mercury Target has Many Advantages but Thermal Shock is a Key Feasibility Issue

	1 MW	2.5MW	5 MW
• Energy/pulse in target (kJ)	10	25	50
• Av. Power Density (MW/m^3)	45	112	224
• Peak SS Power Density (MW/m^3)	157	392	784
• Max. Pulse Power Density (MW/m^3)	5,225	13,062	26,123
• Max. Pulse Temp. Rise Rate (°C/s)	2.8×10^6	7×10^6	14×10^6
• Max. Pulse Temp. Rise (°C)	1.4	3.5	7.0
• Mercury Inlet Temp. (°C)	80	80	80
• Mercury Outlet Temperature (°C)	110	110	110
• Min. Coolant Velocity Required (m/s)	0.7	1.8	3.6
• Required Mercury Flow (kg/s)	144	361	722
• Pressure Drop in Target (kPa)	6.7	35	121
• Pumping Power for Target (W)	71	930	6,464

Mercury Target Containmnet Wall (at the beam window) can be most Conventiently Cooled by Water. Marginal Temperature can be Achieved Through Mercury and Helium Cooling but will Require R&D to Secure Mercury Wetting of the Walls.

	1 MW	2.5MW	5 MW
• Wall Material	316 SS	316 SS	316 SS
• Wall Thickness (mm)	3-5	3-5	3-5
• Vol. Heat Generation (MW/m^3)	91	227	454
• ΔT Across 5mm SS Wall (C)	70	174	348
• ΔT Across 3mm SS Wall (C)	25	63	125
• Max. Wall Temp. (one-sided Mercury)-5mm	325	473	682
• Max. Wall Temp. (two-sided Mercury)-5mm	193	241	303
• Max. Wall Temp. (one-sided Mercury)-3mm	216	280	364
• Max. Wall Temp. (one-sided Helium 10 atm. 50 m/s)-3mm	329	682	1270
• Max. Wall Temp. (one-sided Water)-3mm	140	208	321
• Max. Wall Temp. (Mercury & Helium)-5mm	228	339	495
• Max. Wall Temp. (Mercury & Helium)-3mm	170	225	295

3-43

A Variety of Heat Transfer, Fluid Dynamic, and Structural Codes are Available to us for Performing the ORSNS Design and Analysis

Thermal Conduction-Based Codes:

- HEATING7
- Pthermal (w/PATRAN)
- TOPAZ 2D/3D

Fluid Mechanics-Based Code:

- FLUENT
- FLOW-3D (now CFX-4)
- TEMPEST

Structural-Based Codes:

- ABAQUS
- NASTRAN

Specialized Codes:

- CTH-Shock wave propagation including thermal

We already started the use of HEATING7, FLOW3D, and CTH for analyzing various target concepts (solid and liquid mercury).

Current Base Configuration for the ORSNS Liquid Mercury Target

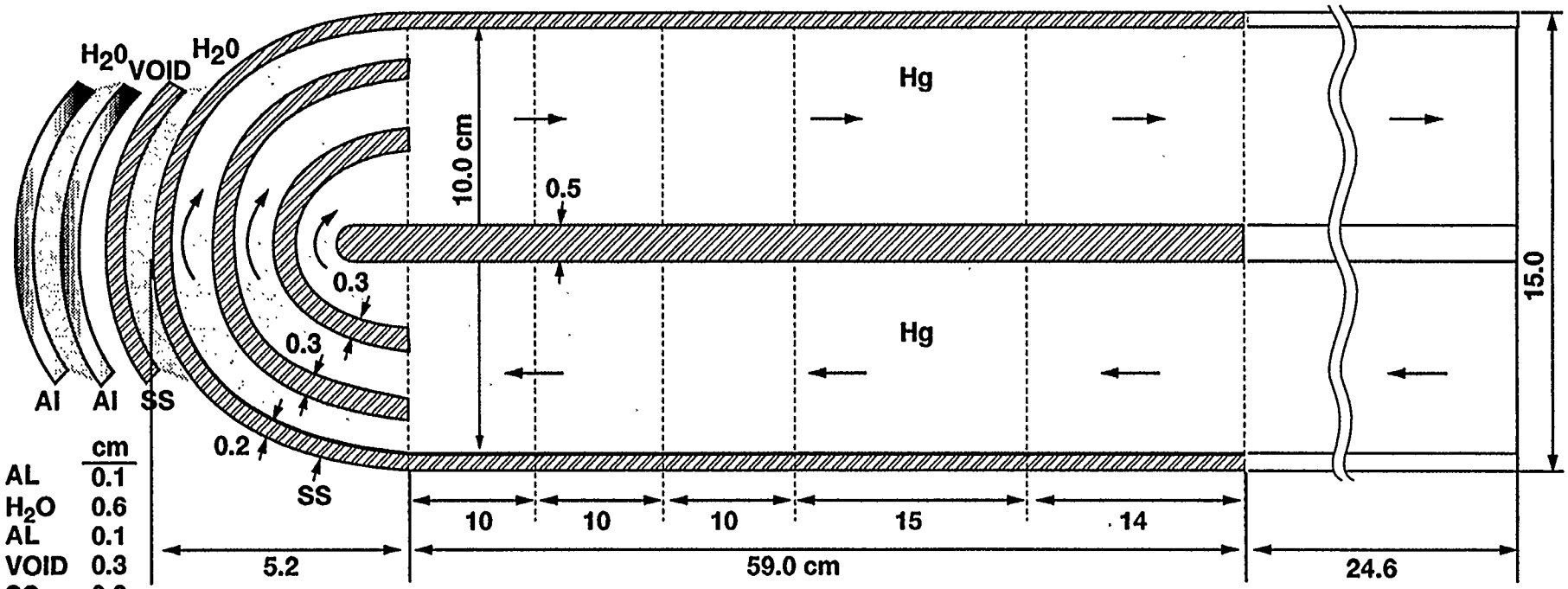

	cm
AL	0.1
H_2O	0.6
AL	0.1
VOID	0.3
SS	0.2
H_2O	0.3
SS	0.2
	1.8

SAME LAYERS ALL ARROUND THE TARGET SHELL

EFG 96-6658

Preliminary CFD (FLOW3D) Simulation of the ORSNS Liquid Mercury Target. Current base case for 5 MW beam power shows recirculation at the tail end of the middle baffle. As a result, "Hot Spots" of 244°C and 163°C for the structure steel and the liquid mercury, respectively, appear at this location.

(2D) || Print || 10 Apr 1998 || m25.plt || CONCEPT 1, 5 MW, h=13,708 W/m**2-K

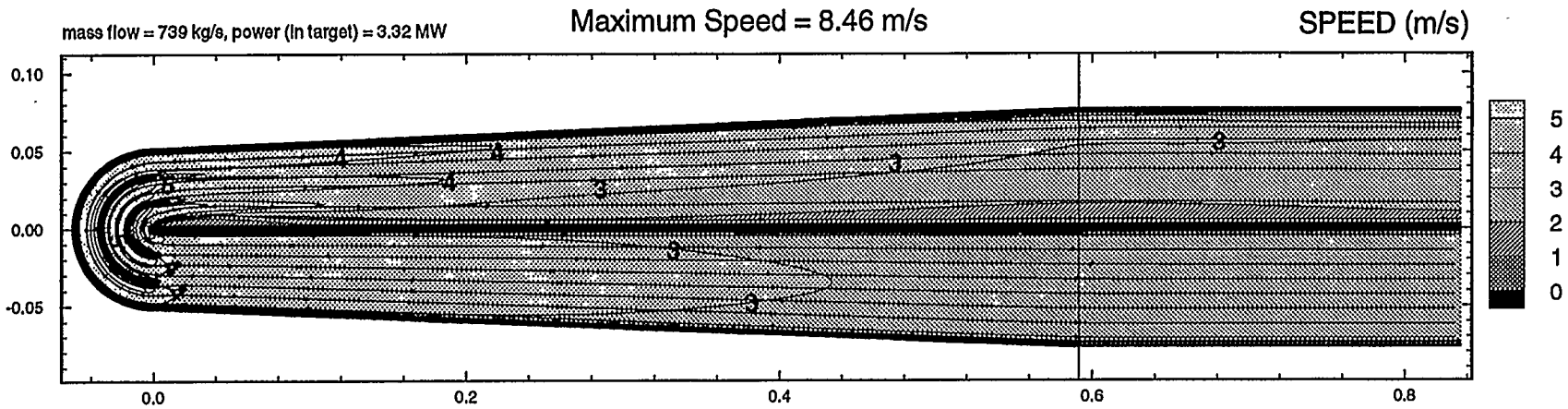

Maximum Temperature in Steel = 517 K at (x,y) = 0.009,0

Maximum Temperature in Mercury = 436 K at (x,y) = 0.005,0.0025

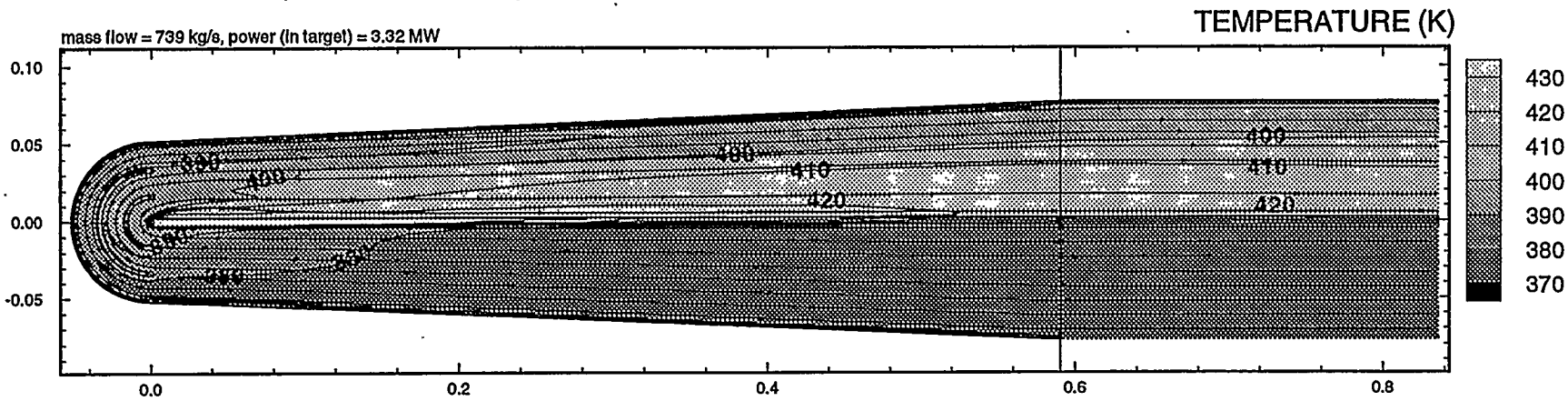

Preliminary CFD (FLOW3D) Simulation of the ORSNS Liquid Mercury Target. Current base case for 5 MW beam power shows recirculation at the tail end of the middle baffle. As a result, "Hot Spots" of 244°C and 163°C for the structure steel and the liquid mercury, respectively, appear at this location.

(2D) || Print || 10 Apr 1996 || m25.plt || CONCEPT 1, 5 MW, h=13,708 W/m**2-K

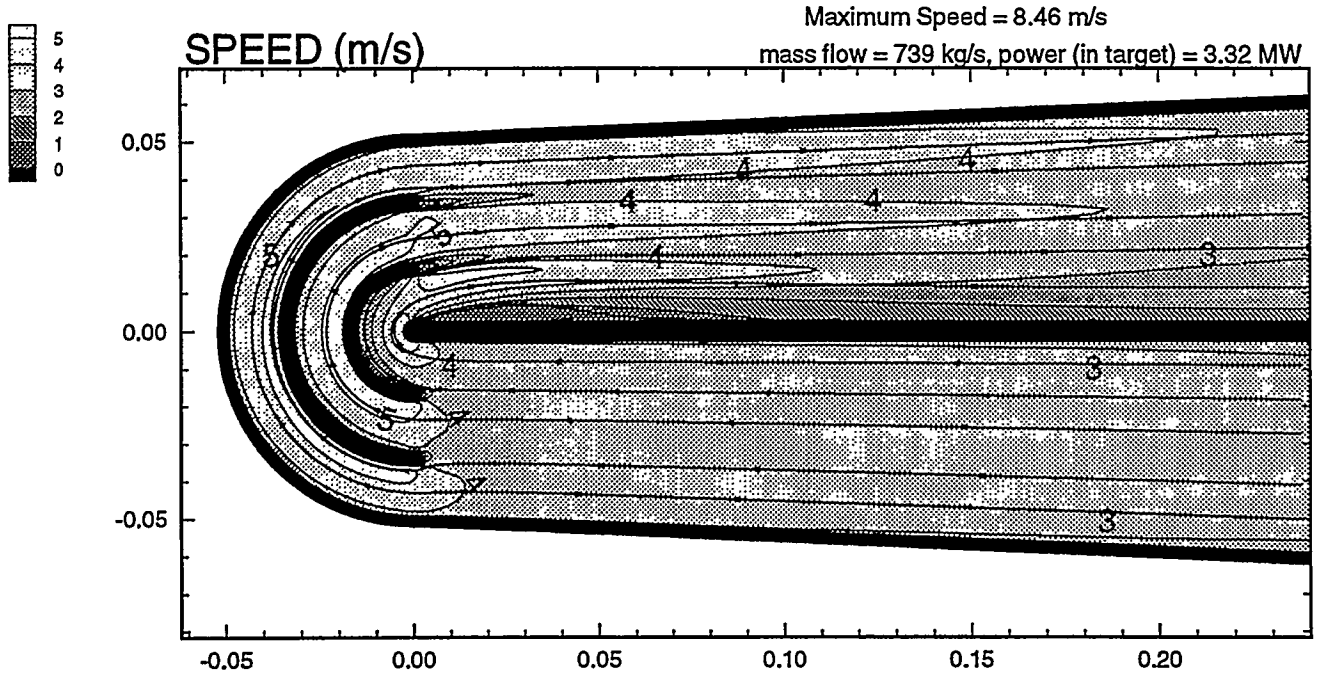

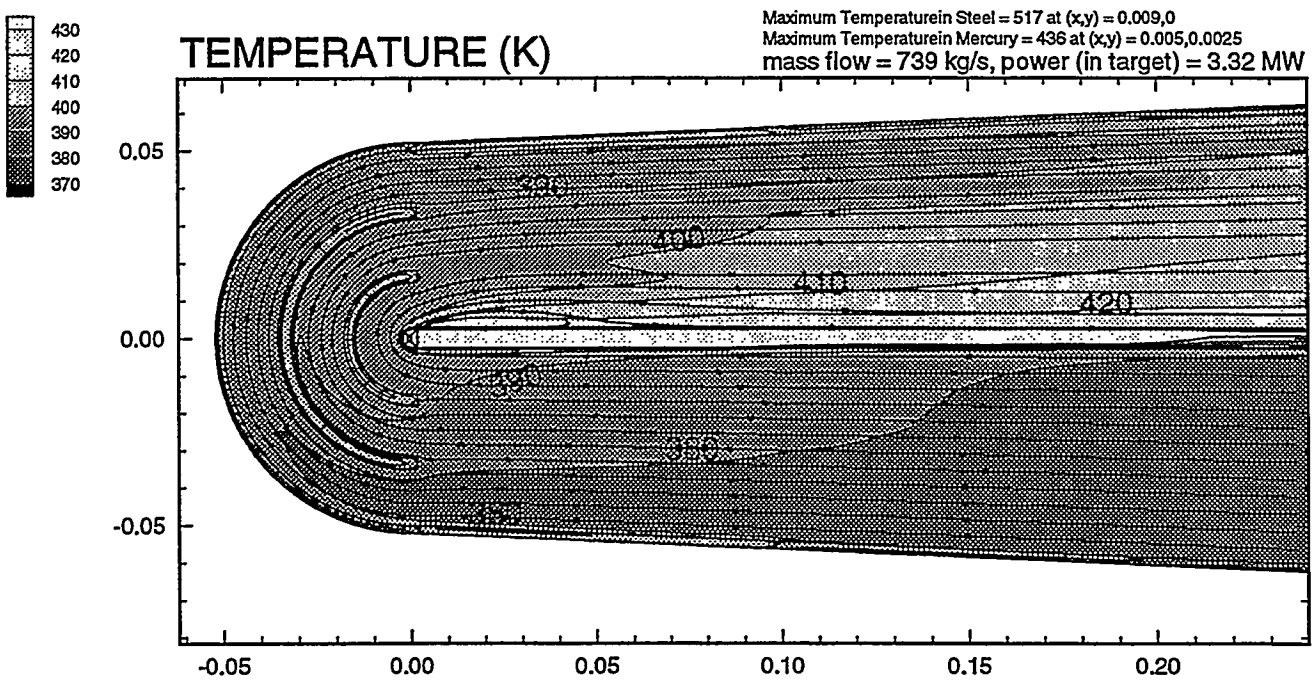

Preliminary CFD (FLOW3D) Simulation of the ORSNS Liquid Mercury Target. Current base case for 5 MW beam power shows recirculation at the tail end of the middle baffle. As a result, "Hot Spots" of 244°C and 163°C for the structure steel and the mercury, respectively, appear at this location.

(2D) || Print || 10 Apr 1996 || m25.plt || CONCEPT 1, 5 MW, h=13,708 W/m**2-K

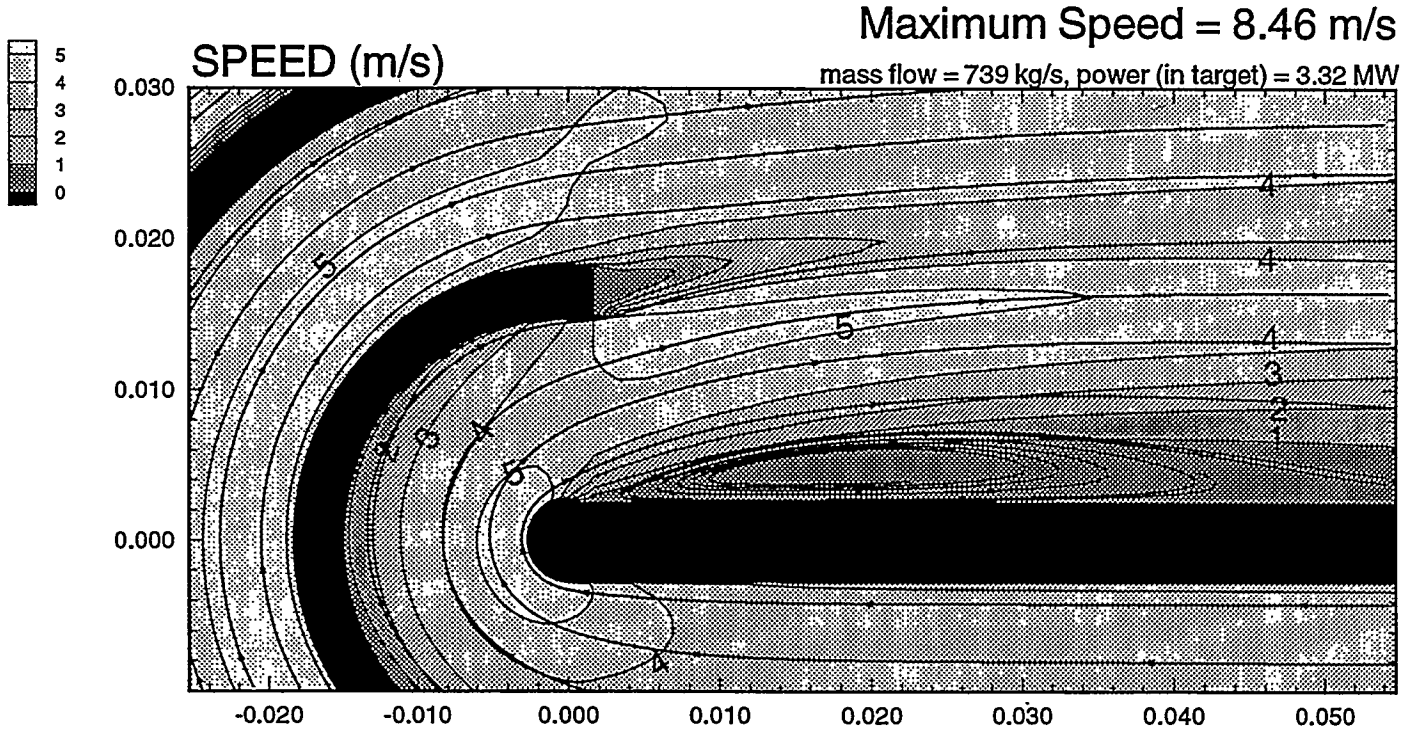

Maximum Temperature in Steel = 517 at (x,y) = 0.009,0
Maximum Temperature in Mercury = 436 at (x,y) = 0.005,0.0025

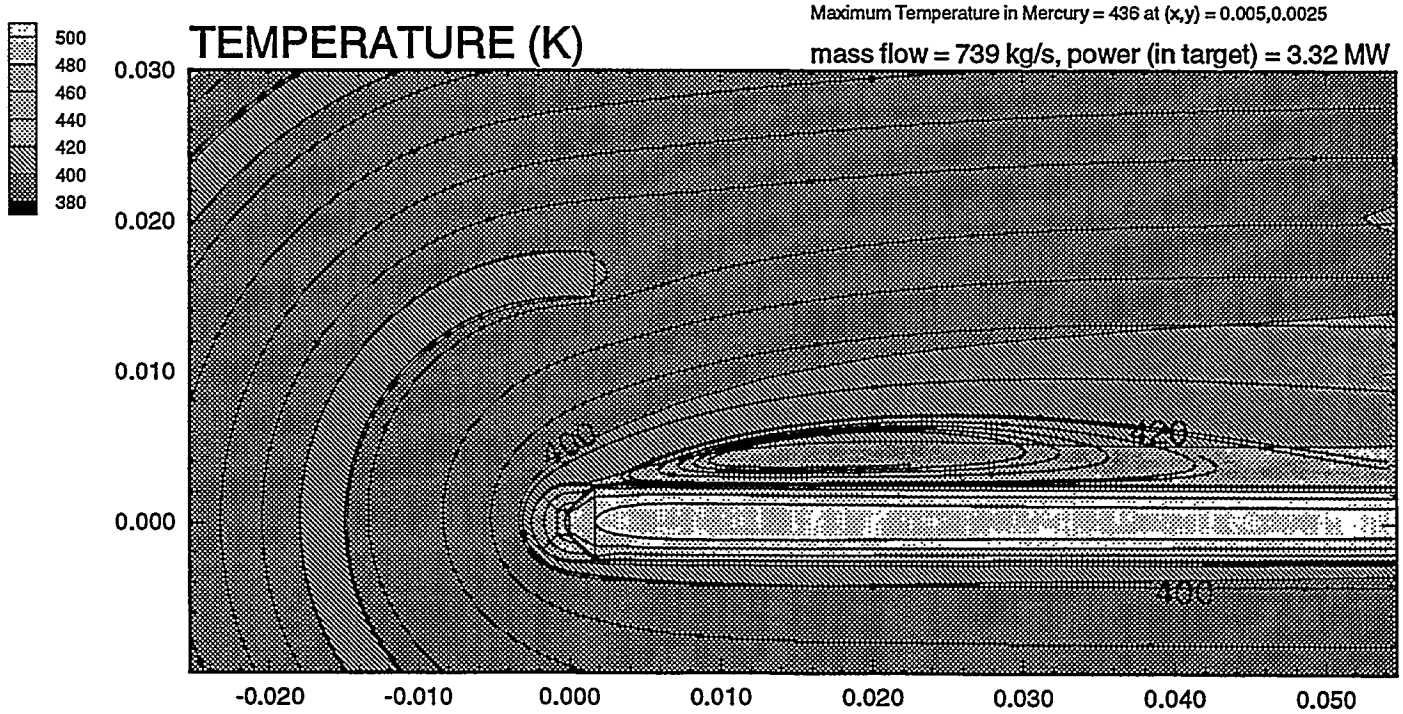

Preliminary CFD (FLOW3D) Simulation of the ORSNS Liquid Mercury Target. Current base case for 1 MW beam power shows recirculation at the tail end of the middle baffle. As a result, quite low and acceptable "Hot Spots" of 173°C and 161 °C for the structure steel and the liquid mercury, respectively, appear at this location.

(2D) II Print II 10 Apr 1996 II m57.plt II CONCEPT 1, 1MW, Adiabatic, mflow = 143.6 kg/s, power = 0.664

Maximum speed = 1.60 m/s

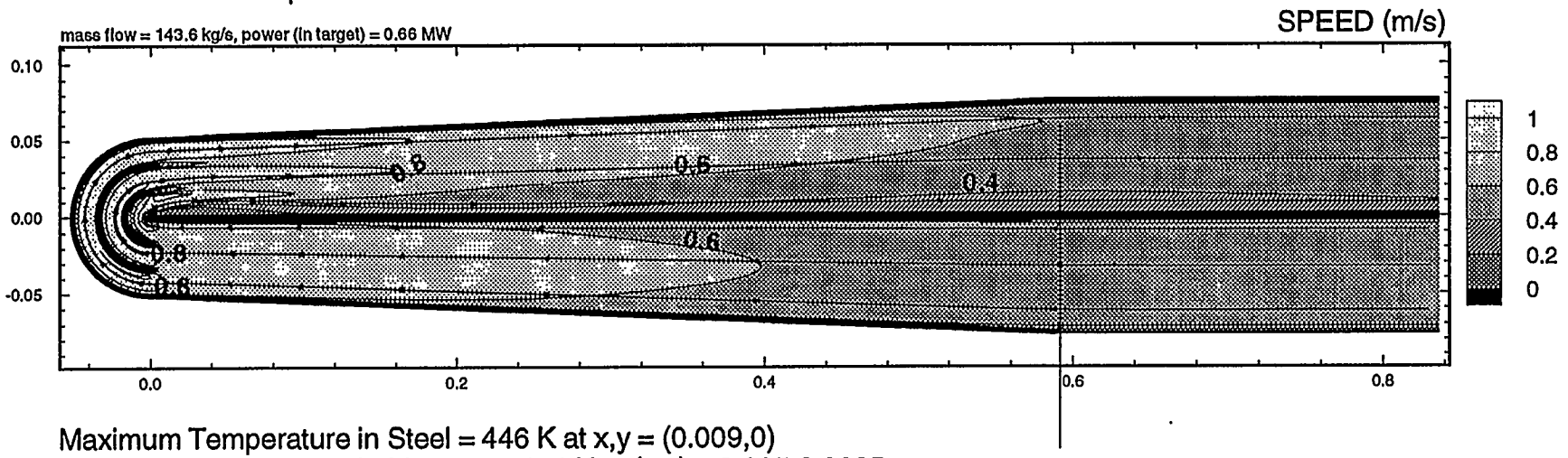

Maximum Temperature in Steel = 446 K at x,y = (0.009,0)
Maximum Temperature in Mercury = 434 K at (x,y) = 0.005,0.0025

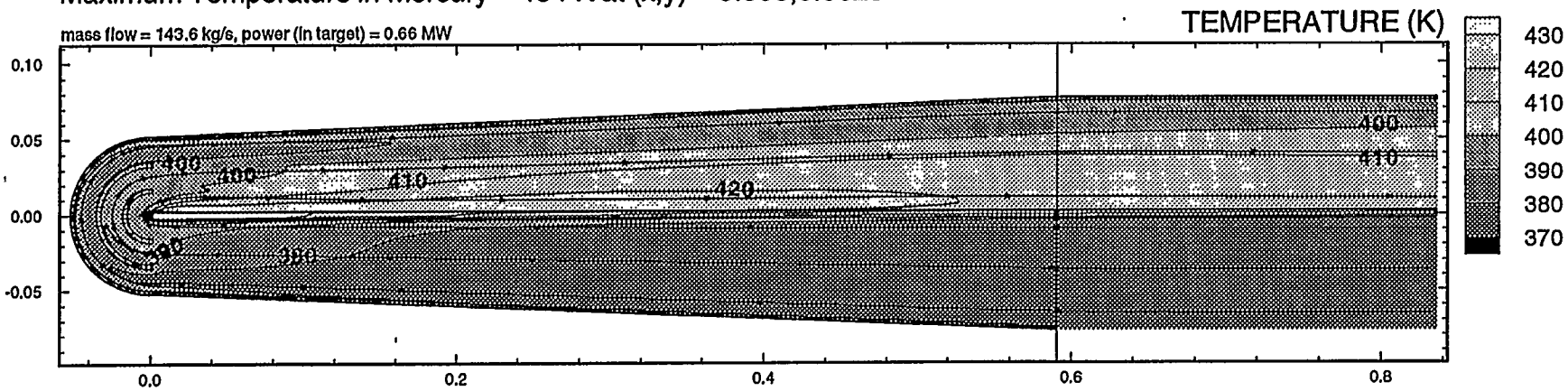

Preliminary CFD (FLOW3D) Simulation of the ORSNS Liquid Mercury Target. Current base case for 1 MW beam power shows recirculation at the tail end of the middle baffle. As a result, quite low and acceptable "Hot Spots" of 173°C and 161°C for the structure steel and the liquid mercury, respectively, appear at this location.

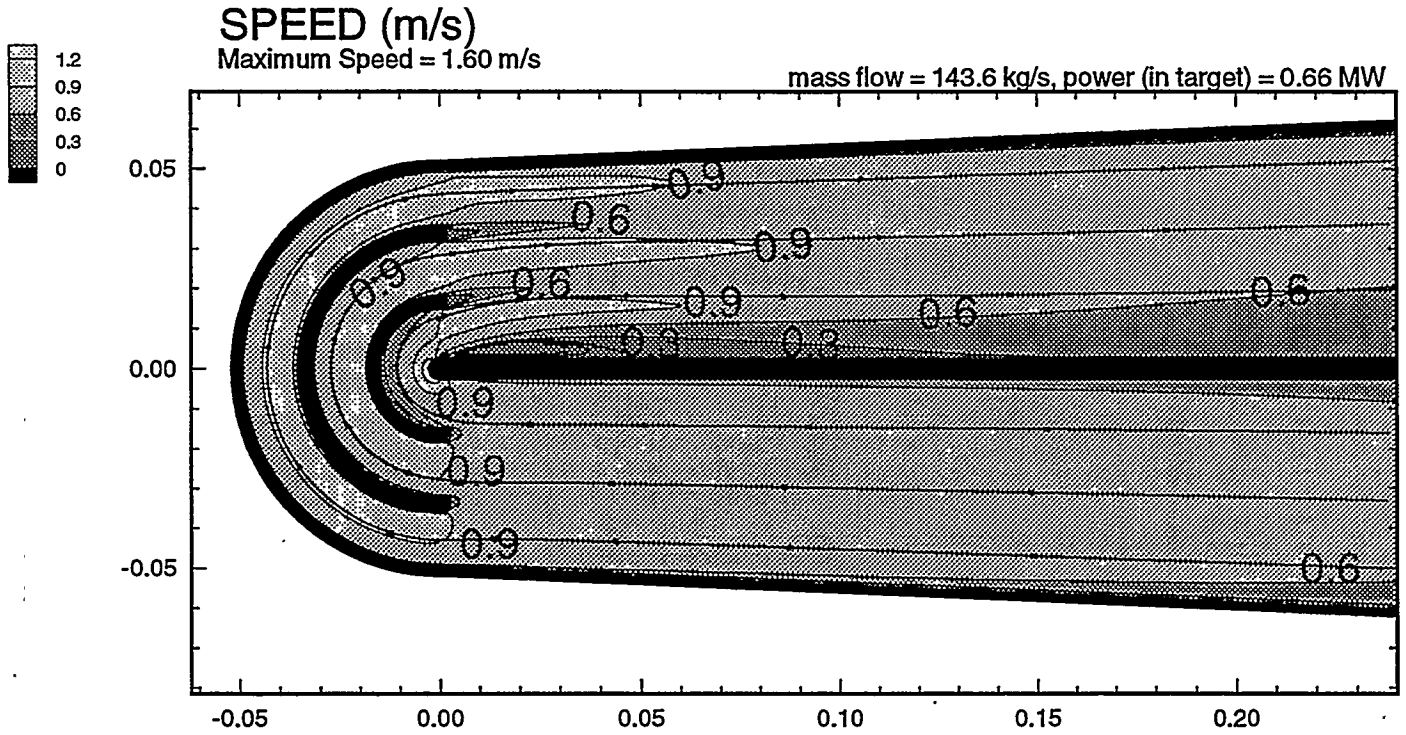

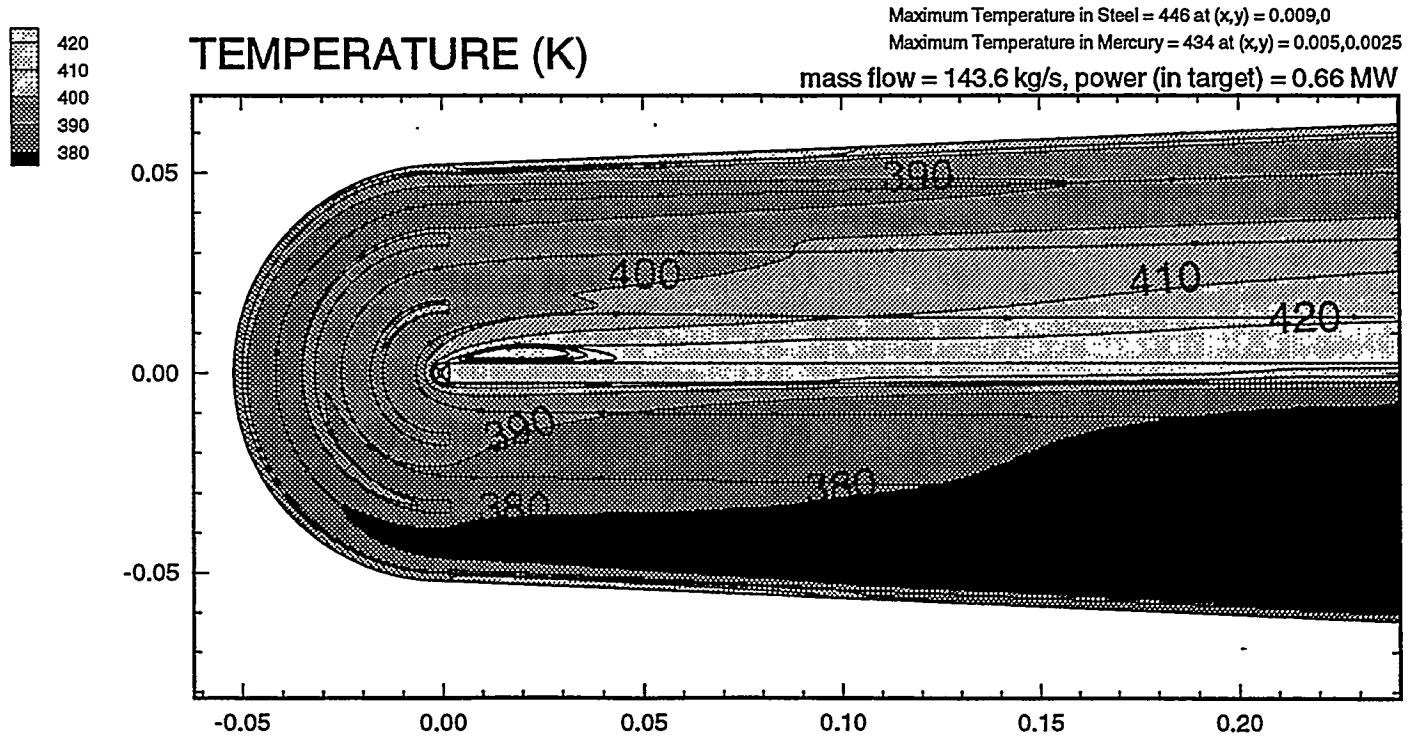

Preliminary CFD (FLOW3D) Simulation of the ORSNS Liquid Mercury Target. Current base case for 1 MW beam power shows recirculation at the tail end of the middle baffle. As a result, quite low and acceptable "Hot Spots" of 173°C and 161°C for the structure steel and the liquid mercury, respectively, appear at this location.

(2D) || Print || 11 Apr 1996 || m57.plt || CONCEPT 1, 1MW, Adiabatic, mflow = 143.6 kg/s, power = 0.664

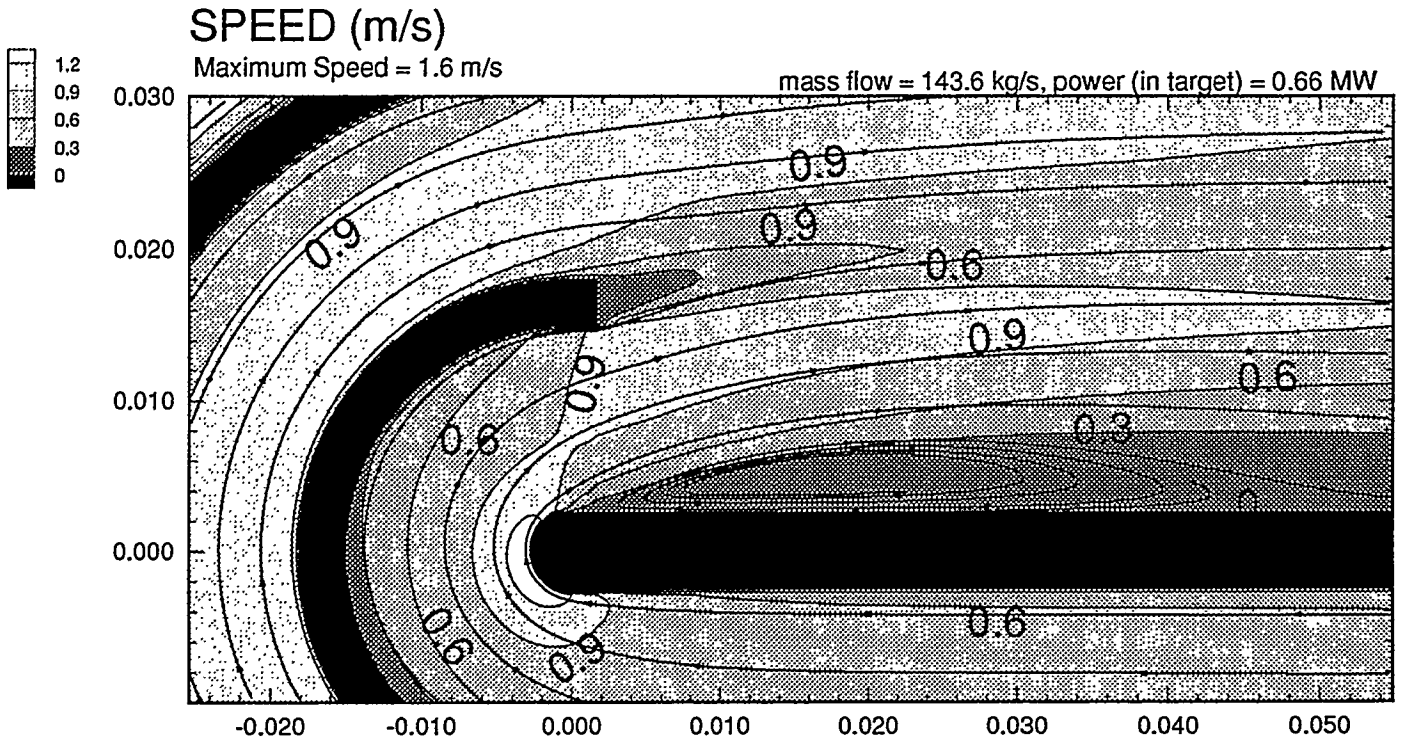

Maximum Temperature in Steel = 446 K at (x,y) = 0.009,0
Maximum Temperaturein Mercury = 434 K at (x,y) = 0.005,0.0025

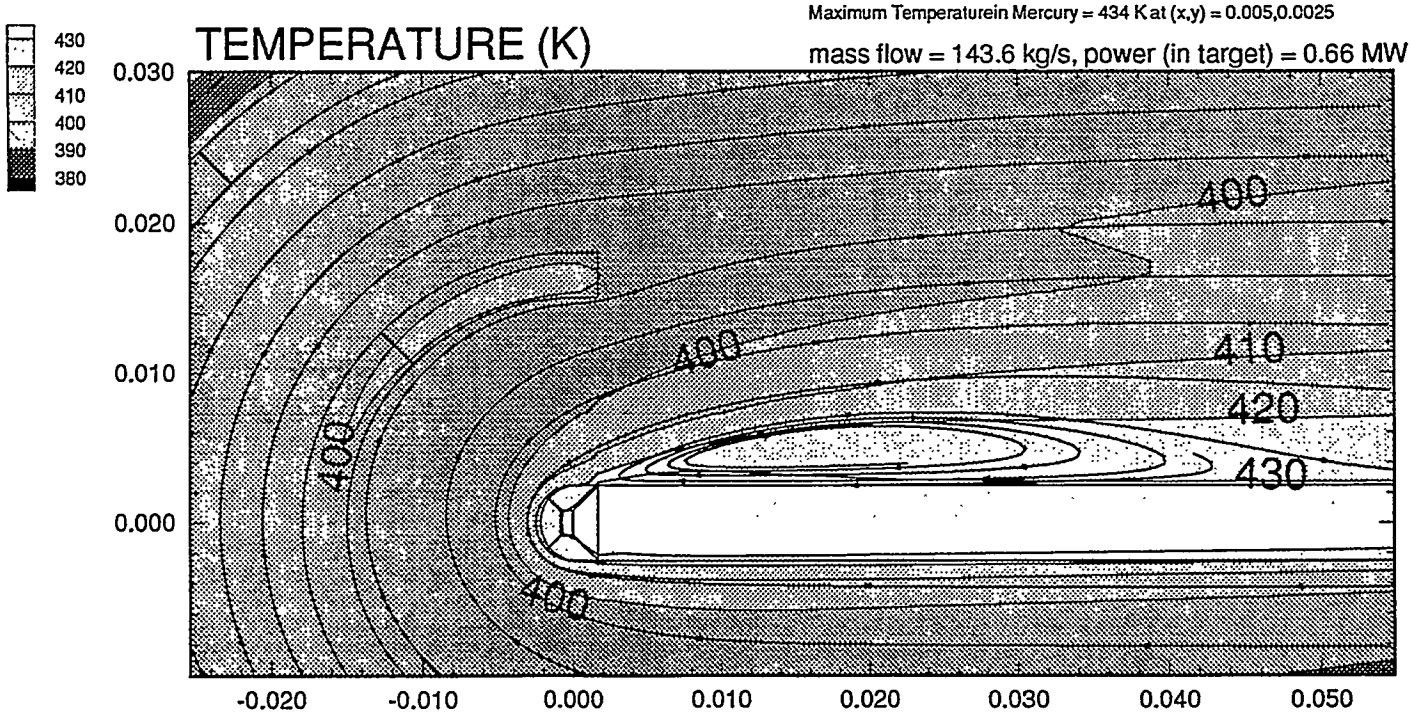

A Number of Alternative Configurations Were Conceived To Overcome Anticipated Issues in The ESS Current Concept

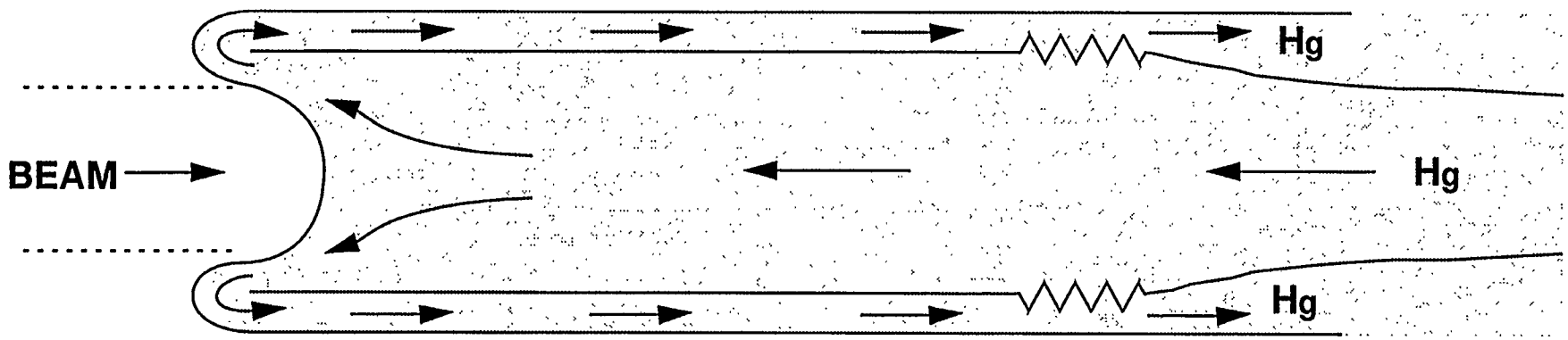

Allows Expansion Through Flexible Inner Walls and Avoid Flow Reversals

EFG 96-6661

Preliminary CFD (FLOW3D) simulation of a proposed concept with flow coming in the middle (Concept #2) for 5 MW beam power shows some recirculation at the tail ends of the top and bottom baffles, but both are outside the beam "path". The stream lines are very smooth and the "Hot Spots" of 146°C and 134°C for the steel and the liquid mercury are quite low.

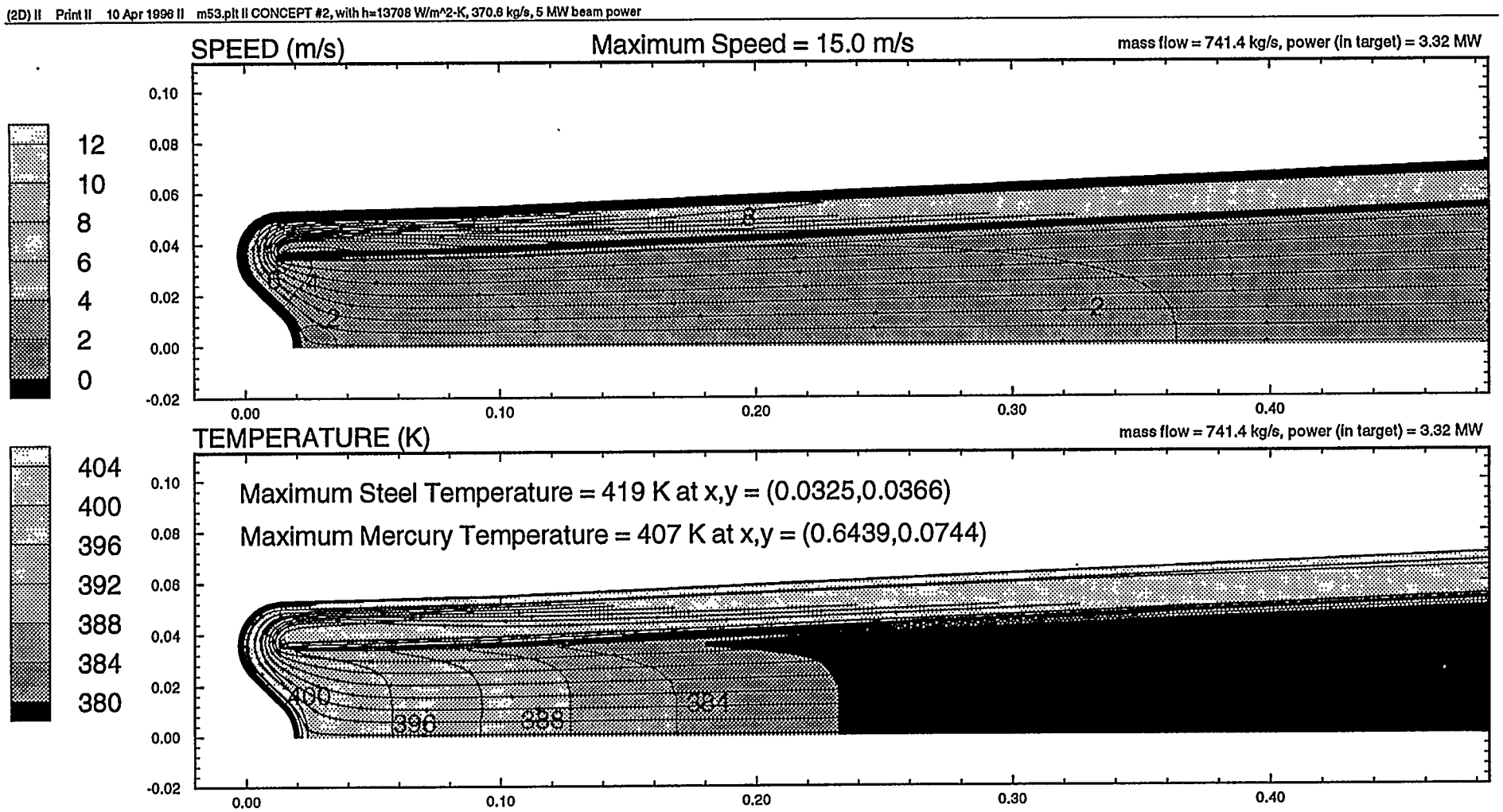

Preliminary CFD (FLOW3D) simulation of a proposed concept with coming in the middle (Concept #2) for 5 MW beam power shows some recirculation at the tail ends of the top and bottom baffles, but both are outside the beam "path". The stream lines are very The stream lines are very smooth and the "Hot Spots" of 146°C and 134°C for the steel and the liquid mercury, respectively, are quite low.

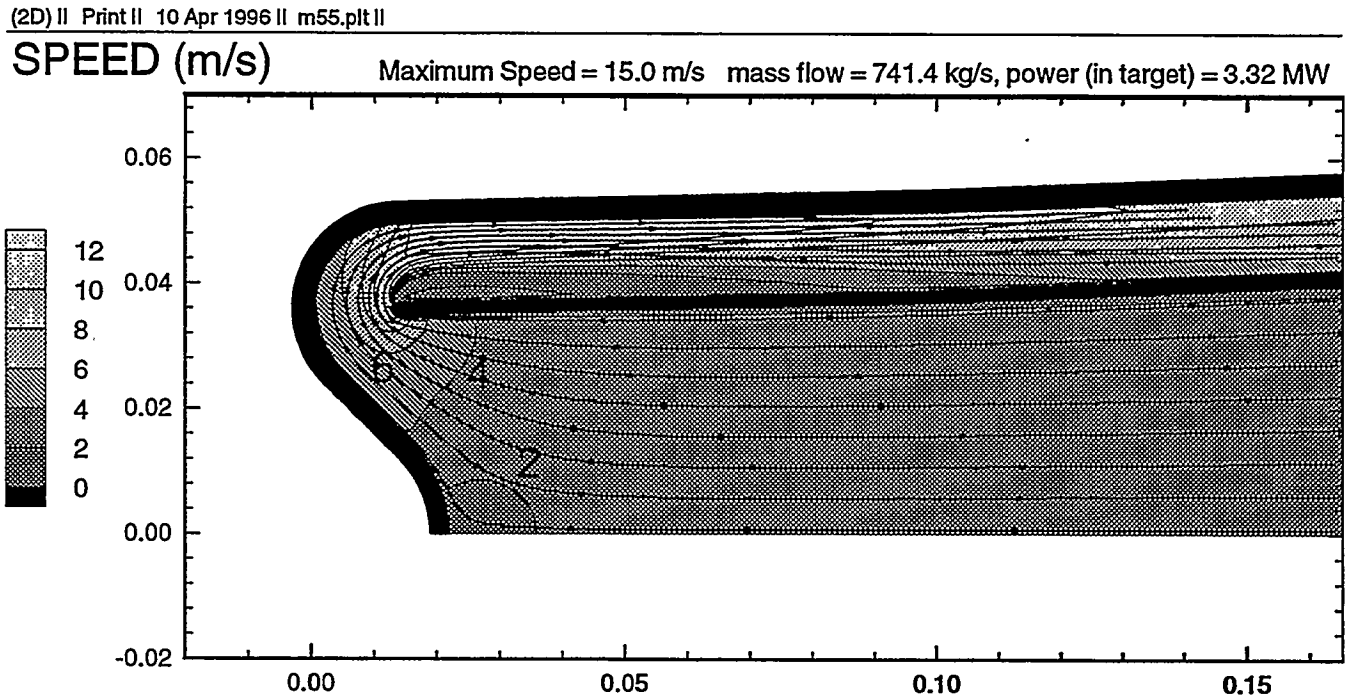

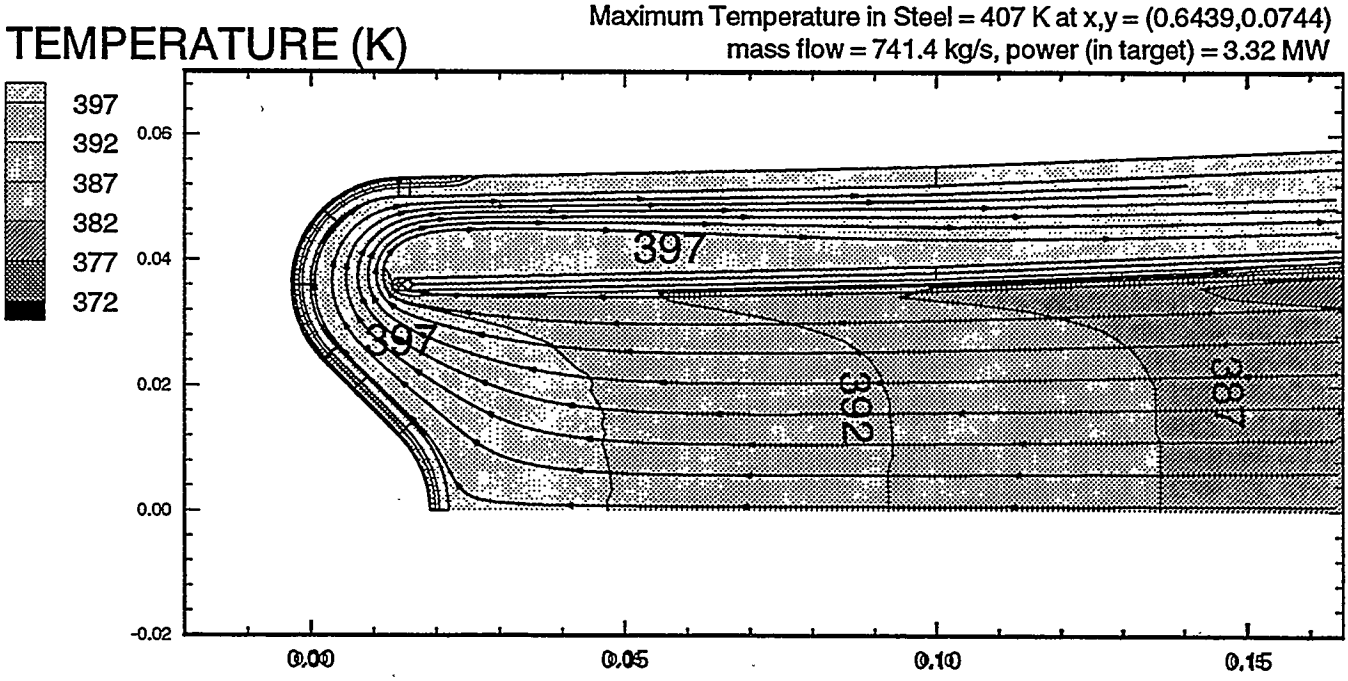

Preliminary CFD (FLOW3D) simulation of a proposed concept with flow coming in the middle (Concpet #2) for 5 MW beam power shows some recirculation at the tail ends of the top and bottom baffles, but both are outside the beam "path". The stream lines are very smooth and the "Hot Spots" of 146°C and 134°C for the steel and the liquid mercury are quite low.

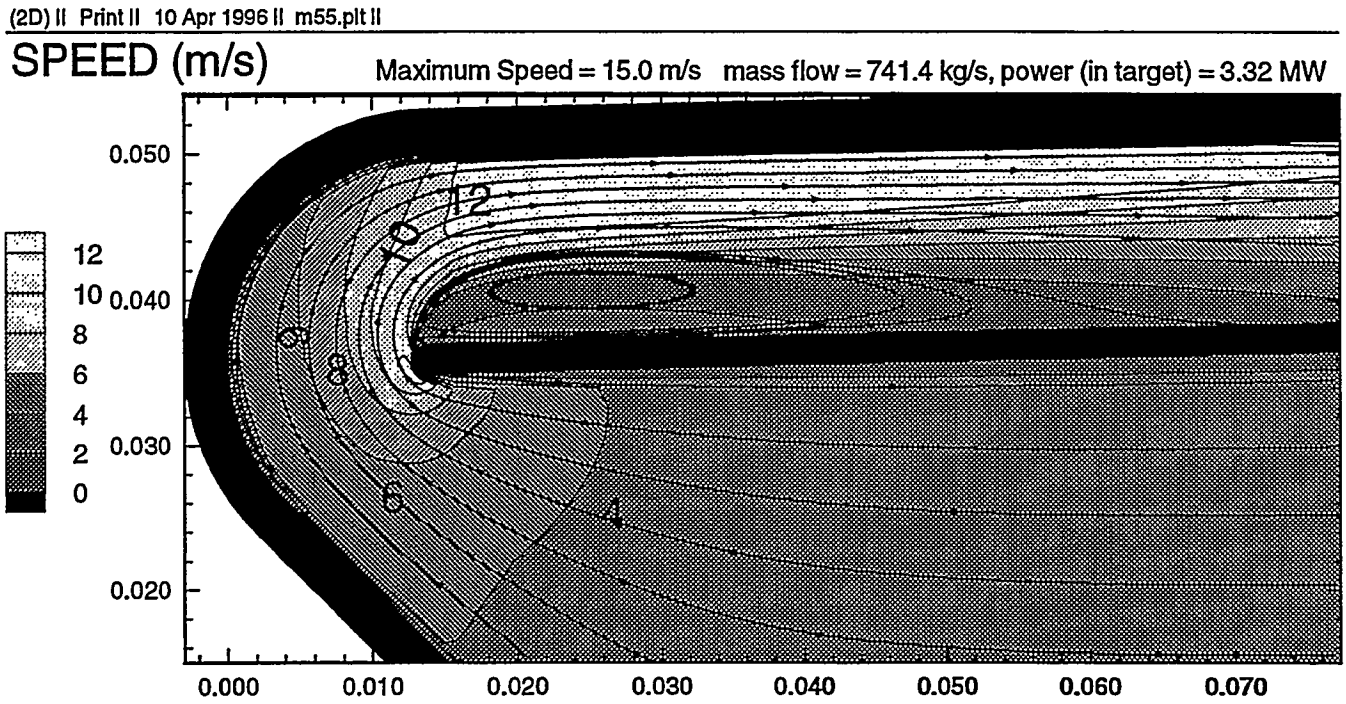

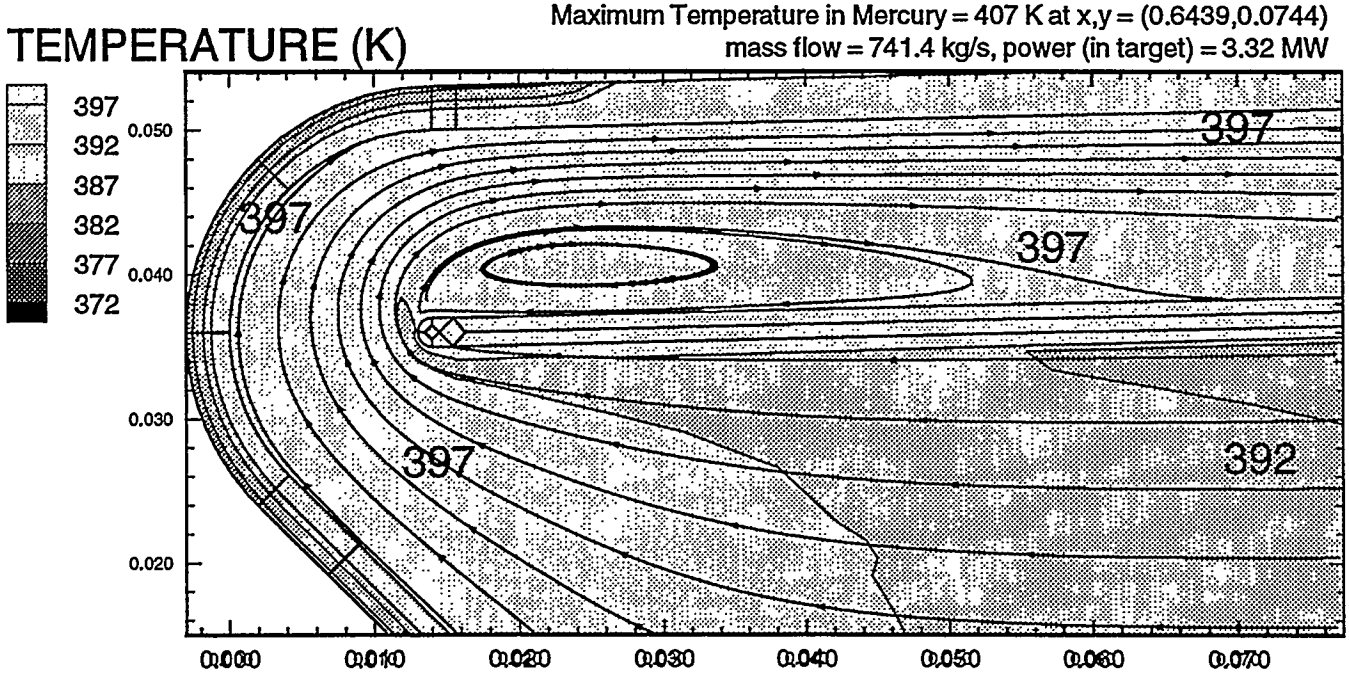

A Number of Alternative Configurations Were Conceived To Overcome Anticipated Issues in The ESS Current Concept

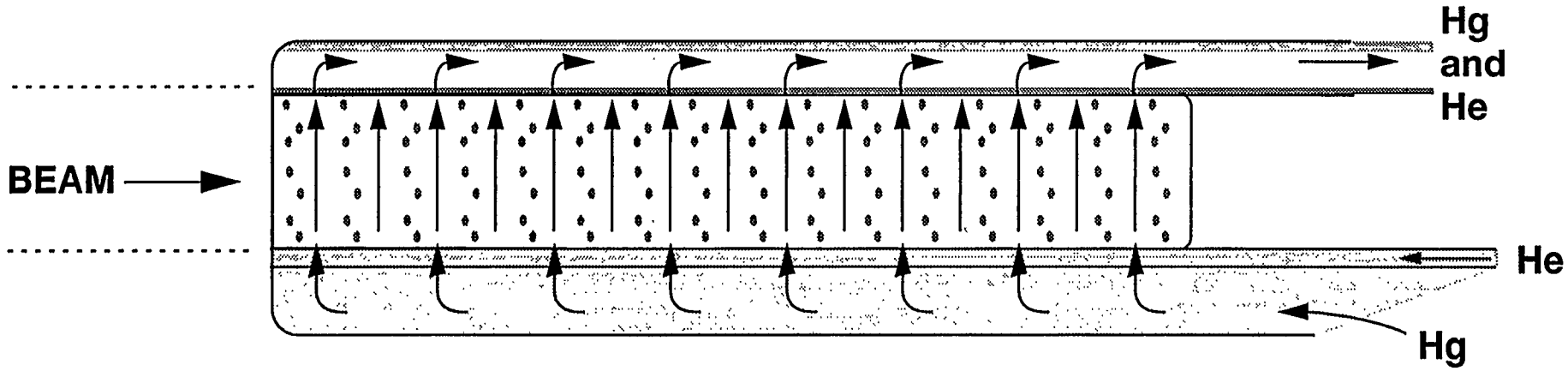

Helps Maintain Uniform He Bubble Distribution for Thermal Expansion: (A Major Issue if Bubbles is the Solution)

EFG 96-6660

Preliminary CFD (FLOW3D) simulation of a proposed concept with vertical upward flow (Concept #3) for 5 MW beam power shows difficulties in proper baffles design resulting in high turbulent flow, many recirculation zones and bypass (short-cut) of the upper return channel.

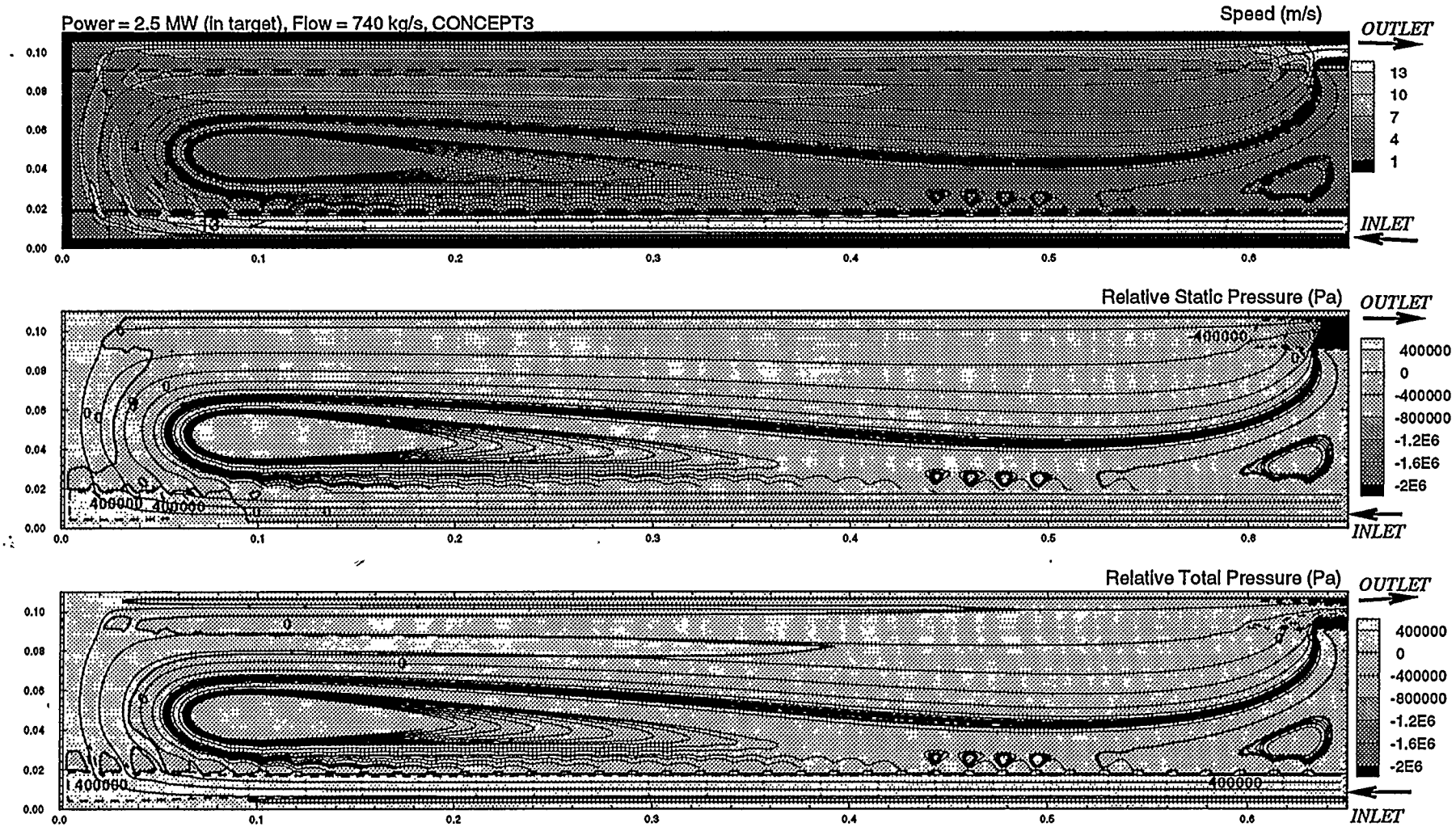

Preliminary CFD (FLOW3D) simulation of a proposed concept with vertical upward flow (Concept#3) for 5 MW beam power shows difficulties in proper baffles design, resulting in high turbulent flow, many recirculation zones and bypass (short-cut) of the return channel.

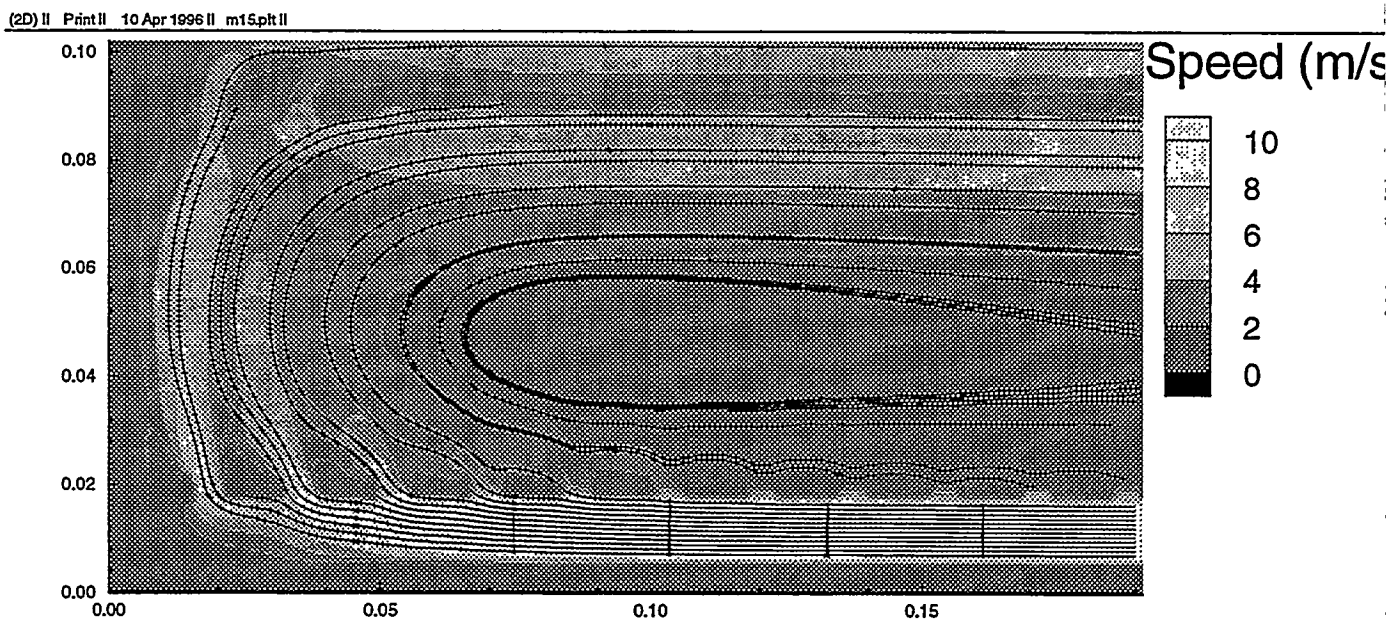

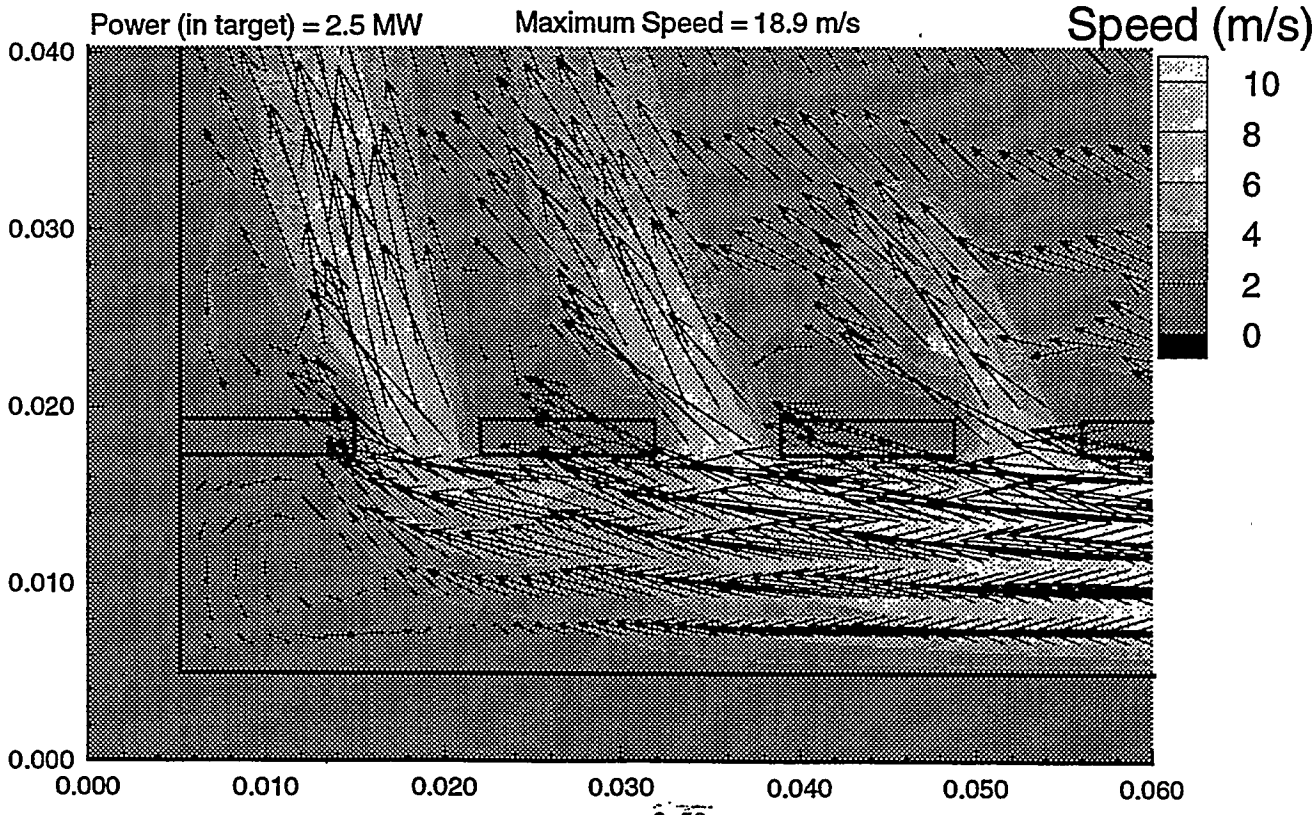

Assuming that proper design of bottom (inlet) and top (outlet) manifolds and their respective baffles can be achieved, Concept #3 shows the potential for smooth, slow, and vertical upward flow, which will coincide well with the direction of He bubbles buoyancy and injection.

(2D) Print 11 Apr 1996 m70 plt

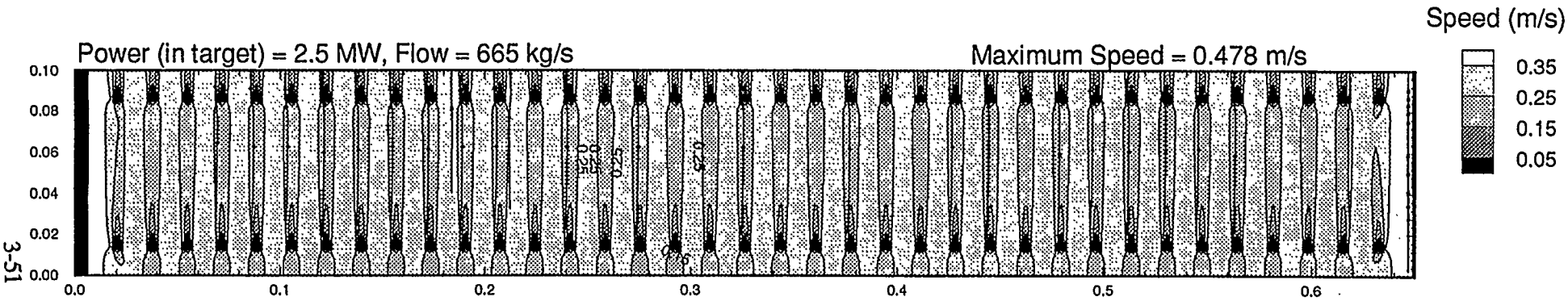

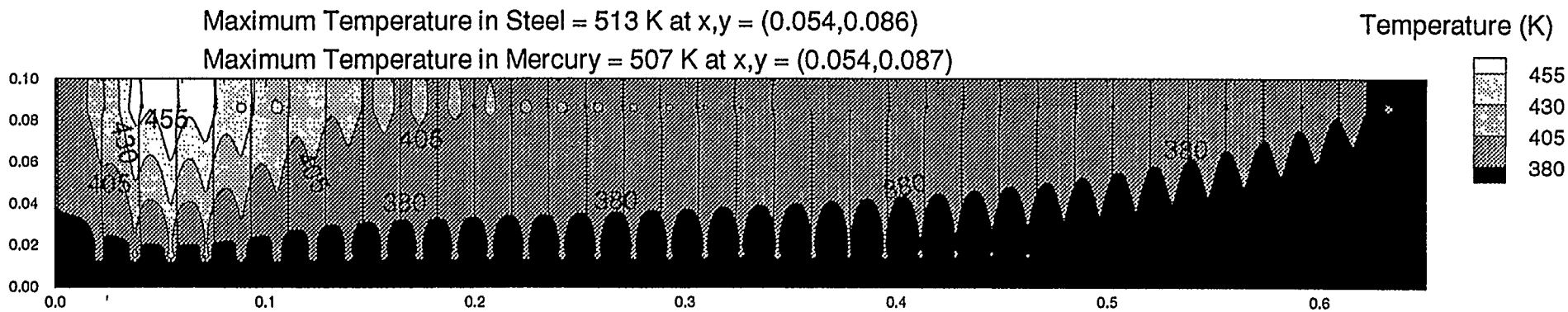

Assuming that proper design of bottom (inlet) and top (outlet) manifolds and their respective baffles can be achieved, Concept #3 shows the potential for smooth, slow, and vertical upward flow, which will coincide well with the direction of He bubbles buoyancy and injection.

(2D) || Print || 11 Apr 1996 || m70.plt ||

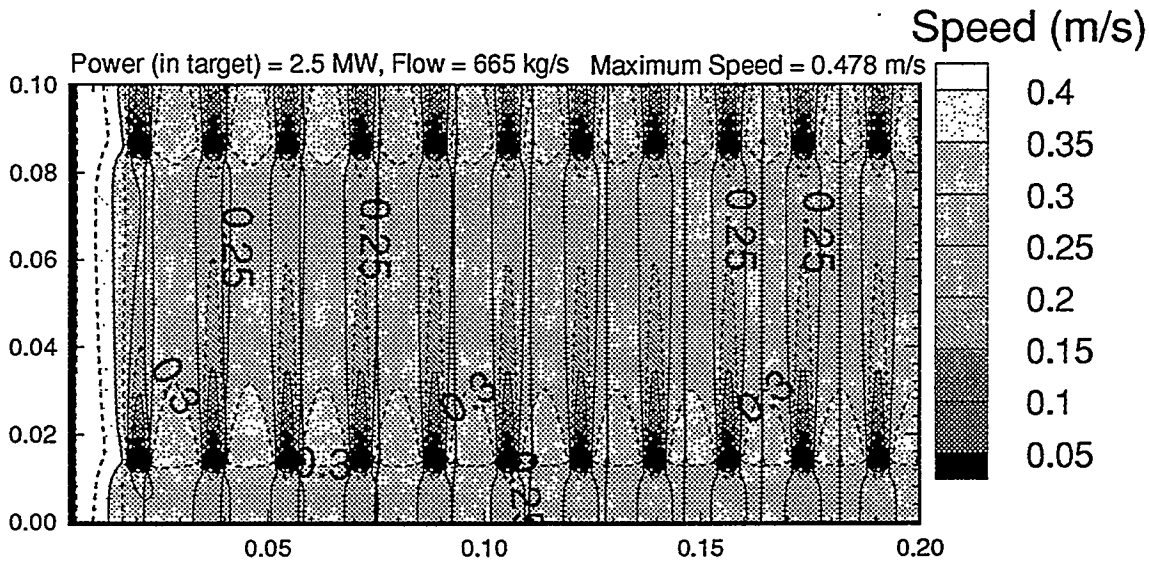

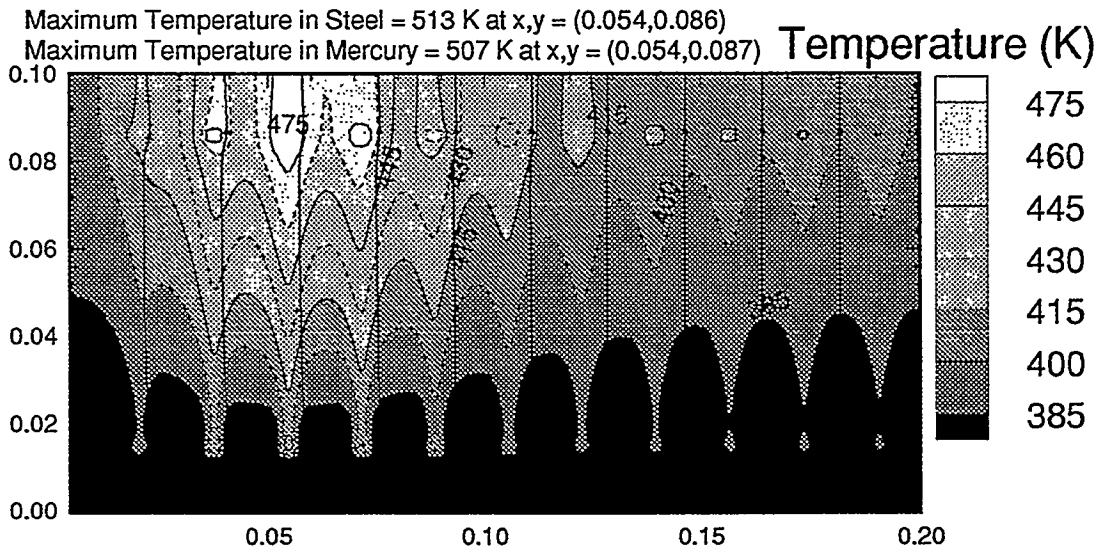

Changes in baffle design and its openings in Concept #3 reduces considerably flow recirculation and stagnation zones behind baffle openings.

(2D) || Print || 10 Apr 1996 || m70.plt ||

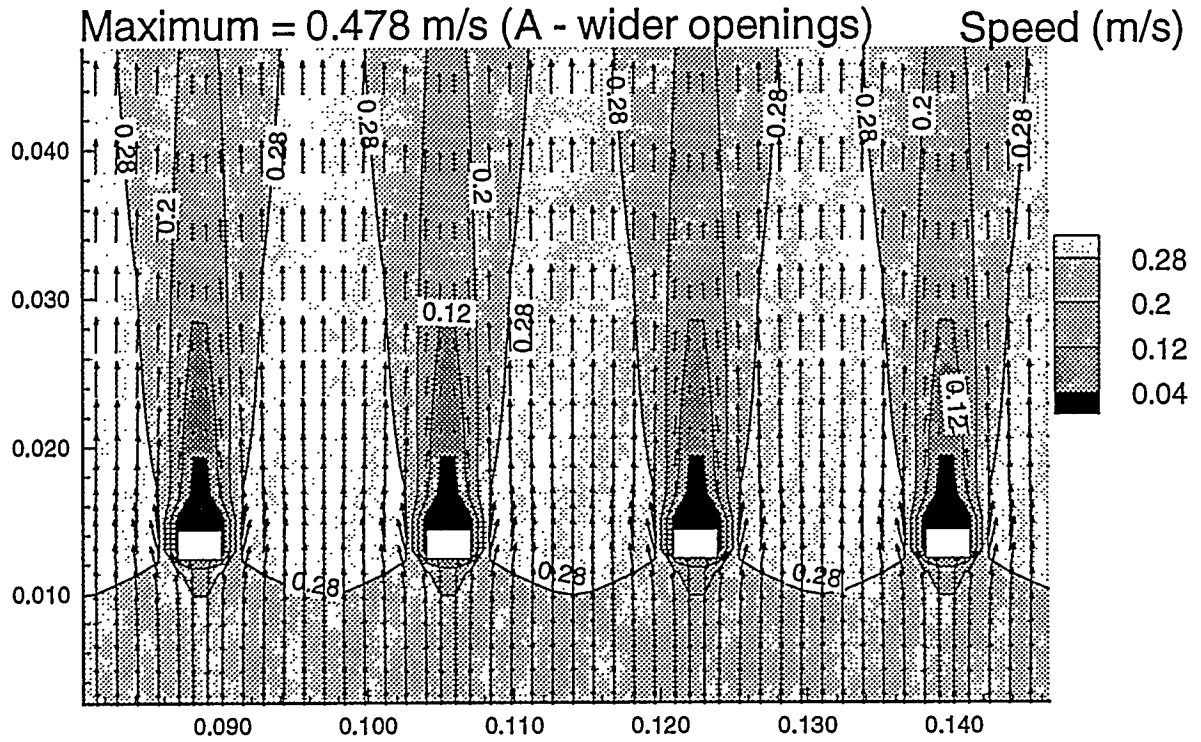

(2D) || Print || 10 Apr 1996 || m40.plt ||

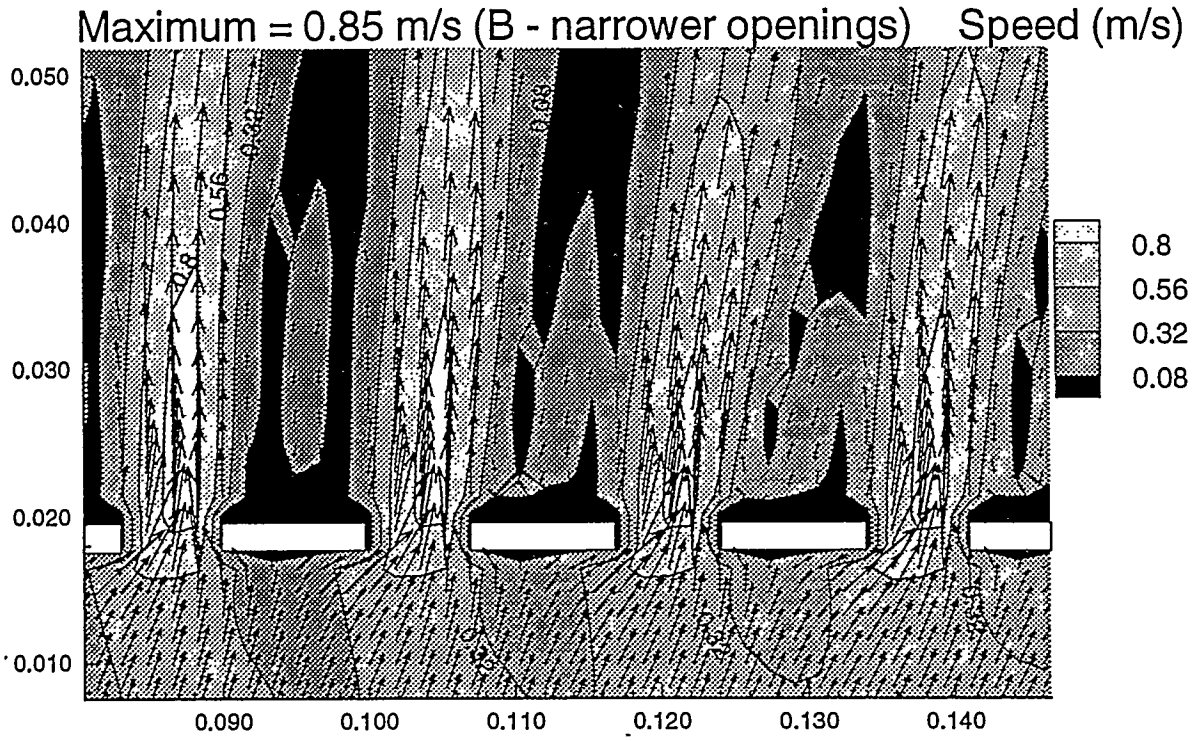

VERY initial CFD (FLOW3D) simulation of He bubbles injection in Concept #1 demonstrates some potential for simulating behavior of He bubbles in flowing Mercury.

Much study and development will be required to be able to "predict", even in a crude way, such a complex phenomenon.

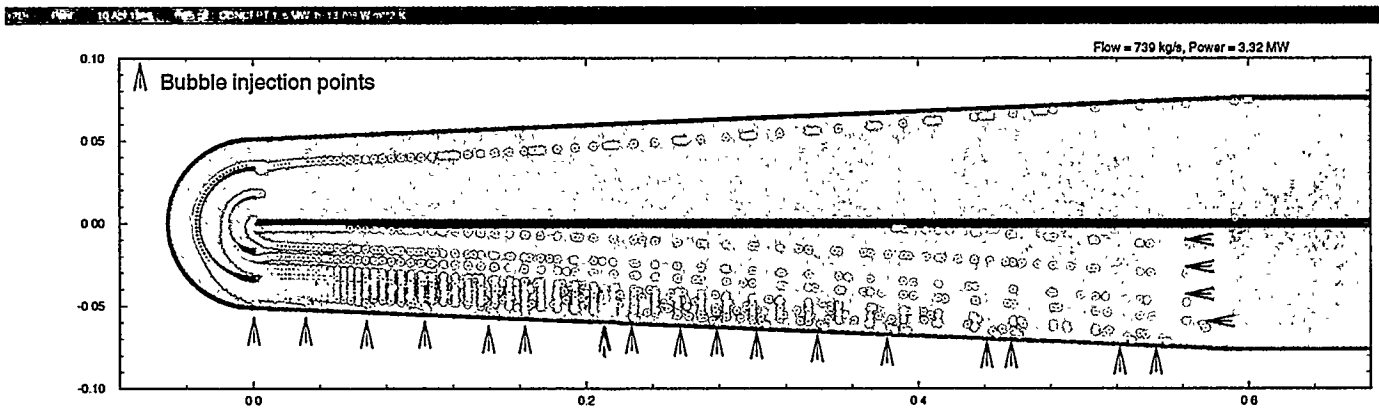

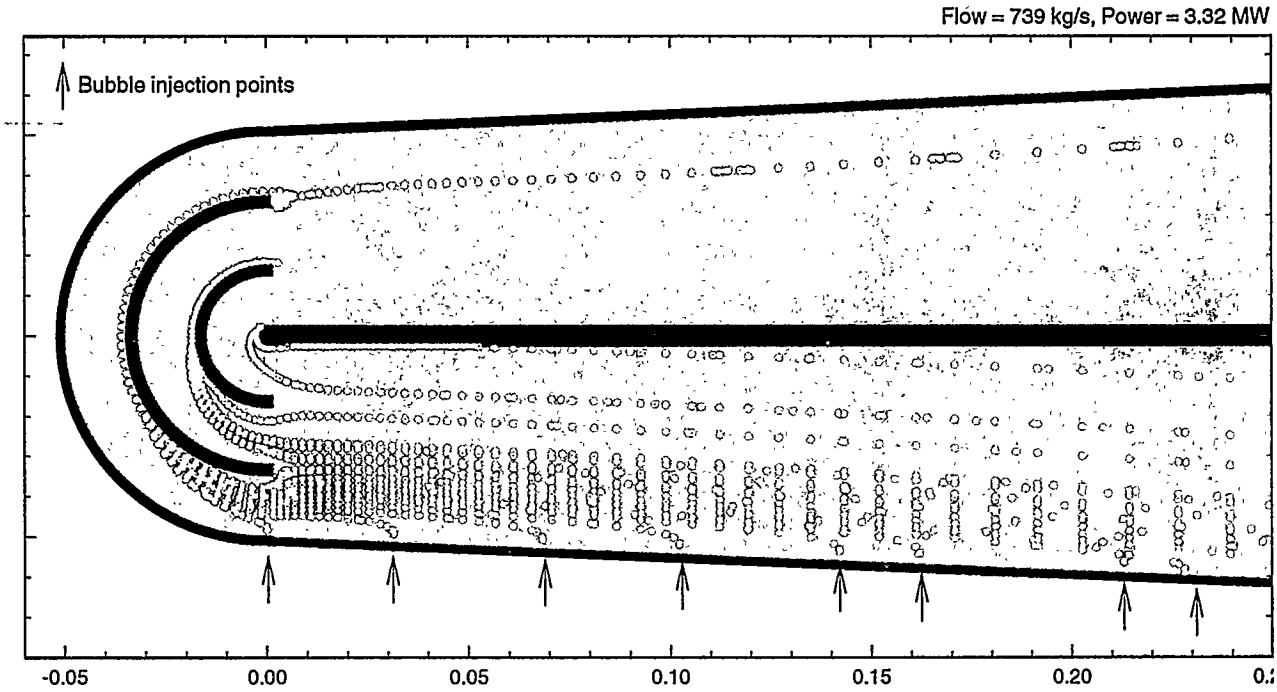

Additional T/H Related Uncertainties to be Considered in the ORSNS Mercury Target

- Uncertainties in Proton Beam (energy deposition) size, shape, and distribution
- "Hot spots" caused by recirculation zones in the mercury
- Possible "hot spots" in the target structure including beam "window"
- Wetting and deposition of Mercury and their effect on thermal/stress
- Helium injection and proper bubble distribution for mitigating thermal shock
- Decay heat, failures, and safety related issues

Safety and Licensing Concerns and Requirements Should be Identified and Incorporated Very Early in The Project and Additional Tasks Defined.

- Tends to drive (or immobilize) project activities
- Has a major effect on project cost
- Need to identify early licensing procedures and by whom
- Need to define additional analytical and R&D tasks based on safety and offset scenarios

A Preliminary List of R&D Tasks for the ORSNS Liquid Mercury Target Was Compiled

-Complete CFD code simulation of the liquid mercury target

*A design tool for various configurations
*Determine flow distribution, flow reversals, stagnation points, and "hot sport"
*Secure proper wall cooling at normal conditions
*Secure proper cooling during non-nominal scenarios
*Simulation work started using FLOW3D

-Full Scale "Mercury Target" loop using WATER.

*Benchmarking the CFD code
*Study flow distributions, pressure drops, etc.
*Might be scaled to simulate mercury
*Existing **THTL** facility at ORNL is available (used for the ANS project)

-Small Scale Mercury Experiment for He Injection and Bubble Distribution

*An important feasibility issue

-A Mercury Test Loop to Study Heat Transfer Coefficients, Friction Factors, etc.

-Full Scale Mercury Target Flow Loop for Confirmation Testing

Summary of Conclusions

- **Preliminary T/H analysis of the ORSNS Liquid Mercury Target has been performed and key T/H parameters were determined.**
- **Three geometrical configurations have been analysed for flow and thermal distribution: one base case and two alternates.**
- **The CFD analysis shows that proper flow distribution can be maintained but fine tuning may be necessary.**
- **Concept #2, with the flow coming in the center, shows the best flow distribution of the three concepts analysed.**
- **If He bubbles will be necessary for mitigating thermal shock, then Concept #3 with vertical flow gives the best chance to maintain proper bubble distribution.**
- **Initial list of T/H R&D Tasks has been developed**

SESSION 4

Thermal Hydraulics, Heat Removal, and Circuit Design (3)

Chairman
S. Lesin

International Workshop on the Technology and Thermal Hydraulics of Heavy Liquid Metals
25.-28. 9. 1996
Schruns, Austria

Thermohydraulic behaviour of the liquid metal target of a spallation neutron source

Y.Takeda PSI

In the presentation, the following three parts of experimental thermohydraulic studies at PSI are presented:

A : Natural circulation in double coaxial cylindrical container
B : Flow around the window
C : Flow in window cooling channels

Part A : The thermohydraulic behaviour of the liquid metal target of the spallation neutron source at PSI has been investigated. The configuration is a natural-circulation loop in a concentric double-tube-type container. The method is based on a one-dimensional loop analysis, and the thermohydraulic behaviour of the target liquid, as well as the total performance of the target, are studied analytically and numerically. These results are verified by two experiments using liquid metal. The results show that the natural-circulation loop concept is valid for the design phase of the target construction, and the current specified design criteria will be fulfilled with the proposed parameter values. The details of both analytical and experimental studies using water and LBE are found in the following publications.

Y.Takeda and W.E.Fischer, "Thermohydraulic behaviour of the liquid-metal Natural-circulation target of the spallation neutron source at Paul Scherrer Institute". Nuclear Science and Engineering, **113**, 287-299 (1993)

Part B : Water experiments were performed for geometry optimisation of the window shape of the SINQ container for avoiding generating recirculation zones at peripheral area and the optimal cooling of the central part of the beam entering window. Flow visualisation technique was mainly used for various window shapes, gap distance between the window and the guide tube edge. A flow mapping study was also performed for quantitative evaluation of the flow pattern and also for a direct comparison with numerical simulation. It was shown that the cusp shape of the central part of the window ensures a smooth flow until the top, which is desirable for heat transfer from the window to the target liquid. For some range of gap distance, it was found that a recirculation zone is generated at the periphery of the window (at the utmost lower part of the annular channel).

Part C : Flows in a narrow gaps of cooling channels of two different types of windows were studied by flow visualisation techniques. One type is a slightly curved round cooling channel and the other is hemispherical shape, both of which have only 2 mm gap distance and the water inlet is located on one side and flows out from the opposite side. In both cases, the central part of the flow area has lower velocity than peripheral area. This is contrary to what was expected for a better cooling at the place where the heat deposition is larger. It was also found that Dean vortices are formed on the curved surface, which may enhance turbulent mixing and thus larger heat transfer rate. However, the influence of the upstream structure is strong so that the structural design must well include this upstream effect.

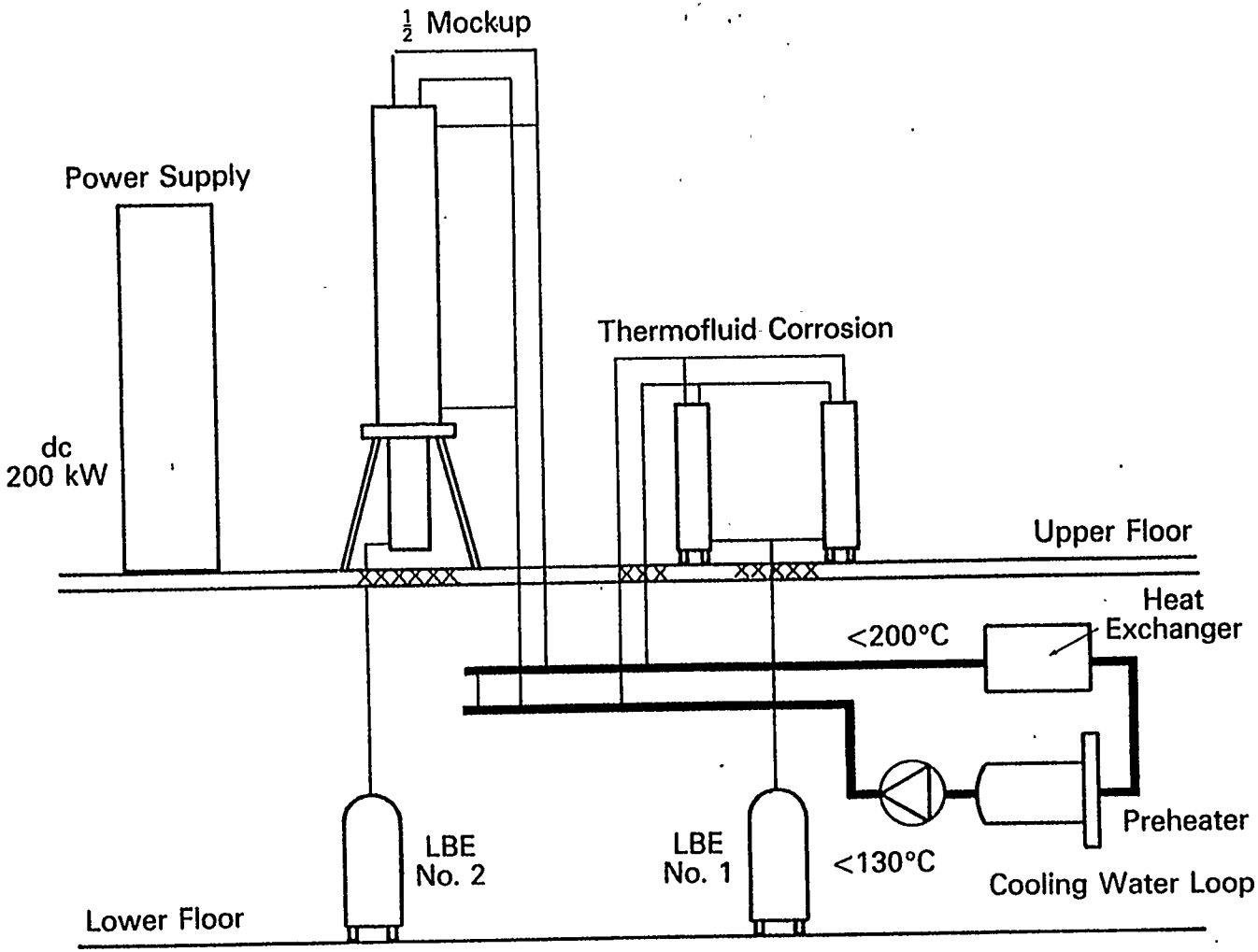

Fig. 10. Schematic of the SSE facility for thermohydraulic dynamics of liquid LBE.

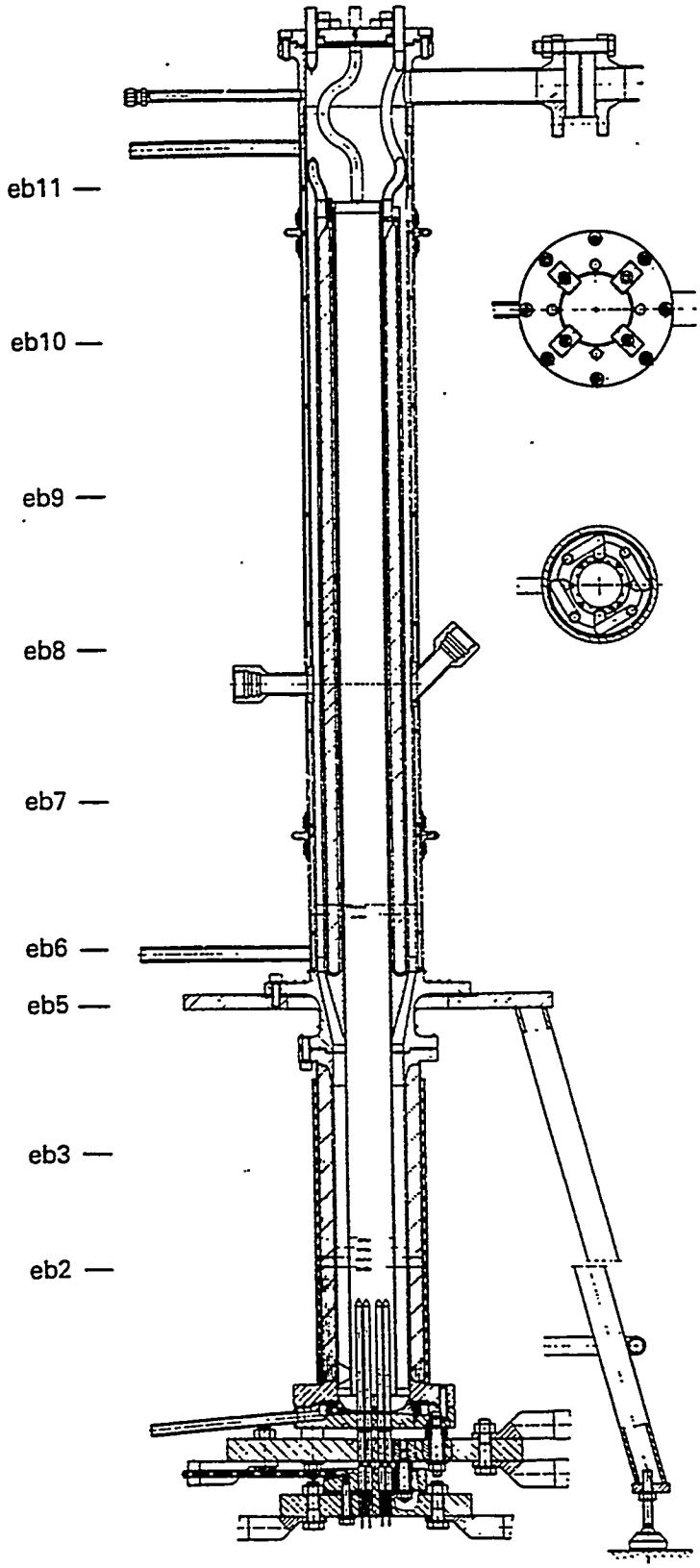

Fig. 11. Detailed schematics of the MUP. The eb numbers show the approximate heights of the temperature measurement. See Fig. 14 for the exact positions.

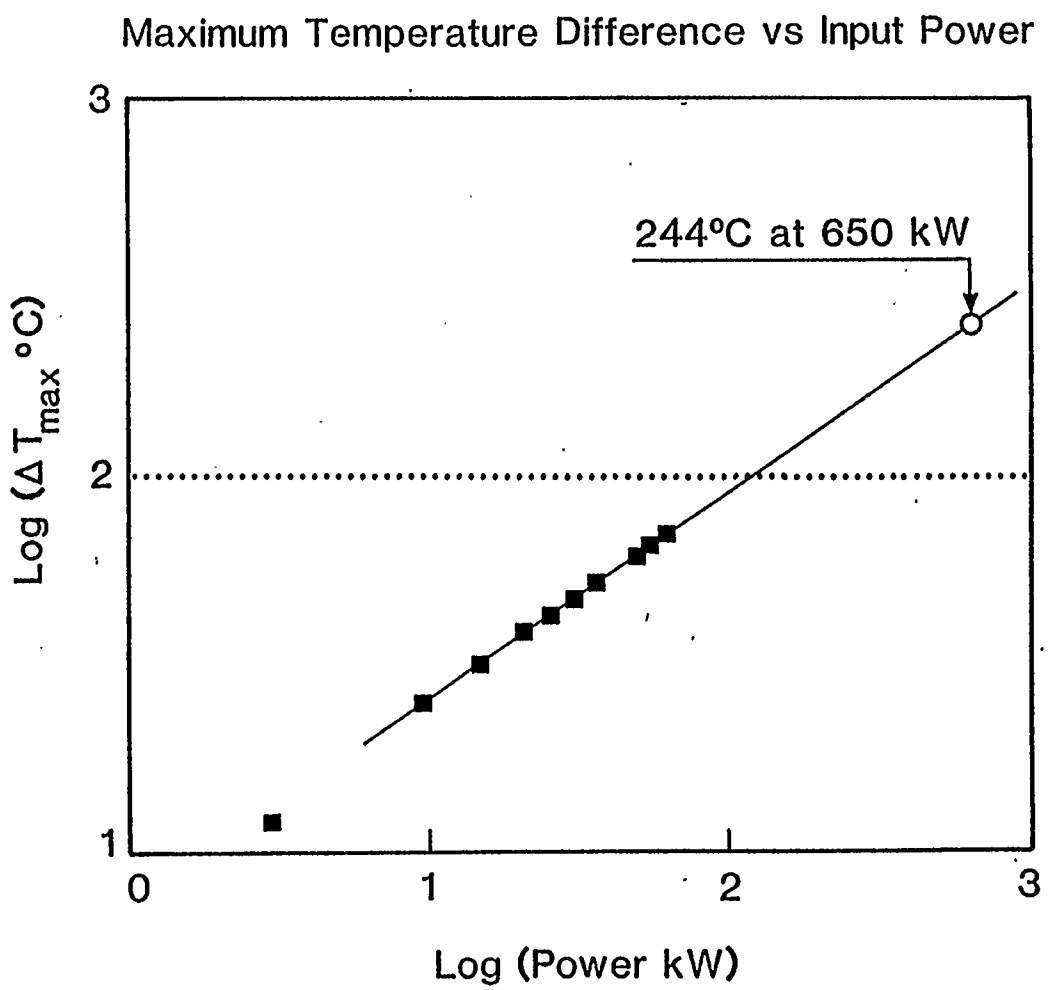
Maximum Temperature Difference vs Input Power
244°C at 650 kW
Log (Δ T_max °C)
Log (Power kW)
3
2
1
0
1
2
3

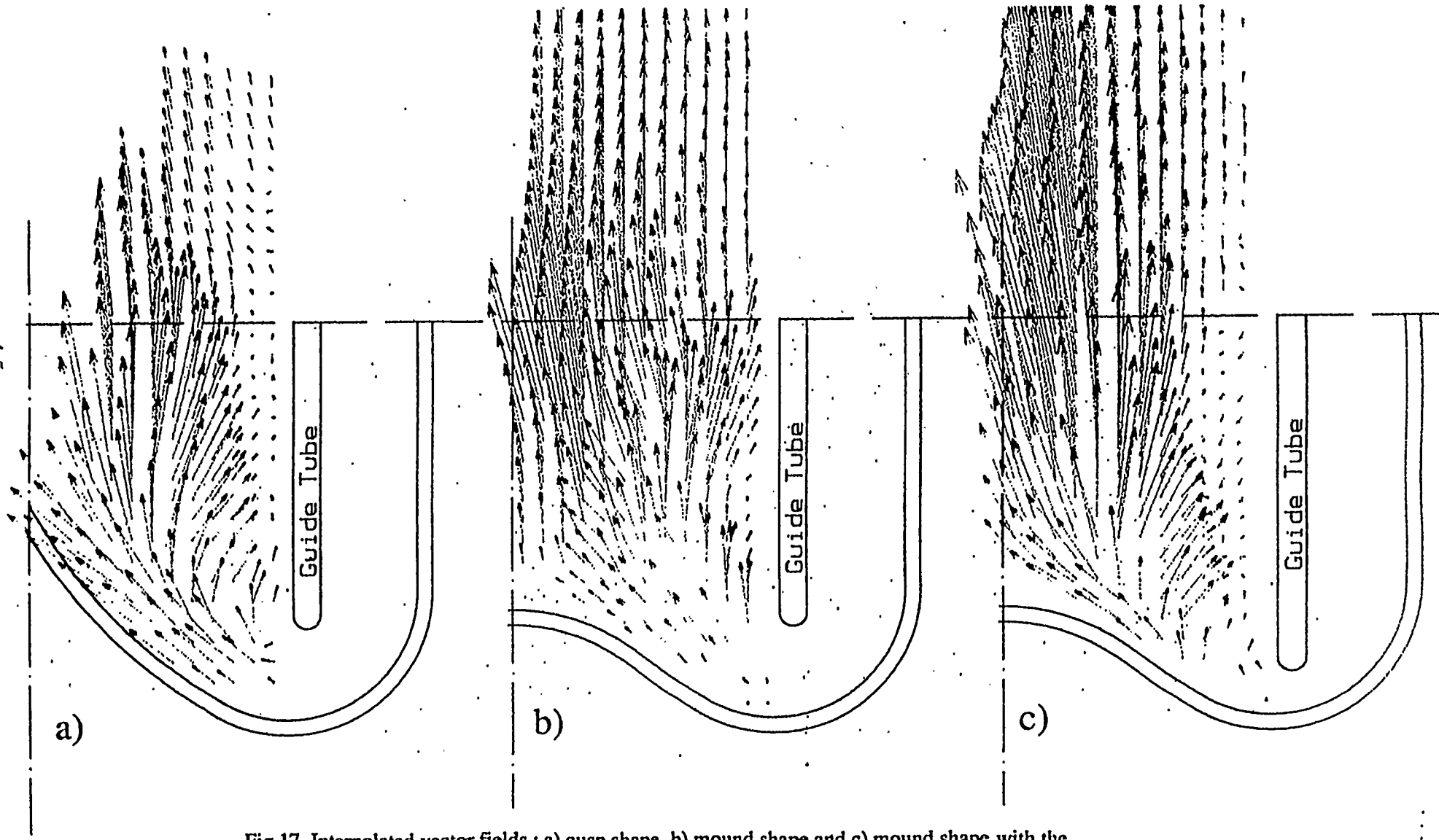

Fig.17 Interpolated vector fields : a) cusp shape, b) mound shape and c) mound shape with the guide tube positioned lower (1/2 to b). Flow rate is 450 l/h for all.

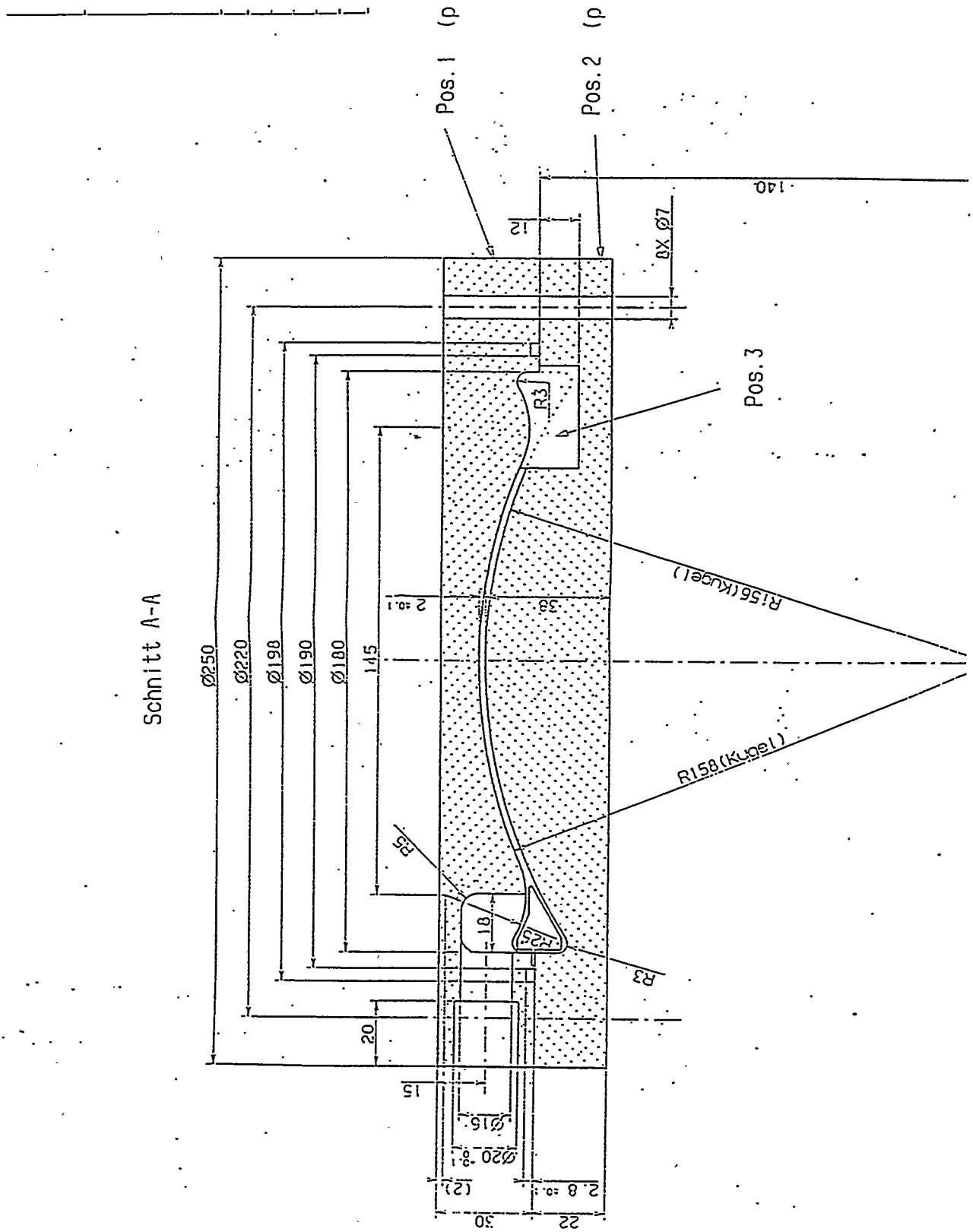

Figure 2b: Schematic of the test section (cross sectional view at A-A')

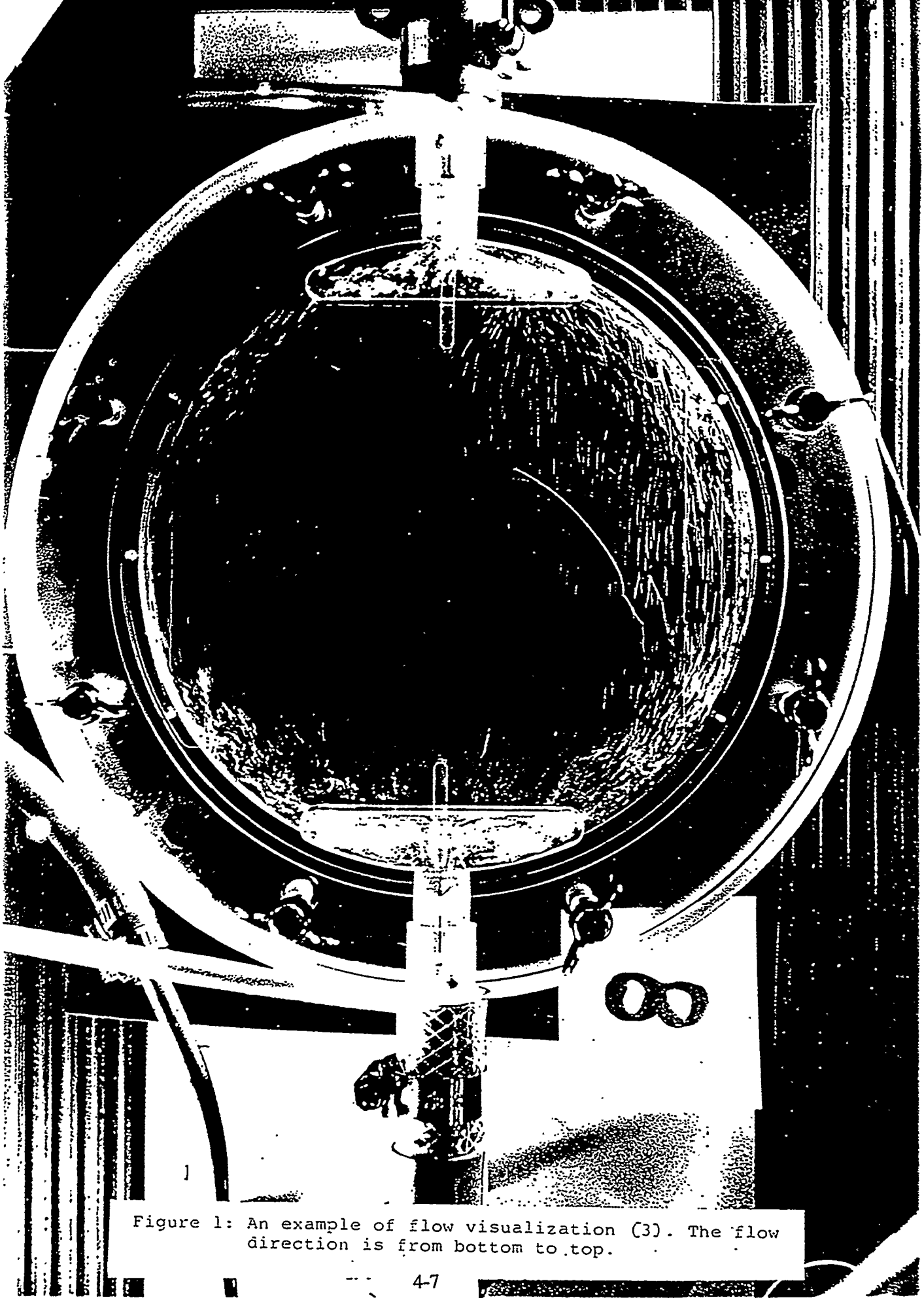

Figure 1: An example of flow visualization (3). The flow direction is from bottom to top.

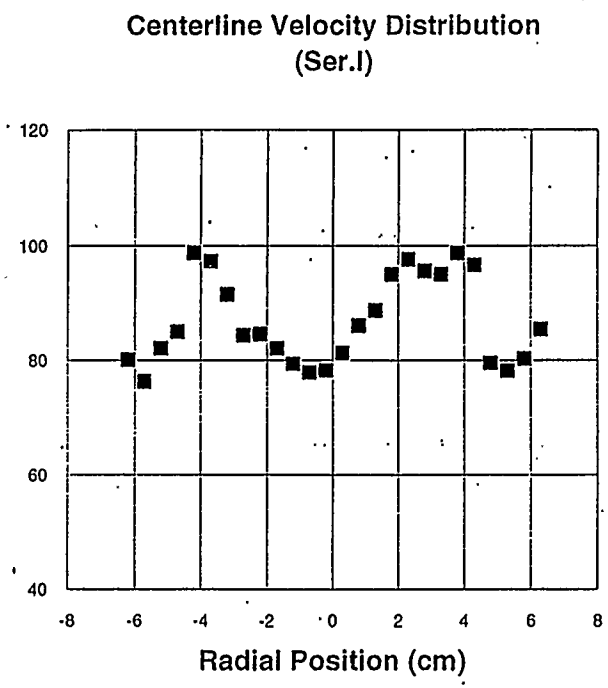

Figure 4: Centerline velocity distribution. The ordinate is the velocity in cm/sec. 1500 l/h with side blockages.

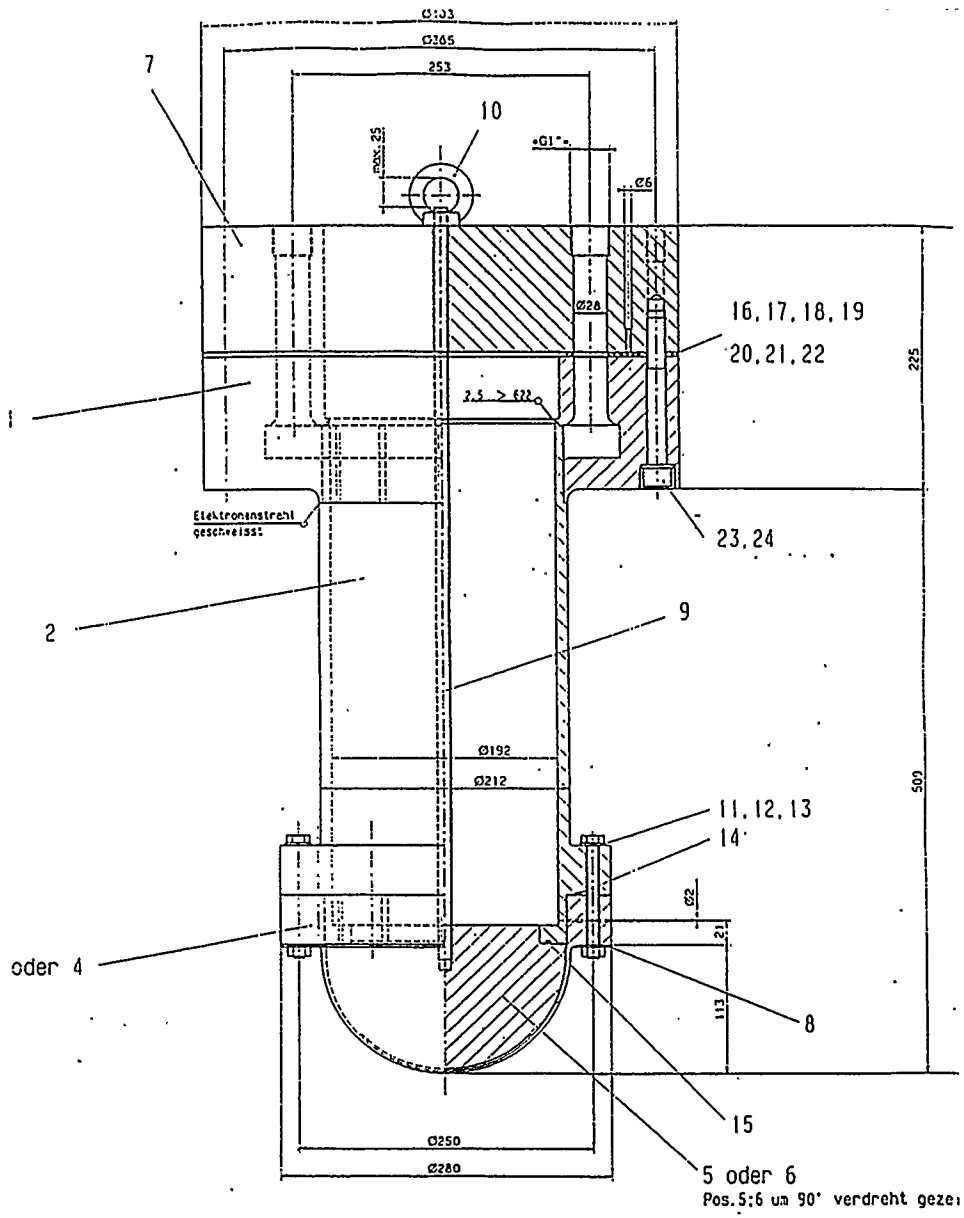

Fig 1 Sketch of the test section

Fig.2 Bottom view. Flow rate is 1.4 *l*/s (Re=8652).
A direction of main flow is from right to left.

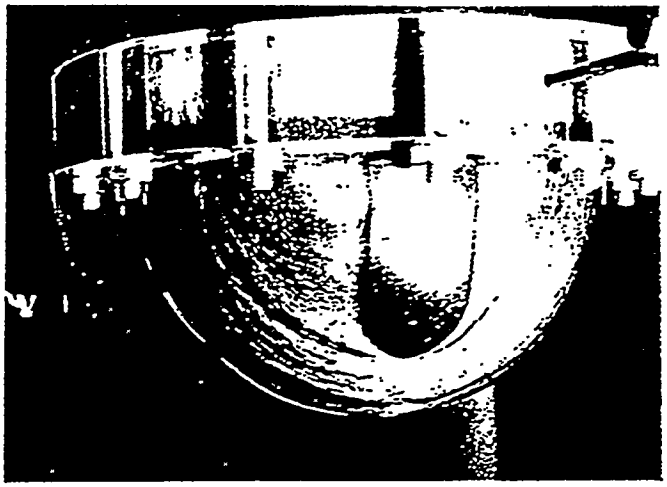

Fig.3 Side view. Flow rate is 1.4 *l*/s (Re=8652).

Contribution to the
International Workshop on the Technology and Thermal Hydraulics of Heavy Liquid Metals

April 24-29, 1996, Schruns, Austria

ENGINEERING ASPECTS OF THE APPLICATION OF STRUCTURAL MATERIALS IN THE 5 MW-ESS-MERCURY-TARGET

Bernd Guttek

Zentralabteilung Technologie
Forschungszentrum Jülich GmbH
Germany

A main problem of the ESS-Hg-target development and the design of the components of its primary Hg-circuit is the choice of structural materials. As designing, calculations and experiments with elected materials take time and are very costy, a preview on their successful application has to be done before as detailed as possible. One aspect on this is to have the knowledge of characteristic values of the structural material candidates under the occuring mechanical and thermal loads, irradiation, corrosion and erosion. Another point is the technology of engineering concerning the manufacturing, welding, surface treatment, and quality control of such parts and components under the demand to reach maximum lifetime.

Present state of the 5 MW-ESS-Hg-target design

Outgoing from the schematic idea of the Hg-target geometry and the Hg-flow arrangement the present state of target design shown in figure 2 and 3 is a result of:

- the target arrangement concept
- the double-walled safety hull concept
- the remote handling concept
- thermal hydraulic Hg-flow calculations
- finite element calculations for the target shell

The target shell with the inner volume of about 20 liters has a wall thickness of 3 mm, which decreases in the beam window area continuously and twodimensionally down to 1 mm in the center. The static pressure of the Hg and the plane structure parts of the shell obligate to:

- reinforce the shell from outside and/or
- reinforce the shell from inside and/or
- pressurize with a definite static pressure the atmosphere outside the target shell

The first option, the outer reinforcement, done by circumferencially running rips, has been examined. Yet for an static pressure difference up to 3 bars between inside and outside the target shell, eight rips, each of them having a cross section of 120 mm^2, are needed.

Knowing more about the Hg-flow arrangement by 3D-Hg-flow calculations run at PSI the three resulting baffle plates and some auxiliary elements could be used to give more stability to the shell from inside. Also, the pressurization of the atmosphere outside the target will be examined; this has to take account the effects on the safety hull. The safety hull surrounds the target shell to guide the Hg to its drain tank in case of a target shell rupture. It is double-walled and cooled by guiding the cooling medium between the walls. Preliminary cooling calculations for its double-walled proton beam window showed that gas cooling by He does not manage to keep material temperatures low enough so that the layout is done for D_2O-cooling. The present design shows both hulls with a wall thickness of 2.5 mm decreasing to 1 mm in the beam window center.
The target is connected to at least three supply lines: one inlet Hg-line, one inlet He-line and one outlet for the Hg-He-mixture. At the moment the design shows three Hg-inlet pipes which may come together to one. The He-line connects to the lower baffle plate through which the He should be injected as bubbles in the Hg-target volume. The safety hull is welded to the main flange which connects to a shielding plug fixed on the trolley which carries the Hg-circuit installations. The necessary two supply lines for D_2O-cooling, crossing the inner safety hull, and the main flange are planned to be connected simultaneously to the shielding plug.

Structural material

The presence of the Hg and the pulsed impact of the proton beam cause different loads on the target shell, especially on the beam window:

	caused by proton beam	caused by Hg	engineering calculations
thermal shock in the beam window	x		x
pressure wave in the Hg	x	x	x
temperature gradients in the window	x		x
static pressure of the Hg		x	x
irradiation damage	x		
corrosion and erosion attack from Hg		x	

Table 1 Different loads on the beam window due to pulsed operation, 5 MW averaged beam power and Hg as target material

The requested properties of the target shell structural material are at least:

- low increase of the DBTT under the present irradiation conditions
- yielding stress at tempertaures of ca. 300°C still about 300 MPa, also when irridiated
- high thermal conductivity
- low linear thermal expansion coefficient
- manufacturing: welding must be possible under limited effort, option of founding is useful

In the present state of the ESS-study, the ESS Target Working Group considers ferritic-martensitic steel from the 'low activation steel'-type (LAS) with the composition:

0.12C 9.5Cr 1W 0.25V 0.08Ta 0.05Ce

as structural material candidate for the target shell. As it is not yet examined but very unlikely that this steel would be water corrosion resistant, the candidate material for both walls of the saftey hull is stainless steel 316SS.

Structure calculations: temperature gradients

The proton beam with an elliptical footprint of 60 mm x 200 mm and 2D-parabolic shape causes in its center under consideration of neutrons a specific heat deposition of 1400 W/cm^3 resulting in a specific energy deposition of 28 J/cm^3 per pulse under an operation with a repitition rate of 50 Hz. The pulse duration is 0.7 µs. The calculation of stresses caused by temperature gradients is done as static calculation.

The present state of results from finite element calculation for the target shell considered the Hg-flow on the inner wall of the target shell under strong simplifications:

- the Hg-temperature is constant
- the heat transfer coefficient is averaged: 22.000 W/m^{2}K

Outside the target shell, vacuum is assumed.

For the comparison of austenitic and ferritic-martensitic steel the following values are used:

	thermal conductivity [W/mK]	linear thermal expansion coefficient [1/K]
austenitic (316SS)	15.5	$1.7 \cdot 10^{-5}$
ferritic-martensitic (LAS)	26	$1.2 \cdot 10^{-5}$

Table 2 Some characteristic values of austenitic and ferritic-martensitic steel

For a center thickness of 1 mm, the maximum von Mises stresses and temperature gradients appearing in the window area are:

	temperature gradient across window thickness [K/mm]	maximum von Mises stresses [MPa]
austenitic, see figure 4	45	140
ferritic-martensitic, see figure 5	30	80

Table 3 Temperature gradient and maximum stress level in the beam window

Structure calculations: static pressure difference

As mentioned in the first section, a static pressure difference between inside and outside the target shell could be arranged. Finite element calculations for the target shell with a reinforcement by rips of a simple geometry (rectangular cross section) had been done assuming a constant static pressure difference for the whole shell:

$$\Delta p_{static} = p_{inside} - p_{outside} = 2.4 \text{ bars}$$

The maximum von Mises stresses *appearing in the window area*, are about 60 MPa (see figure 6). Due to the linear character of the calculations one could add different static loads and/or scale them up.

Figure 6 shows also von Mises stresses due to temperature gradients and static pressure for ferritic-martensitic steel.

Structure calculations: thermal shock in the beam window

In a simple geometry of a flat quadratic plate with the dimensions 100 mm x 100 mm and a thickness of 2 mm first calculations of the dynamic stress state due to the short-pulsed proton beam impact had been run. The finite element model of a quarter plate for this calculation is shown in figure 7. The resulting pictures of the dynamic reponse were recorded on a video tape. For a better comparison with other codes some data have been extracted for the high frequency oscillations, shown in figure 8. For historical reason of the ESS-study the plate material for this calculation had been tantalum.

Young's modul	E	171000	N/mm^2	at 200°C
Poisson number	ν	0.34	---	at 200°C
specific weight	ρ	16.6	kg/dm^3	---
specific heat capacity	c_P	146	J/kg K	at 200°C
linear thermal expansion coefficient	α	$6.6 \cdot 10^{-5}$	1/K	at 200°C
thermal conductivity	λ	58	W/m K	at 200°C
maximum specific energy	w_0	76	J/cm^3	---
length of short axis of beam footprint	x_0	45	mm	---
length of long axis of beam footprint	y_0	45	mm	---

Table 4 Characteristic values of Ta for calculations on stresses caused by thermal shock waves

For a Ta-plate, the specific heat deposition in the beam center of a 2D-parabolic-shaped beam with a round footprint of 90 mm diameter has been assumed as 3800 W/cm^3. The model of the beam impact as a rectangular function is:

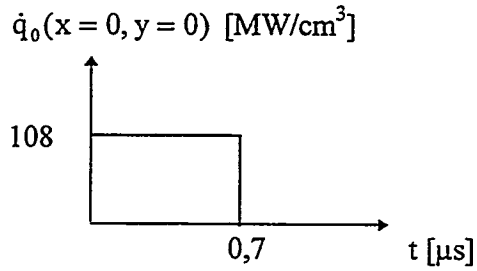

with a specific energy distribution as:

$$w(x,y,z) = \begin{cases} w_0 \cdot \left(1 - \frac{x^2}{x_0^2} - \frac{y^2}{y_0^2}\right) & \text{für } \frac{x^2}{x_0^2} + \frac{y^2}{y_0^2} \le 1 \\ 0 & \text{für } \frac{x^2}{x_0^2} + \frac{y^2}{y_0^2} > 1 \end{cases}$$

Figure 1 Model of proton beam pulse

Structure calculations: conclusion

Giving an overview of the different loads on the beam window for the short-pulsed operation of the 5 MW-ESS-Hg-target one could state at the present state of the calculations:

	stress level [MPa]	frequency	calculations done at
thermal shock in the beam window	60 - 80	MHz	PSI, KFA
pressure wave in the Hg on the beam window	10 - 120 *	kHz	PSI
static pressure of the Hg	60	static	KFA
temperature gradients	80 - 140	static	PSI, KFA

Table 5 Quantitative overview of the different loads on a steel beam window due to pulsed operation, 5 MW averaged beam power and Hg as target material

***): depending on the successful distribution of gas bubbles in the Hg**

Further decisions need:
- more information about the material candidates
- calculations on optimized geometries
- development and validation of codes
- evaluation of the tri-axial stress states under consideration of different frequencies

Future work

Next steps on structure calculations

- on the target shell including the beam window:
  - target shell calculations with optimized structure
  - use of thermal hydraulic data from Hg-flow-calculations done at PSI
  - consideration of the pressure wave caused in the target material
- on the double-walled safety hull including the beam windows:
  - first structure calculations and optimization of geometry
  - 3D-coolant flow calculation
  - use of thermal hydraulic data from coolant flow calculations
- on the target unit (target shell and safety hull)
  - analysis of tri-axial stress states
  - investigation of thermal shock effects in the curved beam windows

Necessary engineering on the Hg-target unit

- choice of structural materials for the target shell and the safety hull
- investigation of possible production and manufacturing of target unit parts
- thermal-mechanical and thermal treatment of structural material and parts
- prototyping for experiments
- design of the flange system for the Hg-, He-, D_2O-lines and the main flange between the safety hull and the shielding plug
- remote handling concept

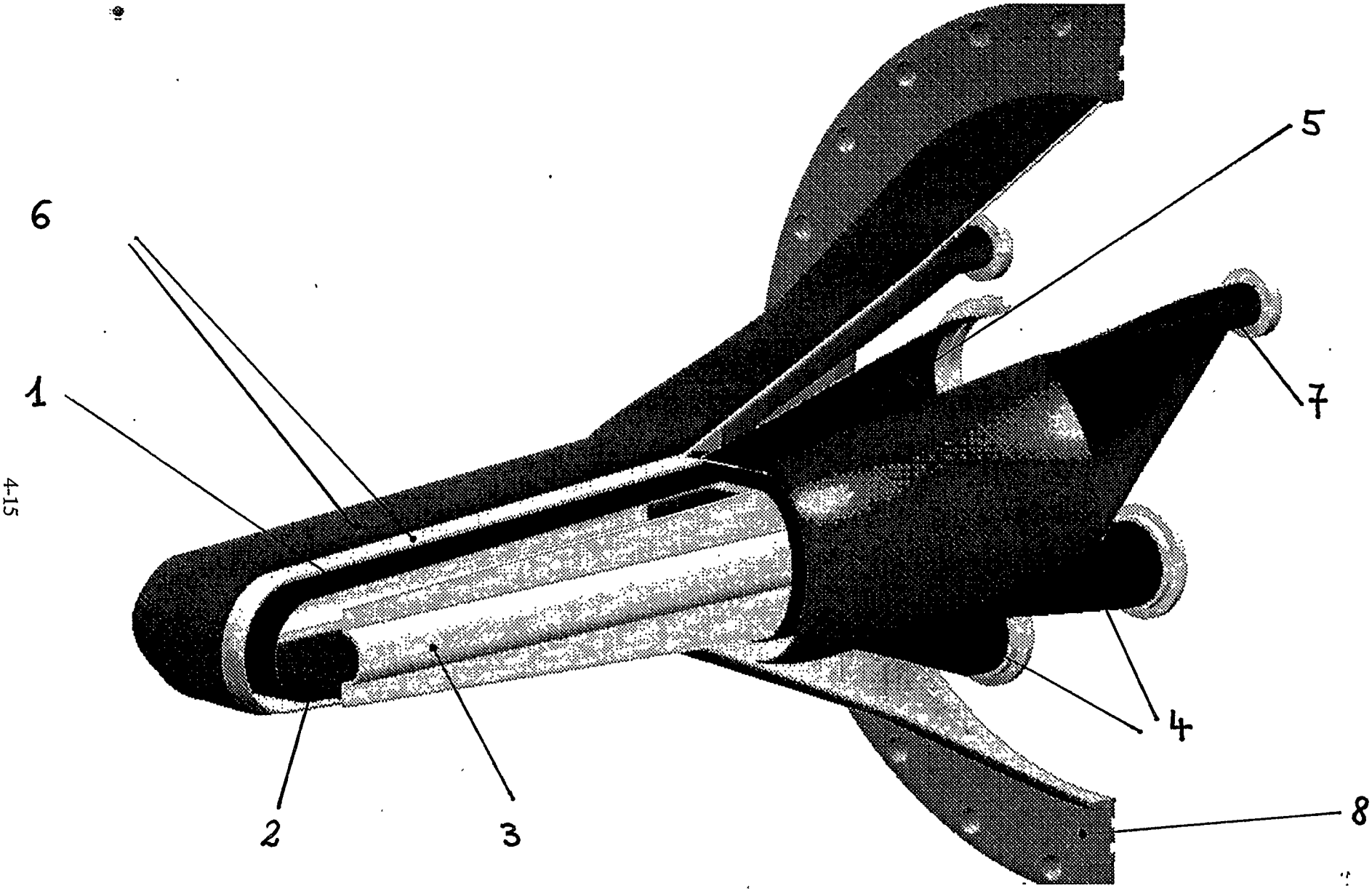

Figure 2 ESS 5 MW Mercury Target
1: target shell, 2: lower baffle plate, 3: side baffle plates, 4: Hg-inlet tubes, 5: Hg/He-outlet tube, 6: double-walled safety hull, 7: D_2O-supply tubes, 8: main flange
scales: the target shell has a depth of 700 mm, the main flange has an inner diameter of 700 mm

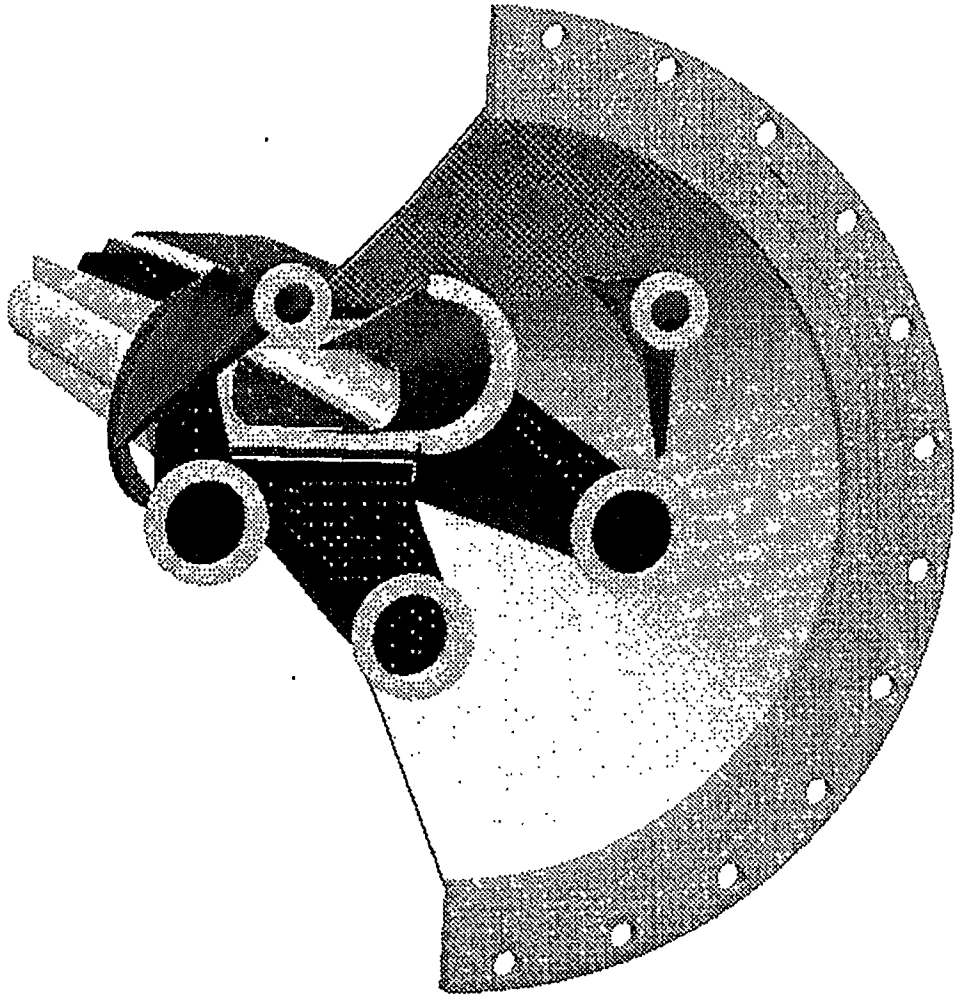

Figure 3 ESS 5 MW Mercury Target
scale: the main flange has an inner diameter of 700 mm

Temperature distribution due to proton beam

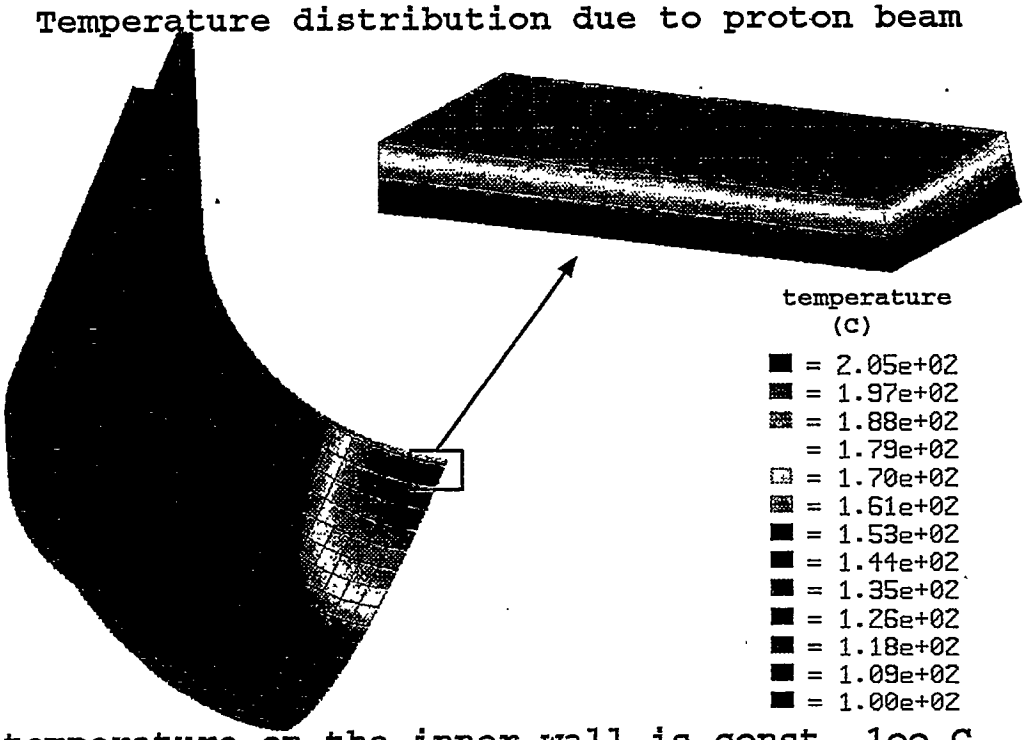

Hg-temperature on the inner wall is const. 1oo C

Von Mises stress due to temperature distribution

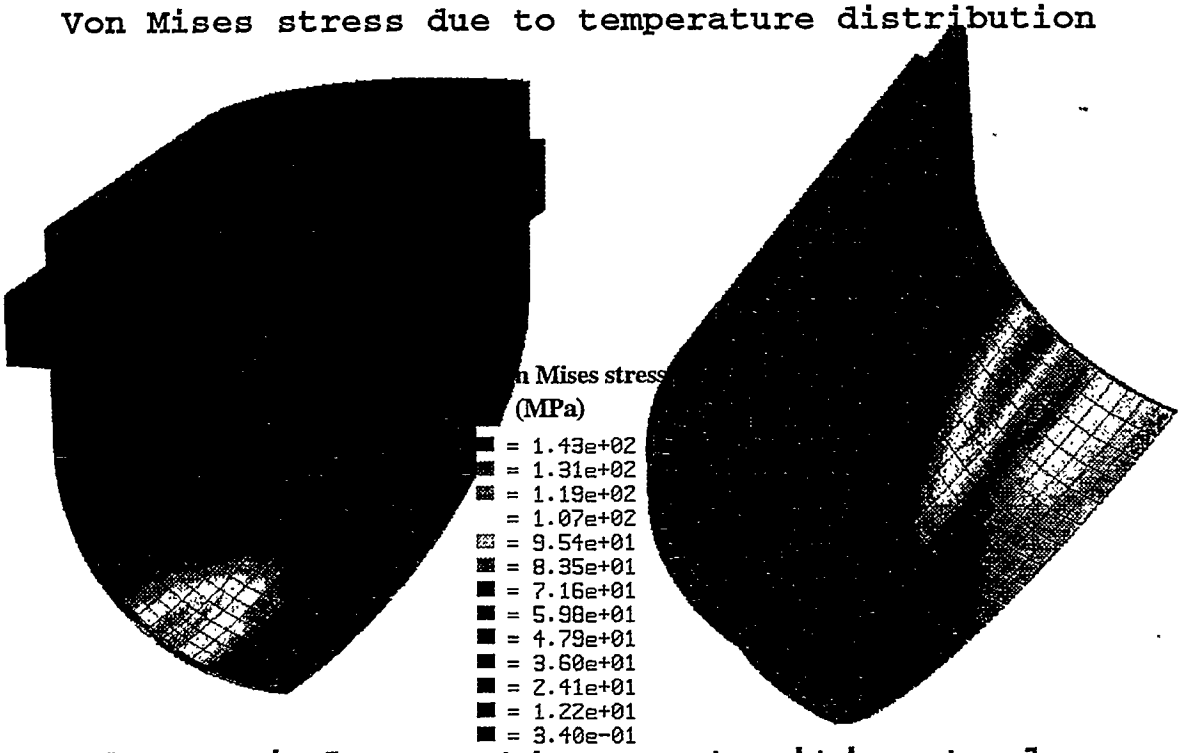

beam window section, austenitic steel

ZENTRALABTEILUNG TECHNOLOGIE (ZAT)	ESS-Hg-Target	04.04.96	Fig 4

Temperature distribution due to proton beam

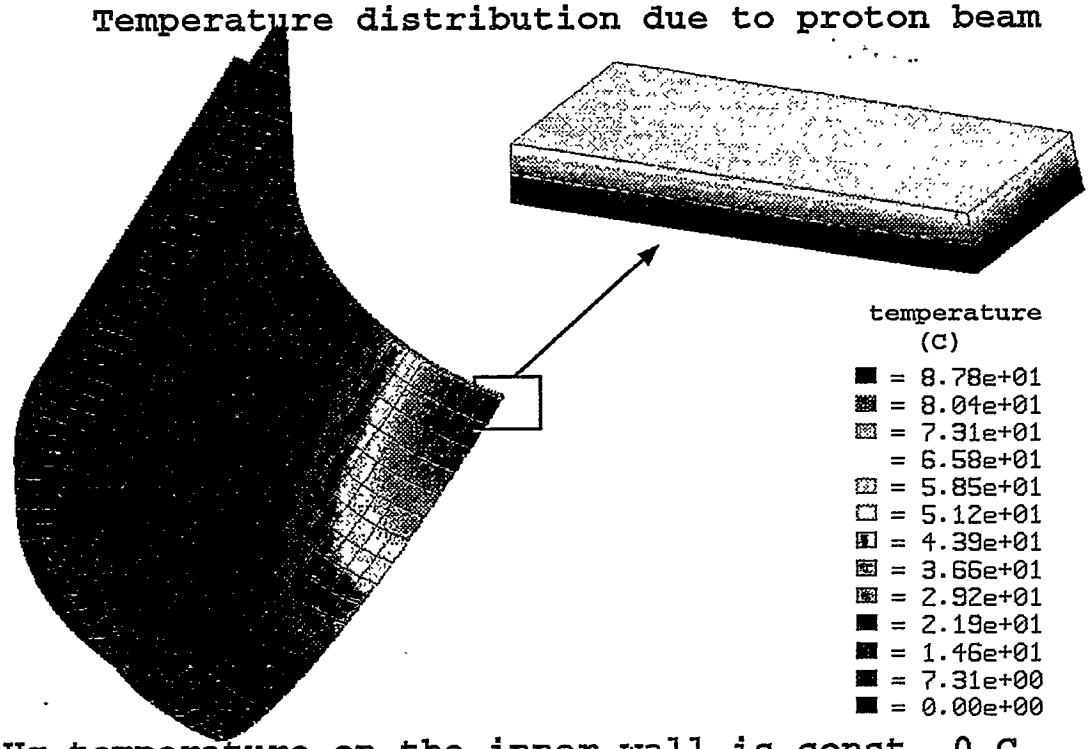

Hg-temperature on the inner wall is const. 0 C

Von Mises stress due to temperature distribution

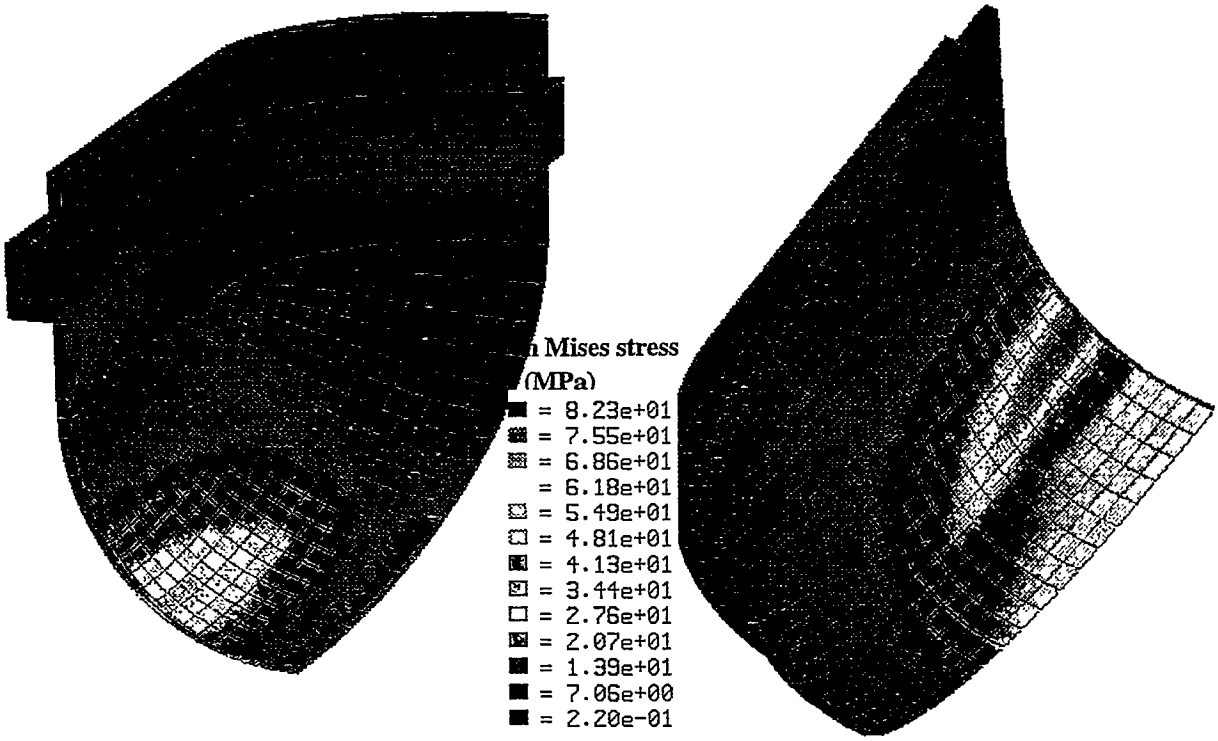

beam window section, ferritic-martensitic steel

ZENTRALABTEILUNG TECHNOLOGIE (ZAT)	ESS-Hg-Target	04.04.96	Fig 5

Von Mises stress due to static pressure

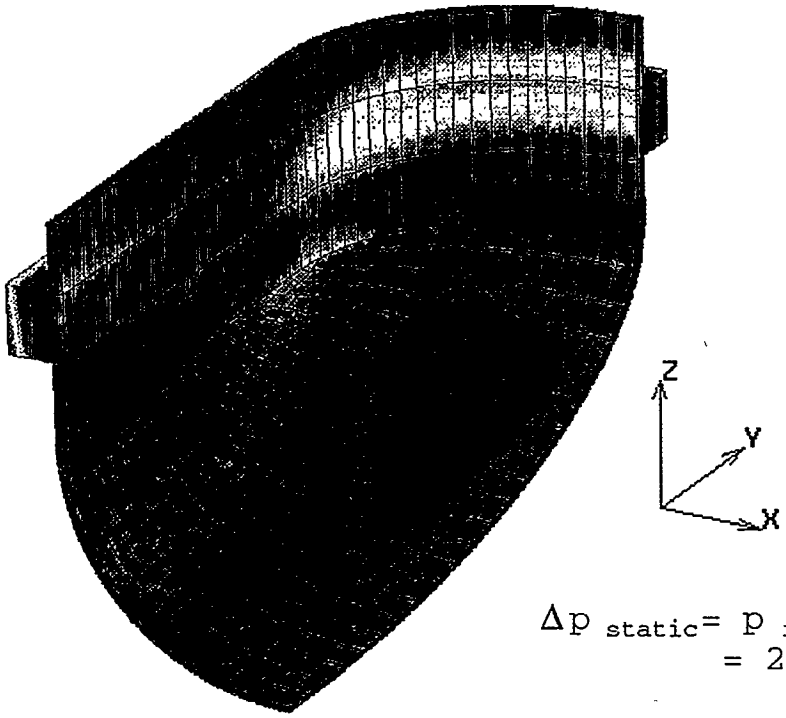

von Mises stress (MPa)
- = 8.56e+01
- = 7.88e+01
- = 7.19e+01
- = 6.51e+01
- = 5.82e+01
- = 5.14e+01
- = 4.45e+01
- = 3.77e+01
- = 3.08e+01
- = 2.40e+01
- = 1.72e+01
- = 1.03e+01
- = 3.46e+00

$\Delta p_{static} = p_{inside} - p_{outside}$
$= 2.4$ bars

Von Mises stress due to static pressure and temperature distribution

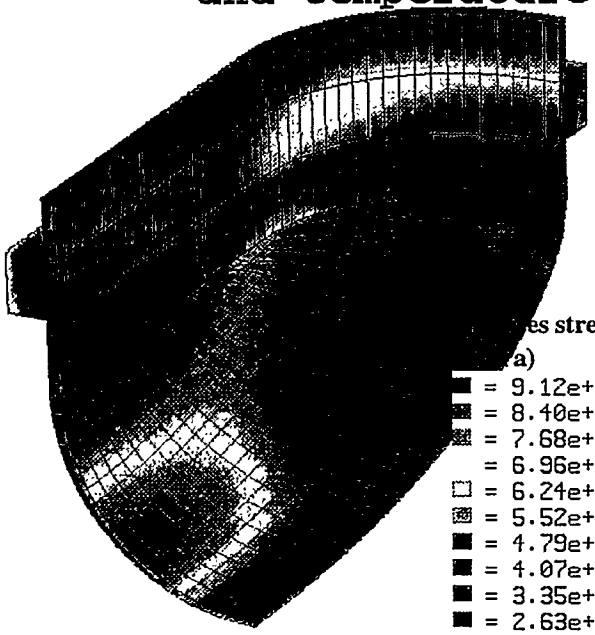

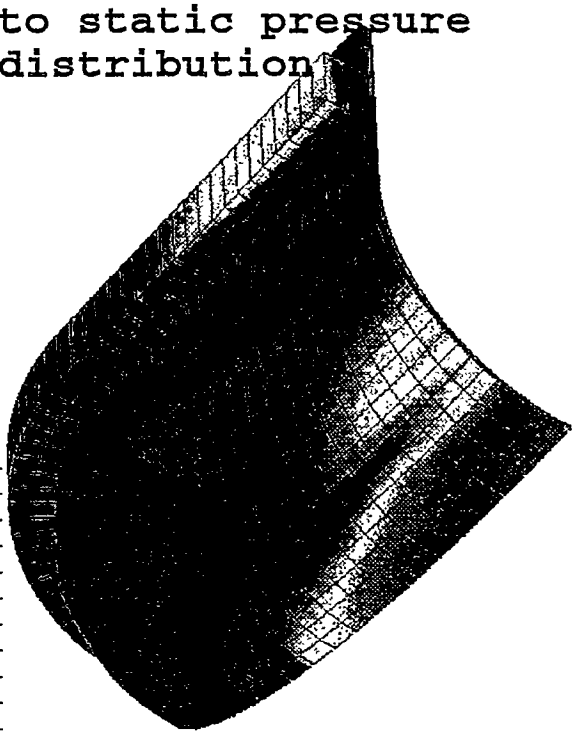

es stress
a)
- = 9.12e+01
- = 8.40e+01
- = 7.68e+01
- = 6.96e+01
- = 6.24e+01
- = 5.52e+01
- = 4.79e+01
- = 4.07e+01
- = 3.35e+01
- = 2.63e+01
- = 1.91e+01
- = 1.19e+01
- = 4.66e+00

view from inside

view from outside

beam window section, ferritic-martensitic steel

ZENTRALABTEILUNG TECHNOLOGIE (ZAT)	ESS-Hg-Target	04.04.96	Fig 6

Finite Element Mesh for One Quarter of a Target Plate

nodal point numbering

reference point for vertical displacements

reference point for stresses

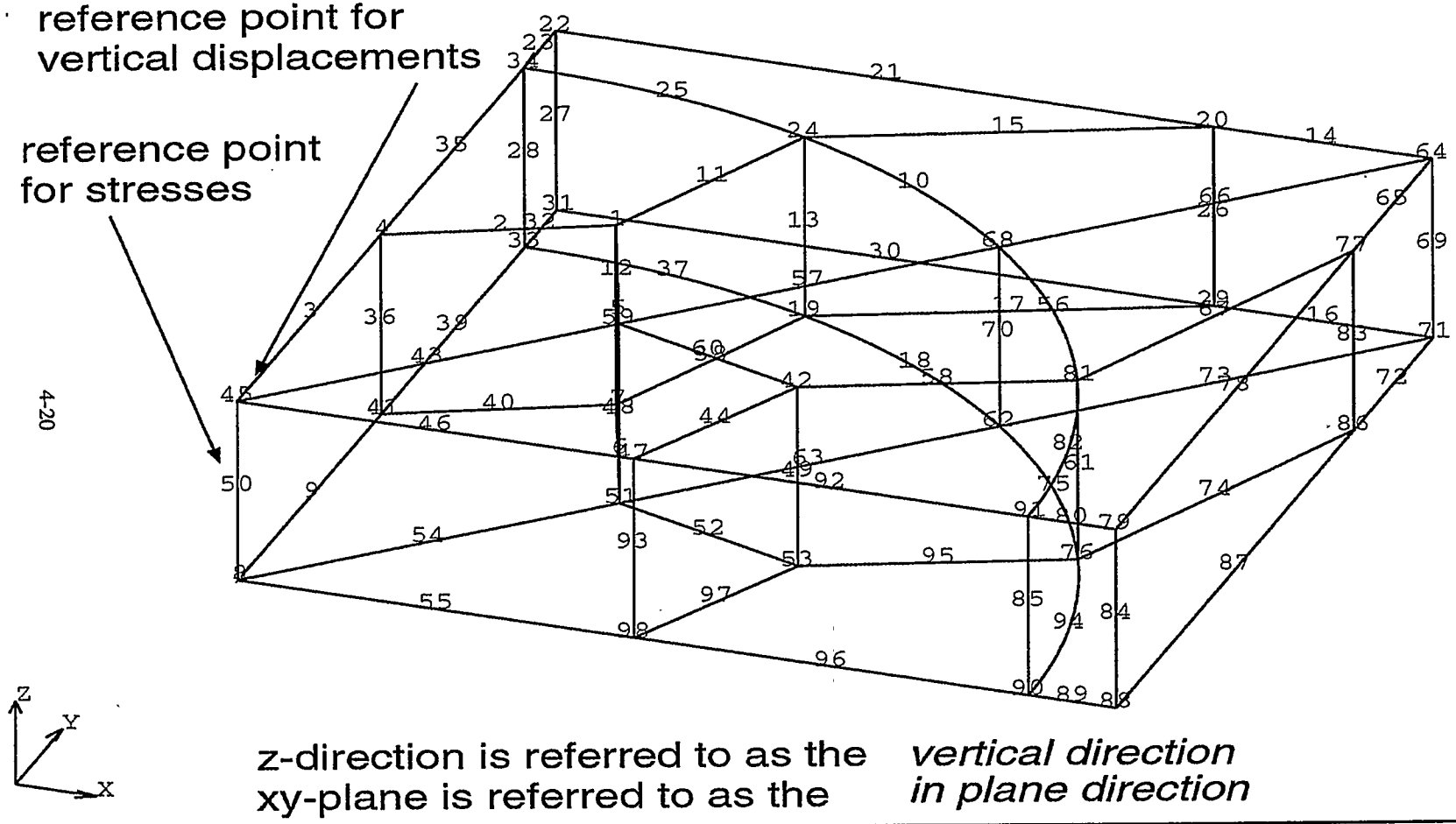

z-direction is referred to as the *vertical direction*
xy-plane is referred to as the *in plane direction*

High Frequency Part of an Oscillating Target Plate

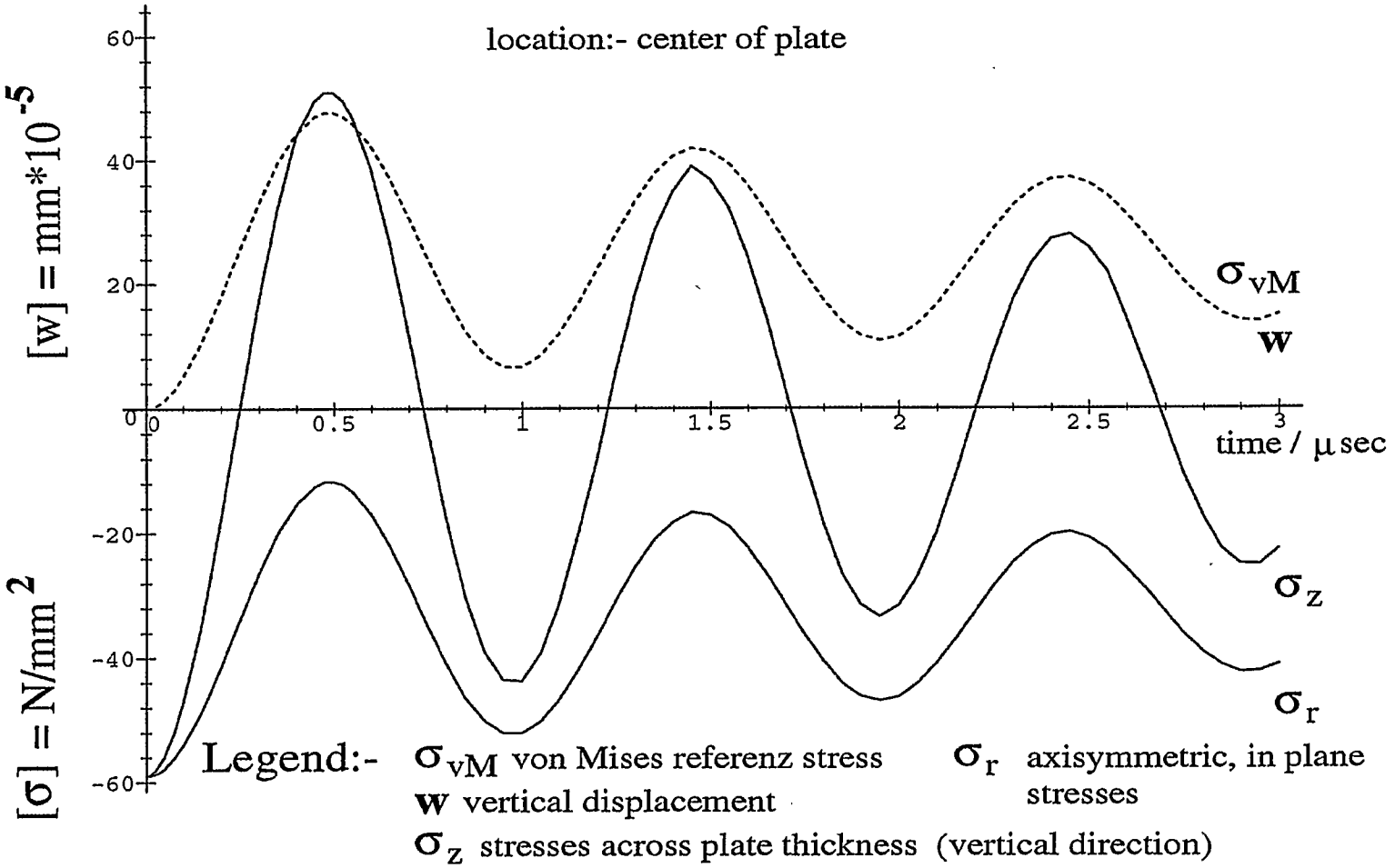

Legend:- σ_{vM} von Mises referenz stress
w vertical displacement
σ_z stresses across plate thickness (vertical direction)
σ_r axisymmetric, in plane stresses

International Workshop on the Technology and Thermal Hydraulics of Heavy Liquid Metals

Abstract

Oak Ridge Spallation Neutron Source (ORSNS) Target Station Design Integration

T. McManamy, R. Booth, J. Cleaves, T. Gabriel, J. Galombos, G. McNutt

The conceptual design for a 1- to 3-MW short pulse spallation source with a liquid mercury target has been started recently. The design tools and methods being developed to define requirements, integrate the work, and provide early cost guidance will be presented with a summary of the current target station design status. The initial design point was selected with performance and cost estimate projections by a systems code. This code was developed recently using cost estimates from the Brookhaven Pulsed Spallation Neutron Source study and experience from the Advanced Neutron Source Project's conceptual design. It will be updated and improved as the design develops. Performance was characterized by a simplified figure of merit based on a ratio of neutron production to costs. A work breakdown structure was developed, with simplified systems diagrams used to define interfaces and system responsibilities. A risk assessment method was used to identify potential problems, to identify required research and development (R&D), and to aid contingency development. Preliminary 3-D models of the target station are being used to develop remote maintenance concepts and to estimate costs.

International Workshop on the Technology and Thermal Hydraulics of Heavy Liquid Metals

Abstract

Oak Ridge Spallation Neutron Source (ORSNS) Target Station Design Integration

T. McManamy, R. Booth, J. Cleaves, T. Gabriel, J. Galombos, G. McNutt

The conceptual design for a 1- to 3-MW short pulse spallation source with a liquid mercury target has been started recently. A major design requirement has been to limit the total project cost to approximately $1B. The design tools and methods being developed to define requirements, integrate the work, and provide early cost guidance will be presented along with a summary of the current target station design status.

An initial design point was selected by a systems code using performance and cost estimate projections. This code was developed recently using cost estimates from the Brookhaven Pulsed Spallation Neutron Source study, experience from the Advanced Neutron Source Project's conceptual design, and other major projects. The code is being updated and improved as the design develops. Cost estimates were then made by the project team and compared with the systems code predictions. Corrections were made both to the code and to the detailed estimates.

The current design point is for a 1-MW facility, with one accumulator ring, one target station, and a beam energy of 1 Gev with a .5 microsecond pulse at 60 Hz. The target station would become the low power/low frequency station in a future upgrade to approximately 5 MW.

A work breakdown structure was developed, with simplified systems diagrams used to define interfaces and system responsibilities. A risk assessment method was used to identify potential problems, to identify required research and development (R&D), and to aid contingency development. Preliminary 3-D models of the target station are being used to develop remote maintenance concepts and to estimate costs.

The target station shielding will be designed for 1 MW operation. An iron shielding region is expected with an outside radius of approximately 5 m, and a height 5-m above and 3-m below the beam center. Approximately 1.5 m of concrete will surround the iron. The proton beam is horizontal, and the mercury target, with a

beryllium reflector, cryogenic hydrogen, and water moderators, will be contained within a 2-m diam safety vessel with shielding between the vessel and the reflector.

In the present concept, the mercury target and water-cooled jacket will be removed horizontally, in a manner similar to ISIS and as proposed for the ESS. The other activated components will be removed vertically and lowered by crane into the hot cells. Water cooling system components will be located under the beam room floor in an area with localized shielding, again similar to the ESS proposal.

ORSNS TARGET STATION
PRINCIPAL DESIGN REQUIREMENTS

- The design is being developed within a limit on the total project cost of approximately $1,000,000,000.
- The intent is to construct a facility operating at approximately 1 MW within the budget limit with a later upgrade to approximately 5 MW.
- The need to design to cost has required the development and use of a systems' code to make preliminary cost estimates for various options and to begin to understand how costs scale.
- The previous conceptual design work done by the other National Laboratories and the ESS team has been very helpful.
- At this time it appears that it is possible, but difficult, to meet the budgetary goal.

Oak Ridge National Laboratory

DESIGN INTEGRATION METHODS

- A Work Breakdown Structure (WBS) has been developed.
- Simplified process diagrams are used to help define interfaces. This was found to be valuable on the Advanced Neutron Source (ANS) Project and other major projects.
- A systems' cost and performance code was developed and is continuing to be updated. The initial costing information was done in cooperation with Brookhaven National Laboratory using information from their conceptual short-pulse spallation source. Other conventional facility cost basis information came from the ANS documentation and other major projects.
- Alternatives selected from the systems' code were estimated by the accelerator, target, and conventional facilities team members. Comparisons with the systems' code resulted in corrections both in the code and in some cases with the first detailed estimates.
- Three-dimensional mechanical models of the target station, site, and building geometry are being used to develop the layout and develop remote handling methods. The models have also been used to define the geometry for the neutronic model of the target assembly.

Oak Ridge National Laboratory

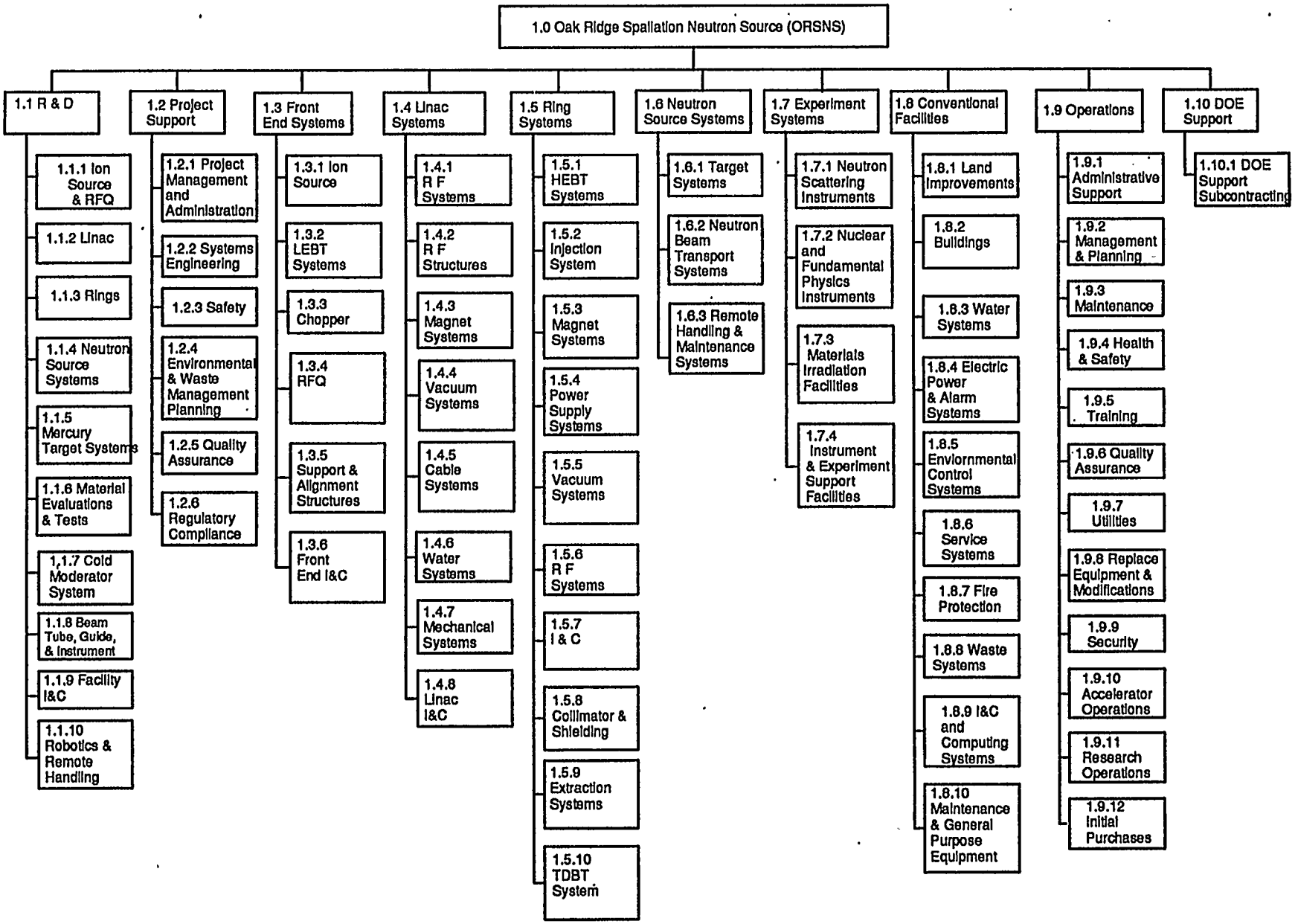
1.0 Oak Ridge Spallation Neutron Source (ORSNS)
1.1 R & D
1.1.1 Ion Source & RFQ
1.1.2 Linac
1.1.3 Rings
1.1.4 Neutron Source Systems
1.1.5 Mercury Target Systems
1.1.6 Material Evaluations & Tests
1,1.7 Cold Moderator System
1.1.8 Beam Tube, Guide, & Instrument
1.1.9 Facility I&C
1.1.10 Robotics & Remote Handling
1.2 Project Support
1.2.1 Project Management and Administration
1.2.2 Systems Engineering
1.2.3 Safety
1.2.4 Environmental & Waste Management Planning
1.2.5 Quality Assurance
1.2.6 Regulatory Compliance
1.3 Front End Systems
1.3.1 Ion Source
1.3.2 LEBT Systems
1.3.3 Chopper
1.3.4 RFQ
1.3.5 Support & Alignment Structures
1.3.6 Front End I&C
1.4 Linac Systems
1.4.1 R F Systems
1.4.2 R F Structures
1.4.3 Magnet Systems
1.4.4 Vacuum Systems
1.4.5 Cable Systems
1.4.6 Water Systems
1.4.7 Mechanical Systems
1.4.8 Linac I&C
1.5 Ring Systems
1.5.1 HEBT Systems
1.5.2 Injection System
1.5.3 Magnet Systems
1.5.4 Power Supply Systems
1.5.5 Vacuum Systems
1.5.6 R F Systems
1.5.7 I & C
1.5.8 Collimator & Shielding
1.5.9 Extraction Systems
1.5.10 TDBT System
1.6 Neutron Source Systems
1.6.1 Target Systems
1.6.2 Neutron Beam Transport Systems
1.6.3 Remote Handling & Maintenance Systems
1.7 Experiment Systems
1.7.1 Neutron Scattering Instruments
1.7.2 Nuclear and Fundamental Physics Instruments
1.7.3 Materials Irradiation Facilities
1.7.4 Instrument & Experiment Support Facilities
1.8 Conventional Facilities
1.8.1 Land Improvements
1.8.2 Buildings
1.8.3 Water Systems
1.8.4 Electric Power & Alarm Systems
1.8.5 Enviornmental Control Systems
1.8.6 Service Systems
1.8.7 Fire Protection
1.8.8 Waste Systems
1.8.9 I&C and Computing Systems
1.8.10 Maintenance & General Purpose Equipment
1.9 Operations
1.9.1 Administrative Support
1.9.2 Management & Planning
1.9.3 Maintenance
1.9.4 Health & Safety
1.9.5 Training
1.9.6 Quality Assurance
1.9.7 Utilities
1.9.8 Replace Equipment & Modifications
1.9.9 Security
1.9.10 Accelerator Operations
1.9.11 Research Operations
1.9.12 Initial Purchases
1.10 DOE Support
1.10.1 DOE Support Subcontracting

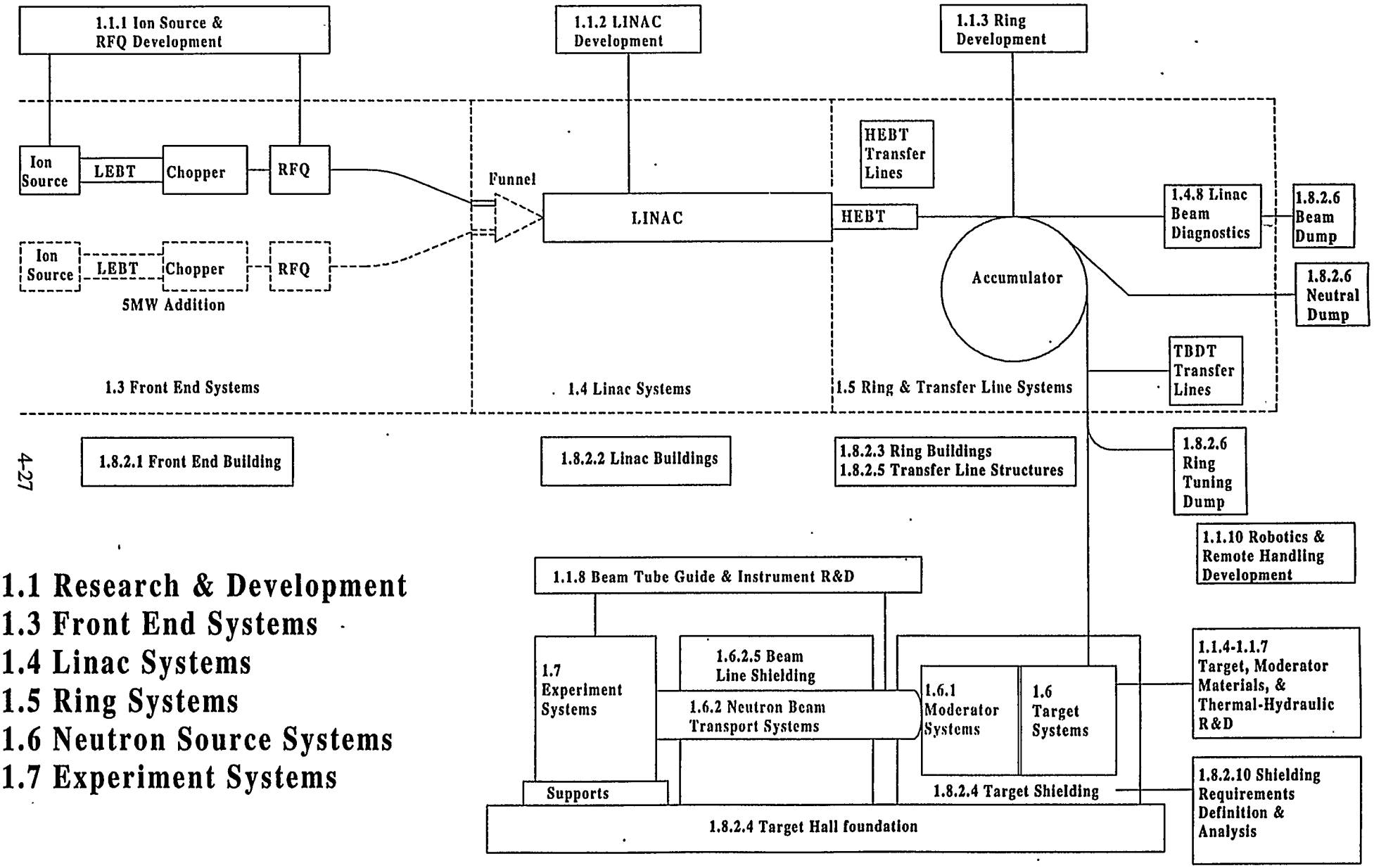

1.1 Research & Development
1.3 Front End Systems
1.4 Linac Systems
1.5 Ring Systems
1.6 Neutron Source Systems
1.7 Experiment Systems

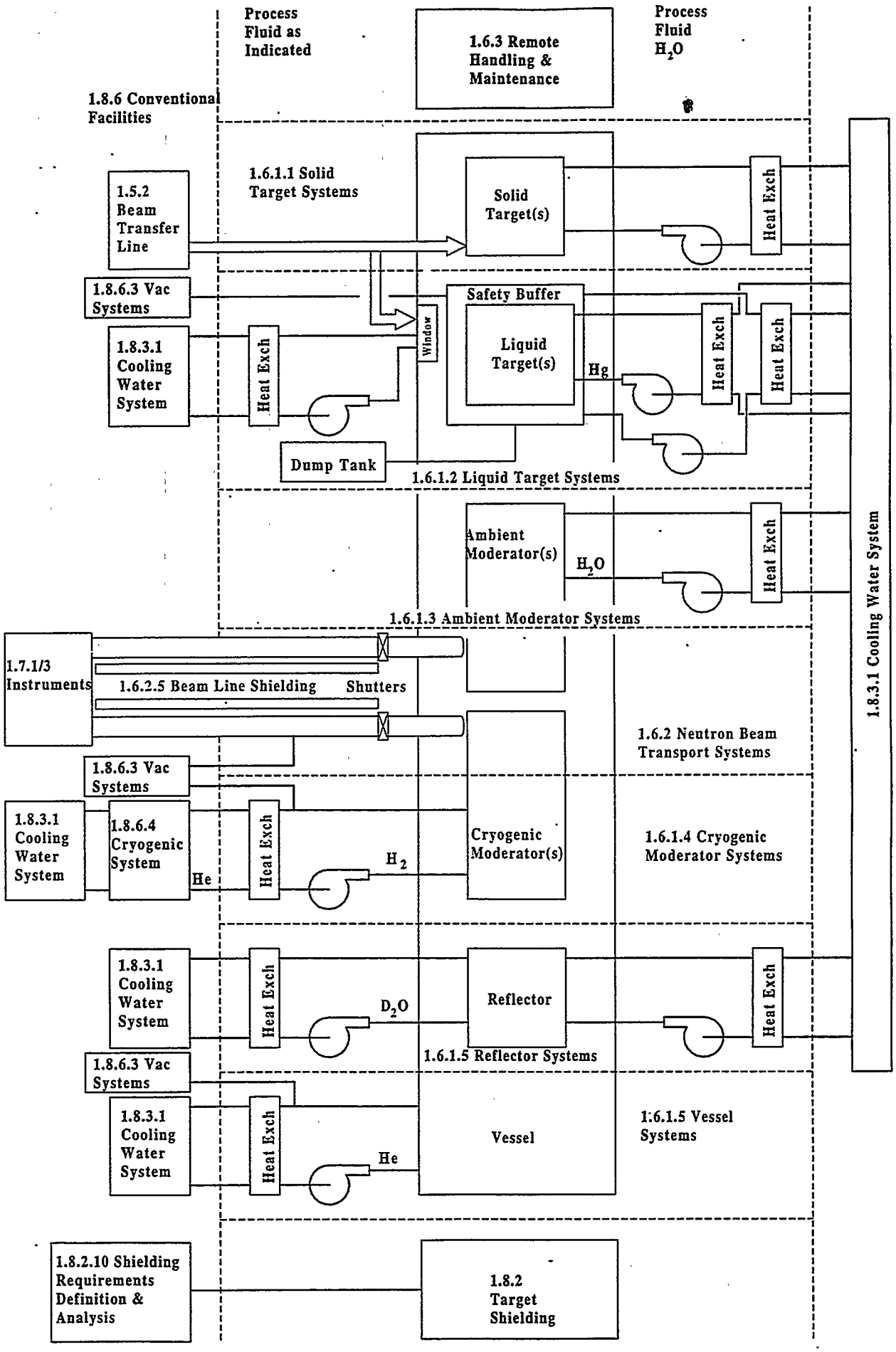

1.6 Neutron Source Systems

ORSNS COST MODEL

The ORSNS cost model integrates sub-system models for all project components

Sub-system Models:

- Accelerator (linac, accumulator ring, synchrotron ring)
- Neutrlon source (target, moderators, instruments)
- Conventional facilities (buildings, plant services, power, ...)
- Other project aspects (R&D, project support, operations, and pre-ops)
- Cost - incorporates input from all other modules

Tools:

- Interactive driver shell
- Optimization
- Risk analysis

Uses:

- Quick cost estimates of alternate design
- Trade studies to indicate trends

Oak Ridge National Laboratory

Design to Cost Model

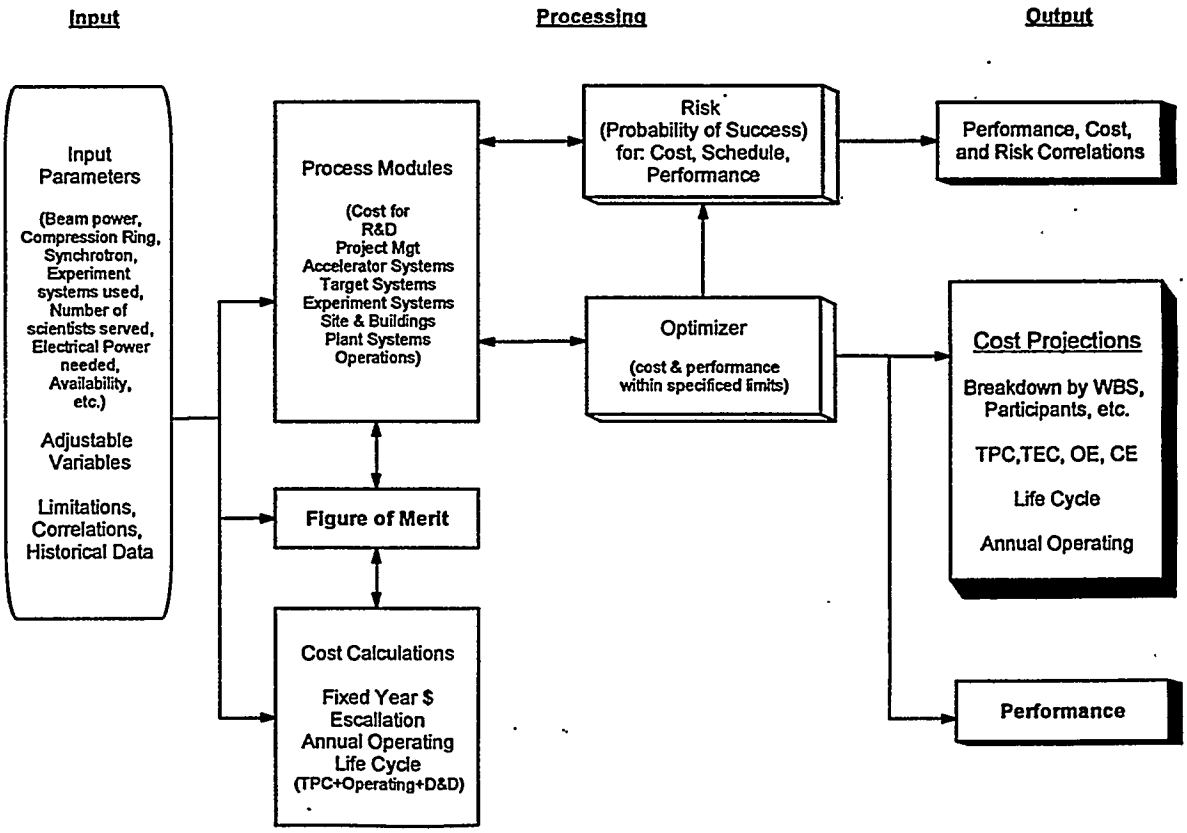

Design to Cost Model

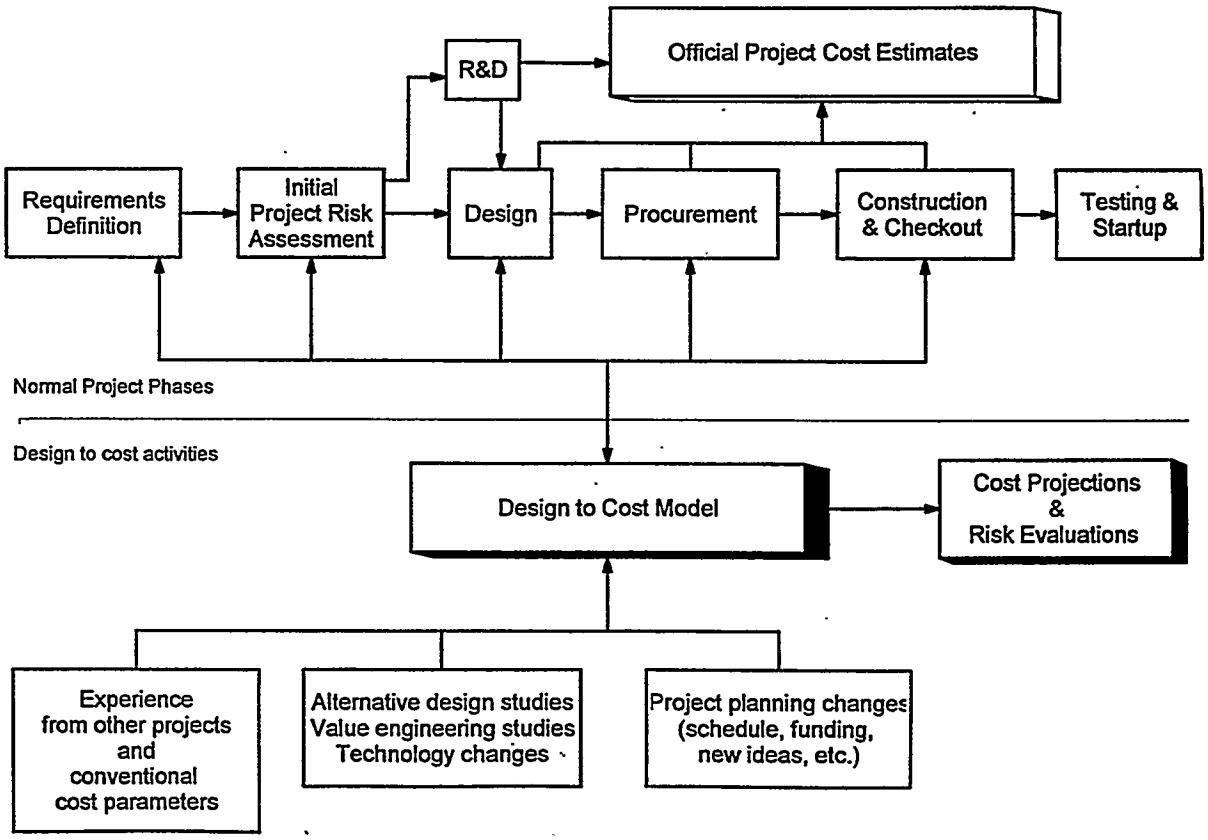

COST OPTIMIZATION EXAMPLE: MINIMUM COST vs. BEAM POWER

Typical problem formulation - accumulator ring option

Fixed configuration, modeling assumptions

- Ion source current, particle loss fractions, ...
- Ring repetition rate (60 Hz)
- Number of rings, number of target stations, ...

Variable input quantities (may be bounded):

- Linac length, gradient, duty factor
- Ring circumference

Constraints on calculated quantities

- Ring filling fraction
- Ring injection time
- Tune shift
- Dipole field limit
- Fixed beam power

Figure-of-merit:

- Minimum cost

Oak Ridge National Laboratory

Cost Optimization Example: Minimum Cost vs. Beam Power

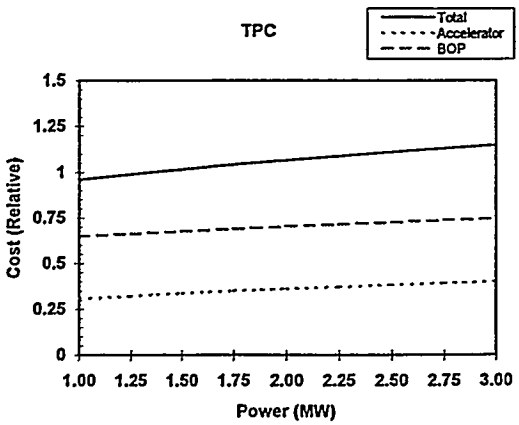

Minimum Cost vs. Power

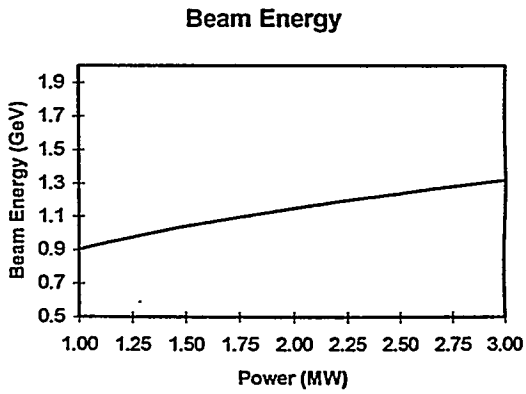

Beam Energy for Minimum Cost

Risk Analysis Example: Cost Uncertainty

- Input: Probability distributions for the cost contingency of all level 2 WBS elements
- Calculate: Probability distribution for the TPC (Total Project Cost).

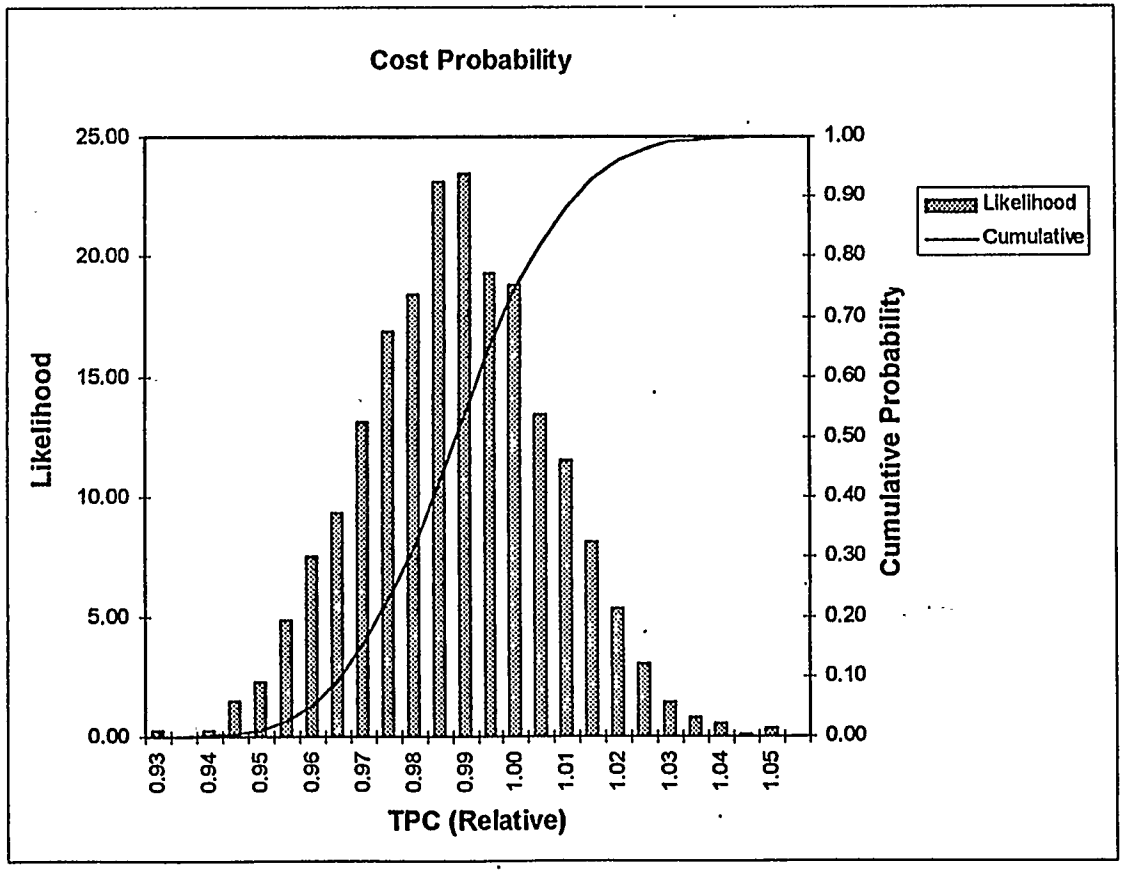

INITIAL OPERATING PARAMETERS

(These are not final but are our best current estimates)

- PROTON BEAM - 1 MW, 1.0 Gev, 60 Hz, .5 micro-second/pulse
- TARGET STATION - One station with shielding for 1 MW. This station will become the low power/low frequency station in an upgrade.
- TARGET TYPE - Liquid Mercury. Potential advantages vs. water-cooled solid target:
  - Increased neutron production
  - Lower decay heat and activation
  - Possible reduction in waste handling
  - Experience for use in a high power upgrade

  Solid target possible backup.
- MODERATORS - 1 liquid hydrogen, 1 ambient light water. Upgrade to 2 hydrogen and 2 light water at each target station.
- NEUTRON BEAM LINES - 18 total per target station, with 4 fully functional at startup
- SCATTERING INSTRUMENTS - Four at startup.
  - High Resolution Powder Diffractometer
  - Two similar to the ISIS MARI instrument
  - One crystal diffractometer similar to the ISIS IRIS instrument

Oak Ridge National Laboratory

PRELIMINARY TARGET STATION CONFIGURATION

- Horizontal Proton Beam
- Liquid Mercury Target
- Beryllium inner reflector with heavy water cooling similar to ISIS - approximately 1m diameter
- An outer 2 m diameter water-cooled reflector/shield - iron or nickel
- An outer 2 m diameter safety vessel with neutron beam windows.
- Bulk shielding with iron from 1m radius to 5m radius, and from 3m below beam center to 5m above beam center. Additional 1.5m concrete shielding outside iron.

Oak Ridge National Laboratory

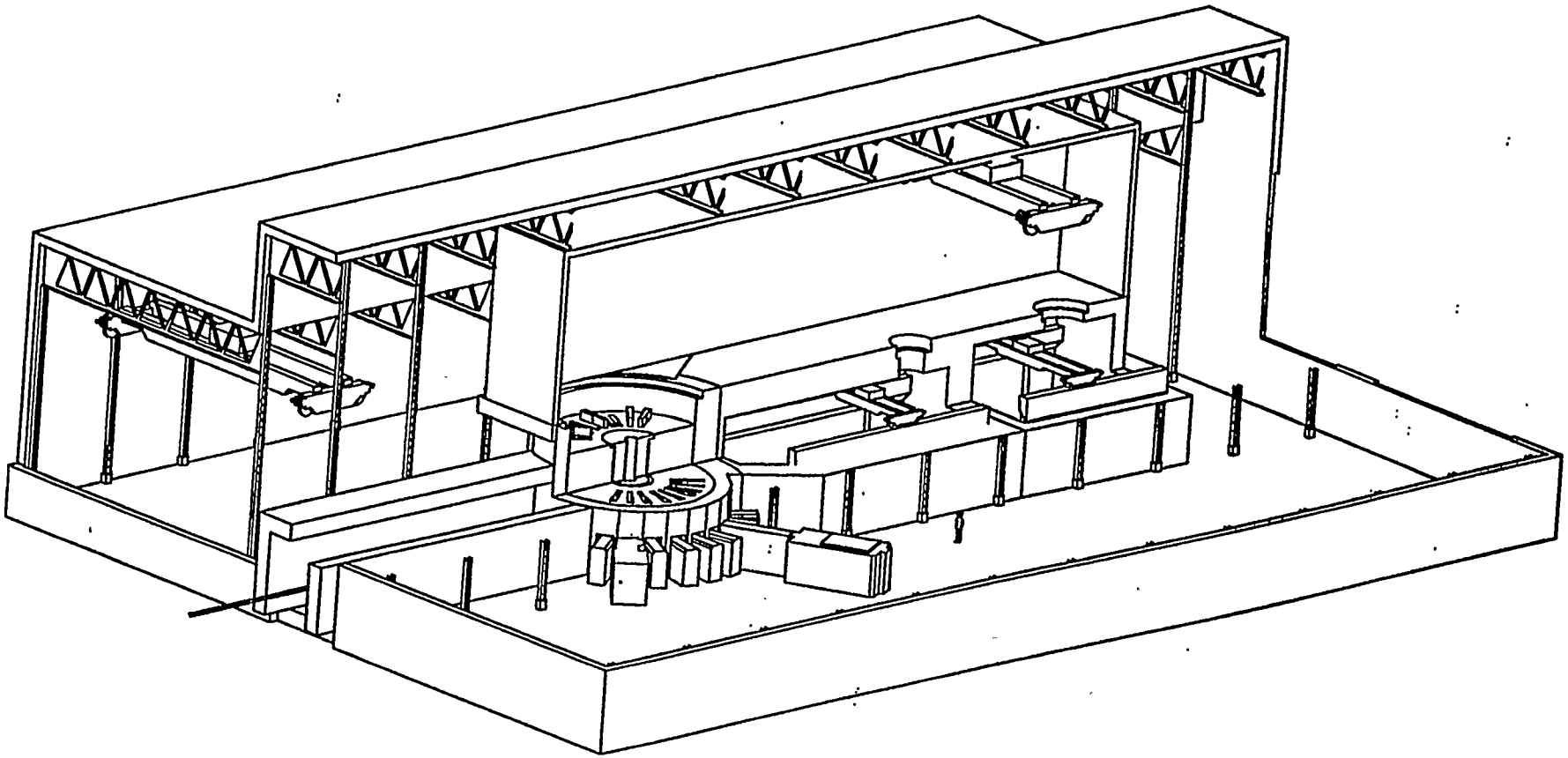

Oak Ridge Spallation Neutron Source
Target Facility

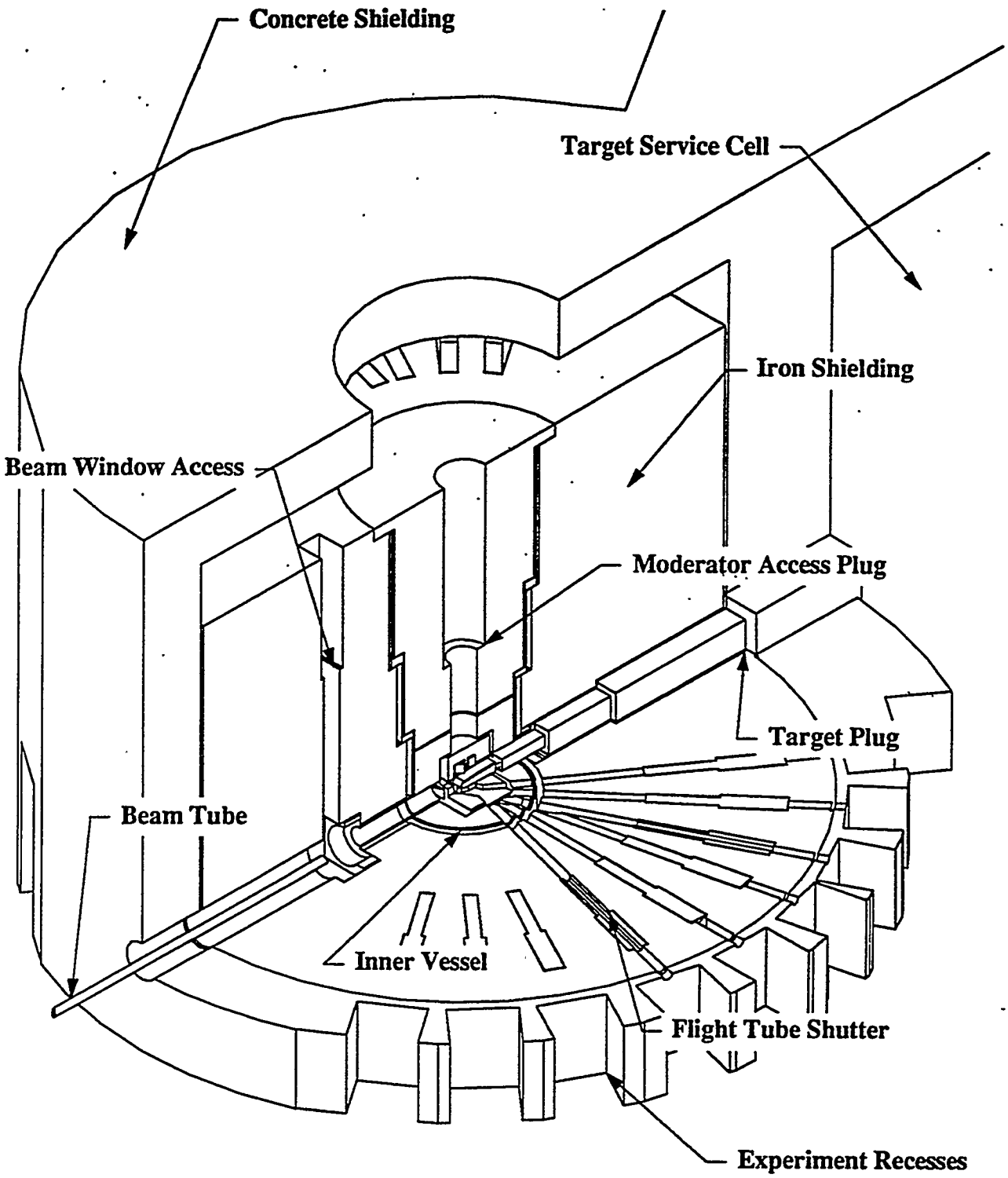

ORSNS Target Assembly

PRELIMINARY TARGET PARAMETERS

- Initial configuration similar to the ESS target
- Separate water-cooled mercury vessel and safety vessel
- 316 SS likely choice for structural material
- Relatively low temperature Mercury loop - 80° to 110°C

Oak Ridge National Laboratory

ORSNS
Liquid Target System Diagram

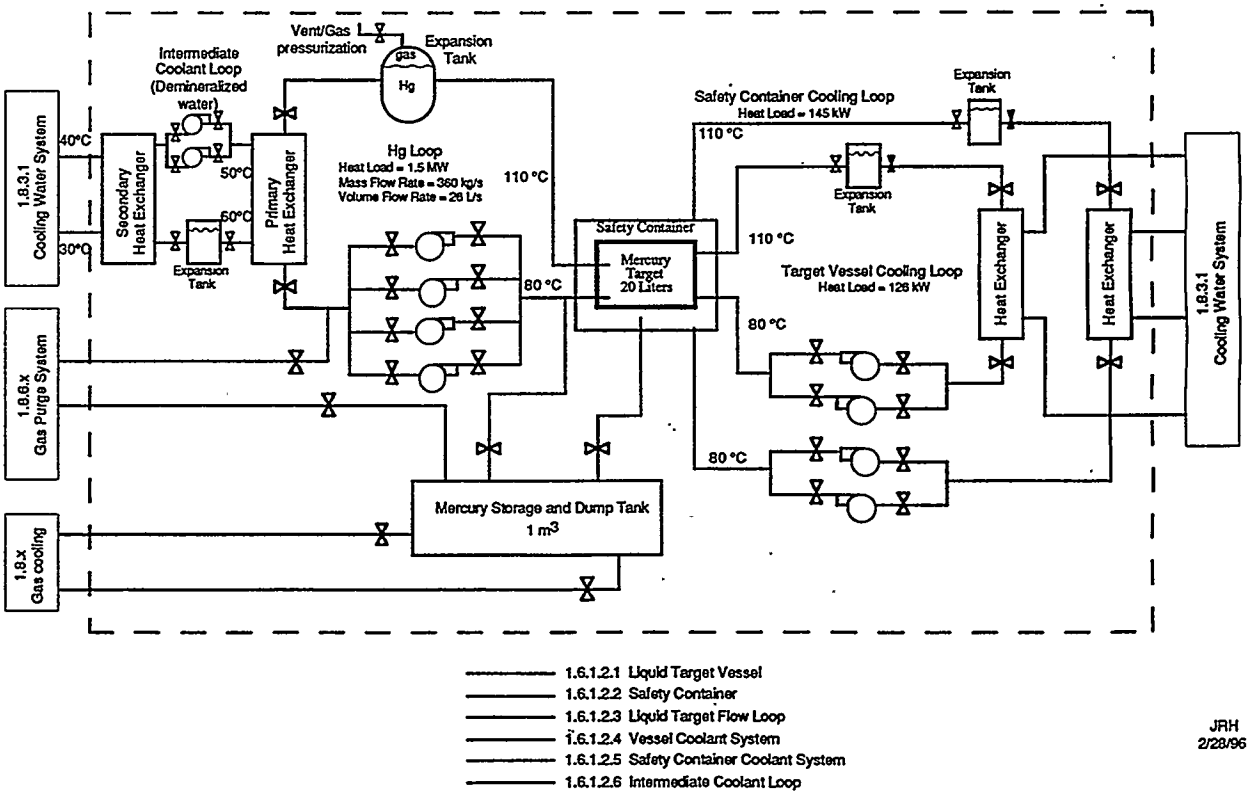

JRH
2/28/96

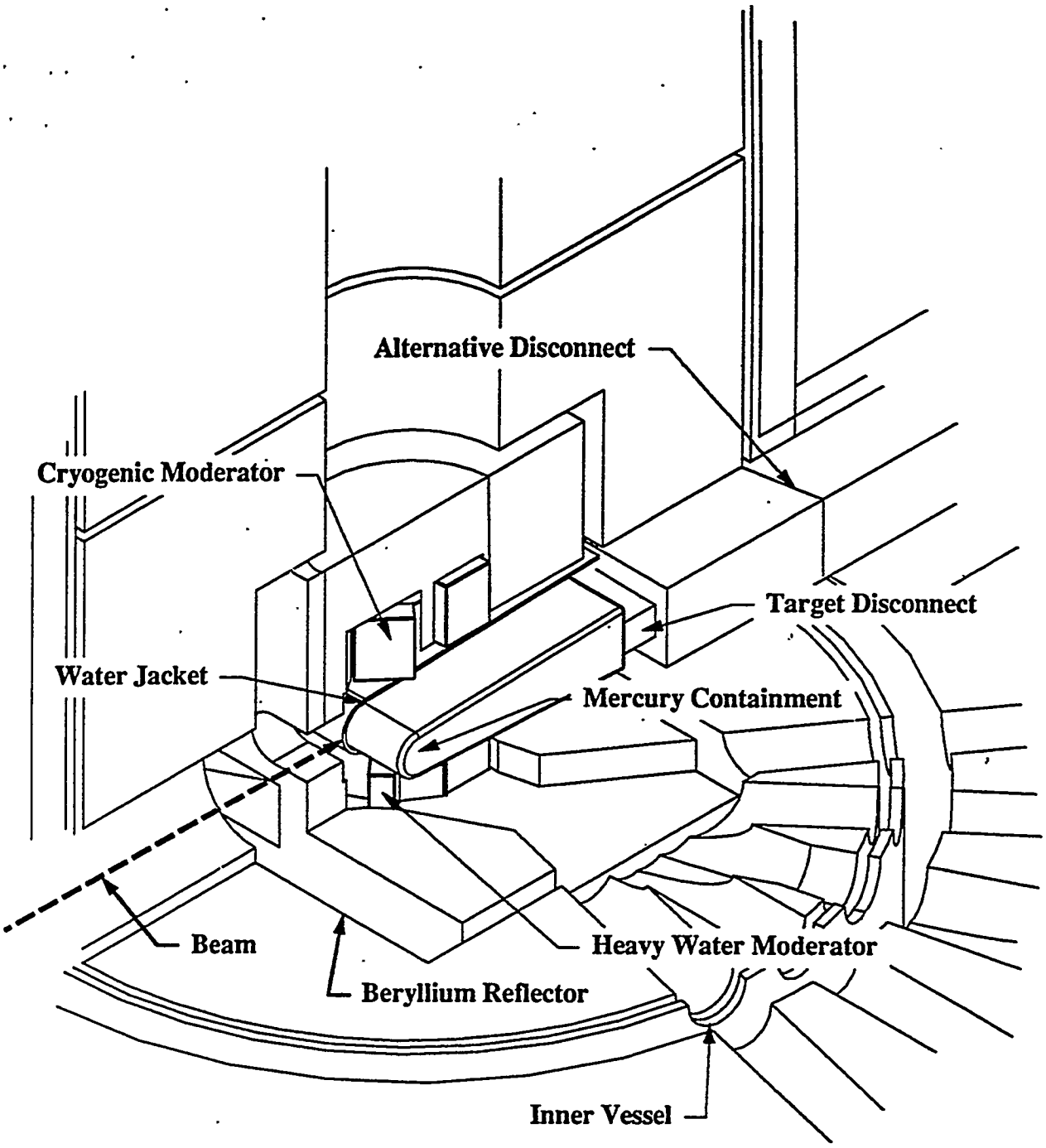

ORSNS
Target Assembly

10b

ORSNS
REMOTE HANDLING PHILOSOPHY

- Avoid remote handling through use of alternative design solutions such as redundancy and local shielding.
- Incorporate ideas and design concepts from ISIS, ESS, PSI, and the LANL long pulse proposal.
- Design for efficient and rapid replacement of modular assemblies; rather than repairing components in-place.
- Plan availability of spares for all key replacement items (e.g., beam windows, shutter drives, and targets)
- Package components in modules with similar repair requirements and rates.
- Incorporate proven and conventional remote handling features to improve reliability and reduce cost.
- Minimize handling paths and procedures (i.e., most modules will be moved vertically with bridge cranes).

Oak Ridge National Laboratory

REMOTE HANDLING

- The design intent is to group components with similar replacement frequencies and where possible to replace activated components rather then to repair in place.
- The current layouts are based on the following component removal paths:
  - Mercury target and safety vessel - horizontal assembly similar to ISIS and ESS concept
  - Proton Beam Window - vertical using PSI type pneumatic seals for easy assembly/disassembly
  - Moderators - vertical with a plug assembly similar to Los Alamos Long Pulse Target Station concept
  - Inner reflector - vertical
  - Neutron Beam Windows - remove bottom 2m of the safety vessel and replace window assemblies in hot cell.
  - Shutters - vertical

Oak Ridge National Laboratory

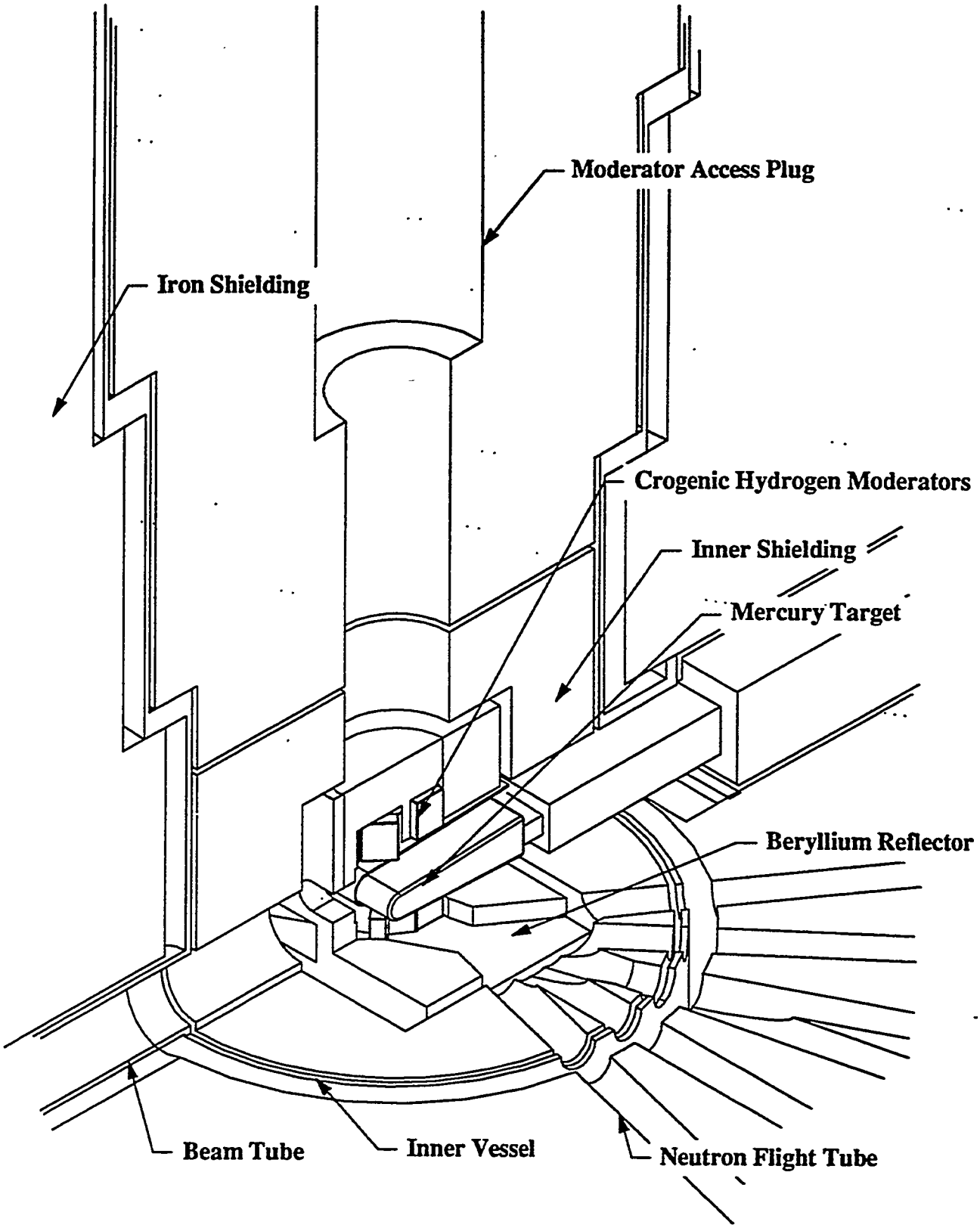

ORSNS
Target Station

10a

Oak Ridge National Laboratory

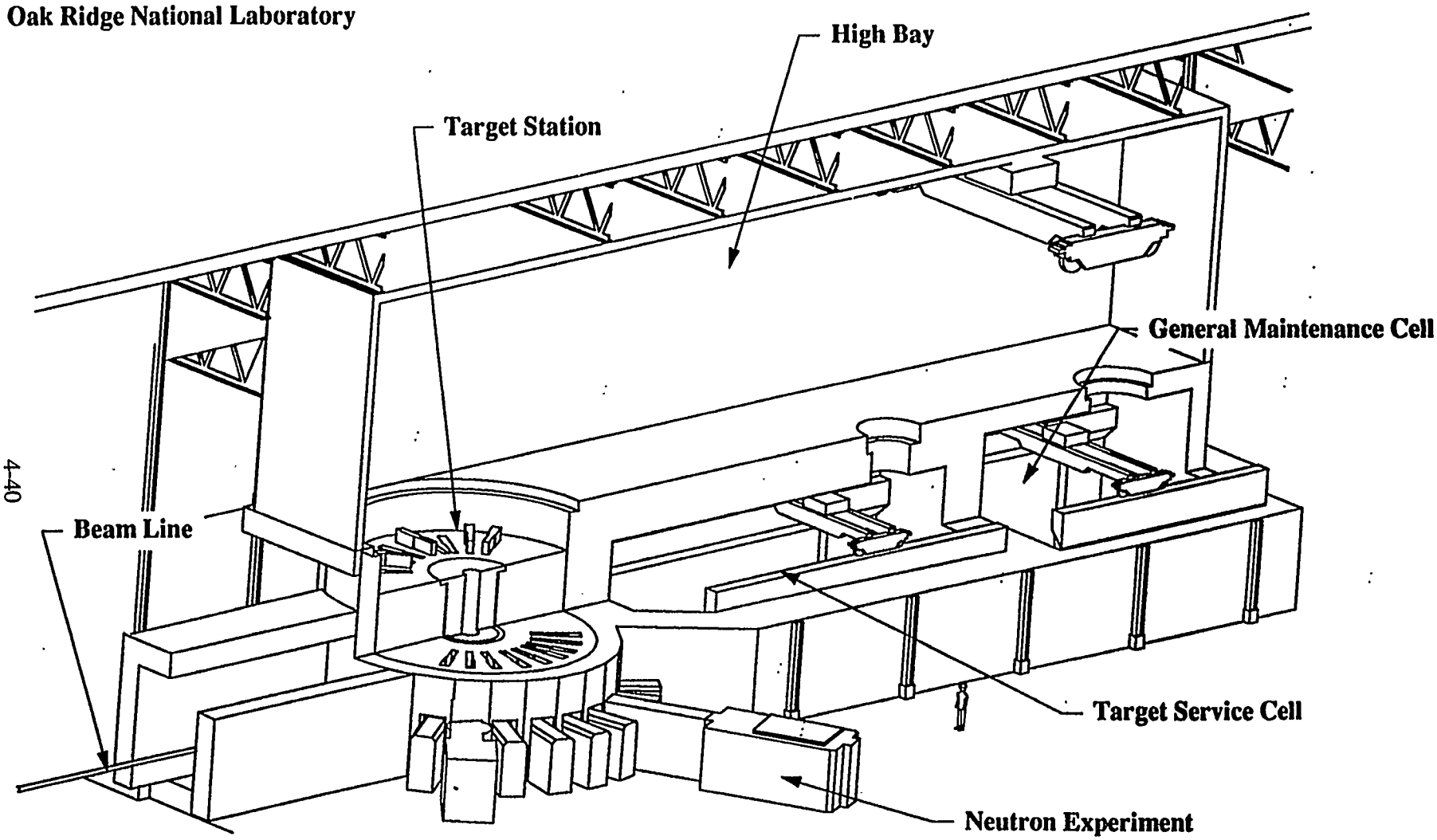

Oak Ridge Spallation Neutron Source
Target Facility

11L

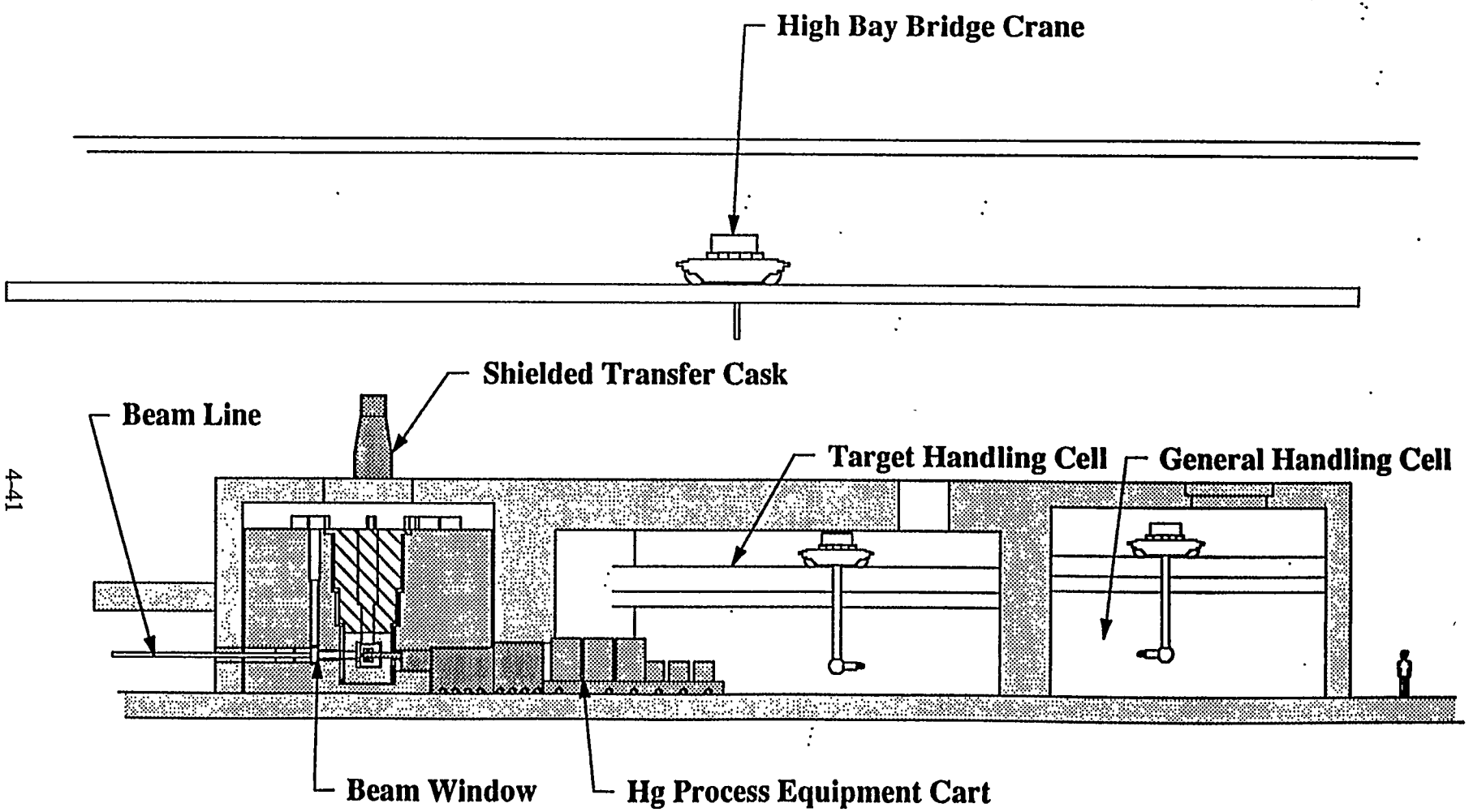

Oak Ridge Spallation Neutron Source
Target Station and Maintenance Cells

SNS-26

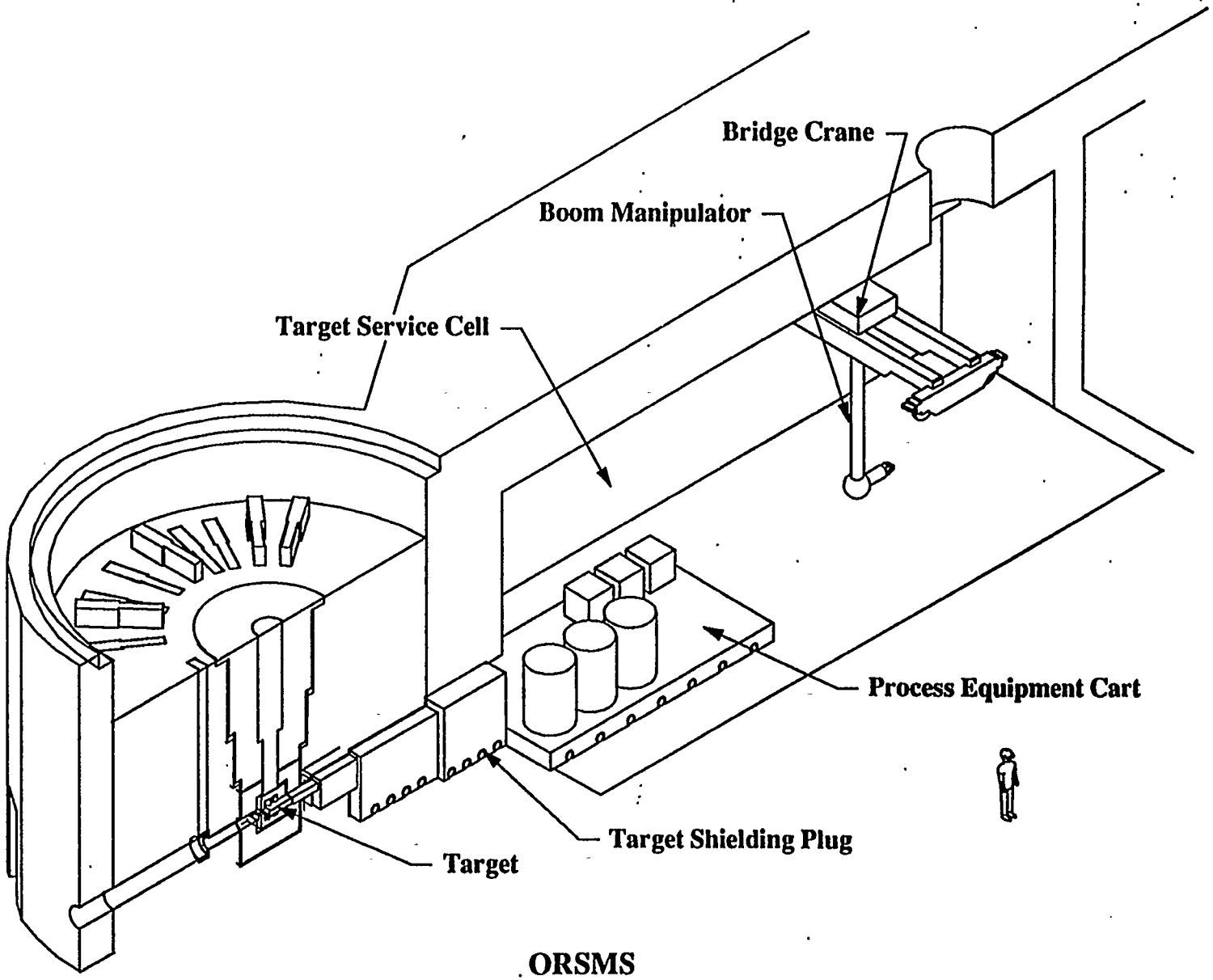

ORSMS
Target System
Target Assembly /Service Cell

C4

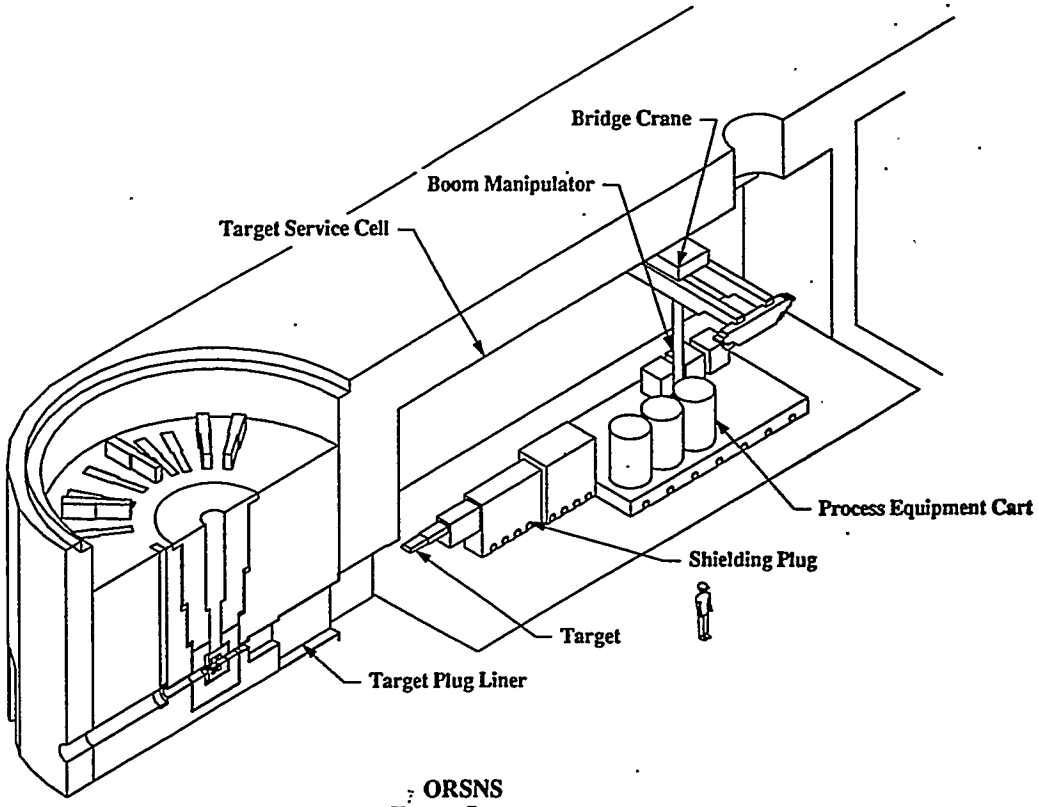

ORSNS
Target System
Target Assembly Retracted Into Service Cell

C3

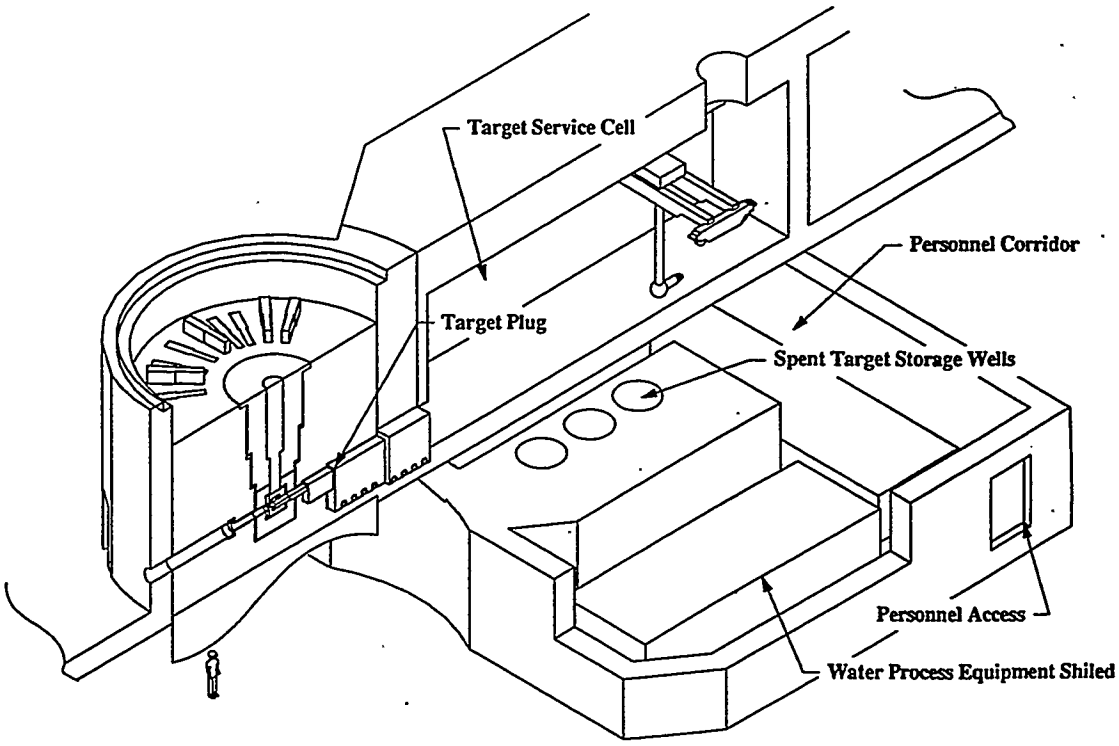

ORSNS
Target Facility
Cooling Water Vault

C6

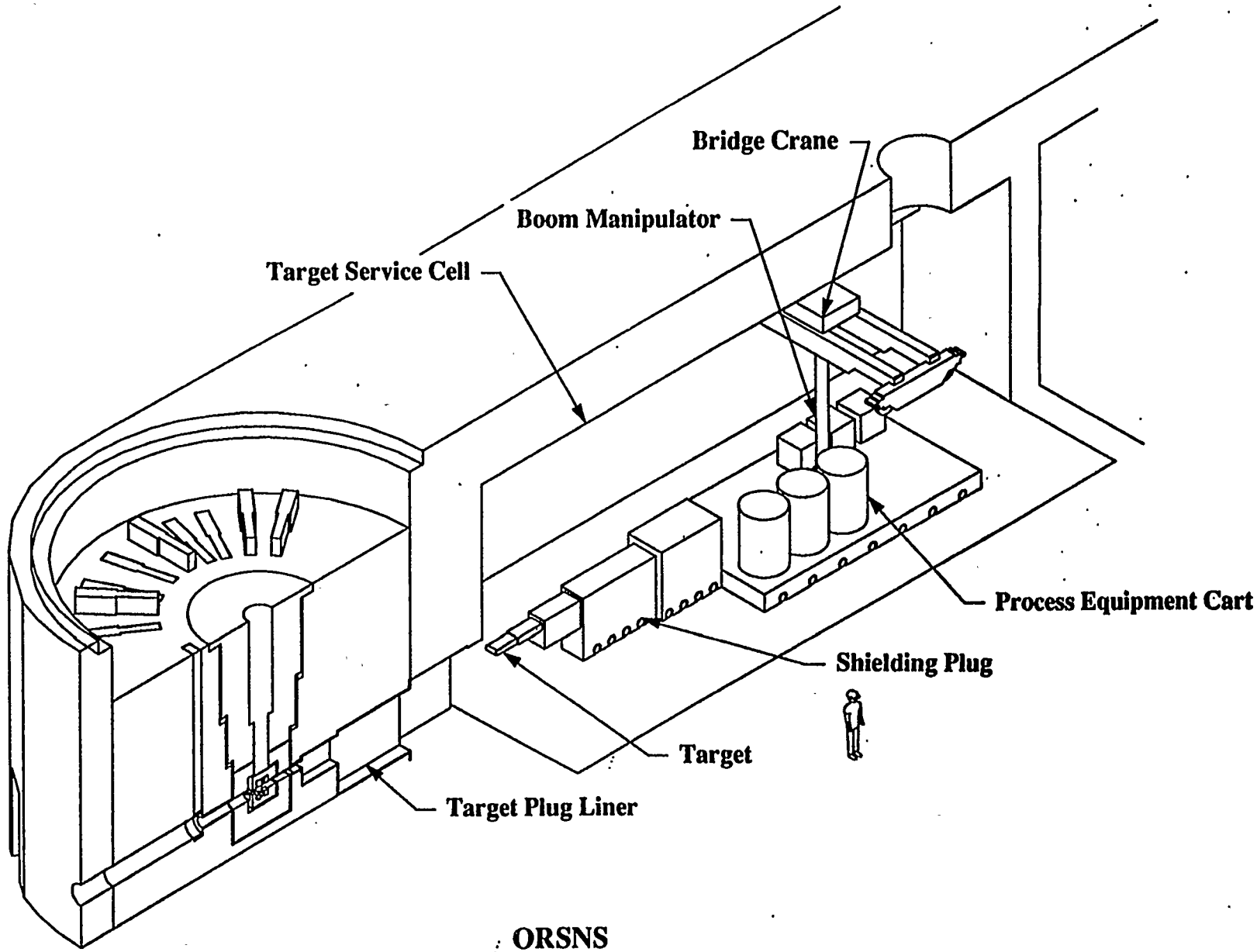

ORSNS
Target System
Target Assembly Retracted Into Service Cell

C3

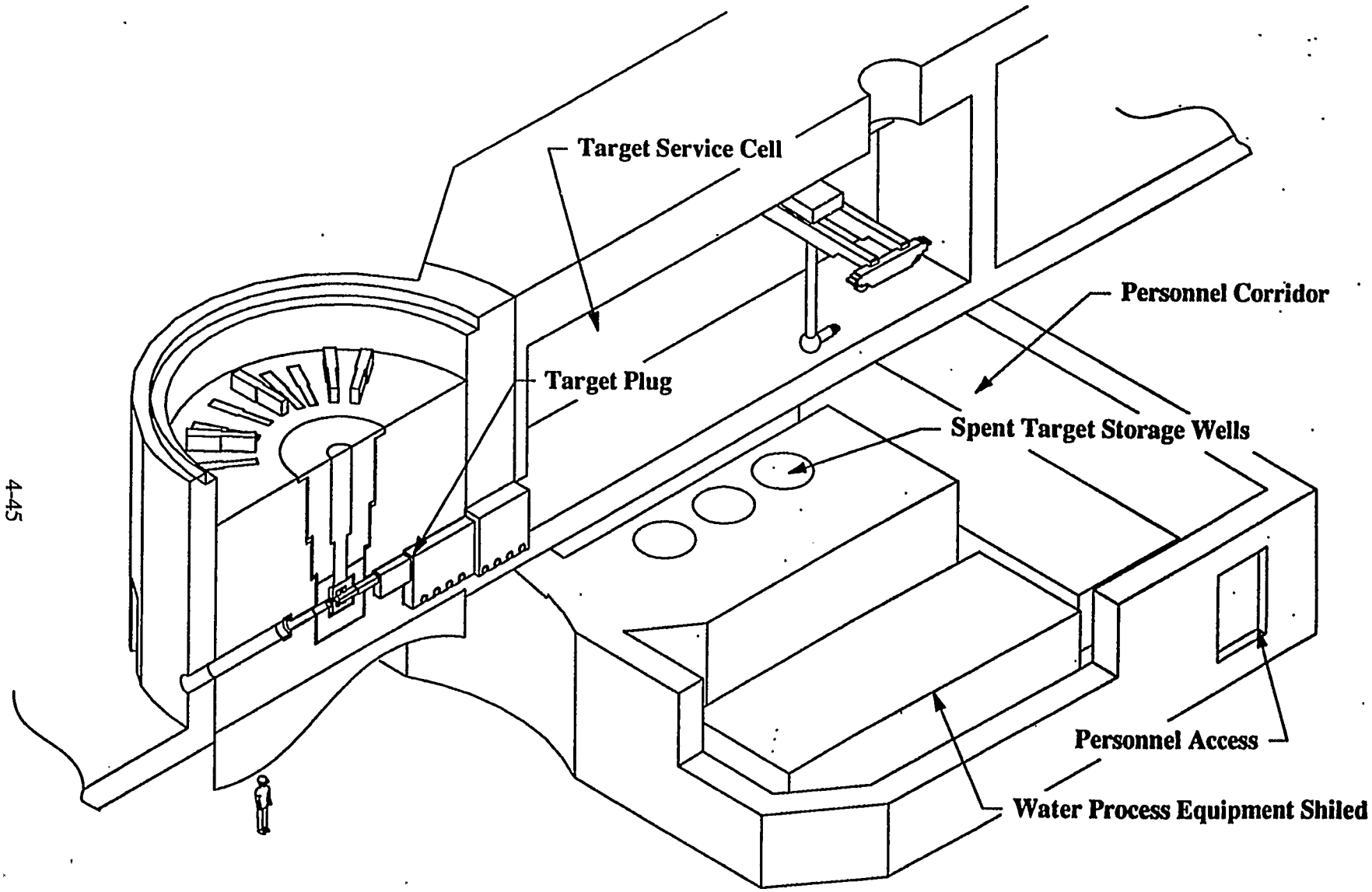

ORSNS
Target Facility
Cooling Water Vault

C6

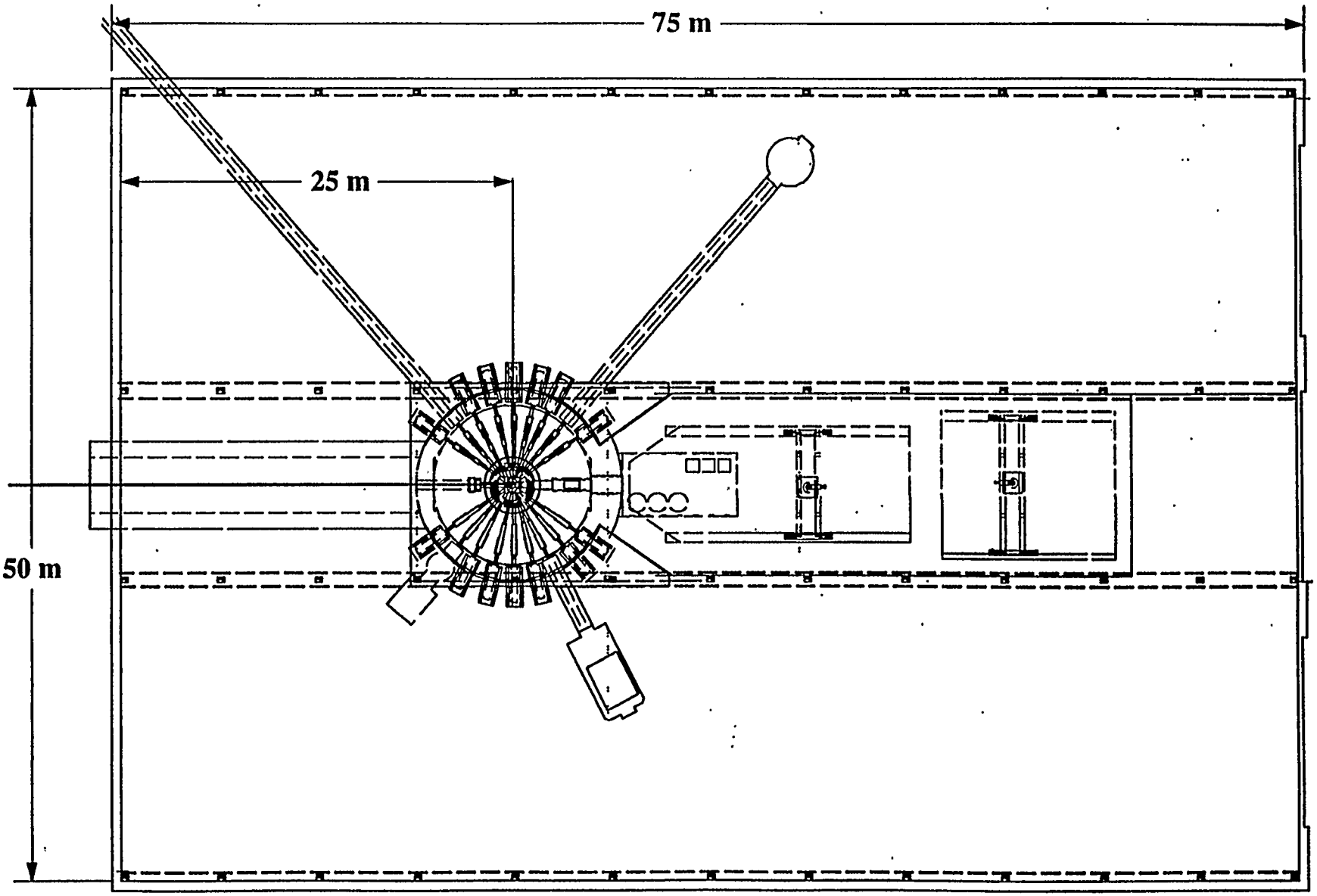

ORSNS
Target Facillity
Plan View

1

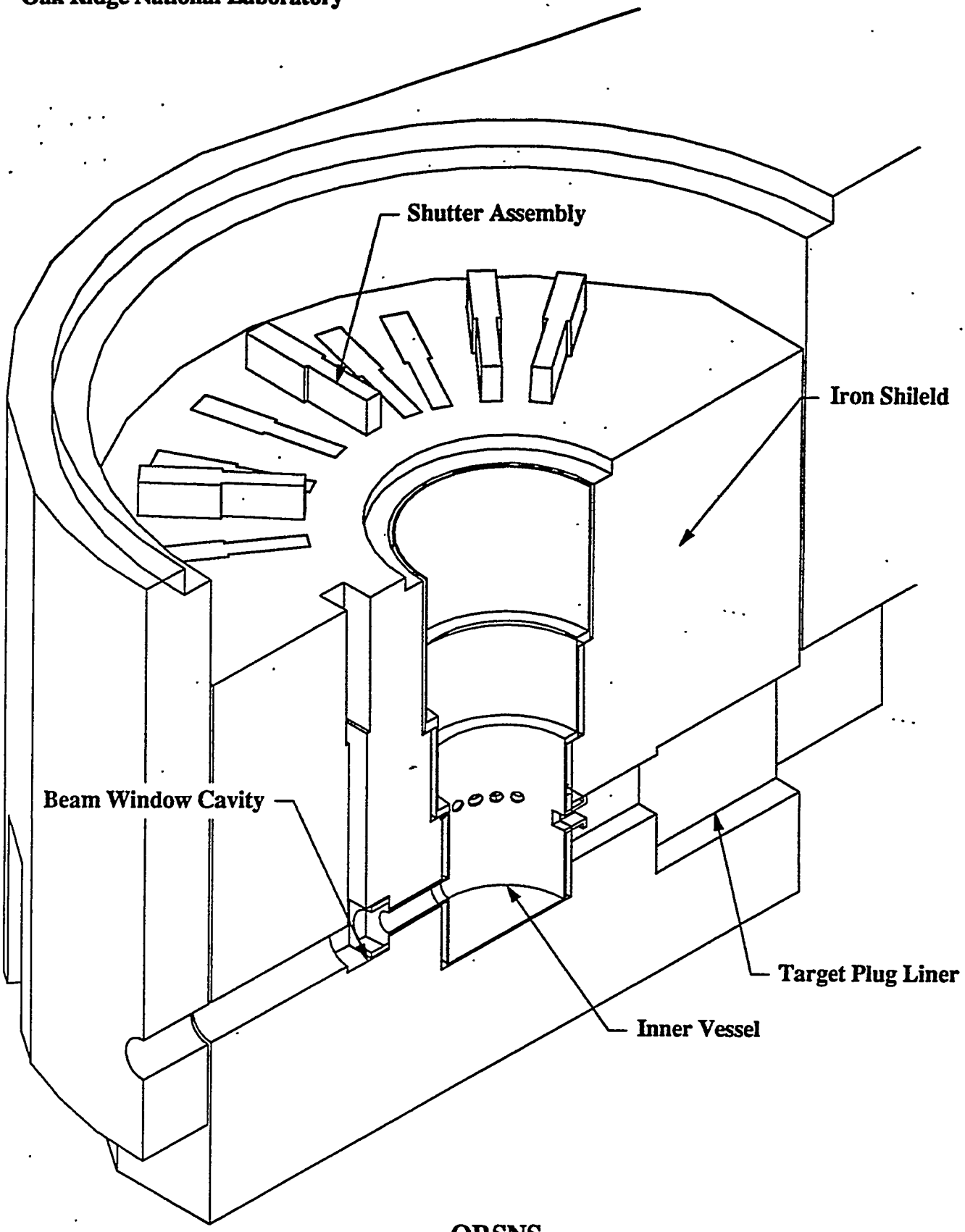

ORSNS
Target Assembly
Active Elements Removed

12

SESSION 5

Structural Materials: Corrosion and Radiation Damage (1)

Chairman
Y. Shubin

COMPATIBILITY OF STRUCTURAL MATERIALS WITH LIQUID BISMUTH, LEAD, AND MERCURY

JOHN R. WEEKS

Guest Senior Metallurgist

Department of Advanced Technology
Engineering Research and Applications Division
Brookhaven National Laboratory

Talk Prepared for the International Workshop on the Technology and Thermal Hydraulics of Heavy Liquid Metals

Schruns, Austria
March 25-28, 1996

bnl
aui

Compatibility of Structural Materials with Liquid Lead, Bismuth, and Mercury

John R. Weeks
Guest Senior Metallurgist
Brookhaven National Laboratory

During the 1950s and 1960s, a substantial program existed at Brookhaven National Laboratory as part of the Liquid Metal Fuel Reactor program on the compatibility of bismuth, lead, and their alloys with structural materials. Subsequently, compatibility investigations of mercury with structural materials were performed in support of development of Rankine cycle mercury turbines for nuclear applications. The present talk will review our understanding of the corrosion/mass-transfer reactions of structural materials with these liquid metal coolants.

Topics to be discussed include the basic solubility relationships of iron, chromium, nickel, and refractory metals in these liquid metals, the results of inhibition studies, the role of oxygen on the corrosion processes, and specialized topics such as cavitation-corrosion and liquid metal embrittlement. Emphasis will be placed on utilizing the understanding gained in this earlier work on the development of heavy liquid metal targets in spallation neutron sources.

OUTLINE

1. THE LMFR PROJECT [1952 (?) - 1962 (?)]

2. MATERIALS SELECTION AND PERFORMANCE

   a. Solubility-Driven Corrosion and Mass Transport
   b. Solubilities of Structural Materials in Bi, Pb, and Their Alloys
   c. Inhibition by Zr and Ti
   d. Role of Oxygen
   e. Liquid Metal Embrittlement
   f. Cavitation by Bi-Pb Coolants
   g. Solubilities and Corrosion by Mercury

3. AREAS FOR FUTURE WORK

---

bnl
aui

THE LIQUID METAL FUELED REACTOR CONCEPT

- Thermal Breeder
- Fuel: U_{233} Dissolved in Liquid Bismuth
- Blankets: $ThBi_2$ Slurry in Bi
- Molten Salt Processing Column
- Lead-Bismuth Secondary Loop to Transport Heat to Boiler
- Graphite Moderator
- Ferritic Steel Piping 2¼% Cr, 1% Mo Steel)

---

bnl
aui

Schematic Thermal Mass Transfer of Fe by a Liquid Metal

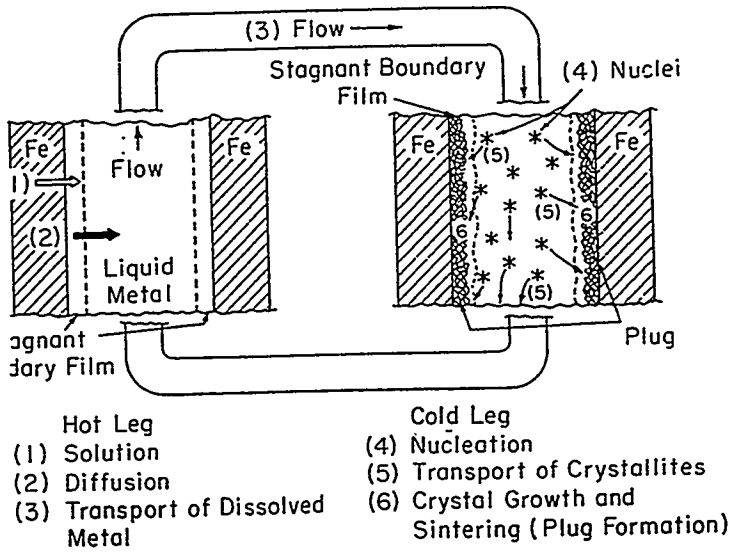

Corrosion and Mass-Transport is Solubility-Driven

---

bnl
aui

CORROSION RATE = α (S_o - S)

where
- **S_o is Solubility of Fe at the Temperature at any Point in the System**
- **S is the Concentration of Fe in Solution at that Point**
- **α is a Function of Velocity**

<u>Note</u>: **Corrosion Rate at T_{max} is a Function of Both T_{max} and T_{min} (Which Controls S).**

---

bnl
aui

SOLUBILITIES IN Bi, Pb, AND THEIR ALLOYS

- Useful Materials Form No Solid Alloys with Bi or Pb
- Monotectic Systems. Mostly BCC Alloys
- Nickel Forms Intermetallic Compounds with Hg, Bi and Pb; Therefore Do Not Use Steels Containing More Than Traces of Ni
- Solubilities of Fe, Cr, Cu, Ni, Ti, and Zr All Highest in Bi, Lowest in Pb, and Intermediate in their Alloys
- Decrease is Approximately Linear on a Plot of Log Solubility vs. % Pb
- Highest Melting Metals do not Dissolve in Bi or Pb
- Mutual Solubility Effects Occur (Fe + Cr in Bi)
- Cr is more Soluble than Fe in Heavy Liquid Metals

bnl
aui

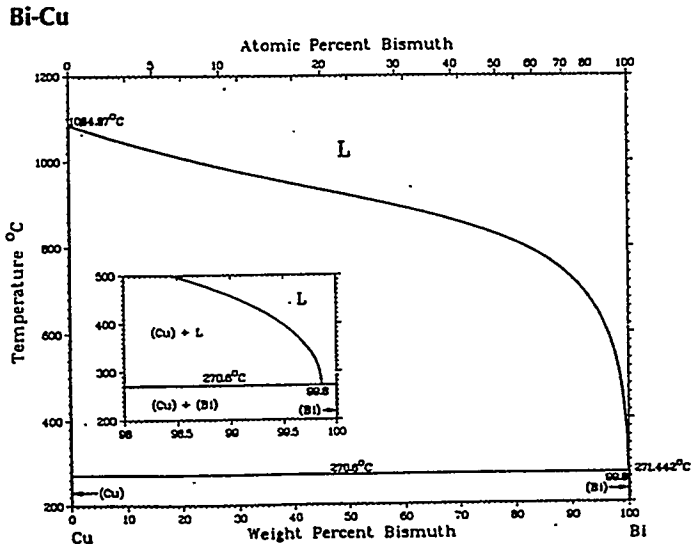

Typical Monotectic System (C_u - B_i)

---

bnl
aui

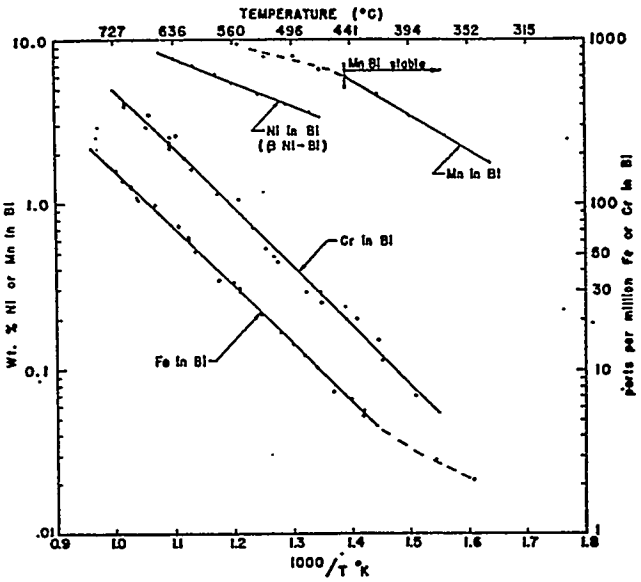

Solubility of Iron, Chromium, Nickel and Manganese in Bismuth

---

bnl
aui

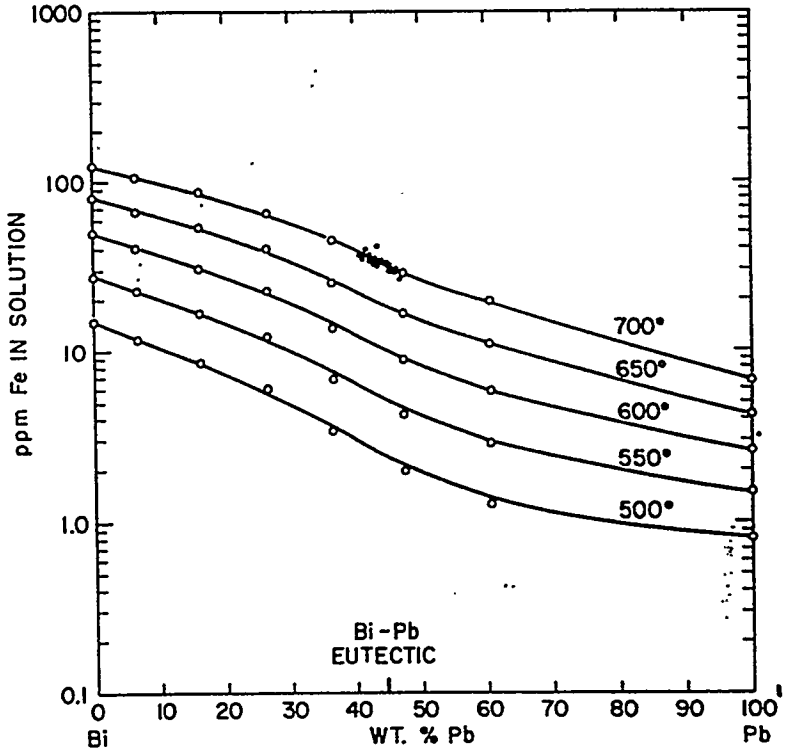

Isotherms of the Ternary Fe-Bi-Pb Liquidus

---

bnl
aui

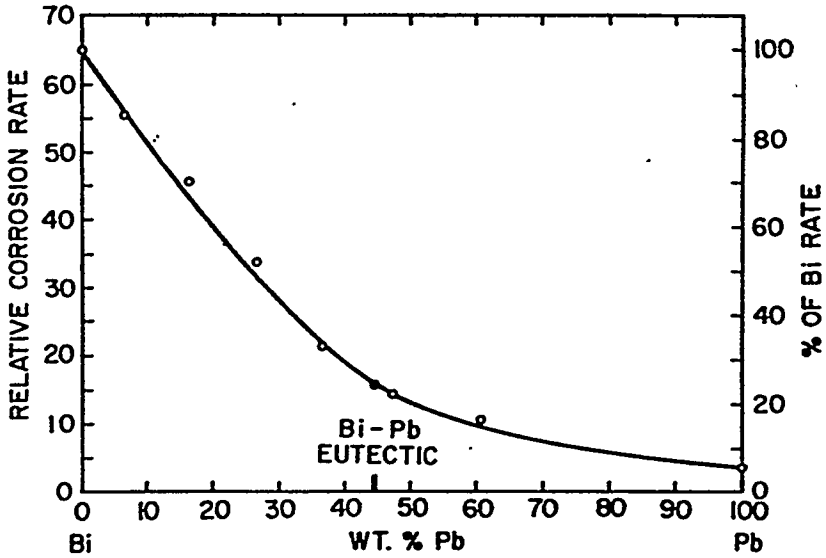

Relative Corrosion Rates of Steels in Bi-Pb Alloys at 650 to 500 C ΔT.
R = α(ΔS). Calculated from Solubility Data

---

bnl
aui

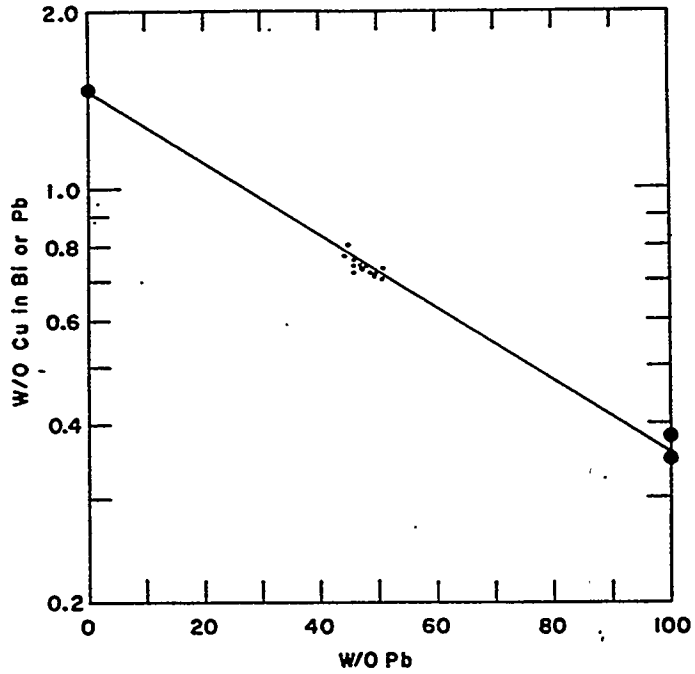

Data on the Cu-Bi-Pb Liquidus

---

bnl
aui

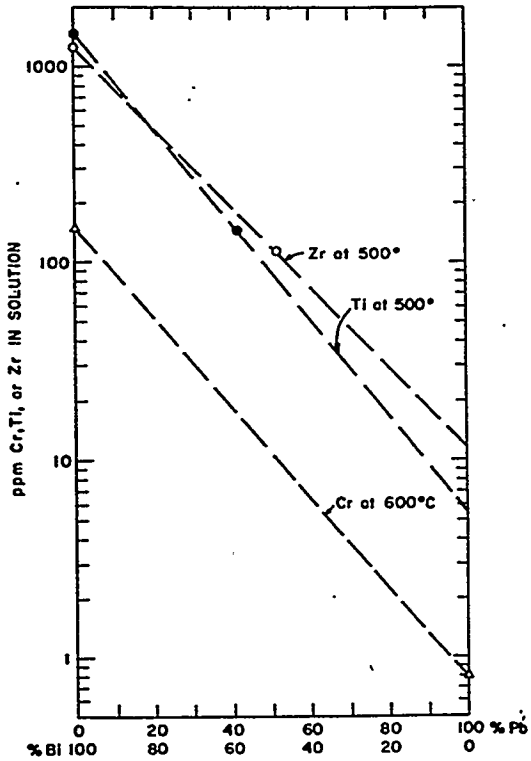

Estimated Liquidus for Cr, Zr, and Ti in Bi-Pb Alloys

---

bnl
aui

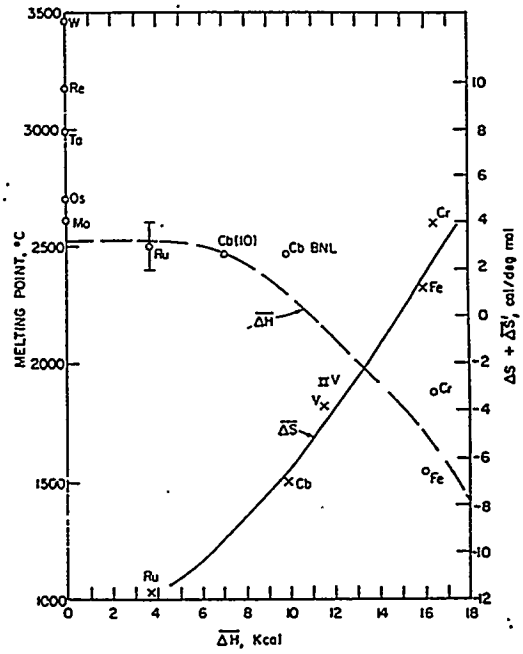

Relationship between Thermodynamic Properties and Melting Point of High-Melting Point Metals

bnl aui

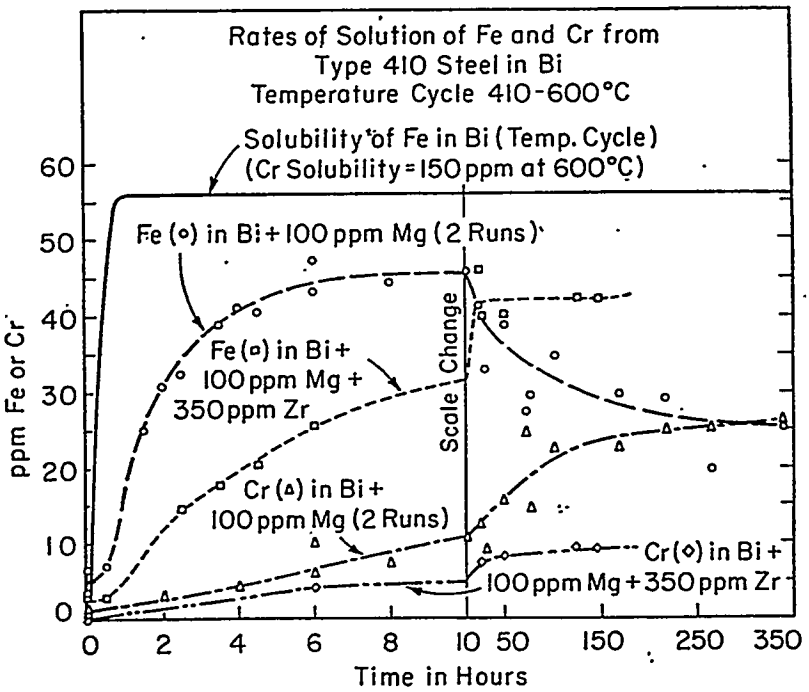

Rate of Solution of Iron and Chromium from Type 410 Steel into Bismuth at 600°C (1110 °F)

bnl aui

INHIBITION OF CORROSION OF STEEL BY Bi-Pb ALLOYS

- Zr and Ti are Both Effective
- Ti Developed at GE for Mercury Systems
- Zr (Which is a Fission Product) Used at BNL
- Zr or Ti React with Steel to Form Surface Layer of, First Zr-Ti-Fe Compound, Later ZrC and ZrN Develop
- Films Inhibit Both Dissolution and Precipitation
- Most Effective (in Bi) at $\Delta T < 100°C$
- Use in Combination with Mg as Deoxidant

---

bnl
aui

ROLE OF OXYGEN

- Oxides of Bi, Pb, and Hg Less Stable than Oxides of Fe or Cr
- No Acceleration of Corrosion or Mass Transfer Due to Oxygen
- Chromium Oxides Can Cause Misleading Results in Small Experiments
- Best to Control Oxygen by Mg Additions
    - Protects Inhibitors
    - Cleans Solid-Liquid Interface

---

bnl
aui

LIQUID METAL EMBRITTLEMENT BY Bi-Pb ALLOYS

- Occurs When Adsorption on the Solid Surface Reduces the Energy Required to Separate Atoms of the Solid to Create New Surfaces
- ΔH (From Solubility Curve) and γ_{SL} Both Reflect This Energy in Monotectic Systems
- $\Delta H/\gamma_{SL} = \overline{V}/d$,cm^2/gm Atom Solute
- Therefore, Low ΔH Suggests Low γ_{SL}, and an Embrittlement is Possible
- In Bi (See Viewgraph 13), Nb and Ru have Lowest ΔH
- Nb is Embrittled by Bi

---

bnl
aui

CAVITATION BY Bi-Pb COOLANTS

- High Density, Low Vapor Pressure
- Careful Design to Eliminate Sharp Corners
- Low Flow Rates

---

bnl
aui

Results from High Velocity Loops

Loop #	Material[a]	Temp. (Bulk) (°C) Max.	Temp. (Bulk) (°C) Min.	Temp. Film (°C) Max.	Temp. Film (°C) Min.	Additive Conc. Mg	Additive Conc. Zr	Additive Conc. U	Time of Test	Flow (gpm)	Remarks
HVL I											
Run 1	2¼Cr–1Mo	520	414	525	400	350	300	920	1026	1·20	No corrosion
Run 2	2¼Cr–1Mo	520	414	525	400	350	350	1000	1026	1·20	Cavitation pits in high velocity test section
Run 3	2¼Cr–1Mo	520	414	525	400	350	300	1000	1006	1·25	No cavitation
→ Run 4	2¼Cr–1Mo	544	417	550	400	350	250	1000	2591	1·1	Severe pits & mass transfer. Loop sectioned
Run 5	1¼Cr–½Mo (loop re-fabricated)	520	445	525	428	350	250	1000	4000[b]		No corrosion—some transfer after 4000 hr operation still in test (3/15/58)
HVL II											
Run 1	2¼Cr–1Mo	520	445	522	427	350	350	1000	7400[b]		Slight pit corr. in welds. Transfer detected after 2500 hr at ΔT. Loop still in operation 7000 hr.
Loop G											
Run 1	2¼Cr–1Mo	525	473	529	458	350	350	1000	938	4·0	Pt. corr. of 4–6 Cr.–1Mo welds. Corr. of AISI 410 SS.
Run 2	2¼Cr–1Mo	525	450	526	435	350	250	900	2500[b]	4·8	No corr. after 2500 hr.

[a] This is the major material of construction. The actual test section is a composite of many materials.
[b] Still in operation. Test time as of 3/15/58.

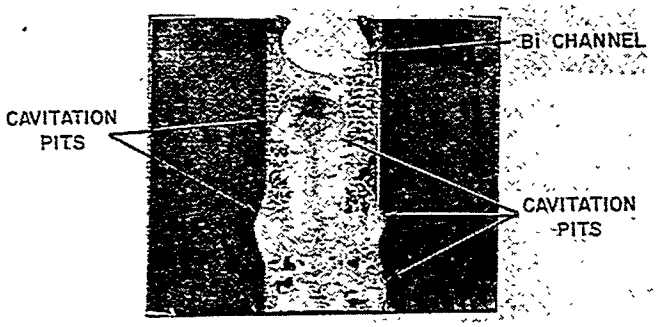

FIG. 15. Cavitation-erosion on downstream side of right angle bend in HVL I Run 2.

C. J. Klamut et al., "Material and Fuel Technology for an LMFR," *Progress in Nuclear Energy, Series IV, Vol. II—Technology Engineering and Safety*, Pergamon Press, New York, 1960, p. 433.

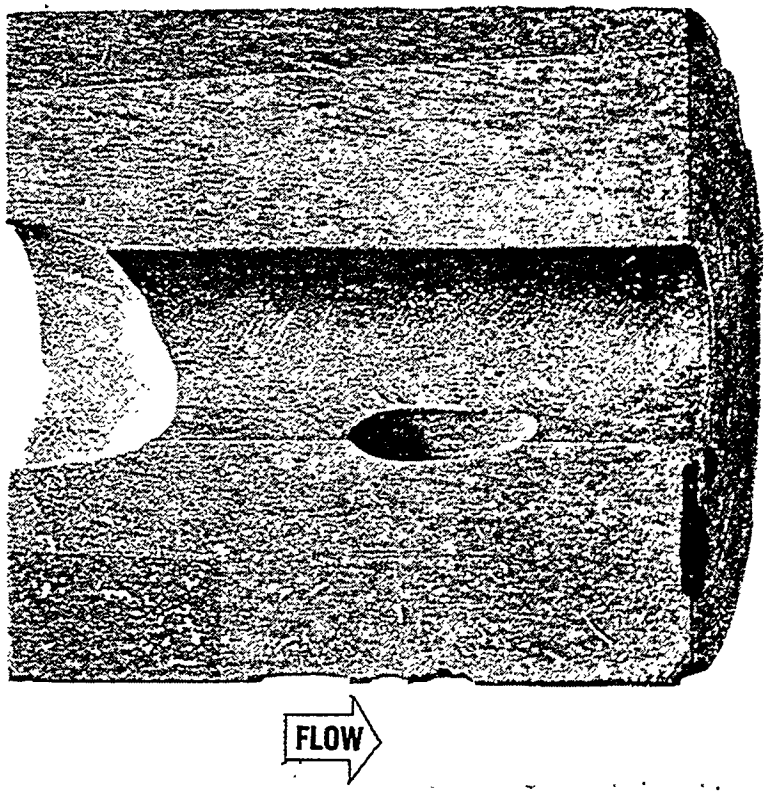

FIG. 17. Attack on annealed 2¼ chromium–1 molybdenum hot test specimen in HVL I Run 4.

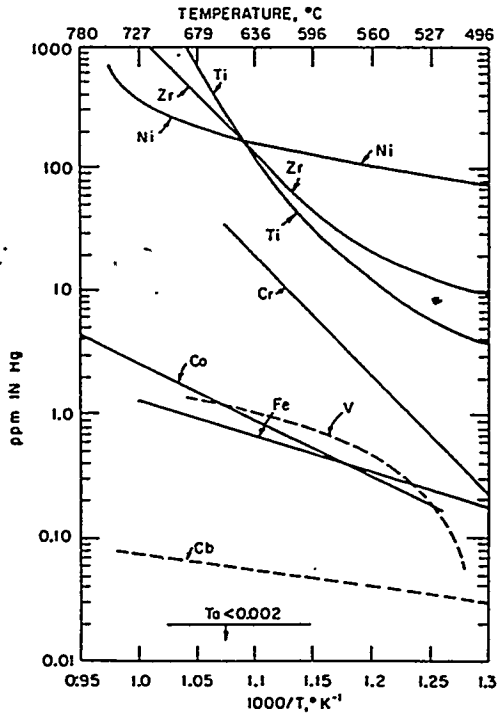

Liquidus Curves of all the Metals Studied Combined to Indicate Relative Solubilities of the Metals in Hg

bnl
aui

Relative Corrosion Rates at 600°C with 100°C Undersaturation

Metal	S_o 600°C (1000/T=1.145) (ppm)	S_o 500°C (1000/T=1.293) (ppm)	$R=\alpha\ (S_{600}-S_{500})$ $\alpha = 10^{(2)}$	R Normalized to $R_{Fe} = 1$
Fe	0.52	0.20	3.2	1.00
Cr	7.0	0.25	67.5	21.1
Ni	130	77	530	166
Co	0.56	0.12[1]	4.4	1.4
V	~0.8	~.005	~7.95	~2.5
Cb	~0.05	~0.03	~0.2	~0.06
Ta	<0.002	<0.002	→0	→0
Ti	47	3.7	433	135
Zr	50	~10	~400	~125

[1] Extrapolated 25°C
[2] For Convenience

bnl
aui

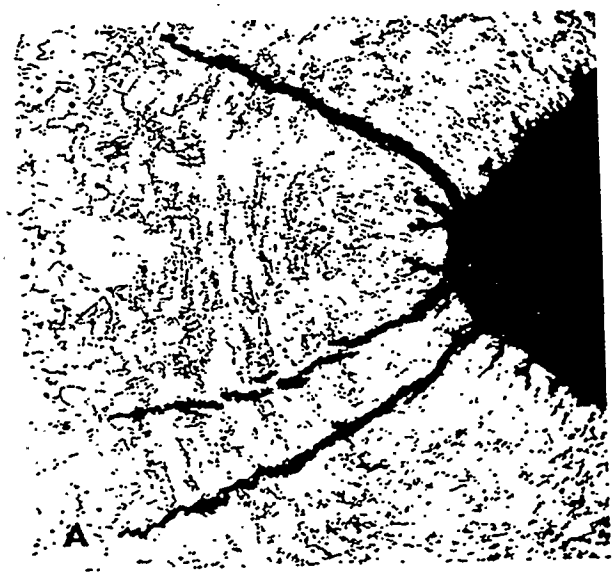

A. Longitudinal Section of Cb-1Zr U-Bend Specimen, Annealed 18 Hours at 1200°C Prior to Being Bent After Contact with Hg 1 Week at 760°C

---

bnl
aui

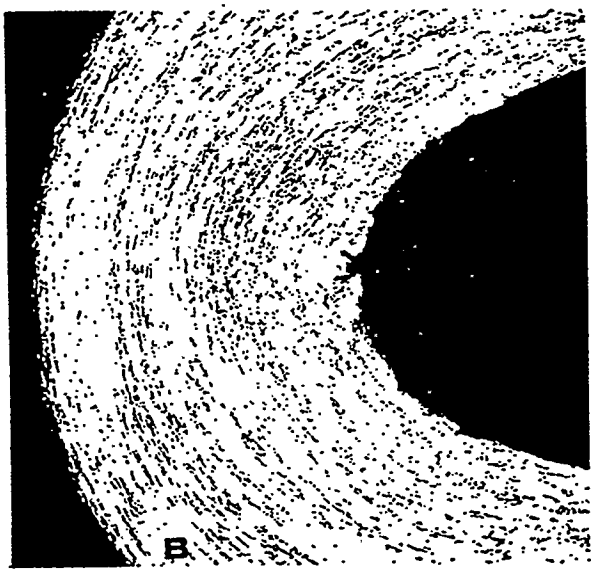

B. Longitudinal Section of Unalloyed Cb U-bend after Contact with Hg 1 Week at 760°C. Both Originally 150X, HNO_3 + HF + H_2O Etched

---

bnl
aui

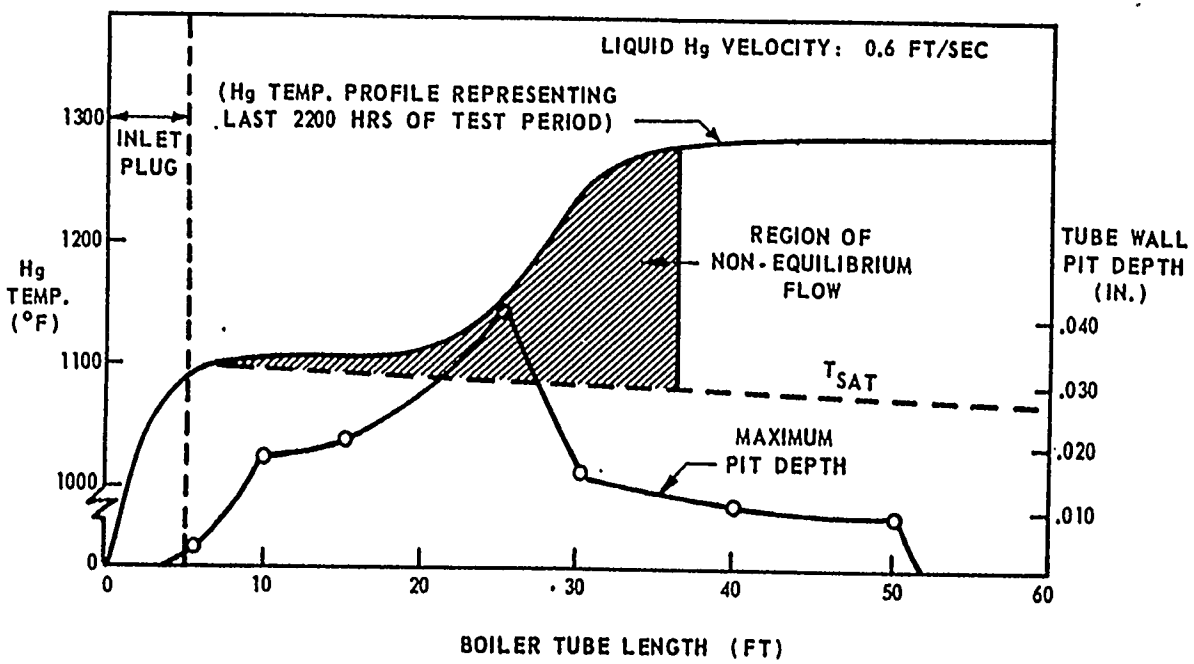

Corrosion in 9 Cr-1 Mo Steel Boiler After 4000 Hours of Test. The Mercury is Heated by NaK

bnl
aui

AREAS FOR FUTURE WORK

- Coatings Inside Pipes
  - Carbonyl - Deposition of Molybdenum
  - Plasma - Spray Deposition of Molybdenum or Tantalum
- Determination of Safe Velocities and/or ΔT's

SELECTED PUBLISHED DOCUMENTS IN THIS AREA

1. J.R. Weeks, "Lead, Bismuth, Tin and Their Alloys as Nuclear Coolants," Nuclear Engineering and Design, 15 (1971), 363-372.

2. C. Williams and R.T. Schomer, "Liquid Metal Fuel Reactor and LMFBR - I," Proc. 2nd Int. Conf. On Peaceful Uses of Atomic Energy 10 (1958), 487.

3. B.R.T. Frost, C.C. Addison, A. Chitty, G.A. Geach, P. Gross, J.A. James, G.J. Metcalfe, T. Raine and H.A. Sloman, "Liquid Metal Fuel Technology," Proc. 2nd Int. Conf. On Peaceful Uses of Atomic Energy 7 (1958), 139.

4. J.R. Weeks and A.J. Romano, "Liquidus Curves and Corrosion of Fe, Ti, Zr, and Cu in Pb-Bi Eutectic Alloy," Corrosion 25 (1969), 130.

5. J.R. Weeks, "Liquidus Curves of Nineteen Dilute Binary Alloys of Bismuth," ASM Trans. Quart. 58 (1965), 302.

6. D.G. Schweitzer and J.R. Weeks, ASM Trans. Quart. 53 (1961), 25.

7. D.G. Schweitzer and J.R. Weeks, ASM Trans. Quart. 54 (1961), 185.

8. J.R. Weeks, ASM Trans. Quart. 58 (1965), 424.

9. J.R. Weeks, ASM Trans. Quart. 58 (1965), 426.

10. J.S. Bryner and M.B. Brodsky, Proc. 2nd Int. Conf. On Peaceful Uses of Atomic Energy 7 (1958), 209.

11. J.R. Weeks and D.H. Gurinsky, "Liquid Metals and Solidification," ed. B. Chalmers (ASM, Cleveland, 1958), 106.

12. A.J. Romano, C.J. Klamut and D.H. Gurinsky, "The Investigation of Container Materials for Bi and Pb Alloys, Part I, Thermal Convection Loops," BNL-811 (T-313) (1963).

13. D.G. Schweitzer and D.H. Gurinsky, Trans. AIME 221 (1961), 192.

14. J.R. Weeks and C.J. Klamut, Nucl. Sci. Eng. 8 (1960), 133.

15. O.F. Kammerer, J.R. Weeks, J. Sadofsky, W.E. Miller and D.H. Gurinsky, Transactions, American Institute of Mining and Metallurgical Engineers 212 (1958), 20.

16. C. Williams and F.T. Miles, "Liquid Metal Fuel Reactor Systems for Power," Chem. Eng. Prog. Symposium Ser. 50 #11 (1954), 245-252.

SELECTED PUBLISHED DOCUMENTS IN THIS AREA *(Continued)*

17. D.H. Gurinsky, "Liquid Metal Fuel Reactors," Reactor Handbook, 2nd Edition, Volume IV, Engineering, Ed. S. McLain and J.H. Martens, Interscience, NY (1964), Chapter 20, 766-804.

18. J.R. Weeks, "Liquidus Curves and Corrosion of Fe, Cr, Ni, Co, V, Cb, Ta, Ti, and Zr in 500-750°C Mercury," CORROSION 23 #4, (April 1967), 96.

19. A.H. Fleitman and J.R. Weeks, "Mercury as a Nuclear Coolant," Nuclear Engineering and Design, 16 #3 (July 1971), 266.

Supplemental Information, John R. Weeks

THE PROPERTIES OF LIQUID METALS

Proceedings of an International Conference held at Brookhaven National Laboratory, Upton, N.Y., U.S.A., 19–23 September 1966, sponsored by the United States Atomic Energy Commission and The International Union of Pure and Applied Physics.

Reprinted from ADVANCES IN PHYSICS Volume 16 Parts 62/63/64 1967

Edited by
P. D. Adams, H. A. Davies and S. G. Epstein

Printed and Published by
TAYLOR & FRANCIS LTD
Red Lion Court, Fleet Street, London, E.C.4

Equation of State and Electrical Resistivity of Liquid Mercury at Elevated Temperatures and Pressures

By D. R. Postill

Department of Physics, Northern Polytechnic, Holloway Road, London, N.7, England

and R. G. Ross and N. E. Cusack

School of Mathematics and Physics, University of East Anglia, Wilberforce Road, Norwich NOR 77H, Norfolk, England

Abstract

Experimental results have been obtained for the density and electrical resistivity of liquid mercury as functions of the independent variables temperature (20°c–1000°c) and pressure (0–1000 bars). Basic equipment for both measurements consisted of a steel vessel containing an internal electrical resistance furnace and pressurized with argon gas. The equation of state was determined with an accuracy of about $\pm\frac{1}{4}\%$ using Archimedes' method by employing a series of totally immersed radioactive sinkers whose rise or fall in the mercury was detected with a γ-ray counter external to the pressure vessel. The electrical resistivity was measured with an accuracy of about $\pm\frac{1}{2}\%$ using a four-lead resistance cell fabricated in fused silica. The two measurements have also been combined to give electrical resistivity at constant volume.

§ 1. Introduction

The work presented here forms part of a programme of research which has the aim of measuring experimentally the properties of a liquid metallic conductor as a function of density.

Toward this end we have made measurements at Birkbeck College, University of London, of the density and electrical resistivity of liquid mercury at temperatures of up to 1000°c together with pressures of up to 1000 bars. This corresponds to a range of density from 13·5 to about 11 g cm^{-3}.

§ 2. Experimental Technique

These measurements were carried out using the high pressure, high temperature equipment shown in fig. 1. This consists of a steel pressure vessel containing an internal electric resistance furnace (1) which is thermally insulated (2) from the steel walls. The steel walls are kept cool by an external water jacket (3), and pressure is raised by pumping argon gas into the vessel.

Figure 2 shows the cells which were used to contain the mercury for the density and resistivity measurements. Both cells were fabricated in fused silica and had re-entrant wells formed in the walls into which

thermocouples were inserted for temperature measurement. Bc had one or more capillary tubes extending into a cool region of th interior so that wherever a free surface of mercury existed in cont the argon gas it was at about room temperature.

Fig. 1

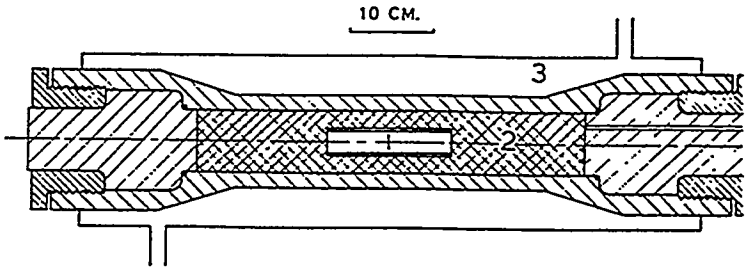

Pressure vessel with internal furnace.

Fig. 2

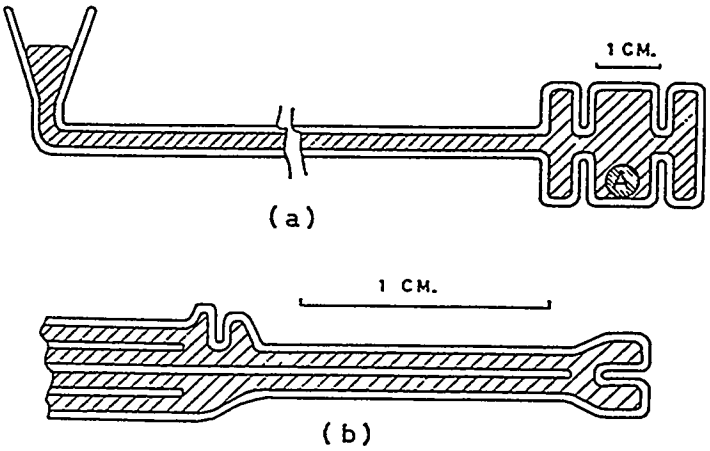

(*a*) Density cell. (*b*) Test length of electrical resistivity cell.

The density cell, fig. 2 (*a*), contained a totally immersed sink about 3–5 mm in diameter, made from TaMo alloy. The sinker wa radioactive so that it emitted γ-rays and by this means its position cell was detectable using a geiger counter and slit system external pressure vessel. The experimental procedure was to adjust the tempe and pressure until the density of the mercury was very nearly ec the known density of the sinker. Then a slight change in tempe would be made so as to cause the sinker to move from the top to the b of the cell, or vice versa, and this movement could be detected usi geiger counter.

Using this procedure the results for the equation of state were obtained in the form of the pairs of P and T which caused the density of the mercury to be just equal to the density of the sinker—in other words, we get P versus T along a line of constant density.

The electrical resistivity was measured using a four-terminal resistance cell the high temperature part of which is shown in fig. 2 (*b*). Conventional methods of d.c. potentiometry were used in the measurements.

Fig. 3

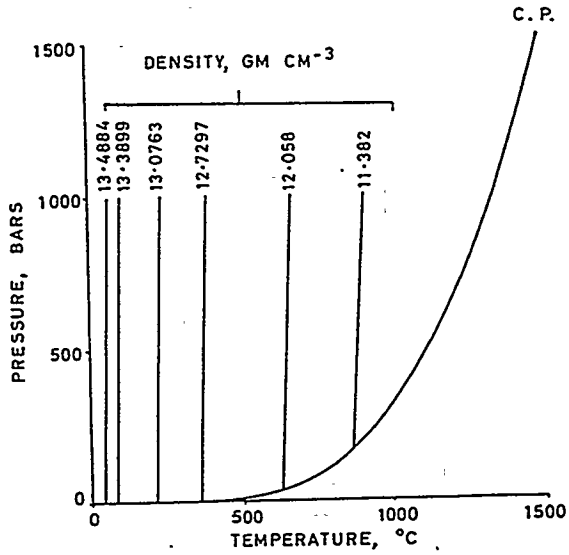

Mercury isochores.

§ 3. Results

The equation of state data obtained are represented in fig. 3. This is a P–T diagram for mercury showing the lines of constant density we have determined, and the boiling curve up to the critical point as determined by Franck and Hensel (1966). Each line of constant density corresponds to an individual sinker of the density given in the diagram. The results for all sinkers have been combined to give a polynomial in P and T which represents the density of liquid mercury over our range of variables to an accuracy which we estimate to be $\pm 0{\cdot}03\%$ up to 400°c and $\pm 0{\cdot}25\%$ in the range 400°c–1000°c.

Relative resistivity was measured as a function of temperature at constant pressure, for a series of pressures, and some of these results are shown in fig. 4. Our results are consistent with those of Franck and Hensel (1966) at higher temperatures to within experimental error, which in our case we estimate to be $\pm 0{\cdot}1\%$ at about 400°c increasing to $\pm 0{\cdot}6\%$ at about 900°c.

It can be seen from fig. 4 that at constant pressure the resistivity incre with increasing temperature, i.e. $(\partial\rho/\partial T)_p$ is positive, and the magni of the derivative also increases with temperature. Our resistivity isc form a family of curves, of which we have shown only two, with the c corresponding to the highest pressure being the lowest, i.e. the effe increasing pressure is to decrease the resistivity at a constant temperat

Fig. 4

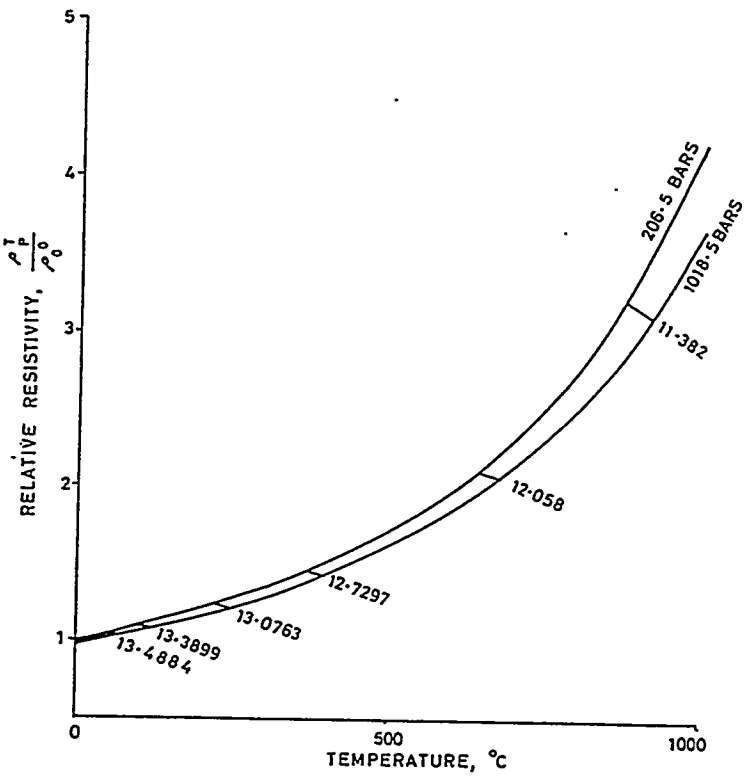

Relative resistivity of mercury along isobars and isochores.

The density and resistivity measurements can be combined to give variation of resistivity with temperature at constant volume, and th resistivity isochores are also shown in fig. 4. We find that in contrast the behaviour at constant pressure, at constant volume the resistiv decreases with increasing temperature, i.e. $(\partial\rho/\partial T)_V$ is negative. can also see from the figure that the negative slope of the isochores increa in magnitude as we go to lower densities and higher temperatures.

This is shown more explicitly in fig. 5, where we plot $(1/\rho_0^0)(\partial\rho/\partial T)_V$ a function of density. The errors increase considerably as we go to lo densities, but it is still possible to conclude that the slope of the resistiv isochores becomes rapidly more negative as we go to lower densities.

Also shown in fig. 5 is $(1/\rho)(\partial\rho/\partial T)_V$, the fractional change of resistivity for unit change of temperature at constant volume. The errors, which are not shown, would be very similar to those for $(1/\rho_0{}^0)(\partial\rho/\partial T)_V$ but by contrast with that quantity, $(1/\rho)(\partial\rho/\partial T)_V$ is nearly constant over our range of measurement. The point shown in parenthesis is calculated from extrapolated density and electrical resistivity data.

Fig. 5

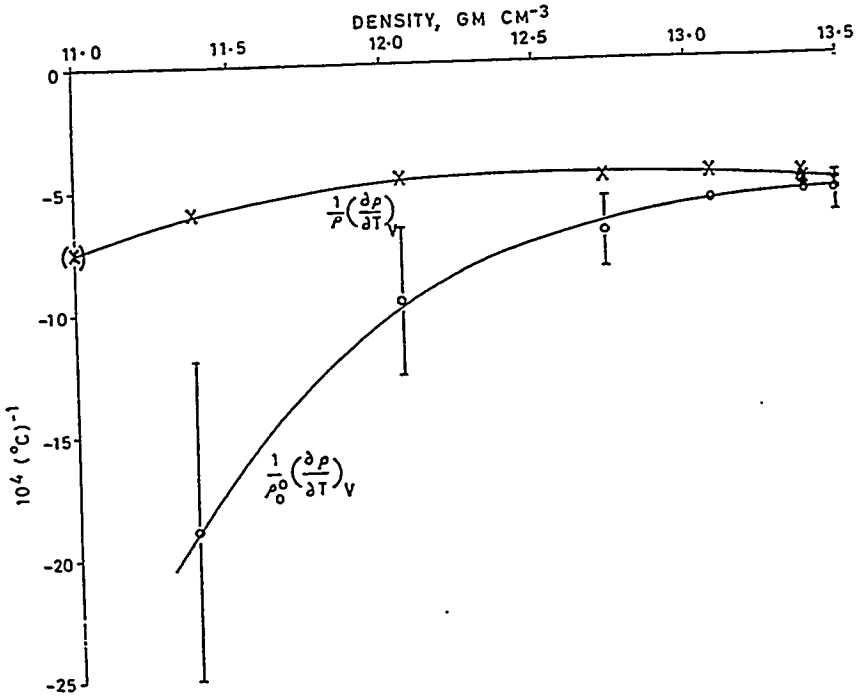

Variation of resistivity at constant volume.

The negative sign of $(\partial\rho/\partial T)_V$ has been known for some time, and may be accounted for in principle either on the Bradley *et al.* (1962) picture, or using the recent Mott (1966) theory of liquid mercury. Although it is not possible to discuss these theories in detail here, we draw attention to the point emphasized by Mott (1966) that it is difficult to see how a simple free-electron picture could be applicable at the lower densities. When the density has dropped to about 11 g cm^{-3} the cube root of the atomic volume, which we might take as a measure of the mean interatomic separation, is approximately equal to the mean free path for electrons as calculated on the free-electron picture, whilst for lower densities the m.f.p. would be less than the interatomic separation.

Returning to the equation of state data, we have calculated the thermal expansion coefficient under various conditions, and our results are shown

in fig. 6. The coefficient is nearly constant at high densities, but begin to rise sharply at temperatures greater than 400°c, which correspond t densities of less than about 12·7 g cm^{-3}. The errors shown on the 1000 ba curve are typical and can be taken to apply to the 200 bar curve also The coefficient at a pressure of 1 bar is much more accurately know and the values shown are taken from the compilation of Bigg (1964).

Fig. 6

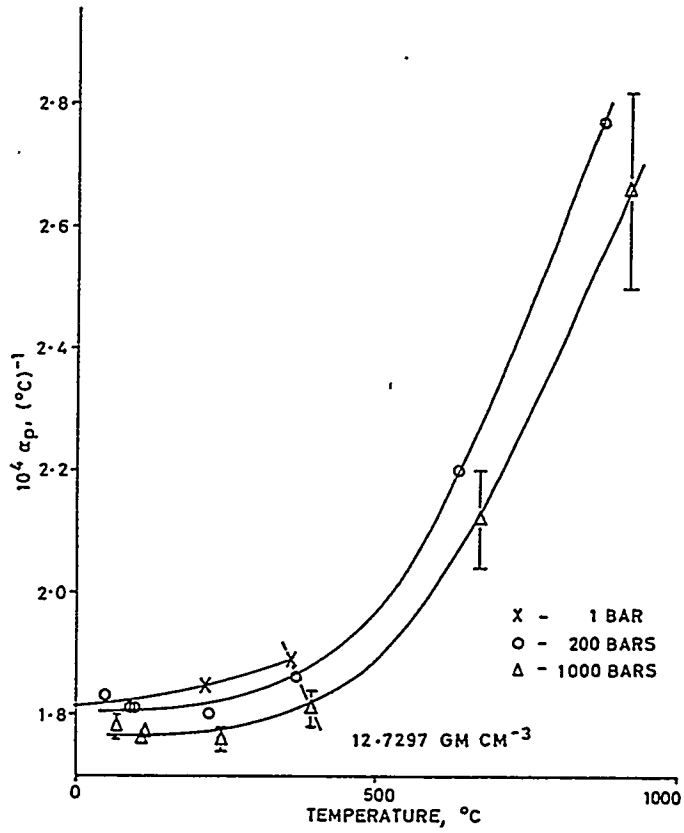

Thermal expansion coefficient of mercury along isobars.

The points given on the three curves have been calculated in such a way as to give us the variation of the thermal expansion coefficient along a line of constant density—for illustration, the 12·7297 g cm^{-3} isochore is sketched in fig. 6. Our results, taken together with the Bigg data, enable us to say that the thermal expansion coefficient decreases as we go along an isochore to higher temperatures and pressures.

The variation of isothermal compressibility with temperature is shown in fig. 7. Again, the errors shown on the 1000 bar curve may be taken to

apply also to the 200 bar curve. Our values near room temperature are in agreement to within experimental error with those of Bridgman (1911), and the compressibility rises fairly sharply to much larger values at higher temperatures and lower densities.

Fig. 7

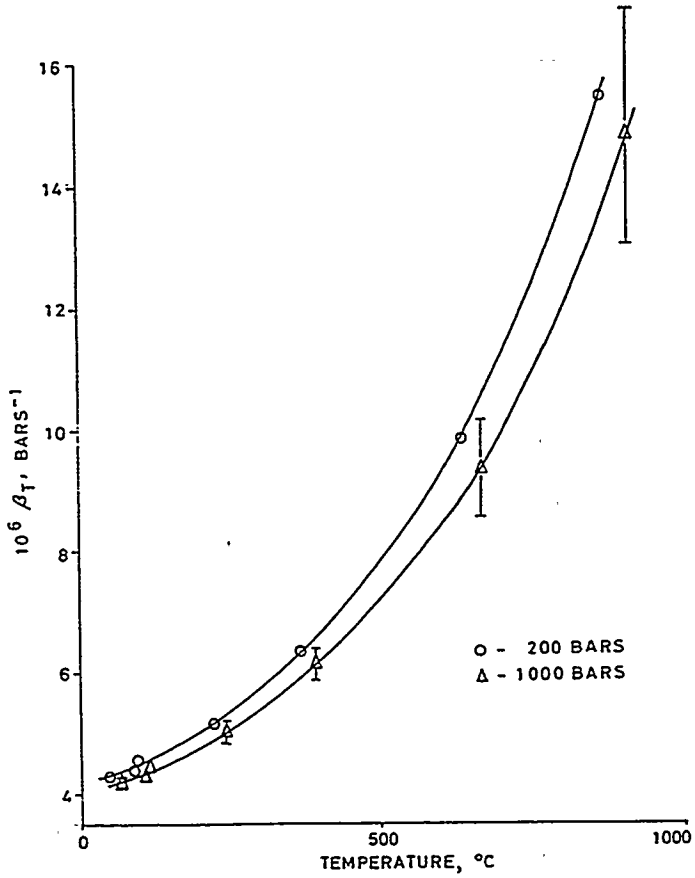

Compressibility of mercury along isobars.

As we pointed out above, our electron transport results could be accounted for theoretically, at least qualitatively, but so far as we are aware the same is not true of our equation of state data.

References

Bigg, P. H., 1964, *Br. J. appl. Phys.*, 15, 1111.
Bradley, C. C., Faber, T. E., Wilson, E. G., and Ziman, J. M., 1962; *Phil. Mag.*, 7, 865.
Bridgman, P. W., 1911, *Proc. Am. Acad. Arts Sci.*, 47, 347.
Franck, E. U., and Hensel, F., 1966, *Phys. Rev.*, 147, 109.
Mott, N. F., 1966, *Phil. Mag.*, 13, 989.

BROOKHAVEN NATIONAL LABORATORY

MEMORANDUM

DATE: October 3, 1962

TO: File

FROM: J.R. Weeks

SUBJECT: Conference with A.J. Nerad and F.J. Norton at GE Research Laboratories

Dr. Nerad directed the Hg boiler development work at GE, which resulted in the design and construction of the Hartford, Kearney, and Portsmouth Hg-boiler power plants. The laboratory work was terminated in 1939, although Nerad is still regularly consulted when troubles are encountered in operation of the Portsmouth plant - the only one still in operation at this date. Shutdown of the Kearney plant was caused by the need for extensive repairs, the improved efficiency of steam cycle plants, and the fact that a $2,000,000 profit could be made by selling their Hg inventory at that time.

During their development program, GE ran over 2,000 harps, both all-liquid and liquid-vapor. They learned early of the aggressive nature of the fresh condensate, and designed both the harps and the Kearney plant so that the fresh condensate would not see steel surfaces. This was accomplished by circulating 90% of the Hg through an all-liquid heat exchanger, and condensing the 10% that was boiled directly into the Hg containing the inhibitors. Nerod sketched his experimental setup as shown below.

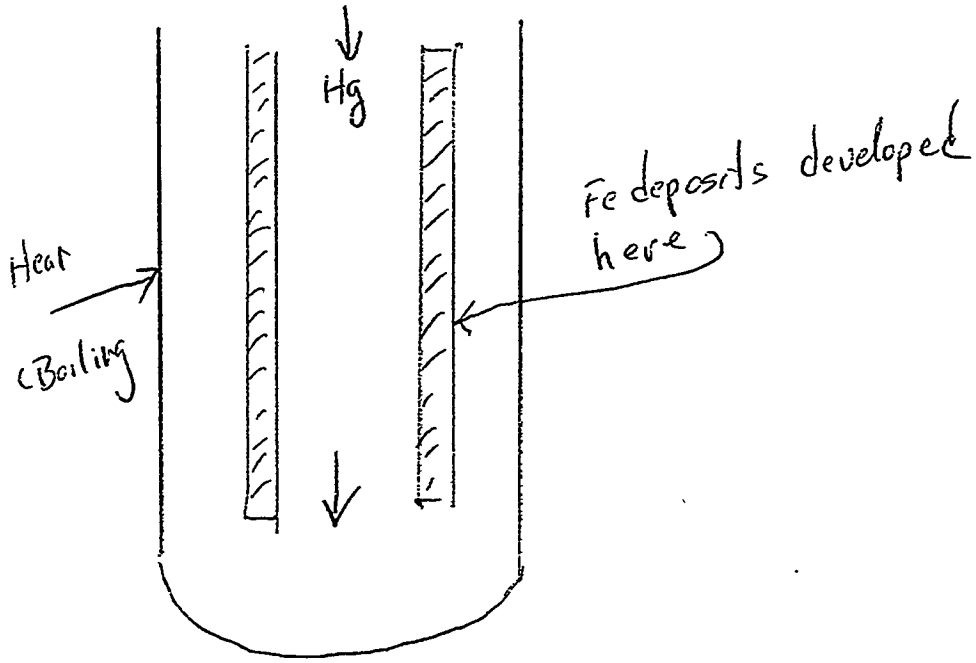

During operation of the Kearney plant, the condensate at the turbine outlet was at a much lower temperature (250°C) than in the loops, and was therefore less aggressive, so this problem was not so serious.

Hg circulation in the plant was 1,200,000 lbs/hr of vapor, and 15-30,000,000 lbs/hr of liquid. The liquid ΔT was approximately 920-885°F.

If the fresh condensate returning from the turbine was allowed to impinge on steel, they found holes eaten in the steel.

All steel attack by Hg observed at GE was transgranular. In rare instances they observed pitting, which they attributed to local wetting, as in the case of corrosion of austenitic steel by Hg containing Ti and Mg inhibitors.

Loop experiments were run at low ΔT (10-15°C) at temperatures ranging up to 800°C; the preferred maximum temperature for loop tests was 650°C.

They studied corrosion at heat fluxes up to 300,000 BTU/ft^2 hr; the average wall rates in the operating boilers were 50 - 100,000 BTU/ft^2 hr. In non-wetted tubes, 30,000 BTU/ft^2 hr was the limit for stable boiling. Nerad described a recent development at Portsmouth where new boiler tubes were flashing - he attributes this to imperfect cleaning of the new tubes resulting in non-wetted conditions.

They designed for thermal stress fatigue, relying upon the mathematician's analysis of the problem.

Their simple laboratory harps were of the types sketched below.

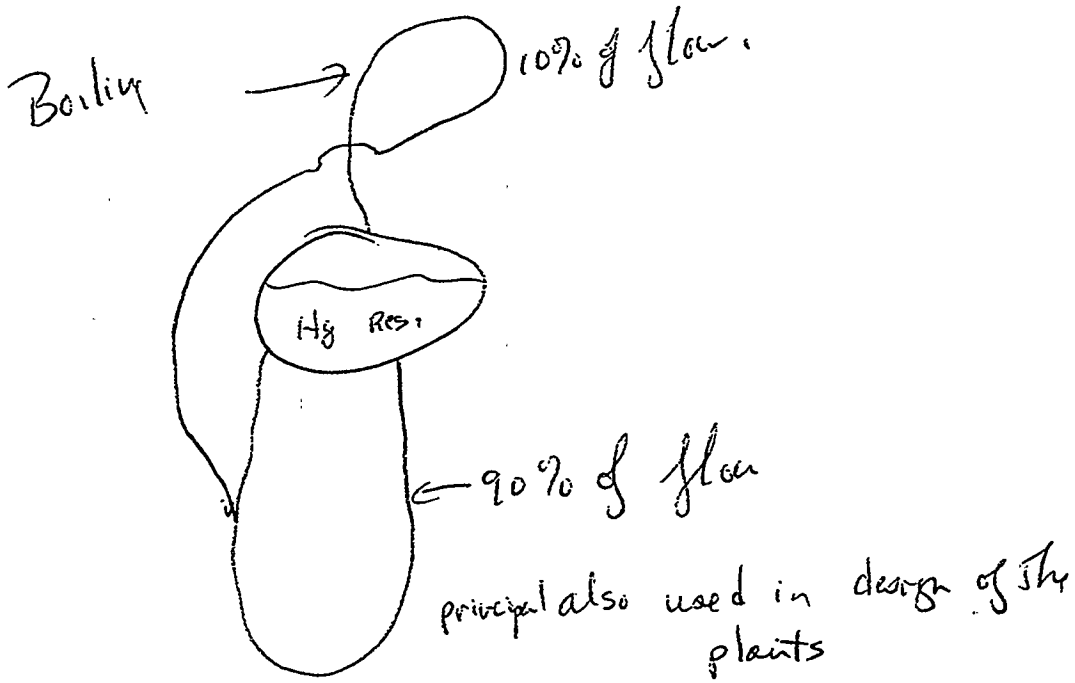

They were not able to obtain stable boiling in a loop of the type we are running.

In the Hartford plant, without inhibitors, they found the corrosion and deposition as sketched below:

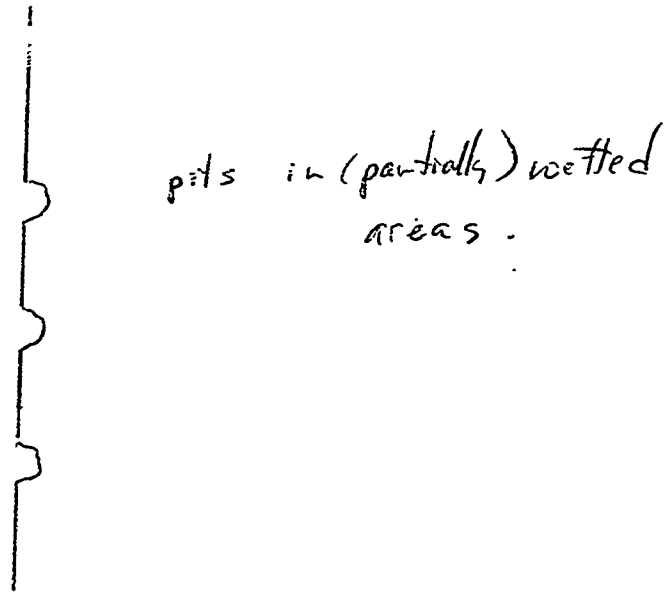

When inhibitors were added, as in the Kearney plant, they saw no corrosion or deposition. However, in the fog boilers in this plant, there was considerable deposition of Mg, Ti, and their oxides.

Their work with inhibitors showed a minimum level of Ti of 0.4 ppm below which inhibition was no longer effected. They needed both Ti and Mg to maintain wetting; with either one alone, they occasionally observed de-wetting of the steel surface. GE preferred Ti to Zr because of the lower inventory required (the minimum Zr concentration was higher). The surface deposits from both were very thin: the maximum observed was 10^{-5}". With either Zr or Ti in the Hg, Nerad could find no other additive that would spoil the inhibitor's effectiveness. They tested every additive in the periodic table that cost less than ~$50.00 per pound.

Additions of Cr and/or Ni to the Hg also protected the boiler surface; they needed to add 0.5% of these to be effective; they got a beautiful Cr-plate on the inside of the steel pipe.

Al additions behaved as follows - there was a critical Al concentration range at which it would protect the steel surface. Below this concentration, Al did not deposit on the surface and corrosion was observed. Above this concentration range, Al would plate out in circular clots on the steel surface, and react with it. When the Al concentration in the Hg is subsequently lowered, the Al would re-dissolve, leaving a circular pit in the area it had been. At very high Al concentrations, the entire steel surface was coated irregularly.

Nerad was very much interested to learn of our Hg work, and congratulated us on our efforts to publish the completed portion of the work. He was quite apologetic for the lack of information in the open literature on the GE work; it had apparently been proprietary for a while, and then it was stale and they were busy with other work.

Nerad felt the inhibition was at least partially due to precipitation inhibition in the all-liquid circuits. At their low ΔT, I agreed that this was likely, and described to him our work in Bi along these lines.

JRW/lh

Compatibility of Materials with Liquid Metal Targets for SNS

J. R. DiStefano, S. J. Pawel, and J. H. DeVan

Several heavy liquid metals are candidates as the target in a spallation neutron source: Hg, Pb, Bi and Pb-Bi eutectic. Systems with these liquid metals have been used in the past and a data-base on compatibility already exists. Two major compatibility issues have been identified when selecting a container material for these liquid metals: temperature gradient mass transfer and liquid metal embrittlement or LME.

Temperature gradient mass transfer refers to dissolution of material from the high temperature portions of a system and its deposition in the lower temperature areas. Solution and deposition rate constants along with temperature, ΔT, and velocity are usually the most important parameters. For most candidate materials mass transfer corrosion has been found to be proportionately worse in Bi compared with Hg and Pb. For temperatures to ~ 550°C, ferritic/martensitic steels have been satisfactory in Pb or Hg systems and the maximum temperature can be extended to ~ 650°C with additions of inhibitors to the liquid metal, e.g. Mg, Ti, Zr. Above ~ 600°C, austenitic stainless steels have been reported to be unsatisfactory, largely because of the mass transfer of nickel. Blockage of flow from deposition of material is usually the life-limiting effect of this type of corrosion. However, mass transfer corrosion at lower temperatures has not been studied.

At low temperatures (usually $\lesssim$150°C), LME has been reported for some liquid metal/container alloy combinations. Liquid metal embrittlement, like hydrogen embrittlement, results in brittle fracture of a normally ductile material. Nickel, aluminum and their alloys are the most susceptible to this phenomenon in mercury systems. Results are cited that indicate type 316 SS is resistant to LME in Hg. However synergisms with hydrogen embrittlement or other forms of radiation-induced embrittlement have not yet been measured.

It has been estimated that a Hg target system in an SNS can be operated at 100 - 250°C. In this range, we believe that an austenitic stainless steel such as type 316 may be the best choice as container material because (1) mass transfer of nickel should be low due to the low system temperature that limits solid state diffusion (2) LME is not expected to occur, and (3) the alloy has a FCC crystal structure and, therefore, does not exhibit a ductile-brittle transition temperature as do the ferritic steels.

Preliminary testing is now underway at ORNL to determine the mass transfer and LME behavior of type 304 SS, type 316 SS, 9 Cr-1Mo steel and several other alloys in mercury as a function of temperature (100 - 250°C). Test systems have been designed and samples obtained. Wetting of the alloy by the mercury has thus far been difficult to attain and maintain.

ORNL DWG 96Z-3281

Compatibility Of Materials With Liquid Metal Targets For SNS

J. R. DiStefano, S. J. Pawel, J. H. DeVan
Oak Ridge National Laboratory
Oak Ridge, Tennessee

International Workshop on the

Technology and Thermal Hydraulics of Heavy Liquid Metals

Schruns, Austria
March 25-28, 1996

ORNL DWG 96Z-3287

Candidate Target System Materials For Oak Ridge Spallation Neutron Source

Component	Candidate Material
Target	Hg, Pb-Bi, Pb
Container	316SS, Mod. 9Cr-1Mo Steel, 9Cr-2W-V-Ta
Window	316SS, Mod. 9Cr-1Mo Steel, 9Cr-2W-V-Ta, Others
Water Jacket Container	316SS, 304SS, Mod9Cr-1Mo Steel, 9Cr-2W-V-Ta, Others: e.g. 6061 Al

ORNL DWG 96Z-3291

Allowable Stress Values Of Conventional Materials As Function Of Temperature

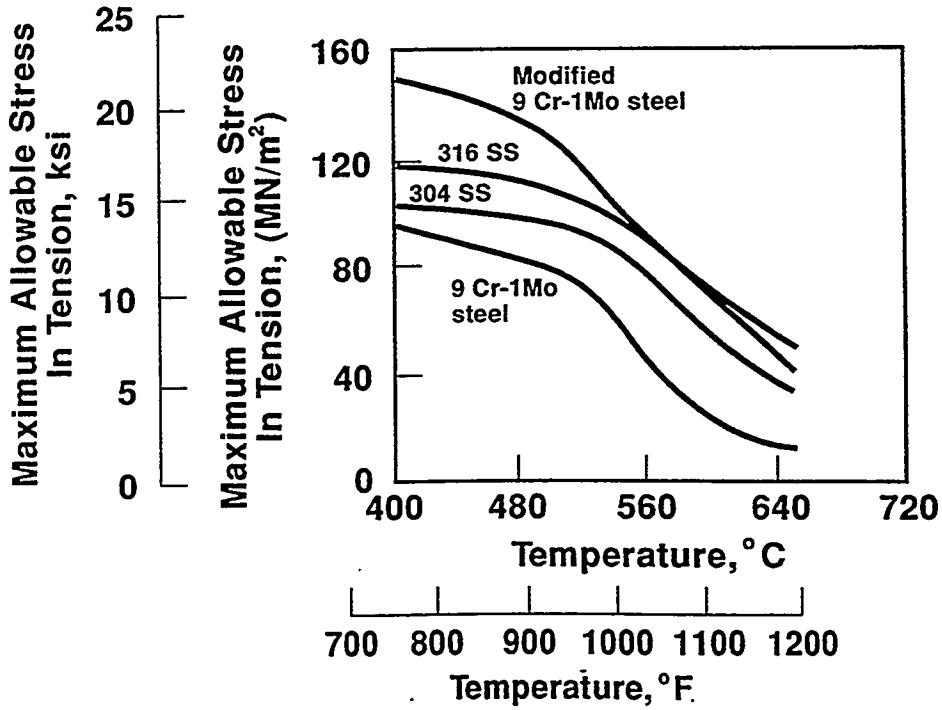

Note: Values are from the ASME boiler and pressure vessel code

ORNL DWG 96Z-3299

A Chart Showing The Various Media In Which Corrosion Is Known To Occur And The Factors That Can Have An Important Influence

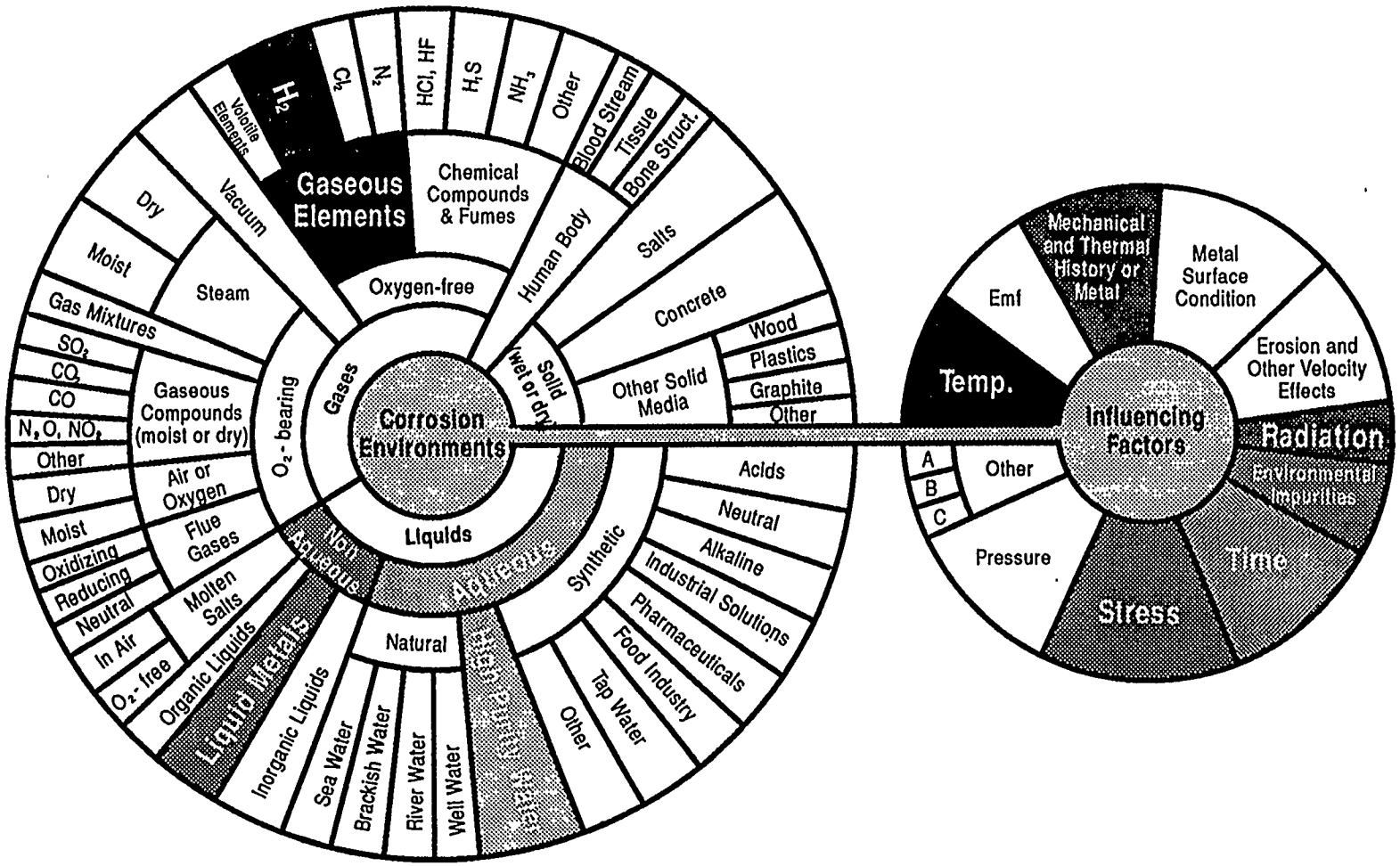

Major Compatibility Issues For Mercury Target System

- Temperature gradient mass transfer
  - Material dissolves at high temperature and precipitates at lower temperatures
  - Driving force is solubility difference in the liquid over the temperature range of the system
  - Important parameters expected to be T, ΔT & solution and deposition rate constants for soluble products in the Hg
- Liquid metal embrittlement (LME) and/or hydrogen embrittlement
  - Brittle failure of normally ductile material when in tension
  - Unique to specific liquid metal/solid material couples. Wide range of materials can be embrittled by hydrogen
  - Sensitive to strain rate, metallurgical factors and temperature

ORNL-DWG 96M-3098

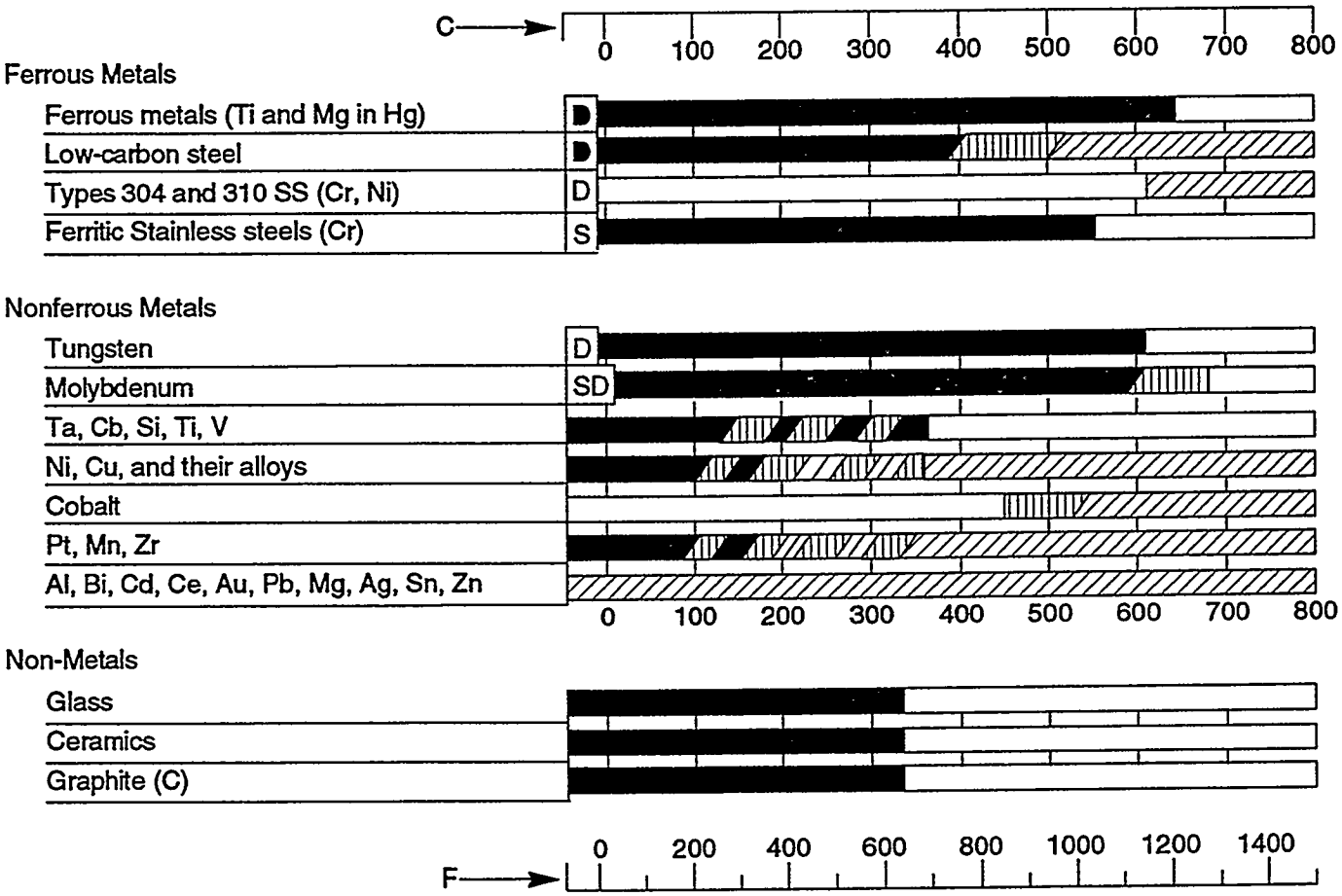

Resistance Ratings (These ratings refer to liquid-metal resistance only - not to temperature-dependent mechanical strength or metallurgical stability):

- GOOD–Consider for relatively long-time use
- –LIMITED–Short-time use only
- –POOR–No structural possibilities
- –UNKNOWN–information inadequate

D – Dynamic mercury harp tests and industriaal boiler tests

D – Dynamic mercury harp tests

S – Static mercury tests

ORNL DWG 96Z-3292

Solubility Of Some Selected Elements In Mercury

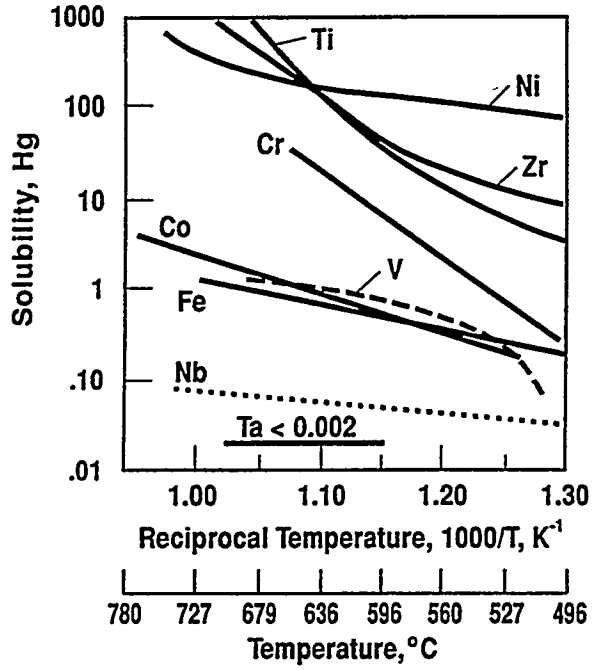

Weeks: Liquidus Curves and Corrosion of Fe, Cr, Ni, Co, V, Cb, Ta, Ti, and Zr in 500° -750 °C Mercury

ORNL DWG 96Z-3293

Comparison Of The Solubility Of Fe in Hg, Pb, and Bi

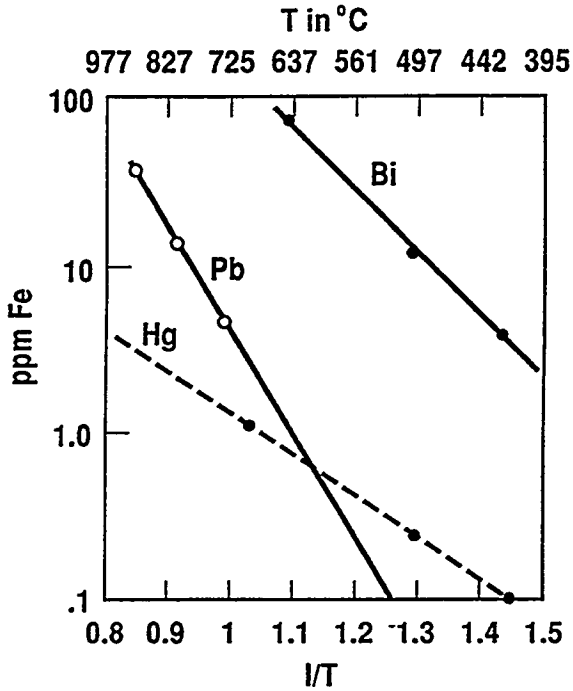

ORNL DWG 96Z-3300

Cold Leg Of 2 1/4 Cr-1Mo Steel Loop Exposed To Lead For 168 h At Max Temperature Of 815 °C With 222 °C ΔT

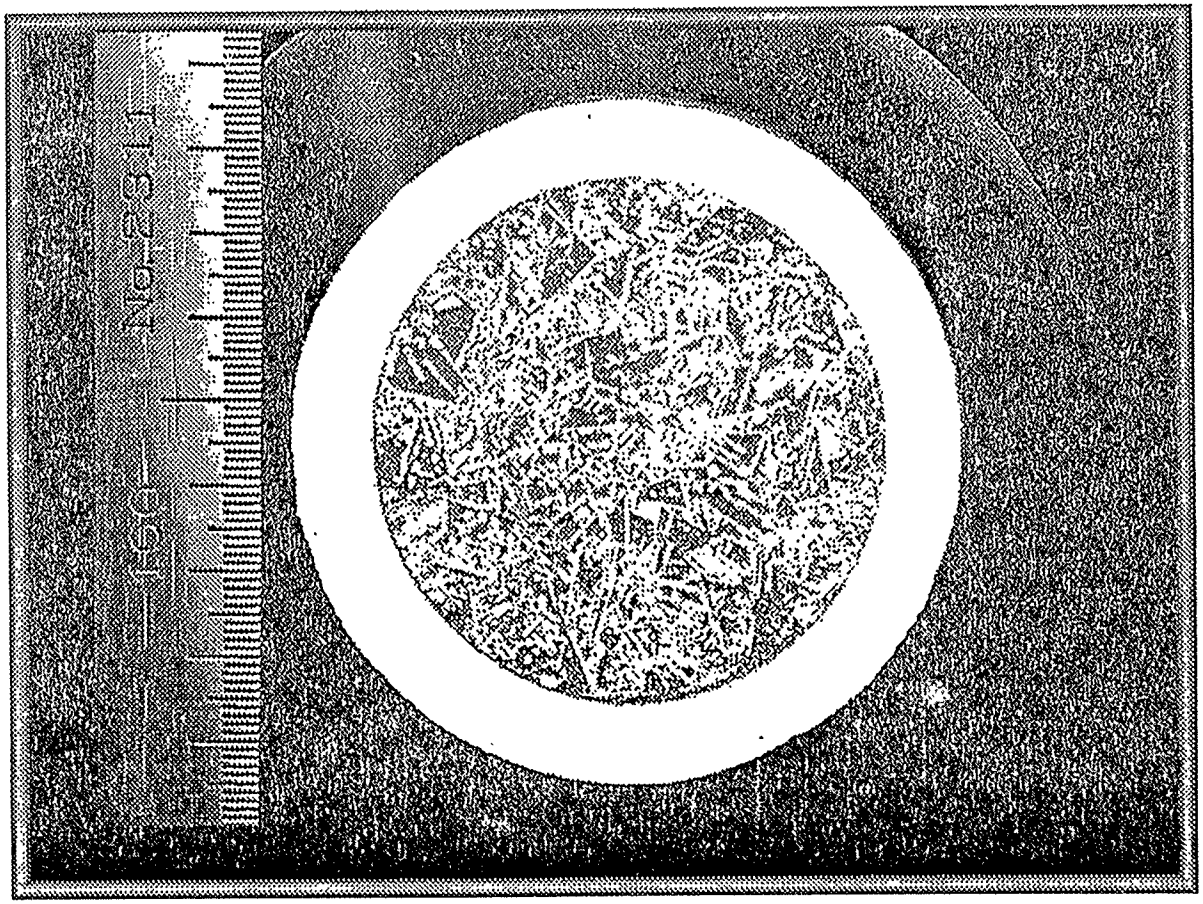

ORNL DWG 96Z-3289

Corrosion Science And Technology Group At Oak Ridge National Laboratory

SCOPE

- Experimental: construct equipment, develop methods, testing
- Failure analysis
- Analytical: material selection, systems analysis, thermodynmamic calculations

Environments:
- Oxidizing and sulfidizing
- Vacuum
- Helium
- Molten salts
- *Liquid metals*

Materials:
- *Steels*
- Superalloys
- Intermetallics
- Refractory metals
- Ceramics and composites

Facilities

- Electrochemical Laboratory (includes noise analysis)
- Autoclaves with recirculating water attached to tensile/fatigue machines
- Microbalance Laboratory for Kinetic Studies
- Controlled Atmosphere Systems (coupons to large-diameter ceramic tubes)
- *Liquid Metal Test Loop Laboratory*

ORNL DWG 96Z-3294

ORNL-TM-13056

ornl

A Review Of The Compatibility Of Containment Materials With Potential Liquid Metal Targets

Oak Ridge National Laboratory

J. R. DiStefano

MARTIN MARIETTA

Results Of Thermal Convection Loop Tests At Oak Ridge National Laboratory Using Lead As A Coolant (ref. 6)

Loop Material	Max Temp (°C)	ΔT (°C)	Time (h)	Max Depth Attack (mm)	Avg. Depth Attack (mm)	Inhibitors
Croloy 2 1/4	654	165	266 [a]	0.025		None
Type 410 Stainless	654	165	1,346 [a]	0.051		None
Croloy 2 1/4	593	110	5,064 [b]	0.203	0.152	None
ASTM Type A-106	593	110	5,064 [c]	0.254	0.178	None
Nb-1Zr clad with type 446 stainless	760	220	5,280	None [d]	None [d]	None
Croloy 2 1/4 [e]	550	120	27,765	None	None	250 Mg + Zr

[a] Loop plugged due to mass transfer of iron and chromium

[b] Did not plug but large amount of dendritic crystals found in cold leg

[c] Flow rate decreased prior to shutdown, indicating cold leg deposition

[d] No measurable hot leg attack; niobium crystals formed in cold leg

[e] Brookhaven National Laboratory operated loop

Summary Of Thermal Convection Loop Tests With Bismuth (ref. 6)

(Conditions: 700 °C maximum hot leg, 90 to 100° C Δ t)

Loop	Loop Material	Specimens	Nominal Li in Bi (%)	Duration (h)	Reason for stopping
1	Quartz	TZM[a]/Ta/Nb/ Nb-1%Zr	0	18	Flow stopped
2	Quartz	TZM/Ta/Nb/ Nb-1%Zr	0	23	Flow stopped
3	Quartz	Mo/TZM	0	3,000	Completed
4	Quartz	Nb/Nb-1% Zr	0	115	Flow stopped
9	Quartz	Fe-5% Mo	0	423	Samples dissolved
11	Quartz	Mo	0.01	3,000	Completed
12	Quartz	T-111	0.01	3,000	Completed
14	Quartz	Graphite	0.01	3,000	Completed
15	Quartz	Mo	0.01	10,000	Completed
17	Quartz	Ta-10% W	0	3,000	Completed
CPML-1	T-111	T-111	2.5	3,000	Completed
CPML-2	Mo	Mo	2.5	8,700	Completed
CPML-4	Mo	Graphite	2.5	3,000	Completed

[a]Mo-0.5% Ti-0.1% Zr.

ORNL DWG 96Z-3298

"Rocker Test"

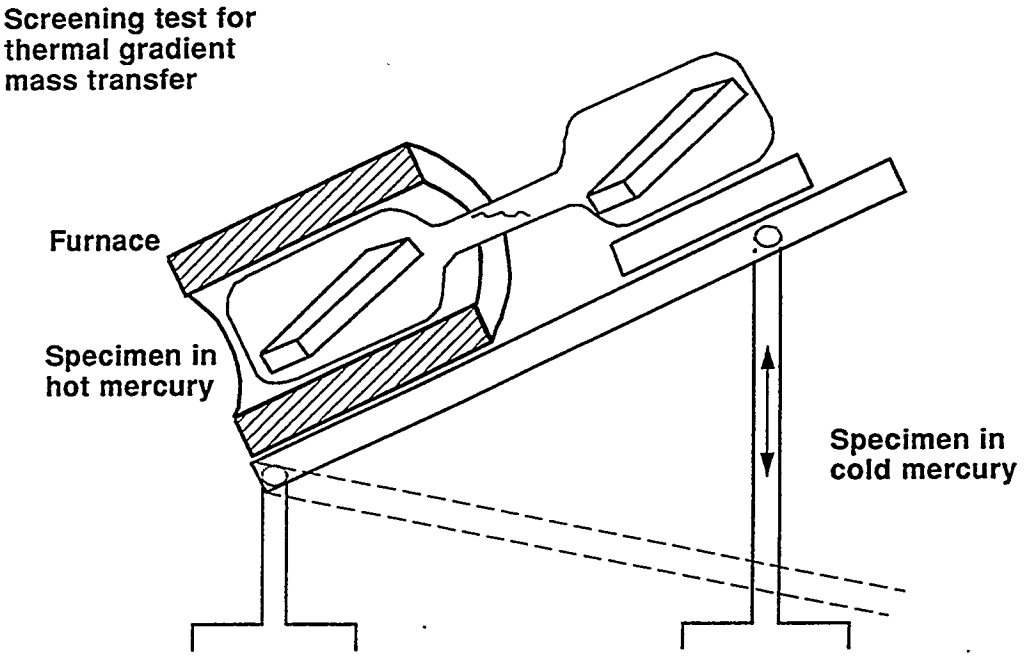

ORNL DWG 96Z-3878

Preliminary Screening Test Matrix

- Test materials
  - 304L, 316L
  - 1020, 9Cr-1Mo
- Coupon conditions
  - Bare
  - Plated (gold)
  - Acid etched
- Hot zone test temperatures
  - 100, 150, 200, 250°C
- Mercury chemistry
  - Pure (triple distilled)
  - Doped (Ti, Mg, others)

ORNL DWG 96Z-3288

Major Compatibility Issues For Mercury Target System

- Temperature gradient mass transfer
  - Material dissolves at high temperature and precipitates at lower temperatures
  - Driving force is solubility difference in the liquid over the temperature range of the system
  - Important parameters expected to be T, ΔT & solution and deposition rate constants for soluble products in the Hg
- Liquid metal embrittlement (LME) and/or hydrogen embrittlement
  - Brittle failure of normally ductile material when in tension
  - Unique to specific liquid metal/solid material couples. Wide range of materials can be embrittled by hydrogen
  - Sensitive to strain rate, metallurgical factors and temperature

ORNL DWG 96Z-3295

Nickel Reduces The Ductility Of Iron-Nickel Alloys In Mercury

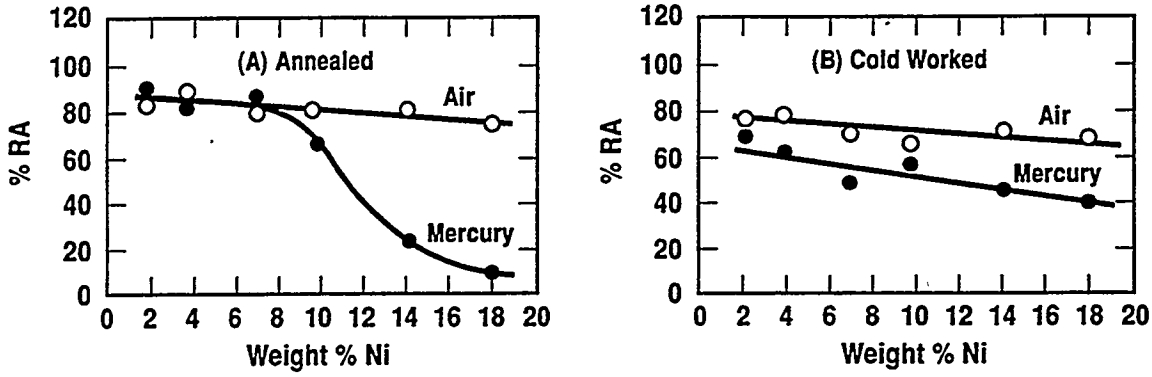

Comparision of reduction in area of tensile samples tested in air with samples tested in mercury. (A) annealed material; (B) cold-worked material.

Hayden and Floreen: The Ductility and Toughness of Iron-Nickel Alloys in Liquid Mercury

ORNL DWG 96Z-3282

Tensile Fracture Characteristics Of Ni and NI Alloys In Mercury At Room Temperature

Material	Environment	
	Air	Mercury
Ni-200	All alloys had ductile cup & cone fractures subsequent to necking. Fracture from microvoid coalescence	Brittle fracture
Monel 400		Complete intergranular embrittlement at low strain rates
Inconel 600		Similar to Ni-200
Inconel 625		Similar to Monel 400
Inconel 718		Intermediate between Ni-200 and Monel 400. Noticeable embrittlement with intergranular failure
Alloy 800/825		Not embrittled; cup & cone failure after necking. (Later fatigue tests showed intergranular cracking)

Price and Good: The Tensile Fracture Characteristics of Nickel, Monel, and Selected Superalloys Broken in Liquid Mercury

ORNL DWG 96Z-3284

Effect Of Mercury

Slow Strain Rate Tests At Room Temperature (5×10^{-6}/sec)

Material	Environment	Time to Failure (h)	Reduction in Area (%)	Comments
304L SS	Air	33	83	No cracking
	Mercury	28	49	Linear cracking
316L SS	Air	37	80	No cracking
	Mercury	38	79	No cracking
Alloy 600	Air	29	72	Linear/Random cracking
	Mercury	24	58	Linear/Random cracking
Alloy 800	Air	24	77	No cracking
	Mercury	26	71	No cracking

Krupowitz: Effect of Heat Treatment on Liquid Metal Induced Cracking of Austenitic Alloys

ORNL DWG 96Z-3283

Slow Strain-Rate Tests Of Aluminum Alloys In Air Versus Mercury

Material	Fractional Time-To-Failure t_{Hg} / t_{Air}		
	Room Temp.	-38°C	-72°C
Al-5083	0.15	.25	1.5
Welded Al-5083	0.12		
Al-3003	0.80		
304 SS	0.60		

McIntyre et. al.: Mercury Attack of Ethylene Plant Alloys

ORNL DWG 96Z-3297

Effect Of Hydrogen On The Ductility Of Monel 400

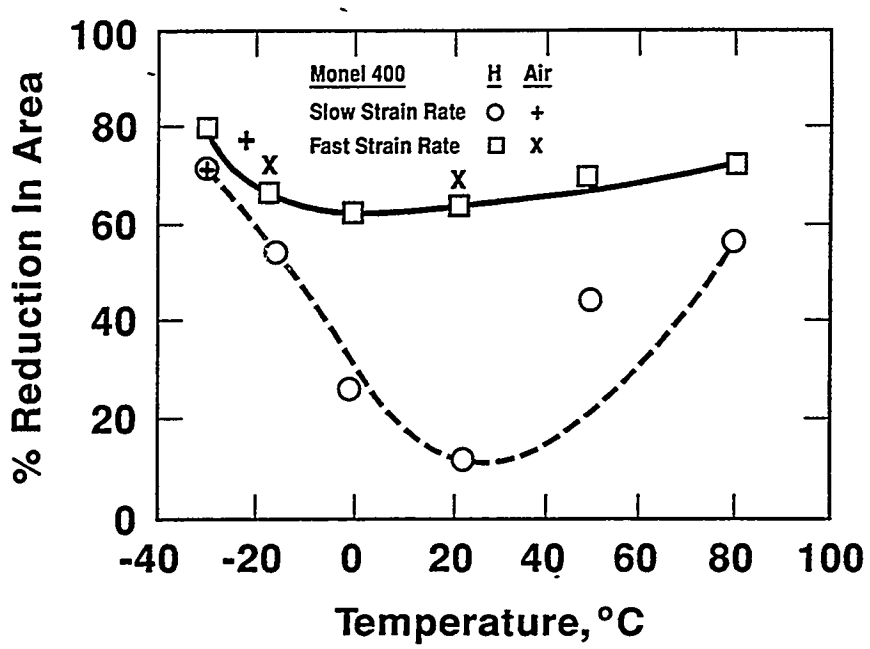

ORNL DWG 96Z-3296

Effect Of Hydrogen

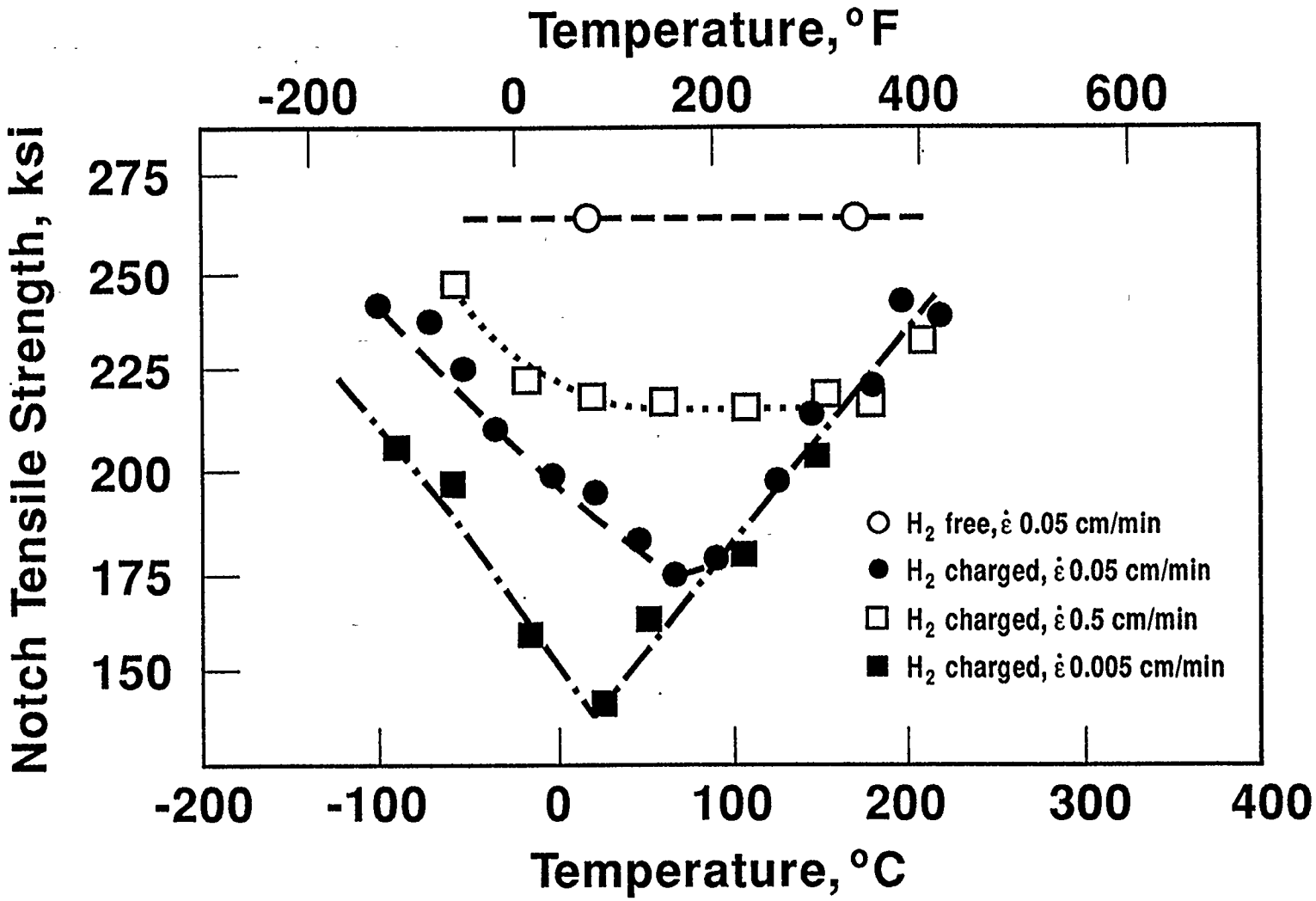

Notch tensile strength of high-strength steel plotted against testing temperature for three strain rates (crosshead speeds).

ORNL DWG 96Z-3879

Mercury Test Container

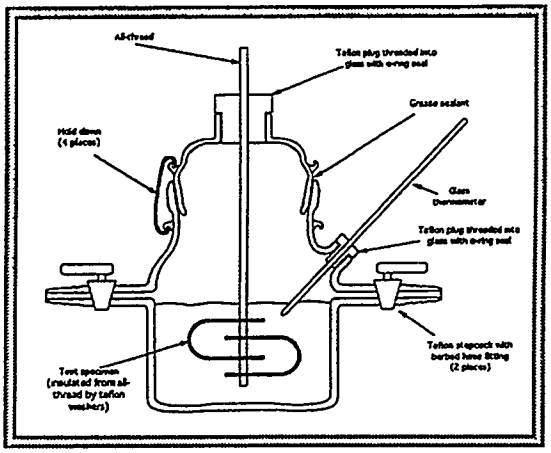

- Preliminary embrittlement tests underway to examine U-bends in Hg
  - Coupons with and without welds across bend apex
  - Emphasis on 304L and 316L but we will also include coupons of 1020, 2.25Cr-1Mo, 9Cr-1MO, 6061Al
  - Embrittlement and weight loss examined as a function of temperature and Hg chemistry

ORNL DWG 96Z-3877

Preliminary Embrittlement Test Results

- U-bends of 304L stainless steel
  - Without gold plating, no wetting, no weight change, no cracking, at ambient or 150° C (72 hr)
  - With 10-12 μm gold plate on "marginal" surface, wetting good but persists only as long as the Au remains on the specimen; no weight change, no cracking at ambient or 150° C (72 hr)

ORNL DWG 96Z-3876

Review Of Past Experience For Stress Corrosion Cracking Of Stainless Steel On Water Side

- Radiolysis
  - Water in proton beam may liberate oxygen and hydrogen
  - This oxygen may contribute to SCC in high temperature water (>200°C)
  - One remedy is overpressuring with hydrogen to recombine with oxygen
- IASCC
  - Some stainless steels suffer radiation-induced segregation and sensitization
  - Low carbon ("L") grade material does not mitigate problem
  - Aggravated by higher neutron fluxes, higher coolant conductivities, and the presence of dissolved oxygen in high temperature (> 200°C) water

ORNL DWG 96Z-3285

Summary

Major compatibility issues have been identified and R&D tasks structured to address them

- What is max T/ΔT for satisfactory containment of Hg target by type 316 SS & other potential materials?
  - How affected by spallation transmutation products in Hg, or container material compositional changes to mitigate radiation damage, etc.?
- If wetting promoters/corrosion inhibitors are needed
  - What concentrations are required?
  - How difficult to control?
  - How affected by spallation transmutation products, wall sputtering, etc.?
- Is LME/HE a factor?
  - If yes, under what conditions?
- How are any of the above affected by radiation or other synergisms?

TYPES OF RADIATION EFFECTS IN MATERIALS

- Short answer
  - Almost everything changes
- Long answer
  - Dimensional
  - Mechanical
  - Electrical
  - Optical
  - Microstructural
  - Phase relationships

    •

    •

    •

PHENOMENA IMPORTANT FOR IRRADIATED STRUCTURAL AND TARGET MATERIALS

- Swelling--Volume expansion by the formation of cavities and/or less dense phases
- Creep--Time-dependent stress-directed shape change in excess of ordinary thermal creep
- Embrittlement--Loss of ductility and associated strengthening; often accompanied by changes in fracture mode

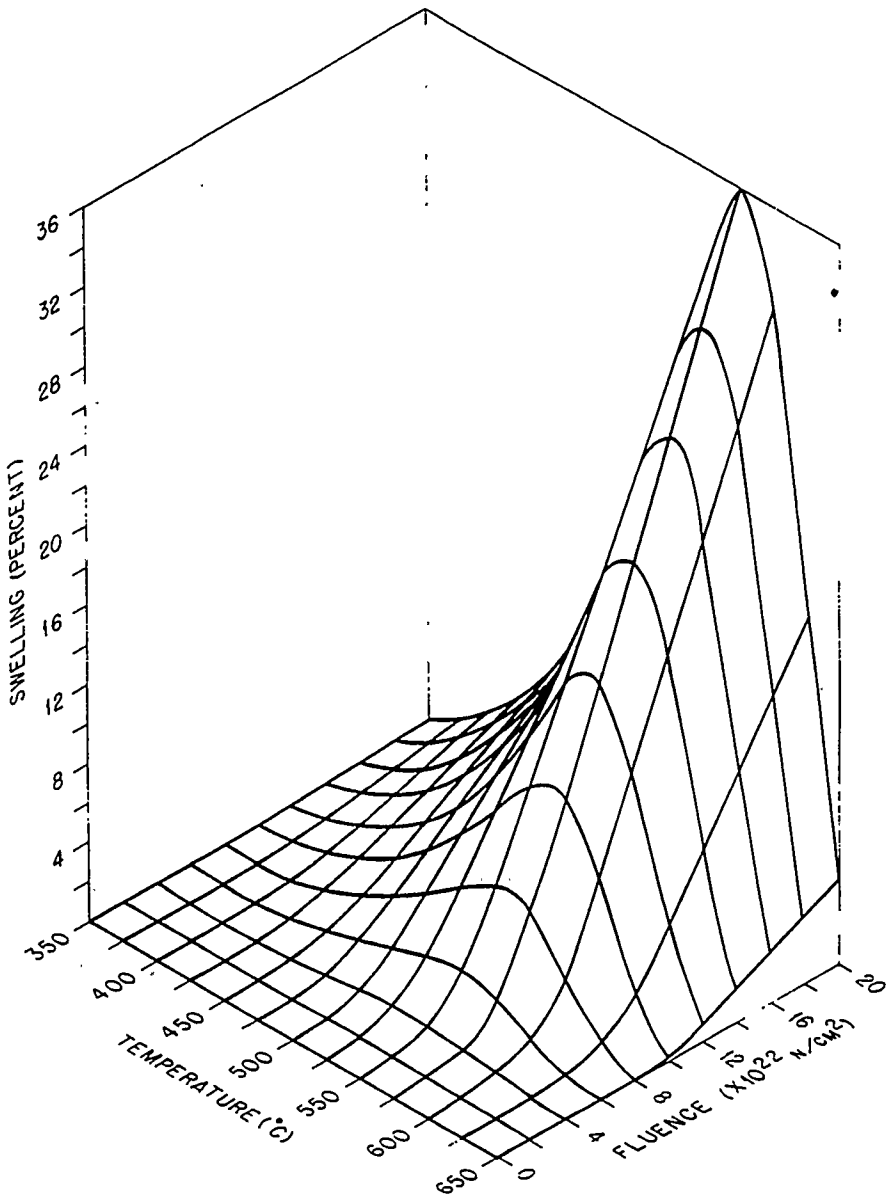

Percent Swelling as Functions of Temperature and Fluence

IMPORTANCE OF SWELLING

- Engineered shapes and dimensions grossly unstable
- Sensitivity to dose, dose rate, and temperature causes non-uniform changes
- May severely limit lifetimes if operational problems are to be avoided

ORNL-DWG 90Z-12681

Alloys Have Been Developed That Show Outstanding Swelling Resistance

Fe-13Cr-15Ni Ternary

(P,Si,Ti,C)-Modified

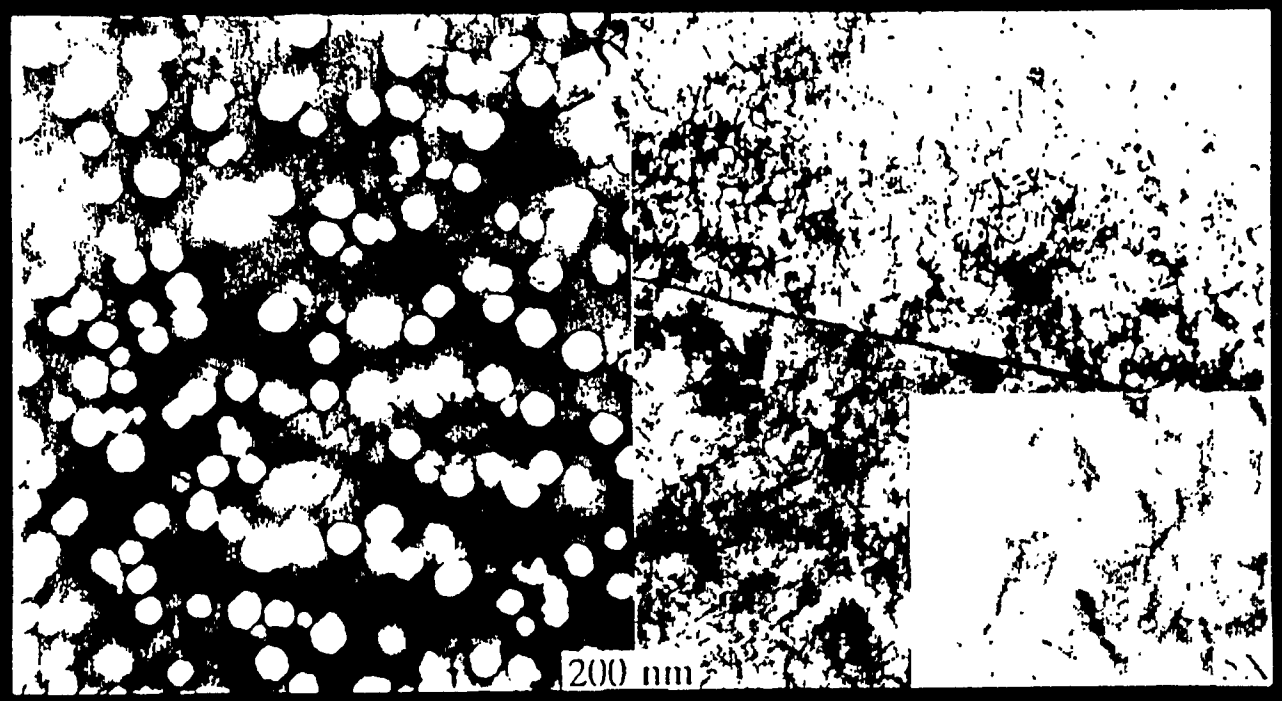

70 dpa/28 appm He at 675C

109 dpa/2000 appm He at 675C

ORNL-DWG 89Z-8929A

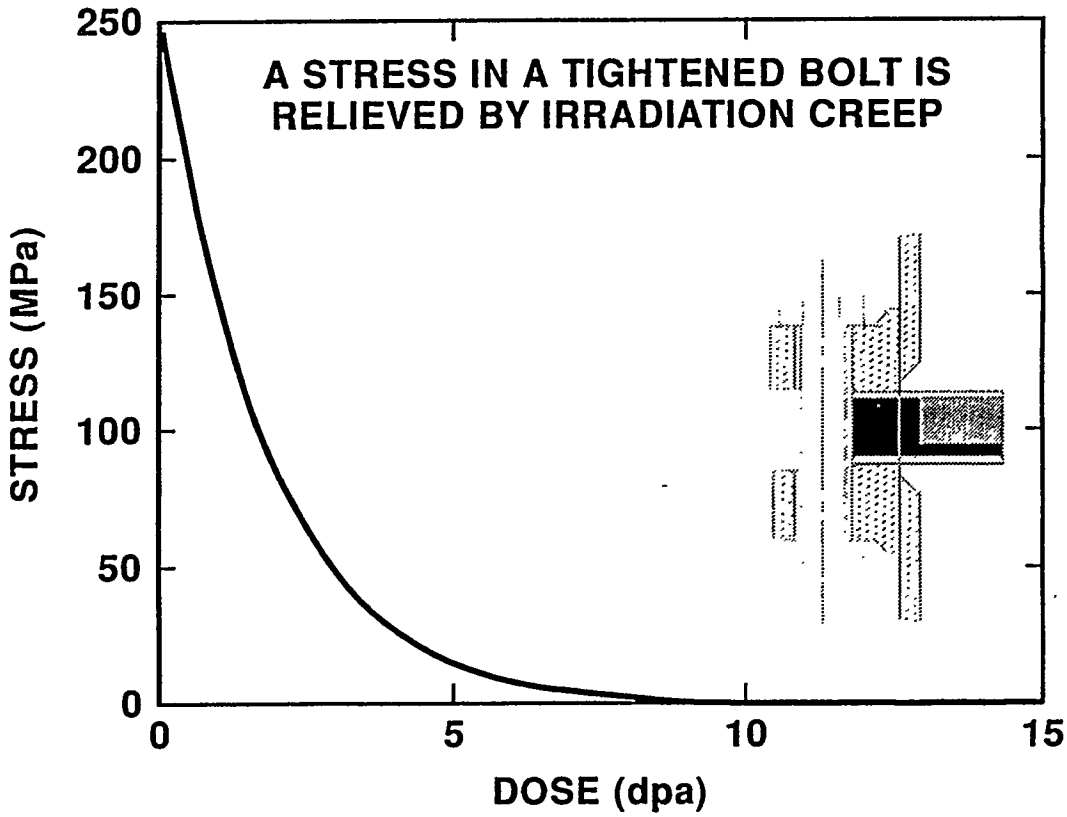

ORNL-DWG 89Z-8250

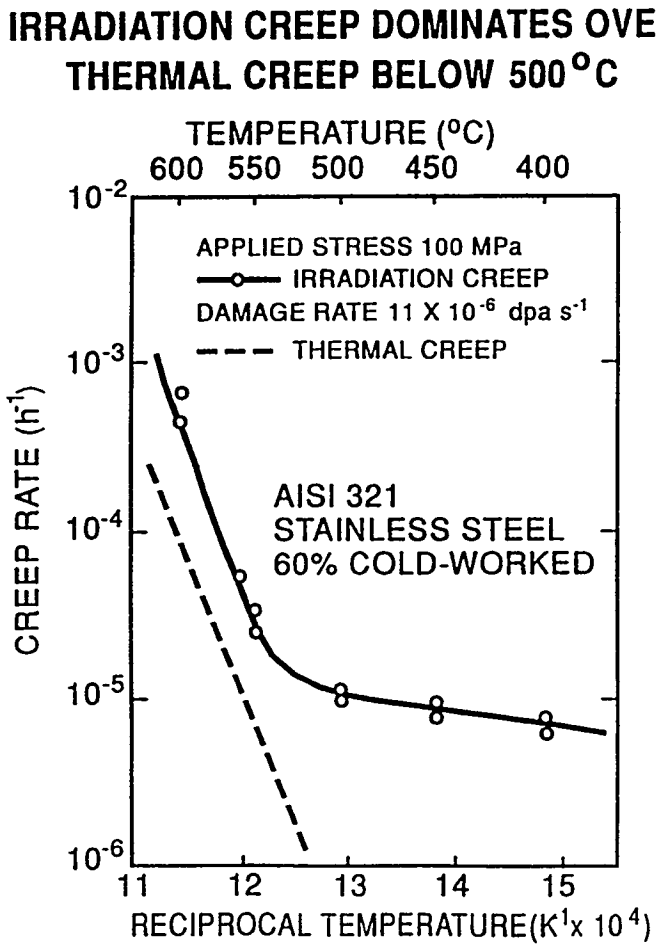

ORNL DWG 96Z-3252

Embrittlement In fcc Alloys

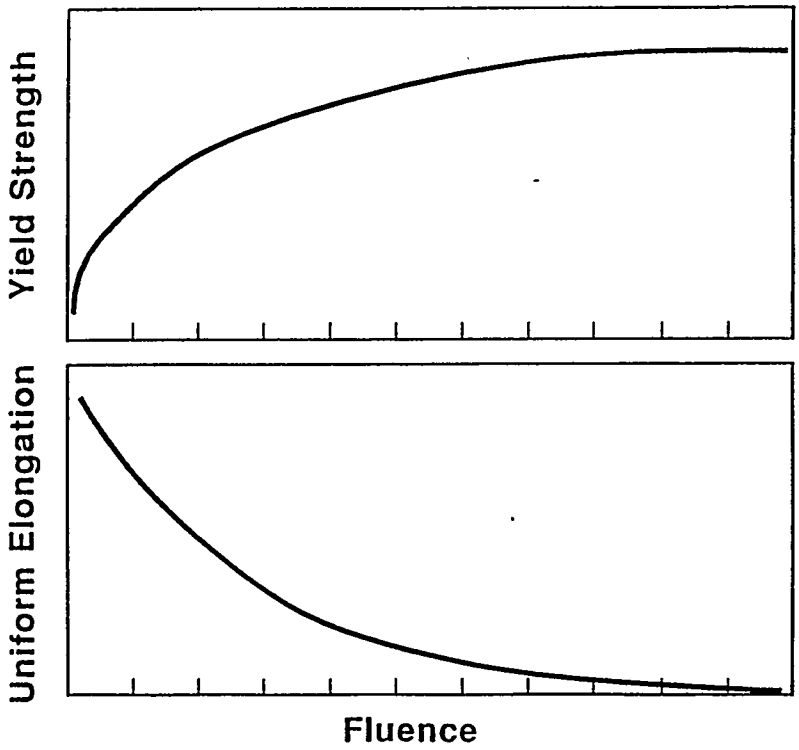

IMPORTANCE OF CREEP

- Engineered stress distributions quickly removed
- Engineered shapes and dimensions grossly unstable
- May be beneficial in relaxing stresses caused by differential swelling

ORNL DWG 96Z-3253

Embrittlement In bcc Alloys

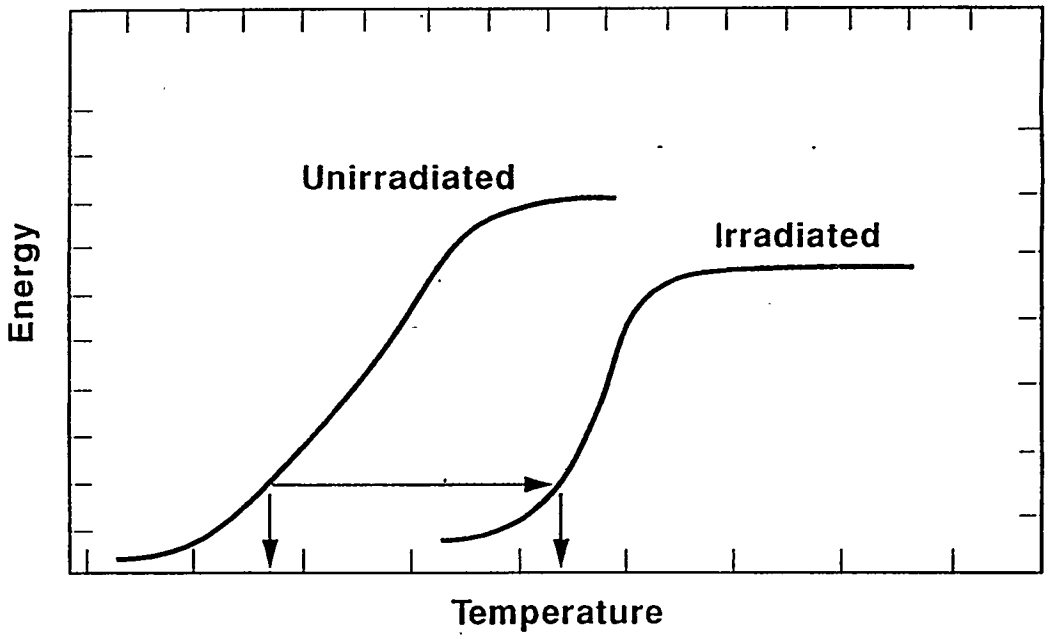

IMPORTANCE OF EMBRITTLEMENT

- Potential for gross failure of engineering structures
- Possible crack formation and loss of vacuum or coolant integrity
- May necessitate early replacement of components to avoid failures

ORNL-DWG 91Z-14711

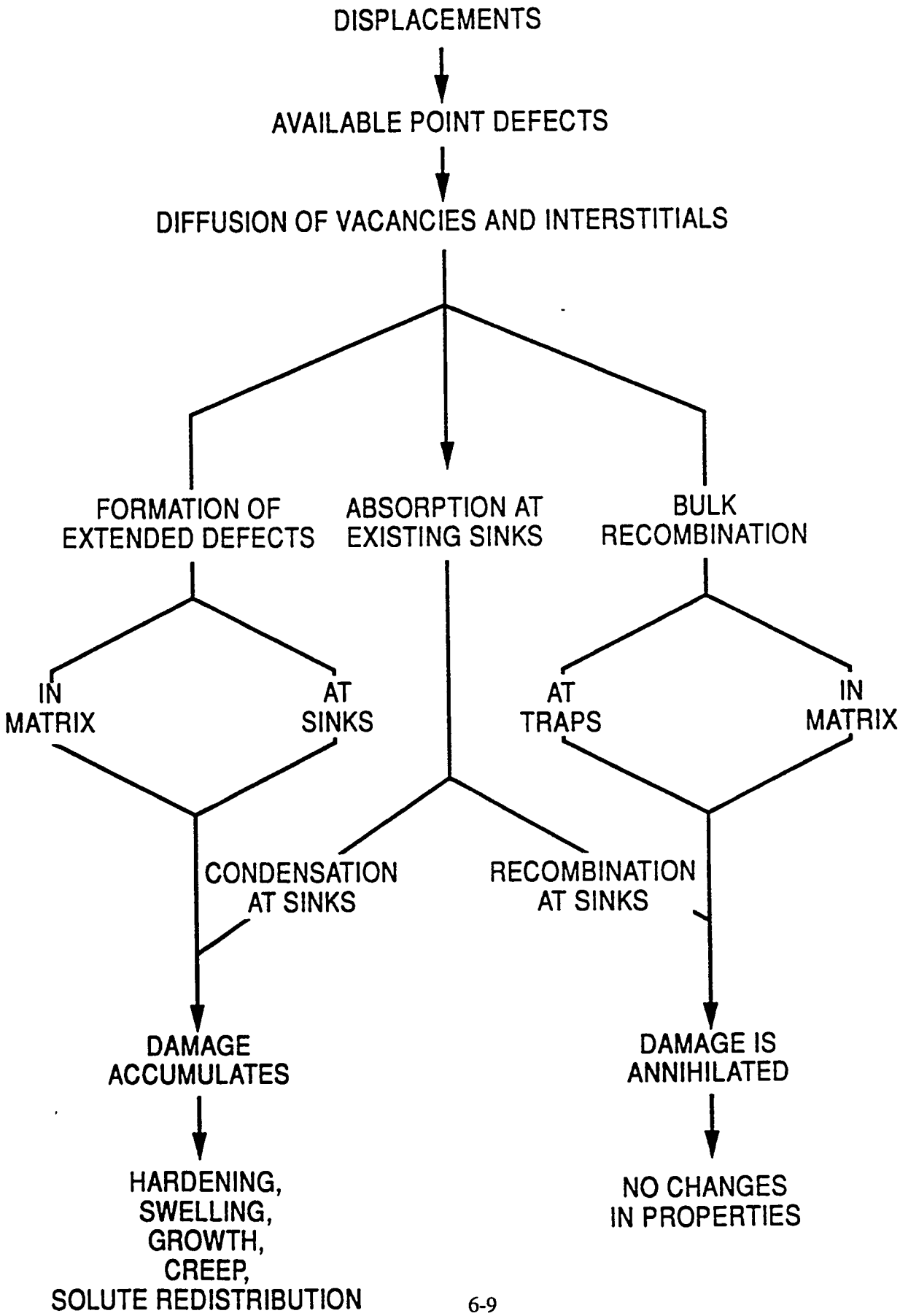

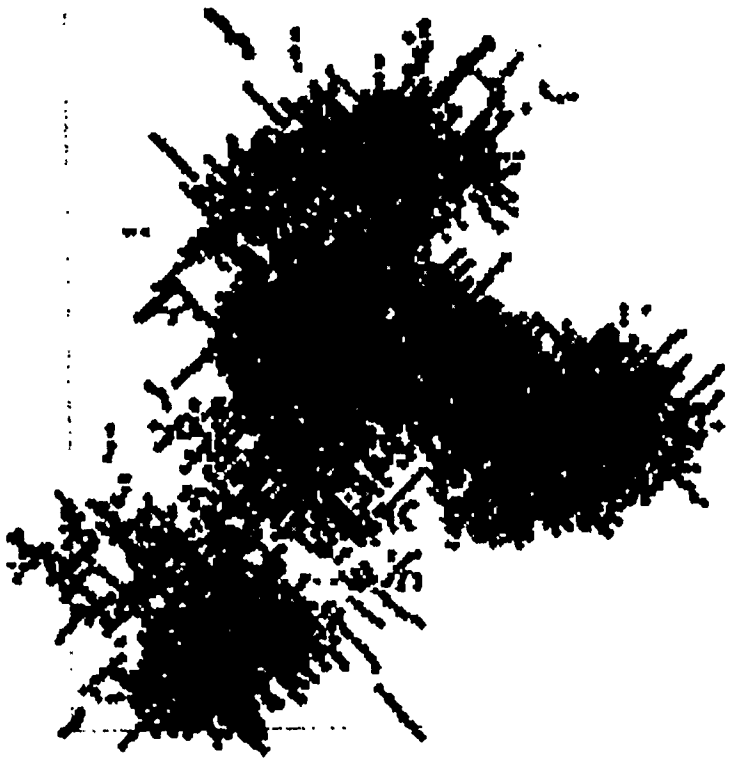

20 keV cascade
in iron at 100K

Near peak damage,
t=0.26 ps

Atom block is 50
unit cells on each
side, contains
250,000 atoms

~11,000 Frenkel pair

1 nm

- vacancy
- interstitial

EVOLUTION OF MICROSTRUCTURE UNDERLIES CHANGES IN MACROSCOPIC PROPERTIES

CAVITIES
DISLOCATIONS
PRECIPITATES
→ *SWELLING*

DISLOCATIONS
DISLOCATION LOOPS
→ *CREEP*

PRECIPITATES
VACANCY CLUSTERS
INTERSTITIAL CLUSTERS
POINT DEFECT-SOLUTE CLUSTERS
DISLOCATION LOOPS
GAS BUBBLES
→ *EMBRITTLEMENT*

DIMENSIONAL AND MECHANICAL PROPERTY CHANGES CAUSED BY DISPLACEMENT OF ATOMS

- The unit of displacement dose is the displacement per atom (dpa)
- One dpa is the dose at which, on average, each atom has been displaced from its lattice position once
  - Example: Highest fast flux reactors produce ~10^{-6} dpa/s
- In the most demanding applications, structural materials will see displacement doses up to 100 dpa

ORSNS WILL BE MUCH DIFFERENT FROM FISSION AND FUSION

- Extremely high particle energies
- Combined protons and neutrons
- High helium and hydrogen production rates
  - SNS 200 appm He/dpa
  - Fusion 10 " "
  - Fast Fission 0.2 " "
- Production of wide range of solid impurities
- Pulsed beam delivery schedule
  - Pulsed radiation damage
  - Pulsed pressure waves

ORNL DWG 96Z-3280

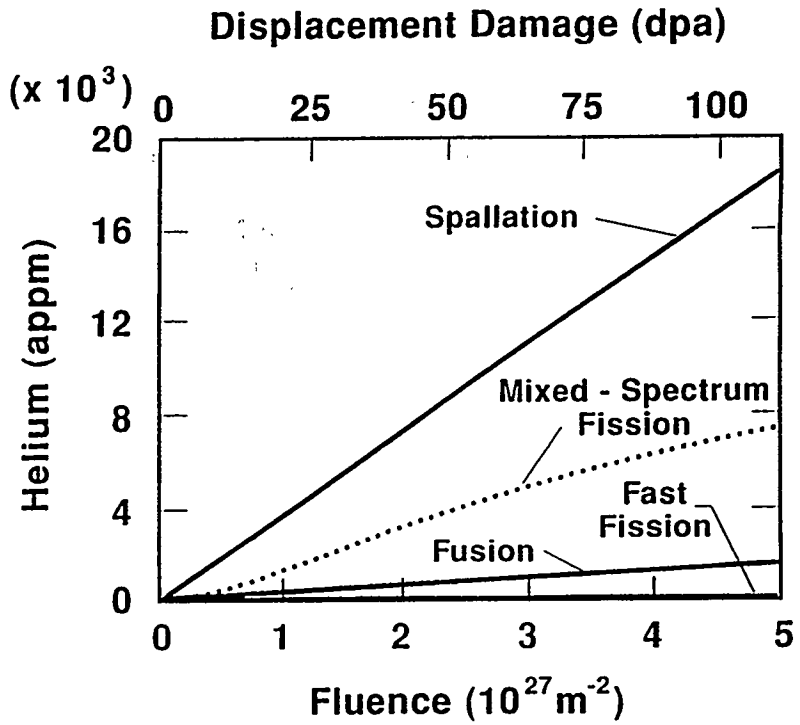

ORSNS MERCURY TARGET DAMAGE CALCULATIONS

Assumed Conditions

- 1 MW on target (1.2 GeV, 0.83 mA)
- 90 % of beam in 7 x 20 cm^2 area (flat)
- One year (1.6 x 10^{23} total protons)
- Front surface, "stainless steel"

*Preliminary Results**

Particle Energy	Displacement Damage, dpa	Helium, appm/dpa	Hydrogen, appm/dpa
All	8	54	552
n, p > 20 MeV	69 %	98 %	99 %
n < 20 MeV	31 %	2 %	1 %

*Calculations by Johnson, Charlton, and Barnes, ORNL

Effects of particle flux, beam shape and location on target

Facility	Max proton flux, μA/cm²	Beam Energy, GeV	Damage, dpa/y Front	Damage, dpa/y Centre
ORSNS (flat)	5	1.2	8	
" (shaped)	~15	1.2	~24	
" (5MW)	~75	1.2	~120	
ATW	50	1.6	35*	360†
LAMPF	~30	0.8	20‡	

* Window, p only
† Total damage
‡ Experiment completed on Inconel 718

ORSNS MERCURY TARGET DAMAGE CONSIDERATIONS

- Damage and gas production depends upon location on wall--expected to be higher at other points
- He production cross-section is a factor of 3 to 4 lower than experiment (Green, et al.) for Fe, using HETC
- Recent calculations for 750 MeV protons on Fe give similar (3 to 4) discrepancies using HETC or LAHET
- How to compare with experimental data for H?
- Two step reaction with thermal n's may add significantly more He
  - $^{58}Ni(n,\gamma)^{59}Ni(n,\alpha)^{56}Fe$

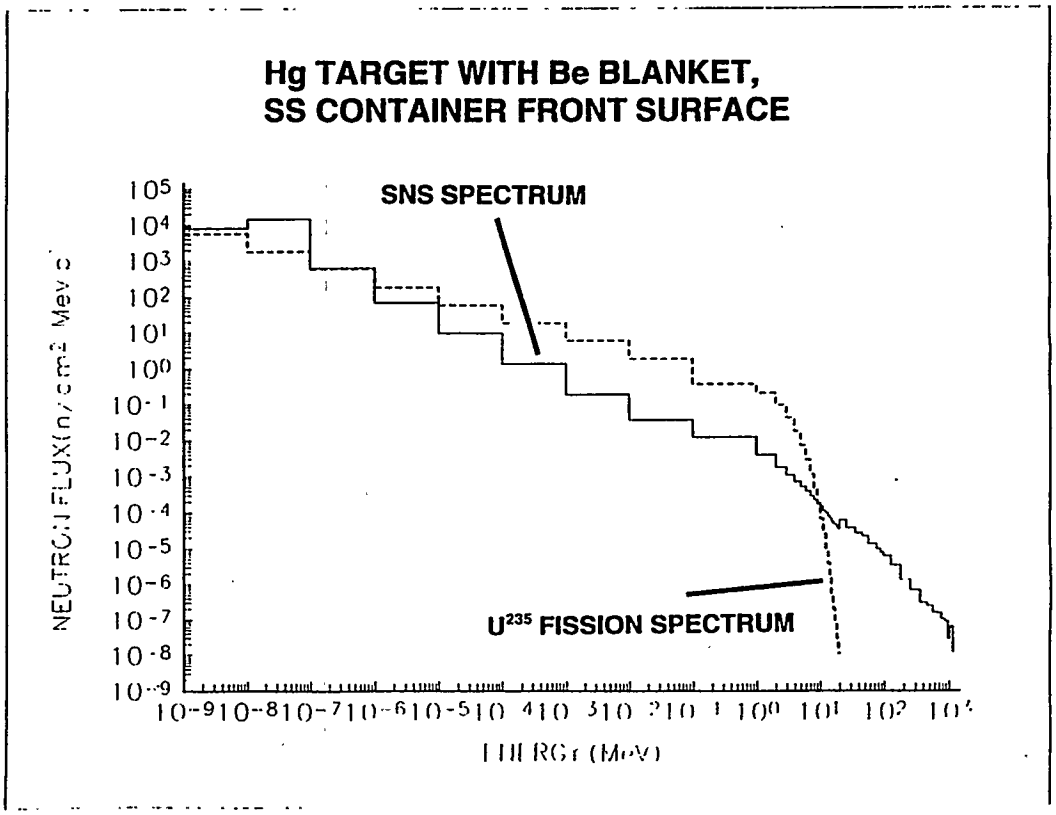

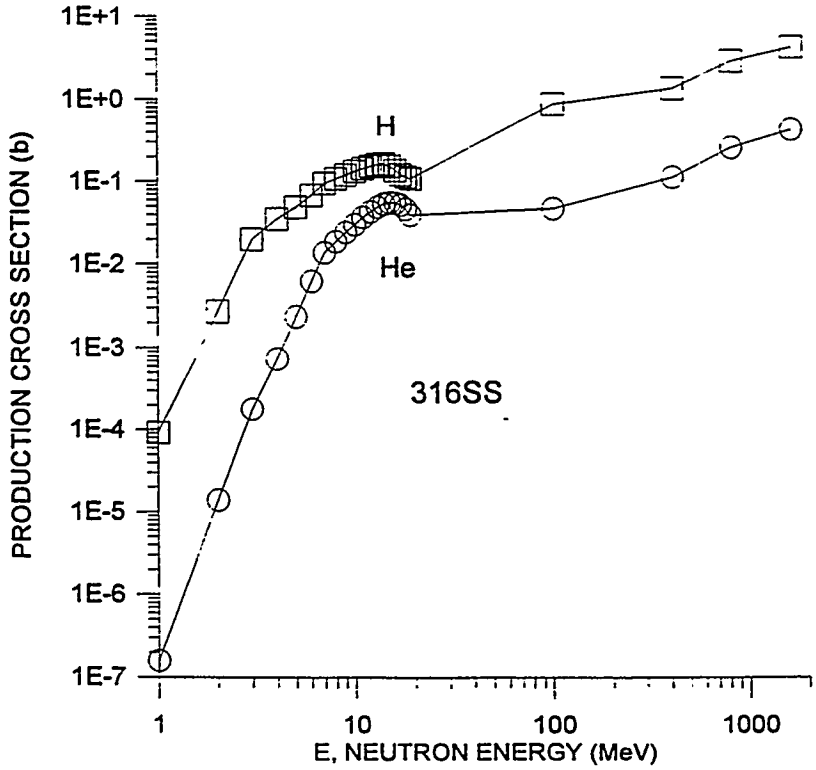

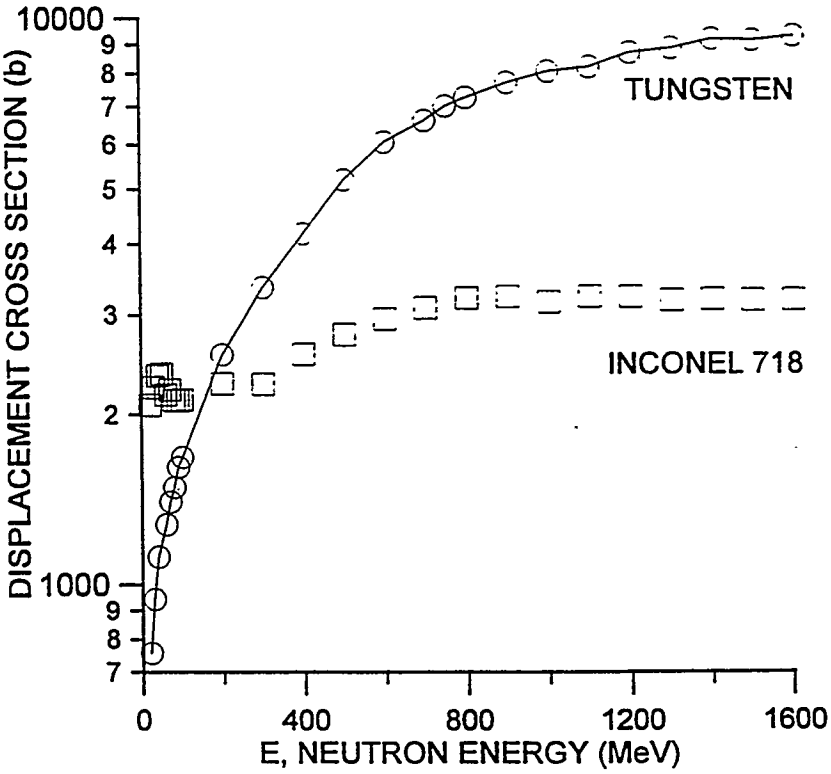

DISPLACEMENT CROSS SECTION FOR TUNGSTEN AND INCONEL 718 AS A FUNCTION OF NEUTRON ENERGY, ASSUMING THRESHOL DISPLACEMENT ENERGIES OF 90 AND 40 eV, RESPECTIVELY.

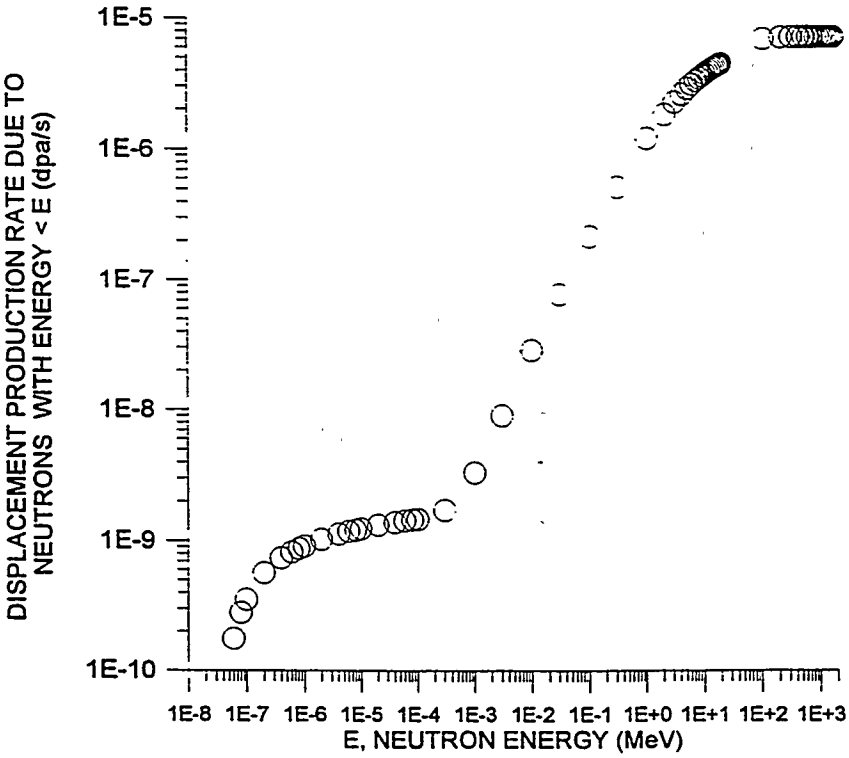

Displacement production rate versus neutron energy for 316 stainless steel (Fe - 18 wt% Cr - 10 wt% Ni). Files: c:\graf4win\ss\sskdspl4.grf, c:\graf4win\ss\sskdspl4.dat, and c:\excel5\ss\sskdsp&l.xls, Sheet 7.

OUTLOOK FOR MATERIALS IRRADIATION BEHAVIOR

- **Spallation Neutron Source irradiation conditions are unusual in terms of previous experience**
- **Performance data in more conventional environments ranges from extensive (stainless steels, aluminum alloys) to meager (tungsten, tantalum, . . .)**
- **Performance data in SNS environments ranges from sparse to non-existent**

HELIUM EXACERBATES RADIATION DAMAGE IN MATERIALS

- Triggers swelling
- Changes precipitation
- Causes or aggravates grain boundary embrittlement
- Increases hardening that may lead to loss of ductility

unirradiated

irradiated

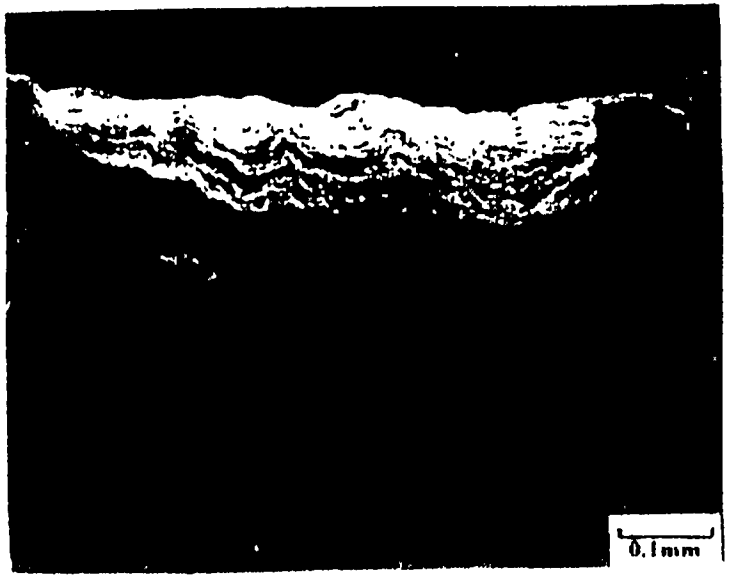

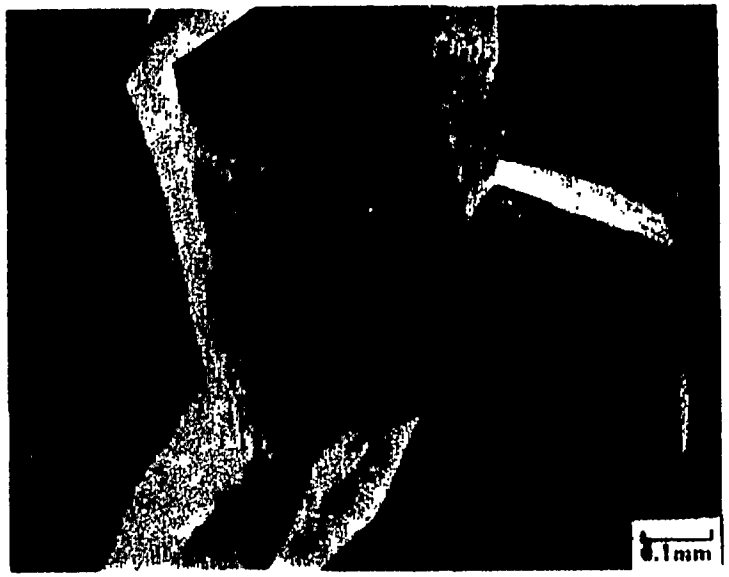

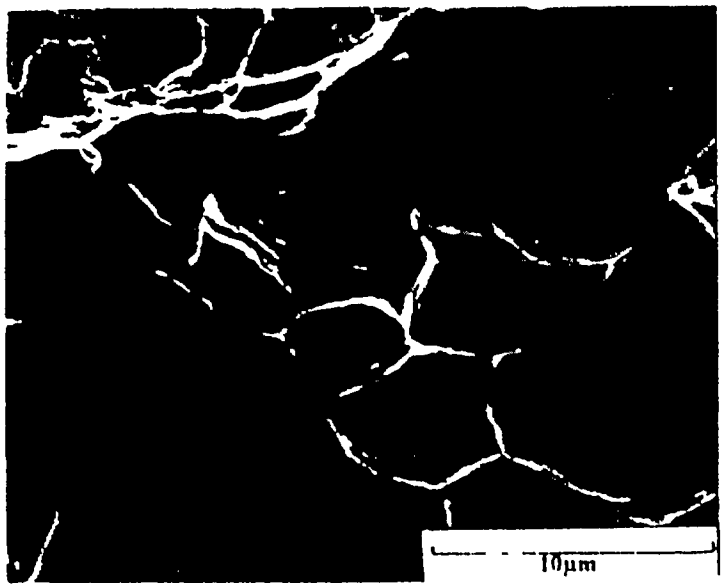

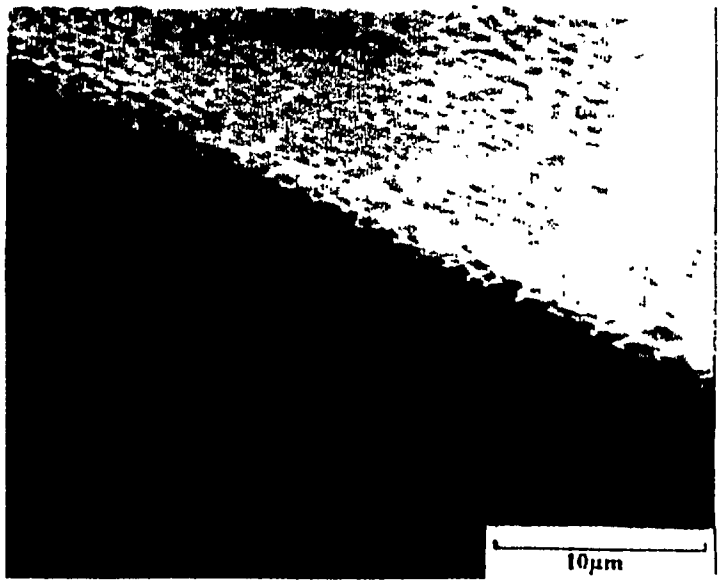

MATERIALS ISSUES FOR ORSNS TARGET

- Avoid component failures
- Achieve satisfactory lifetimes
  - Select and qualify materials
  - Obtain informed lifetime estimates

COMPONENTS CONSIDERED

- Target/coolant container
- Target elements and target cladding
- Beam windows
- Support structures/plumbing
- Moderator containers
- Beam tubes
- Materials irradiation facility

MATERIALS OF INTEREST FOR TARGETS, WINDOWS, STRUCTURAL MATERIALS

- Stainless steels
- Ferritic martensitic steels
- Tantalum
- High nickel alloys (Inconel 718)
- Tungsten
- Aluminum alloys
- Zirconium alloys
- Beryllium

MATERIALS-RELATED ISSUES FOR THE CONTAINER

- Radiation damage
- Compatibility
- Pressure pulse
  - Single pulse damage
  - Fatigue

RADIATION EFFECTS TASKS

- Analyze existing fission, fusion and ion irradiation data
- Irradiate candidate materials in spallation environments as available
- Perform reactor experiments in reactors (e.g., HFIR, HFBR) to attain high damage dose and using tricks to boost production of He and H
- Use ORNL's triple ion facility to determine combined effects of radiation damage, high He, high H and cycling on evolving microstructures
- Participate in international collaborations

CONTAINER MATERIALS

- Austenitic stainless steels
  - Suitable for operation (only?) at low temperature in contact with Hg
  - Entire target system can be designed for lower temperature operation
  - Better aqueous corrosion resistance
  - Non-magnetic
- Ferritic/martensitic steels
  - Better compatibility with Hg at high temperature
  - Stronger
  - Better thermal conductivity
  - Lower helium transmutation rate
  - Lower residual radioactivity

Radiation Hardening in Austenitic Stainless Steel is Accompanied by Significant Changes in the Stress-Strain Relationships

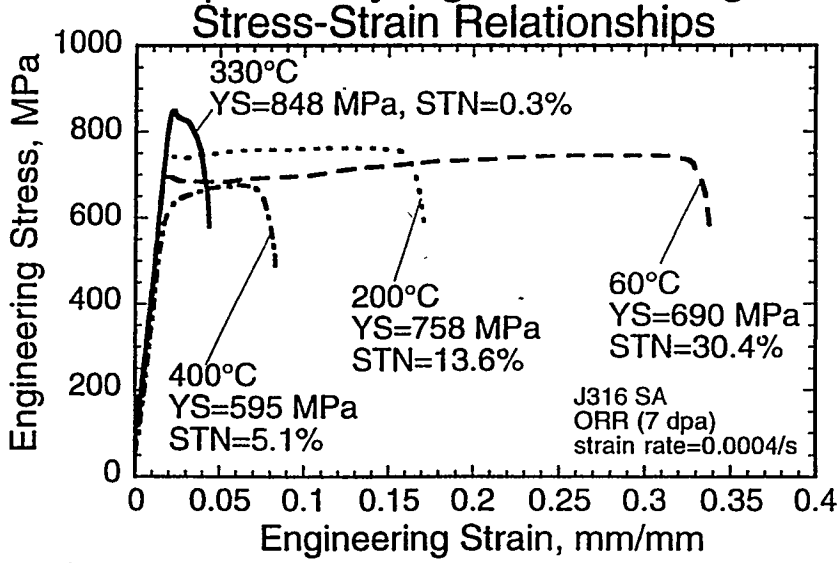

- For T≤200°C: yield drop, low work hardening rates, high total elongation, ductile failure mode
- For T=330°C: yield drop, no work hardening, rapid failure with STN < 1%, ductile failure mode

Damage-Temperature Map Can Be Used to Define the Regime of Low Ductility

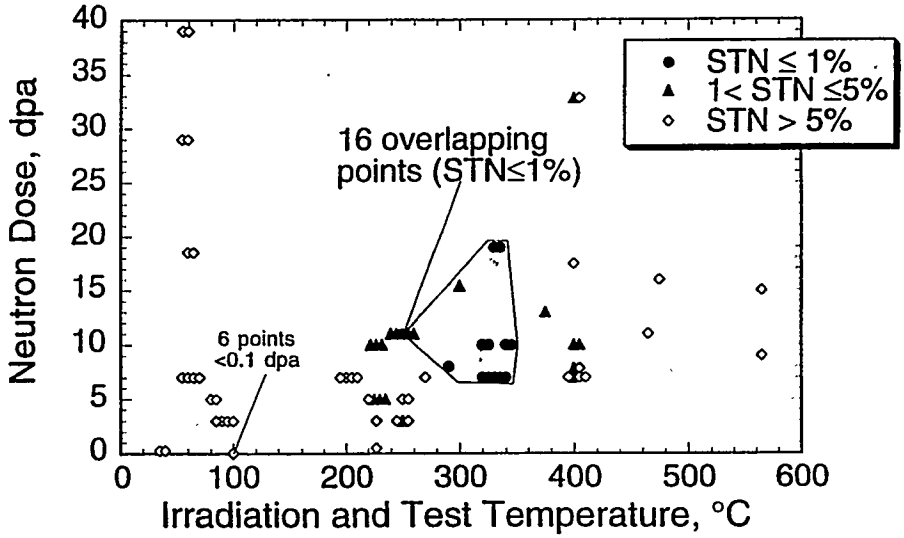

- STN>5%: ASME code rules apply
- 1%<STN<5%: "semi-brittle"
- STN<1%: "brittle" (zero strain hardening capacity)

Tensile Properties of Annealed 316 Austenitic Steels, Neutron-Irradiated and Tested at <100°C

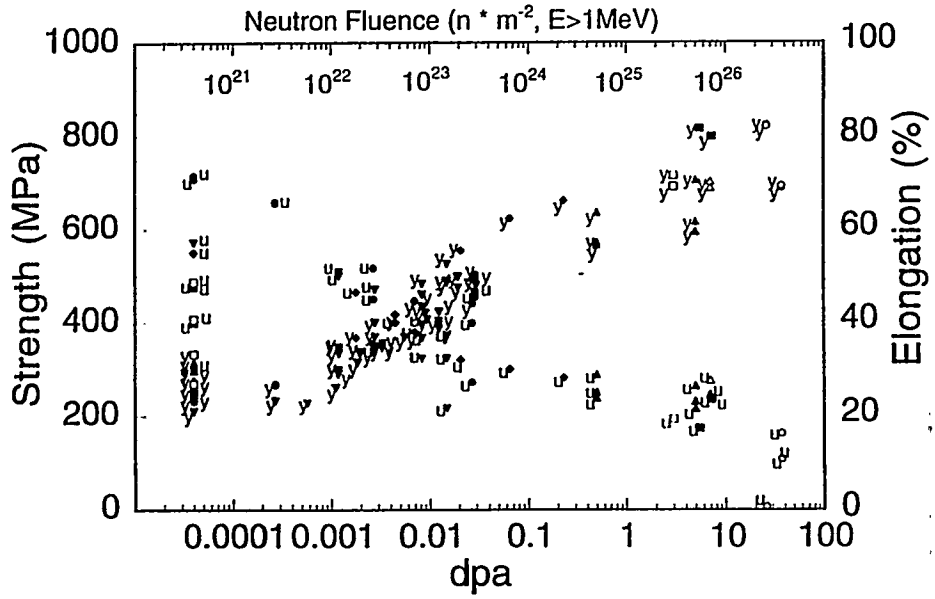

AFTER MODERATE IRRADIATION DOSE, DBTT SHIFTS IN FERRITIC STEELS CAN BE LARGE

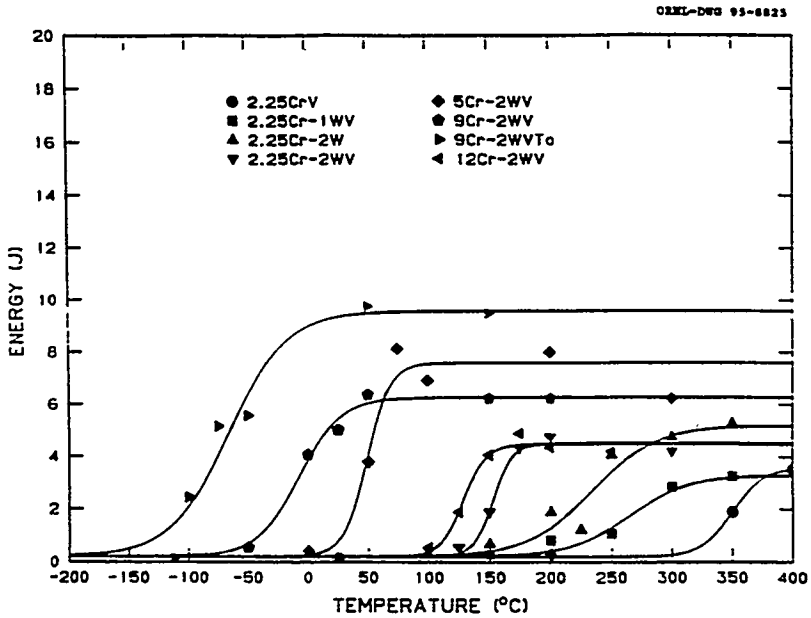

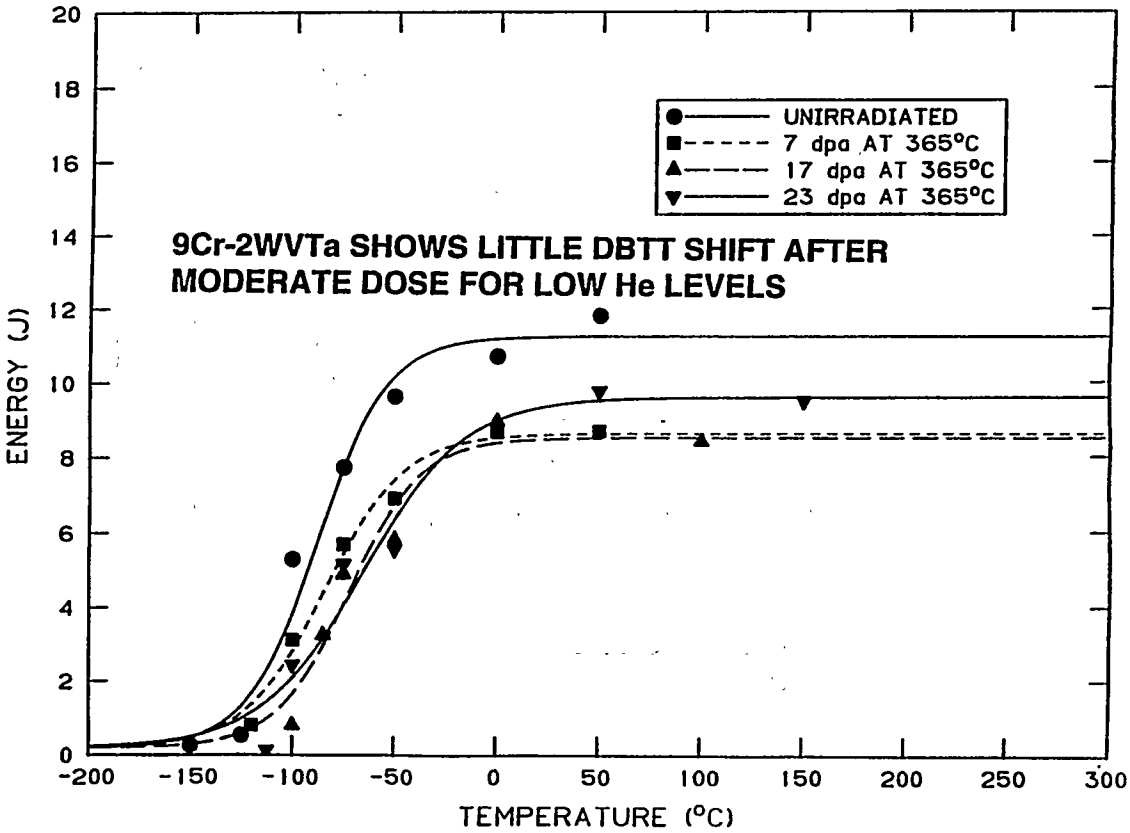

Helium Effects are Studied by Irradiation in HFIR

- Irradiation of nickel-containing steels in HFIR produces helium by two-step reaction of ^{58}Ni with thermal neutrons in mixed spectrum of HFIR
- 9Cr-1MoVNb contains ≈0.1% Ni; 12Cr-1MoVW contains ≈0.5% Ni
- 9Cr-1MoVNb and 12Cr-1MoVW with 2% Ni were also irradiated (2% Ni gives He:dpa ratio comparable to tokamak)
- Irradiation in HFIR has little effect on tensile behavior relative to irradiation in a fast reactor where little helium is produced
- A larger effect on Charpy impact behavior has been observed on steels irradiated in HFIR than in a fast reactor (FFTF and EBR-II)
- The effect has been attributed to the helium generated in HFIR

ORNL-DWG 90Z-14440A

9Cr-1MoVNb STEEL IRRADIATED IN HFIR

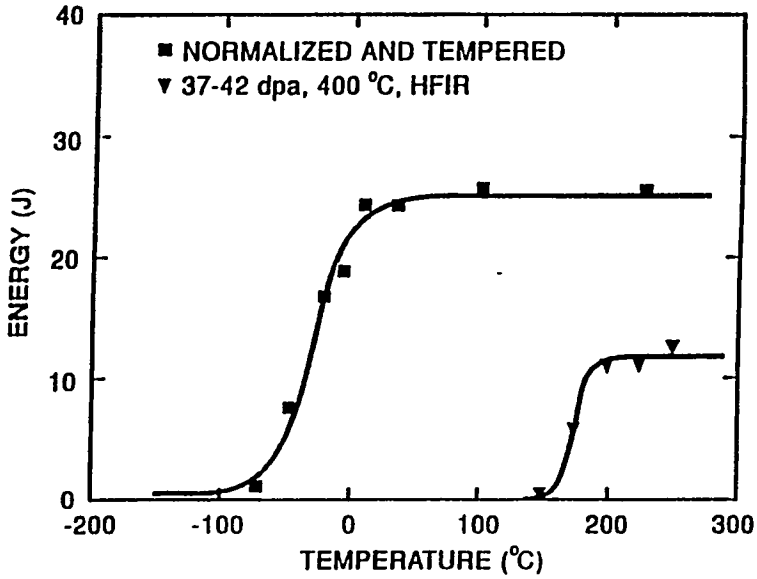

- SHIFT IN DBTT: 204°C AT 400°C IN HFIR
- SHIFT IS MUCH LARGER THAN IN EBR-II
- SHIFT FOR 9Cr-1MoVNb-2Ni WAS 348°C

ORNL-DWG 90Z-9764

SHIFT IN DBTT IN EBR-II AND HFIR FOR 9Cr-1MoVNb STEEL

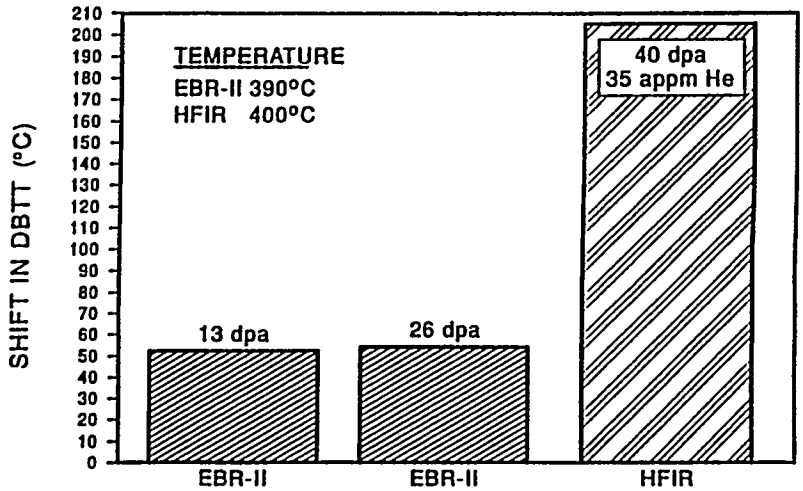

- SATURATION OF SHIFT IN DBTT OBSERVED IN SPECIMENS IRRADIATED IN FAST REACTOR (EBR-II), WHERE LITTLE HELIUM IS PRODUCED
- SATURATION VALUE OBSERVED IN FAST REACTOR IRRADIATION DOES NOT APPLY TO STEEL IRRADIATED IN HFIR, WHERE HIGH CONCENTRATIONS OF HELIUM ARE PRODUCED
- CONCLUSION IS THAT DIFFERENCE BETWEEN SPECIMENS IRRADIATED IN HFIR AND EBR-II IS CAUSED BY HELIUM

GOALS

- Extend our extensive-database yet limited-environment experience in radiation effects to spallation conditions
- Systematic irradiations in fission reactors for materials and irradiation conditions relevant to SNS
- Tie-point irradiations in high energy accelerators
- Special multiple-ion irradiations to assess high dose, high-hydrogen and irradiation cycling effects

NEW ENVIRONMENTS LEAD TO NEW RADIATION EFFECTS

Environment	Date	Discovery
Fast neutrons	1950's	Irradiation creep
Fast neutrons	1960's	Swelling
Fast neutrons	1970's	Changes in phase stability
High He transmutation rate	1950's-1970's	Embrittlement
Fast neutrons,	1980's	"Transient" interstitial creep
Pulsed irradiation	1980's	Changes in microstructure, phase stability, swelling
Hard-γ fields	1990's	Embrittlement
Ultra-high transmutation rates	??	
Large (GeV) span in neutron energies	??	

International Workshop on the Technology and
Thermal Hydraulics of Heavy Liquid Metals
Schruns, Austria
March 25-28, 1996

Martensitic/ferritic Steels as Container Materials for Liquid Mercury Target of ESS

Yong Dai

Paul Scherrer Institut, 5232 Villigen PSI, Switzerland

ABSTRACT

In the previous report [1], the suitability of steels as the ESS liquid mercury target container material was discussed on the basis of the existing database on conventional austenitic and martensitic/ferritic steels, especially on their representatives, solution annealed 316 stainless steel (SA 316) and Sandvik HT-9 martensitic steel (HT-9). Compared to solution annealed austenitic stainless steels, martensitic/ferritic steels have superior properties in terms of strength, thermal conductivity, thermal expansion, mercury corrosion resistance, void swelling and irradiation creep resistance. The main limitation for conventional martensitic/ ferritic steels (CMFS) is embrittlement after low temperature (≤380°C) irradiation. The ductile-brittle transition temperature (DBTT) can increase as much as 250 to 300°C and the upper-shelf energy (USE), at the same time, reduce more than 50%. This makes the application temperature range of CMFS is likely between 300°C to 500°C. For the present target design concept, the temperature at the container will be likely controlled in a temperature range between 180°C to 330°C [2]. Hence, CMFS seem to be difficult to apply. However, solution annealed austenitic stainless steels are also difficult to apply as the maximum stress level at the container will be higher than the design stress [1,3,4]. The solution to the problem is very likely to use advanced low-activation martensitic/ferritic steels (LAMS) developed by the fusion materials community though the present database on the materials is still very limited.

LAMS are considered tentative candidate materials for the first wall of future fusion reactors. R&D of LAMS have been emphasized since the late 1980s. LAMS have similar physical properties (e.g. thermal conductivity and thermal expansion) and strength as compared to CMFS. The mercury corrosion resistance of them are expected to be the same as or even better than those of CMFS as there is no Ni content in LAMS.

The main advantages of LAMS are that, firstly, the long-term residual radioactivity of CMFS after irradiation will be reduced, and secondly, LAMS have much better fracture properties in terms of lower DBTT and higher USE for unirradiated materials and, more important, less changes in DBTT, USE and fracture toughness after irradiation at low tempertures. The degradation in ductility and fracture toughness after irradiation are also less than those of CMFS. LAMS are, therefore, considered as the most feasible materials for the ESS mercury target container.

However, the definitive conclusion can be made only till a number of important issues being clarified. Firstly, irradiation effects produced by high energy proton irradiation. As the limited existing results on steels after high energy proton irradiation are at low doses, ≤~1 dpa, the results at high doses are needed. These results will be also useful for understanding helium embrittlement effects because high energy protons produce much more helium than neutrons in steels, especially in martensitic/ferritic steels. Secondly, mercury corrosion in steels at low temperatures (<~350°C) is little known though the corrosion rate is expected to be smaller or even much smaller than that at higher temperatures. The key issues such as stress corrosion cracking and irradiation assisted stress corrosion cracking of the material should be well understood before the material is chosen for the container. Finally, the distribution of stress and temperature at the beam window and other parts of the container should be known.

Above needs will be achieved partly in near future. Two PSI windows of martensitic steel DIN 1.4926 (similar to HT-9) irradiated in LAMPF to a peak dose of ~9 dpa and one 304 stainless steel window from ISIS Ta target of similar dose will be studied in KFA Jülich this year. Corrosion and stress corrosion cracking tests have been started in stationary mercury in PSI. Tests in mercury loops will be also performed this year. In long term, several kinds of austenitic and martensitic/ferritic steels, including some LAMS, will be irradiated in Los Alamos National Laboratory to a peak dose of about 20 dpa. The results should be obtainable in three or four years. Irradiation assisted stress corrosion cracking tests will be also planed.

PART-I INTRODUCTION

Mechanical and Radiation Loads at the Beam Entry

Mechanical load:

- Hg flow
- Temperature gradient
- Stress wave

Radiation load (calculated by using HETC code):
For an Fe base alloy container

- The irradiation damage:
  ~ 0.15 dpa/day by p^+
  ~ 0.3 dpa/day by $(p^+ + n)$
- The transmutation elements produced by p^+:
  ~ 1400 appm H/dpa ⇒ 210 appm H/day
  ~ 300 appm He/dpa ⇒ 45 appm He/day

Desirable properties of materials for Hg Target Container

High heat load capability

- High thermal conductivity
- Low thermal expansion

Mechanical properties

- High tensile and creep strength
- Adequate ductility and fracture toughness
- Resistance to fatigue crack growth

High resistance to radiation effects

- Low swelling and irradiation creep
- Minimal losses in ductility, impact properties and fatigue lifetime

High resistance to Hg corrosion

Materials considered

- **Martensitic/ferritic steels:**
  Conventional steels:
  HT-9, 9Cr-1Mo, MANET and EM10.
  Low-activation steels:
  9Cr-2W, Optimax, Optifer, F82H, JLF

- **Solution annealed 316 type austenitic stainless steel (SA 316)**

Chemical compositions of some CMFS, LAMS and 316 stainless steel

Steel	Cr	Ni	Mn	Mo	W	Nb	Ta	V	C	Si	Fe
HT-9	12.0	0.50	0.50	1.00	0.50	-	-	0.33	0.02	0.40	bal
MANET	10.8	0.92	0.7	0.77	-	0.16	-	0.20	0.14	0.37	bal
9Cr-1MoVNb	8.61	0.09	0.37	0.90	-	0.07	-	0.21	0.08	0.11	bal
EM10	8.76	0.18	0.48	1.05	-	-	-	-	0.10	0.37	bal
F82H	7.65	-	0.50	-	2.0	-	0.04	0.18	0.09	0.09	bal
JLF-1	9.0	-	0.50	-	2.0	-	0.07	0.2	0.10	0.05	bal
9Cr-2WVTa	8.72	-	0.43	-	2.09	-	0.07	0.23	0.10	0.23	bal
Optimax	9.24	-	0.56	0.09	0.96	-	0.08	0.24	0.09	0.02	bal
Optifer	9.3	-	0.5	-	0.96	-	0.07	0.26	0.10	0.06	bal
AISI 316	17.3	13.7	1.64	2.26	-	-	-	-	0.05	0.56	bal

PART-II COMPARISON BETWEEN AUSTENITIC STAINLESS STEELS AND CONVENTIONAL MARTENSITIC / FERRITIC STEELS

Thermal conductivity and expansion:

	HT-9	AISI 316
Thermal conductivity:	24 W $m^{-1}K^{-1}$	16 W $m^{-1}K^{-1}$
Thermal expansion coef.:	1.1×10^{-5} K^{-1}	1.6×10^{-5} K^{-1}

Yield and tensile strengths of unirradiated HT-9 and SA 316

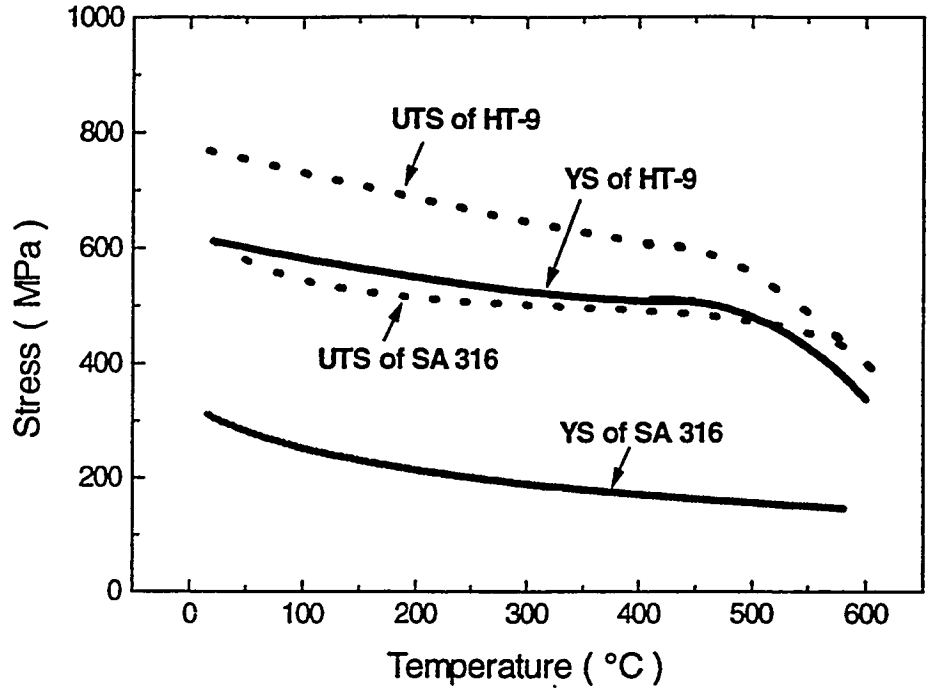

Swelling in HT-9, AISI 316 and D9

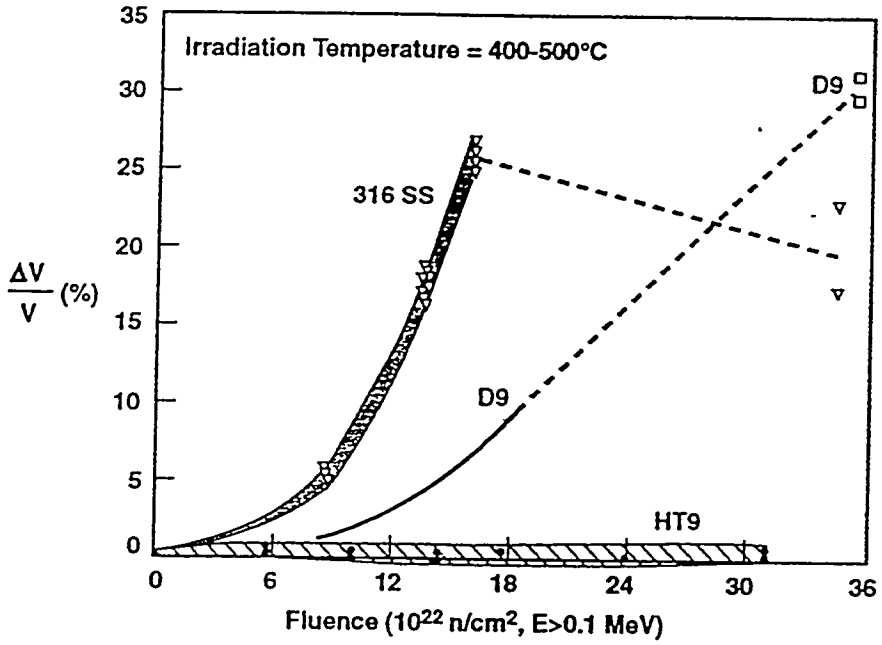

*Irradiation performed in EBR-II [5]

Irradiation creep in HT-9, AISI 316 and D9

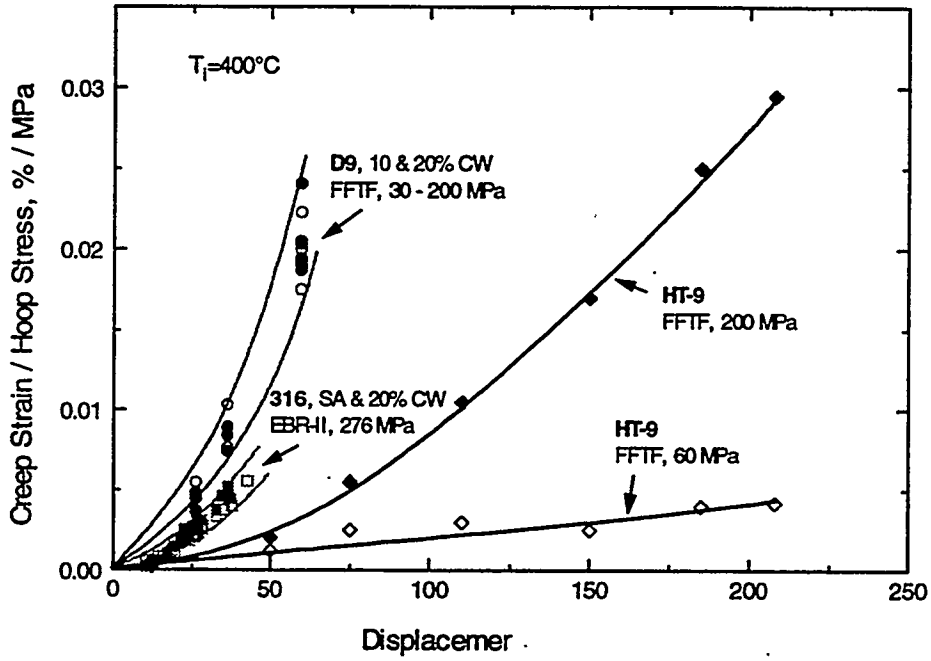

Normalized creep strain in HT-9, AISI 316 and D9. Data from [6-8]

Irradiation effects on tensile properties of HT-9

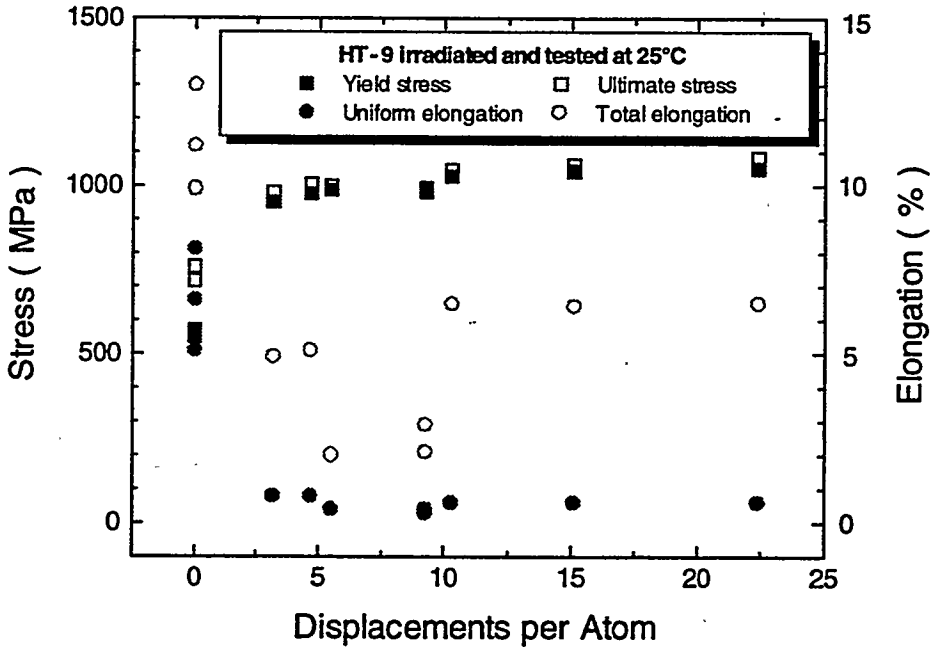

Change of tensile properties of HT-9 after irradiation at 50°C in HFIR and tested at 25°C [10].

Irradiation effects on the fracture toughness of HT-9

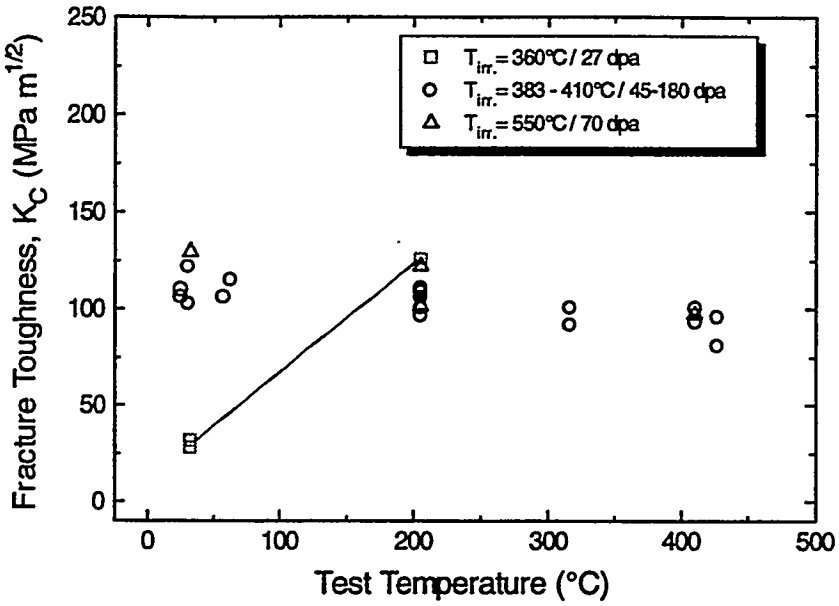

Fracture toughness of HT-9 after fast neutron irradiation tested at different temperature [11,12].

Irradiation effects on the DBTT of some CMFS

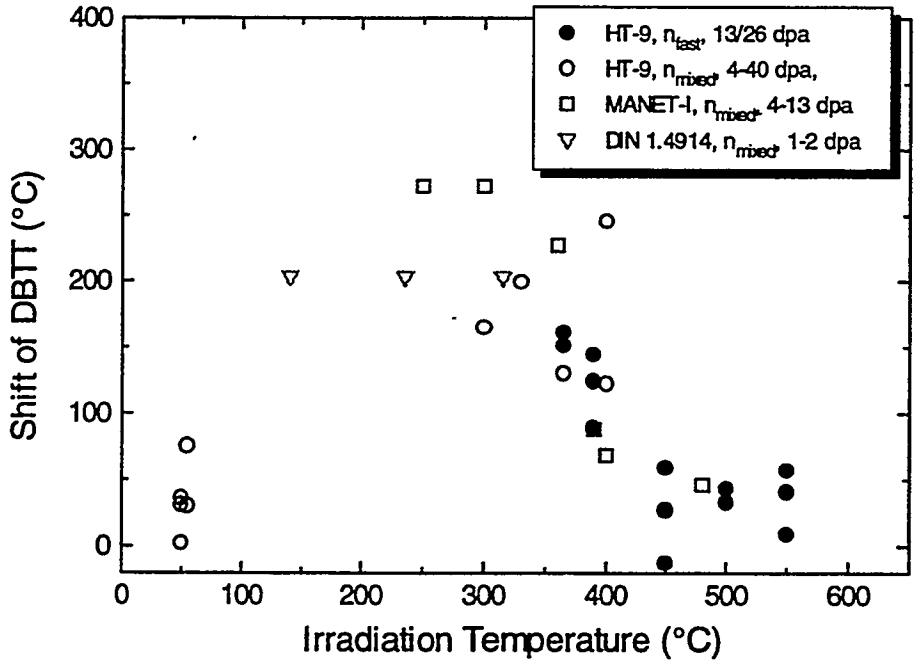

Shift of the DBTT of different martensitic/ferritic steels after fast and mixed-spectrum neutron irradiation [1].

Helium effects on DBTT in 9Cr-1MoVNb

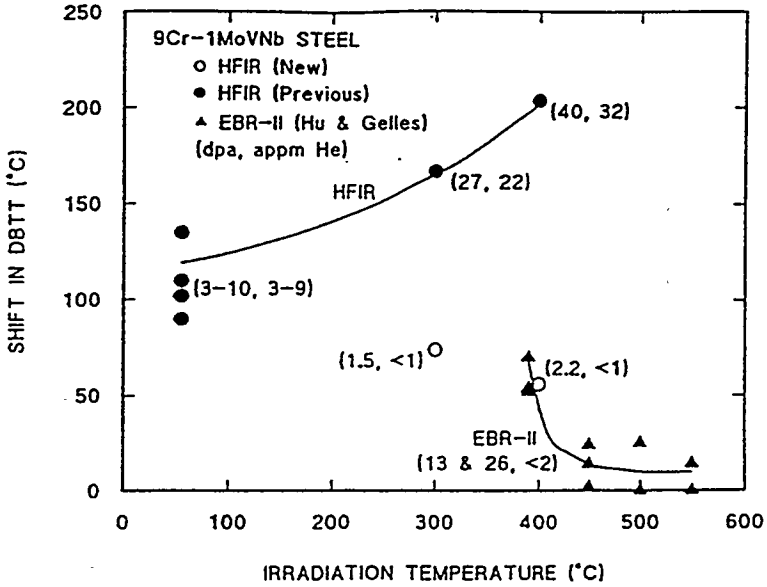

Shift of DBTT versus irradiation temperature for 9Cr-1MoVNb irradiated in HIFR and EBR-II. The difference between HIFR and EBR-II irradiation results was attributed to helium concentration [13].

Hydrogen effects in DIN 1.4914

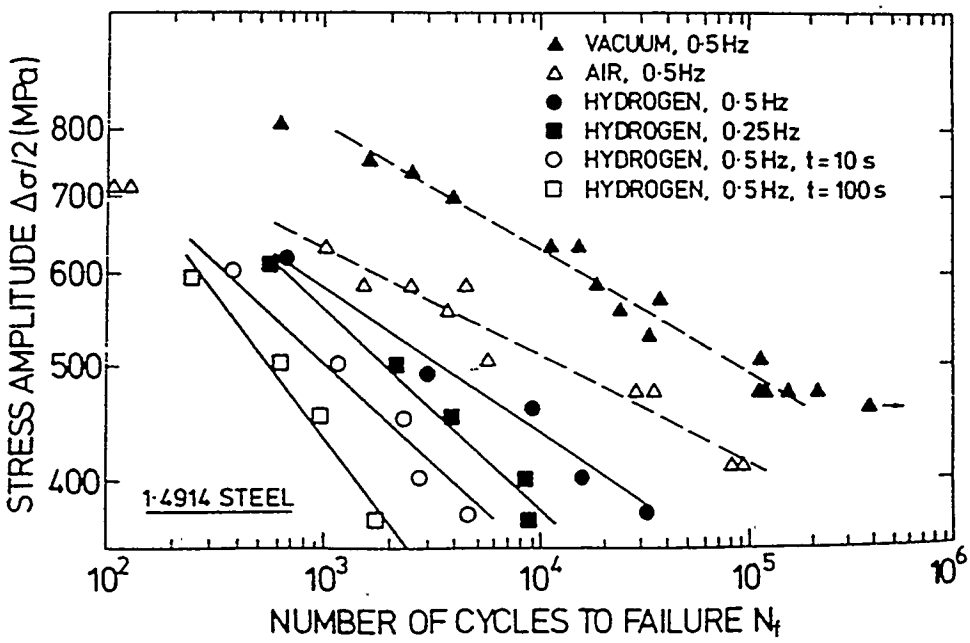

Fatigue lifetime as a function of stress amplitude for DIN 1.4914 tested at room temperature in vacuum, air and hydrogen [14]. Note the large reduction of the lifetime in the hydrogen cases.

Mercury corrosion in different steels

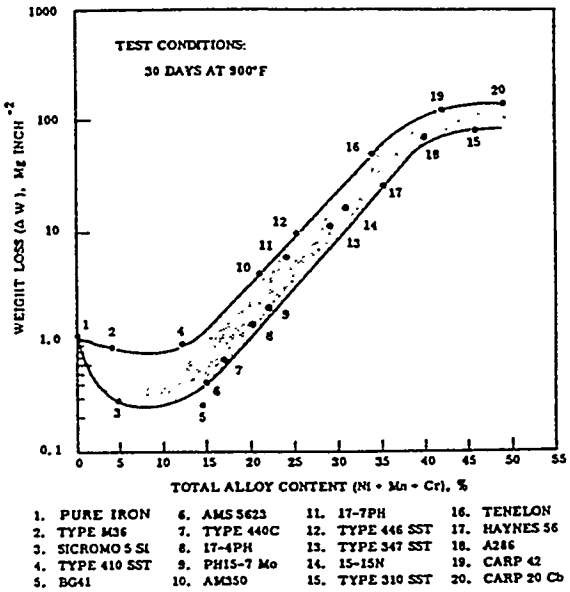

Effect of total Ni, Mn and Cr alloy content of iron base alloys on mercury corrosion at 900 F (482°C) [9]. Note the total Ni, Mn and Cr content of martensitic/ferritic steels is generally less than 15% but that of austenitic steels is about 35%, therefore, it can be seen the corrosion rate of austenitic stainless steels is much higher.

Application ranges of HT-9 and SA 316

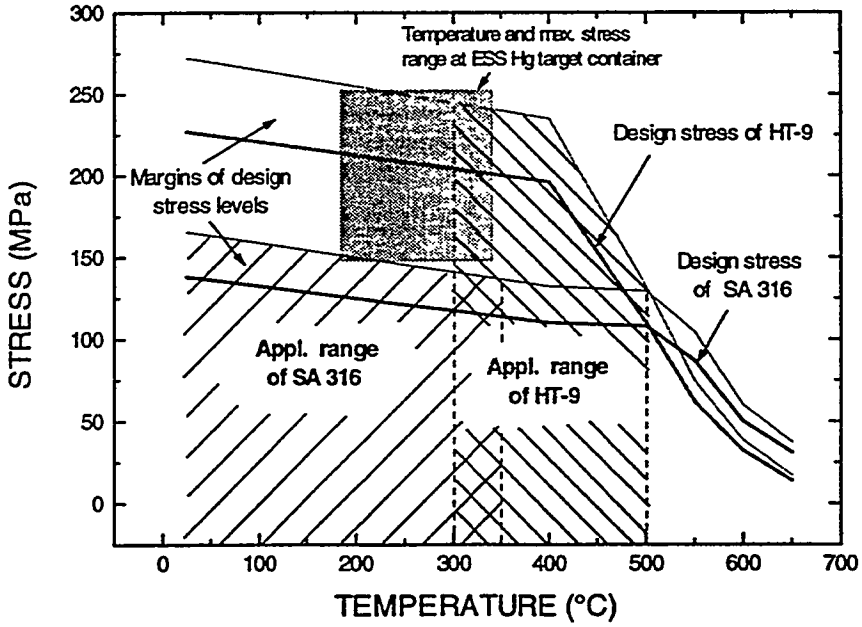

Sketch showing design stress and temperature range for SA 316 and HT-9, as well as the temperature and max. stress range at the ESS Hg target container. Note that in this case both solution annealed stainless steels and CMFS are difficult to apply.

PART-III IRRADIATION EFFECTS IN LOW-ACTIVATION MARTENSITIC/FERRITIC STEELS

Irradiation effects on tensile properties

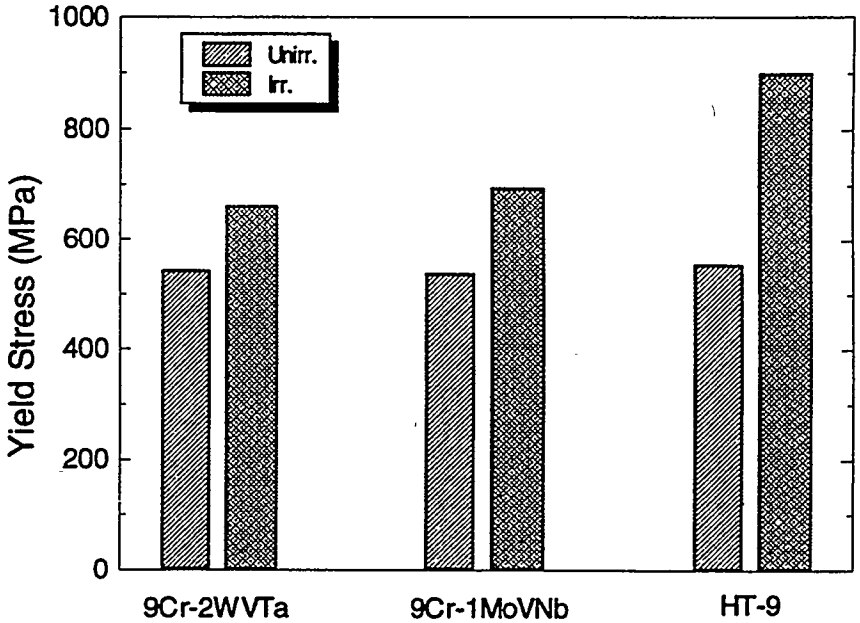

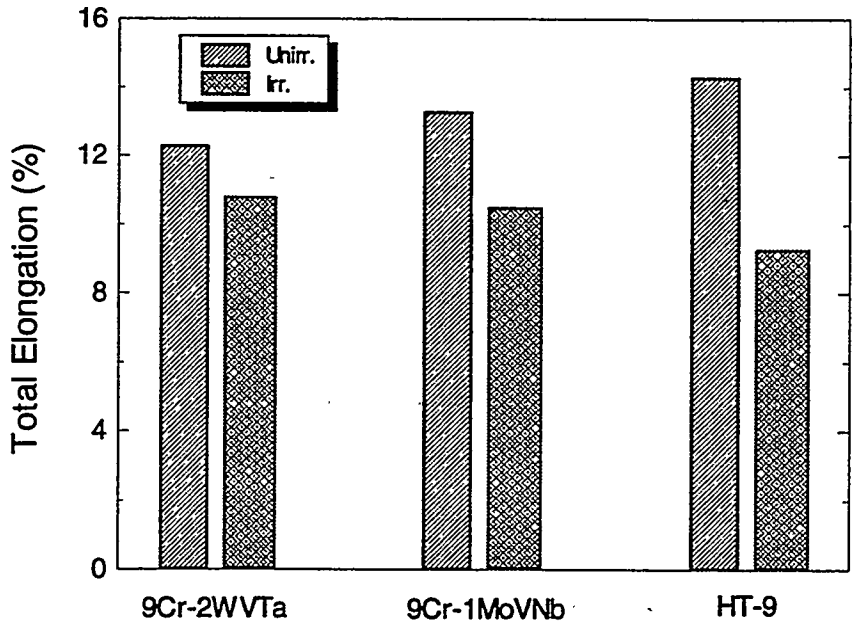

Yield stresses and total elongations of 9Cr-2WVTa, 9Cr-1MoVNb and HT-9 before and after irradiation at 365°C of 7 dpa in FFTF [15]. Note the LAMS 9Cr-2WVTa has smallest changes in both yield stress and total elongation.

Irradiation effects on impact properties in 9Cr-2WVTa and HT-9

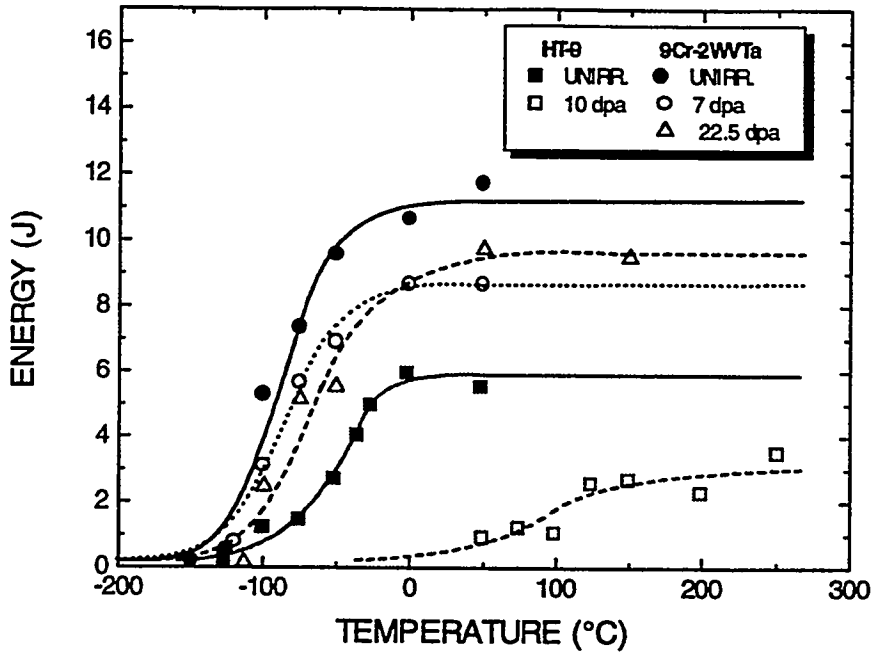

Charpy impact curves for 1/3 size HT-9 and 9Cr-2WVTa specimens after irradiation at 365°C in FFTF [16,17]. Note the low DBTT and high USE in unirradiated 9Cr-2WVTa and much less changes in DBTT and USE after fast neutron irradiation.

Irradiation effects on fracture toughness in F82H and HT-9

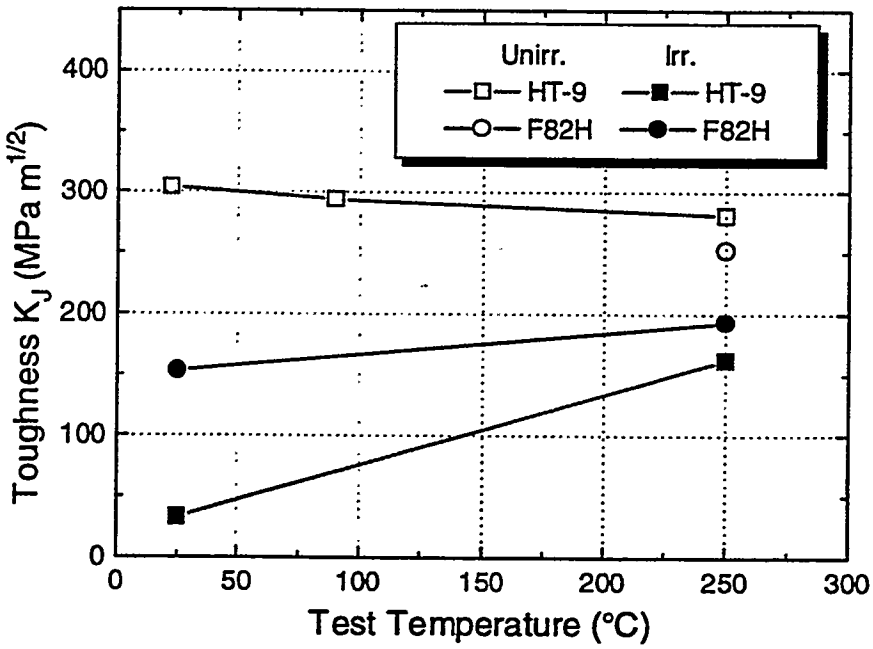

Fracture toughness in HT-9 and F82H before and after irradiation at 250°C to 3 dpa in HFIR [18].

Irradiation creep in LAMS and CMFS

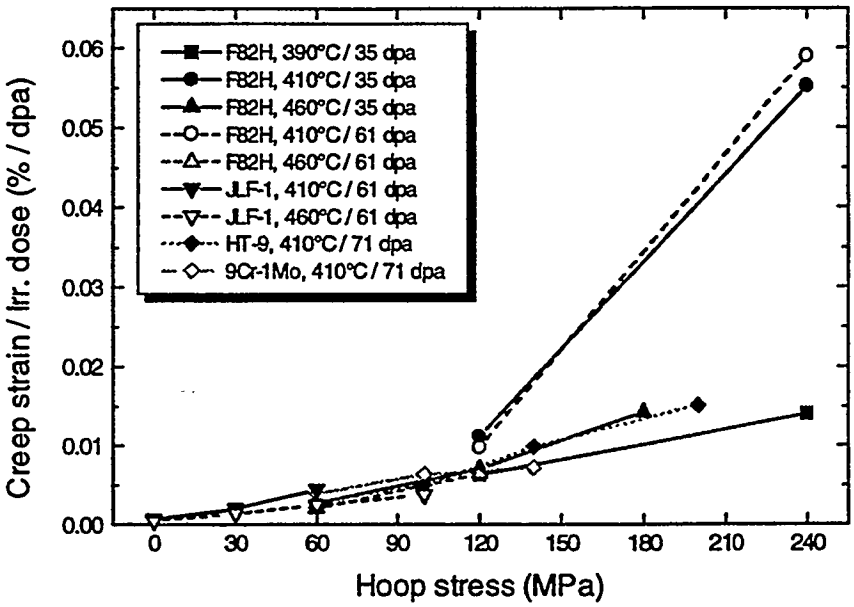

Normalized creep strain in F82H, JLF-1, HT-9 and 9Cr-1MoVNb irradiated in FFTF. Data quoted from [8, 19,20]

Application ranges of LAMS and CMFS

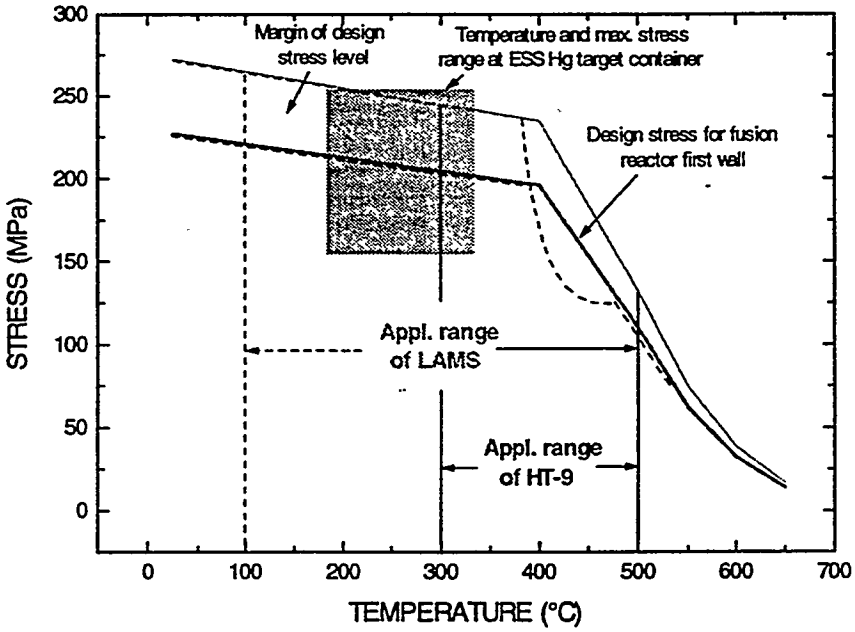

Sketch showing design stress and temperature range for LAMS and CMFS (HT-9), as well as the temperature and max. stress range at the ESS Hg target container. Note that the low temperature limit of LAMS may be extended as low as about 100°C based on the fast neutron irradiation data. The information from high energy proton irradiation is needed to make a definitive conclusion.

Summary:

- With improved fracture properties, advanced low-activation martensitic/ ferritic steels are considered as the most feasible materials for the ESS mercury target container.

- Conventional martensitic/ferritic steels can be applied in a range from about 300°C to 500°C with relatively high stress, and solution annealed austenitic stainless steels can be applied in a range of temperature up to about 350°C but at low stress levels.

REFERENCES

[1] Y. Dai, Proc. of ICANS-XIII, (PSI, Switzerland, 1995), p. 604.
[2] T. Dury, this proceedings.
[3] K. Skala and L.P. Ni, this proceedings.
[4] B. Guttek, this proceedings.
[5] F.H. Huang, in *Effects of Radiation on Materials: 16th Inter. Sym.*, (ASTM STP 1175, 1993), p. 575.
[6] L.C. Walters, G.L. McVay and G.D. Hudman, in: *Proc. of Inter. Conf. on Radiation Effects in Breeder Reactor Structural Materials*, (AIME, New York, 1977), p.277.
[7] F.A. Garner, M.L. Hamilton, C.R. Eiholzer, M.B. Toloczko and A.S. Kumar, in *Effects of Radiation on Materials: 16th Inter. Sym.*, (ASTM STP 1175, 1993), p. 696.
[8] M.B. Toloczko, F.A. Garner and C.E. Eiholzer, *J. Nucl. Mater.* **212-215** (1994) 604.
[9] J.F. Nejedlik and E.J. Vargo, *Corrosion*, **20** (1964) 384.
[10] R.L. Klueh and J.M. Vitek, *J. Nucl. Mater.* **161** (1989) 13.
[11] F.H. Huang and M.L. Hamilton, *J. Nucl. Mater.* **187** (1992) 278.
[12] F.H. Huang, in *Effects of Radiation on Materials: 15th Inter. Sym.*, (ASTM STP 1125, 1992), p. 1267.
[13] R.L. Klueh and D.J. Alexander, *J. Nucl. Mater.* 218 (1995) 151.
[14] J.I. Shakib, H. Ullmaier, E.A. Little, R.G. Faulkner, W. Schmitz and T.E. Chung, *J. Nucl. Mater.* **212-215** (1994) 579.
[15] R.L. Klueh and D.J. Alexander, *J. Nucl. Mater.* 218 (1995) 151.
[16] R.L. Klueh and D.J. Alexander, in: Effects of Radiation on Materials: 15th Intern. Sym., (ASTM STP 1125), 1992, p.1256.
[17] R.L. Klueh and D.J. Alexander, ICFRM-7, to be published in J. Nucl. Mater..
[18] D.J. Alexander,et al., *Fusion Materials Semiannual Progress Report*, (DOE/ER-0313/16, ORNL, 1994), p. 173.
[19] A. Kohyama, Y. Kohno, K. Asakura, M. Yoshino, Mater. Trans. JIM, vol. 34, (1993) 1061.
[20] A. Kohyama, Y. Kohno, K. Asakura, M. Yoshino, C. Namba, and C.R. Eiholzer, J. Nucl. Mater. **212-215** (1994) 751.

SESSION 7

Pulsed Operation and Gas Admixture (1)

Chairman
E. Yefimov

Pressure waves in liquid mercury target from pulsed heat loads and the possible way controlling their effects

Liping Ni and Karel Skala
Paul Scherrer Institute, CH-5232 Villingen, Switzerland

1. Abstract

In ESS project liquid metals are selected as the main target materials for the pulsed spallation neutron source. Since the very high instantaneous energy is deposed on the heavy molten target in a very short period time, pressure waves are generated. They travel through the liquid and cause high stress in the container. Also, additional stress should be considered in the wall which is the result of direct heating of the target window. These dynamic processes were simulated with computational codes with the static response being analized first. The total resulting dynamic wall stress has been found to have exceeded the design stress for the selected container material. Adding a small amount of gas bubbles in the liquid could be a possible way to reduce the pressure waves.

2. Introduction

The selection of a liquid metal target is based on convective heat removal from reaction zone and good production of neutron ([1]). Fig. 1 shows a conceptural design of ESS liquid target in pulsed spallation sources. The proton beam with very high power (100 kJ per pulse) is injected into the target during a very short period time at a high repetition rate (1 μs at 50 Hz). About 56% of the beam energy are deposited in the target material and converted into heat, which causes a sudden temperature increase and a rapid local pressure rise. The effects of pressure waves on the structural integrity of the container have become the main problem from the design point of view.

3. Simulation model (PSI-code)

As shown in Fig. 2, during the very short pulse period, the thermal expansion is strongly prevented by the surrounding materials, as a result, the local pressure in the isochorically heated liquid goes up rapidly. This pressure is the cause of acceleration of the surrounding material whose velocity is obtained via an integration over time. The motion of this material will reduce the pressure, giving rise to feedback between the volume elements in the target. The pressure wave will thus propagate through the compressible material with the velocity of sound. It passes through the non-heated zones of the target and reaches the wall where it causes mechanical stress. Due to the elastic properties of the wall it will be reflected back into the material in the liquid and the pressure waves could be either increased or decreased as the results of superposition with the reflected waves.

The detailed modeling of this dynamic process has been reported in reference [2]. The governing equations of the simulation are conservation of mass and energy and the equation of motion. The pressure rise is derived to be:

$$\Delta p = K \{c_p/c_v\} \Delta V/V_0 \qquad (1)$$

where

$$K = V_0 \{\partial p/\partial V\}_T$$

is the isothermal bulk modulus of the liquid and ΔV is the volume change during the pressure wave propagation. Because of the tensile strength of the wall, the pressure gives rise to stresses in the wall material which are the sum of the direct pressure load on a surface element and stresses due to the influence of neighbouring elements. The bending stress is calculated in analogy to the case of a beam with two fixed ends under lateral displacement.

In the container wall, especially on the window top centre of the target, an additional stress wave is created through the direct heating of the beam. Also, this dynamic response could be calculated using above model with the Youngs' modulus and the poisson-ratio of the container materials.

The total wall stress is therefore the sum of these two parts: one from the pressure wave in the liquid and another from the stress wave through direct heating. The simulation code (PSI-code) uses finite difference method and gives many possibilities of the boundary conditions and terget geometries.

4. Dynamic response of the pressure waves in the mercury target

As an illustrative example, here we show the simulation results of a cylindrical target with an elastic dome-shaped window, in which mercury is the target material. The cylinder has a inside diameter of 200mm, a height of 620mm and the wall thickness of 3mm. The beam power distribution is taken essentially as an exponential along the beam axis (or the depth of the target) and as a parabolic in the radial direction of a beam diameter of 110mm.

Fig 3 shows the dynamic stress distribution from the dome window to the cylindrical wall for three different time points after the pulse. In the dome window area there are some complicated vibrations with high peak stresses (about 480 MPa at t=55µs !). These instataneous stresses can also be found in Figs.4 and 5. Fig. 4 shows the stress distribution as a function of time at different depths. In contrast to the curve I=3, which presents the immediate response of the pressure waves, curves I=16 and I=31 indicate a reaction delaying of ca. 20µs. That means, it takes 20µs for the pressure wave to reach the wall, and the pressure rise is moderated through the non-heated zone of liquid. Therefore the stresses in cylinder wall are smaller then that in the dome window. All results show clearly that the peak stresses have already exceeded the design stress of about 200 MPa for the selected container material !

5. Effects of gas bubble on the pressure waves

According to equation (1) the pressure rise in the liquid is directly proportional to the bulk modulus K. Considering the fact that gases can be compressed more easily than solids or liquids, we may expect that a small volume of gas bubble ε can be continuously injected into the region where the interaction between the liquid and proton beam takes place. The modulus of elasiticity for the mixture can be derived as:

$K_{mix} = \{ 1/K + \varepsilon/(np) [p_0/p]^{1/n} \}^{-1}$

which is a function of the bulk modulus of the liquid K, the volume fraction of gas bubble ε, the initial and instantaneous pressures (p_0 and p), and the gas exponent n. Since K is usually very large (for mercury $K=2.77*10^{10}$ [N/m^2]), the high pressure level could be moderated even for very small values of ε. Figs. 6 and 7 give stress response after adding a volume of 3% helium gas bubbles and the results are much better. The stress level on the wall has droped almost by two orders of magnitude, and the resulting stress is far below the design criterion especially in the dome area. The stress rise along the depth is caused by the hydrostatic pressure and for the optimum volume of gas further investigation is needed.

6. Dynamic response of the target window

Only the dome-shaped target window has been calculated since it is the main affected area by the direct heating. For the same reason the most interesting point is the top centre of the window. The structural response has been simulated using both the PSI-code and a commercial code named ANSYS, the latter is a finite element general purpose code capable of performing analyses where nonlinear and large displacement effects are involved. A good agreement of the results from both codes has been found.

Because of the symmetry of geometry and power distribution, a quasi three dimensional ANSYS-element (PLANE 42) was used. The static thermal stress was analized first. Fig. 8 shows the hoop stress at the dome centre area (window 1 in isolines) and the displacement (window 2, where the displacement changes were enlarged 499 times) in which the dashed lines presents original and the solid lines the changed structure. It can be seen that hoop stress in the outside surface is tensile and in the inside compressive.

The dynamic analysis was done using Newmark time integration method and the results are shown in spherical coordinate system. Fig. 9 gives the radial stress and hoop stress at the top centre of the dome as a function of time. The radial stress is in this situation predominant and it reaches a maximum of about 78 MPa. The radial stress distributions at two time points („1" for t=1.5μs and „2" for t=2μs) can be seen in Fig. 10, which indicate tensile stresses at t=1.5μs and compressive stress at t=2μs in the middle line. The results indicate a maximum hoop stress of 39% of the design stress.

7. Conclusions

Through the simulation studies of the structure response of the target we may conclude that the container wall endure two parts of stresses, one is the dynamic stress due to pressure waves in the liquid and the other is the thermal stress through direct heating. In our case, the maximum thermal stress reaches 39% of the design criterion, but the wall stresses due to the pressure waves are much higher and could be very serious for the container design. Adding a small volume fraction of helium gas bubble could reduce pressure level of about two orders of magnitude.

References

[1] G.S.Bauer:"ESS-Liquid Metal Target Studies: Status report". March, 1995

[2] K. Skala and G.S. Bauer:" on the pressure wave problem in liquid metal tergets for pulsed spallation neutron souces, 2nd Status report". Oct. 1995

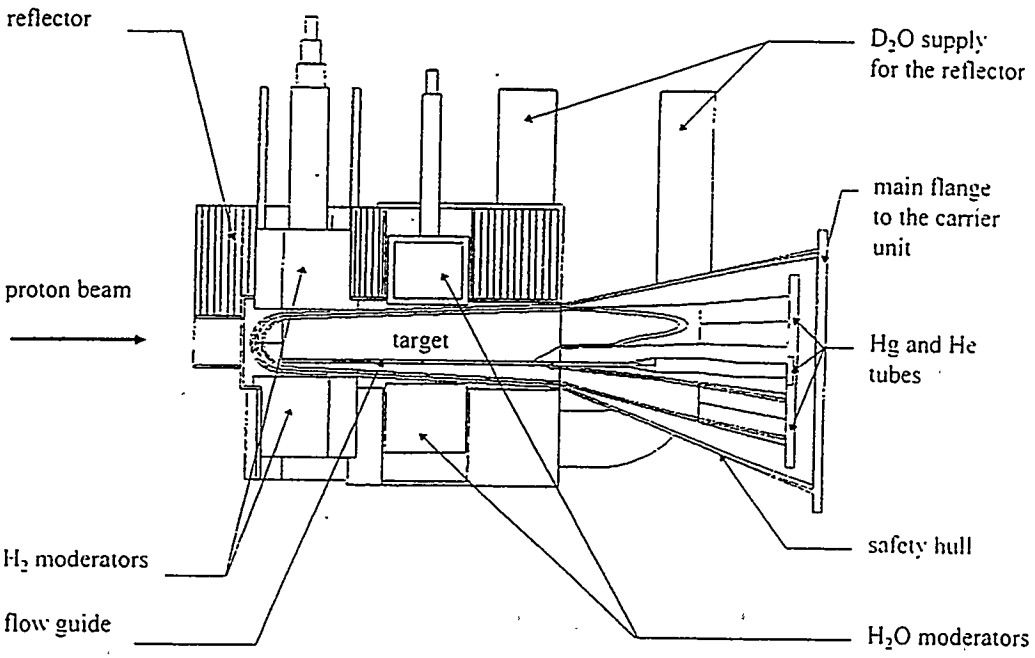

Fig.1 Schemetic concept of the ESS liquid metal target

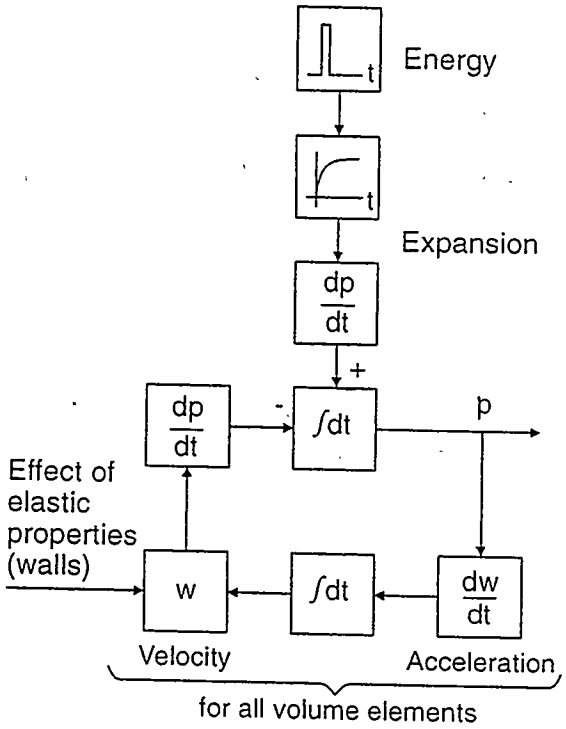

Fig. 2 Simulation procedure of pressure waves in a liquid metal target

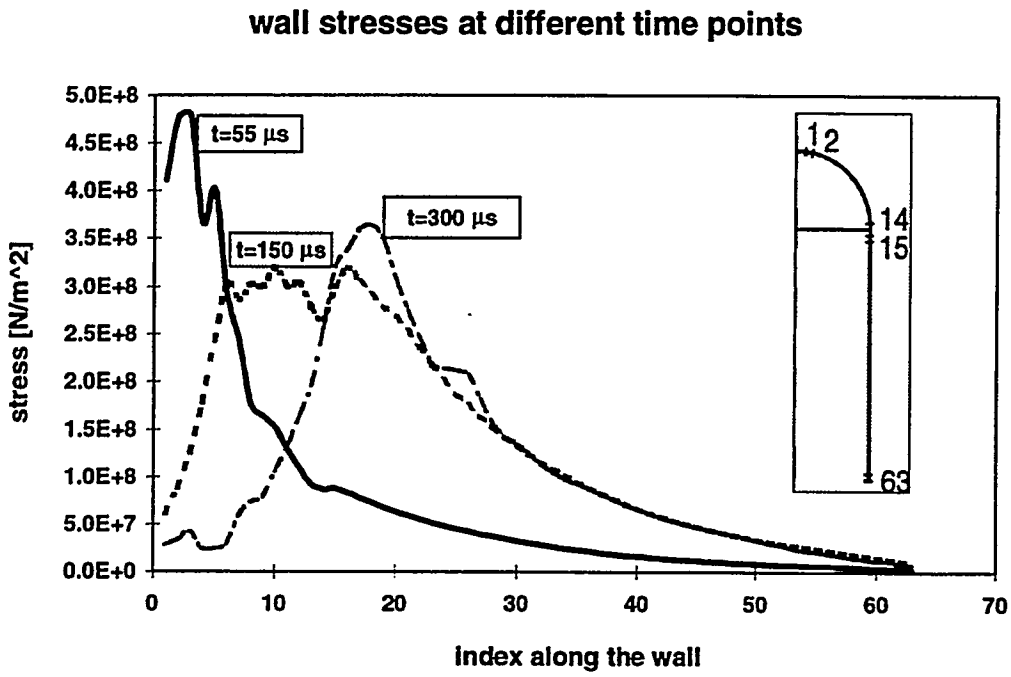

Fig. 3 Wall stresses at different time points.

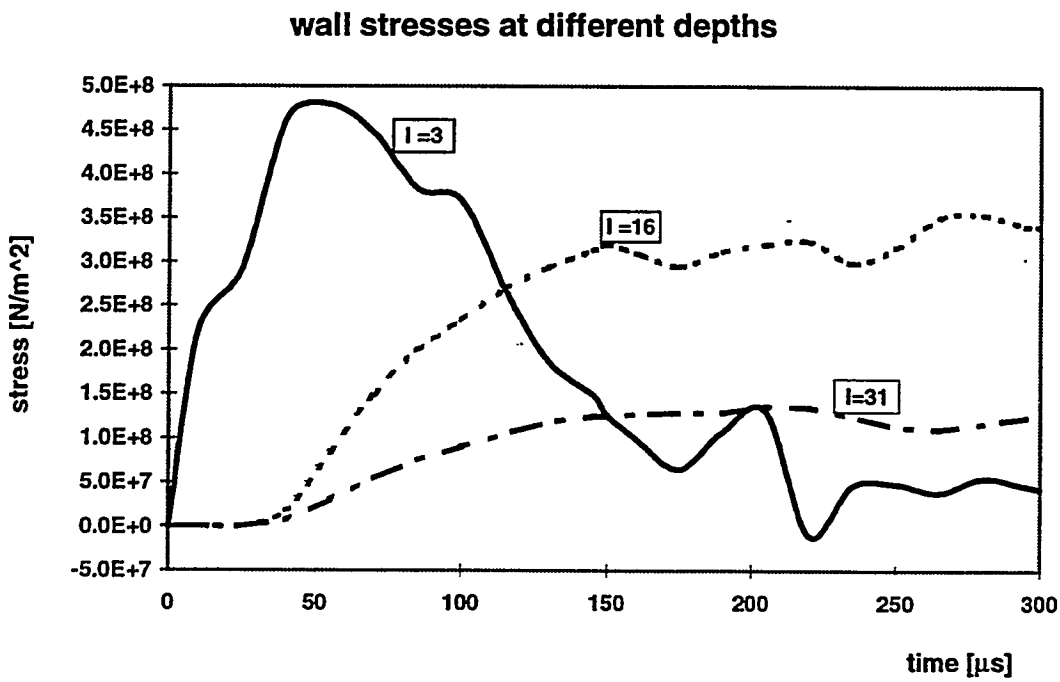

Fig. 4 Stress histories on the wall at different depths

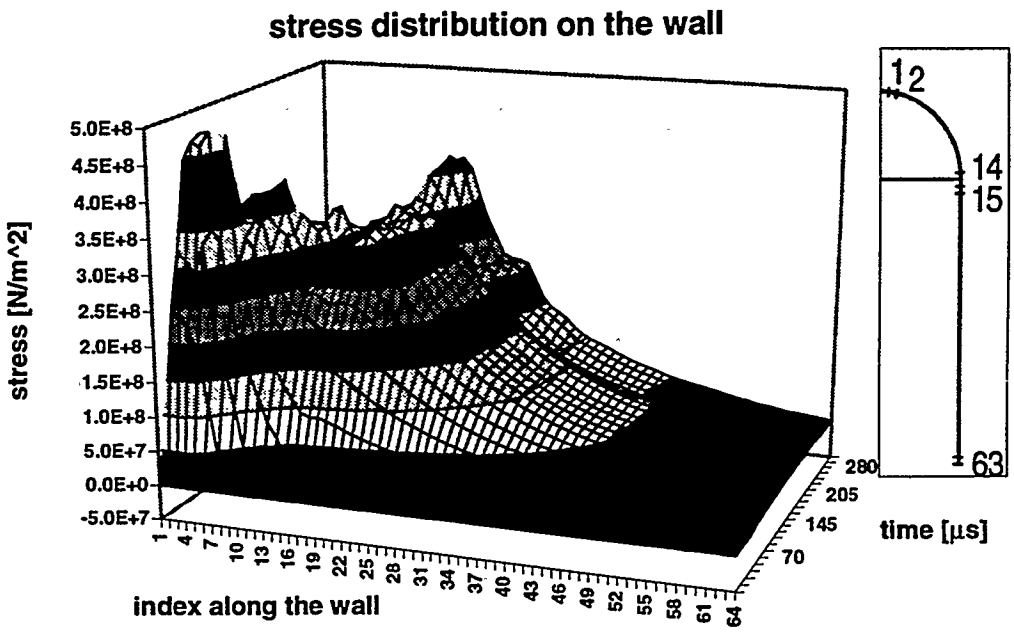

Fig. 5 Stress distribution on the wall without the effect of gas bubble

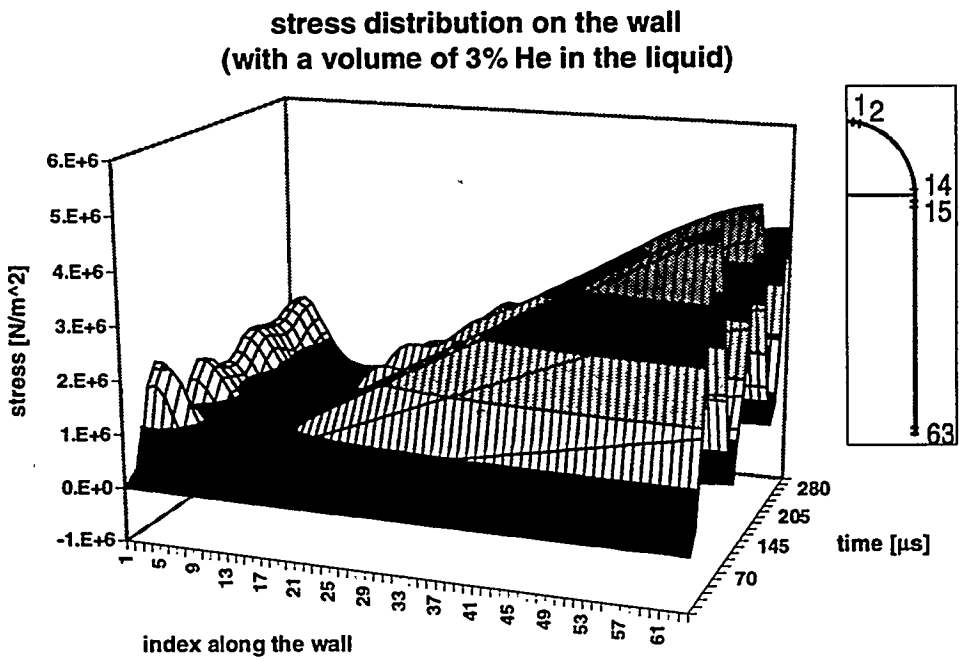

Fig. 6 Stress distribution on the wall with the effect of gas bubble

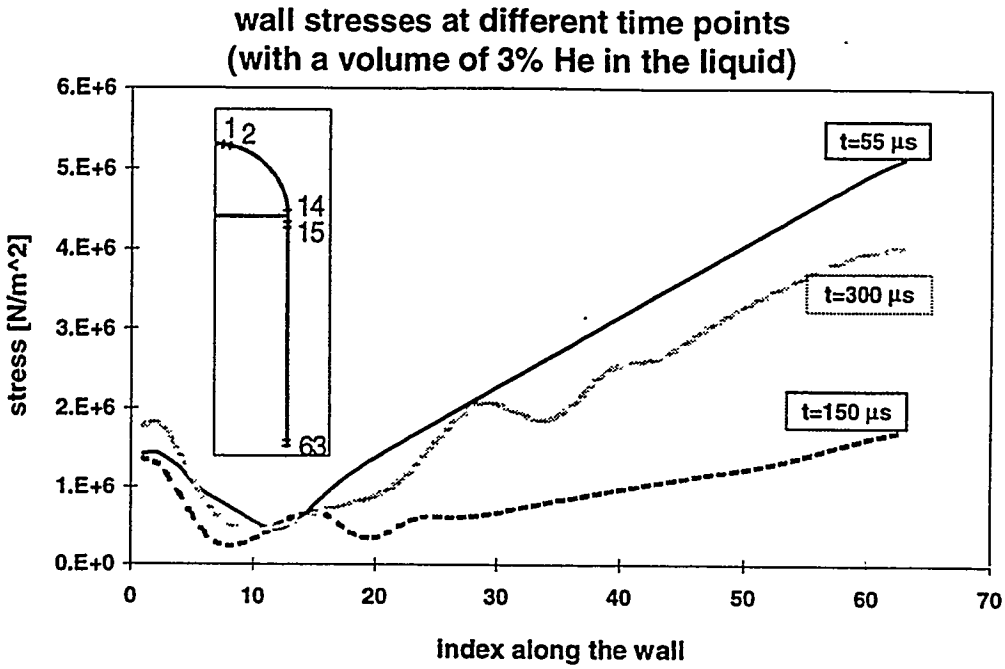

Fig. 7 Wall stresses at different time points with effects of gas bubble

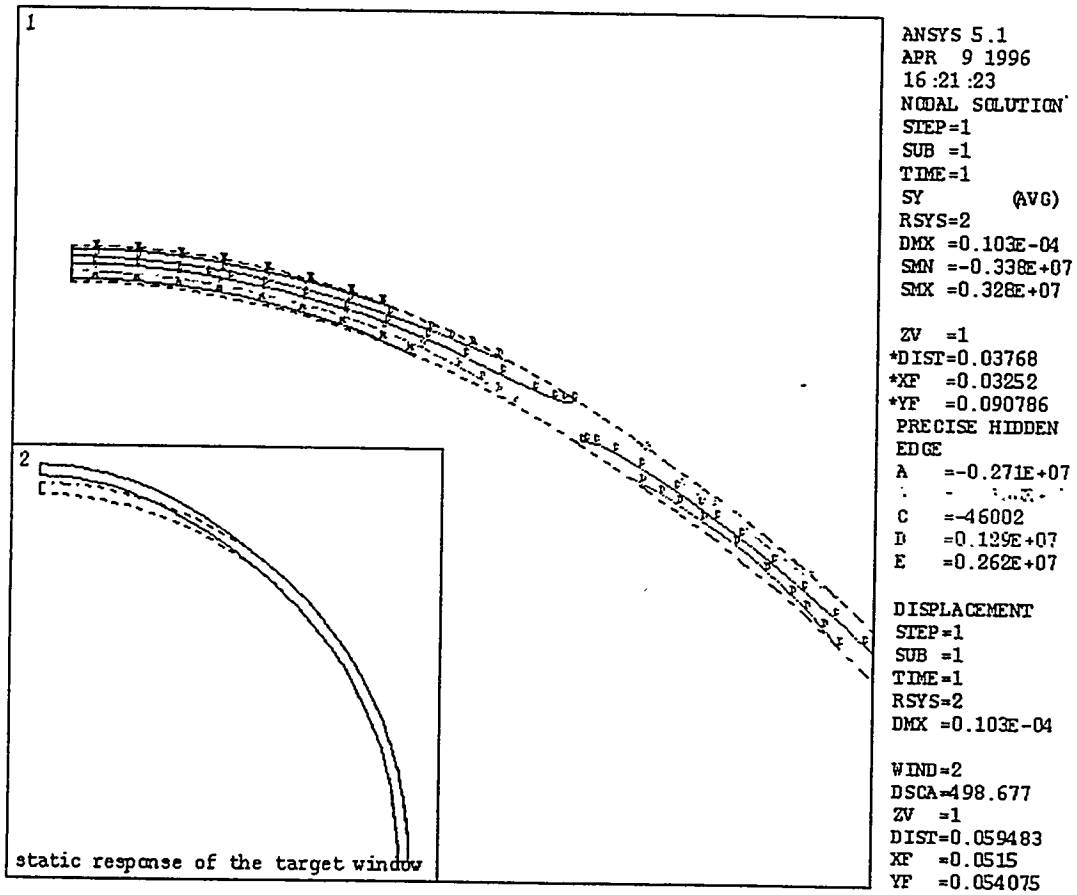

Fig. 8 Hoop stress 1 and displacement 2 in the static analyses of the target window

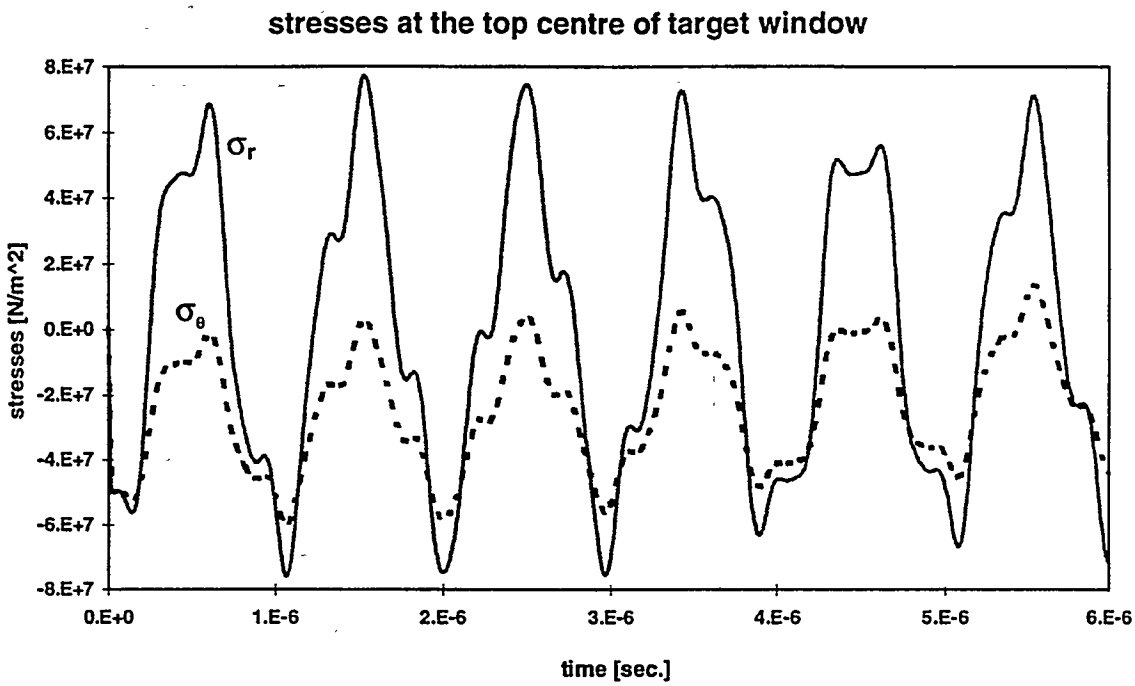

Fig. 9 Radial stress σ_r and hoop stress σ_θ at the top centre of the target window.

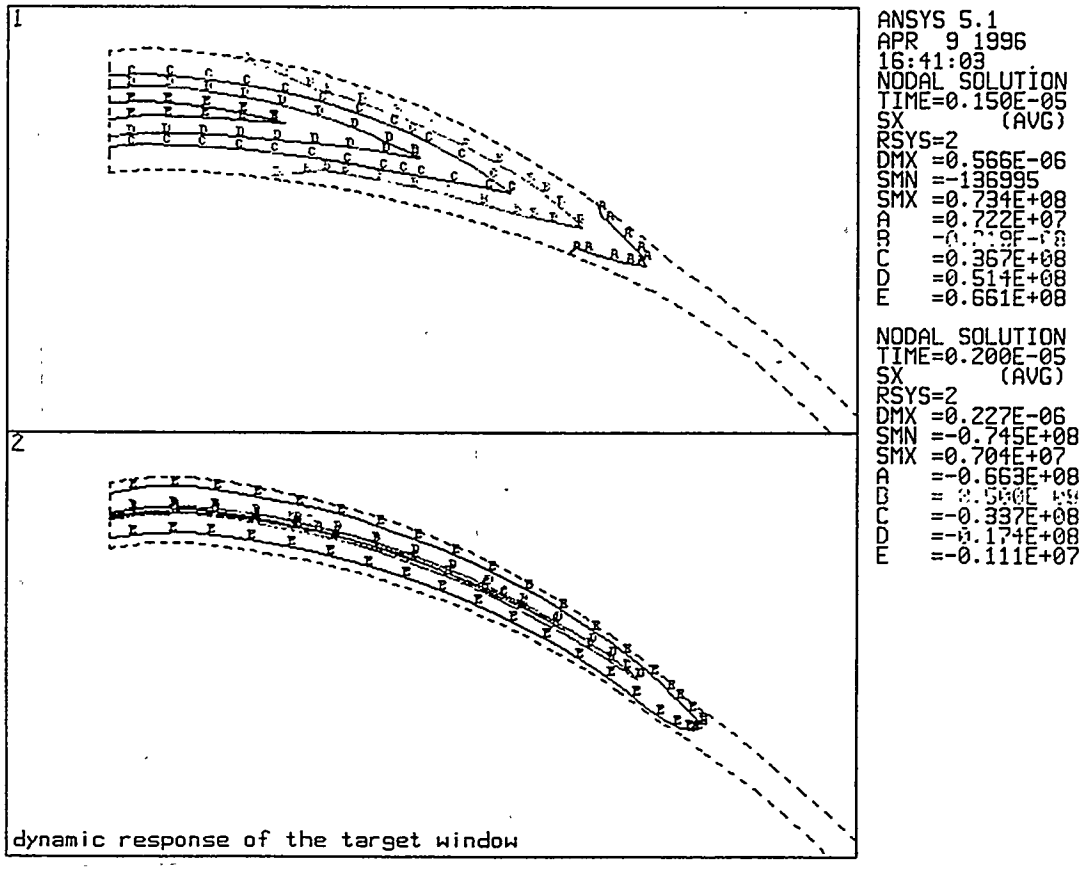

Fig. 10 Radial stress distribution at two time points (1- t=1.5μs and 2- t=2μs)

Integrated Modeling / Analyses of Thermal-Shock Effects in SNS Targets*

by

R. P. Taleyarkhan & J. Haines
Oak Ridge National Laboratory

In a spallation neutron source (SNS), extremely rapid energy pulses are introduced in target materials such as mercury, lead, tungsten, uranium, etc. Shock phenomena in such systems may possibly lead to structural material damage beyond the design basis. As expected, the progression of shock waves and interaction with surrounding materials for liquid targets can be quite different from that in solid targets.

The purpose of this paper is to describe ORNL's modeling framework for "INTEGRATED" assessment of thermal-shock issues in liquid and solid target designs. This modeling framework is being developed based upon expertise developed from past reactor safety studies, especially those related to the Advanced Neutron Source (ANS) Project. Unlike previous separate-effects modeling approaches employed (for evaluating target behavior when subjected to thermal shocks), the present approach treats the overall problem in a coupled manner using state-of-the-art equations of state for materials of interest (viz., mercury, tungsten and uranium). That is, the modeling framework simulataneously accounts for localized (and distributed) compression pressure pulse generation due to transient heat deposition, the transport of this shock wave outwards, interaction with surrounding boundaries, feedback to mercury from structures, multi-dimensional reflection patterns & stress induced (possible) breakup or fracture.

A preliminary model has already been developed to assess and gage the temporal and spatial phenomena arising in typical SNS target disks (made with tungsten or uranium) for a 5-MW SNS facility. Preliminary analysis of results indicate that central regions in the energy deposition zone quickly rise in temperature to about 800 K (in tune with adiabatic heatup, and will remain there, as expected, because the thermal transit time is so much larger than the microsecond pulse duration). Extremely large compression and tensile pressure pulses were noted to be developed (in the GPa range) that vary spatially and temporally. The preliminary analysis did not include modeling of material fracture. However, it was noted that the initial compression wave is followed by the target material (in some sections) going into significant tension, which, in some cases may go beyond the ultimate tensile stress. This would indicate a significant propensity for material breakup either from fracture or ductile tearing in selected locations.

Modeling and analyses have also begun for liquid mercury targets. Insightful, but simple experiments are also being planned for validation studies. This work includes investigation of shock wave absorption from gases introduced which could provide for significant mitigation potential. Results obtained from on-going studies for liquid and solid target designs for the ORSNS are presented at the SNS Workshop for stimulating discussions and intellectual partnership development with efforts elsewhere.

(*) - Prepared by the Oak Ridge National Laboratory, Oak Ridge, TN 37831 operated by Lockheed Martin Energy Research Corp., for the U.S. Department of Energy under contract DE-ACO5-960R2264

Acknowledgements

The authors wish to acknowledge the valuable discussions and encouragement provided by Colin West. Also, useful insights and planning-related thoughts resulting from conversations with Tony Gabriel, Doug Selby and M. Siman-Tov are acknowledged.

Integrated Modeling/Analyses of Thermal Shock Effects in SNS Targets

by

R. P. Taleyarkhan & J. Haines

Oak Ridge National Laboratory
Oak Ridge, TN 37831, USA

March, 1996

Prepared for Presentation & Discussions at Intl. Workshop on the Technology and Thermal-Hydraulics of Heavy Liquid Metals

Prepared by the Oak Ridge National Laboratory, Oak Ridge, TN 37831 operated by Lockheed Martin Energy Research Corp.,for the U.S. Department of Energy under Contract No. DE-ACO5-960R2264

PRESENTATION WILL HIGHLIGHT

o OVERVIEW OF RELATED WORK FOR RESEARCH REACTORS

o RESULTS OF ASSESSMENTS FOR 5-MW SNS SOLID TARGETS

- Uranium
- Tungsten

o CURRENT WORK FOR MERCURY TARGETS

- Model development for "INTEGRAL" simulations of thermal shock
- "PRELIMINARY / DRAFT" analyses & results
- Uncertainties and need for focussed experimentation
- Focussed R&D

EXTREMELY RAPID STRAIN RATES CAN READILY LEAD TO MATERIAL BREAKUP

o IMPACT DYNAMICS

- Karate chop

- Hyper-velocity impact of missiles against targets

o RAPID HEATUP-INDUCED BREAKUP (Single shock or fatigue-induced)

- Past analysis of rapid heatup transients of thin research reactor U-Al plates

** TREAT experiments

** ORNL-JAERI collaborative experiments in NSRR facility (via ANS Project)

o RELATED PROJECTS HAVE HELPED TO DEVELOP IN-HOUSE EXPERTISE

- Steam explosion dynamics in HFIR and ANS (incl. fluid-structure interactions) (in conjunction with failure envelope development)
- Hydrogen detonation in containments (and fluid-structure interactions)
- Explosively formed projectiles

PARALLELS CAN BE DRAWN WITH REACTORS

Parameter	Reactors	Liquid SNS Targets
Fluid within Structural Boundary	Yes	Yes
Cause of pressure rise	Melt dispersion and steam formation	High energy beam heats up Hg, Pb,Steel, etc.
Time span of energy deposition	milliseconds	microseconds
Concerns	Gross failure of structures, and containment integrity threats	Structural damage
Primary Issues	Safety	Design / Operation

7-13

Oak Ridge National Laboratory - G. R. Gilpatrick & J. Stokes, SNS

Relevant Past Assessments & Insights Derived

- As can be noted, except for mode of energy deposition and time-scale of events the technical challenges to be faced for assessing steam explosions and thermal-shock phenomena in SNS targets remains the same

- Our past work has demonstrated the importance of conducting "INTEGRAL" evaluations which couple shock transport phenomena in the liquid with feedback & multi-material motion and response of restraining structures
  - Important effects related to shock dissipation, amplification,focussing, and multi-dimensional material response features may be entirely overlooked <u>if decoupled</u>
  - We plan to conduct "INTEGRAL" assessments for ORSNS

Oak Ridge National Laboratory - G. R. Gilpatrick & J. Stokes, SNS

Some Examples & Results

- o Research Reactor Safety Studies (ANS, HFIR at ORNL)

  - Vapor explosions from hypothetical explosive interactions of molten fuel-water in the core region of the ANS reactor
  - Detailed models were developed for multi-dimensional representation of shock generation, transport and interactions with surrounding structures & development of failure curves

- o Sample results of assessments of steam explosion event in HFIR (due to postulated flow-blockage-induced fuel melt)

  - 50 MJ of thermal energy deposited in core region of reactor over 1 ms
  - Note: -Large deformations of downcomer tube and pressure contours in system
    -CTH code system utilized for this study

HFIR EXPLOSION STUDIES MODEL

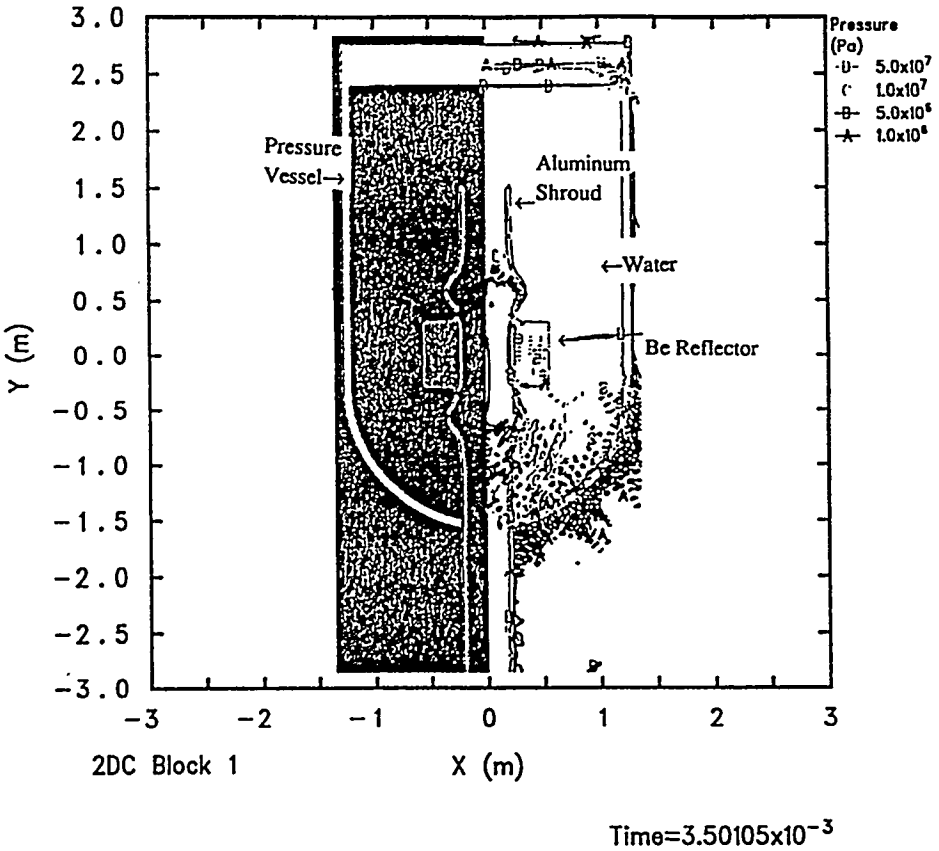

PRELIMINARY ANALYSIS FOR 5 MW-SNS

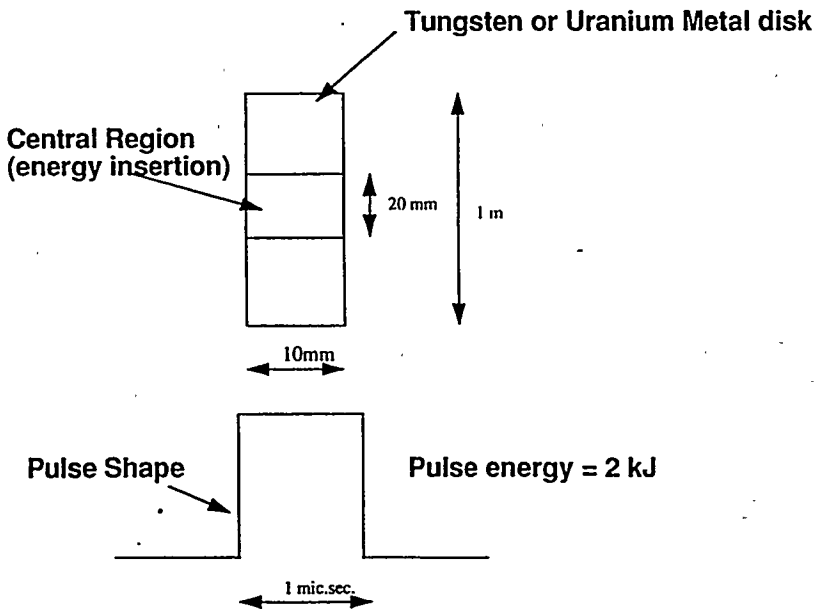

2-D AXISYMMETRIC CTH MODEL

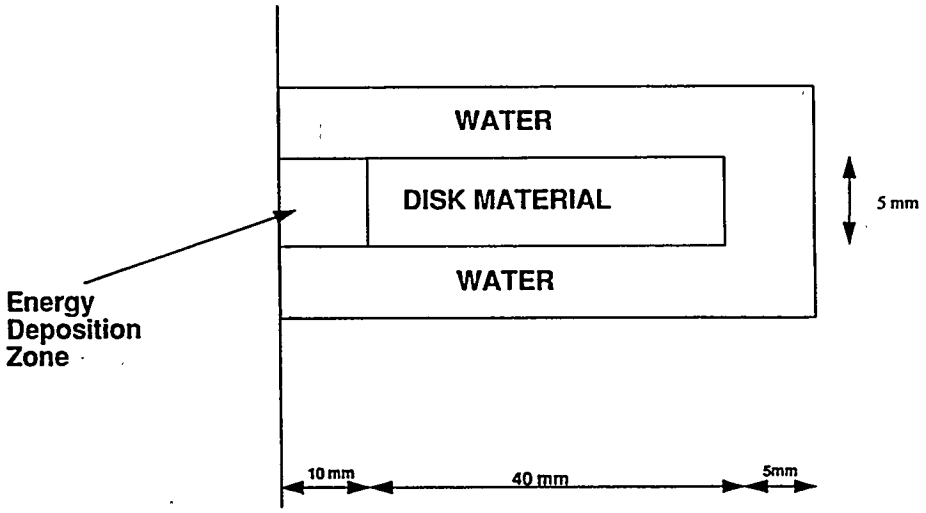

TRACER POINTS

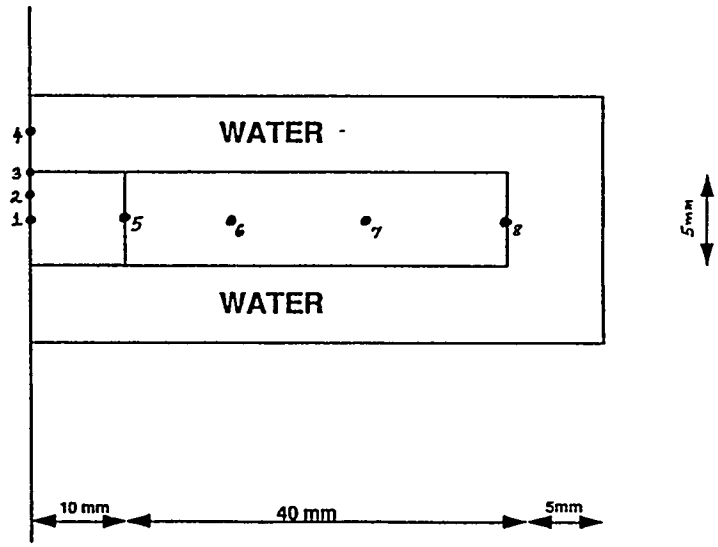

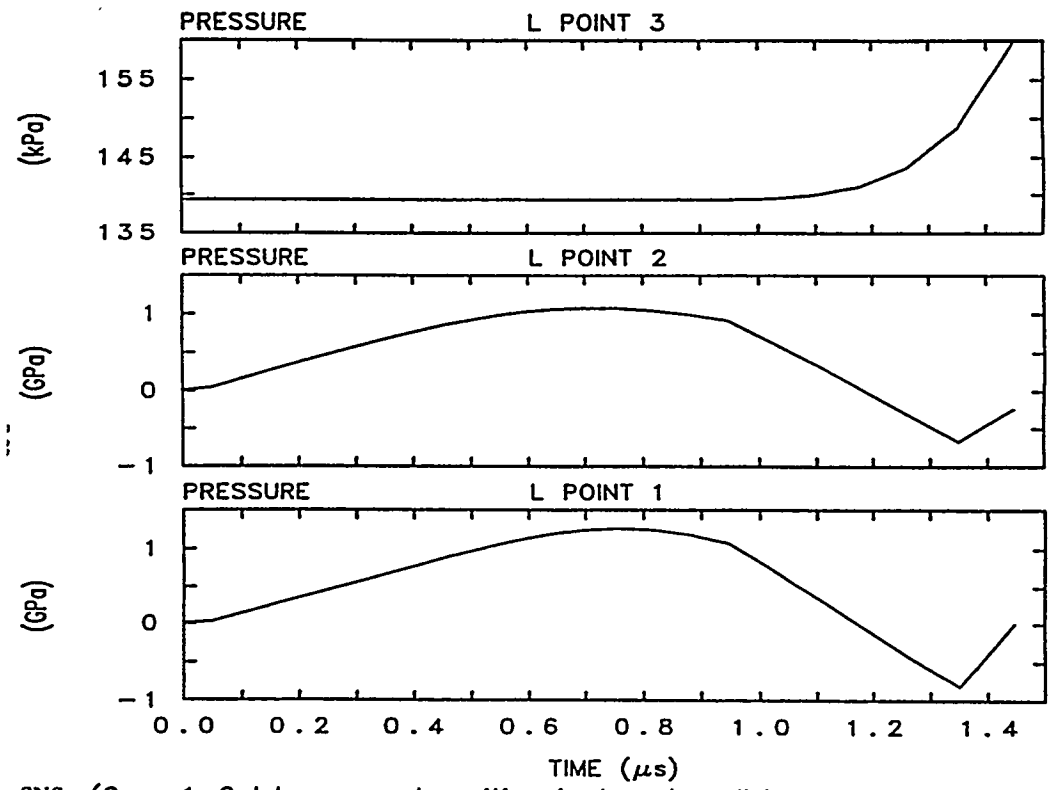

SNS. (Case 1: 2 kJ energy deposition in tungsten disk surrounded by wa

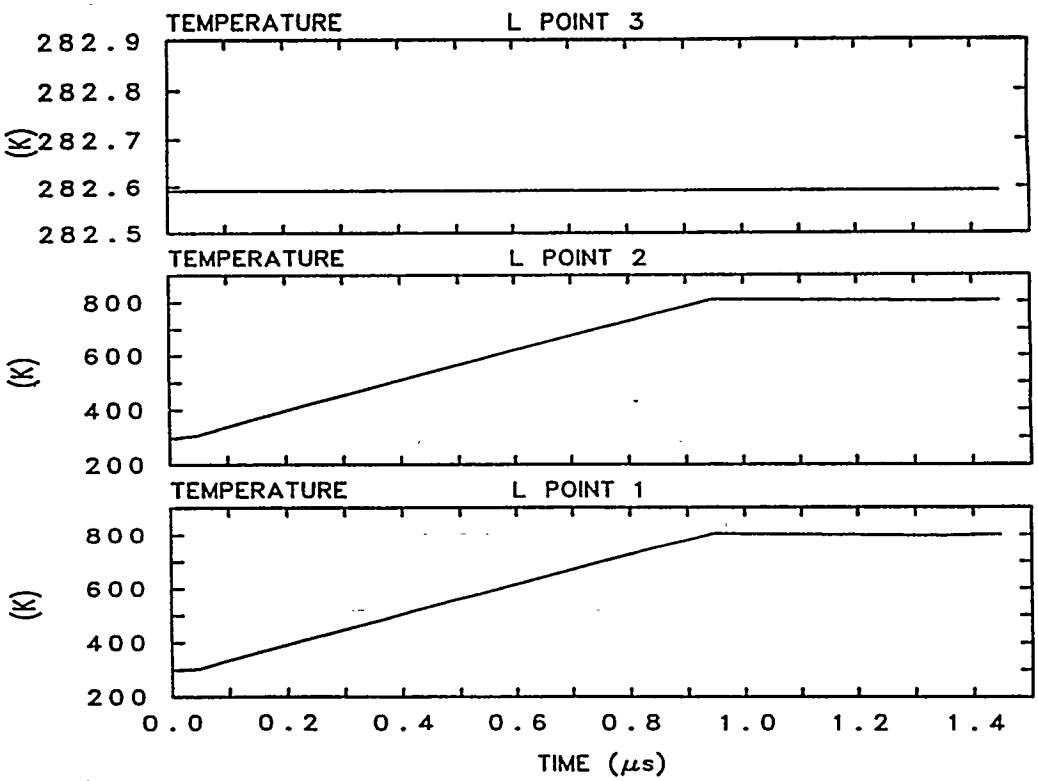

SNS (Case 1: 2 kJ energy deposition in tungsten disk surrounded by wa

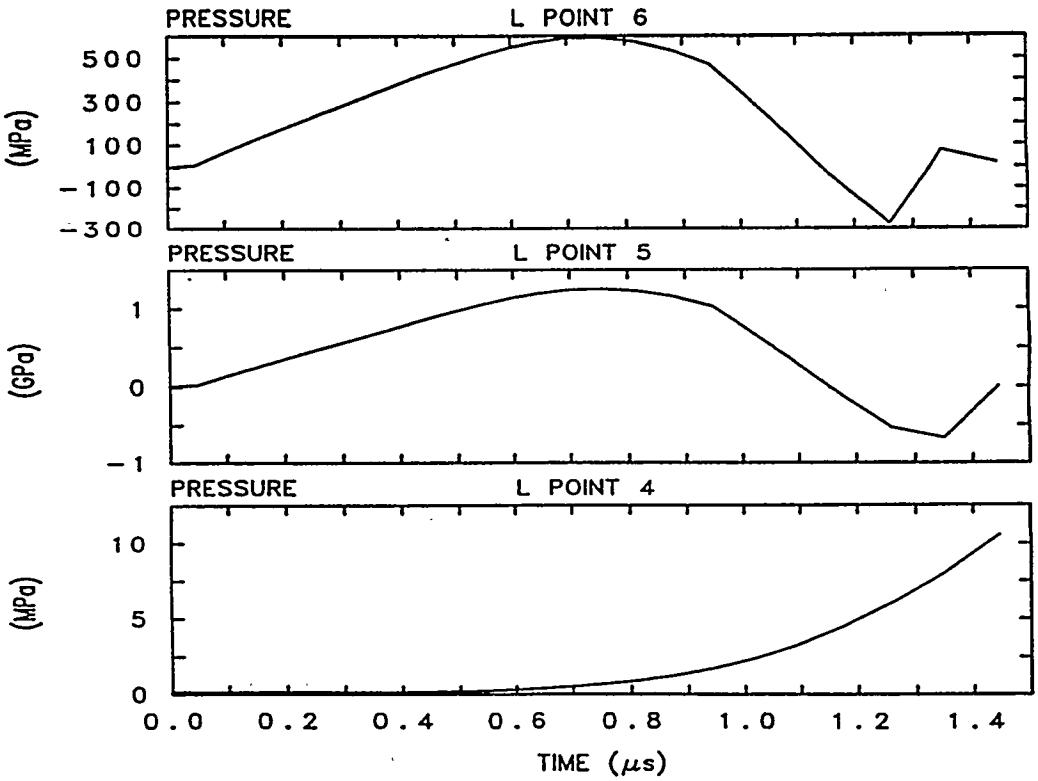

SNS (Case 1: 2 kJ energy deposition in tungsten disk surrounded by wa

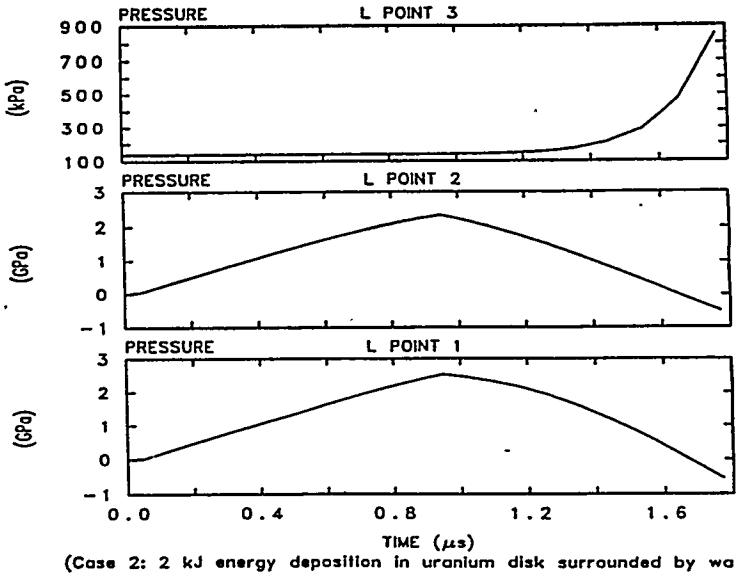

(Case 2: 2 kJ energy deposition in uranium disk surrounded by wa

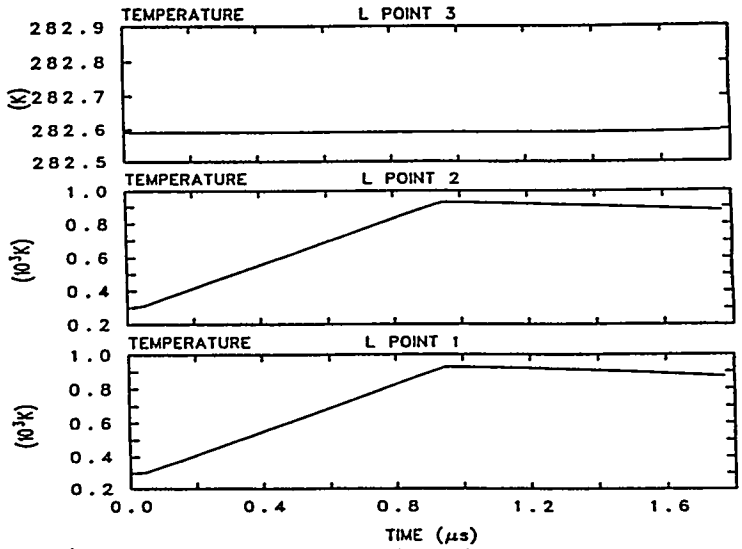

(Case 2: 2 kJ energy deposition in uranium disk surrounded by wa

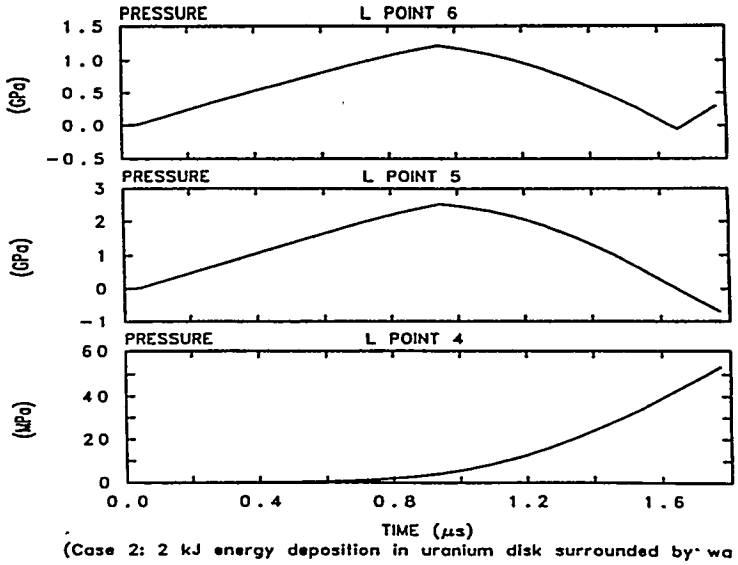

(Case 2: 2 kJ energy deposition in uranium disk surrounded by wa

PRELIMINARY MODELING FOR ORSNS

- o MODELING IS BEING DONE IN STAGES
  - Start with simple geometry (cylinder with hemispherical dome filled with mercury)
  - Use existing equation-of-state (Mie-Gruniesen form) for Hg
  - Evaluate impacts of:
    - Time scale of energy deposition
    - Energy deposition magnitude and spatial distribution (Hg & Steel)
    - Pressure boundary material form and thickness
    - Central flow-separators / baffles in Hg
  - Use insights and R&D results to develop 3-D design modeling framework
- o DEVELOP UNDERSTANDING FOR:
  - Magnitude of thermal-shock issues for ORSNS
  - Suitability of current design tools and EOS for application to ORSNS design
  - Need for mitigative measures & focussed R&D plan development

"PRELIMINARY" MODEL

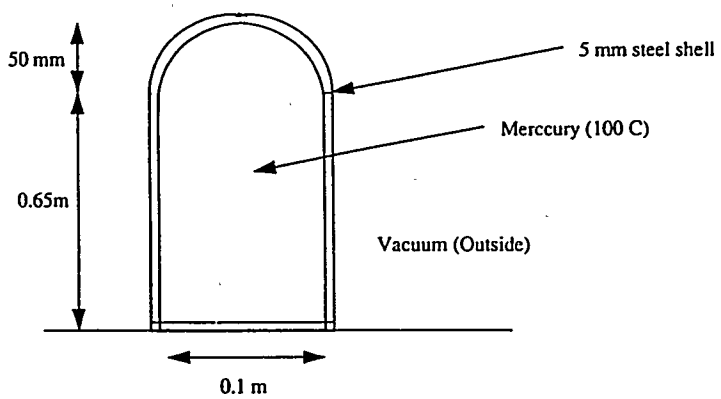

Notes:
1) Volumetric Energy Deposition Magnitude = 1.34 kJ / kg ** presently only in Hg
2) Time span of Energy Deposition = 0.58 mic.sec.
3) Mie-Gruniesen EOS for Hg; ANEOS for steel
4) Perfect wettability assumed

*** Limitations of use of Mie-Gruniesen EOS form should be (and have been) recognized ***

KEY POINTERS & CHECKS

o SANITY CHECKS FOR 1.34 kJ/kg ENERGY DEPOSITION

- Expected Temperature Rise = ~ 7 K
-- Expected Compression Pressure Rise ~ 35 MPa
-- Static Hoop Stress Buildup = ~ 35 x 50 mm / 5 mm = 350 MPa
-- Equivalent Strain Displacement Computations:

Elastic Modulus ~ 200 GPa
Strain for 350 MPa ~ 300 MPa / 200 GPa ~ 0.15%
Lateral Displacement ~ .0015 x 50 mm = .075 mm

Yield Stress at 100 C ~220 MPa (for SS 316)
Strain at Yielding ~ 0.11%
Lateral Displacement ~ .0011 x 50 = .055mm

---> For yielding to take place lateral displacement should exceed ~ .055mm

**** NOTE: RESULTS ARE PRELIMINARY ****

Oak Ridge National Laboratory - R.R. Coltharp & J. Cohen, 1/96

RESULTS PRESENTED

o IN FOLLOWING PLOTS WE SHOW VARIATIONS OF HYDROSTATIC STRESS (PRESSURE) LEVELS - TOTAL STRESS TENSOR COMPONENTS ARE UNDER STUDY

o VARIABLES PRESENTED

- Pressures (hydrostatic) in Hg and steel
  *** Note: Significant Rarefaction Waves in Hg ***
- Max. / Min. principal stresses in steel
- Temperature variations in Hg
- Density variations in Hg
- Velocity of steel material at key locations in shell
- Displacements of steel material at key locations in shell
  ** this parameter to be used to draw preliminary conclusions on yielding, etc. ***

Oak Ridge National Laboratory - R.R. Coltharp & J. Cohen, 1/96

Tracer Point Locations

Point	Co-ordinates	Material	Location
1	(0., 1.375)	Hg	Centerline at base
2	(0., 30)	Hg	Centerline at mid-plane
3	(0., 60)	Hg	Centerline at top of cylindrical region
4	(0., 64)	Hg	Centerline right below the top steel surface
5	(4.6,1.4)	Hg	Next to steel wall at base
6	(4.6, 30)	Hg	Next to steel wall at midplane
7	(4.6, 60)	Hg	Next to steel wall at top of cylindrical region
8	(0., 65.08)	Steel	Inner surface of steel dome at centerline
9	(0., 65.25)	Steel	Middle of steel dome at centerline
10	(0.,65.4)	Steel	Outer portion of steel dome at centerline
11	(5.08, 1.4)	Steel	Inner steel surface at base of cylinder portion
12	(5.25,1.4)	Steel	Middle section of steel cylinder at base
13	(5.42,1.4)	Steel	Outer section of steel cylinder at base
14	(5.08,30)	Steel	Inner steel surface at midplane of cylinder portion
15	(5.25,30)	Steel	Middle section of steel cylinder at midplane of cylinder
16	(5.42,30)	Steel	Outer section of steel cylinder at midplane of cylinder
17	(5.08,60)	Steel	Inner steel surface at top of cylinder portion
18	(5.25,60)	Steel	Middle section of steelat top of cylinder portion
19	(5.42,60)	Steel	Outer section of steel cylinder at top of cylinder portion

Oak Ridge National Laboratory - A. R. Tidquist & J. Rates, 1/94

POSITION OF TRACER POINTS

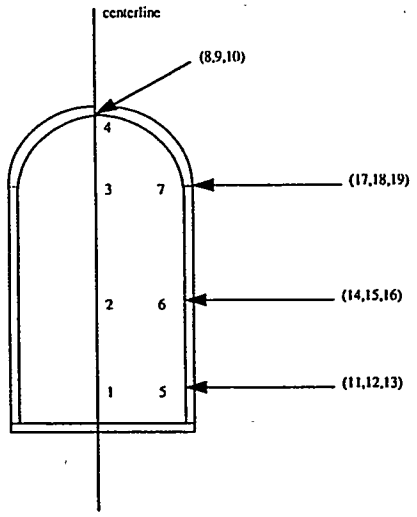

Oak Ridge National Laboratory - A. R. Tidquist & J. Rates, 1/94

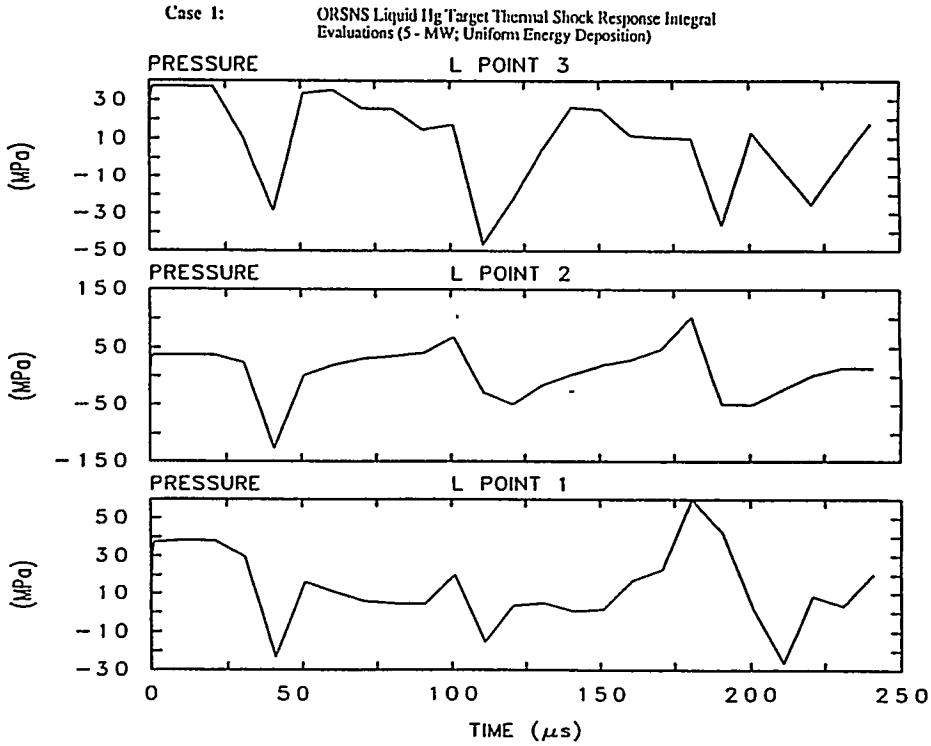
Case 1:
ORSNS Liquid Hg Target Thermal Shock Response Integral Evaluations (5 - MW; Uniform Energy Deposition)
PRESSURE
L POINT 3
(MPa)
30
10
-10
-30
-50
PRESSURE
L POINT 2
150
50
-50
-150
PRESSURE
L POINT 1
50
30
10
-10
-30
0
50
100
150
200
250
TIME (μs)

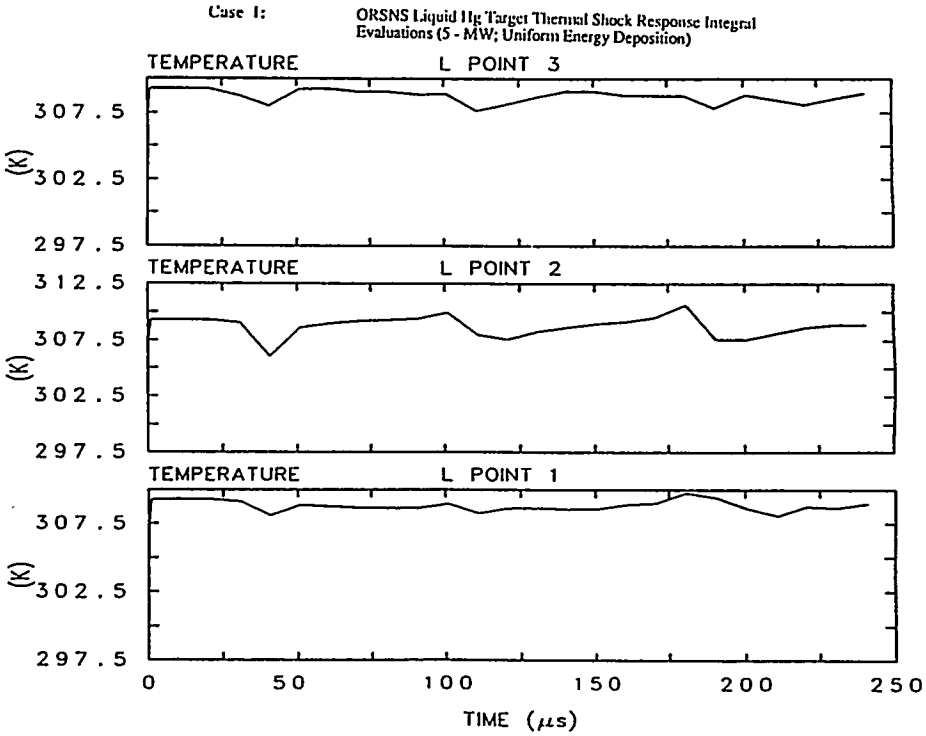
Case 1:
ORSNS Liquid Hg Target Thermal Shock Response Integral Evaluations (5 - MW; Uniform Energy Deposition)
TEMPERATURE
L POINT 3
(K)
307.5
302.5
297.5
TEMPERATURE
L POINT 2
312.5
307.5
302.5
297.5
TEMPERATURE
L POINT 1
307.5
302.5
297.5
0
50
100
150
200
250
TIME (μs)

Case 1: ORSNS Liquid Hg Target Thermal Shock Response Integral Evaluations (5 - MW; Uniform Energy Deposition)

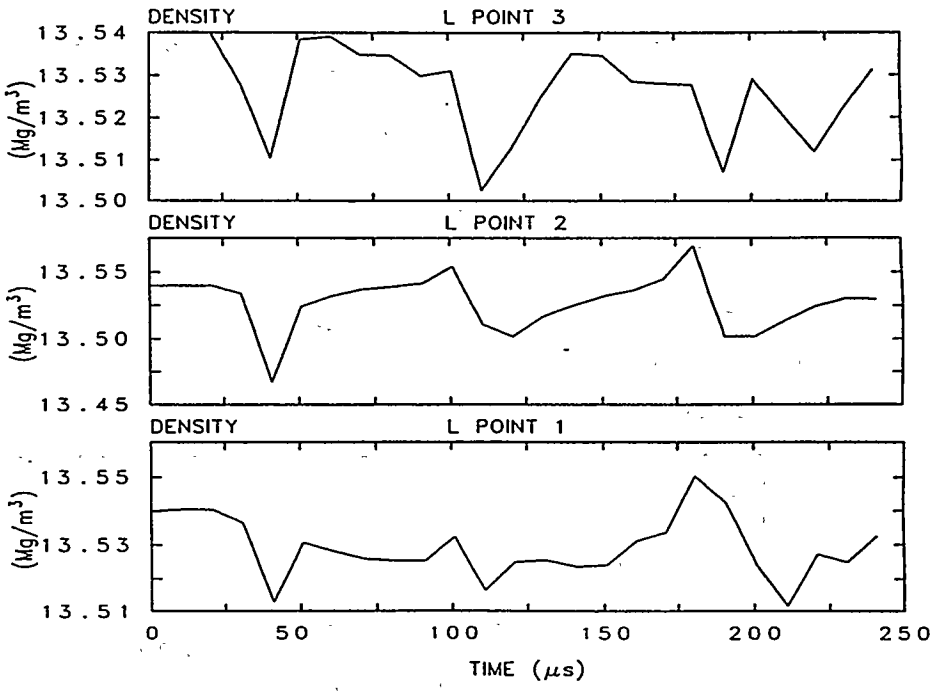

Case 1: ORSNS Liquid Hg Target Thermal Shock Response Integral Evaluations (5 - MW; Uniform Energy Deposition)

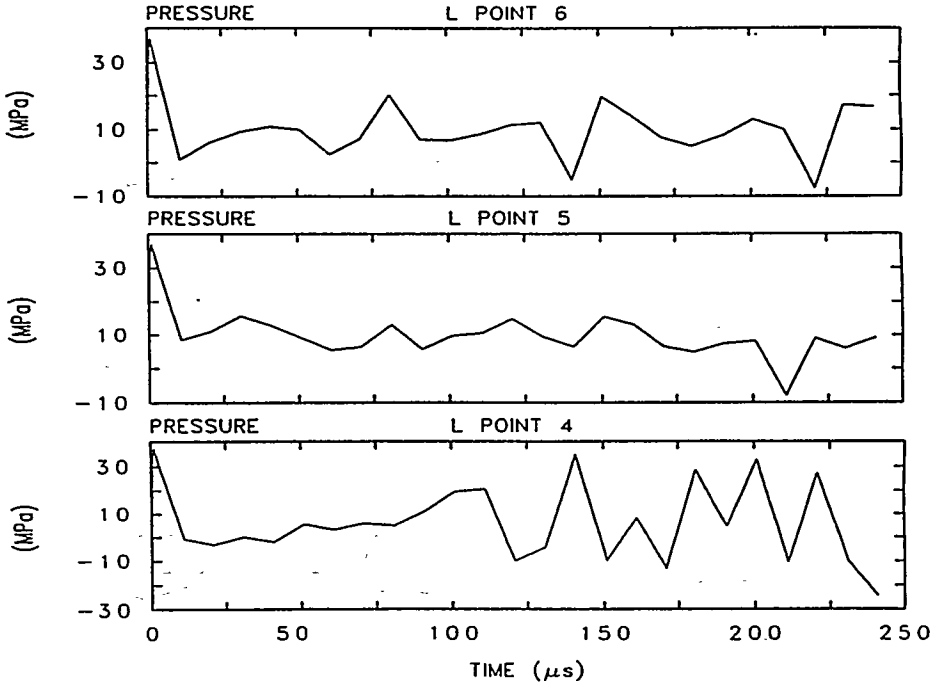

Case 1: ORSNS Liquid Hg Target Thermal Shock Response Integral Evaluations (5 - MW; Uniform Energy Deposition)

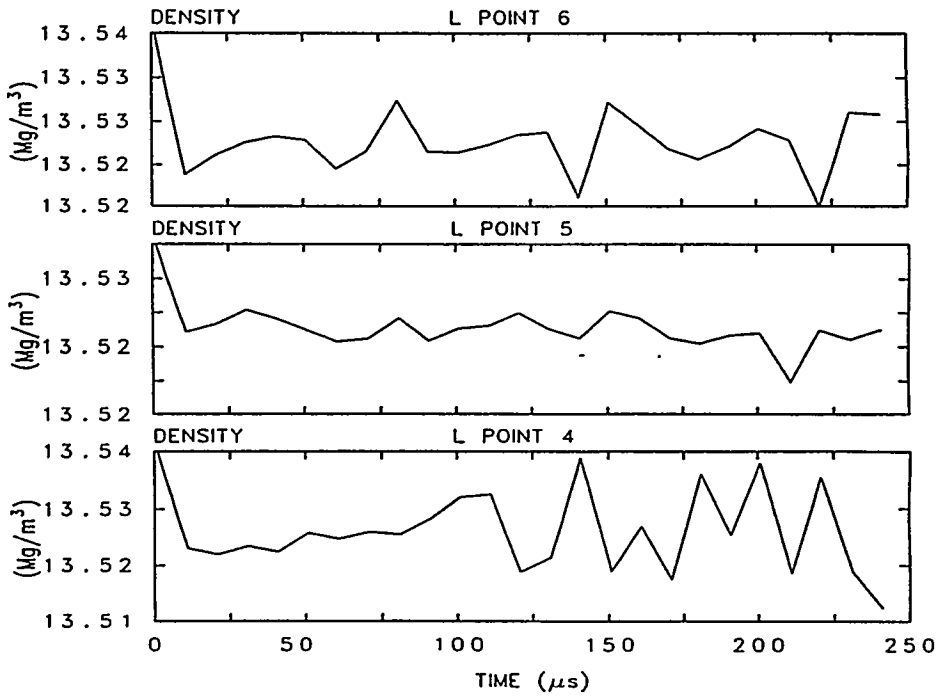

Case 1: ORSNS Liquid Hg Target Thermal Shock Response Integral Evaluations (5 - MW; Uniform Energy Deposition)

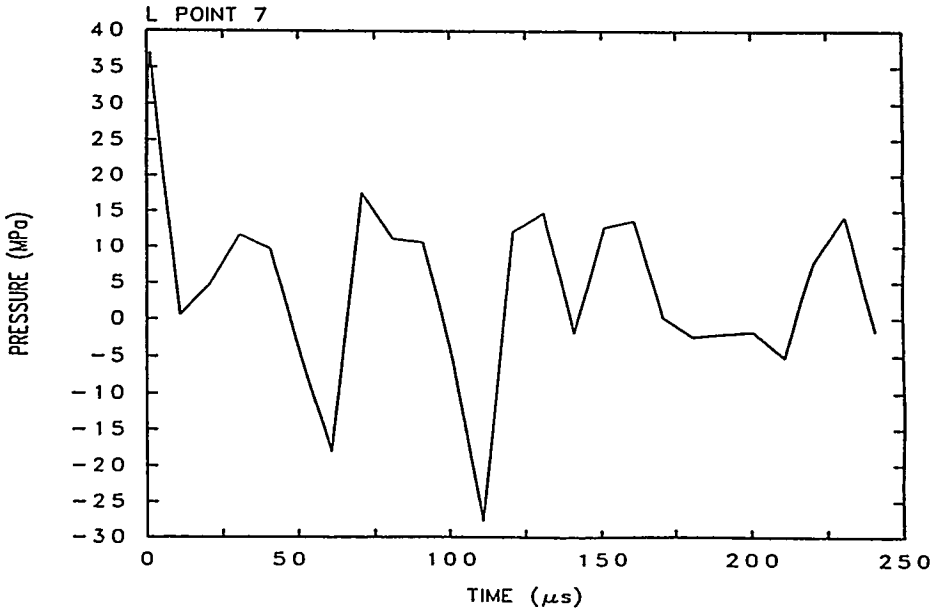

Case 1: ORSNS Liquid Hg Target Thermal Shock Response Integral Evaluations (5 - MW; Uniform Energy Deposition)

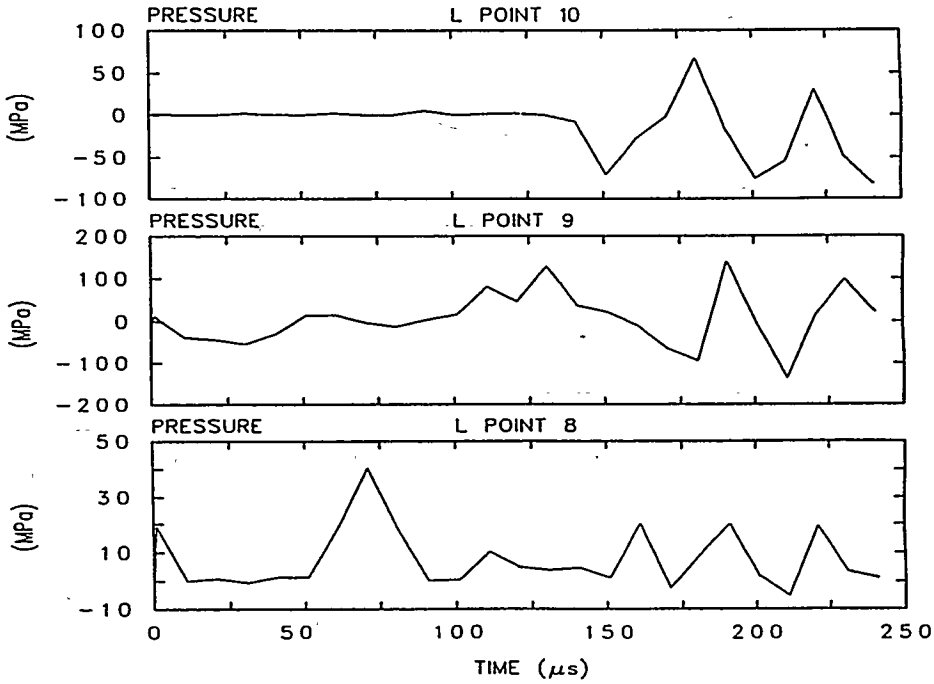

Case 1: ORSNS Liquid Hg Target Thermal Shock Response Integral Evaluations (5 - MW; Uniform Energy Deposition)

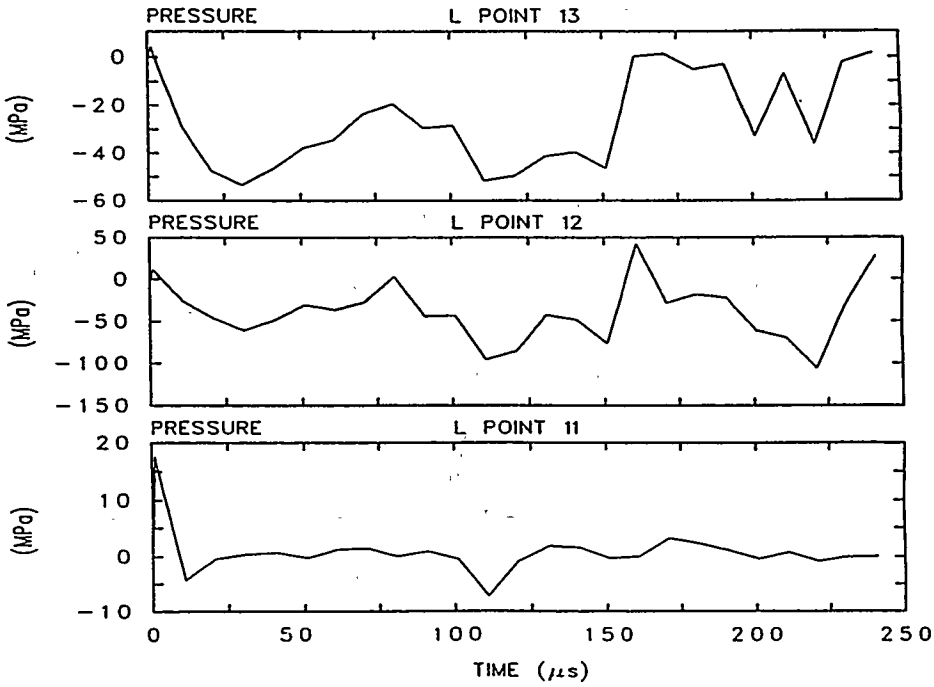

Case 1: ORSNS Liquid Hg Target Thermal Shock Response Integral Evaluations (5 - MW; Uniform Energy Deposition)

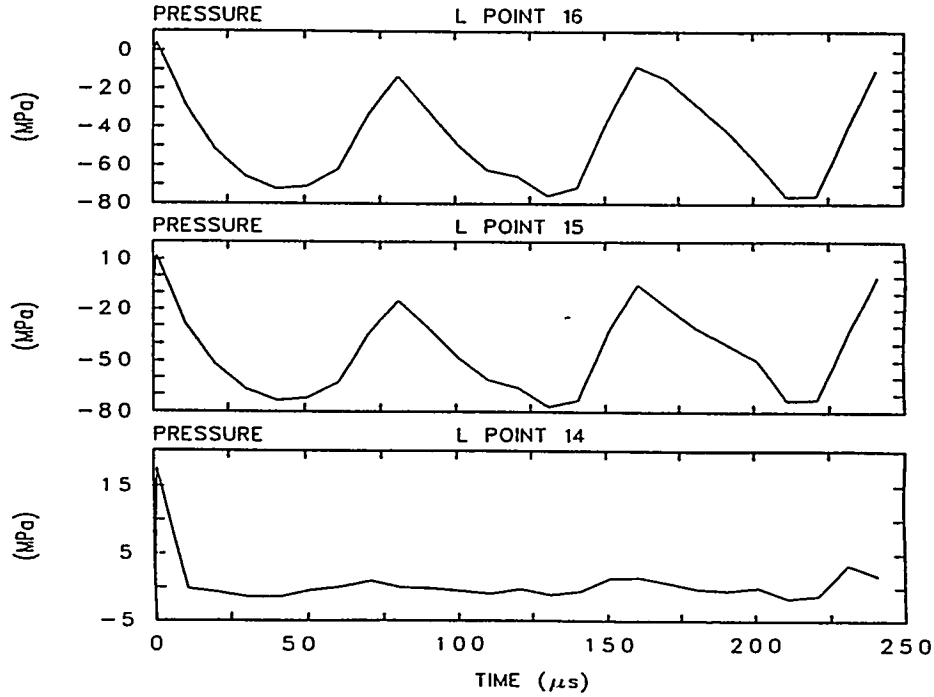

Case 1: ORSNS Liquid Hg Target Thermal Shock Response Integral Evaluations (5 - MW; Uniform Energy Deposition)

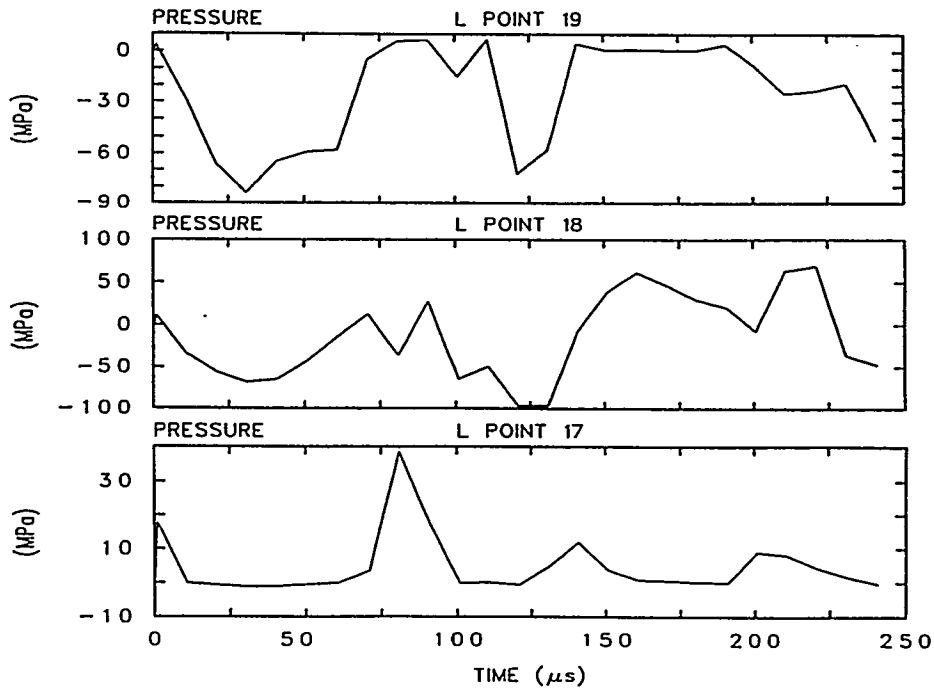

Case 1: ORSNS Liquid Hg Target Thermal Shock Response Integral Evaluations (5 - MW; Uniform Energy Deposition)

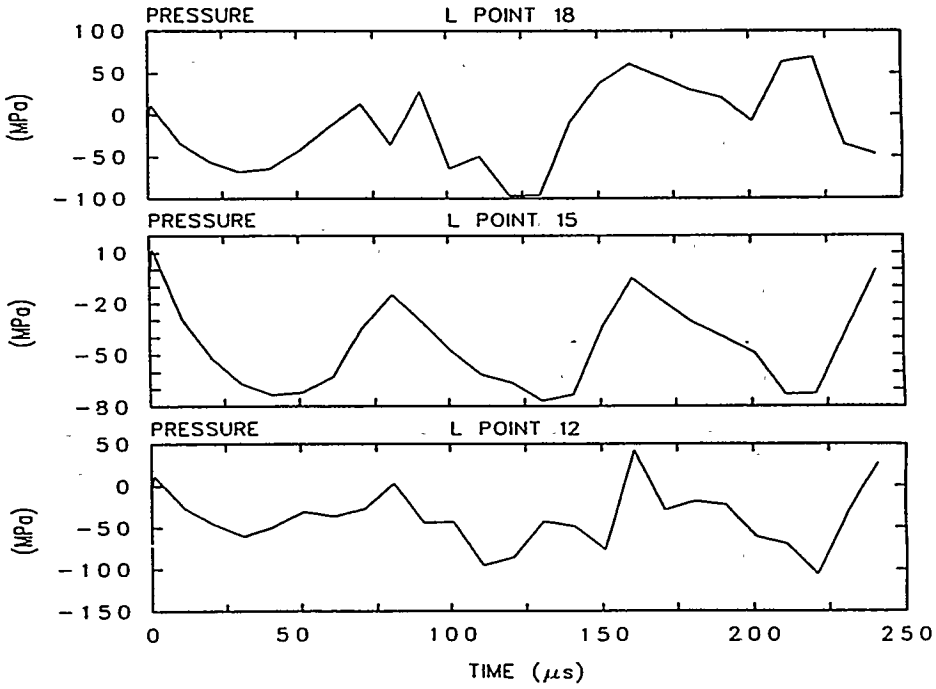

Case 1: ORSNS Liquid Hg Target Thermal Shock Response Integral Evaluations (5 - MW; Uniform Energy Deposition)

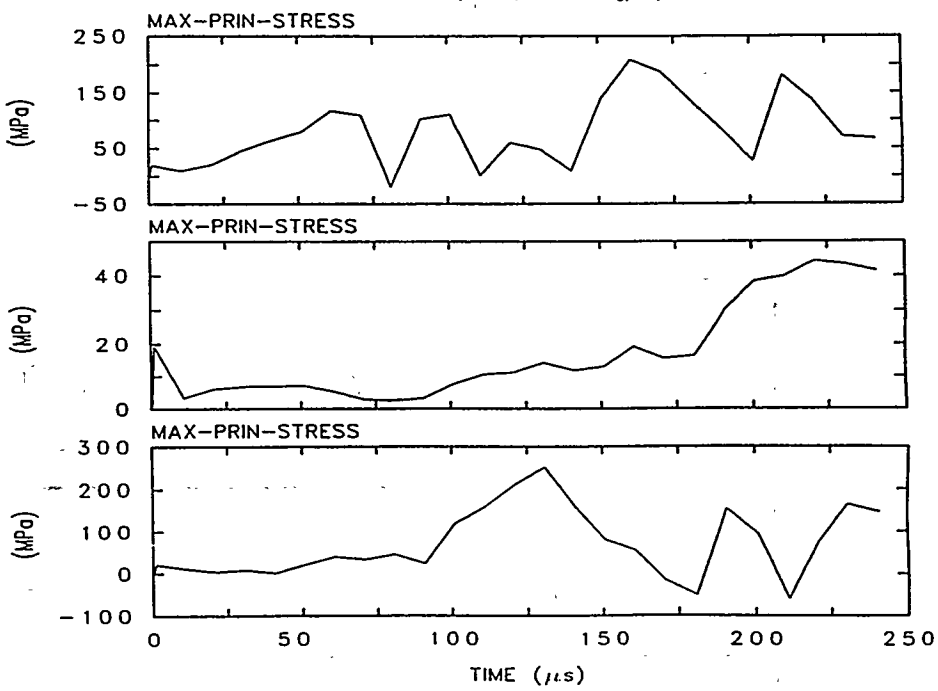

Case 1: ORSNS Liquid Hg Target Thermal Shock Response Integral Evaluations (5 - MW; Uniform Energy Deposition)

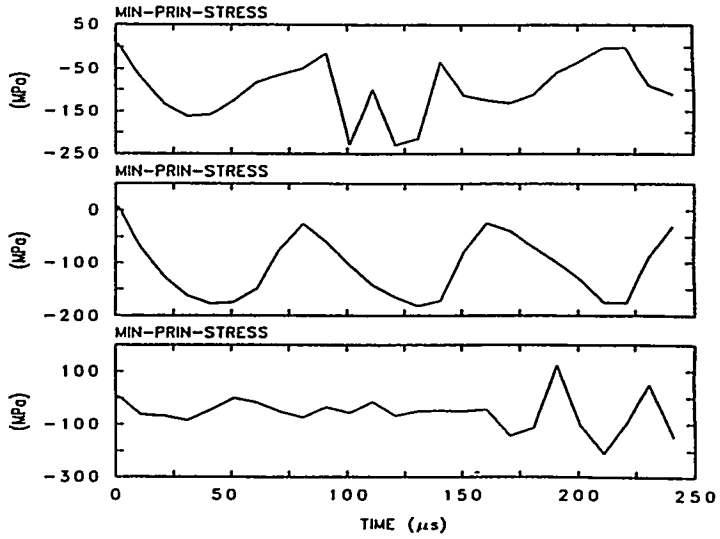

Case 1: ORSNS Liquid Hg Target Thermal Shock Response Integral Evaluations (5 - MW; Uniform Energy Deposition)

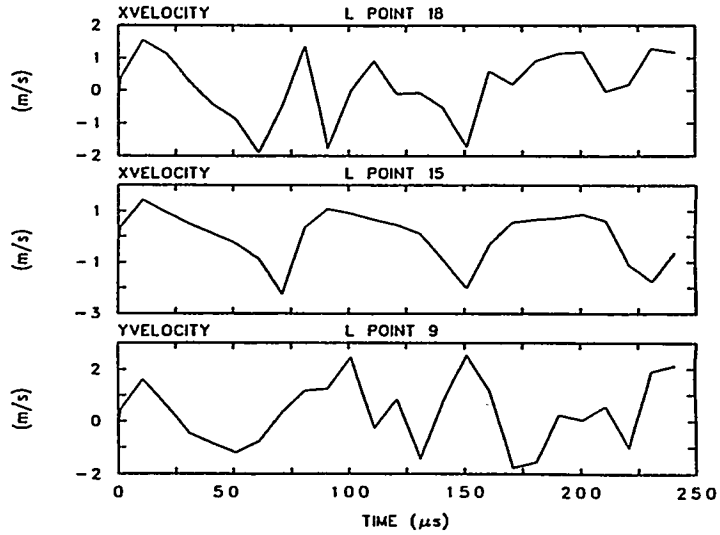

Case 1: ORSNS Liquid Hg Target Thermal Shock Response Integral Evaluations (5 - MW; Uniform Energy Deposition)

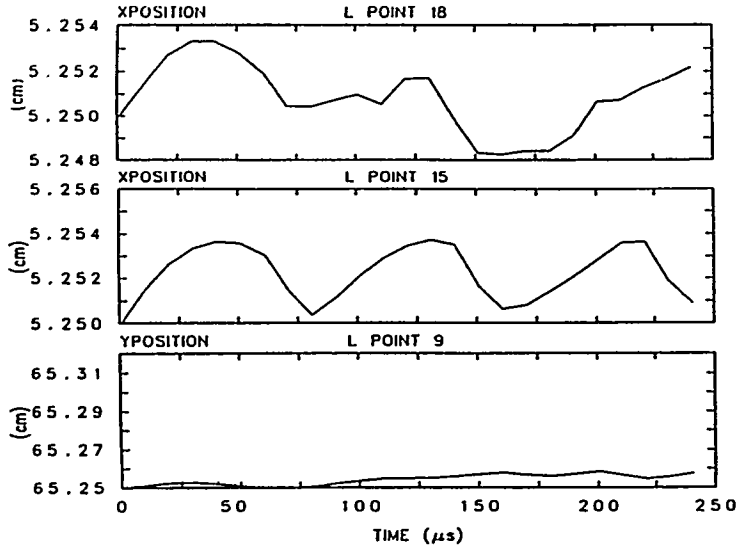

FUTURE THERMAL SHOCK R&D WORK UNDER PLANNING STAGES

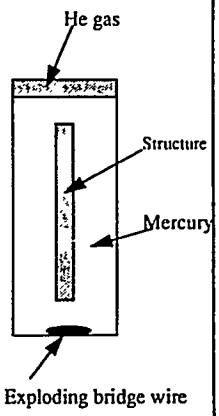

o Pressure-Pulse Tests (point energy deposition source)

- 2-D cylindrical geometry
- To develop key benchmarking & validation data (shock transport at Hg-Steel & Hg-Steel-He interfaces)
- To update EOS for Hg (incl. wettability effects)
- To evaluate impact of geometry
- To evaluate impact of gases

o Testing in ORELA

- To build upon pressure-pulse tests and investigate impact of volumetric energy input

o Cyclic Shock Tests & Analyses

- To evaluate impact of cyclic, short-duration pulsing on life and failure of steels

o Testing for Mitigative Features (e..g., He bubble injection)

IN SUMMARY

o PARALLELS CAN BE DRAWN BETWEEN PAST ORNL WORK & TECHNOLOGY NEEDED FOR ADDRESSING THERMAL-SHOCK ISSUES FOR SNS

o MODEL FOR RAPID HEATUP FOR A SAMPLE DISK MADE WITH TUNGSTEN and URANIUM METAL (w/o zircalloy sheet) REVEAL

- Significant spatial gradients in compressive and tensile stresses are noticed (as also significant temperature gradients)
- Loading stresses / strains in Uranium metal appears to be more severe
- Significant tensile stresses are built up (beyond ultimate strength) which implies distinct possibility of ductile tearing / void fromation and growth (coupled with fatigue-induced fracture).

o PRELIMINARY (conservatively-scoped) WORK FOR Hg TARGET INDICATES

- Significant rarefaction potential exists for liquid Hg region
- Current EOS (Mie-Gruniesen form) needs updating for current application
- Significant tensile stresses and gradients can be expected in steel shell
- Strain & stress levels may exceed yielding conditions
- Focussed R&D is needed for benchmarking & validation of design tool & framework for application to ORSNS conditions

© Oak Ridge National Laboratory - G. R. Fitzpatrick & J. J. Roman, 5/96

SESSION 8

Pulsed Operation and Gas Admixture (2)

Chairman
E. Yefimov

Generation and characterization of gas bubbles in liquid metals

S. Eckert*, G. Gerbeth*, H. Langenbrunner#, W. Witke*

* *Research Centre Rossendorf (RCR), 01314 Dresden, P.O. Box 510119*
\# *Dresden University of Technology (TUD), Institute for Fluid Mechanics*

Extended Abstract

There is an ongoing research performed in the RCR on local transport phenomena in turbulent liquid metal (LM) duct flows exposed to external magnetic fields. In this context so-called MHD flow phenomena can be observed, which are unknown in usual hydraulic engineering. The field of interest covers also the influence of magnetic fields on the behaviour of liquid metal - gas mixtures. Profound knowledge on these LMMHD two-phase flow plays an important role in a variety of technological applications, in particular, in the design of Liquid-Metal MHD generators or for several metallurgical processes employing gas-stirred reactors. However, the highly empirical nature of two-phase flow analysis gives little hope for the prediction of MHD two-phase flows without extensive experimental data.
A summary is given about our research activities focussing on two directions:

(a) Momentum transfer between gas and liquid metal in a bubbly flow regime
⇨ to investigate the influence of the external magnetic field on the velocity slip ratio S[1)]
(b) Pecularities of the MHD turbulence
⇨ to use small gas bubbles as local tracers in order to study the turbulent mass transfer

Concerning point (a) a programme was performed including experimental as well as modelling aspects. The closure of any two-phase flow model is necessarily based on semi-empirical closure laws, which have to be validated for LMMHD two-phase flows.
Our model is one-dimensional and restricted to a bubbly flow regime. In order to describe the motion of a multitude of bubbles in a liquid metal we partly followed and extended the papers of KAMIYAMA [1] and MOND, SUKORIANSKY [2] which are founded on the well-known VAN WIJNGARDEN model of bubbly flow. For a detailed description of the model we refer to [3]. The main results of the calculations can be summarized as following: The effect of a transverse as well as a longitudinal magnetic field on the drag coefficient of a single bubble was taken into account. As result a monotonous decrease of the slip ratio with increasing field strength was found in the longitudinal case. In the transverse case we have to deal with two opposite effects. The drag coefficient of the bubble will also be enhanced by the field influence, but on the other hand the electromagnetic forces brake the liquid metal if the flow and the field lines have not the same direction.
The calculated outcomes were checked experimentally. Measurements have been carried out at the sodium facility in Rossendorf (sodium/argon, transverse field) and at the mercury loops in Grenoble (mercury/nitrogen, transverse field) and Riga (mercury/nitrogen, longitudinal field), respectively. By means of single- and double-wire resistivity probes the local void fraction and

---

1) slip ratio $S = v_{gas}/v_{liquid}$

the local bubble velocity were measured. The probes are connected with a traversing mechanism allowing to move the probe over the channel cross section and to obtain the mean void fraction by integration. In the case of the transverse field configuration the agreement between model and experiment is satisfactory. On the contrary, the measurements in the mercury/nitrogen two-phase flow passing a longitudinal magnetic field cannot confirm the prediction of the slip reduction by the influence of the $\bar{B}$-field. However, the reason is that due to the low electrical conductivity of mercury (compared to liquid sodium) it was not able to reach the parameter region, where the corresponding closure law is valid ($10 \leq N_b \leq 80$, see also the Table 1).

Point (b) is directed to the investigation of the features of MHD turbulence in ducts. If a turbulent liquid metal flow is exposed to a strong magnetic field, it seems obvious to expect that the turbulent velocity fluctuations are suppressed by the very efficient electromagnetic damping. However, many extensive experimental studies [4-6] revealed the survival of turbulent perturbations with a distinct anisotropy of the flow structure showing a tendency to become two-dimensional. Because of the anisotropy of the electromagnetic dissipation term the vortices will be scarcely damped over long distances if their axes are aligned with the magnetic field direction [7].
For the investigation of the mass transfer in a turbulent sodium MHD flow small argon bubbles were injected by a single orifice in the centre of the channel and further upstream the distributions of the local void fraction were measured. Due to the bouyancy effect the gas bubbles can be considered as passive tracers only rough approximately. The advantage of this procedure is the relative simple measuring method. In view of the hard conditions for the employed materials in liquid sodium (200°C) it is generally a serious problem to perform local measurements. The obtained bubble distributions show the expected anisotropic shape. An quantitative description of the experimental situation was given by a calculation of turbulent dispersion coefficients perpendicular as well as parallel to the field lines.

References

[1] Kamiyama, S. , "Analysis of Two-Phase MHD flow in converging-diverging ducts", *Proceedings of the 4th Beer-Sheva Seminar, Jerusalem, Israel 1984*, *AIAA*, Vol. 100, 1985, pp. 304-316

[2] Mond, M. , Sukoriansky, S. , "An analytical model for bubbly flow" , *Proceedings of the 4th Beer-Sheva Seminar, Jerusalem, Israel 1984*, *AIAA*, Vol. 100, 1985, pp. 329-339

[3] Eckert, S. , Gerbeth, G. , Thibault, J.P. , Mihalache, G. "Some aspects of LMMHD Two-Phase Flow: MHD Generator Configuration" *Proceedings of the 7th Beer-Sheva Seminar, Jerusalem, Israel 1993*, Magn. Gidrodin.

[4] Branover, H.H. , Slyusarev, N.M. , Scherbinin, E.V. , "Some results of measuring turbulent pulsation of velocity in a mercury flow in the presence of a transverse magnetic field", *Magn. Gidrodin.*, Vol. 1, 1965, p. 33

[5] Branover, H.H. , Gelfgat, Yu.M. , Kit, L.G. , Platnick, E.A. , "Effect of a transverse magnetic field on the intensity profiles of turbulent velocity fluctuations in a channel of rectangular cross section", *Magn. Gidrodin.*, Vol. 3, 1974, p. 41

[6] Hua, H.M. , Lykoudis, P.S. , "Turbulence measurements in a magneto-fluid-mechanic channel", *Nuclear Science and Engineering*, Vol. 54, 1974, p. 445

[7] Sommeria, J. , Moreau, R. , "Why, how and when MHD turbulence becomes two-dimensional", *J. Fluid Mech.*, Vol. 118, 1982, pp. 507-518

Generation and characterization of gas bubbles in liquid metals

S. Eckert*, G. Gerbeth*, H. Langenbrunner#, W. Witke*

** Research Centre Rossendorf, 01314 Dresden, P.O. Box 510119*
 # Dresden University of Technology, Institute for Fluid Mechanics

Outlook:

- ☞ Status of the work regarding liquid metal two-phase flows at RCR (specific case: influence of an external magnetic field ⇨ MHD)
- ☞ Competence of the RCR group to contribute to the ESS-project

RCR-Activities: LMMHD Two-Phase Flows

Goal: To study

(a) the influence of an external magnetic field on the momentum transfer between the gas and the liquid in a bubbly flow regime

(b) the gas bubble dispersion in MHD channel turbulence

Approach:

- ☞ simple one-dimensional model in order to predict the average behaviour of the LMMHD Two-Phase Flow
- ☞ measurements of the local void fraction α in order to extract informations about the slip ratio S
  the turbulent dispersion coefficients

Experimental facilities:

- Sodium loop (NATAN), Research Centre Rossendorf
  ⇨ sodium/argon, transverse magnetic field
- Mercury loop, Institute de Mechanique de Grenoble
  ⇨ mercury/nitrogen, transverse magnetic field
- Mercury loop. Institute of Physics Riga-Salaspils
  ⇨ mercury/nitrogen, longitudinal magnetic field

Dimensionless flow parameters

- Reynolds number $\quad Re_b = \frac{\rho v L}{\eta}$
- Hartmann number $\quad Ha_b = B_0 L \sqrt{\frac{\sigma}{\eta}}$
- Stuart number $\quad N_b = \frac{Ha_b^2}{Re_b} = \frac{\sigma B_0^2 L}{\rho v}$

with

L - characteristic length scale ⇦ bubble diameter

v - characteristic velocity ⇦ rel. bubble velocity $(v_{gas} - v_{liquid})$

B_0 - intensity of the external magnetic field

ρ, σ, η - material parameters of the two-phase flow
$(\rho = \alpha \rho_{gas} + [1-\alpha]\rho_{liquid})$

α - void fraction

Bubbly flow model I: geometry and assumptions

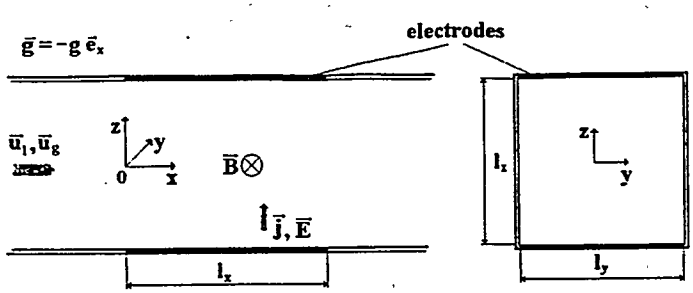

figure 1: considered MHD generator configuration

Assumptions:

- The flow is:- *isothermal* (large heat capacity of the liquid metal)
  - *steady*
- The gas phase:- is *an ideal gas.*
  - consists of *spherical bubbles* of a mean radius r(x).
  - *no aggregation or breakup* of bubbles
- There is *no mass transfer* between the phases (i.e. no evaporation or condensation).
- The *induced magnetic field* is assumed to be *neglegible.*
- The electrodes in the both sides are *perfect conductors.*

Bubbly flow model II: system of equations

continuity: $\frac{d\left[(1-\alpha)u_l\right]}{dx}=0$, $\frac{d(\alpha\rho_g u_g)}{dx}=0$

combined momentum equation:

$$\alpha\rho_g u_g\left(\frac{du_g}{dx}\right)+(1-\alpha)\rho_l u_l\left(\frac{du_l}{dx}\right)=-\frac{dp}{dx}-\left[\alpha\rho_g+(1-\alpha)\rho_l\right]g-f_R+(\vec{j}\times\vec{B})_x$$

equation of motion of a single bubble:

$$\frac{d(\rho_g V_b u_g)}{dt}=-V_b\left(\frac{dp}{dx}\right)-\rho_g V_b g-F_D-F_{VM}$$

where $F_D=0.5\rho_l\pi r^2 C_D(u_g-u_l)\left|u_g-u_l\right|$ drag force

$$F_{VM}=0.5\rho_l u_g\frac{d\left[V_b(u_g-u_l)\right]}{dx}$$ virtual mass force

bubble's mass conservation and equation of state:

$$\rho_g r^3=const., \qquad \frac{p}{\rho_g}=const.$$

Bubbly flow model III: closure laws

a) momentum equation:

- wall draging - f_R → Lockhart-Martinelli modelling
- $\left(\vec{j}\times\vec{B}\right)$

apparent electrical conductivity of the Two-Phase flow σ_t

Maxwell $\sigma_t=\sigma_l\frac{2(1-\alpha)}{2+\alpha}$

Petrick/Lee $\sigma_t=\sigma_l\,exp(-3.8\alpha)$

definition of the load factor

$$K(x)=-\frac{E_z}{u_l B_0}=\frac{U_e}{u_l B_0 l_z}=\frac{IR_{ext}}{u_l B_0 l_z}$$

+ current density (Ohm's law)

$$j_z=\sigma_t(E_z+u_l B_0)$$

$$\left(\vec{j}\times\vec{B}\right)_x=-\sigma_t B_0^2 u_l\left[1-K(x)\right]$$

b) equation of motion of a single bubble:

- interfacial dragging - C_D (drag coefficient of the TP flow)

drag coefficient of a single bubble C_{Ds}

transverse magnetic field

$C_{Ds}=C\,(1+0.7\sqrt{N_b})$

($10^3\le Re_b\le 8.6\,10^3$, $0\le N_b\le 1.5$)

($20\le Re_b\le 5\,10^2$, $0\le N_b\le 2.3\,10^3$)

longitudinal magnetic field

$C_{Ds}=0.33\sqrt{N_b}$

($10^3\le Re_b\le 2.5\,10^5$, $10\le N_b\le 80$)

C_D relating to C_{Ds} → $C_D=C_{Ds}(1-\alpha)^4$

Bubbly flow model IV: main results

- transverse magnetic field: ⇨ two effects

  1) B-field has an braking effect on the liquid metal (~ B^2)
  2) B-field enhances the drag coefficient C_{Ds} (~ B)

- longitudinal magnetic field:

  An effect of the magnetic field on the mean flow does not occur
  ⇨ monotonous decrease of the slip with increasing field strength

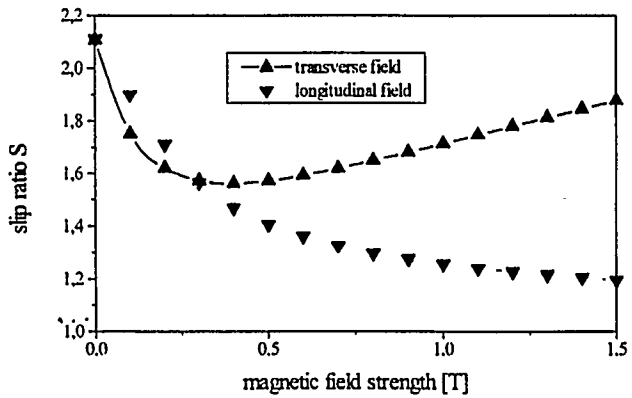

slip ratio S as a function of the transverse and the longitudinal magnetic field. respectively, calculated for a sodium/argon flow with $\bar{v}_{So}$= 0.1 m/s

Experiment sodium loop (Rossendorf)

- rough scetch of the experimental configuration:

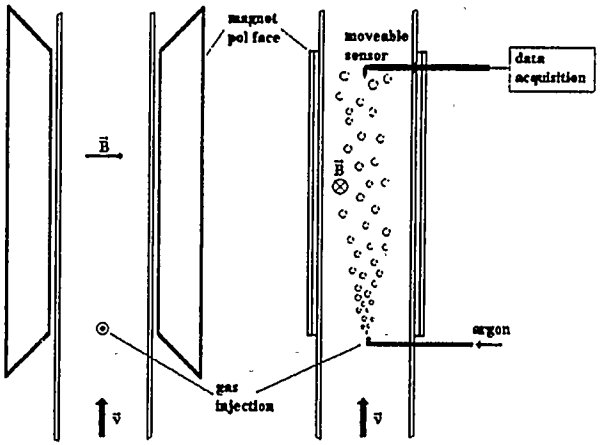

- vertical channel with rectangular cross section (45×50 mm²)
- single gas injector, distance injector - probe: 290 mm
- volumetric quality $\beta < 0.1$ ⇨ bubbly flow regime
  ($\beta = Q_g/(Q_g+Q_l)$)
- sodium velocity 0.1...0.3 m/s ⇨ Re = 9300...27900
- transverse magnetic field, length: 320 mm
  B_{max}: 0.45 T ⇨ Ha = 0...2750,
  N = 0...800 (Re = 9300)

(Here the nondimensional parameters are related to the characteristic scales of the facility)

Experimental results: sodium/argon flow

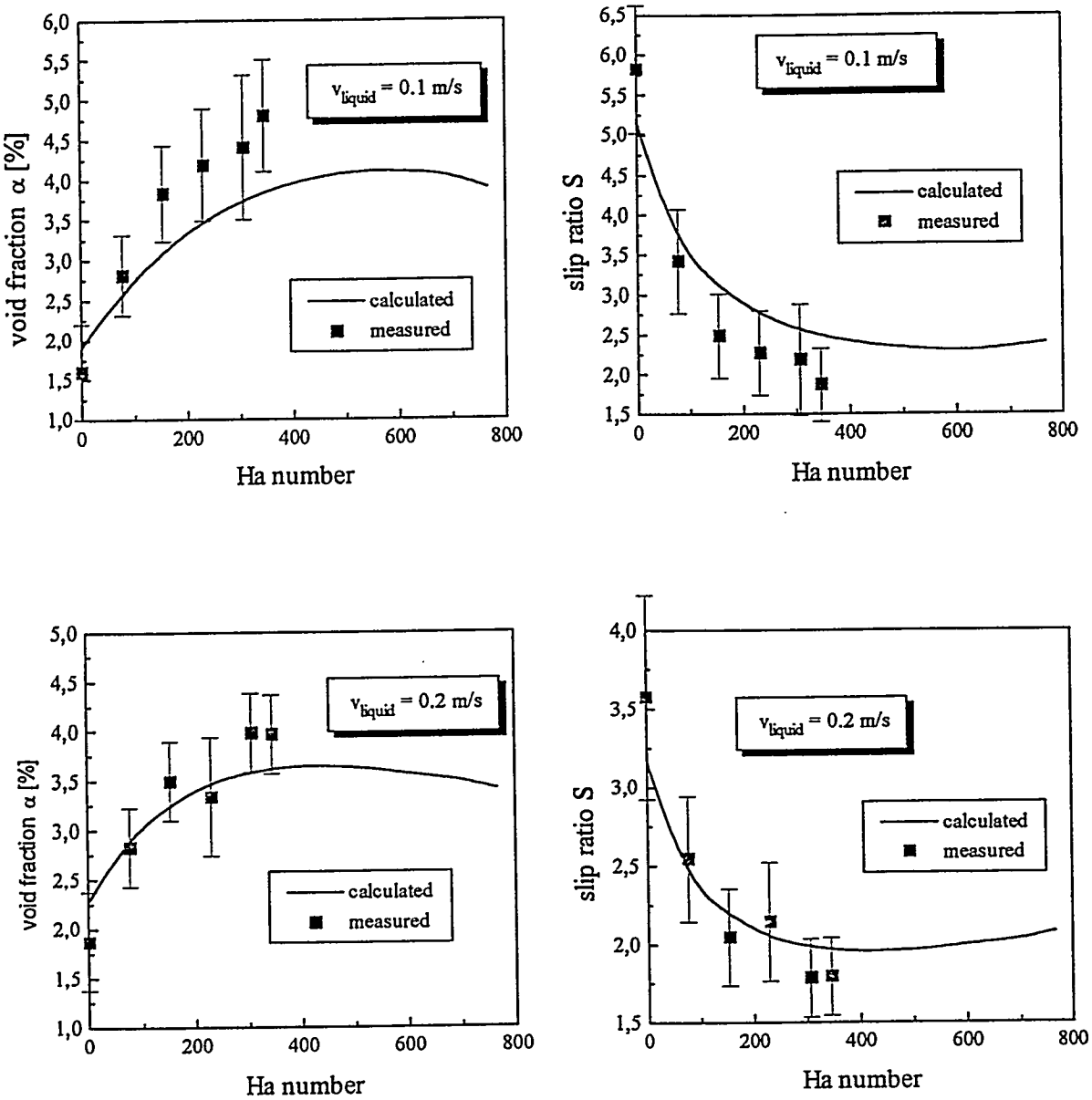

$$\text{slip ratio } S = \frac{v_{gas}}{v_{liquid}} = \frac{\beta[1-\alpha]}{\alpha[1-\beta]} \quad ; \quad \text{volumetric quality } \beta = \frac{\dot{Q}_{gas}}{\dot{Q}_{gas} + \dot{Q}_{liquid}}$$

Experiment: mercury loop (Riga-Salaspils)

- scheme of the facility:

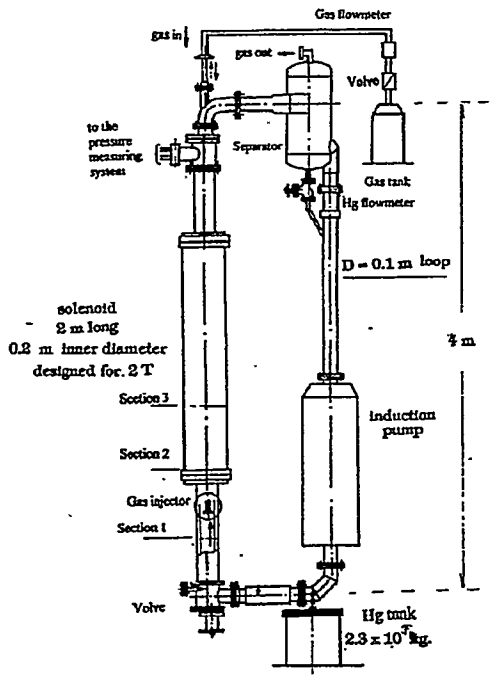

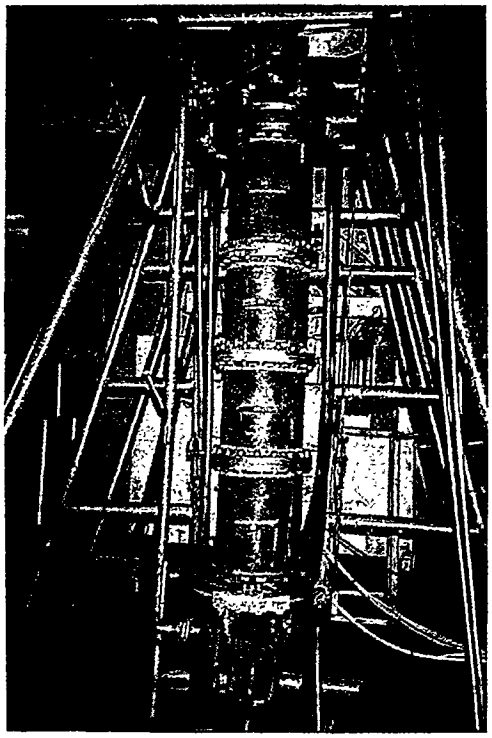

- vertical tube (∅ = 0.1 m, L = 4 m) as test section
- injection of the bubbles through a single orifice
- distance injector - probe: 0.5 and 1 m
- mercury velocity 0...0.09...0.18 m/s ⇨ $Re_{max} = 163000$
- longitudinal magnetic field, $B_{max} = 0.9$ T ⇨ $Ha_{max} = 2300$
- variations of the mean liquid velocity, the gas flow rate, the magnetic field strength as well as the installation positions of the injector and the probes
- two variants: (a) one single probe moveable along a cirular line in the cross section
  (b) array of 16 sensors (rotatable mounted)

Experimental results: mercury/nitrogen flow (longitudinal field)

serie (a) (moveable single-wire probe)

- results show the same qualitative tendency as predicted by the calculations

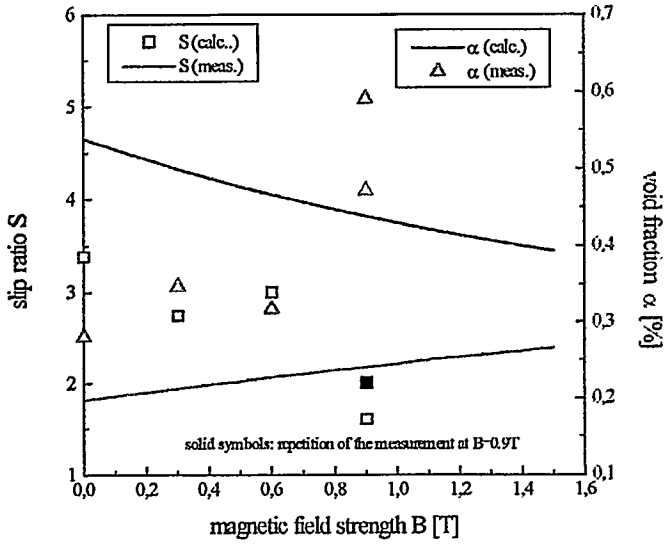

serie (b) (multichannel measurements, 16 single-wire probes)

- disagreement between model and experimental results

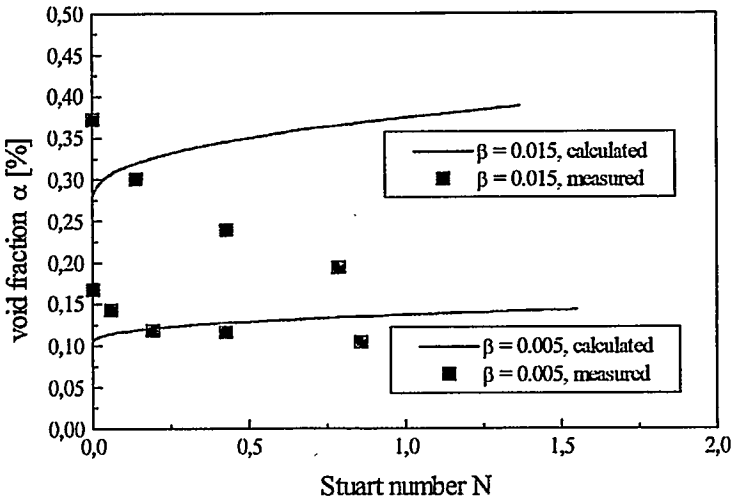

Table 1: comparison between the experimental situations of the mercury/nitrogen facility (Grenoble) and the sodium/argon facility (Rossendorf) with respect to the main material properties and resulting nondimensional parameters

	mercury/nitrogen facility of IMG	sodium/argon facility of RCR
temperature [°C]	20	200
ρ_l [kg/m³]	$1.36\ 10^4$	$9.03\ 10^2$
μ_l [N/sm²]	$1.50\ 10^{-3}$	$4.57\ 10^{-4}$
σ_l [1/Ωm]	$1.00\ 10^6$	$7.46\ 10^6$
p (channel inlet) [Pa]	$5.40\ 10^5$	$2.20\ 10^5$
ρ_g [kg/m³]	6.24	2.42
$\beta = Q_g/Q_l$	0.24	0.015
d_H [m]	0.0175	0.0474
Re	240000	$10^4...10^5$
Re_b	65000	1500...5500
Ha	0...350 (B_0=0.77T)	0...2750 (B_0=0.45T)
Ha_b	0...120	0...350
N	0...0.5	0...800
N_b	0...0.22	0...80

Some features of the MHD turbulence in ducts

- Agreement between friction measurements and the law for a laminar flow above a critical ratio Ha/Re
- Persistence of turbulent fluctuations for Ha/Re > $(Ha/Re)_{cr}$
  very slow decay on large distances
- Energy spectra with a characteristic k^{-3}-slope (enstrophy cascade)
- Two-dimensionality of the flow ($v_\parallel << v_\perp, \frac{\partial}{\partial_\parallel} << \frac{\partial}{\partial_\perp}$):
  Fluctuations become highly correlated along the direction of the field lines.
  Elongation of the vortices in field direction: $L_\parallel = \sqrt{N} \cdot L_\perp$
- Crucial role of the boundary conditions perpendicular to the field:
  Electrical conductivity of the wall material influences the closure of the electric currents ⇨ minimizing of the electromagnetic damping if the walls are insulating
- Origin of the turbulent fluctuations by entry effects or the use of turbulence promoters

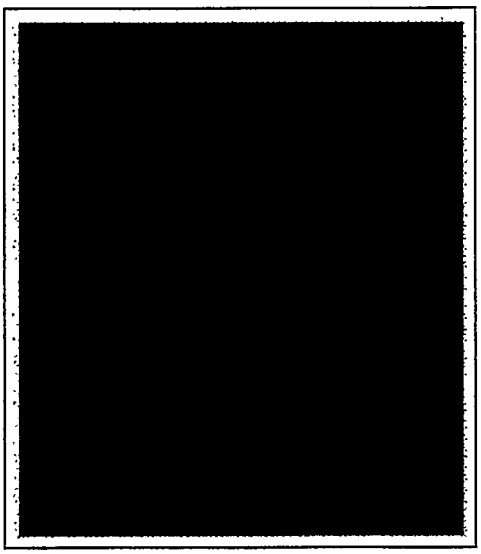

a) Ha = 300, N = 10

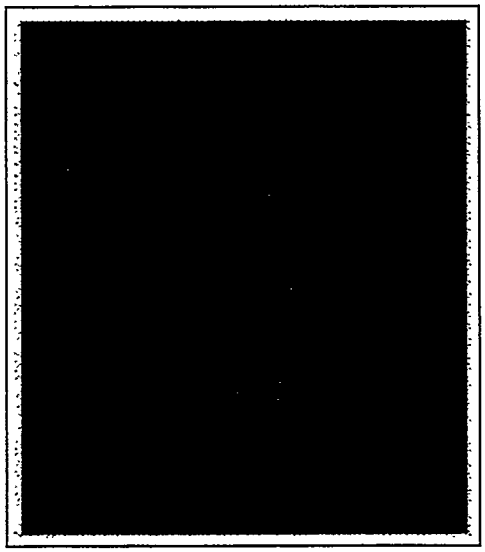

b) Ha = 845, N = 77

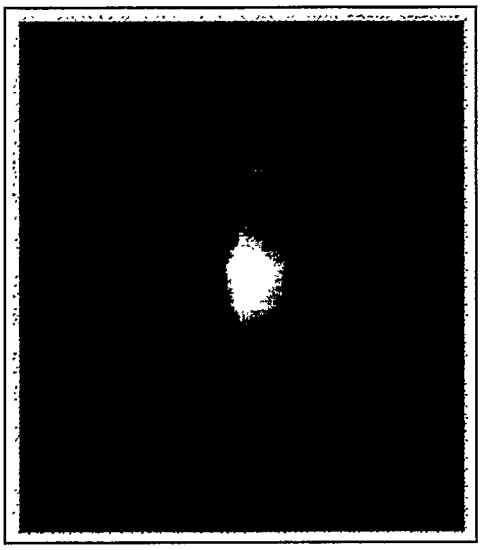

c) Ha = 1505, N = 244

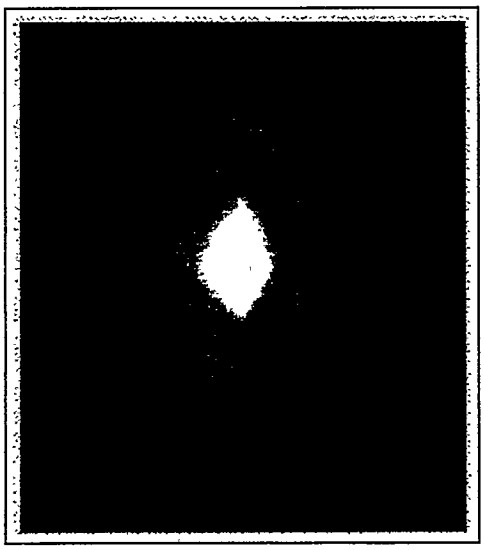

d) Ha = 2410, N = 625

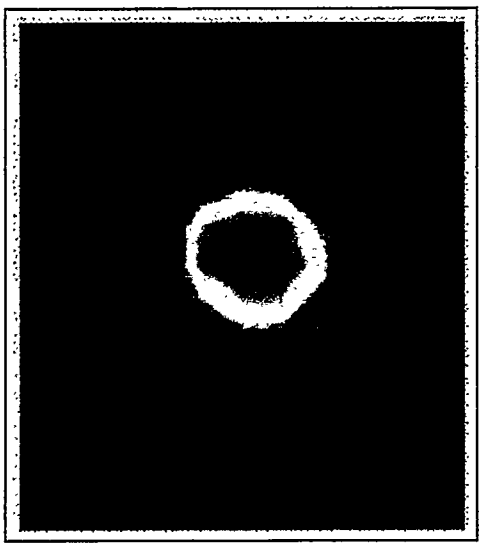

e) Ha = 2710, N = 790

→ direction of the B-field →

Experimental results of the
void fraction distributions
at Re = 9300
transverse field, single injector

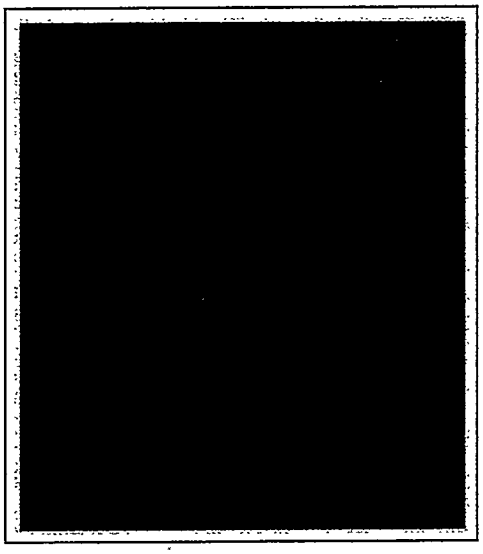

a) Ha = 0, N = 0

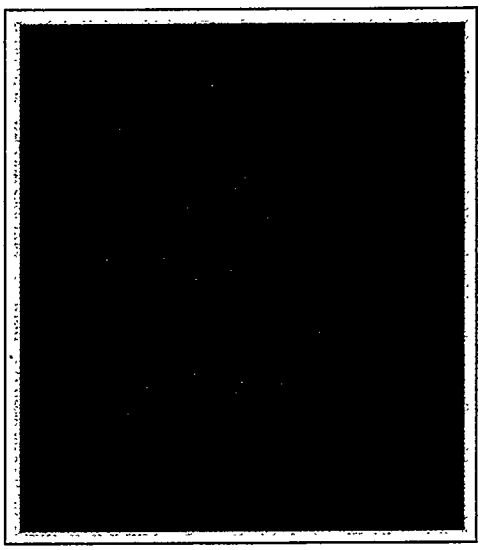

b) Ha = 600, N = 19

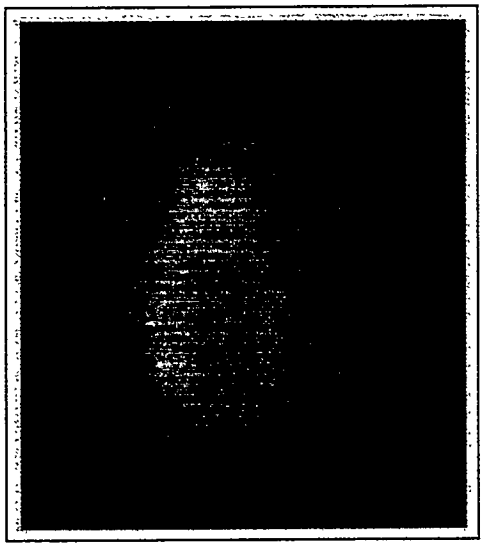

c) Ha = 1200, N = 78

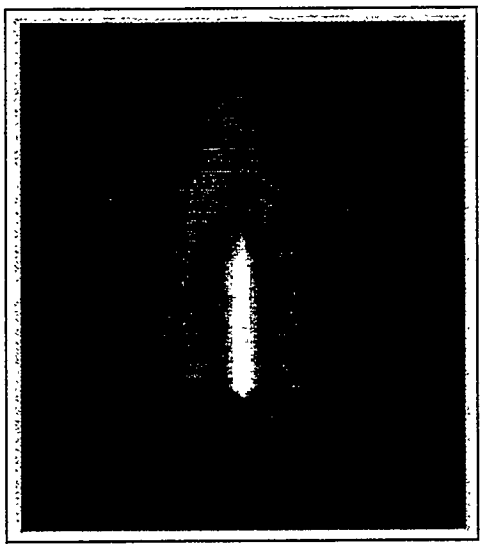

d) Ha = 1505, N = 122

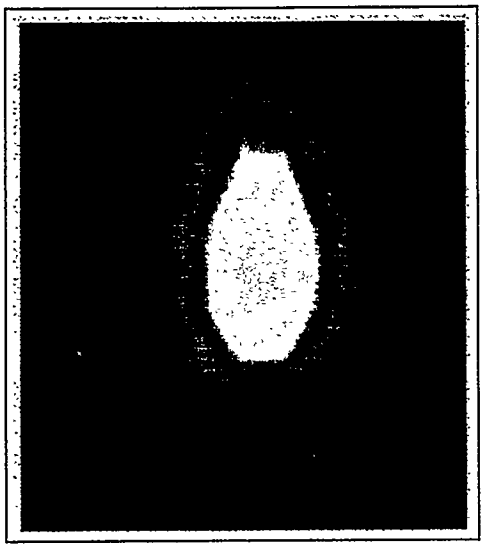

e) Ha = 2110, N = 239

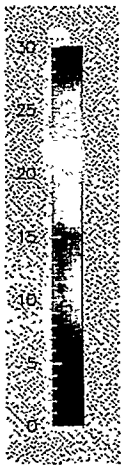

→ direction of the B-field →

Experimental results of the
void fraction distributions
at Re = 18600
transverse field, single injector

Experimental results: void fraction distributions

- mercury loop, longitudinal magnetic field, single injector
- $\bar{v}_{liquid} = 0.09 m/s$, $\dot{Q}_{gas} = 2.66 \cdot 10^{-5} m^3/s$ ⇨ $\beta = 0.015$

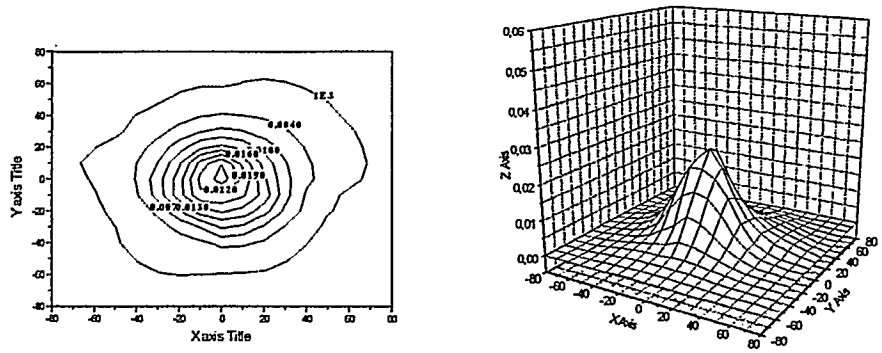

B = 0 T

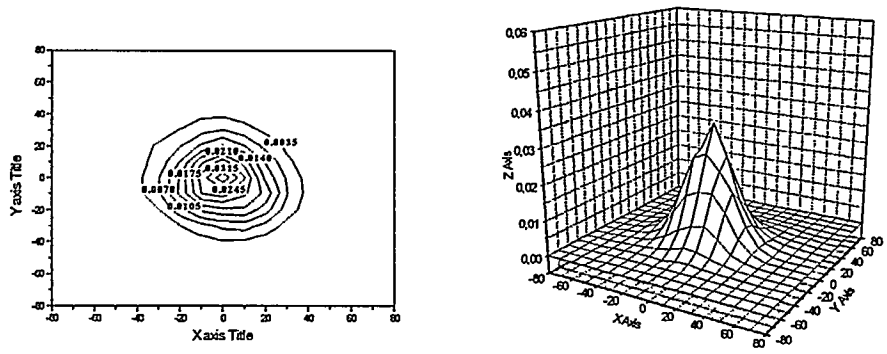

B = 0.3 T

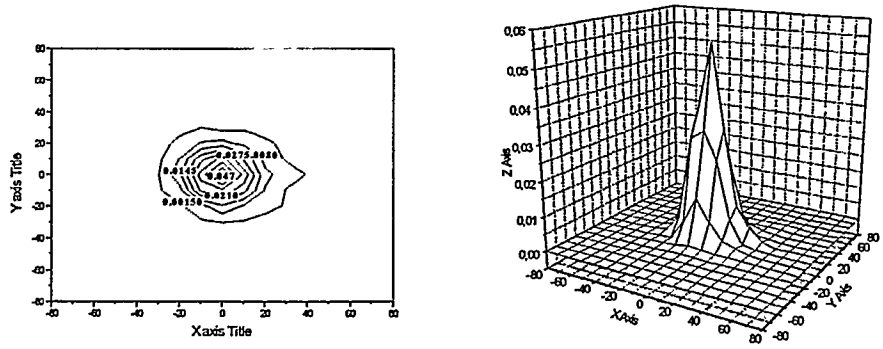

B = 0.9 T

RCR-Competence

- Measuring techniques for pure LM and LM-Gas Flows
  (own developments, only few techniques on market)
- Modelling and / or numerical simulation of LM and LM-Gas Flows
- Controlled influence of LM and LM-Gas Flows by external magnetic fields

Options:

☞ LM stirring not by bubbles, but by alternating magnetic fields

☞ Magnetic stirring in addition to bubbling in order to avoid safely any local overheating

☞ Contactless handling by magnetic fields

Local measuring techniques

- potential probe
  - measuring quantity: liquid velocity
  - work only with external magnetic field
  - selfmade
- single-wire resistivity probe
  - measuring quantity: void fraction α
  - selfmade
- double-wire resistivity probe
  - measuring quantity: interface velocity (bubble velocity and size)
  - selfmade
- micromagnet probe
  - measuring quantity: liquid velocity
- optical fibre probe
  - measuring quantity: temperature (silicium, gallium)
    pressure ?
    void fraction α (mercury, sodium)
  - problem: probes based on electrical measurements can show considerable errors in strong temperature gradients

Experimental study of two - component flow structure "lead - bismuth - gas".

B.F.Gromov, Yu.I.Orlov, M.I.Sotov, G.P.Poletaev.
State Scientific Centre of Russian Federation-
Institute of Physics and Power Engineering
249020 Obninsk, Russia.

There is possibility of realization of two - component flow "liquid metal - gas" in circuit with lead-bismuth. This can take place because of gas entrapment from the coolant free surface, leakage in water cooled system, deliberated insertion of gaseous mixtures during special technology processing.

Appearance of two - component flow can influence on operation of both the whole installation and its assemblies.

In this report investigation results of formation mechanism are presented for downward two - component flow "liquid metal - gas".

Experiments were carried out on experimental facility ÑÂÒ - 3M.

A two - electrode sensor on the basis of transit time method was used for study of flow structure.

The following values were measured at the distance 2m from gas insertion point: bubble velocities, gas concentration gradient, frequency of bubbles running and change of bubble maximum dimensions along tube diameter.

It was revealed that by low gas concentrations (<1%) gas was mainly concentrated in the flow centre and bubbles diameter did not exceed 2mm. With gas concentration increase larger bubbles with diameter up to 10 mm arised near tube wall. Under flow velocity more that 0.6 m/s immobile bubbles or bubbles moving opposite flow were not observed.

International Workshop, Schruns, Austria
March 25-28,1996

Experimental study of two-component flow structure " lead - bismuth - gas".

Gromov B.F., Orlov Y.I., Sotov M.I., Poletaev G.P.

State Scientific Centre of Russia
Institute of Physics and Power Engineering,
249020 Obninsk, Russia

Reasons for two-component flow formation:

- spontaneous gas capture on surface liquid metal ;
- leakages of cooling water systems;
- special gas insertion to flow during some technological operations;

Two-component flow formation can influence on thermohydraulic operation regimes of both the whole sistem, and separate sistem blocks.

Research results of experimental study have been presented in this report for descending two-component flow structure of " Pb - Bi - gas" with gas concentration ~ 1% vol.

Scheme of circulation facility.

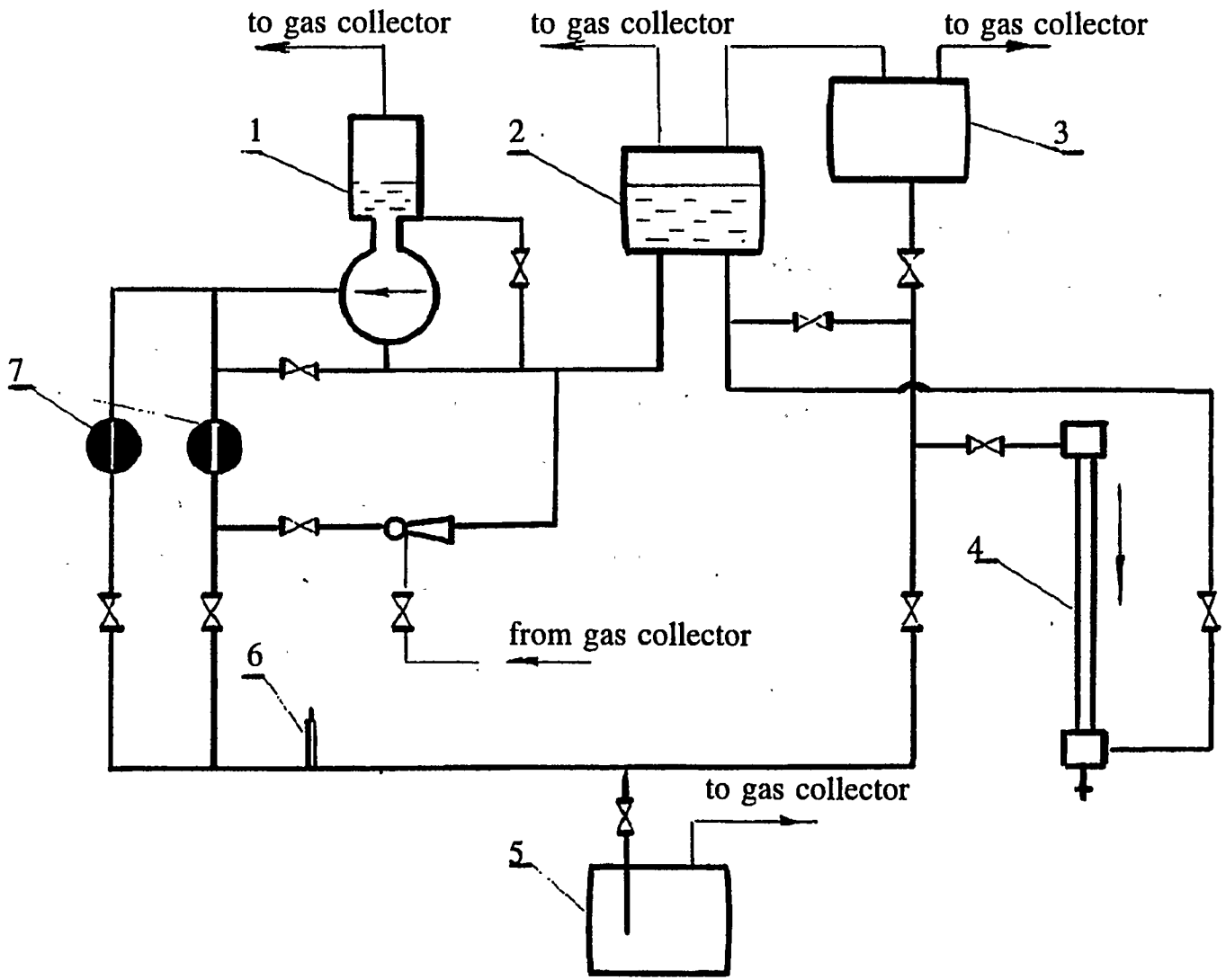

Fig. 1.

1 - pump, 2 - separator, 3 - measuring capacity, 4 - working section, 5 - tank, 6 - controller of oxygen activity, 7 - magnetic flowmeter.

Probe construction.

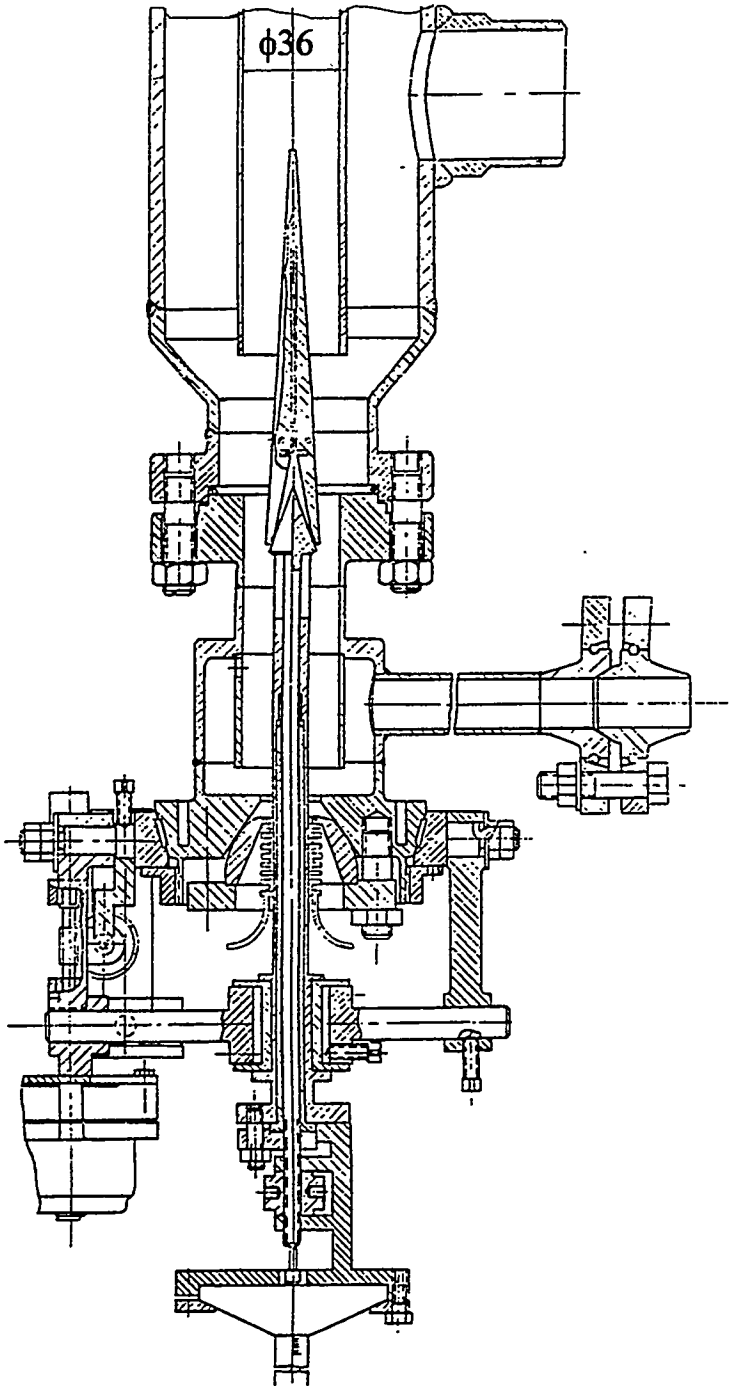

Fig. 2.

Probe construction of electrode.

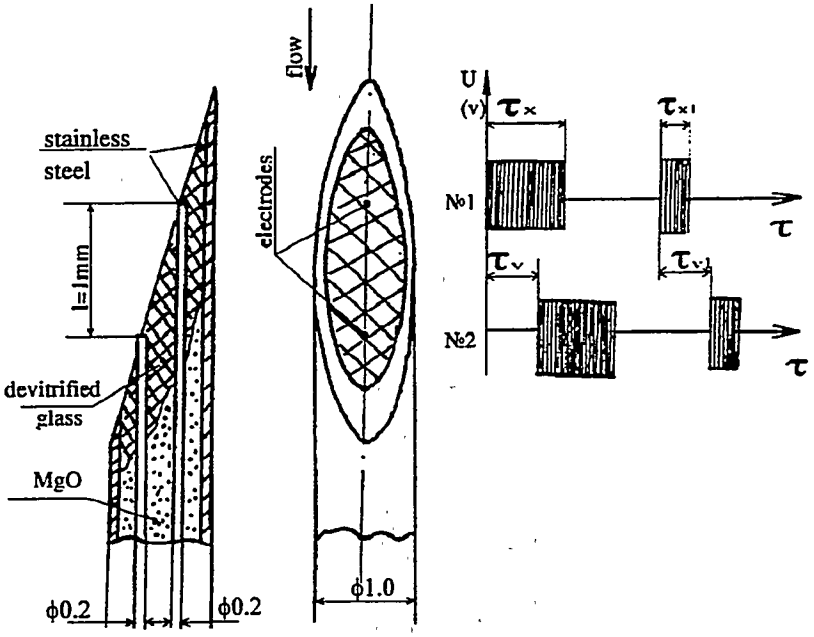

Fig. 3.

Distribution of time intervals.

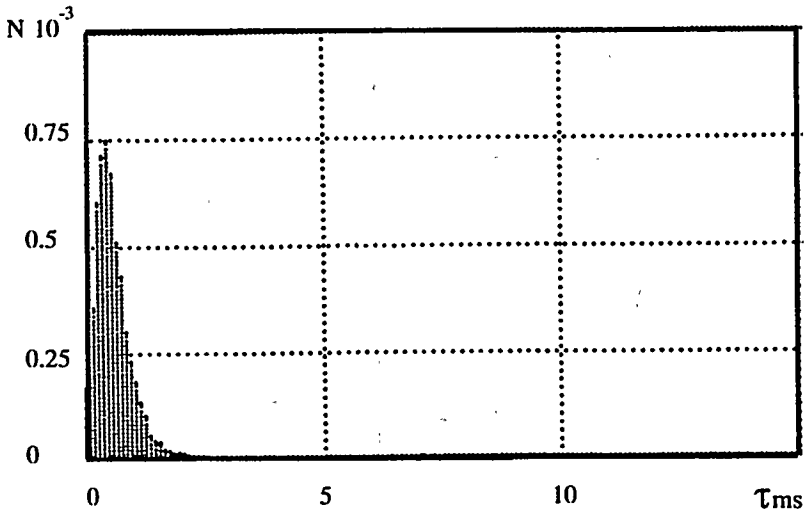

Fig. 4.

R = 4mm; $Q_L = 3.21m^3/h$; $Q_G = 31.8nl/h$;

Distribution of bubble velocity.

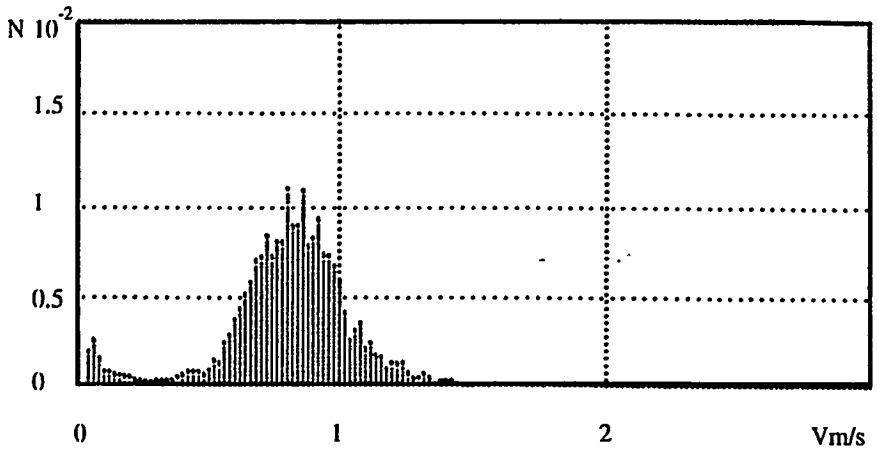

Fig. 5.

R = 4mm; $Q_L = 3.21 m^3/h$; $Q_G = 31.8 nl/h$;

Distribution of chord .

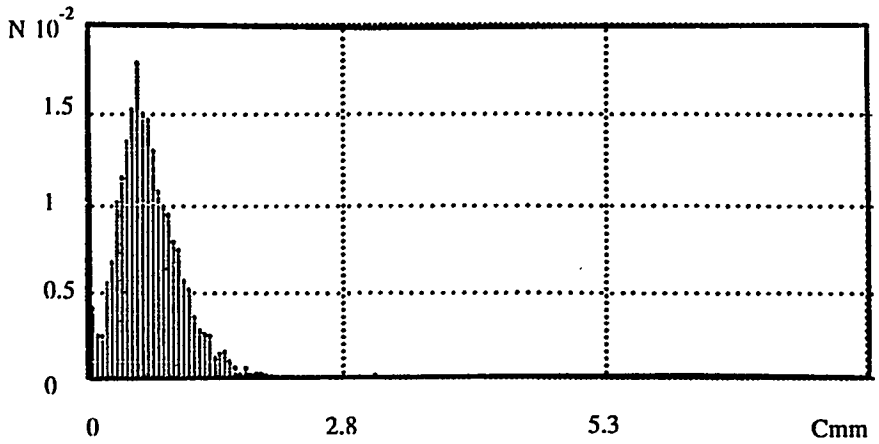

Fig. 6.

R = 4mm; $Q_L = 3.21 m^3/h$; $Q_G = 31.8 nl/h$;

Structure of descending two-component flow.

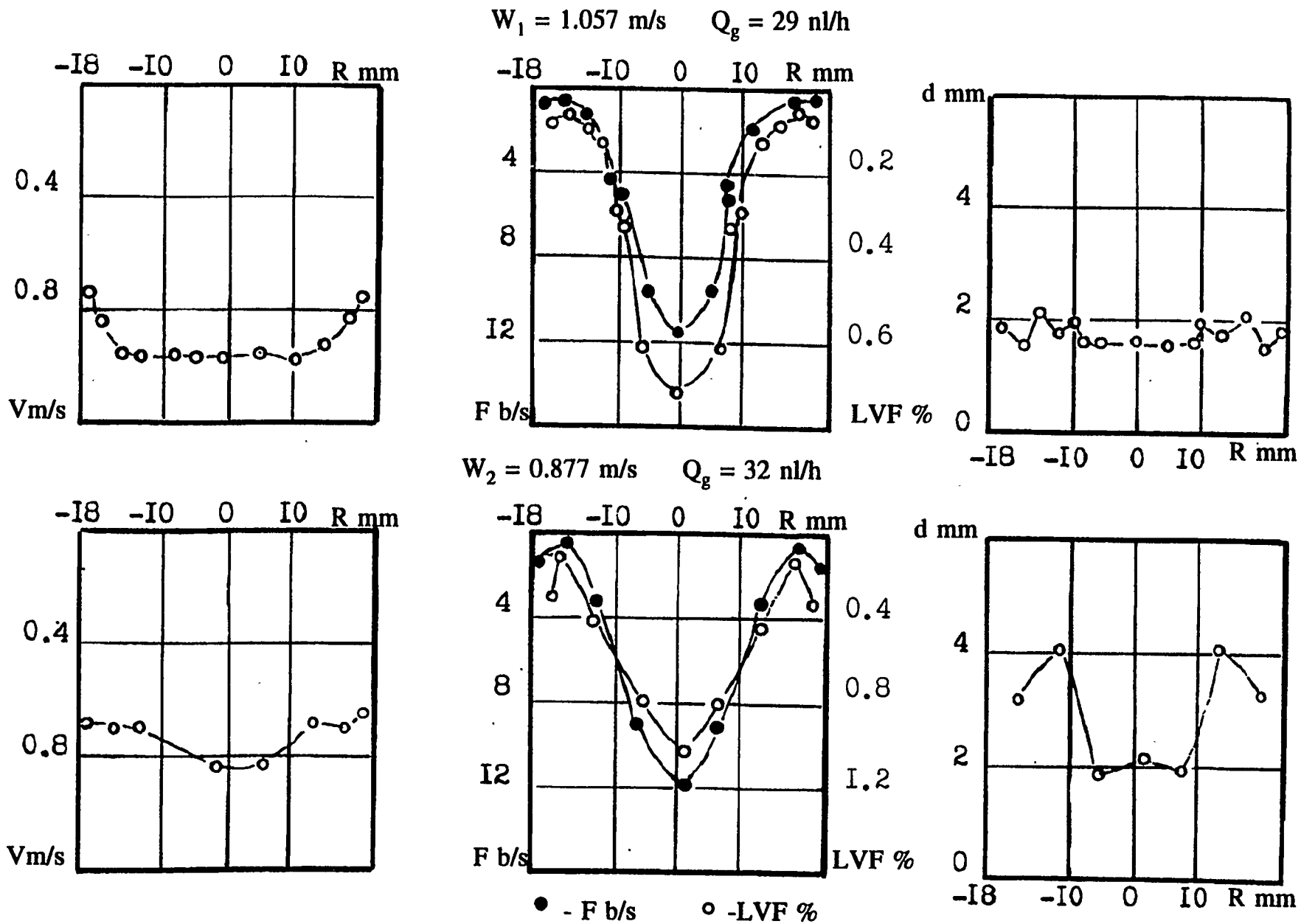

Fig. 7.

Automated Working Plase (A.W.P.) for research of the two-phase flow structure

A.W.P.is designed for automatization of collection and experimental data initial processing on research of two-phase flows structure with using electrocontact method of gas phase fixing.

Electrocontact conductivity gauge is used as a first measuring transducer. Gauge transforms aggeregate condition of the medium to closed or open state of contacts managing the electrical circuit. Electrical circuit opens and produces voltage impulse, when a bubble gets to the sensitive element of gauge. Bubble dimensions and flow rate determine duration of the voltage impulse.

Two-channel gauge allows to determine bubble rates using the time of base distance passing.

Range:

of measured time intervals _	_ 0.025-400 millis
of_measured bubbles rates_	0.00625-10 m/s
of measured bubbles chords_	_ 0.125-200 mm

Tecnical facilites of A.W.P. allows to get the following two- phase flow characteristics:

time intervals distribution of gauge sensitive element being in gas;

time intervals distribution of bubbles passing of electrocontect gauge base distance;

distribution bubbles rates in the flow;

distribution of bubbles chords dimensions.

Package of applied programs developed provides the following possibilites of A.W.P.:

definition of local volume gas content;

graphic presentetion of measurement results;

output of experimental data and results of processing onto the several carriers.

International Workshop on the Technology and
Thermal Hydraulics of Heavy Liquid Metals
Schruns, Austria
25-28 March, 1996

Comments on the Possibility of Cavitation in Liquid Metal Targets for Pulsed Spallation Neutron Sources

J. M. Carpenter
IPNS, Argonne National Laboratory

Abstract

When short pulses of protons strike the volume of a liquid target, the rapid heating produces a pressurized region which relaxes as the pressure wave propagates outward. Skala and Bauer[1] have modeled the effects of the pressure wave impinging on the container walls of a liquid mercury target under ESS conditions. They find that high pressures and high wall stresses result if the medium is uniform, nearly incompressible liquid. The pressure and the stresses are much reduced if the liquid contains bubbles of helium, due to their high compressibility. However, according to the calculation, the pressure still reaches an atmosphere or so at the surface, which reflects the compressive wave as a rarefaction wave of the same magnitude. Even such modest underpressures can lead to the growth of bubbles (cavitation) at or near the surface, which can collapse violently and erode the container surface. It is necessary to avoid this. Leighton[2] provides a wide ranging discussion of pressure waves in bubbly media, which may provide insights into the nature and control of cavitation phenomena. The paper surveys some of the relevant information from that source.

References

1. K. Skala and G. S. Bauer, ICANS XIII, p 559-576 (1995).

2. T. G. Leighton, *The Acoustic Bubble*, Academic Press, 1994.

Why Liquid Targets?

Heat removal by mass transport

Material cycling enables removal of spallation products

Self healing aginst
- Radiation damage
- Material failure due to stress or shock ...

OR?

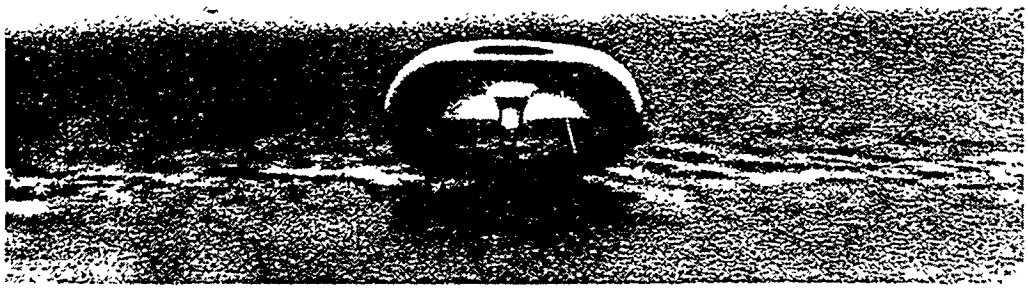

Figure 5.50 Jet formation during the collapse of an oscillating gas–vapour bubble at low pressure (0.04–0.05 bar) in a 60-Hz sound field. The bubble size is approximately 0.2 cm. (Photograph courtesy of Professor LA Crum, University of Mississippi, previously published in reference [362].)

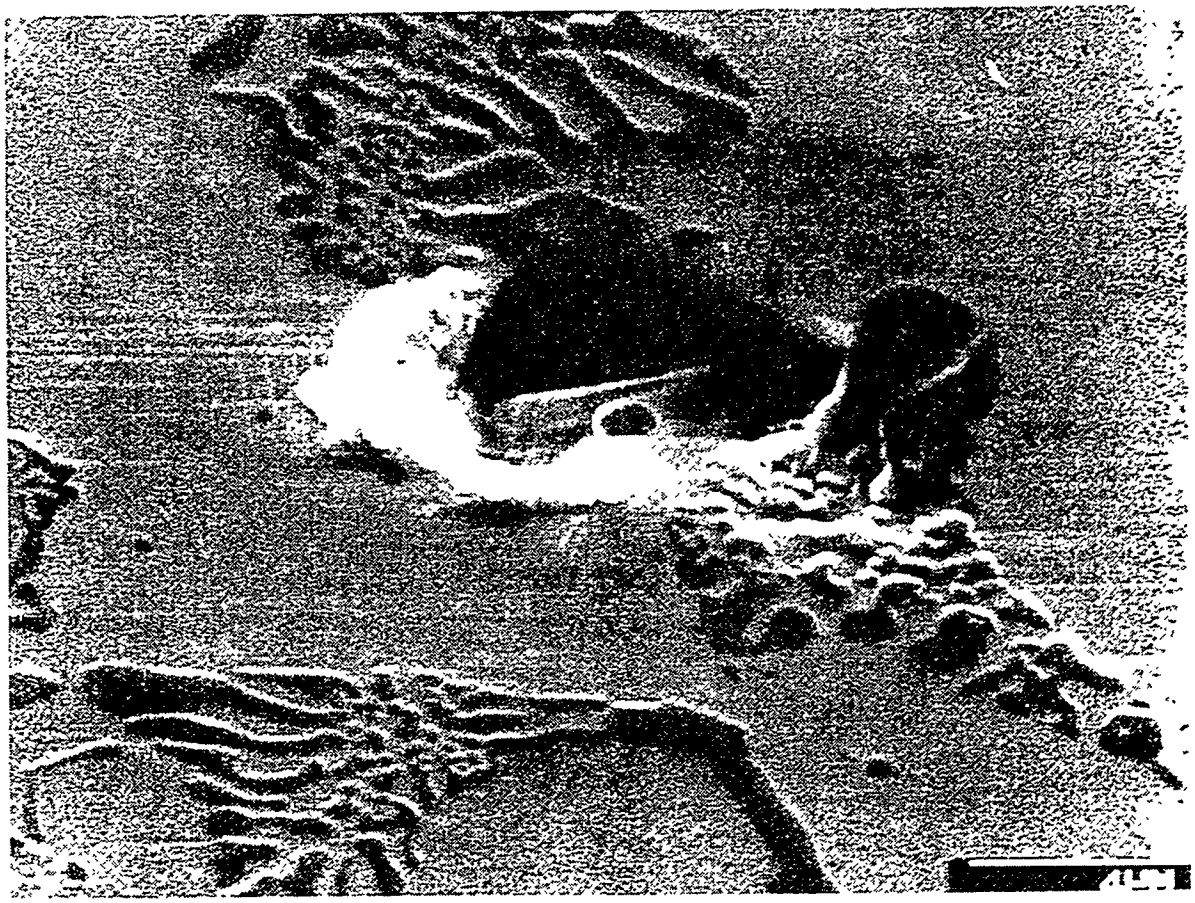

Example of cavitation damage at a surface.

Elastic Energy

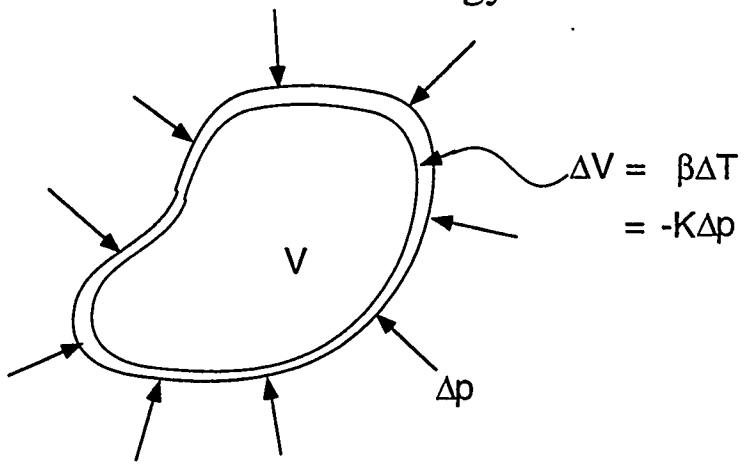

$$\Delta V = \beta \Delta T$$
$$= -K\Delta p$$

Elastic energy required to compress volume V by increment dV

$$dE_{el} = pdV$$

Compressibility

$$dV = \left(\frac{\partial V}{\partial p}\right) = V\frac{1}{V}\left(\frac{\partial V}{\partial p}\right) = VKdp;\ K \equiv \frac{1}{V}\left(\frac{\partial V}{\partial p}\right)$$

Elastic energy

$$E_{el} = \int_0^{\Delta p} dE_{el} = VK\int_0^{\Delta p} pdp = \frac{1}{2}VK\Delta p^2$$

Thermal expansion

$$\Delta V = \alpha V \Delta T$$

Change in pressure to compensate

$$\Delta p = \frac{\Delta V}{\left(\frac{\partial V}{\partial p}\right)} = \frac{1}{K}\frac{\Delta V}{V}$$

Temperature rise

$$\Delta T = \frac{\varepsilon}{\rho C}$$

Finally,

$$\Delta p = \frac{\beta \Delta T}{K}$$

$$E_{el} = \frac{1}{2}V\frac{\alpha^2 \Delta T^2}{K} = V\frac{\alpha^2 \varepsilon^2}{2K\rho^2 C^2}$$

Goes as <u>square</u> of deposited energy!

It is easy, up to a point, to compute the pressure on the liquid container due to rapid deposition of thermal energy. Skala and Bauer calculated the stress due to an ESS pulse in a liquid Hg target and found that the stress in the container wall would exceed the allowable stress in the steel vessel. Adding a small volume fraction of gas bubbles might be a way to suppress the generation of pressure waves, they found.

Sound Speeds

$$c=\sqrt{B/\rho} \quad ; \quad B=\frac{1}{\frac{1}{V}\frac{\partial V}{\partial p}}$$

Gas: pV^{κ} = constant

κ = polytropic exponent

$B = \kappa p$

$$c_{gas}=\sqrt{\frac{\kappa p}{\rho_{gas}}}$$

Liquid: $$c_{liq}=\sqrt{\frac{B_{liq}}{\rho_{liq}}}$$

Bubbly liquid:

$$c_{Bub}=\sqrt{\frac{\kappa p}{\rho_L\{VF\}}} \qquad \text{large } \{VF\}$$

$$\approx c_{liq}\left\{1-\frac{1}{2}\{VF\}\frac{\rho_{liq}c_{liq}^2}{\kappa p}\right\} \qquad \text{small } \{VF\}$$

$$c_{Bub}\approx c_{liq}\left\{1+\frac{\{VF\}}{2}\frac{c_{liq}^2\rho_{liq}}{\kappa p}\right\}^{-1} \qquad \text{not -so- small } \{VF\}$$

(BUT these relationships apply only for LOW ω!)

{VF} = void fraction

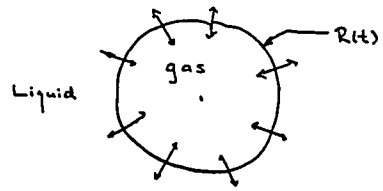

Bubble Frequency

$R(t) = R_0 + R_\varepsilon e^{i\omega 0 t}$

No surface tension, inviscid, adiabatic approx. (Minnaert theory)

Resonant frequency

$$\nu_0 = \frac{1}{2\pi R_0}\sqrt{\frac{3\kappa p}{\rho_{liq}}}$$

For He, $\kappa = \gamma = 5/3$ (adiabatic)

Hg $\rho_{liq} = 13.5\text{x}10^3 \text{kg/m}^3$

and p = 1 atm.

$\nu_0 R_0 = .97$ m/sec

$\nu_0 \sim 1.$kHz if $R_0 = 1.$ mm

Bubbly Medium is Dispersive! ($c = c(\omega)$)

$$c(\omega) = c_{liq}\left[1 - 2\pi c_{liq}^2 \int_{R_0=0}^{\infty} \frac{R_0}{\omega 2} \frac{(\omega_0/\omega)^2 - 1}{\left(\left(\frac{\omega_0}{\omega}\right)^2 - 1\right)^2 + d^2} N(R_0) dR_0\right]$$

d = damping factor

Gives same result as low {VF} case when $\omega \to 0$.

What does this mean?

The usual discussion of sound waves in bubbly media is couched in terms of sound speeds $c(\omega)$, attenuation + propagation of small amplitude pressure waves $\rho(x,t) = e^{i(kx-\omega t)}$ and linear approximation

The usual calcuation of pressure shocks is a finite-element solution of the full non-linear Navier-Stokes equations

$$\rho \frac{D\vec{v}}{Dt} = \rho \vec{g} - \vec{\nabla} p + \eta \nabla^2 \vec{v}$$

DIFFERENT LANGUAGES!

Our problem has two time scales

Bubble period $1/\nu_o$ (msec)

Sound transit time l/"c" (?)

and two length scales

Bubble radius R_0 (mm)

Macroscopic target dimension l (m)

The bubbly medium is stiff for high frequencies: bubbles "scatter" propagating waves; the medium is compliant for low frequencies

SESSION 9

Safety Issues

Chairman
J. Carpenter

ENERGY RELEASE, BEAM ATTENUATION RADIATION DAMAGE, GAS PRODUCTION AND ACCUMULATION OF LONG-LIVED ACTIVITY IN Pb, Pb-Bi AND Hg TARGETS

Yu.N.Shubin, IPPE, Obninsk, Russia

ABSTRACT

The calculation and analysis of the nuclei concentrations and long-lived residual radioactivity accumulated in Pb, Pb-Bi and Hg targets irradiated by 800 MeV, 30 mA proton beam have been performed. The dominating components to the total radioactivity of radionuclides resulting from fission and spallation reactions and radiative capture by both target nuclei and accumulated radioactive nuclei for various irradiation and cooling times were analyzed. The estimations of spectral component contributions of neutron and proton fluxes to the accumulated activity were carried out. The contributions of fission products to the targets activity and partial activities of main long-lived fission products were evaluated. The accumulation of Po isotopes due to reactions induced by secondary alpha-particles were found to be important for the Pb target as compared with two-step radiative capture. The production of Tritium in the targets and its contribution to the total targets activity was considered in detail. It is found that total activities both targets are close one another.

The problems connected with the energy release and beam attenuation in the accelerator-target window for various materials were analyzed for incident proton energies 800 MeV. The radiation damage of the window and accumulation of Hydrogen and Helium was considered also. It seems that titanium window is preferable as compared with stainless steel or tungsten due to less energy losses.

The analysis performed permits to make following conclusions:

1. Main contribution to the target activity is due to not Po isotopes, but other isotopes that are formed in spallation reactions.
2. Total activity of Pb and Pb-Bi targets are close one another.
3. The dominant contribution to the target activity is due to high energy (>20 MeV) parts of neutron and proton spectra. It is in this energy region thorough analysis of nuclear data is needeed.
4. The contributions of fission products to the target activity comprize 10-15% of total activity, well known long-lived isotopes make the largest contributions.
5. The contributions of (α,xn) reaction to polonium activity of Pb target may be a few times higher than that of double neutron capture.
6. Tritium accumulation is approximately equal in all targets and its contribution to the total activity is as high as 50% for lead target at cooling times from 3 till 30 years and 2 times lower than the same figure for lead-bismuth target for the same time interval.
7. Calculation and analysis of the activatiion of mercury target showed that at cooling time interval up to one year the mercury target activity exceeds that for lead and

lead-bismuth target. The activities of all targets are close at cooling times up to 5000 years. For larger cooling times activity of lead and lead-bismuth targets is 2 or 3 order of magnitude higher than for mercury target.

8. It should be noted that to total activities of mercury, lead and lead-bismuth targets contribute different radionuclides.
   The comparision between targets shows that the use of mercury target enables to diminish the long-lived activity as compared with lead and lead-bismuth targets considerabley
9. Main part of the energy released by the beam in a thin window is connected with ionization losses. Nuclear interactions increase ionization losses by some 10-15%.
   Attenuation of the intensity of proton beam per cm of window thickness is approximately equal for both materials: 6.5% for steel and 3.9% for titanium.
   The analysis demonstrated that replacement of stainless steel by titanium results in decrease of energy release by a factor of 1.7 for the same window thickness. Estimates of energy release done by various groups agree within the accuracy of calculations which is 15-20%.
10. Significant discrepancies exist in published evaluations of radiation damage of target windows. In particular, the estimates carried out in JAERI and BNL for designs with comparable integral proton fluxes differ by more than an order of magnitude. There is no detailed description of operating experience with the dividing windows of the accelerator LAMPF in available publications. The main reason of differences in radiation damage evaluations is the discrepancy in calculated spectra of secondary particles produced in nuclear collisions. Considerable work is needed to remove the discrepancy and test calculation results by comparison with experimental data.
    There is difference of a few times between the evaluations of hydrogen and helium accumulation in the window. To improve the situation more reliable evaluations are needed of the cross sections of the emission of all hydrogen and helium isotopes in the material of the window.

INTRODUCTION

Various properties of hybrid electronuclear systems that can be used to utilize plutonium or to transmute long-lived radioactive waste, in a large degree depend on target characteristics: safety, lifetime and productivity as neutron source. This part of the system was investigated less in comparison with already existing accelerators and blankets of various types. That is why the analysis of characteristics such as energy release, beam attenuation, radiation damage and gas production in the target window and, at last, the accumulation of various elements, other than target material, and activity of target due to produced various isotopes is necessary for the feasibility investigation to construct the system as a whole. Below we analyze the status of the problem and estimate the target characteristics for concrete examples of Pb, Pb-Bi and Hg targets. The target has cylindrical form: 100 cm length, 50 cm diameter, filled with liquid lead or mercury (natural content) or lead-bismuth eutectics: 44.5% lead and 55.5% bismuth. The target is separated from ionguide by window having 20 cm diameter, constructed of stainless steel or titanium and having 2-5 cm thickness. The proton beam is distributed uniformly on the window surface.

1. ENERGY RELEASE AND BEAM ATTENUATION IN THE WINDOW

Main part of the energy released by the beam in a thin window is connected with ionization losses. Nuclear interactions increase ionization losses by some 10-15%. Total energy release in steel or titanium is shown in Table 1.

Table 1. Energy release in the target window.

Beam		Energy release, kWt/mm	
Energy, MeV	Current, mA	Stainless steel	Titanium
800	30	45.0	25.4
1600	60	79.2	45.5

Attenuation of the intensity of proton beam per cm of window thickness is approximately equal for both materials: 6.5% for steel and 3.9% for titanium.

The analyses demonstrated that replacement of stainless steel by titanium results in decrease of energy release by a factor of 1.7 for the same window thickness. Estimates of energy release done by various groups agree within the accuracy of calculations which is 15-20%.

2. GAS PRODUCTION IN THE WINDOW

The evaluated cross sections for the (p,xp) and (p,xα) reactions on ^{56}Fe can be taken from ENDF/B-IV and MENDL-2 [1] cross section data libraries for the energies up to 1000 MeV. The difference of evaluated cross sections for alpha-particle production is about 20%. Keeping in mind this accuracy and taking fluence $1.85 \cdot 10^{22}$ p/cm^2 year we get for alpha-particle accumulation the value of $0.98 \cdot 10^{-2}$ α/atom·year. According to proton yield evaluation the accumulation of hydrogen is approximately 6 times more than alpha-particle accumulation. For thin window approximately one half of alpha-particles and 2/3 of all protons will escape the window. On the other hand

other particles such as deuterons, tritons and helium-3 will be accumulated also. The cross sections for these are evaluated with considerably larger errors than alpha-particle emission cross section. Taking into account the uncertainties noted one can take as an evaluation for hydrogen and helium accumulation the values given above. The uncertainties of such evaluations are probably not less than 50%.

When we go to the proton energy 1600 MeV and to doubled fluence one should expect the increase of hydrogen and helium accumulation by factor four.

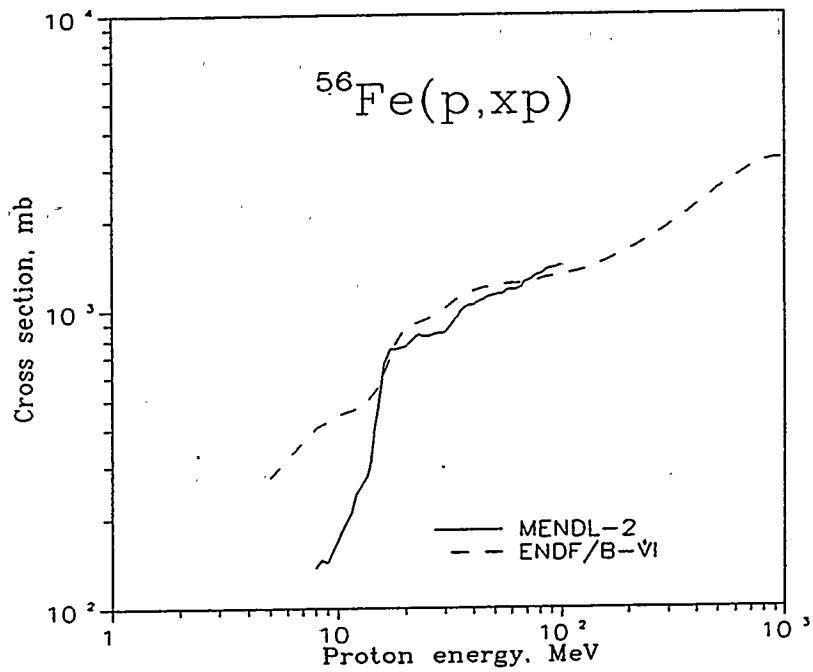

Figure 1. Cross-section for ^{56}Fe(p,xp) reactions.

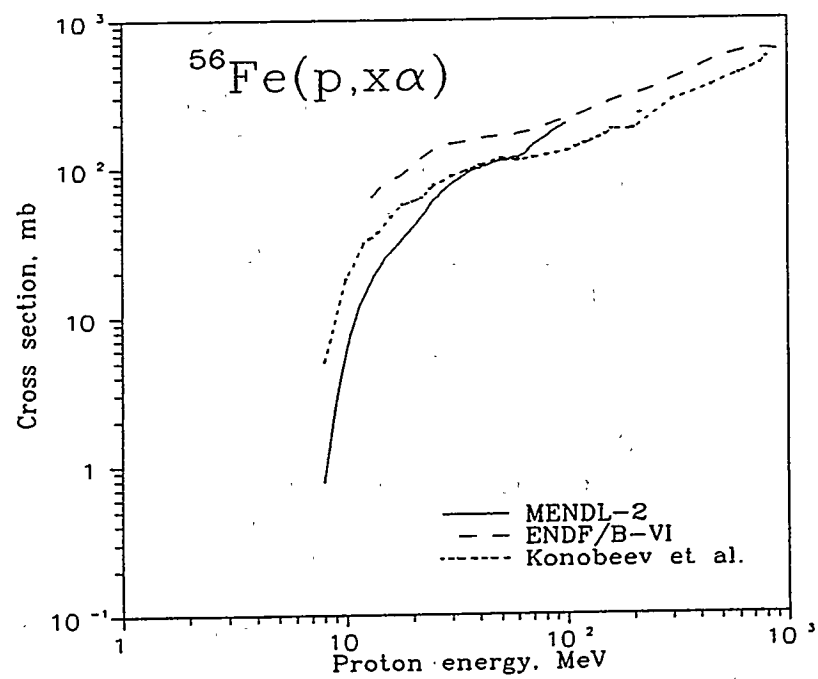

Figure 2. Alpha-particle production cross section for ^{56}Fe(p,xα) reactions

Table 2. Gas production in the window

Ref.	R,cm	$\Phi_p, 10^{15}$	H, 10^3 appm	He, 10^3 appm	He', 10^3 appm	He", 10^3 appm
[2]	23	0,146	10	3	2.7	11
[3-4]	8	0,312	35	3.5	6	1.1-1.6
	10	0,5			10	
	10	1,2			25	

3. RADIATION DAMAGE OF TARGET WINDOW

The experimental data on target window radiation resistance for high energy protons are reviewed and analyzed in the paper of Ireland J.R. [5]. On the base of these data conclusion was made that the replacement of the window in the project of transmutation installation will be necessary only in a half of a year (if it will be necessary at all). This conclusion is not so evident due to some reasons:

1. The technology requirements to the window, cooled by liquid metal, and to the window in front of beam trap, that was the base of the conclusion, are different (the thickness of the window was not given).
2. The linear dependence of the window lifetime on the intensity of the processes occurring (heat release, radiation damage, gas production) was assumed. It was proposed to compensate the threefold intensity increase by fourfold decrease of the lifetime (for the same window design).

The results of the radiation damage calculations, that are defined by the values of the displacement per atom and hydrogen and helium accumulation, are shown in Table 3, where the results of Ref. [2] (OMEGA project), Refs. [3,4] (BNL project) and also the estimates on the base of Ref. [6] are given. The thickness of all windows was taken 0.5 cm, structural material was stainless steel. In the last column of Table 3 the values of displacements per atom in a year are given that were calculated using relation: $dpa' = \sigma_d \cdot \Phi_p \cdot T$, where σ_d - the displacement cross section, was taken equal 3200 barn [6], T is the number of seconds in a year. The authors of paper [2] used the NMTC/JAERI codes, in Refs. [3,4] the LAHET and HTAPE codes were used. We see that the results of estimations not only are different, but contradict each other: to twice as larger fluence corresponds smaller (by order of magnitude) value of the displacement per atom. Our results are given in the last two lines. We see that the discrepancies between different gas production estimates are not so large as compared with the values of dpa but are not negligible. Thus, the calculations of the radiation damage of the target window, that is important for technology problems, are rather sensitive to be a touchstone for the intercomparison of various approaches and codes, for the test of validity of the assumptions used in calculation and analysis.

Table 3. Radiation damage evaluations for window.

Refs.	R,cm	E,GeV	I,мA	$\Phi_p, 10^{15}$	dpa/year	dpa'/year
[2]	23	1,5	39	0,146	60	15
[3-4]	8	1	10	0,312	6,07-8.8	32
	10	1	25	0,5		51
	10	1	60	1,2		123

4. THE ANALYSIS OF LONG-LIVED RADIOACTIVITY IN LEAD AND LEAD-BISMUTH TARGETS

Lead and lead-bismuth are considered as most probable target materials for intense neutron source in accelerator driven transmutation problem. The analysis of radioactive nuclei accumulation was performed in a several papers [5,7,8]. The results of the calculations reduced to the same irradiation conditions differ some-times by a few orders of magnitude. In particular, in paper [8] the activity value for dominating isotope ^{210}Po ($T_{1/2}$ = 138 d) in lead-bismuth target has been obtained that exceed the results of other authors more than 10 times. Such significant discrepancies can be due to cross sections used for some channels of isotope accumulation. That is why it is important to have reliable tested libraries of evaluated data on the one hand and to clear up the reasons of discrepancies in calculations on the other hand. We have carried out calculations of activity accumulation for lead and lead-bismuth targets irradiated by 800 MeV, 30 mA proton beam. Main component were determined of the long-lived residual radioactivity of lead and lead-bismuth targets and dominating channels were investigated of the reactions producing those activity components. We founded out the reason of discrepancies in calculation results. Analysis was made of the contribution of fission products to the target's activity and partial activities of main long-lived fission products were evaluated. The accumulation of Po isotopes due to reactions induced by secondary α-particles has been estimated.

4.1 METHOD OF CALCULATIONS AND DATA

The nuclides concentrations in the targets have been defined by solving the system of differential equations:

$$dN_i(t)/dt = \sum_{k \neq i} \left(\lambda^r_{ik} + \lambda^d_{ik}\right) \cdot N_k(t) - \left(\lambda^r_i + \lambda^d_i\right) \cdot N_i(t), \qquad (1)$$

where $N_i(t)$ is the concentration of i-th nuclide at time t, λ^r_{ik} and λ^d_{ik} are nuclear reaction and decay rates, consequently, resulting in the transmutation of k-th nuclide to i-th, λ^r_i is the rate of transmutation of nuclide "i" in nuclear reactions, λ^d_{ik} is the radioactive decay rate of this nuclide. The nuclear reaction rates λ^r_{ik} and λ^r_i in equation (1) are defined as follows:

$$\lambda^r_{ik} = \sum_j \int \sigma^{(j)}_{ik}(E) \cdot \varphi^{(j)}(E) dE, \qquad (2)$$

$$\lambda^r_i = \sum_j \int \sigma^{(j)}_{abs,i}(E) \cdot \varphi^{(j)}(E) dE, \qquad (3)$$

where $\varphi^{(j)}(E)$ is the type "j" incident particle spectral current density, $\sigma^{(j)}_{ik}$ is formation cross section for nuclide "i" when nuclide "k" is irradiated by particles of j type. $\sigma^{(j)}_{abs,i}$ is the cross section equal to the difference of total nonelastic cross section and inelastic scattering cross section for particles considered on nuclei of "i" type.

The spectra of neutrons and protons calculated in papers [8,9] were used. The neutron cross sections for reactions at energies below 20 MeV have been taken from ADL library [10]. For neutron reactions at 20-100 MeV and for proton reactions up to 100 MeV the data of MENDL library [11] have been taken. The cross sections at energies higher than 100 MeV have been defined using the Silberberg-Tsao approximate relations [12].

4.2 RESULTS AND DISCUSSION

4.2.1 DOMINATING COMPONENTS OF THE LONG-LIVED ACTIVITY OF THE TARGET.

The results of calculations of the total activity and activities of some most important nuclides for the lead and lead-bismuth targets are shown in Figs. 3, 4. For one year irradiation of the target without heat exchanger ^{210}Po ($T_{1/2}$=138 d) concentration is $3.1 \cdot 10^{-7}$ g/kg for lead target and $5.9 \cdot 10^{-3}$ g/kg for lead-bismuth target which is about 1000 times lower than the results obtained for this isotope in the same conditions in earlier calculations by the INPE group [8]. We found out that this discrepancy, as well as less important differences for other Po isotopes, are due to the use in INPE calculations of cross sections of $^{209}Bi(n,\gamma)$ reaction overestimated by a factor of 1000. The use of correct cross sections removes the discrepancies in the results for the accumulation of radioactive isotopes of Bi and Po. From Figs. 3, 4 one can see that various isotopes of Pt, Au, Hg, Tl, Pb and Bi make more significant contribution to the long-lived ($T_{1/2}$>100 d) activity than ^{210}Po isotope for both targets. The activity accumulations were calculated for both lead and lead-bismuth targets and the nuclides with atomic number Z=72÷84 and half-life $T_{1/2}$>6 min. were taken into account (about 170 nuclides). The nuclides making main contributions to the total activity of the targets after different cooling times were identified. The resulting long-lived activities of the dominating isotopes are presented in Tables 4 and 5. The isotope ^{195}Au (half-life $T_{1/2}$=186 days) provides main contribution in the cooling time range 10 days 1 year together with the isotope ^{204}Tl (half-life $T_{1/2}$=3.78 years, begins to dominate after 3 years). The ^{193}Pt contribution becomes significant later. For lead target the ^{210}Po contribution is by a few orders of magnitude lower than the contribution of those isotopes.

Alternative isotopes dominate also in lead-bismuth target activity for the same range of cooling times. The ^{210}Po activity is only 2.5 times lower than the activity of ^{195}Au. After three years the total activity is determined by ^{207}Bi nuclide ($T_{1/2}$=32.2 years).

Table 4. Total and partial activities (Ci/kg) in lead target for primary proton beam energy 800 MeV and current 30 mA after a year of irradiation for cooling times indicated in the Table.

Cooling time	180 days	2 years	20 years	100 years
Total activity	$1.037 \cdot 10^{2}$	$2.699 \cdot 10^{1}$	1.987	$5.960 \cdot 10^{-1}$
Po-210	$6.076 \cdot 10^{-4}$	$3.910 \cdot 10^{-5}$	$2.772 \cdot 10^{-7}$	$2.306 \cdot 10^{-8}$
Bi-207	$1.652 \cdot 10^{-1}$	$1.607 \cdot 10^{-1}$	$1.157 \cdot 10^{-1}$	$2.690 \cdot 10^{-2}$
Pb-202	$5.404 \cdot 10^{-3}$	$5.404 \cdot 10^{-3}$	$5.403 \cdot 10^{-3}$	$5.397 \cdot 10^{-3}$
Tl-204	$1.922 \cdot 10^{1}$	$1.469 \cdot 10^{1}$	$5.899 \cdot 10^{-1}$	-
Hg-194	$1.306 \cdot 10^{-1}$	$1.304 \cdot 10^{-1}$	$1.273 \cdot 10^{-1}$	$1.144 \cdot 10^{-1}$
Au-194	$1.306 \cdot 10^{-1}$	$1.304 \cdot 10^{-1}$	$1.273 \cdot 10^{-1}$	$1.144 \cdot 10^{-1}$
Pt-193	1.297	1.270	$9.899 \cdot 10^{-1}$	$3.268 \cdot 10^{-1}$

The comparison of the activities of lead and lead-bismuth targets irradiated by 800 MeV protons for one year demonstrates that the total activities of the targets begin to differ significantly only after one year. They are determined by the formation

of long-lived bismuth isotopes in the (n,2n) and (n,3n) reactions in lead-bismuth target (^{207}Bi and, for very long times, ^{208}Bi). In the targets irradiated for a month total activity after 1 day of cooling is significantly lower than in the targets irradiated for a year, but relative contributions of individual isotopes remain the same.

Table 5. The same as in Table 4 for lead-bismuth target

Cooling time	180 days	2 years	20 years	100 years
Total activity	$1.087 \cdot 10^{2}$	$3.438 \cdot 10^{1}$	$1.240 \cdot 10^{1}$	3.042
Po-210	$1.119 \cdot 10^{1}$	$7.117 \cdot 10^{-1}$	$9.349 \cdot 10^{-6}$	$7.778 \cdot 10^{-7}$
Po-208	1.578	1.101	$1.497 \cdot 10^{-2}$	$7.573 \cdot 10^{-11}$
Bi-207	$1.573 \cdot 10^{1}$	$1.530 \cdot 10^{1}$	$1.102 \cdot 10^{1}$	2.561
Tl-204	9.201	7.030	$2.824 \cdot 10^{-1}$	$1.761 \cdot 10^{-7}$
Hg-203	$2.201 \cdot 10^{-1}$	$6.150 \cdot 10^{-5}$	-	-
Hg-194	$1.059 \cdot 10^{-1}$	$1.057 \cdot 10^{-1}$	$1.032 \cdot 10^{-1}$	$9.276 \cdot 10^{-2}$
Au-195	$4.815 \cdot 10^{1}$	6.206	$1.032 \cdot 10^{-1}$	-
Pt-193	1.096	1.073	$8.362 \cdot 10^{-1}$	$2.761 \cdot 10^{-1}$

4.2.2 ANALYSIS OF THE CONTRIBUTIONS OF THE PROTON AND NEUTRON SPECTRAL COMPONENTS TO THE ACCUMULATING ACTIVITY

To evaluate correctly the possible uncertainties of the calculations and the influence of cross section data errors on the results it is necessary to analyze the spectral contributions of neutrons and protons to the accumulating activities.

The components of the long-lived radioactivity in lead and lead-bismuth targets, accumulating due to the (p,xn) and (n,xn) reactions, are presented in Tables 6 and 7 for the case of incident proton energy 800 MeV and 30 mA current. The activities induced by the soft part of neutron spectra with En < 20 MeV are also presented. These results indicate that the dominating long-lived activities determined by platinum, gold, mercury and thallium isotopes are formed by hard components of proton and neutron spectra with the energies above 20 MeV.

The soft component of neutron spectrum with the energies below 20 MeV corresponding to 96.6% of the total neutron flux makes some 10^{3}-10^{4} times lower contribution to the total long-lived activity ($T_{1/2}$ > 1000 days) than protons and neutrons from the hard part of the spectra comprising less than 4% of the total flux of the particles.

It must be pointed out however that the accumulation of long-lived isotopes ^{207}Bi ($T_{1/2}$=$1.39 \cdot 10^{4}$ days), ^{208}Bi ($T_{1/2}$=$1.34 \cdot 10^{8}$ days) and ^{210}Po ($T_{1/2}$=138 days) is due to the (n,γ) reaction on soft neutrons. The total activity of those isotopes is more than 1000 times lower than that of gold, mercury and thallium for lead and lead-bismuth targets for cooling times longer than 1 year.

Our analysis demonstrates that the possible uncertainties of the results of calculations of the long-lived activity of the targets are determined by the errors of the cross sections of the threshold reactions at intermediate energies of protons and neutrons (20-100 MeV). The new version of MENDL library has been developed in IPPE [1]. Working out the MENDL-2 library we took into account the preequlibrium emission of clusters, the pair correlations, shell and collective effects in nuclear level density on the base of the unified superfluid model. The library has been tested on experimental data for the threshold reactions.

Table 6. Total and partial activities (Ci/kg) produced by various spectral components in lead target for incident proton beam of the energy 800 MeV and current 30 mA after a year of irradiation for cooling times indicated in the Table.

Cooling time (days)	Spectral component				
	< 1 MeV	< 20 MeV	< 100 MeV	Total n activity	Total p activity
10	$1.094 \cdot 10^{-3}$	1.497	$7.835 \cdot 10^{1}$	$1.609 \cdot 10^{2}$	$2.251 \cdot 10^{2}$
30	$7.065 \cdot 10^{-4}$	$1.519 \cdot 10^{-1}$	$2.065 \cdot 10^{1}$	$6.685 \cdot 10^{1}$	$1.740 \cdot 10^{2}$
180	$3.243 \cdot 10^{-4}$	$6.178 \cdot 10^{-2}$	8.878	$3.152 \cdot 10^{1}$	$7.214 \cdot 10^{1}$
730	$2.235 \cdot 10^{-5}$	$4.686 \cdot 10^{-2}$	6.452	$1.297 \cdot 10^{1}$	$1.399 \cdot 10^{1}$
18500	$1.122 \cdot 10^{-6}$	$2.901 \cdot 10^{-3}$	$1.255 \cdot 10^{-2}$	$2.206 \cdot 10^{-1}$	$7.667 \cdot 10^{-1}$
36500	$9.562 \cdot 10^{-7}$	$2.519 \cdot 10^{-4}$	$8.467 \cdot 10^{-3}$	$1.385 \cdot 10^{-1}$	$4.580 \cdot 10^{-1}$

Table 7. The same as in Table 6 for lead-bismuth target

Cooling time (days)	Spectral component				
	< 1 MeV	< 20 MeV	< 100 MeV	Total n activity	Total p activity
10	$2.526 \cdot 10^{1}$	$3.710 \cdot 10^{1}$	$3.689 \cdot 10^{2}$	$4.755 \cdot 10^{2}$	$2.980 \cdot 10^{2}$
30	$1.805 \cdot 10^{1}$	$2.370 \cdot 10^{1}$	$1.235 \cdot 10^{2}$	$1.704 \cdot 10^{2}$	$1.665 \cdot 10^{2}$
180	8.343	$1.358 \cdot 10^{1}$	$2.936 \cdot 10^{1}$	$4.661 \cdot 10^{1}$	$6.198 \cdot 10^{1}$
730	$5.307 \cdot 10^{-1}$	2.995	$1.721 \cdot 10^{1}$	$2.194 \cdot 10^{1}$	$1.250 \cdot 10^{1}$
18250	$1.756 \cdot 10^{-5}$	$9.408 \cdot 10^{-1}$	5.496	6.026	1.148
36500	$1.751 \cdot 10^{-5}$	$3.793 \cdot 10^{-1}$	2.212	2.462	$5.885 \cdot 10^{-1}$

4.2.3 CONTRIBUTION OF THE FISSION PRODUCTS INTO LONG-LIVED ACTIVITY

To take into account the contribution of the fission products into targets activity it is necessary to include a lot of additional nuclides into kinetic equations. In our calculations we considered only the nuclides with half-lives longer than 5 hours.. The empirical Zilberberg-Tsao [12] formulae were used to determine fission product yields for fission induced by high energy protons and neutrons. The resulting total long-lived activities are given in Table 8 as well as total activities of lead and lead-bismuth targets irradiated for a year by the beam of 800 MeV protons. The results demonstrate that fission products increase the activity of both targets by 10-15% for cooling times under 2 years and less than by 10% for longer cooling times. Well known long-lived isotopes ^{90}Sr, ^{137}Cs, $^{98,99}Tc$ and ^{129}I make largest contributions.

Table 8. Fission products activities and the total activities (Ci/kg) produced in lead and lead-bismuth targets by incident proton beam with the energy 800 MeV and current 30 mA after a year of irradiation for various cooling times.

Cooling time	Lead target		Lead-bismuth target	
	Fission products	Total activity	Fission products	Total activity

(days)	(Z<50)		(Z<50)	
30	$7.545 \cdot 10^{1}$	$3.505 \cdot 10^{2}$	$8.108 \cdot 10^{1}$	$4.496 \cdot 10^{2}$
180	$2.255 \cdot 10^{1}$	$1.386 \cdot 10^{2}$	$2.458 \cdot 10^{1}$	$1.449 \cdot 10^{2}$
365	$1.065 \cdot 10^{1}$	$7.405 \cdot 10^{1}$	$1.172 \cdot 10^{1}$	$7.996 \cdot 10^{1}$
730	4.925	$3.401 \cdot 10^{1}$	$2.937 \cdot 10^{-1}$	$4.084 \cdot 10^{1}$
18250	$1.087 \cdot 10^{-1}$	1.117	$1.129 \cdot 10^{-1}$	6.948
36500	$4.261 \cdot 10^{-2}$	$6.491 \cdot 10^{-1}$	$4.518 \cdot 10^{-2}$	2.960

Figures 7, 8 show the contribution to the target activity due to fission products for lead and lead-bismuth targets, consequently. It should be noted out that the contributions to the activity due to light nuclides have been calculated taking into account the formation of tritium up to 20 MeV only. The ^{3}H contribution due to high energy neutrons and protons can change this result.

4.2.4 EVALUATION OF POLONIUM ACCUMULATION DUE TO PB(α,xn) REACTIONS.

The equilibrium intensities and spectra of alpha-particles produced in the target were evaluated as well as the accumulation of the polonium isotopes in the reactions induced by those particles. The results of calculations are presented in Table 9. The results indicate that the contribution of this channel of the polonium isotopes formation by Pb(α,xn) reactions may be a few times higher than that of double neutron capture. It is necessary to point out that those processes are induced by high energy particles formed due to the preequilibrium emission which is usually not taken into account in the models of intranuclear cascade. So further investigation of the role of this mechanism seems to be important for the reliable evaluation of the polonium activities accumulated in lead target irradiated by high energy protons. The calculation results indicate also that taking these processes into account may lead to the reassessment of relative contribution of various polonium isotopes into the total activity which may be important for the estimates of residual heat, the contamination of accelerator beam tract and for designing of on-line cleaning of liquid targets.

Table 9. Long-lived Po isotopes yields (g/kg) due to the (α,xn) reaction for lead target irradiated by 800 MeV, 30 mA proton beam for various irradiation times.

Isotope yield	Sample irradiation time				
g/kg	10 days	30 days	6 months	1 year	2 years
^{208}Po	$4.5 \cdot 10^{-7}$	$1.4 \cdot 10^{-6}$	$7.8 \cdot 10^{-6}$	$1.5 \cdot 10^{-5}$	$2.7 \cdot 10^{-5}$
^{209}Po	$2.8 \cdot 10^{-7}$	$8.5 \cdot 10^{-7}$	$5.2 \cdot 10^{-6}$	$1.0 \cdot 10^{-5}$	$2.1 \cdot 10^{-5}$
^{210}Po	$9.6 \cdot 10^{-8}$	$2.8 \cdot 10^{-7}$	$1.2 \cdot 10^{-6}$	$1.8 \cdot 10^{-6}$	$2.0 \cdot 10^{-6}$

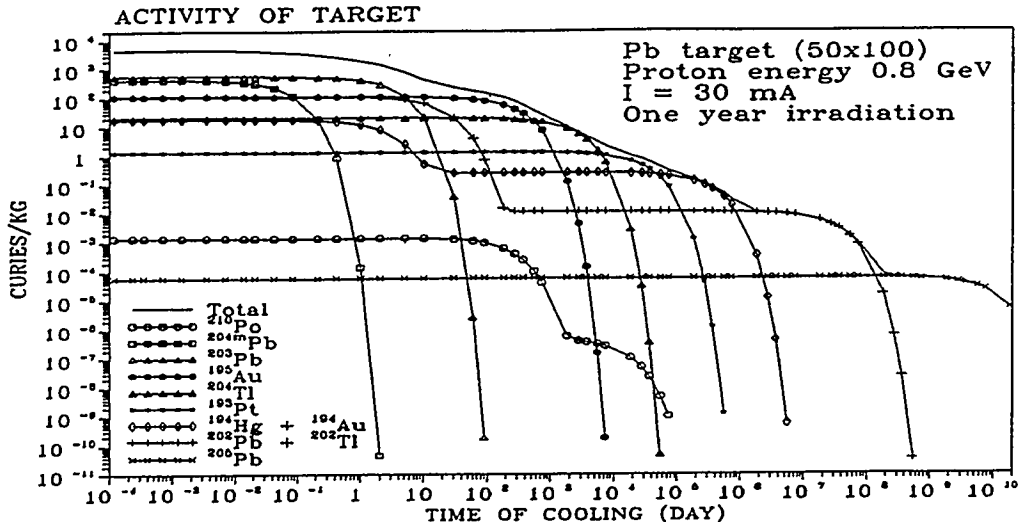

Figure 3. Total and partial activities of lead target as a function of cooling time.

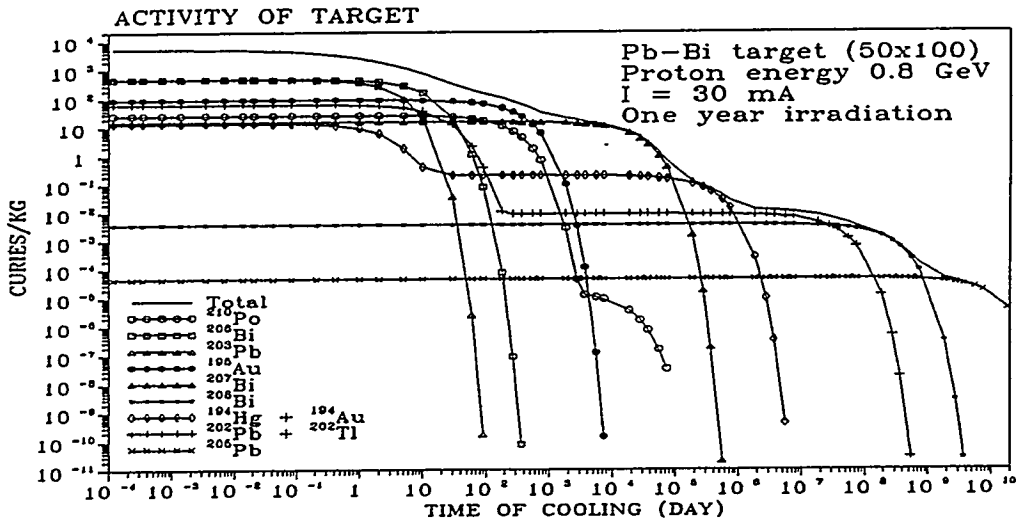

Figure 4. The same as in Fig. 3 for lead-bismuth target.

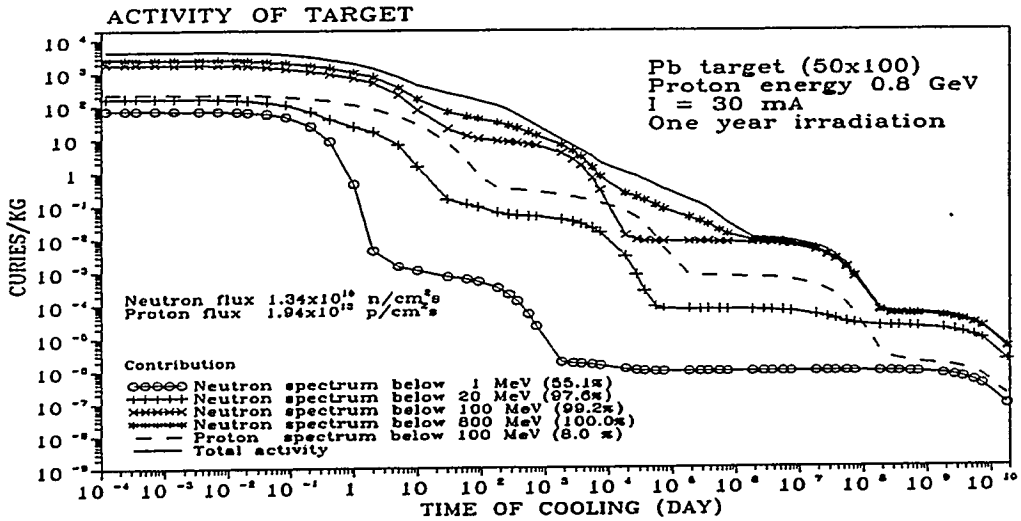

Figure 5. Activity of lead target due to various spectral components.

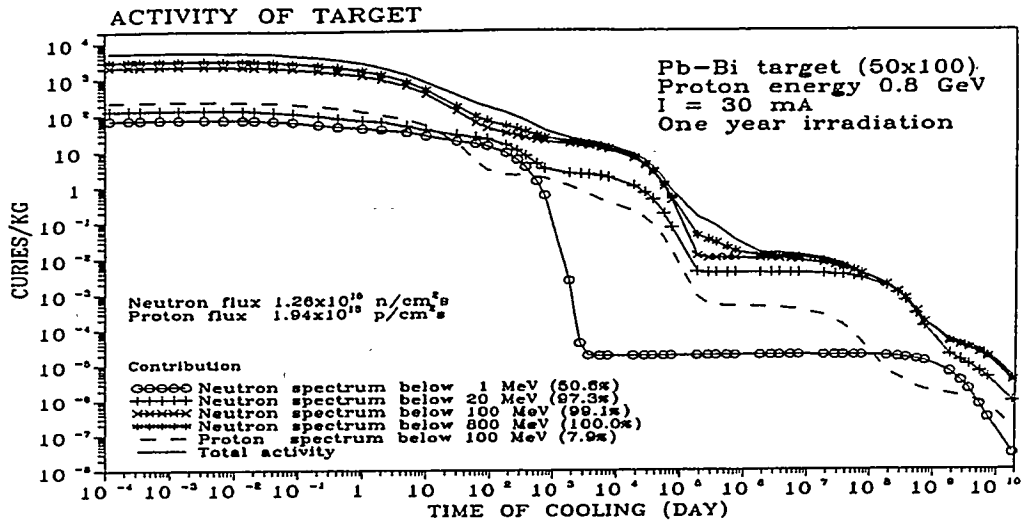

Figure 6. The same as in Fig. 5 for lead-bismuth target.

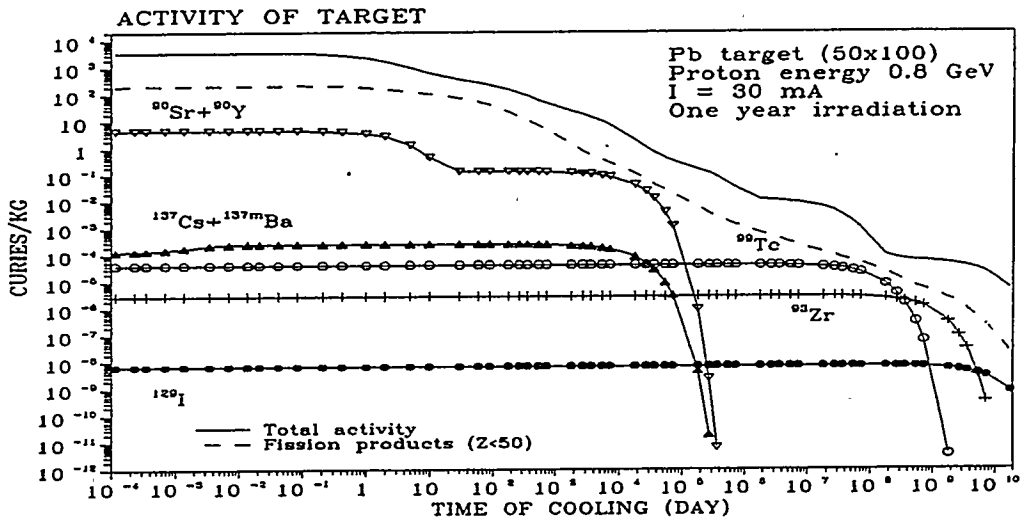

Figure 7. Activity of lead target due to fission products.

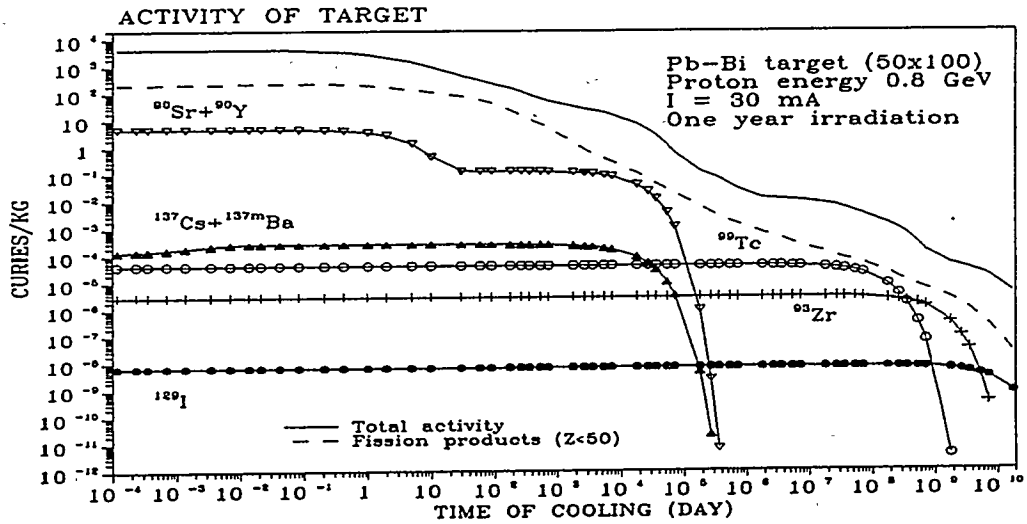

Figure 8. The same as in Fig. 7 for lead-bismuth target.

4.2.5 ANALYSIS OF TRITIUM ACCUMULATION IN THE TARGET

Tritium accumulation in the target requires special consideration due to special ecological dangers associated with this isotope. Tritium production in the reactions induced by the soft neutrons was analyzed in earlier reports. To determine its accumulations in the reactions with high energy protons and neutrons it is necessary to have reliable enough evaluations of tritium production cross sections for nucleon energies above 100 MeV.

Experimental data available for lead and bismuth isotopes [14-22] were analyzed together with different evaluations of tritium yields. ENDF/B-VI evaluation describes observable tritium production cross sections about 800 MeV satisfactorily but is in sharp disagreement with the experimental data available below 100 MeV. Semiempiric approximation of tritium production cross sections for high energy neutron and proton reactions [13] on lead and bismuth isotopes was developed on the base of experimental data and ADL-3 recommended values for the neutron energies below 20 MeV. Comparison of various evaluations with experimental data for neutron and proton induced reactions are shown in Figs. 9-12.

The results of the calculations of the total activities of lead and lead-bismuth targets as well as tritium contributions to this activity using this approximation are presented in Tables 10 and 11 tritium accumulation is approximately equal in both targets and its contribution to total activity is as high as 50% for lead target at cooling times from 3 to 30 years and is 2 times lower than the same figure for lead-bismuth target for the same time interval.

Table 10. Total activity and tritium activity (Ci/kg) of the lead target for 800 MeV, 30 mA primary proton beam after a year of irradiation for cooling times indicated in the Table.

Cooling time	180 days	2 years	20 years	100 years
Total activity	$1.530 \cdot 10^{2}$	$4.723 \cdot 10^{1}$	7.112	$7.021 \cdot 10^{-1}$
H-3	$1.443 \cdot 10^{1}$	$1.326 \cdot 10^{1}$	4.821	$5.370 \cdot 10^{-2}$

Table 11. The same as in Table 10 for lead-bismuth target.

Cooling time	180 days	2 years	20 years	100 years
Total activity	$1.584 \cdot 10^{2}$	$5.319 \cdot 10^{1}$	$1.629 \cdot 10^{1}$	2.853
H-3	$1.450 \cdot 10^{1}$	$1.332 \cdot 10^{1}$	4.843	$5.395 \cdot 10^{-2}$

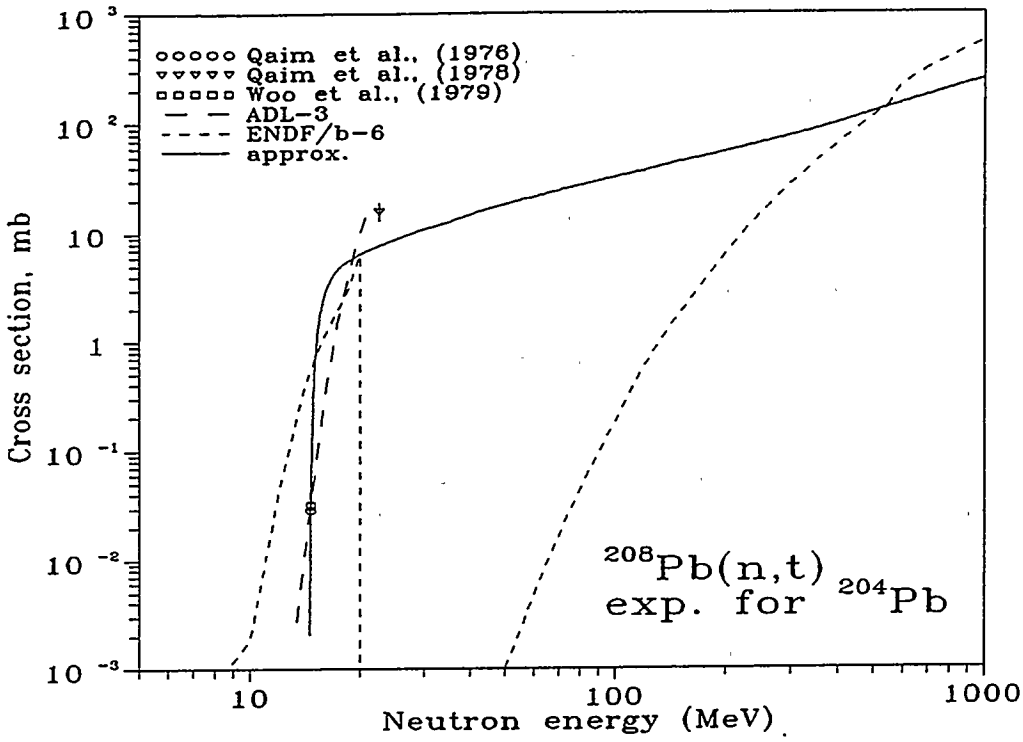

Figure 9. Tritium production cross section for neutron induced reactions on lead.

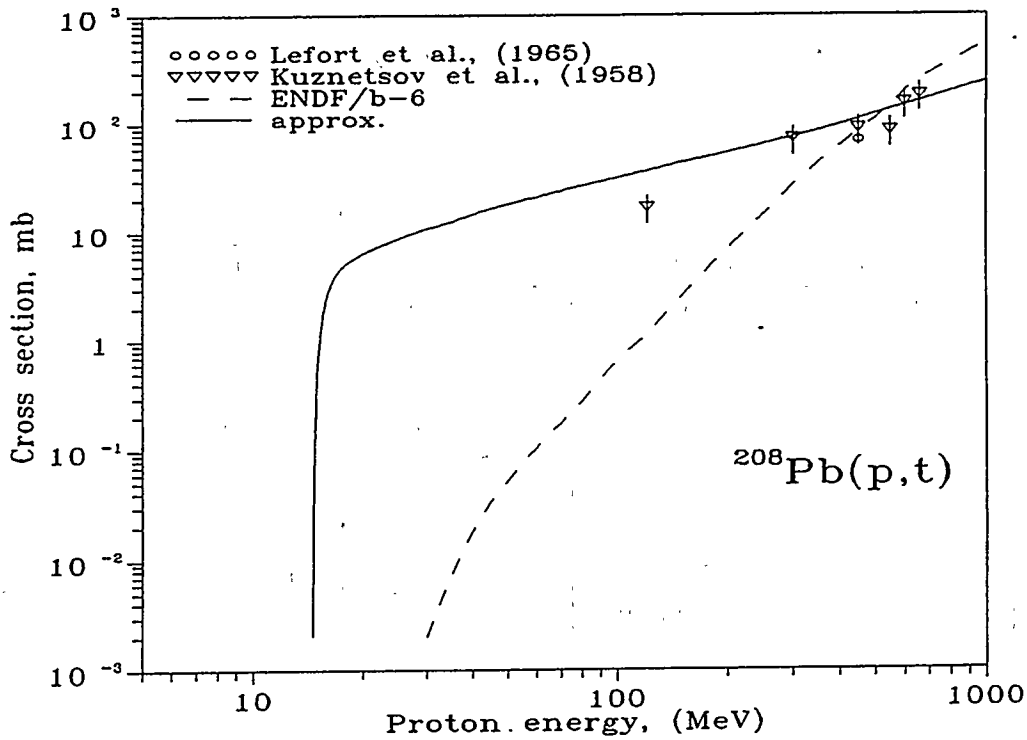

Figure 10. Tritium production cross section for proton induced reactions on lead.

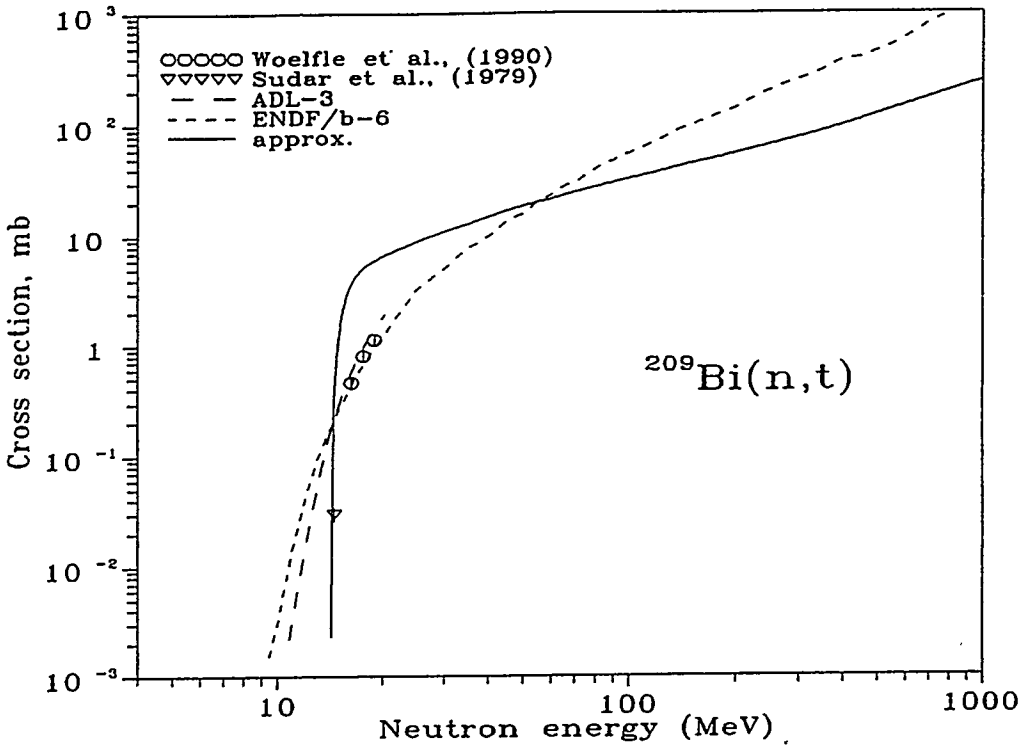

Figure 11. Tritium production cross section for neutron induced reactions on bismuth.

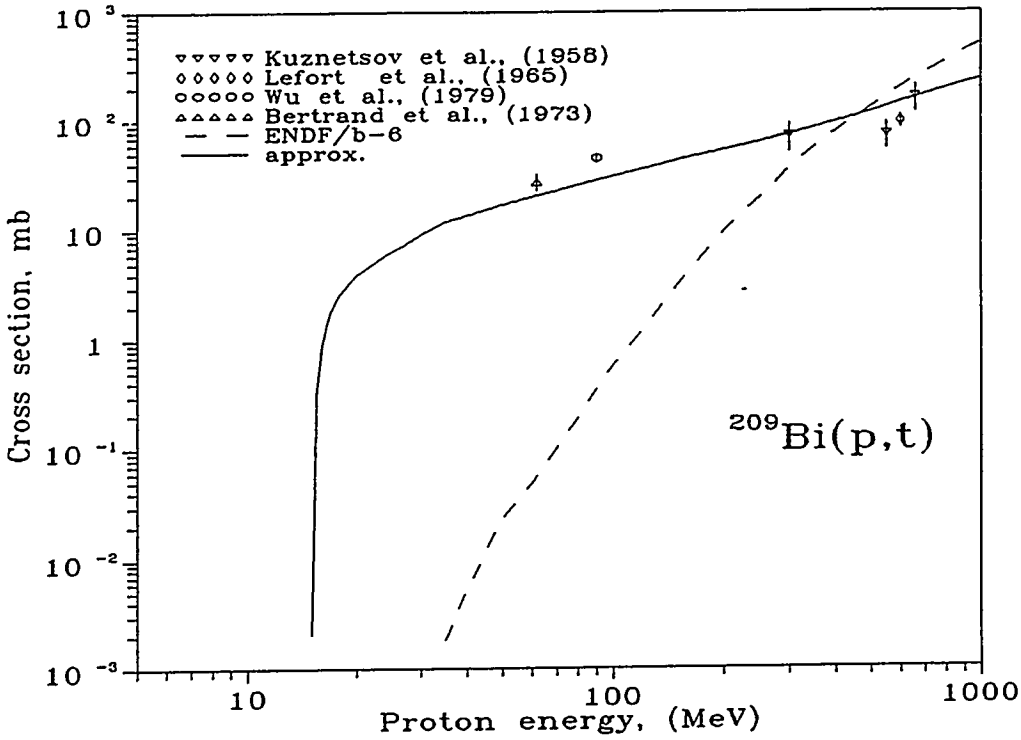

Figure 12. Tritium production cross section for proton induced reactions on bismuth.

5. THE ANALYSIS OF LONG-LIVED RADIOACTIVITY IN MERCURY TARGET

The another perspective material for target that is analyzed in various laboratories is mercury. The calculations and analysis of the target activity for the same irradiation conditions was carried out. The concentration of 658 nuclei with atomic number Z≥1-82 and life-time $T_{1/2}$≥5 hours was taken into account in the calculations. The high energy fission and tritium production processes have been considered also. The resulting long-lived activities of the dominating isotopes are presented in Tables 12, 13 and 14.

The activities of mercury target and also the activities of lead and lead-bismuth targets are compared in Fig. 16. One can see that mercury target activity exceeds that for lead and lead-bismuth targets at cooling times up to one year by factor 3-10. At cooling times up to 5000 years the activities of all targets are close one another. The long-lived activities (T>5000 years) of lead and lead-bismuth targets are 2-3 orders of magnitude higher than for mercury target. Fig. 17 shows the activities of radionuclides produced in nuclear reactions except fission, that give highest contributions to total mercury activity for various cooling times. The activity of most important fission products is shown in Fig. 18. At cooling times up to 1 year the contributions of ^{203}Hg and ^{195}Au are dominant. Next 10 years the activity is determined by tritium and for larger times is determined by ^{194}Hg and daughter nuclei. At cooling times more than 10^6 years the activity is due to long-lived fission products: ^{99}Tc, ^{93}Zr etc..

It should be noted that to the total activities of mercury, lead and lead-bismuth targets contribute different radionuclides. At an exception the contributions of ^{195}Au and ^{194}Hg(+^{194}Au) to the total activities for all targets are important.

The comparison of various target activities shows that the use of mercury target enables to diminish the long-lived activity as compared with lead and lead-bismuth targets considerable.

Table 12. Total and partial activities (Ci/kg) in mercury target for primary proton beam energy 800 MeV and current 30 mA after a year of irradiation for cooling times indicated in the Table.

Cooling time	180 days	2 years	20 years	100 years
Total activity	$7.433\cdot10^{2}$	$5.570\cdot10^{1}$	8.682	$1.695\cdot10^{-1}$
Hg-203	$4.559\cdot10^{2}$	$1.274\cdot10^{-1}$	-	-
Au-195	$1.708\cdot10^{2}$	$2.202\cdot10^{1}$	$5.190\cdot10^{-10}$	-
Pt-193	3.626	3.551	2.767	$2.286\cdot10^{-1}$
Au-194	$3.809\cdot10^{-1}$	$3.790\cdot10^{-1}$	$3.700\cdot10^{-1}$	$3.333\cdot10^{-1}$
Hg-194	$3.809\cdot10^{-1}$	$3.790\cdot10^{-1}$	$3.700\cdot10^{-1}$	$3.333\cdot10^{-1}$
Re-185m	$1.158\cdot10^{-1}$	$1.158\cdot10^{-1}$	$1.158\cdot10^{-1}$	$1.158\cdot10^{-1}$
Re-186g	$1.158\cdot10^{-1}$	$1.158\cdot10^{-1}$	$1.158\cdot10^{-1}$	$1.158\cdot10^{-1}$
Pt-190	$2.100\cdot10^{-9}$	$2.100\cdot10^{-9}$	$2.100\cdot10^{-9}$	$2.100\cdot10^{-9}$

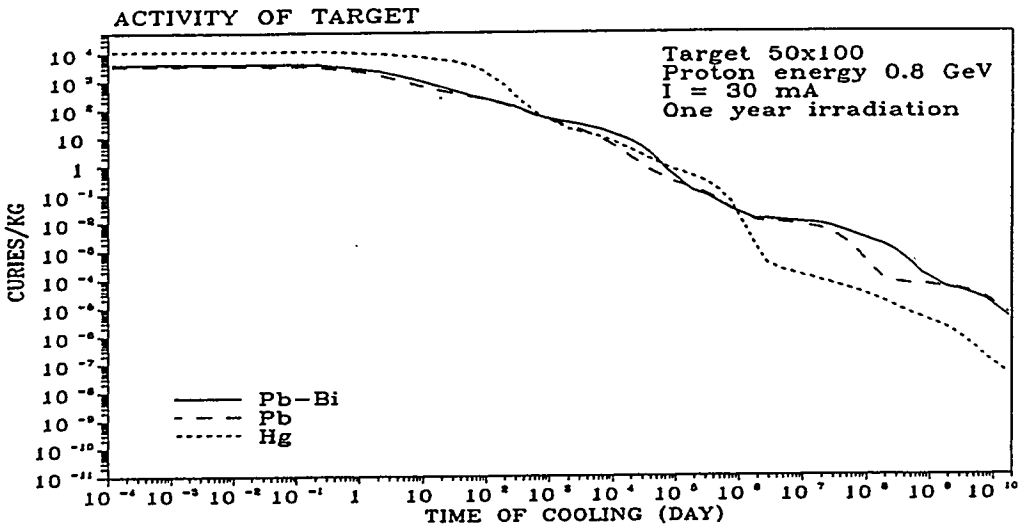

Figure 13. Total target activities for mercury, lead and lead-bismuth.

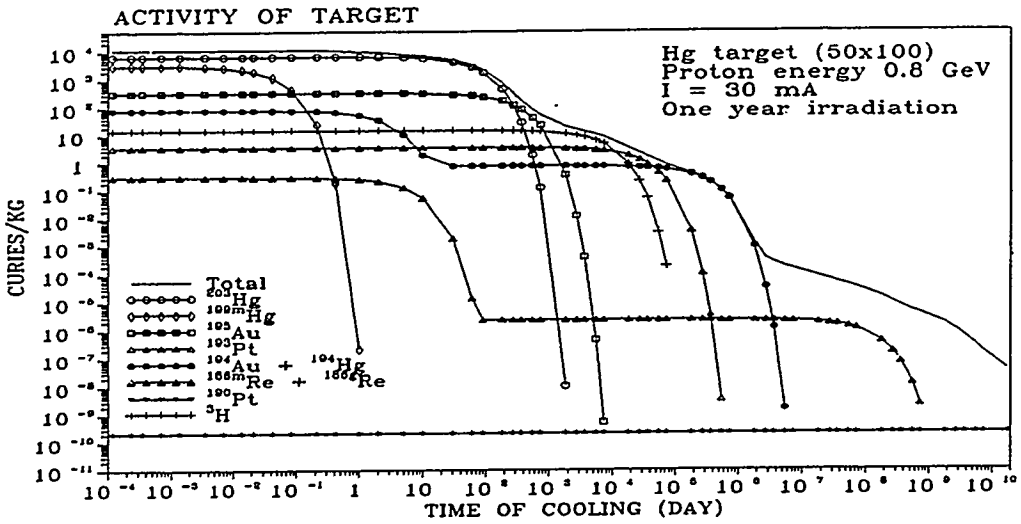

Figure 14: Total and partial activities of mercury target as a function of cooling time.

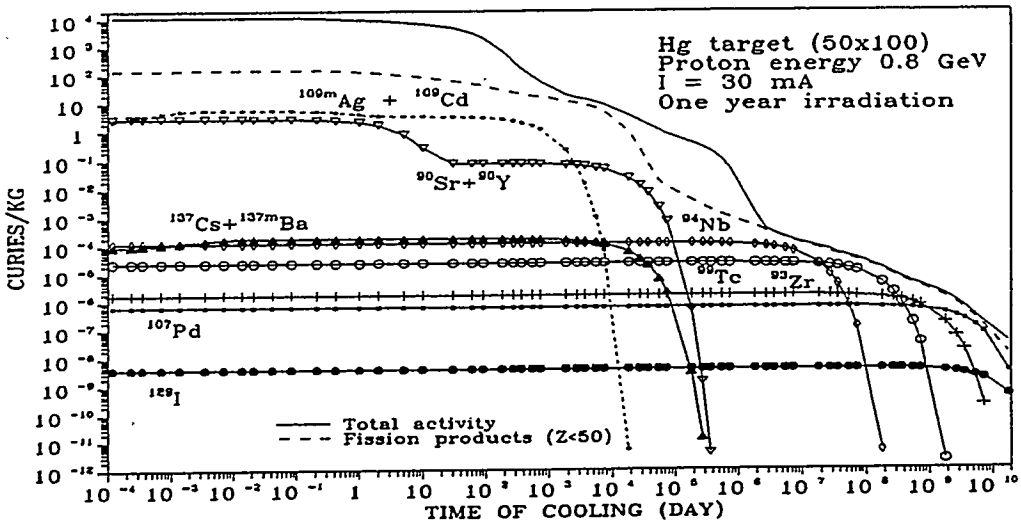

Figure 15. Activity of mercury target due to fission products.

Table 13. Fission products activities and the total activities (Ci/kg) produced in mercury targets by incident proton beam with the energy 800 MeV and current 30 mA after a year of irradiation for various cooling times.

Cooling time	30	180 days	2 years	20 years	100 years
Total activity	$4.921 \cdot 10^3$	$7.433 \cdot 10^2$	$5.571 \cdot 10^1$	8.682	1.695
Z<50	$6.306 \cdot 10^1$	$2.879 \cdot 10^1$	$1.617 \cdot 10^1$	5.001	$8.084 \cdot 10^{-2}$

Table 14. The same as in Table 10 for mercury target.

Cooling time	180 days	2 years	20 years	100 years
Total activity	$7.433 \cdot 10^2$	$5.571 \cdot 10^1$	8.682	1.695
H-3	$1.449 \cdot 10^1$	$1.331 \cdot 10^1$	4.84	$5.39 \cdot 10^{-2}$

CONCLUSIONS

1. Main contribution to the target activity is due to not Po isotopes, but other isotopes that are formed in spallation reactions.
2. Total activity of Pb and Pb-Bi targets are close one another.
3. The dominant contribution to the target activity is due to high energy (>20 MeV) parts of neutron and proton spectra. It is in this energy region thorough analysis of nuclear data is neededed.
4. The contributions of fission products to the target activity comprize 10-15% of total activity, well known long-lived isotopes make the largest contributions.
5. The contributions of (α,xn) reaction to polonium activity of Pb target may be a few times higher than that of double neutron capture.
6. Tritium accumulation is approximately equal in all targets and its contribution to the total activity is as high as 50% for lead target at cooling times from 3 till 30 years and 2 times lower than the same figure for lead-bismuth target for the same time interval.
7. Calculation and analysis of the activatiion of mercury target showed that at cooling time interval up to one year the mercury target activity exceeds that for lead and lead-bismuth target. The activities of all targets are close at cooling times up to 5000 years. For larger cooling times activity of lead and lead-bismuth targets is 2 or 3 order of magnitude higher than for mercury target:
8. It should be noted that to total activities of mercury, lead and lead-bismuth targets contribute different radionuclides.
   The comparision between targets shows that the use of mercury target enables to diminish the long-lived activity as compared with lead and lead-bismuth targets considerabley
9. Main part of the energy released by the beam in a thin window is connected with ionization losses. Nuclear interactions increase ionization losses by some 10-15%.

Attenuation of the intensity of proton beam per cm of window thickness is approximately equal for both materials: 6.5% for steel and 3.9% for titanium.
The analysis demonstrated that replacement of stainless steel by titanium results in decrease of energy release by a factor of 1.7 for the same window thickness. Estimates of energy release done by various groups agree within the accuracy of calculations which is 15-20%.

10. Significant discrepancies exist in published evaluations of radiation damage of target windows. In particular, the estimates carried out in JAERI and BNL for designs with comparable integral proton fluxes differ by more than an order of magnitude. There is no detailed description of operating experience with the dividing windows of the accelerator LAMPF in available publications. The main reason of differences in radiation damage evaluations is the discrepancy in calculated spectra of secondary particles produced in nuclear collisions. Considerable work is needed to remove the discrepancy and test calculation results by comparison with experimental data.
There is difference of a few times between the evaluations of hydrogen and helium accumulation in the window. To improve the situation more reliable evaluations are needed of the cross sections of the emission of all hydrogen and helium isotopes in the material of the window.

REFERENCES

1. Shubin Yu.N., Lunev V.P., Konobeyev A.Yu., Dityuk A.I., Cross Section Data Library MENDL-2 to Study Activation and Transmutation of Materials Irradiated by Nucleons of Intermediate Energies. Voprosy Atomnoj Nauki I Techniki. Yadernie Constanti, 1995, No1, p.3.(in russian).
2. Takizuka T. et al. Conceptual Design of Transmutation Plant. Workshop on Nuclear Transmutation of Long-Lived Nuclear Power Radiowastes. July 1-5, 1991. Obninsk. p.79.
3. Harada H. et al. Transmutation of Fission Products and Transuranium by High Energy Neutron. PSI-Proceedings of Specialists' Meeting 92-02, ISSN 1019-6447, p. 383.
4. Takashita H. et al. Transmutation of Long-Lived Radioactive Nuclides. Global-93, September 12-17, 1993, Seattle, Washington, Proceedings, p.797.
5. Ireland J.R. ATW Aqueous Base-Case Target/Blanket System Design. The Los Alamos Accelerator Transmutation of Nuclear Waste (ATW) Concept, Los Alamos, April 15-16, 1992, ed. E.D.Arthur, **v1**.
6. Konobeyev A.Yu., Korovin Yu.A. BISERM - cross section data library for the analysis of radiation damage for structural materials, irradiated by nucleons with energy up to 800 MeV. At. Energy 1992, **v.72**, No 2, p. 190.
7. Dementyev A.V., Sobolevsky N.M. SHIELD - a Monte-Carlo Hadron Transport Code. in Proceedings of Specialists' Meeting Intermediate Energy Nuclear Data: Models and Codes. Paris, France 1994, p.237.
8. Artisyuk V.V., Konobeyev A.Yu., Korovin Yu.A., Pereslavtsev P.E., Long-lived radionuclide formation in Lead and Lead-Bismuth targets irradiated by high energy protons. Izvestiya Vuzov, Yadernaya Energetica, 1994, v.1, p.41 (in russian).
9. Artisyuk V.V., Calculation investigations of experimental and power facilities. Collected volume of works of general and special physics. Obninsk Institute of Power Engineering, Obninsk, 1993, No5, p.60. (in russian).
10. Grudzevich O.T., Zelenetsky A.B., Ignatyuk A.V., Pashchenko A.B., Catalogue of ADL-3 Library. Voprosy Atomnoj Nauki I Techniki. Yadernie Constanti, 1993, No3-4, p.3.(in russian).
11. Shubin Yu.N., Konobeyev A.Yu., Korovin Yu.A., Lunev V.P., Masterov V.S., MENDL - Activation Data Library for Intermediate Energies. IAEA-NDS-136 Rev.0,May 1994.
12. Silberberg R., Tsao C.H. Astrophysical Journal Supplement, 1973, Series No 220 (I), 25, p.315; Series No 220(II), 25, p.335.
13. Konobeyev A.Yu., Korovin Yu.A., Tririum production in materials from C to Bi irradiated with nucleons of intermediate and high energy., Nucl.Instr.Meth., **v.B92**, p.103 (1993).
14. Qaim S.M., Stocklin G. Investigation of (n,t) reactions at 14.6 MeV and an analysis of some systematic trends in the cross section data. Nucl.Phys.,**v.A257**, p.233 (1976).

15. Qaim S.M., Woelfle R. Triton emission in the interactions of fast neutrons with nuclei. Nucl.Phys., **v.A295**, p.150 (1978).

16. Woo T.W., and Salaita G.N., Production Cross Sections for (n,t) Reactions in ^{40}Ca, ^{54}Fe, ^{86}Sr, ^{89}Y, ^{102}Pd, ^{112}Sn, ^{106,114}Cd, ^{130}Te, ^{139}La, ^{204}Pb and ^{205}Tl with 14.6 MeV Neutrons. Nuclear Cross Sections for Technology.,(Proc. of Knoxwille conference (Ed. Fowler J.L., Johnson C.H., Bowman C.D. 1980)) p.853 (1979).

17. Woelfle R., Qaim S.M., Liskien H., and Widera R., Systematic studies of excitation functions of (n,t) reactions on medium and heavy mass nuclei., RCA, **v.50**, p.5 (1990)

18. Sudar S., and Chikai J., Measurement of (n,t) cross sections at 14 MeV and calculation of excitation functions for fast neutron reactions., Nucl.Phys., **v.A319**, p.157 (1979).

19. Bertrand F.E., Peele R.W., Complete Hydrogen and Helium Particle Spectra from 30 to 60 MeV Proton Bombardment of Nuclei with A=12 to 209 and Comparison with Intranuclear Cascade Model. Phys.Rev., **v.C8**,p.1045 (1973).

20. Wu J.R., Chang C.C., Holmgren H.D., Charged particle spectra: 90 MeV protons on ^{27}Al, ^{90}Zr and ^{209}Bi., Phys.Rev., **v.19**,p.698 (1979).

21. Кузнецов В.В., Мехедов В.Н., Образование трития в металлах под действием протонов с энергией 120-660 МэВ. ЖЭТФ, **т.35**, с.587 (1958).

22. Lefort M., Cohen J.P., Dubost H., and Tarrago X., Evidence for Nucleon Clustering from High-Energy Reactions., Phys.Rev., **v.139B**, p.1500 (1965).

Polonium problem in lead-bismuth flow target.

D.V.Pankratov, E.I.Yefimov, M.I. Bugreev
State Scientific Centre of Russian Federation-
Institute of Physics and Power Engineering
249020 Obninsk, Russia.

Alpha - active polonium nuclides Po -198 ÷ Po - 210 are formed in a lead-bismuth target as results of reactions $Bi^{209}(n,\gamma)Bi^{210} \rightarrow Po^{210}$, $Bi^{209}(p,xn)Po^{210} \rightarrow Po^{210-x}$ (x=1÷12), $Pb^{208}(\alpha,xn) \rightarrow Po^{210-x+2}$ (x=2÷14). The most important nuclides are Po-210 ($T_{1/2}$ =138.4 day), Po-209 ($T_{1/2}$ =102 years) and Po-208 ($T_{1/2}$ =2.9 years). Polonium activity of the circuit for SINQ - conditions is about 15,000 Ci after 1-year operation.

Polonium radiation hazard is connected with its output from the coolant and formation of aerosol and surface alpha - activity after the circuit break-down for repair works or in accidents.

The experiments carried out in SSC RF - IPPE and analysis of available literature information demonstrated that polonium evaporation from lead-bismuth takes place in the chemical form of Pb Po which volatility at temperature interval 200 - 800 ^{0}C is as much as 10,000 ÷ 100 times less than the one of metallic polonium. At 200 ^{0}C polonium evaporation rate into vacuum is 2×10^{-8} (Ci/m^2 s)/(Ci/kg), at 800 ^{0}C it is as much as 10^6 times higher.

Possibilities of polonium removal from a target circuit were analysed by means of vacuum sublimation and alkaline extraction. The first way requires creation of high temperature potentially dangerous devices. The data on high efficiency of alkaline extraction when the coolant was passing through melted mixture of NaOH and KOH were obtained in SSC RF - IPPE.

One of the important issues of polonium removal system creation is containing and storing polonium removed. Its storage in solidified alkaline is not expedient because of secondary neutron formation as a result of (α,n) - reaction on oxygen and sodium nucleus. The estimations carried out demonstrated that by polonium concentration ~ 100 Ci/l neutron current on the container surface can reach ~ 10^4 n/cm^2 s.

Concentration and storage of polonium in solidified lead-bismuth seems the most convenient. The calculations demonstrated that in a 100 l container 50,000 Ci of polonium can be stored (as much as 3 times more than 1-year polonium product in SINQ-conditions) under temperature in the container less than melting point of lead-bismuth (the wall temperature is about 100 ^{0}C).

Fields of possible use of lead-containing melts in nuclear power engineering

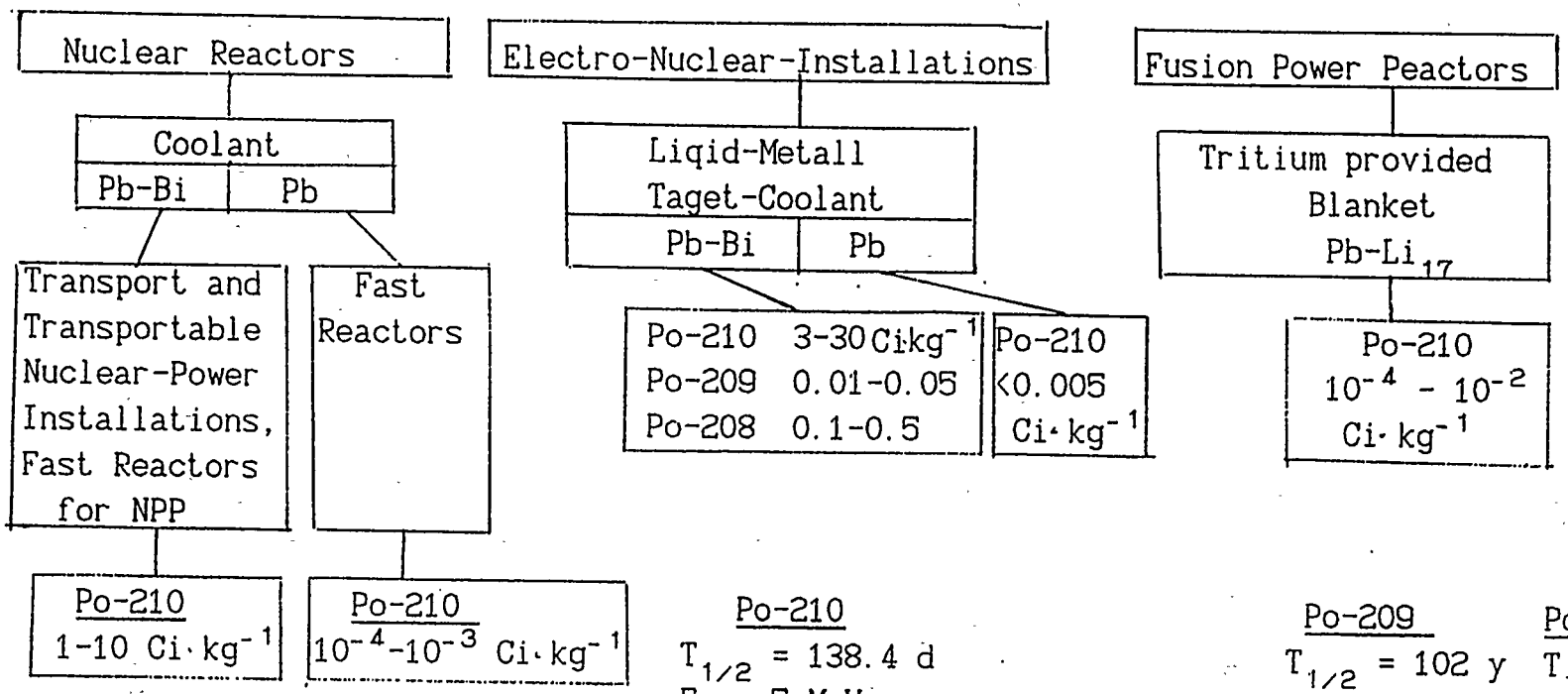

generated by
$Bi^{209}(n,\gamma)Bi^{210} \xrightarrow[\sim 5d]{\beta^-} Po^{210}$
$Pb^{208}(n,\gamma)Pb^{209} \xrightarrow[\sim 3h]{\beta^-} Bi^{209}$

Bi in Pb ~ 1ppm

Po-210
$T_{1/2}$ = 138.4 d
E_α = 5 MeV
Permissible limit concentration (Cat. A, personnel) $9.3 \cdot 10^{-14}$ Ci·l⁻¹
Permissible limit surface contamination (Cat. A, personnel) 200 $cm^{-2} \cdot min^{-1}$

Po-209
$T_{1/2}$ = 102 y
E_α = 4.9 MeV

Po-208
$T_{1/2}$ = 2.9 y
E_α = 5.2 MeV

generated by
Bi (p, xn)
Pb (α, xn) et al
neutrons from blanket
$Bi^{209}(n,\gamma)Po^{210}$

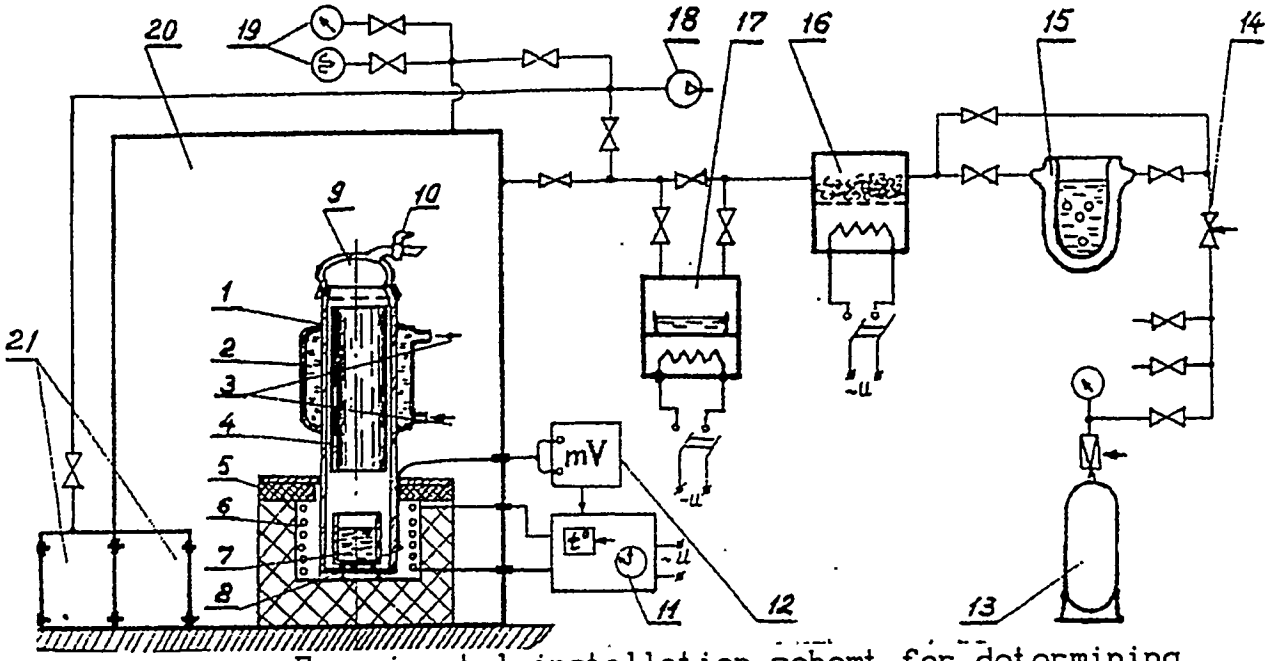

Experimental installation schemt for determining polonium and mercury evaporation rates by heating of lead and lead-bismuth samples irradiated.

N O T A T I O N :

1. - quartz vessel, ø ~ 40 mm, h ~ 240 mm,
2. - cooler,
3. - input and output of cooling water,
4. - copper foil screen,
5. - electric furnace thermal isolation,
6. - furnace heater,
7. - sample in the quartz glass, ø ~ 20 mm, h ~ 40 mm,
8. - hot thermal junction to control temperature,
9. - vessel lid,
10. - lid valve,
11. - electric furnace control device, definition of temperature and time behaviours,
12. - e m f thermocouple meter, mV,
13. - high pressure gas balloon,
14. - gas flow rate controller,
15. - liquid-nitrogen trap for moisture and condensed admixtures,
16. - trap for oxygen with heated copper oxide,
17. - trap for moisture and oxygen with alkaline,
18. - forevacuum pump,
19. - pressure-gauge and thermocouple vacuum gauge,
20. - protective chamber,
21. - transfer drawer.

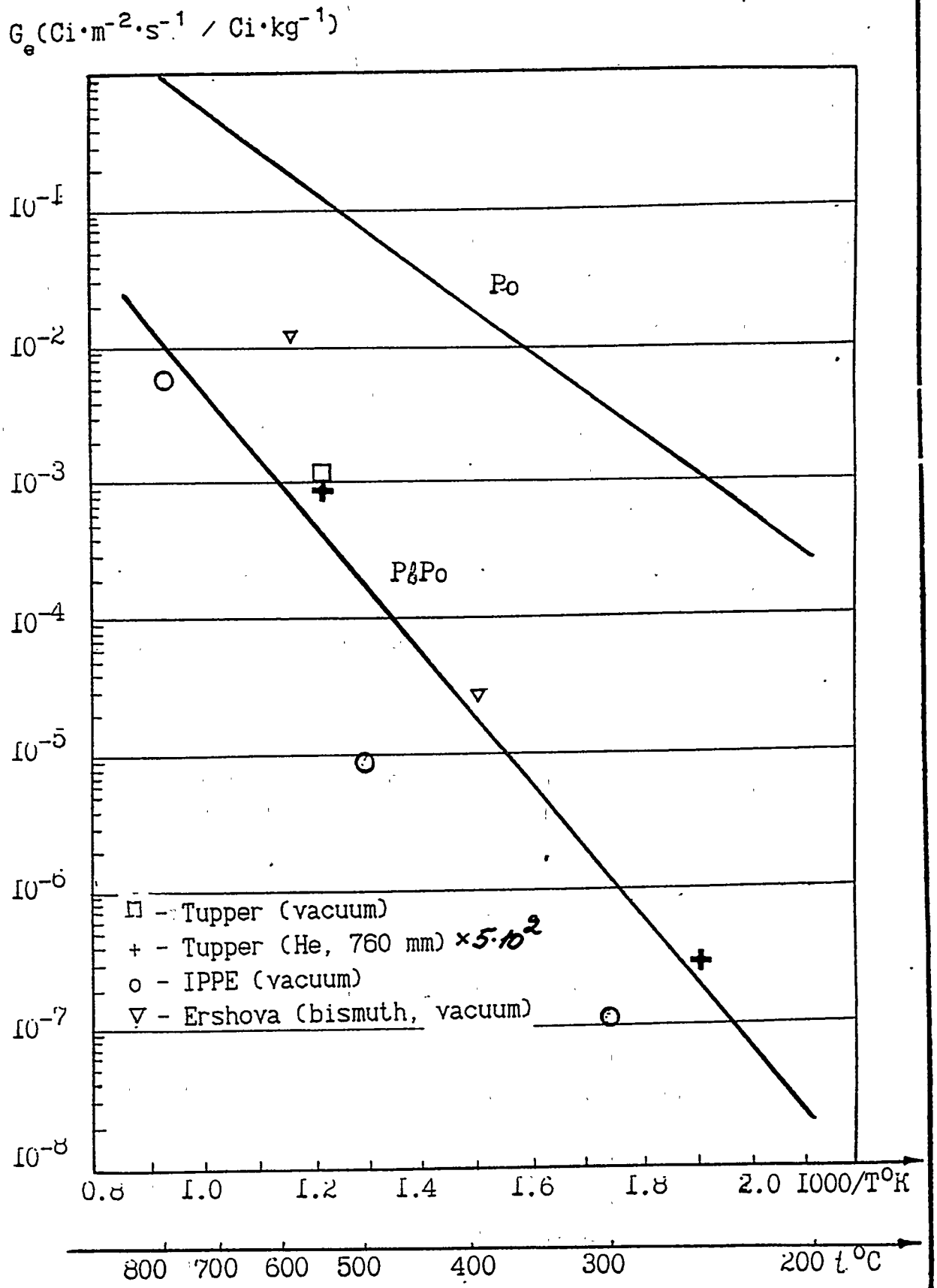

Evaporation rates for polonium from molten Pb-Bi in vacuum,

Vapor pressure, Pa

Po (metall) $\lg P_s = 9.3545 - 5377/T$ (438 - 745°C)
$\lg P_s = 9.46 - 5440/T$ (368 - 604°C)

PoPb $\lg P_s = 9.06 - 7270/T$ (640 - 850°C)

$$q_v = (4.38 \cdot 10^{-3} \cdot K(T) \cdot P_s(T) \cdot a \cdot M_0) / \sqrt{MT}$$

q_v - evaporation rate in vacuum, Bq $m^{-2}s^{-1}$

K(T) - accomodation coefficient, K = 1.5, t = 300°C
K = 0.1, t = 550°C

$P_s(T)$ - vapor pressure, Pa,
a - activity of coolant, Bq kg^{-1},
M_0 - molecular mass of coolant,
M - molecular mass of evaporative.

$$q_c = q_v \beta$$

q_c - evaporation rate in covergas (Ar, He),
β - shielding coefficient,
($\beta \sim 2 \cdot 10^{-3}$, P_c = 760 mm Hg - R.Tupper et al)
($\beta \sim 10^{-3}$, P_c = 760 mm Hg - Feuerstein et al)

$$q_{Po} = q_{Bi}\ \varepsilon$$ (Ershova et al)

$$PbPo + H_2O \longrightarrow Pb + PoH_2$$

$$q_{PoH_2} \sim (1.5 - 2.0) \cdot 10^{-10}\ Ci(Ci \cdot s)^{-1}$$

(air hymidity x = 90 %, t = 20°C, V = 5 cm s^{-1})

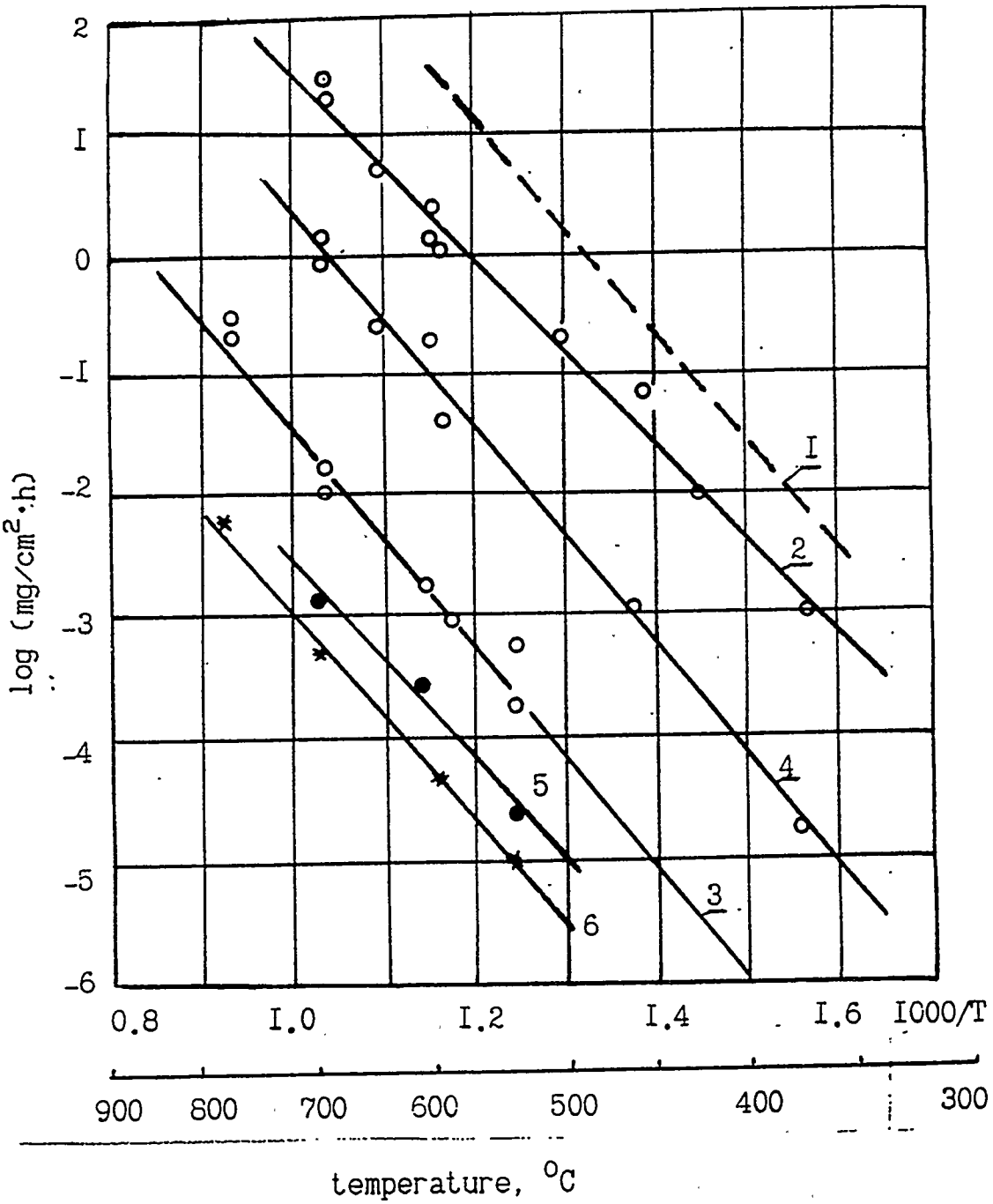

Evaporation rates for lithium and lead from molten Pb-17Li.
1- calculated maximum rate for Pb, 2- Pb in vacuum,
3- Pb in Ar and He, 4- Li in vacuum, 5- Li in Ar,
6- Li in He.

Feuerstein et al

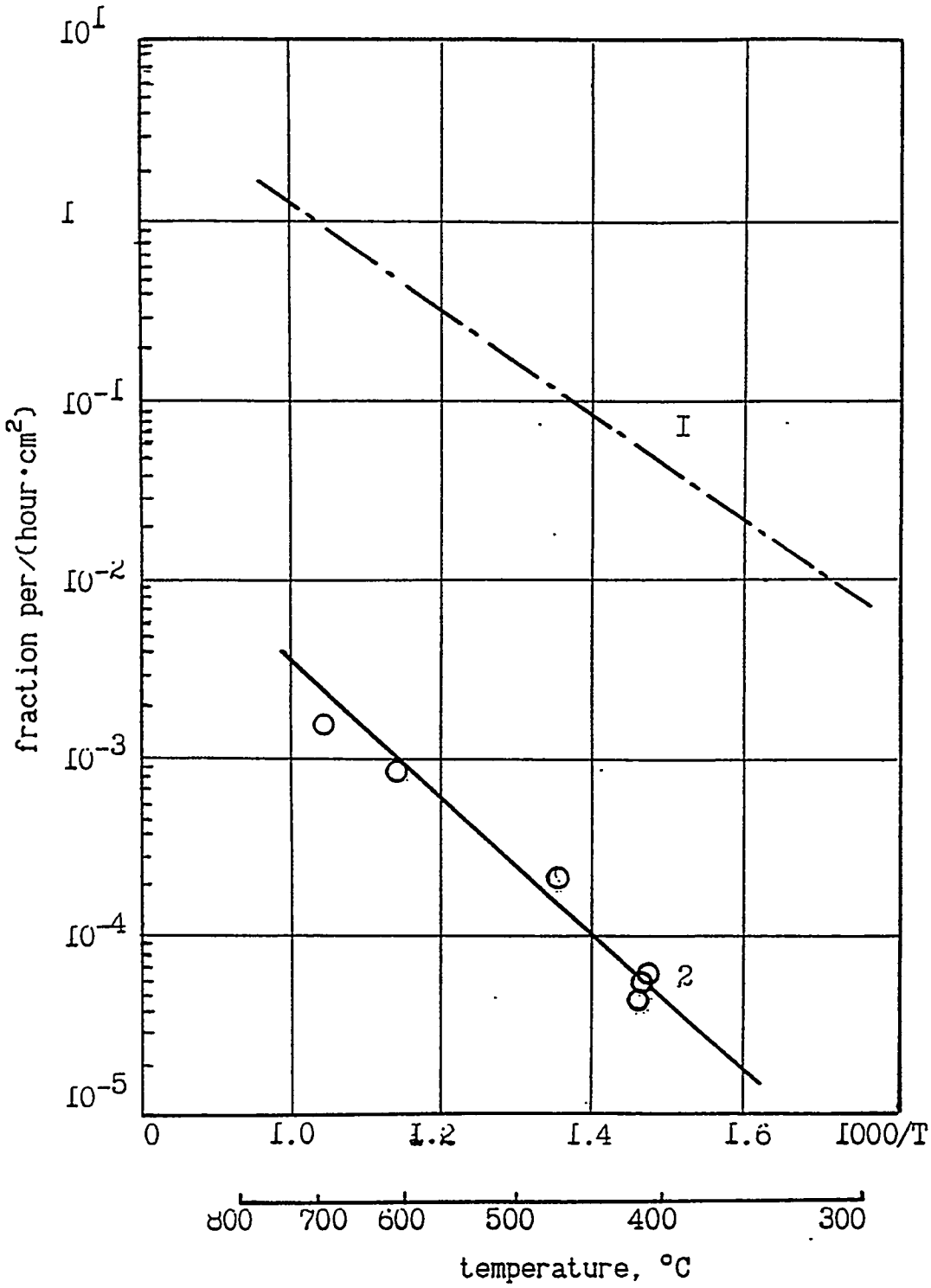

Evaporation fraction of Po-210 in vacuum, using 130 g of the eutectic.

1- calculated for the evaporation of polonium metai,

2- for the evaporation of lead polonide,

0- experimental results.

Feuerstein et al

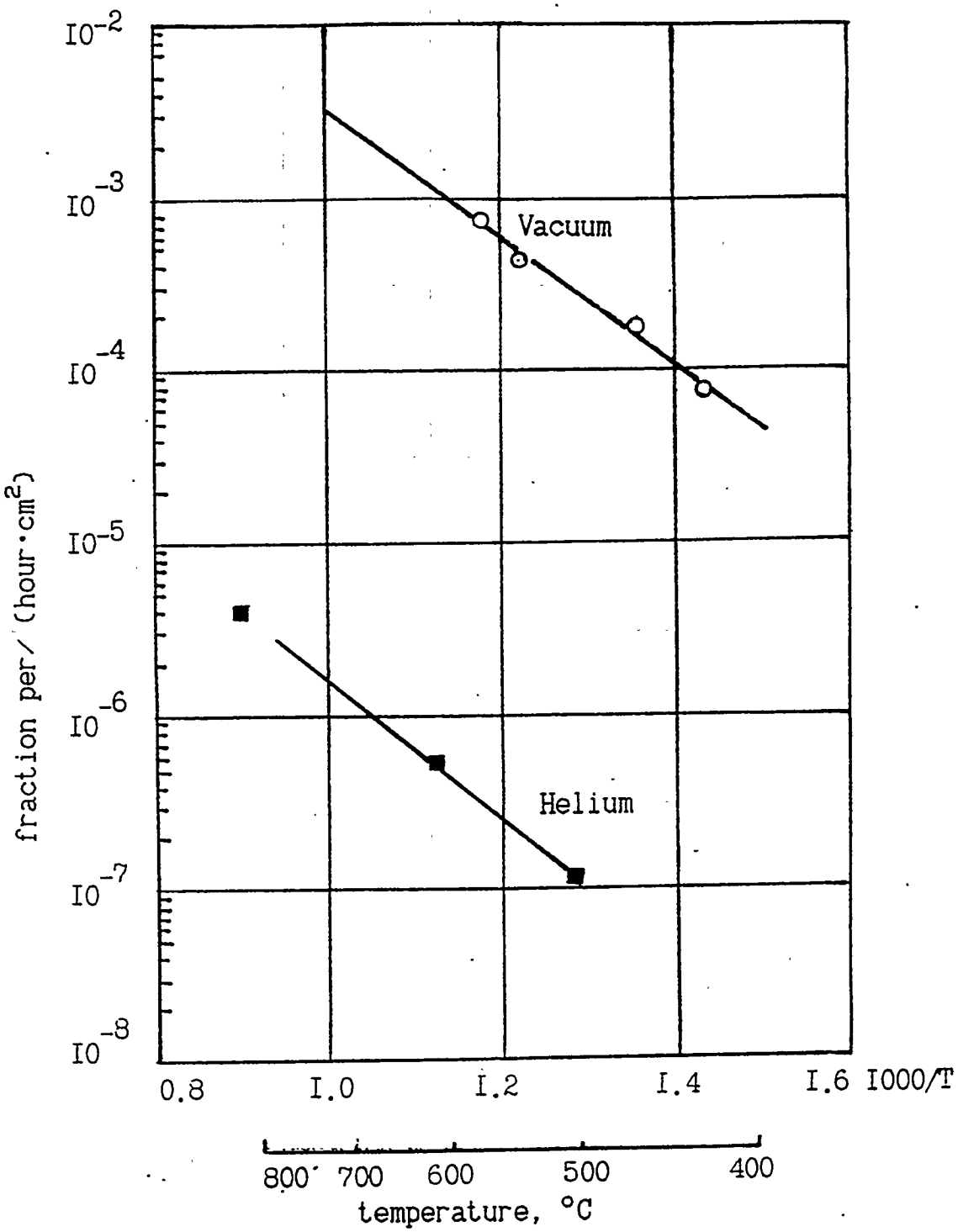

Evaporation rate of Po-210 from molten Pb-17Li in vacuum and helium.

Feuerstein et al

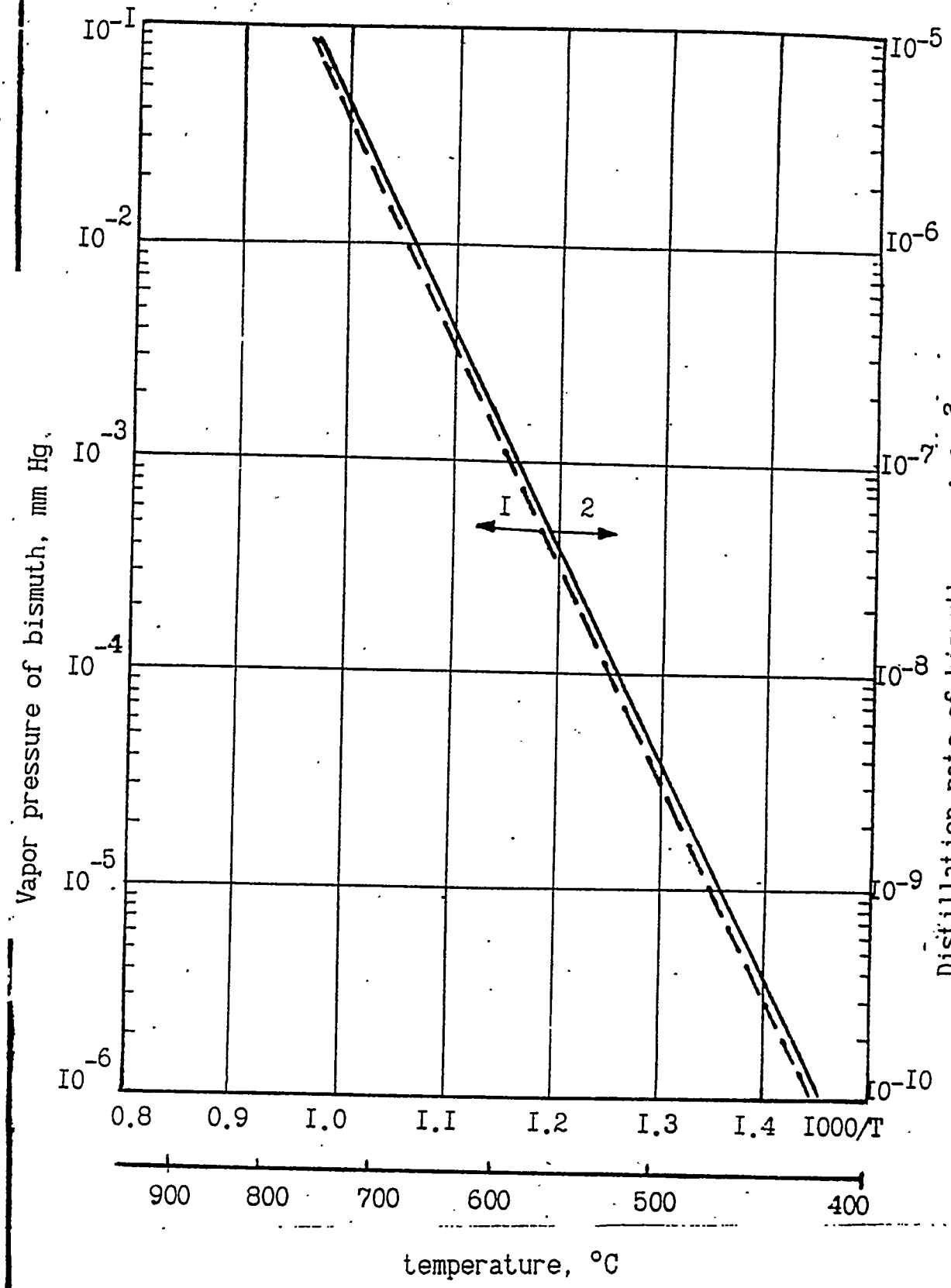

Vapor pressure and distillation rate of bismuth.

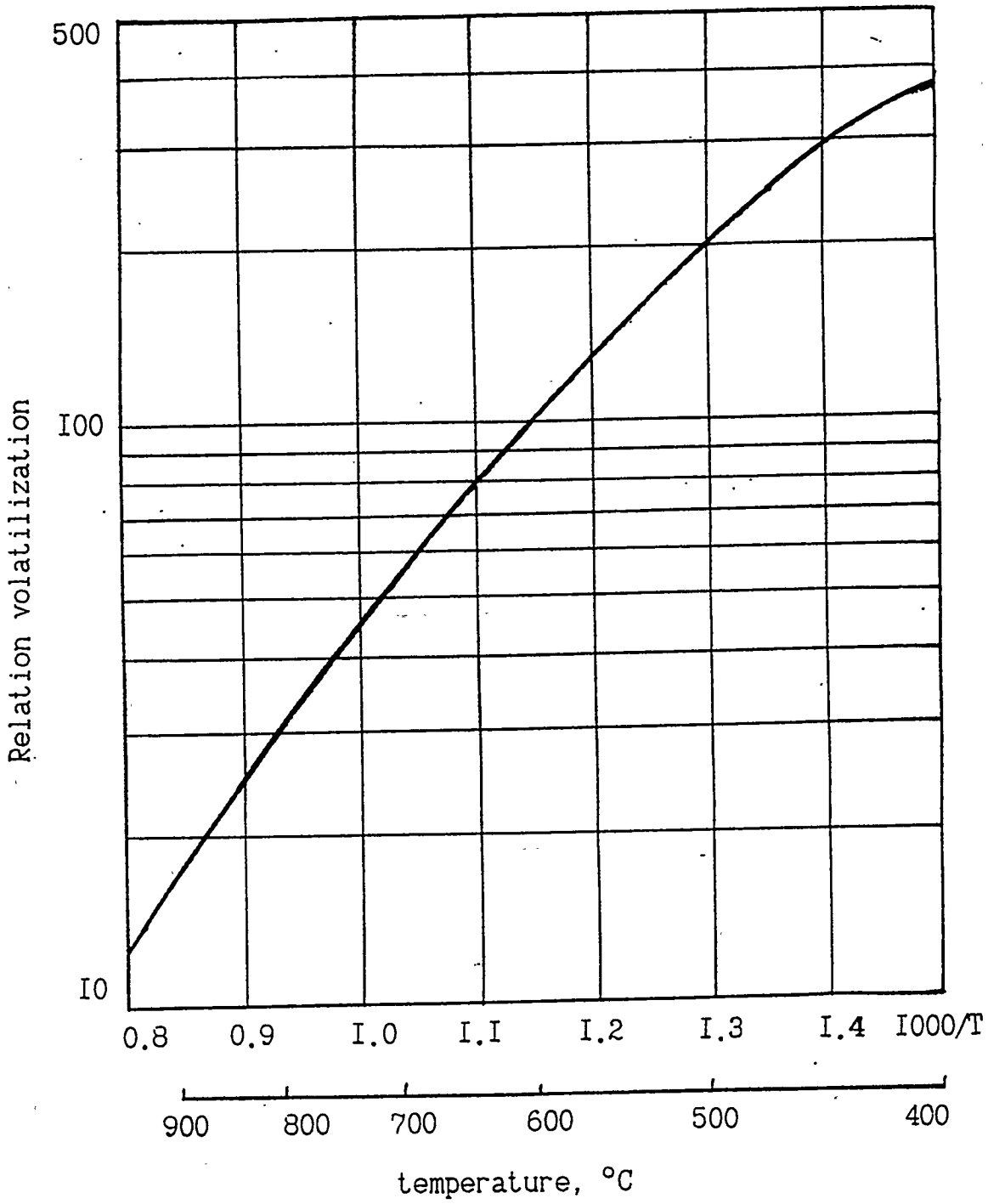

Relation volatilization of polonium from bismuth.

SESSION 10

R&D Needs and Options (1)

Chairman
Y. Gelfgat

International Workshop on the Technology and Thermal Hydraulics of Heavy Liquid Metals
March 25-28 1996, Schruns, Austria

Needs and Opportunities for CFD-Code Validation

B. L. Smith
Thermal-Hydraulics Laboratory
Paul Scherrer Institute
Würenlingen and Villigen
Switzerland

The conceptual design for the ESS target [1] consists of a horizontal cylinder containing a liquid metal – mercury is considered in the present study – which circulates by forced convection and carries away the waste heat generated by the spallation reactions. The protons enter the target via a beam window, which must withstand the thermal, mechanical and radiation loads to which it is subjected. For a beam power of 5MW, it is estimated that about 3.3MW of waste heat would deposited in the target material and associated structures. It is intended to confirm, by detailed thermal-hydraulics calculations, that a convective flow of the liquid metal target material can effectively remove the waste heat and avoid any threat to the structural integrity of the target and its components due to overheating.

The present series of Computational Fluid Dynamics (CFD) calculations has indicated that a single-inlet Target design leads to excessive local overheating [2], but a multiple-inlet design, Fig. 1, is coolable [3]. With this option, inlet flow streams, two from the sides and one from below, merge over the target window, cooling the window itself in crossflow and carrying away the heat generated volumetrically in the mercury with a strong axial flow down the exit channel. The three intersecting streams form a complex, three-dimensional, swirling flow field in which critical heat transfer processes are taking place. In order to produce trustworthy code simulations, it is necessary that the mesh resolution is adequate for the thermal-hydraulic conditions encountered and that the physical models used by the code are appropriate to the fluid dynamic environment. The former relies on considerable user experience in the application of the code, and the latter assurance is best gained in the context of controlled benchmark activities where measured data are available. Such activities will serve to quantify the accuracy of given models in the code and to identify potential problem areas for the numerical simulation which may not be obvious from global heat and mass balance considerations. The basis and outline of a series of tests which will serve this purpose are given in the accompanying oral presentation, and some salient points are included below.

The main objective of the COVE (COde Validation Experiments) programme is to provide high quality experimental data for use in validating the CFD calculations undertaken in the context of the design and safety case of the ESS Liquid Metal Target. It should be emphasised that the experiments in the COVE series should not be regarded as prototypic scale model tests, which would be of limited value for general code validation purposes. Rather, they are simplified tests where conditions are chosen to isolate, and magnify, the physical phenomena the experiment is designed to examine. In this way the test sequence can proceed without being subject to minor design changes originating from the ESS project, though an awareness of major changes should be maintained by periodic review of the test programme.

The simulant materials to be used for the tests will be: water, liquid sodium and, possibly, NaK. Tests will be conducted cold and with (electrical) window heating. All tests utilize existing facilities at PSI. The water tests are aimed at providing visual information regarding the fluid dynamics of the intersecting input streams, to quantify the role played by turbulent heat transfer from the heated window to the fluid in the absence of heat conduction effects (high Prandtl number), and to evaluate the turbulence models in the code. In liquid sodium heat conduction effects in the boundary layer over the window are exaggerated compared to mercury because of the higher thermal conductivity (lower Prandtl number), but experimental conditions can be arranged so that this effect may be investigated in isolation from, or coupled with, turbulent boundary layer heat transfer. The role of the buoyancy force on fluid flow and heat transfer over the window is also magnified compared to mercury because of the large coefficient of volumetric expansion in sodium, so this

effect can be examined.

From the code point of view, the tests will aim towards simplicity and unambiguous modelling rather than towards a high degree of realism in regard to the latest ESS design. There should be as few 'adjustable parameters' as possible, otherwise the validation process is degraded. Experiments will proceed on a step-by-step basis such that each new feature is examined first in isolation, but later in combination with other (validated) models where feed-back effects are suspected. In addition, the test programme should not be regarded as *inexorable*; that is, defined and carried out in isolation from the accompanying analysis. Rather, it will be the responsibility of the COVE project co-ordinator to ensure that experiments and analysis proceed in parallel, providing a forum for interaction, so that the tests can be modified where indicated. Finally, active liaison with the ESS project management will be maintained with a view to steering the COVE tests in the direction of a final prototypic experiment using mercury or NaK (intermediate Prandtl number).

Since the tests in the COVE series are intended to provide high quality data for code validation purposes, numerical simulation of each test in the series will form an integral part of the study. Data from the experiments will be used to test whether the simulation code basically copes with the various fluid dynamic processes encountered. Flow deceleration over the curved window may induce boundary layer separation, instabilities, Görtler vortices and, in extreme conditions, local flow reversal. Such behaviour will be evident from the measured temperatures on the window surface and from the visual data from the water tests. Buoyancy effects can be assessed by varying the window heating rate, particularly for the sodium tests where more power may be used. The expansion from the inlet channel exits over the window, the convergence of flow streams from the sides and the sharp changes in direction could create flow instabilities. Combined with heating, these could also affect the structure of the boundary layer over the window, and hence the heat transfer across it. Overall heat exchange between window and coolant will only be adequately predicted by the code if the detailed structure of the boundary layer is correct. If points of discrepancy are noted, it might be necessary to carry out more basic tests in order to isolate the problem areas. Overall, the validation process is aimed at increasing the degree of confidence in the ESS simulations being carried out in support of the design work and safety case.

If a 1-1 scaling is maintained between the actual window design and the COVE test section, once a computational mesh has been assembled it can be used with minor modifications for the analysis of all the experiments in the series. It is anticipated, therefore, that a pre-test calculation can be performed for each experiment. Such mesh adaptation as proven necessary from post-test analyses will become inherent for the pre-test calculations of succeeding experiments, so that by the end of the test programme a highly refined mesh, capable of resolving the thermal-hydraulic processes encountered, will have evolved. This experience will pass over directly to the final analysis of the ESS target proper. Parallel, semi-analytic work to scope the basic phenomena and increase understanding will also be carried out.

The goal of the validation programme is to confirm that the CFD tools can reproduce the overall flow characteristics, identify local hot-spots, and predict adequately the temperature and velocity distributions observed in the experiments. If points of discrepancy do arise, these will be itemised, and underlying causes identified and rectified, where possible. Any unresolved discrepancies will be noted and kept in mind during the CFD analysis of the ESS Target. There should be sufficient flexibility in the experimental programme definition to allow for some repeat tests to be carried out to clarify problem areas in the modelling.

1. Bauer, G. S. (ed.) *ESS-Liquid Metal Target Studies, 2nd Status Report*, Oct. 1995.

2. Smith, B. L. *Thermal Hydraulics of the Liquid Metal Target*, Paper T-14, Proc. ICANS-XIII and ESS-PM4, Weinfelden, Oct. 16-19, 1995.

3. Dury, T. V. & Smith, B. L. *Theoretical Investigation of the Thermal Hydraulic Behaviour of a Slab-Type Liquid Metal Target*, Session 3 of this Workshop.

ESS Thermal Hydraulics
Code Validation Tests

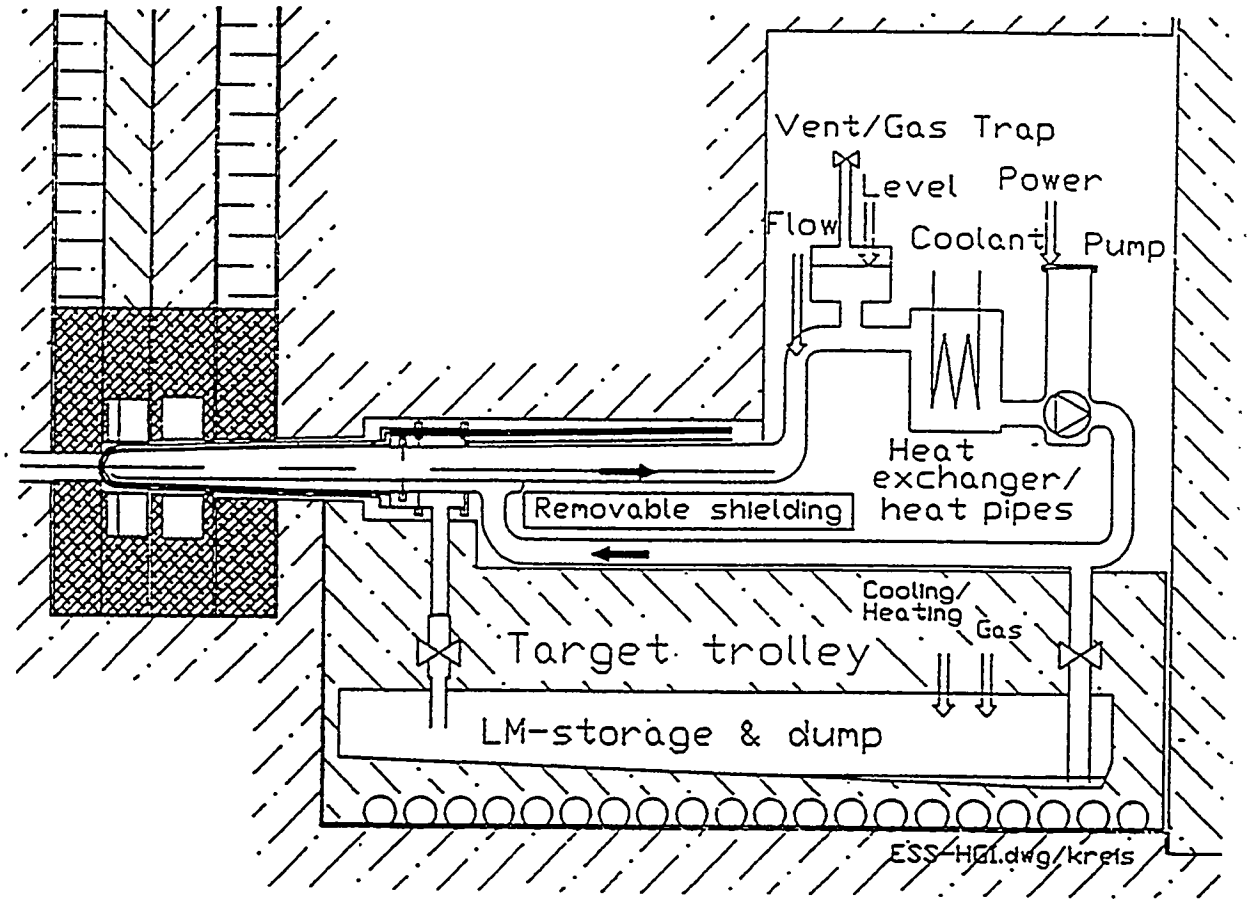

Schematic of ESS Liquid Metal Target Components
(Beam Power 5MW, Waste Heat 3.3MW)

Necessary to demonstrate coolability of target configuration to avoid:

- boiling of the mercury;
- overheating of the structures.

ESS Thermal Hydraulics
Code Validation Tests

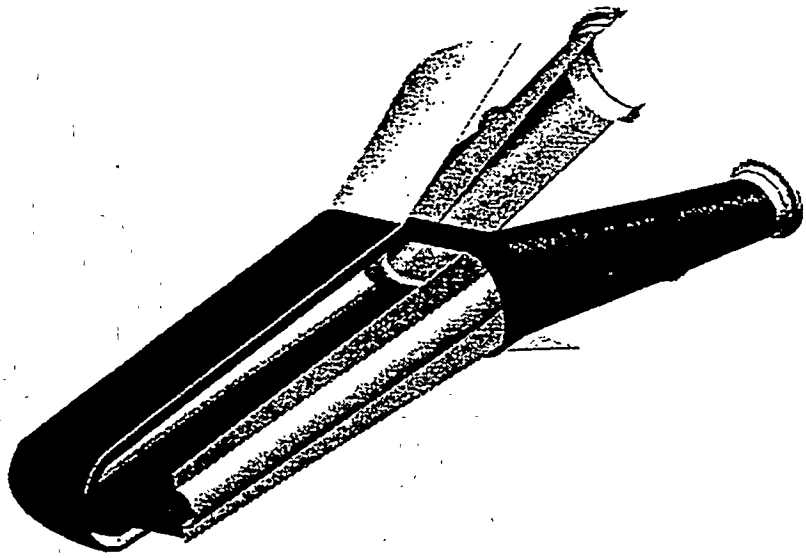

Multiple-Inlet Target Design

Detailed thermal-hydraulic calculations are being performed to:

- demonstrate target coolability;
- provide pressure and temperature data for structural analysis;
- optimize design.

Phenomena to be investigated:

- Complex fluid dynamic interaction of converging inlet streams;
- Turbulent heat tranfer from window to coolant;
- Bulk fluid heating by proton beam;
- Recirculating flow regions;
- Pressure drops;
- Boundary layer development and stability.

ESS Thermal Hydraulics
Code Validation Tests

Principal analysis tool: CFDS-FLOW3D.

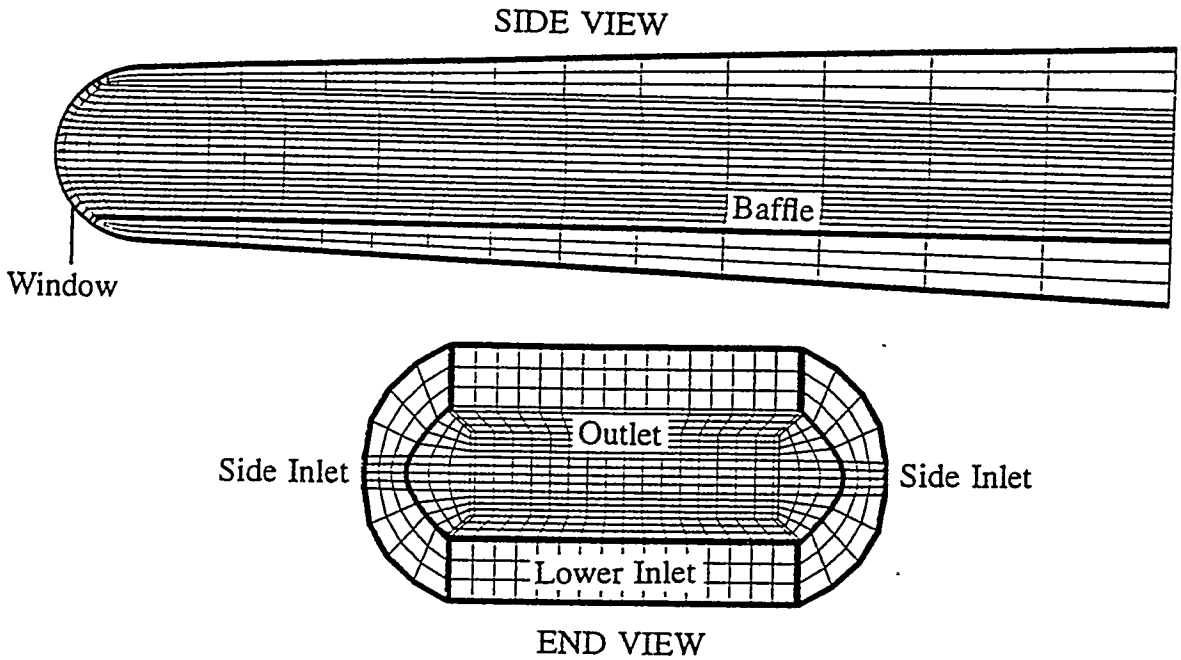

Typical Mesh Layout for ESS Simulation

Questions:

1. Is the computation mesh independent?
2. Are there other numerical errors?
3. Are the physical models appropriate?

Answers:

1. User experience; use different mesh layouts.
2. Vary BCs, FD schemes, convergence criteria, cross-check with a second code (ASTEC).
3. Comparison with controlled validation experiments.

The CFDS-FLOW3D Code
(AEA Technology)

Description

- Transient or Steady-State Fluid Flow
- Heat Transfer and Buoyancy
  Conduction in Solid Regions
- Single- and Multi-Phase Models
- Particle Transport Model
- Compressible or Incompressible
- Combustion
- Temperatures, Velocities, Chemical Species
- Laminar or Turbulent Flows
  (Large Re k-ϵ, Low Re k-ϵ, RSM, ASM)
- Complex 2-D and 3-D Geometry
- Finite Element Mesh
- Finite Volume Solution Algorithm
  (After Transforming to Rectangular Grid)
- Implicit Time Differencing
- Multi-Grid Linear Equation Solver
- Own Pre- & Post-Processors
  SOPHIA-2, JASPER-2

The ASTEC Code
(AEA Technology)

- Transient Single-Phase Thermal Hydraulic Code
- Finite Volume Solution Algorithm
- Complex 3-D Geometry
- Compressible or Incompressible Flow
- Calculates Temperatures, Velocities, Concentrations
- Laminar or Turbulent ($k - \epsilon$ Model) Flow
- Full Tensor Porous Medium Model
- Fully Implicit Time-Differencing
- Hybrid, Skew Upwind Differencing for Advection terms (Reduces Numerical Diffusion)
- Free Surface Tracking Algorithm
- Radiation Effects included for Heat Transfer Calculations
- Parallel (Transputer) or Vector Versions
- Own Pre-Processor (SOPHIA)
- Own Post-Processor (JASPER)

ESS Thermal Hydraulics
Code Validation Tests

Necessary to distinguish between **Prototype** and **Validation** experiments.

PROTOTYPE EXPERIMENTS

- Dynamic and thermal similarity (Re, Pr, Gr, Pe, etc.);
- 1-1 scale using actual materials (Hg);
- Useful as confirmatory test

Such tests are generally **not useful** for code validation purposes since all phenomena are intermingled. If code simulation is not satisfactory, it is very difficult to trace the origins of the modelling deficiencies.

VALIDATION EXPERIMENTS

- Series of simple, structured tests of increasing complexity;
- Relevant phenomena are first studied in isolation;
- Measurable effects are amplified, if possible, to provide good data;
- Phenomena combined in a step-by-step manner, increasing realism.

At each stage of the validation procedure on additional phenomenon is added and the consequences examined. Shortcomings in code modelling are more readily traced by this method, and the appropriate action taken (change, modify or develop new models). The series ends with a final, prototype experiment. At the end of the validation exercise the code can be used with confidence in further simulations, parameter studies, etc.

ESS Thermal Hydraulics
Code Validation Tests

RATIONALE OF EXPERIMENTS:

- 1-1 scale in the appropriate geometry;
- Dynamic Similarity (same Re);
- Isothermal and heated tests;
- Water tests (large Pr) for visualization purposes;
- Liquid sodium tests (small Pr);
- Final confirmatory test using Hg or NaK (intermediate Pr);
- Water tests utilize existing WALO facility at PSI;
- Na tests utilize existing NALO facility at PSI;
- NaK test possible with minor modifications to the NALO loop;
- Hg tests may need to be done elsewhere (or a new loop built).

ESS Thermal Hydraulics
Code Validation Tests

WATER EXPERIMENTS

1. Laminar, Isothermal

- Simple physical models;
- Modelling deficiencies are numerical in origin;
- Optimization of mesh, FD schemes, BCs, convergence criteria;
- Transient studies if flow instabilities occur.

2. Laminar, Heated

- Low power only (no subcooled boiling);
- Influence of (weak) buoyancy forces;
- (Weak) heat transfer by conduction only.

3. Turbulent, Isothermal

- Study of turbulent flow phenomena: stagnation, BL separation and reattachment, recirculation, swirling, mixing layers, wakes;
- Evaluation of turbulence models;
- Curvature effects on turbulent BLs.

4. Turbulent, Heated

- Heat transfer by turbulence only;
- Mixing of hot and cold streams, plumes;
- Buoyancy effect on turbulent BL.

ESS Thermal Hydraulics
Code Validation Tests

SODIUM EXPERIMENTS

1. Laminar, Isothermal

- Calibrate velocity measurement devices;
- Otherwise, covered already by water tests.

2. Laminar, Heated

- Medium power tests;
- Influence of buoyancy forces;
- Heat transfer by conduction only.

3. Turbulent, Isothermal

- Evaluation of turbulence models;
- Curvature effects on turbulent BLs.
- But, only useful if good velocity measurements available.

4. Turbulent, Heated

- High power tests;
- Heat transfer by turbulence and conduction;
- Effect of (strong) buoyancy forces on BLs;
- Evaluation of turbulence model with buoyancy effects.

ESS Thermal Hydraulics
Code Validation Tests

PROTOTYPE EXPERIMENT

- Final, confirmatory test;
- Correct combination of phenomena;
- Validated models;
- Strengthens safety case for target.

Assessment of the Neutron Cross Section Database for Mercury for the ORNL Spallation Source

L. C. Leal, R. R. Spencer, D. T. Ingersoll, and T. A. Gabriel
Oak Ridge National Laboratory
Bldg 6011, MS 6370
P. O. Box 2008
Oak Ridge, TN 37831
Phone: (423)-574-5281
Fax: (423)-574-3527

ABSTRACT

Neutron source generation based on a high energy particle accelerator has been considered as an alternative to the canceled Advanced Neutron Source project at Oak Ridge National Laboratory. The proposed technique consists of a spallation neutron source in which neutrons are produced *via* the interaction of high-energy charged particles in a heavy metal target. Preliminary studies indicate that liquid mercury bombarded with GeV protons provides an excellent neutron source. Accordingly, a survey has been made of the available neutron cross-section data. Since it is expected that spectral modifiers, specifically moderators, will also be incorporated into the source design, the survey included thermal energy, resonance region, and high energy data. It was found that data of individual isotopes were almost non-existent and that the only evaluation found for the natural element had regions of missing data or discrepant data. Therefore, it appears that to achieve the desired degree of accuracy in the spallation source design it is necessary to re-evaluate the mercury database including making new measurements.

During the presentation the currently available data will be presented and experiments proposed which can lead to design quality cross sections.

Neutron Cross-Section Data for Mercury

Background

The use of a high energy particle accelerator to generate neutron sources is being considered as an alternative to the canceled Advanced Neutron Source project at Oak Ridge National Laboratory. The proposed technique consists of a spallation neutron source in which neutrons are produced by allowing high-energy charged particles to interact with a heavy metal target. A key part in the analysis and design of such a device is the choice of the target material. Preliminary studies performed at ORNL indicate that liquid mercury provides an excellent neutron source and has several thermo-mechanical advantages over solid target materials. To assess how the neutrons collimate in various directions, it is necessary to accurately determine the neutron flux in the surrounding target and moderator areas, which will require calculations involving neutron-mercury interactions.

Comments on the Available Nuclear Data for Mercury

The isotopic abundances of natural mercury (Hg) are given in Table 1, which shows that natural mercury has seven major important isotopes. As a general rule, materials with atomic mass number, A, greater than 80, as is the case of mercury, have resonance structure in the neutron cross sections starting in the energy range of a few eV and extending all the way into the keV range. In order to properly characterize the neutron flux, it is necessary that the resonance effects are accounted for in the energy dependence of the cross sections. The approach that best provides a way to characterize the resonance effects is the evaluation of the neutron cross sections to determine the resonance parameters which can be used to reproduce the very detailed structure of the cross sections in the resonance region.

A survey of the neutron cross section data for mercury has been recently performed. It was found that there are no total cross section data available for the individual mercury isotopes. A major benefit from this effort could be the determination that the most effective spallation target is one in which certain isotopes of mercury have been either enhanced or separated out. There are total cross section data for natural mercury from an evaluation performed about 25 years ago tailored for particular applications at that time. The available data are not continuous and not consistent, when different data sets are compared. In addition, the capture cross sections of the individual isotopes were measured for neutron energies above 2.5 keV; however, these data could not be analyzed since transmission data were not available from which neutron widths could be derived.

Proposed Tasks

To achieve the degree of accuracy demanded in the design of the spallation neutron source, it is proposed that a new evaluation of the neutron cross sections for mercury be performed. The proposed tasks will consist of (1) measuring the transmission and capture cross section for the mercury isotopes using time-of-flight techniques, (2) analyzing the experimental data to determine resonance parameters, and (3) using the resonance parameters to generate pointwise and multigroup cross section libraries.

1) Neutron Cross-Section Measurements

The time-of-flight technique is undoubtedly the most powerful method available today to measure neutron cross sections. It allows one to identify resonance structures which are fundamental properties of the cross sections. The Oak Ridge Linear Accelerator (ORELA) provides a world-class cross section measurement capability. It is based on the time-of-flight method and is a unique machine in the sense that it provides the best resolution neutron cross section data in the world. Highly qualified ORELA personnel provide the expertise to perform cross section measurements.

2) Nuclear Data Analysis and Evaluation

Neutron cross section evaluations at ORNL are performed with the computer code SAMMY. SAMMY is a multilevel multi-channel R-matrix resonance analysis program based on the Bayes approach. SAMMY is responsible for about 40 % of the neutron cross section evaluations in the latest version of the Evaluated Nuclear Data File, ENDF/B-VI. SAMMY was written at ORNL and has been frequently used by ORNL personnel in several areas.

To represent mercury cross sections with resonance parameters, SAMMY will be used to analyze the seven mercury isotopes listed in Table 1. For each isotope, the analysis will be performed by evaluating the experimental transmission and capture data.

3) Cross-Section Libraries Generation

The new evaluated mercury data will be processed for application in neutronic calculations of the spallation neutron source. The effort will include the data generation in multigroup and pointwise form for use in deterministic and Monte Carlo computer codes.

ISOTOPE	ABUNDANCE (%)
Hg^{196}	0.15
Hg^{198}	10.1
Hg^{199}	17.0
Hg^{200}	23.1
Hg^{201}	13.2
Hg^{202}	29.65
Hg^{204}	6.8

Table 1. Mercury Isotope Compositions.

Target assembly enclosed in the Berylium reflector

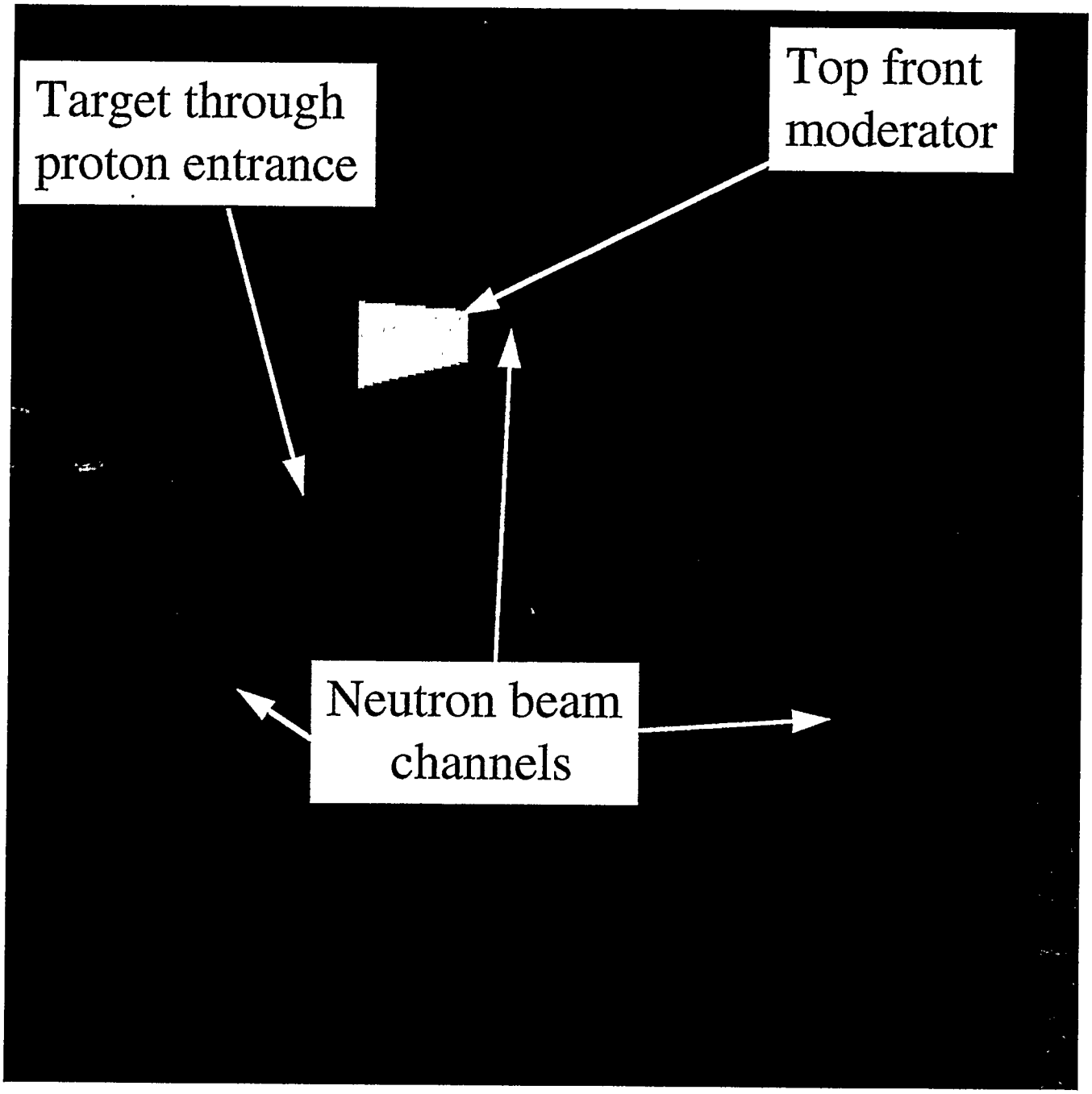

Target, moderators and the beam channels as viewed from the bottom

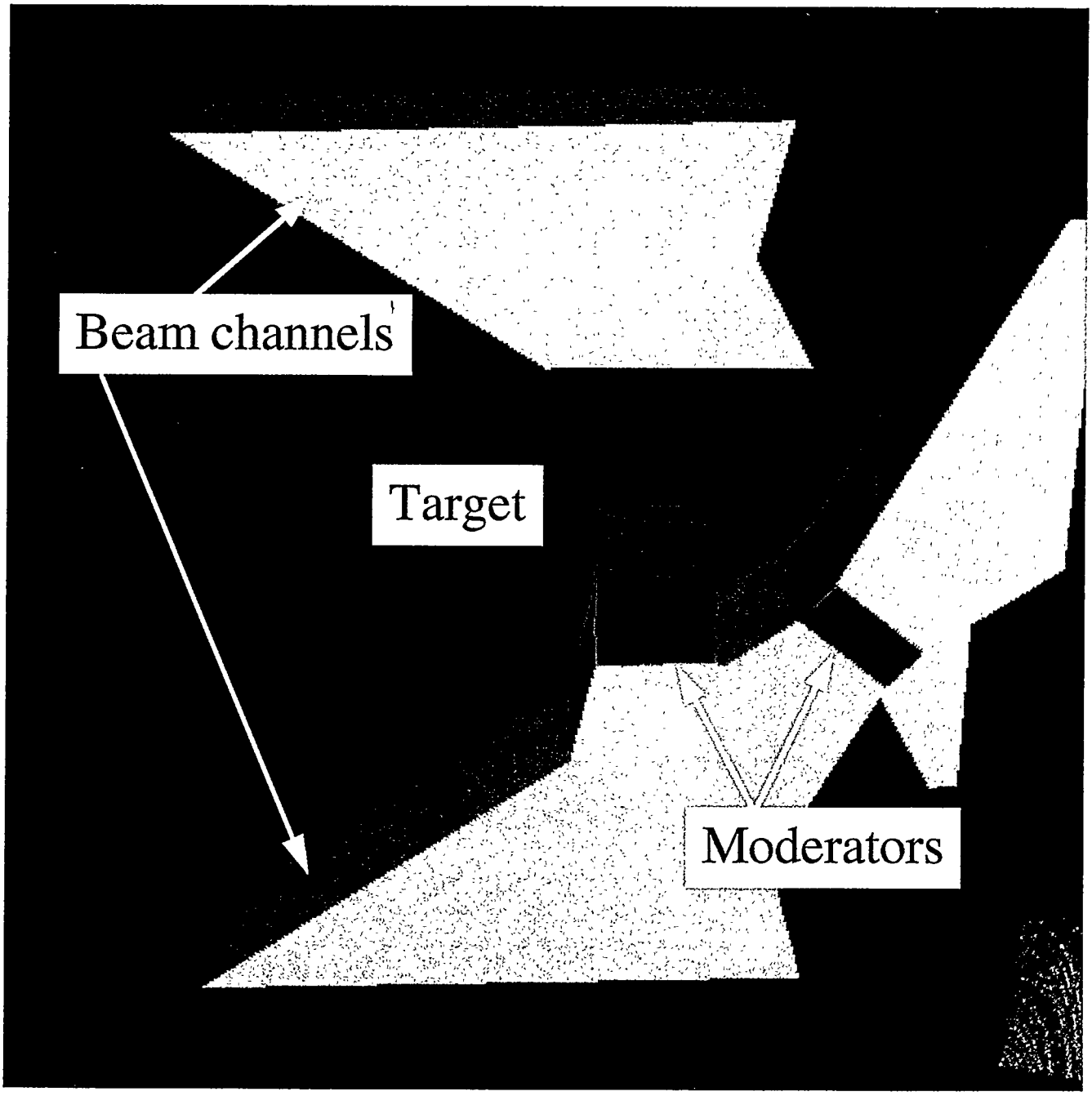

Neutronic Comparison-Hg,W,Ta
Coupled moderators

	Cryogenic		Ambient	
Target	J(n/p)	Ratio	J(n/p)	Ratio
Hg	.254	1.35	.290	1.35
W	.220	1.17	.252	1.17
Ta	.188	1.00	.215	1.00

Part of the difference between Hg and W or Ta is due to the 35% D_2O target content for W or Ta.

Cryogenic(ambient) means the neutrons coming from a face on a cryogenic (ambient) moderator are being counted

Thermal Flux Comparison
ESS[1] Flux and ORSNS "Effective"[2] Flux
5MW

Cryogenic

Target	ϕ_{th}^{ORSNS}	R	ϕ_{th}^{ESS}	R
Hg	2.94×10^{14}	1.35	3.91×10^{14}	1.23
W	2.54×10^{14}	1.17	3.53×10^{14}	1.10
Ta	2.17×10^{14}	1.00	3.19×10^{14}	1.00

Ambient

Target	ϕ_{th}^{ORSNS}	R	ϕ_{th}^{ESS}	R
Hg	3.35×10^{14}	1.35	2.29×10^{14}	1.51
W	2.91×10^{14}	1.17	1.67×10^{14}	1.10
Ta	2.48×10^{14}	1.00	1.52×10^{14}	1.00

Units: ϕ_{th} (n/cm^2-sec)

[1]ESS results from D. Filges, R.D. Neef and H. Schaal "Nuc. Studies of Different Target Systems for ESS", ICANS-XIII

[2]ORSNS "effective" fluxes were converted from 2π steradian current calculations. The differing distances from the target to the moderator were also corrected for.

FAST AND THERMAL NEUTRON FLUXES OF Ta, W, and Hg TARGETS

Target	Φfast [n/cm² • s • 5 MW]		Φthermal [n/cm² • s • 5 MW]	
	upstream Moderator	downstream Moderator	upstream Moderator	downstream Moderator
Tantalum	$7.25 \cdot 10^{13}$	$2.30 \cdot 10^{13}$	$3.19 \cdot 10^{14}$	$1.52 \cdot 10^{14}$
Tungsten	$6.42 \cdot 10^{13}$	$2.14 \cdot 10^{13}$	$3.52 \cdot 10^{14}$	$1.67 \cdot 10^{14}$
Mercury	$8.31 \cdot 10^{13}$	$3.52 \cdot 10^{13}$	$3.91 \cdot 10^{14}$	$2.29 \cdot 10^{14}$

D. Filges, R. D. Neef, and H. Schaal, Forschungszentrum Jülich GmbH, Institute für Kernphysik, D-52425 Jülich, Germany, "Nuclear Studies of Different Target System for the European Spallation Source (ESS)," ICANS-XIII, 13th Meeting of the International Collaboration on Advanced Neutron Sources, October 11-14, 1995, Paul Scherrer Institut, 5232 Villigen PSI, Switzerland

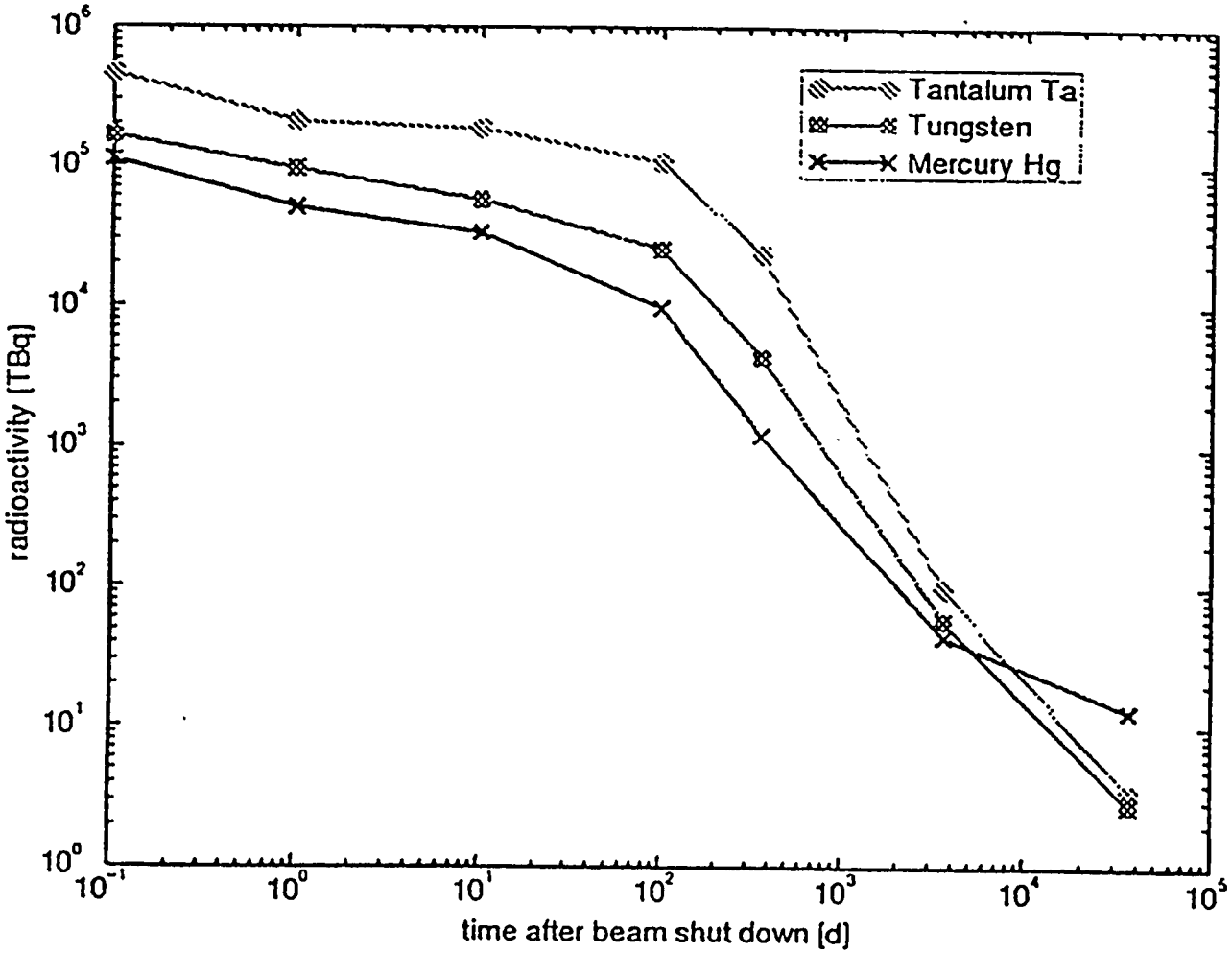

Activation in Ta, W, and Hg Target as a Function of Time After Beam Shut Down

D. Filges, R. D. Neef, and H. Schaal, Forschungszentrum Jülich GmbH, Institut für Kernphysik, D-52425 Jülich, Germany, "Nuclear Studies of Different Target System for the European Spallation Source (ESS)," ICANS-XIII, 13th Meeting of the International Collaboration on Advanced Neutron Sources, October 11-14, 1995, Paul Scherrer Institut, 5232 Villigen PSI, Switzerland

Neutron Spectrum
Cryogenic Moderator

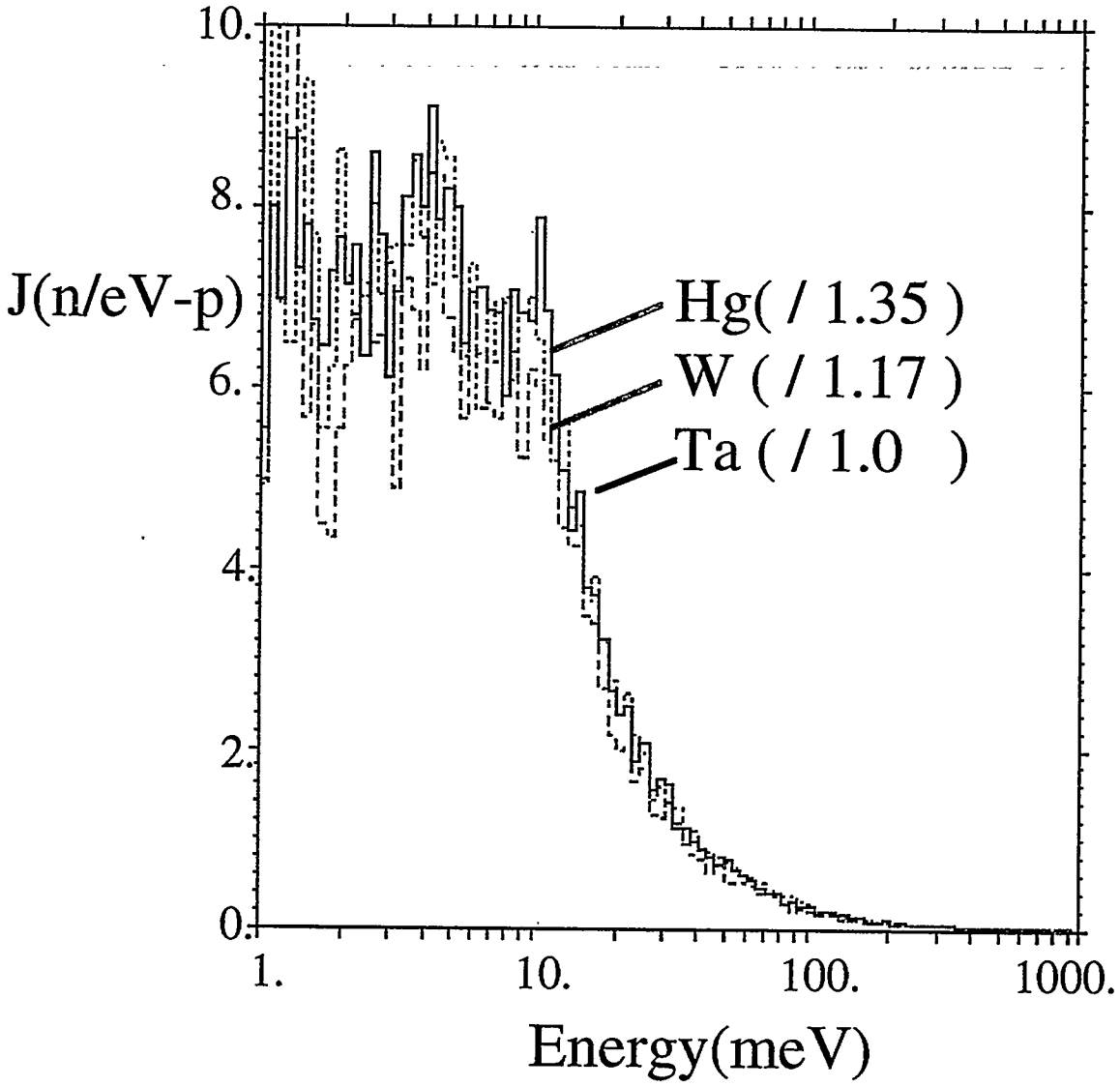

Pulse
Cryogenic Moderator

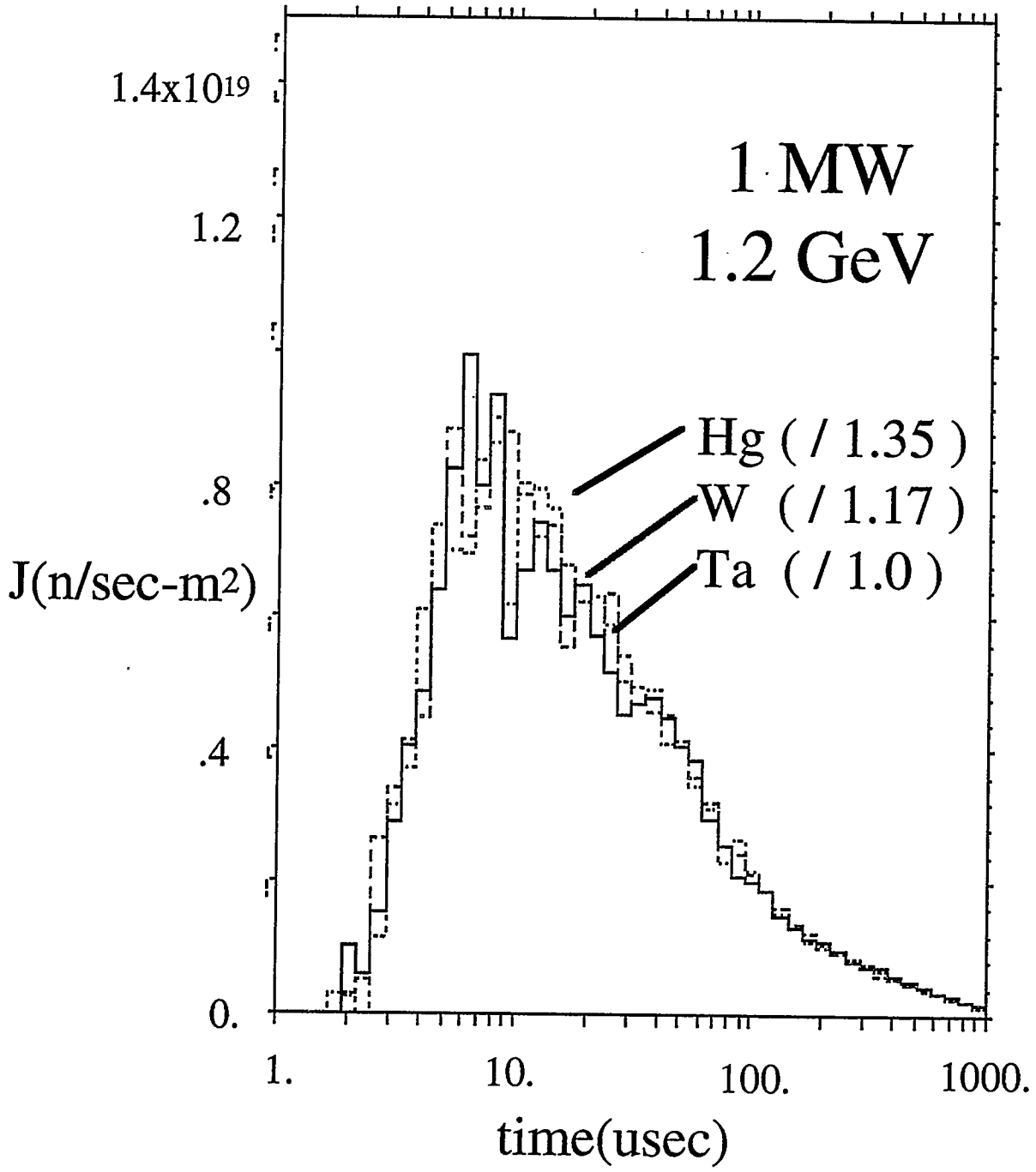

Neutron Spectrum
Ambient Moderator

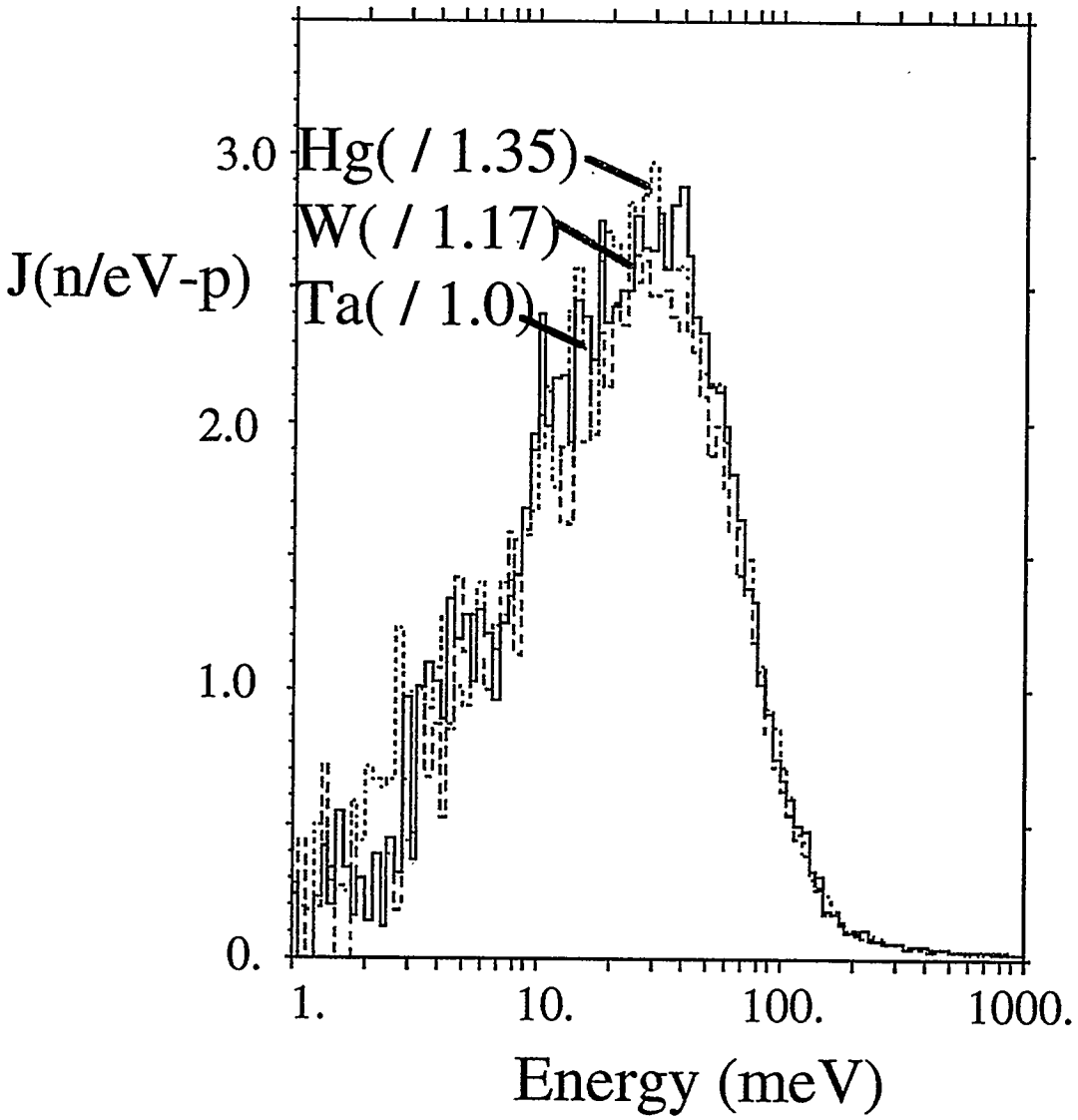

Pulse
Ambient Moderator

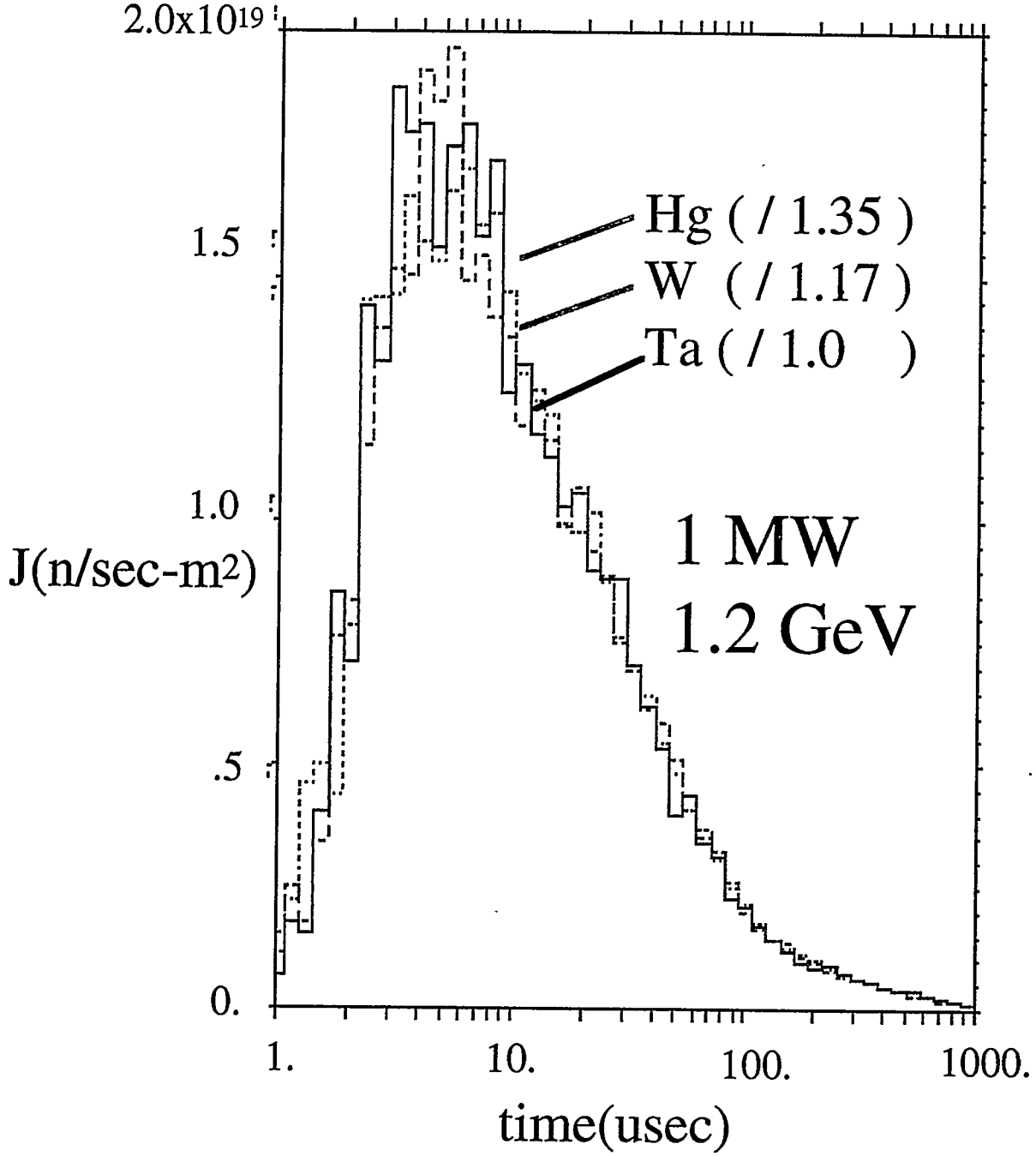

IMPORTANCE OF THE MERCURY NEUTRON CROSS SECTIONS IN THE ORNL SPALLATION NEUTRON SOURCE (ORSNS) DESIGN

- Liquid mercury is the proposed target for the ORSNS;
- High energy protons (E > 1 GeV) interacting with mercury produces a cascade of spallation products including neutrons from several MeV down to the eV range (thermal range);
- Characterization of the interaction and slowing down of these neutrons with the mercury is critical in the design of the ORSNS;
- The goal of the ORSNS is to produce thermal neutrons which are collimated toward targets in the experimental guide hall. These neutrons are produced in the mercury and from interactions of the epithermal neutrons in the target, moderators and reflector regions. An accurate representaion of neutron spectrum in the mercury is essential.
- In addition to the neutron spectrum in the target, the design of the ORSNS also depends on the by-products produced in the spallation process. Activation products must be accurately accounted for in the design since the ORSNS will have a mercury loop to recirculate and purify the mercury entering the target.

MERCURY CROSS SECTION DATA

- A Cross Section Evaluation for Mercury is Available in a MCNP library:

  It is the only evaluation available

  Features:
  - Natural mercury
  - Energy range: 10^{-4} eV to 30 MeV
  - Cross Section representation: Pointwise representation at a temperature of 300 K
  - Cross Section reactions: Total, Capture and Scattering

- Comparisons of the MCNP total cross sections were made with experimental data retrieved from the Nuclear Data Center at Brookhaven National Laboratory data bank. Figures 1 through 7 show the MCNP evaluation (solid line) compared with the experimental data (crosses) from 10^{-4} eV up to 30 keV. Above 500 eV, evaluated and experimental are very discrepant.

- The Mercury cross section must be known with a high degree of accuracy. As an example, the neutron heating at a given location is proportional to $E*\sigma(E)$.

  Calculated values of $E*\sigma(E)$ for the MCNP evaluated total cross section and for the experimental data obtained from the Nuclear Data Center at Brookhaven Lab, integrated from 10^{-4} eV to 30 keV (assuming a flat-flux distribution) are:

  MCNP: 6.2×10^{8} eV.barns

  Exp : 8.3×10^{8} eV.barns

  MCNP calcuation is approximately 33 % lower than the experimental results.

NEED FOR MEASUREMENTS AND EVALUATION

- The current state-of-the-art mercury data are inadequate. There is considerable disagreement with measured data, especially in the epithermal and thermal regions of importance to the ORSNS;

- Mercury has seven major isotopes (Table 1). Experimental data for individual isotopes of mercury are non-existent. Isotope cross sections are needed to quantify the amount of activation products;

- The design of a very accurate spallation source requires accurate neutron-mercury interaction cross sections;

- The latter can be achieved if new cross section measurements are performed in conjunction with new evaluations of resonance region parameters;

- Features of a resonance parameter representation of the cross section:

  - reproduces the very detailed structure of the cross sections in the resonance region
  - temperature effects on the cross section properly accounted for

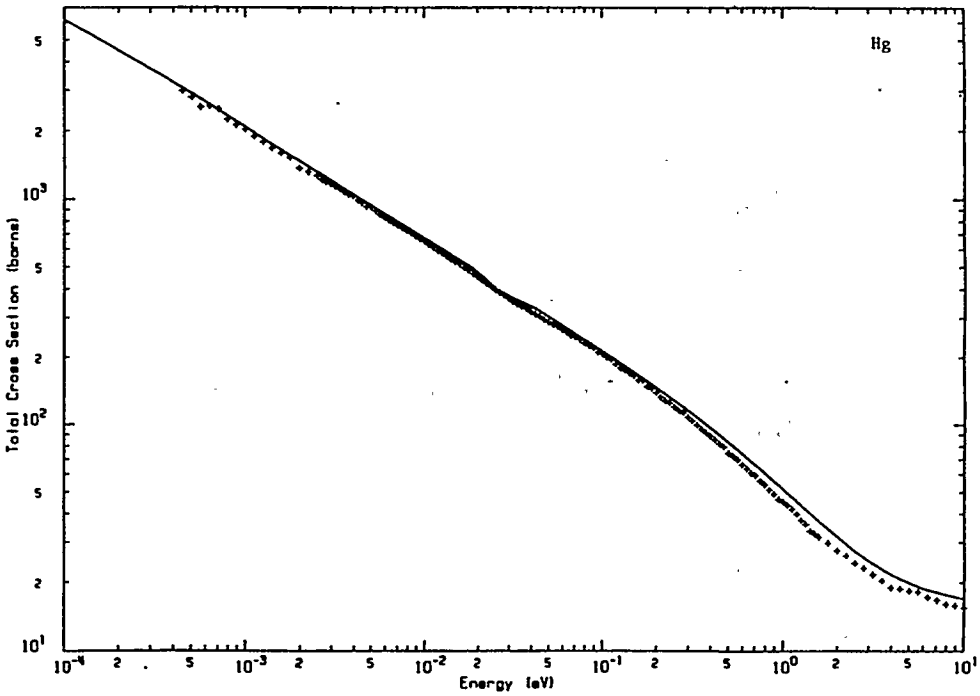

Fig. 1. Comparison between the MCNP Evaluated Total Cross Section (solid line) and Experimental data (crosses) in the Energy Range 1.0^{4} eV to 10 eV.

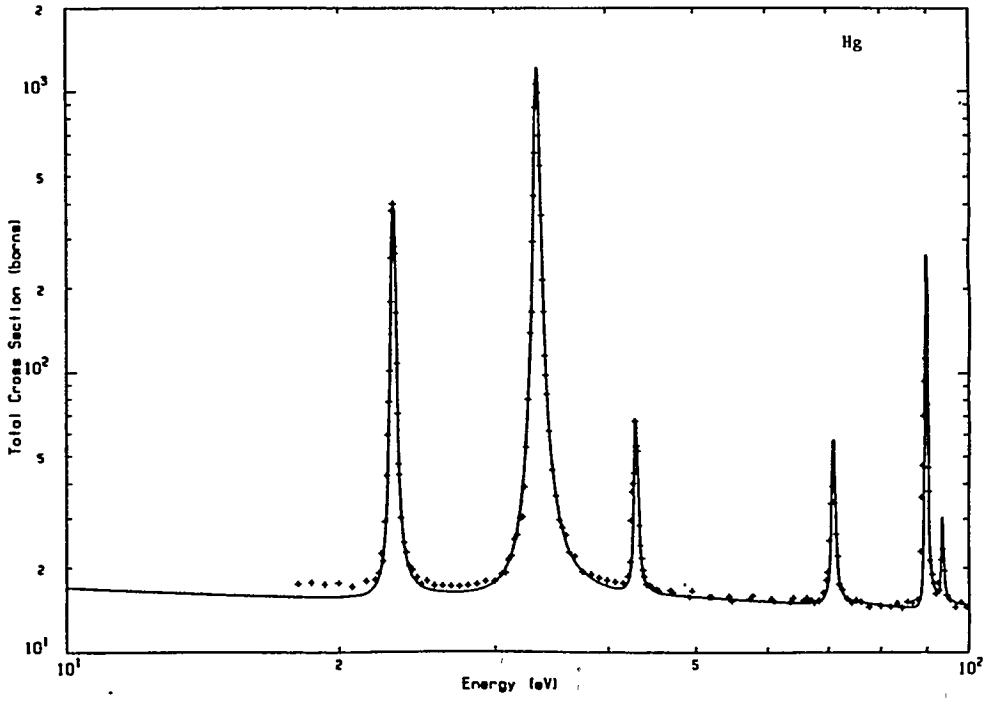

Fig. 2. Comparison between the MCNP Evaluated Total Cross Section (solid line) and Experimental data (crosses) in the Energy Range 10 eV to 100 eV.

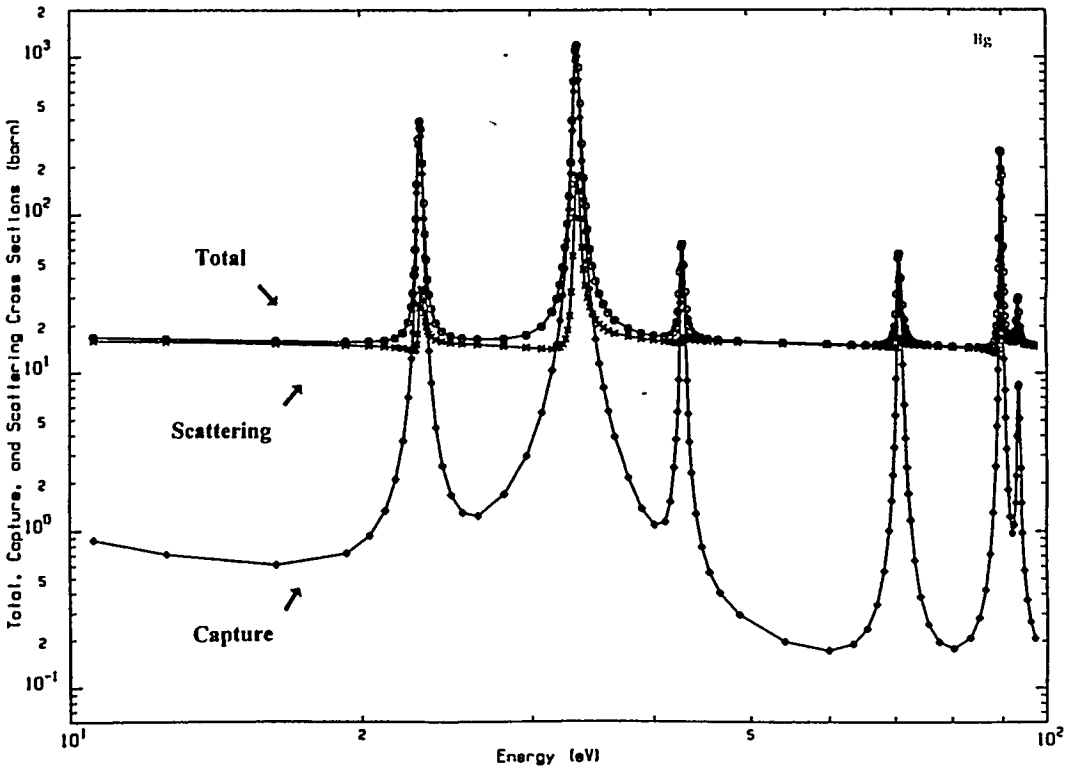

01-Feb-1995 09:09

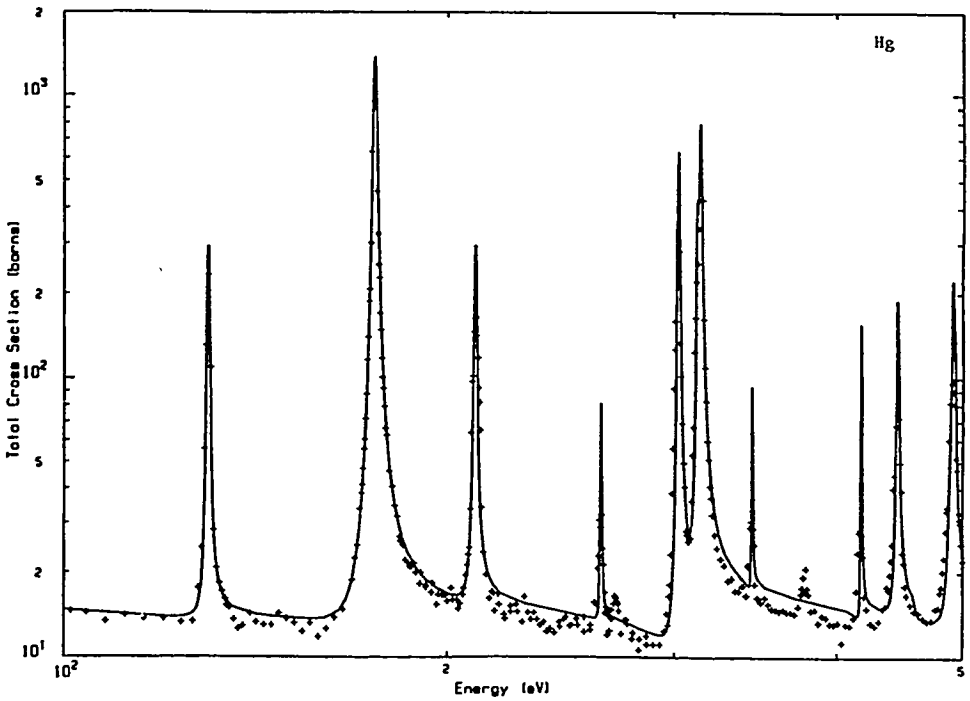

Fig. 3. Comparison between the MCNP Evaluated Total Cross Section (solid line) and Experimental Data (crosses) in the Energy Range 100 eV to 500 eV.

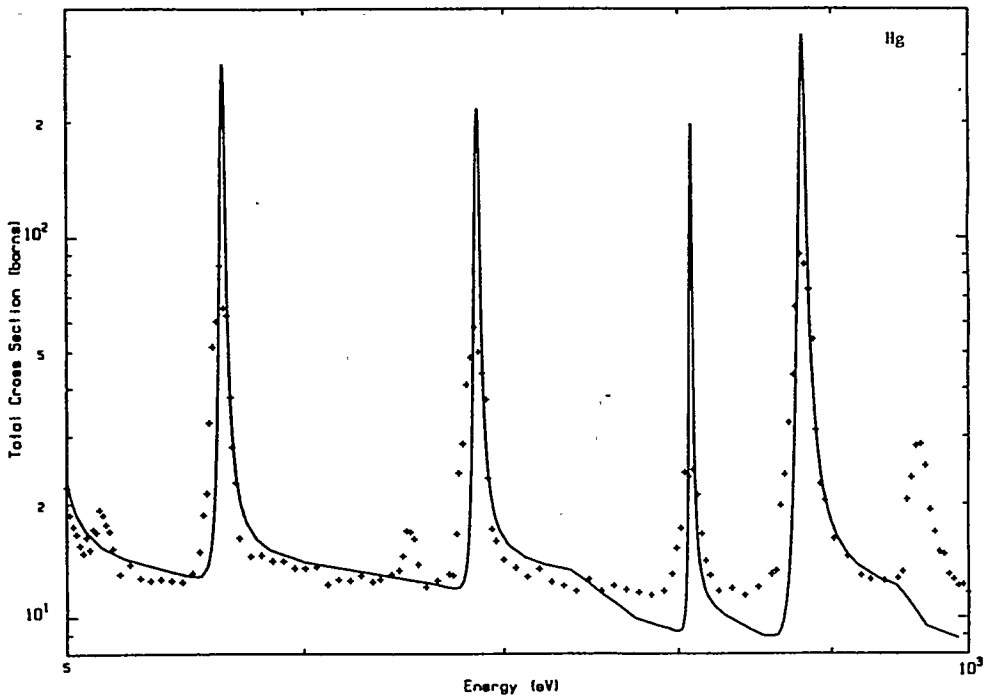

Fig. 4. Comparison between the MCNP Evaluated Total Cross Section (solid line) and Experimental data (crosses) in the Energy Range 500 eV to 1000 eV.

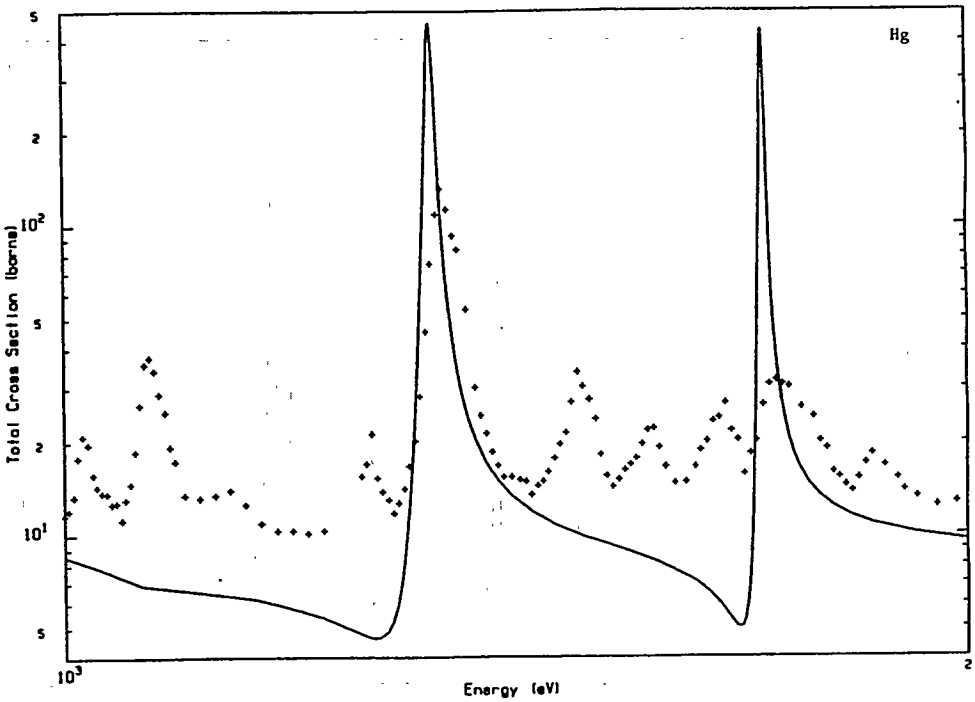

Fig. 5. Comparison between the MCNP Evaluated Total Cross Section (solid line) and Experimental data (crosses) in the Energy Range 1000 eV to 2000 eV.

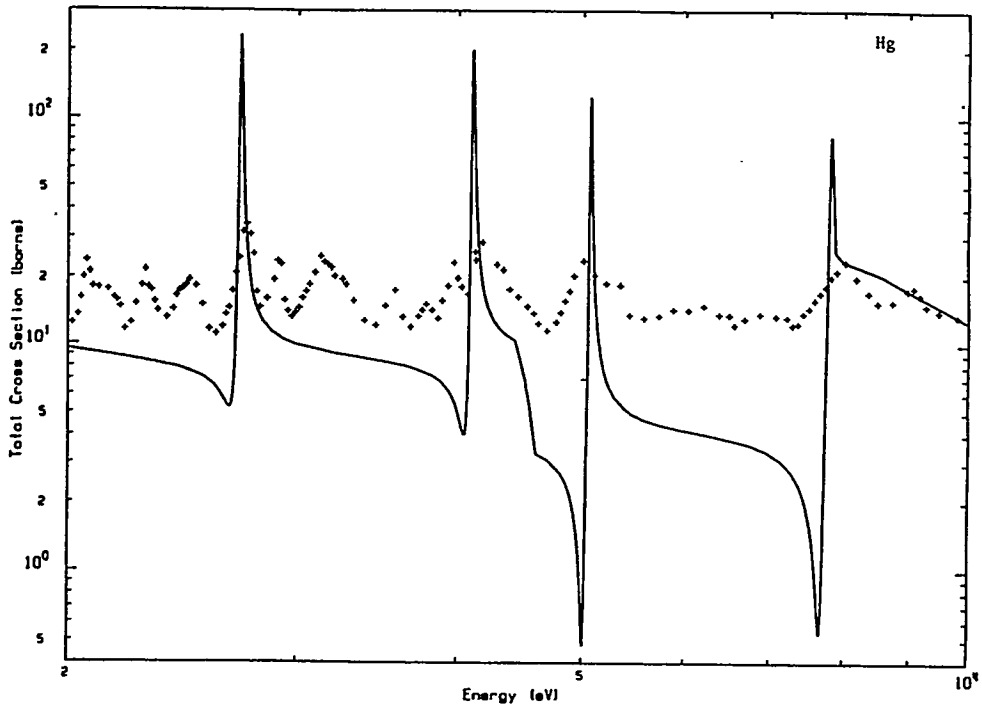

Fig. 6. Comparison between the MCNP Evaluated Total Cross Section (solid line) and Experimental data (crosses) in the Energy Range 2 keV to 10 keV.

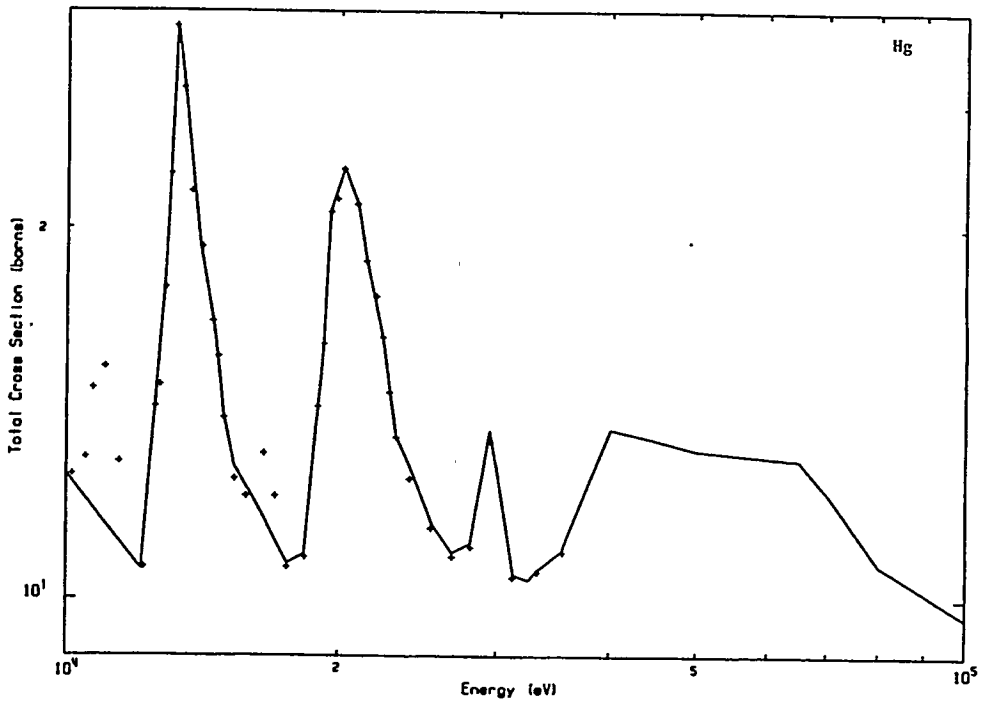

Fig. 7. Comparison between the MCNP Evaluated Total Cross Section (solid line) and Experimental data (crosses) in the Energy Range 10 keV to 100 keV.

ISOTOPE	ABUNDANCE (%)
Hg^{196}	0.15
Hg^{198}	10.1
Hg^{199}	17.0
Hg^{200}	23.1
Hg^{201}	13.2
Hg^{202}	29.65
Hg^{204}	6.8

Table 1. Mercury Isotope Compositions.

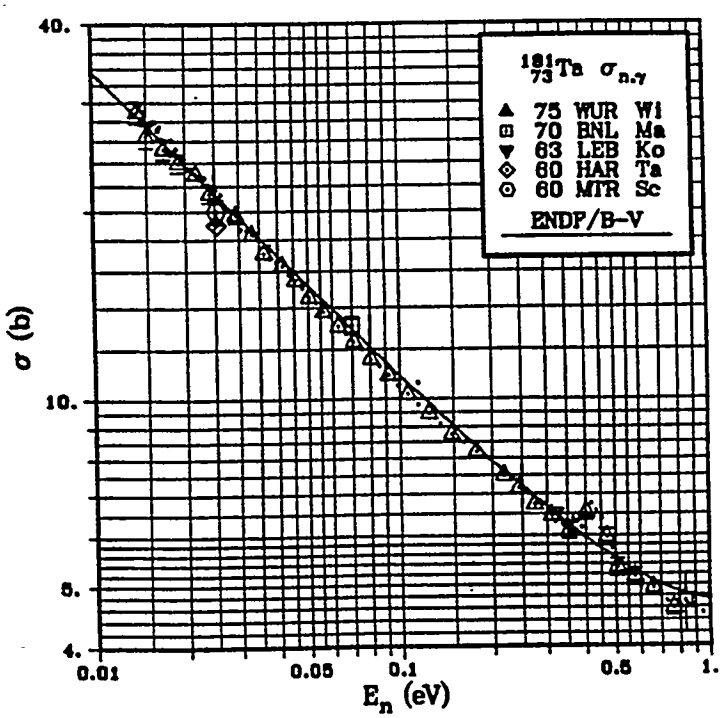

Neutron Capture Cross Section for Ta in the 0.01- to 1.0-eV Energy Range

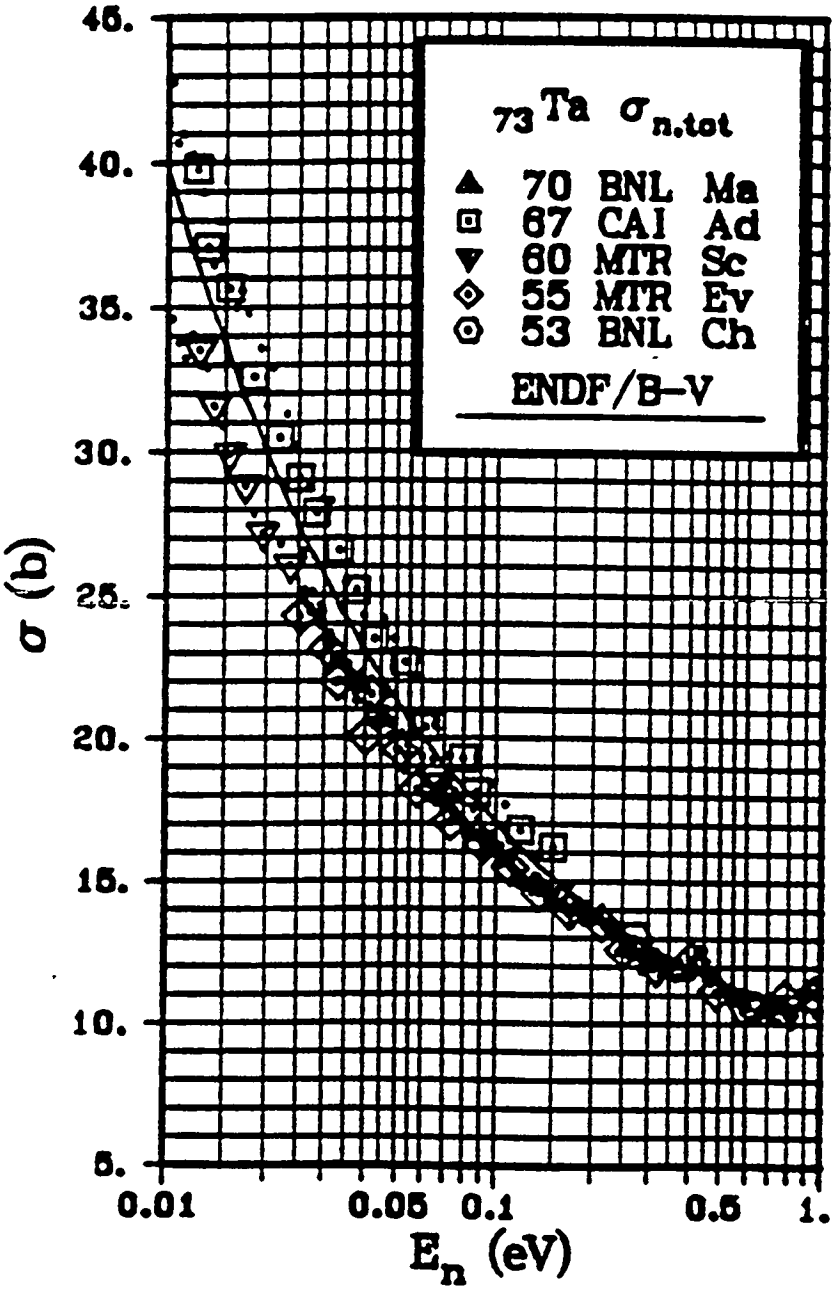

Neutron Total Cross Section for Ta in the 0.01 - to 1.0 eV Energy Range

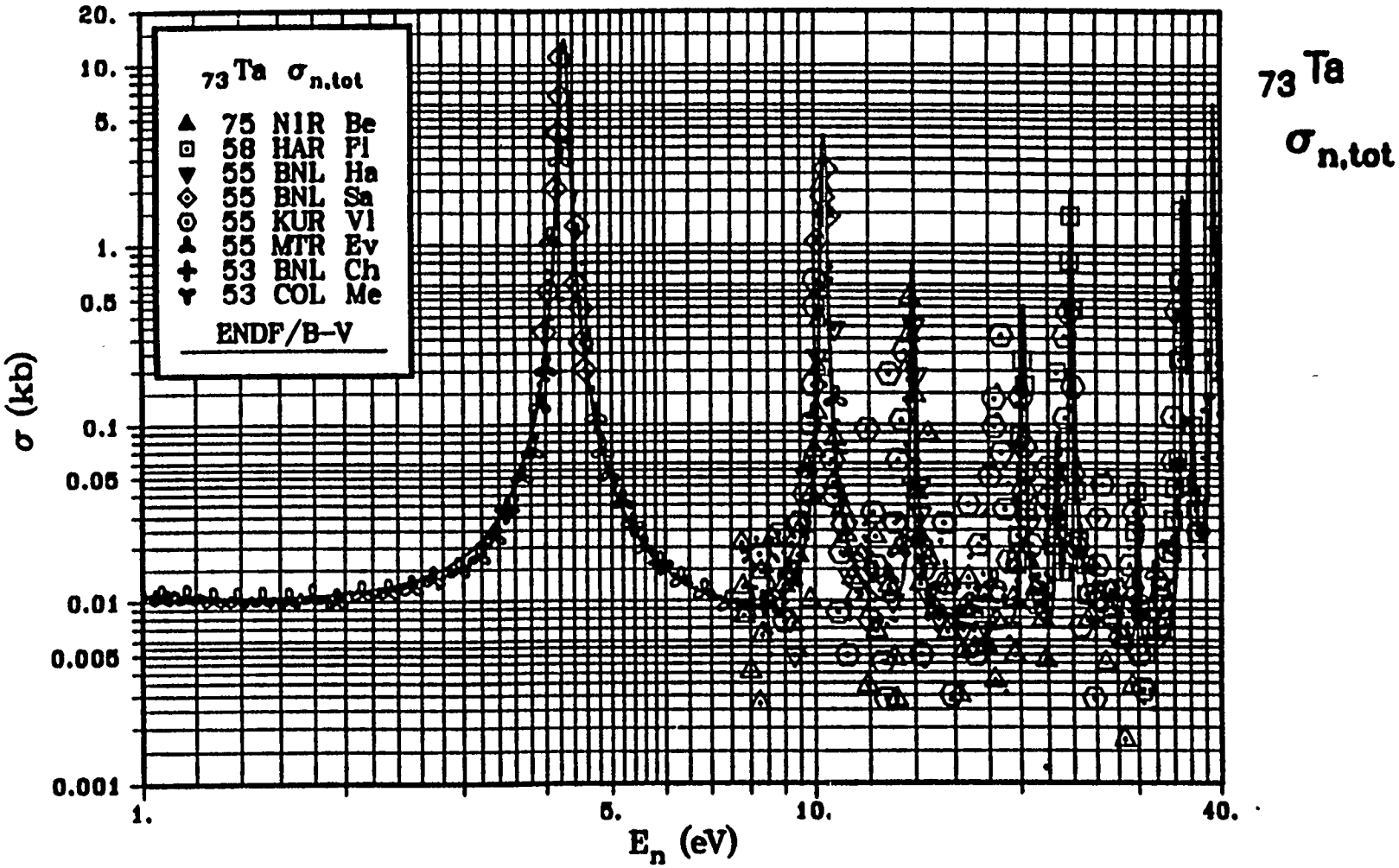

Neutron Total Cross Section for Ta in the 1.- to 40.-eV Energy Range

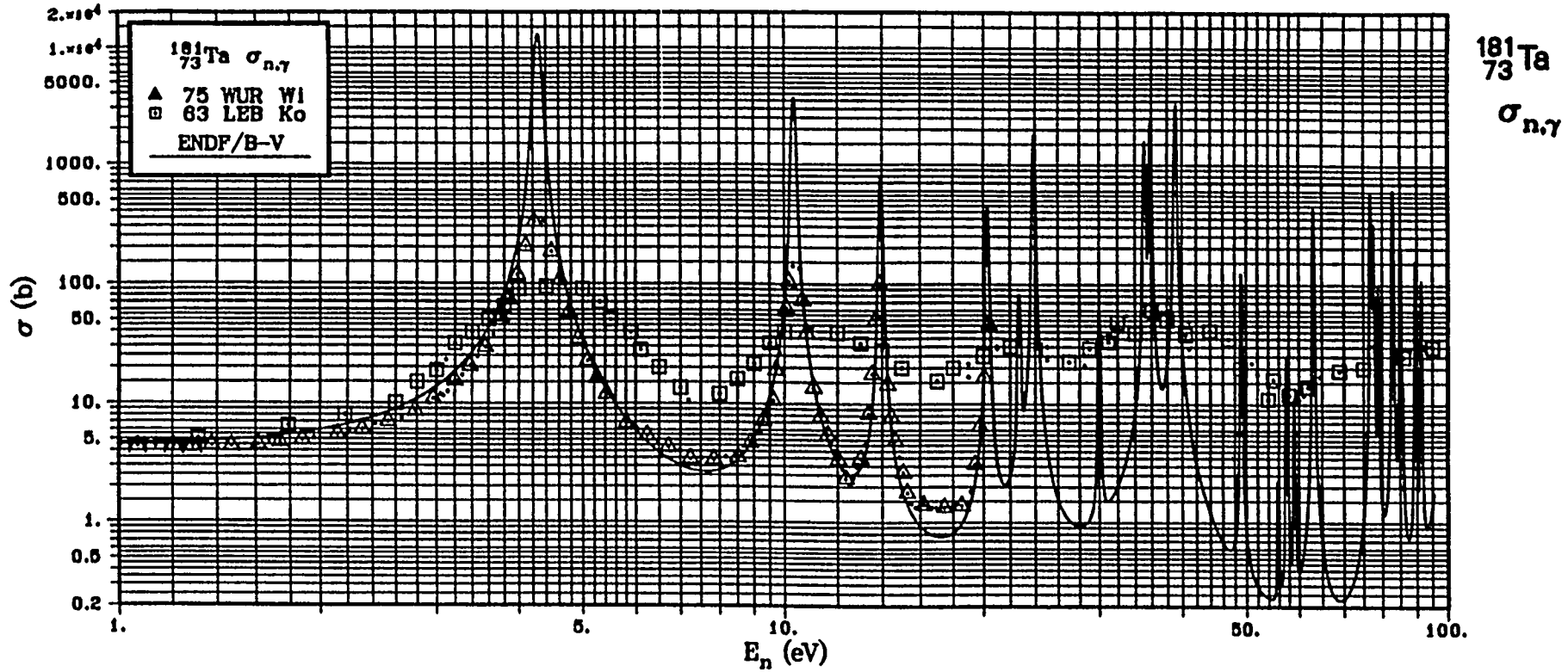

Neutron Capture Cross Section for Ta in the 1- to 100-eV Energy Range

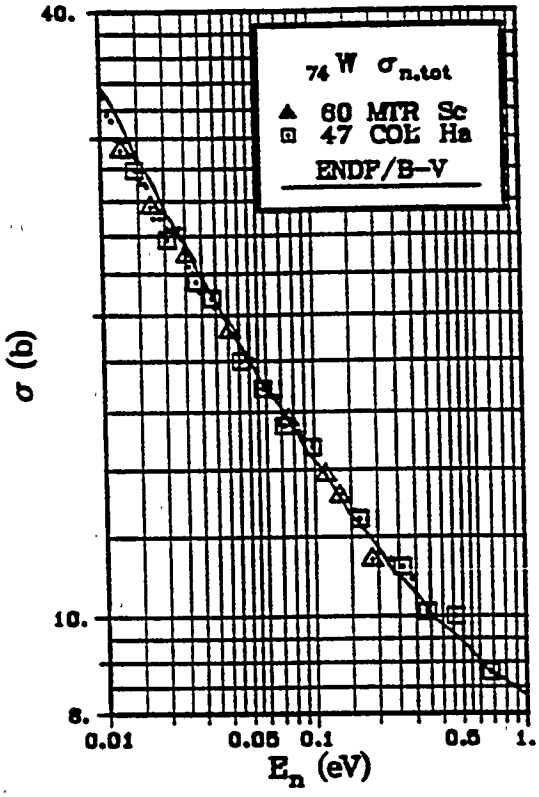

Neutron Total Cross Section for W in the .01- to 1.0- eV Energy Range

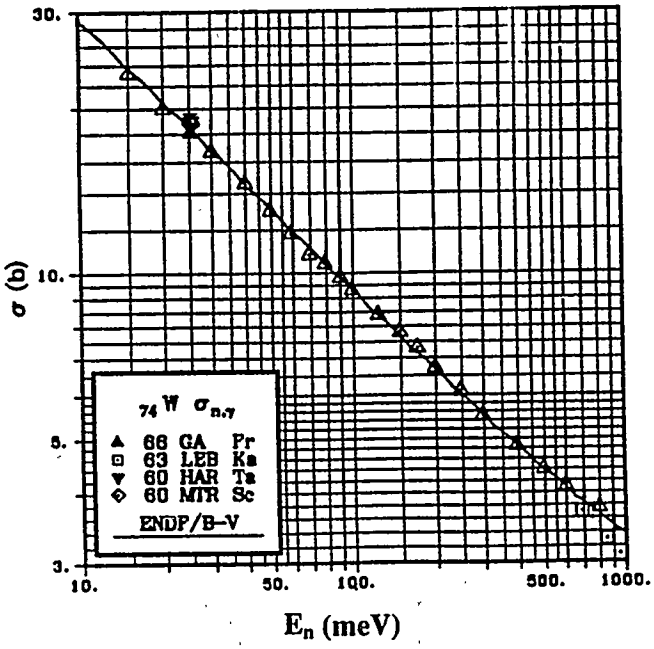

Neutron Capture Cross Section for W in the 10- to 1000 meV Energy Range

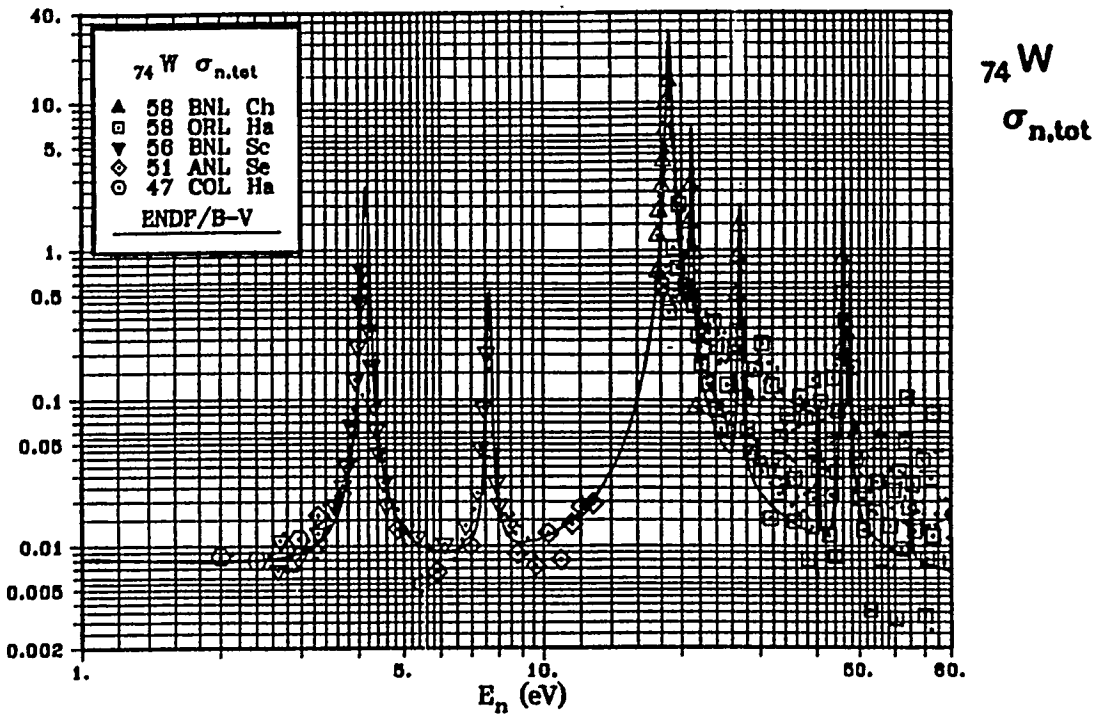

Neutron Total Cross Section for W in the 1- to 80. eV Energy Range

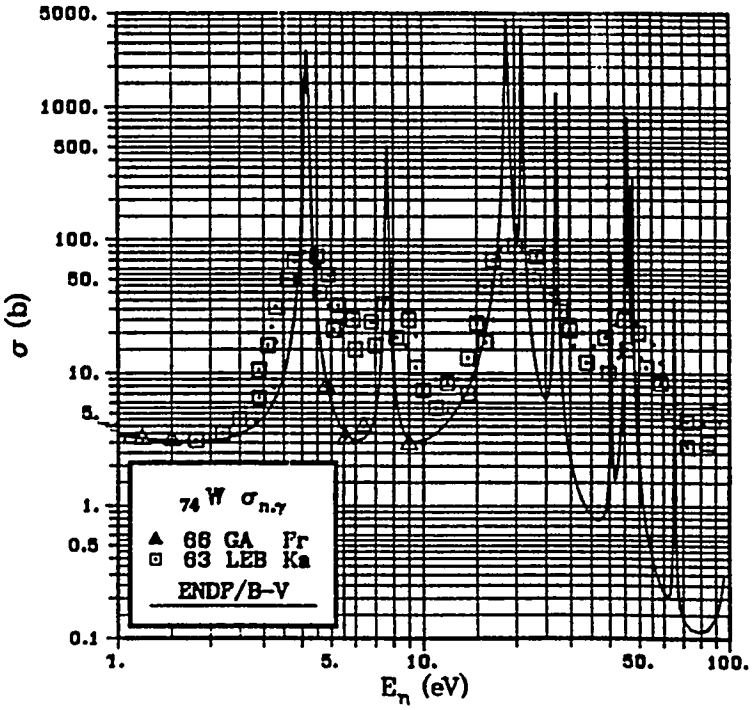

Neutron Capture Cross Section for W in the 1.- to 100. -eV Energy Range

Mercury Target R&D for the Oak Ridge Spallation Neutron Source

J. R. Haines, J. DiStefano, K. Farrell, T. A. Gabriel, L. K. Mansur,
S. Pawel, P. Rittenhouse, M. Siman-tov, R. Taleyarkhan

Presented at the
International Workshop on the
Technology and Thermal Hydraulics of Heavy Liquid Metals
Schruns, Montafon Valley, Austria
by
John Haines
March 27, 1996

ornl

MERCURY TARGET R&D FOR THE OAK RIDGE SPALLATION NEUTRON SOURCE

J. R. Haines, J. DiStefano, K. Farrell, T. A. Gabriel,
L. K. Mansur, S. Pawel, P. Rittenhouse, M. Siman-Tov, R. P. Taleyarkhan
Oak Ridge National Laboratory

The conceptual design for the Oak Ridge Spallation Neutron Source (ORSNS) incorporates liquid mercury as its reference target material. A flowing liquid target was selected mainly because of the increased power handling capability possible with the convective transport process. The major reasons for choosing mercury as the liquid target material are because it: (1) is a liquid at room temperature, (2) has good heat transport properties, and (3) has a high atomic number and mass density resulting in high neutron yield and source brightness.

Since liquid targets are not widely utilized in presently operating accelerator targets and because of the challenges posed by the intense, pulsed thermal energy deposition (~ 20-100 kJ deposited during each 1-10 μs pulse), considerable R&D is planned for the mercury target concept. The key feasibility issue that will be addressed in early R&D efforts are the effects of the thermal shock environment, which will include development and testing of approaches to mitigate these effects. Materials compatibility and ES&H issues associated with the use of liquid mercury are also of major importance in early R&D efforts.

A brief description of the mercury target design concept, results of initial evaluations of its performance characteristics, identification of its critical issues, and an outline of the R&D program aimed at addressing these issues will be presented.

* Oak Ridge National Laboratory, managed by Lockheed Martin Energy Research Corp. for the U.S. Department of Energy under contract number DE-AC05-96OR22464.

ORSNS Target Design Decision Matrix

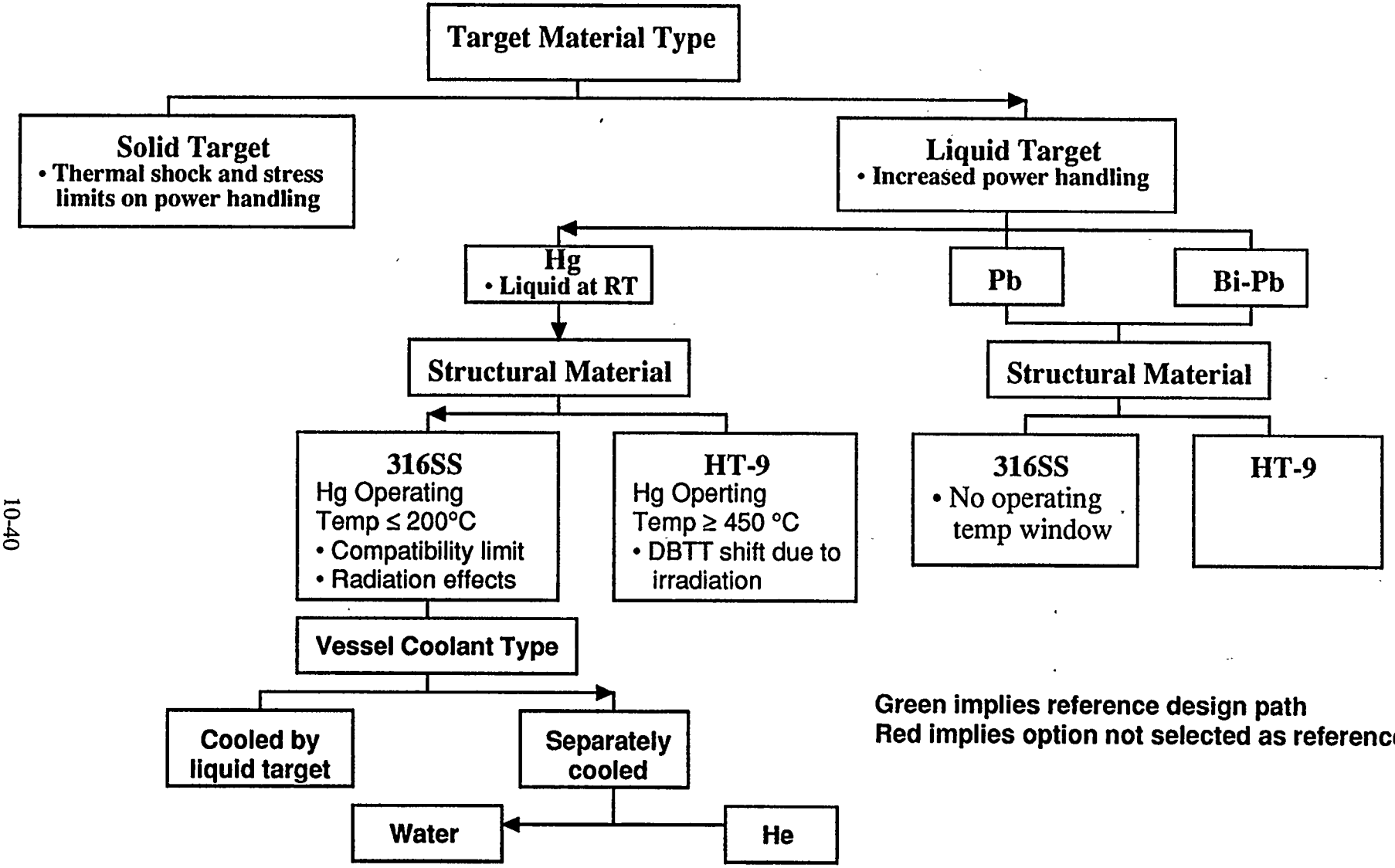

Green implies reference design path
Red implies option not selected as reference

Key Remaining Issues

- Thermal shock loads on vessel
- Irradiation lifetime of 316SS

ORSNS
Liquid Target System Diagram

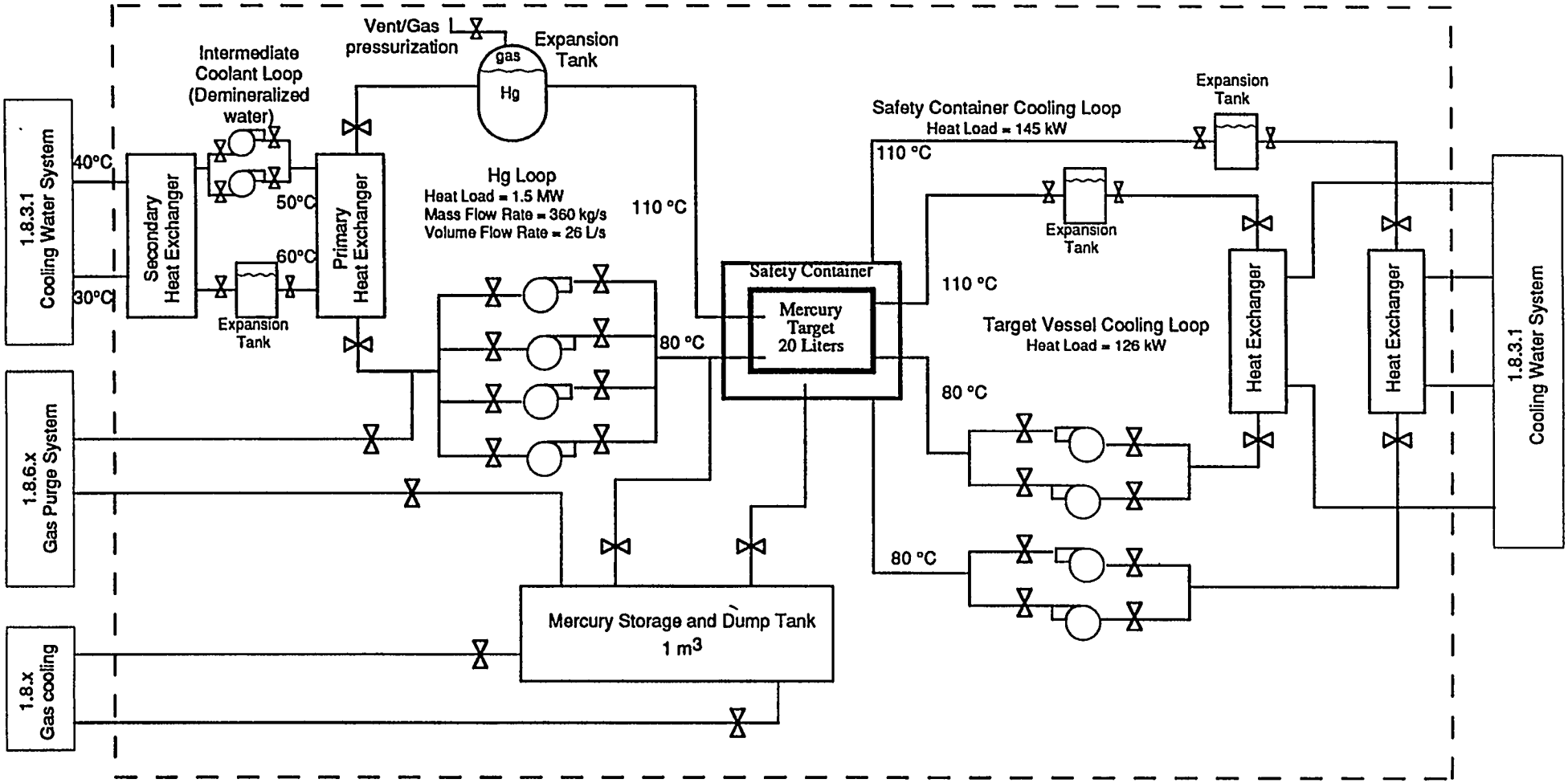

1.6.1.2.1 Liquid Target Vessel
1.6.1.2.2 Safety Container
1.6.1.2.3 Liquid Target Flow Loop
1.6.1.2.4 Vessel Coolant System
1.6.1.2.5 Safety Container Coolant System
1.6.1.2.6 Intermediate Coolant Loop

JRH
2/28/96

Why Use a Liquid Target?

- High heat removal capability - convective transport with a flowing liquid

- No structural radiation damage to the target material - target material is reusable

Why Mercury?

- Liquid at ambient temperatures
- High neutron yield (high atomic number)
- High density leading to high source brightness
- Some materials compatibility information exists
  - Should not be a limitation at low temperatures
- Easy to purify
- No extremely long-lived isotopes
- High thermal neutron absorption
  - May be an advantage for the type of experiments proposed for a pulsed source

ornl

Critical Issues for the ORSNS Mercury Target

- Thermal shock
  - Pressure pulse in Hg
  - Thermal shock of structural material
  - Need for He injection and if needed, how do we inject the He?
- Steady state power handling
  - Hot spots caused by recirculation zones
  - Cooling of target wall/window material
- Radiation damage to structural enclosure materials
- Compatibility between Hg and other Target System materials
- Helium and hydrogen solubility in Hg
- Wetting of Hg
- Low-energy cross-sections for Hg

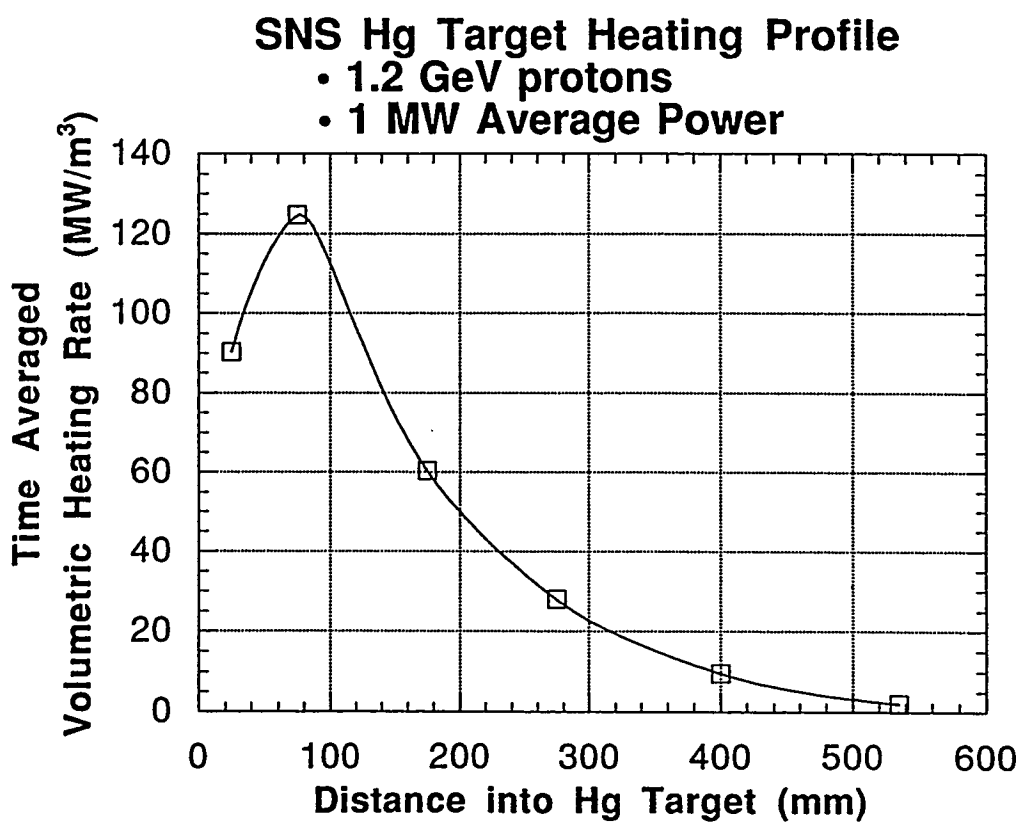

Thermal Effects During a Single-Pulse

- Mercury target volume ~ 20 L
- Repitition rate = 60 Hz

Proton Beam Power (MW)	Power Density (MW/m^3)		Energy Density (MJ/m^3)		Temperature Rise (K)	
	Ave	Peak*	Ave	Peak*	Ave	Peak*
1	50	195	0.83	3.25	0.44	1.72
2	100	390	1.67	6.50	0.88	3.44
5	250	975	4.17	16.25	2.20	8.60

* Includes an additional peaking factor of 1.5

"Thermal Shock" Is Caused By the Intense Heating Pulse

- Let's examine some characteristic time scales:
- Speed of sound for Hg = c_{Hg}~ 1,450 m/s
  - Characteristic time for a compression wave to travel through the target = t_s ~ 0.05 m / 1450m/s ~ 50 μs
- Residence time for Flowing Hg
  - Flow length ~ 1 m, Velocity ~ 2 m/s
  - Residence time = t_r ~ 0.5 s --- Hg is in the target for ~ 30 pulses
  - Time scale for heating = $t_{on} << t_r \Rightarrow$ Hg is essentially static during the heating process
- Since $t_{on} << t_r$ or t_s, the fluid cannot expand during the heating process $\Rightarrow$ isometric process $\Rightarrow$ volume remains the same, pressure increases
- Pressure wave propogates through the mercury

ornl

Thermal Shock Loads Are A Concern

- During the short-time scale associated with the beam pulse (~ 0.5 μs), the fluid cannot expand
- The local pressure increase associated with this compression of the fluid is given by:

$$\Delta P = \Delta T \ \beta / \kappa$$

β = coefficient of volume expansion = 1.8×10^{-4} /K for Hg
κ = isothermal compressibility = 4×10^{-5} /MPa for Hg

Proton Beam Power (MW)	Peak Temp Rise (°C)	Virtual Volume Change, ΔV/V (%)	Peak Pressure Rise (MPa)
1	1.7	0.03	8
2	3.4	0.06	15
5	8.6	0.15	39

- If this load is static and appears everywhere in the target, the structure will fail at 5 MW (Stress ~ 390 MPa compared to a yield stress of 210 MPa for 316 SS)
- The damping of the pressure pulse in unheated regions of the target and dynamic nature of the load tend to mitigate this loading condition
- Tests and analysis of this problem are required to examine this phenomenon and determine the feasibility of using a liquid target with this type of cyclic loading
- Using helium gas bubbles has been proposed as a possible solution to this problem

ornl

SNS Mercury Target System Design and Fabrication

Task	FY 96	FY 97	FY 98	FY 99	FY 00	FY 01	FY 02
Conceptual Design							
Preliminary Design							
Final Design							
Procurement and Fabrication							
Installation and Checkout							

Mercury Target System Development

R&D Tasks	FY 96	FY 97	FY 98	FY 99	FY 00	FY 01	FY 02
Thermal-hydraulic tests and analysis							
CFD Simulation of target							
Create central mercury handling facility							
Develop Hg diagnostics and instrumentation							
Flow distribution tests (water)							
Mercury thermal hydraulic parameter tests							
Full-scale mercury tests (no pulsed heating)							
Thermal shock tests and analyses							
Pressure Pulse Tests							
Thermal Shock Tests on ORELA							
Benchmark model analyses of mercury target							
Cyclic Shock Evaluations							
Thermal Shock Mitigation Tests and Analyses							
Erosion/corrosion tests and analyses							
Planning and design of corrosion tests							
Procure/Install corrosion loop							
Shakedown/Startup of corrosion loop							
Perform corrosion tests							

Near-Term Hg R&D Efforts

- Pressure pulse tests - benchmark thermal shock models
- Thermal shock and power handling tests on ORELA
- Start thermal-hydraulic calculations in preparation for testing
- Materials compatibility tests can easily be included as part of these efforts

Hg Pressure Pulse Testing

- Create localized pressure pulse
  - Use an existing ORNL/FED gas gun to create a pressure pulse in a Hg containing vessel

    ---or---
  - Use an exploding wire
- Use strain gauges to measure response of the vessel and pressure transducers to measure response in Hg
- "Benchmark" with thermal shock models (ORNL & ESS?)
- Rationale for these tests:
  - Establishes credibility of models and verifies Hg equation of state
  - Hg handling experience
  - Simple, fast, and inexpensive - takes advantage of existing equipment

ornl

ORELA Experiment

- A small experiment (~ 1/10 scale) at ORELA may provide insight on many of the critical issues for a Hg target
- ORELA parameters

  Electron energy ~ 150 MeV
  Energy per pulse ~ 30 J
  Pulse duration ~ 30 ns
  Beam size ~ 5-10 mm diameter
  Rep rate ~ 600 pulses per second

- Effective range of EM cascade for 150-MeV electrons in Hg is ~ 100 mm
- A Hg target with dimensions of 10 mm x 10 mm x 100 mm can be used in ORELA

Parameter	ORSNS Target*	ORELA Target
Volume (L)	20	0.01
Energy per pulse (J)	3.3×10^4	30
Energy density (MJ/m^3)	1.7	2-3
Avg. Power Density (MW/m^3)	100	up to 1,800
Pulse Duration (μs)	0.5	0.03
Characteristic time for sonic speed (μs)	3.5	3.5

* 2 MW average beam power

Conclusion: We can achieve the desired temperature rise per pulse (thermal shock) and steady state heating conditions

Concern:
- Reduced scale size makes extrapolation to the SNS difficult - must use this experiment to improve understanding of physical processes and "benchmark" models

Concluding Remarks

- Liquid mercury is an attractive ORSNS target material
  - Liquid at room temperature
  - High heat removal capability
  - High neutron yield and source brightness
- A mercury target design concept and its associated R&D issues are being identified
- Thermal shock of the mercury and its resulting mechanical loading of the target wall is an especially critical issue
- An experiment in ORELA or high energy electrical discharge testing are under consideration as means for simulating the intense heating
- If required, injection of helium bubbles must be examined as a means for mitigating the thermal shock effects

ornl

SESSION 11

R&D Needs and Options (2)

Chairman
Y. Gelfgat

International Workshop on the Technology and Thermal Hydraulics of Heavy Liquid Metals
25.-28. 9. 1996
Schruns, Austria

Heavy Liquid Metals : Research programs at PSI

Y.Takeda PSI

R & D programs at PSI under way for thermohydraulics, thermal shock and material test for mechanical properties. In the presentations the following two parts were focused:

A : SINQ LBE target
B : ESS Mercury target

SINQ LBE Target : The phase II study program for SINQ is planned. A new LBE loop is being constructed. The study has following three objectives:

Pump study : In order to ensure a flow of LBE inside the double tube container, especially for a higher flow velocity around the window, and to maintain a continuous flow during the beam interruption, an Electromagnetic pump is considered to be integrated into a SINQ target. Due to its relatively low efficiency, various types, shapes and configurations of EM pump are to be tested.

Heat pipe performance test : An idea to use heat pipes in the target cooling system is for decoupling the primary liquid metal circuit and the secondary water cooling circuit, which may be beneficial to attain a larger safety margin for the radioactive system in the event of water laekage into a high temperature liquid metal. The theoretical study of construction of the heat pipes are under way and the prototype heat pipe will be fabricated. The performance test is planned in the test loop.

Mixed convection experiment : In order to find an optimal configuration of the additional flow guide for window cooling, mixed convection around the window is to be studied. The experiment will be started using water and then with LBE.

ESS Mercury target : For ESS target study, the following experimental studies are planned, some of which are exampled by trial experiments. This includes following studies:

(1) Flow around the window : Flow mapping around the hemi-cylindrical window will be made for optimising the flow channels and structures,

(2) Geometry optimisation for minimizng a recirculation zone behind the edge of the flow separator,

(3) Flow induced vibration and buckling problem for a optimised structure of the flow separator and

(4) Gas-liquid two-phase flow will be studied by starting to establish the new experimental method of measuring various kinds of two-phase flow characteristics.

R & D Programs at PSI

Thermohydraulics

Numerical	**ASTEC, FLOW3D**	**T. Dury, (B. Smith)**
Experimental	**Water, Hg,**	**Y.Takeda**

Thermal shock **ANSYS + DYNA** **L.Ni**

Material study - Mechanical properties

Hg, Stationary, with Flow **Y.Dai**

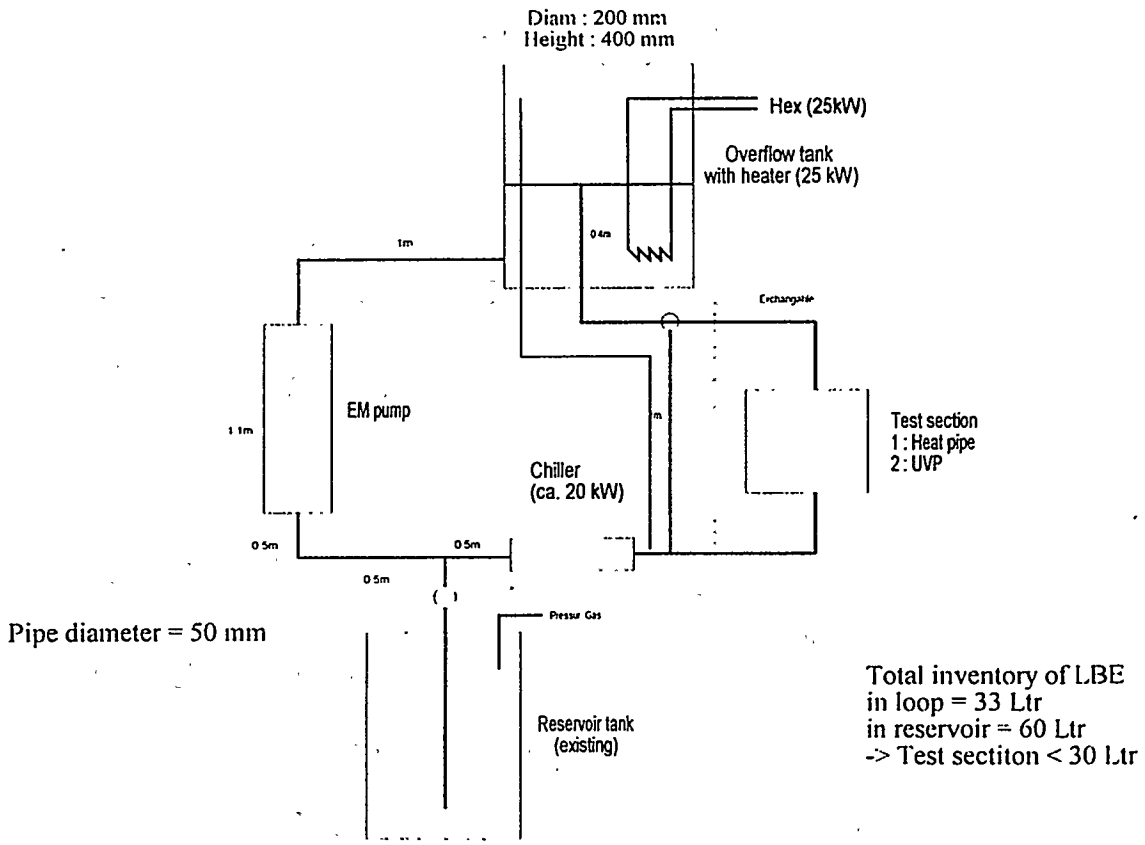

An illustration of the planned LBE loop for the phase II study of SINQ target.

SINQ liquid metal target with integrated EM pump

EM Pump is a linear induction type.
A coil section might be designed as two cylindridal shells, which are detachable to the side. A return path is by two connecting legs between the top plenum and the lower section.
By this configuration, the EM pump can be integrrated into the SINQ LM target without immersing this component in the radioactive liquid.

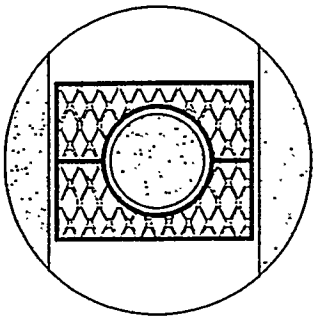

A-A'

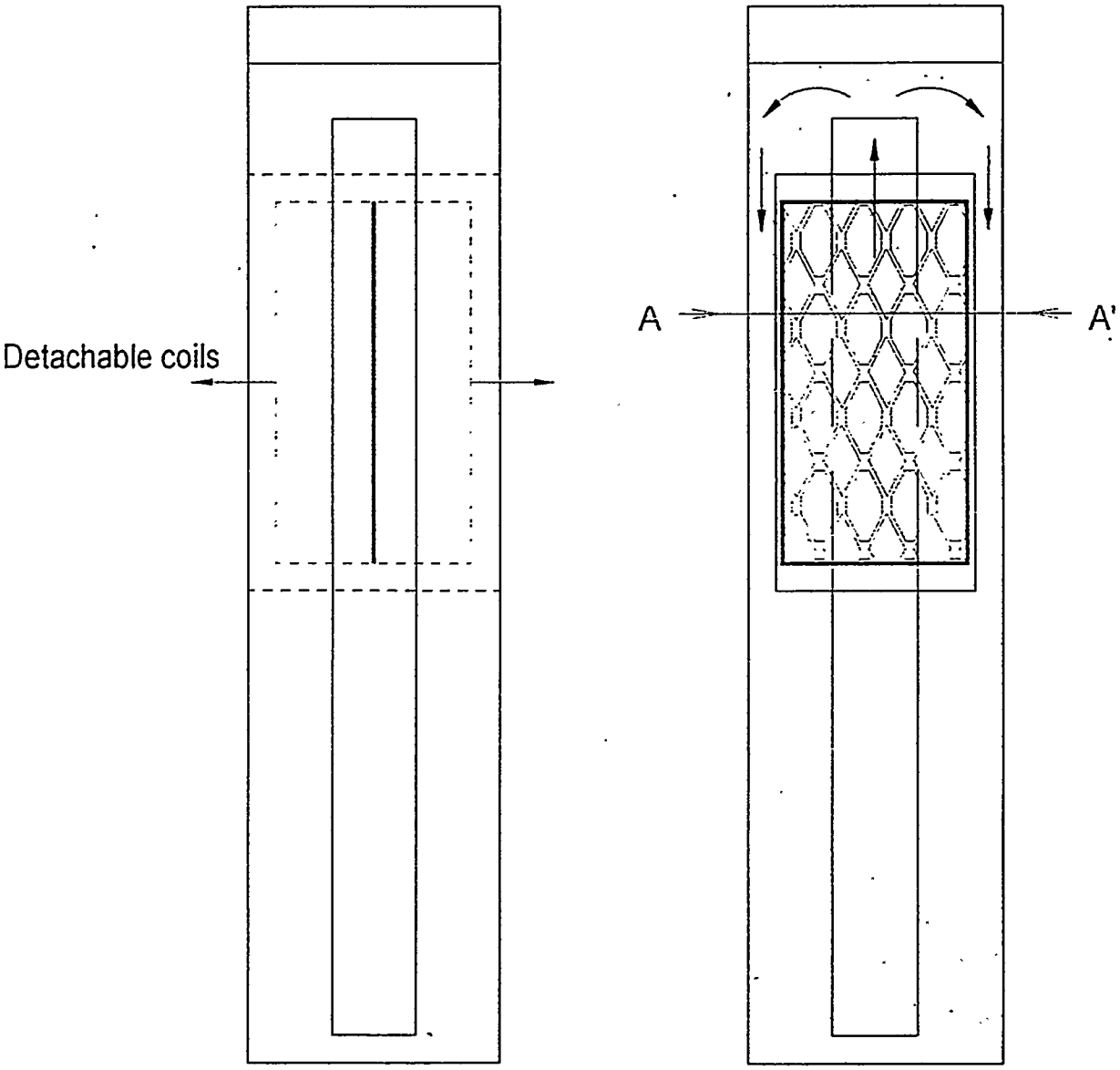

SINQEM.skd

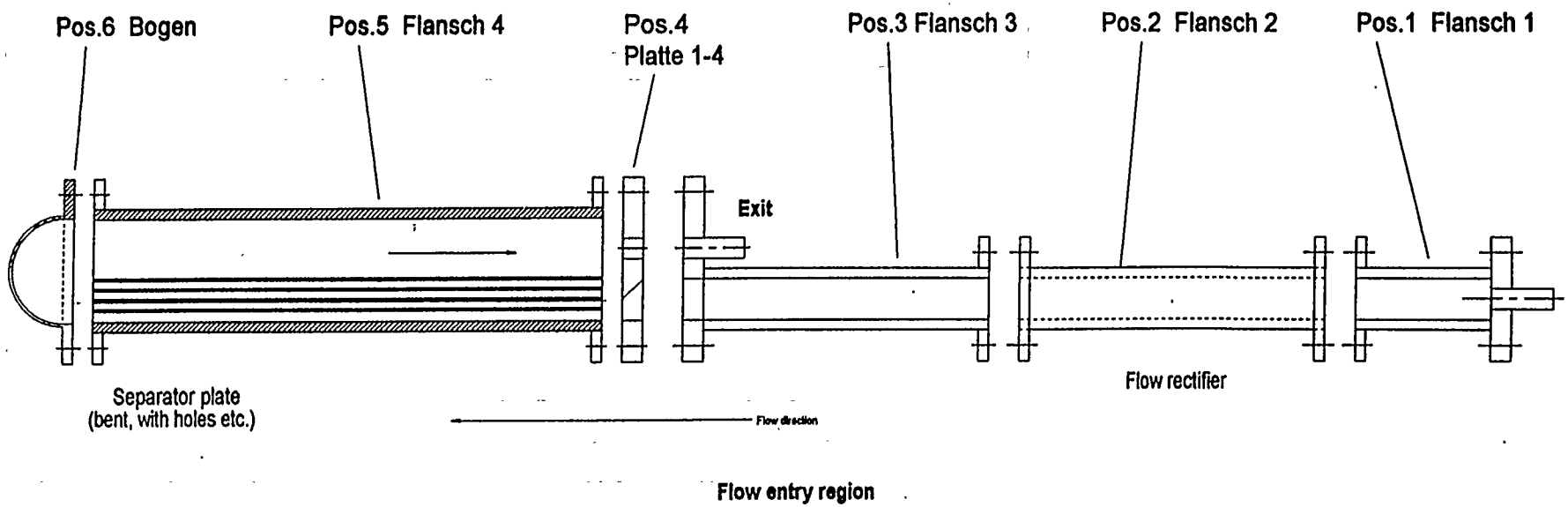

A water model for ESS horizontal target : Flow study around the hemi-cylindrical window.

ESS - TARGET

30 5 95 mh

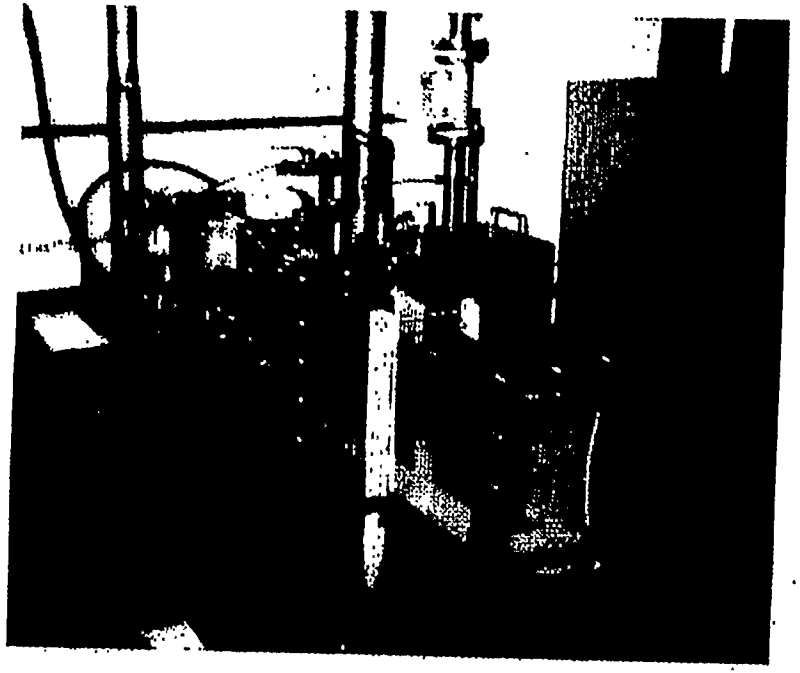

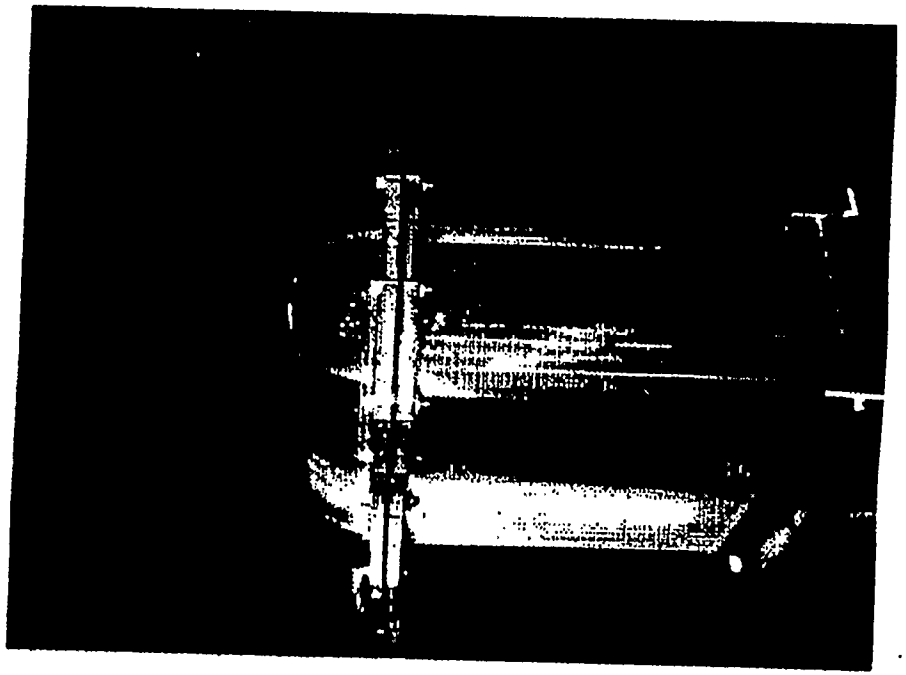

A water model for ESS horizontal target : Flow study around the hemi-cylindrical window.

Flow Mapping - UVP

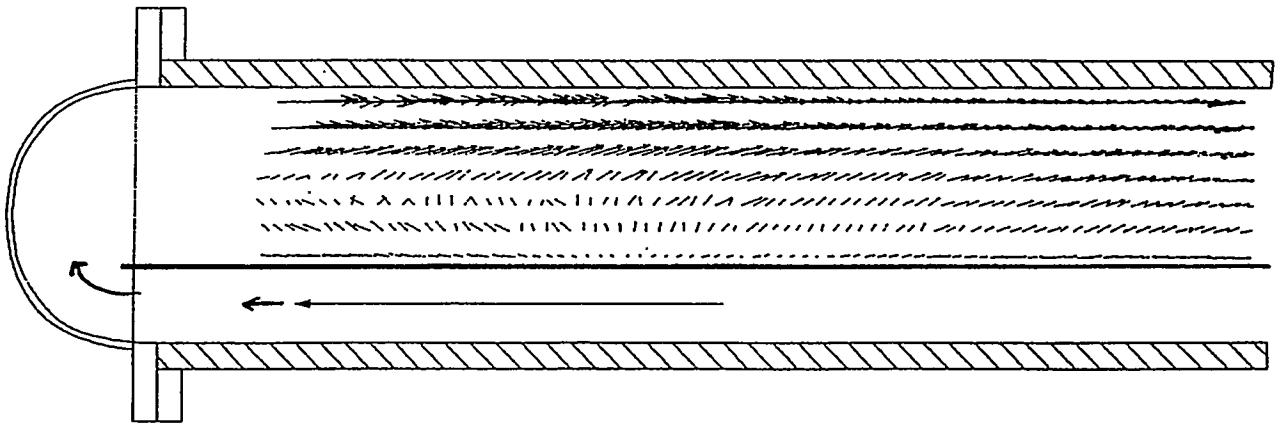

An example of a flow mapping on the recirculation in a water model for ESS horizontal target.

He-Hg Two-Phase Flow

Objective : To realize a homogeneously dispersed flow (He in Hg)

What have to be done :

Method of bubble generation
Metliod to study a distribution of bubbles
Influence of flow geometry on the distribution

Strategy :

Water experiment : Visualization + Ultrasound method
Hg experiment : Ultrasound method

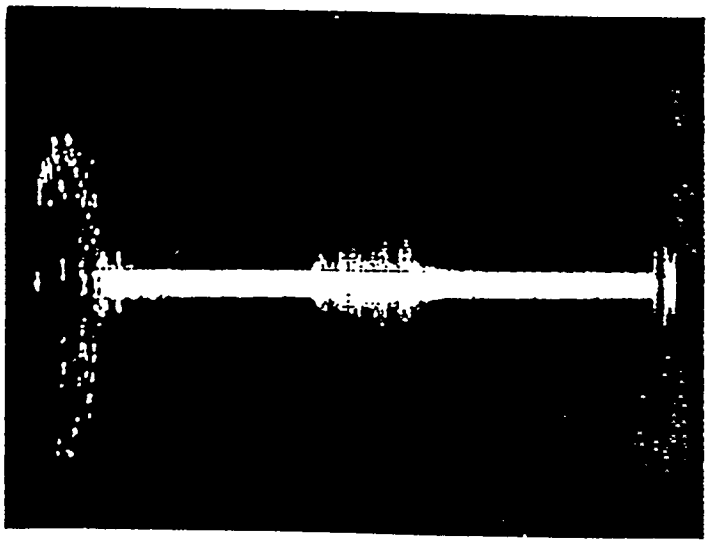

Echo signals reflected by bubbles in a bubbly sheet. Top to bottom at various heights above the bubble generator. The bubbly sheets is widened as rising.

Observation of gas bubble behaviour in flowing liquid metal

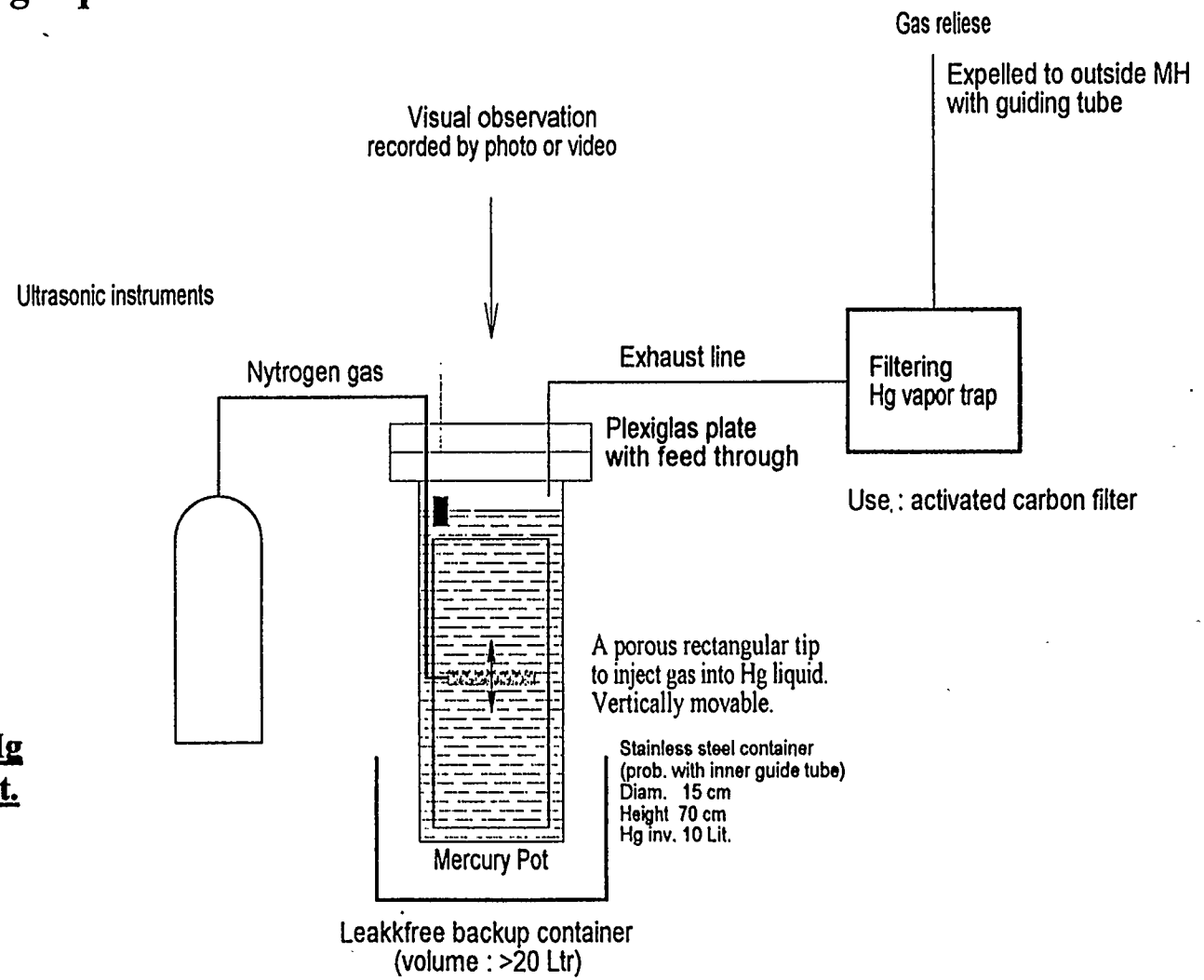

Illustration of the experimental setup for He-Hg two-phase flow measurement. (under construction)

LM2P01.skd

LM-Research opportunities and activities at Beer-Sheva

S. Lesin

Solmecs (Israel) Ltd/Center for MHD Studies
Ben Gurion University of the Negev
P.O. Box 653
Beer Sheva, 84105, Israel

For the
Workshop on the Technology and Thermal Hydraulics of Heavy Liquid Metals
March 24 - 28, 1996

EXTENDED ABSTRACT

Energy conversion concepts based on liquid metal (LM) magnetohydrodynamic (MHD) technology was intensively investigated at the Center for MHD Studies (CMHDS), in the Ben-Gurion University of the Negev in Israel.

LMMHD energy conversion systems operate in a closed cycle as follows: heat intended for conversion into electricity is added to a liquid metal contained in a closed loop of pipes. The liquid metal is mixed with vapor or gas introduced from outside so that a two-phase mixture is formed. The gaseous phase performs a thermodynamic cycle, converting a certain amount of heat into mechanical energy of the liquid metal. This energy is converted into electrical power as the metal flows across a magnetic field in the MHD channel. The thermodynamic working fluid after separation from the LM is reversed to initial conditions by cooling, pumping and heating.

Those systems where the expanding thermodynamic fluid performs work against gravitational forces (natural circulation loops) and using heavy liquid metals are named ETGAR systems.

The development of the ETGAR technology, which began in 1980 at the CMHDS and supported by Solmecs Israel Ltd., includes the following R&D activities:

1. Investigation of Physical Phenomena, mainly two-phase flow (liquid-gas), mixing, separation, wetability, boiling, MHD and turbulence.

2. Development of a Universal Numerical Code for the Two Phase flow data analysis, Parametric Studies, Optimization and Design of the systems.

3. Material studies, mainly corrosion in liquid lead.

4. Building and testing small and medium-scale systems.

A number of different heavy-metal facilities have been specially constructed and tested with fluid combinations of mercury and steam, mercury and nitrogen, mercury and freon, lead-bismuth and steam and lead and steam.

The pipe diameters vary from 2.7 cm to 20.3 cm. Since the experimental investigation of such flows is a very difficult task and all the known measurement methods

are incomplete and not fully reliable, a variety of experimental approaches have been developed. In most experiments, instantaneous pressure distributions along the height of the upcomer were measured and the average void fraction was calculated numerically using the one-dimensional equation for the two-phase flow.

The research carried out at the CMHDS led to significant improvements in the characterization of the two-phase phenomena expected in the riser of ETGAR systems. One of the most important outcomes is the development of a new empirical correlation which enables the reliable prediction of the velocity ratio between the LM and the steam (slip), the friction factor, as well as of the steam void fraction distribution along the rizer.

In view of the importance of reducing the size of the bubbles for maintaining a small slip ratio, a number of studies have been undertaken, investigating a means to influence the liquid-gas interface phenomena (surface tension, stability, etc.). The studies convincingly demonstrate the possibility of substantially influence the interface and thus lower the size of the bubbles.

The three hey components, the mixer, separator and MHD generator, have been intensively tested regarding their performance characteristics, prediction and optimization of design.

Mixers of different design were tested with a variety of working fluids. Two main questions have been addressed: (1) the possibility to influence the size of the bubbles along the height of the upcomer, and (2) minimizing pressure losses in the mixer. It turned out that no substantial differences in bubble size occurred when completely different mixer designs were used (mixers with injection in the opposite directions, etc.). It is possible to say that the two-phase flow has a very short "memory" about the conditions of its inception. The resulting conclusion was that preference should be given to a mixer design which minimizes the possibility of plugging by impurities. The jet mixer best fits this condition.

The separator of an ETGAR system has to provide a complete separation between the two phases while simultaneously preserving a maximal possible fraction of kinetic energy. Different types of separators were tested and analyzed. These include designs based either on gravitational forces or centrifugal forces (in which the flow rotates in a stationary structure). New separator designs which offer attractive performance were developed.

Several engineering problems regarding the handling of the liquid metal have been solved in the CMHDS together with selection of construction materials solutions resulting from the operation of the mentioned experimental systems.

As a conclusion it can be said that great R&D opportunities are existing in the CMHDS by using the existing experimental systems and the wide experience gained in handling heavy liquid metals.

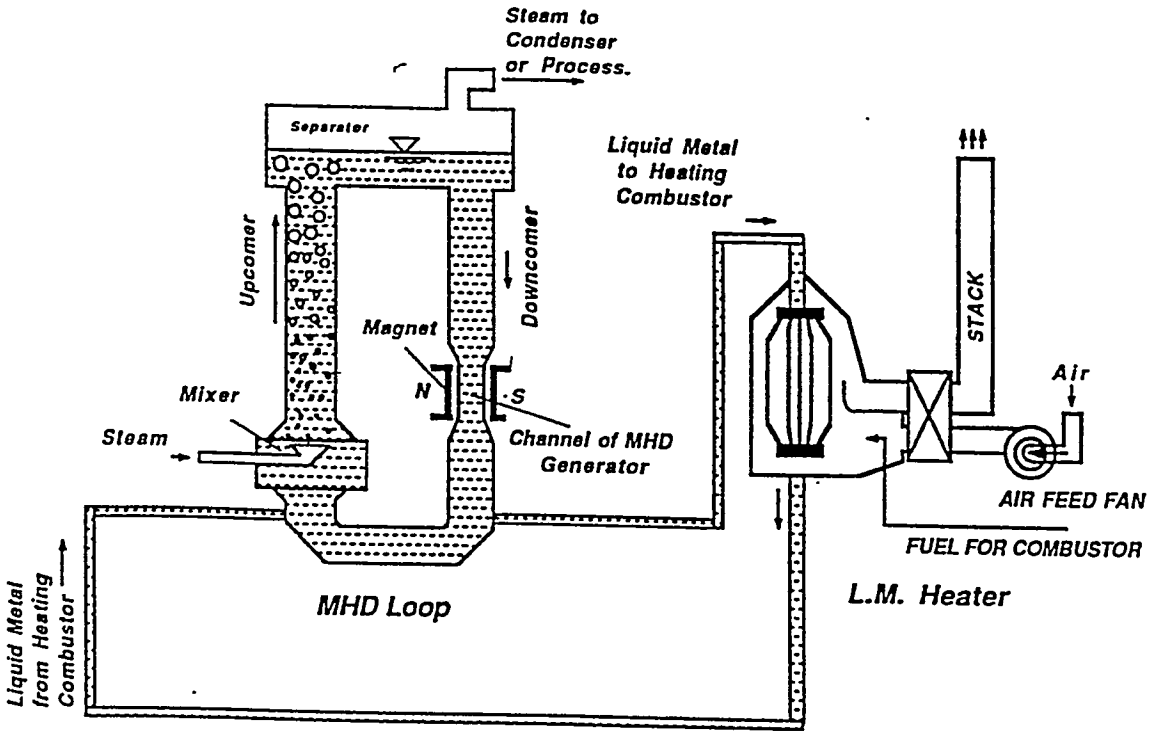

GENERAL SCHEMATIC OF THE ETGAR LMMHD POWER CONVERSION PLANT

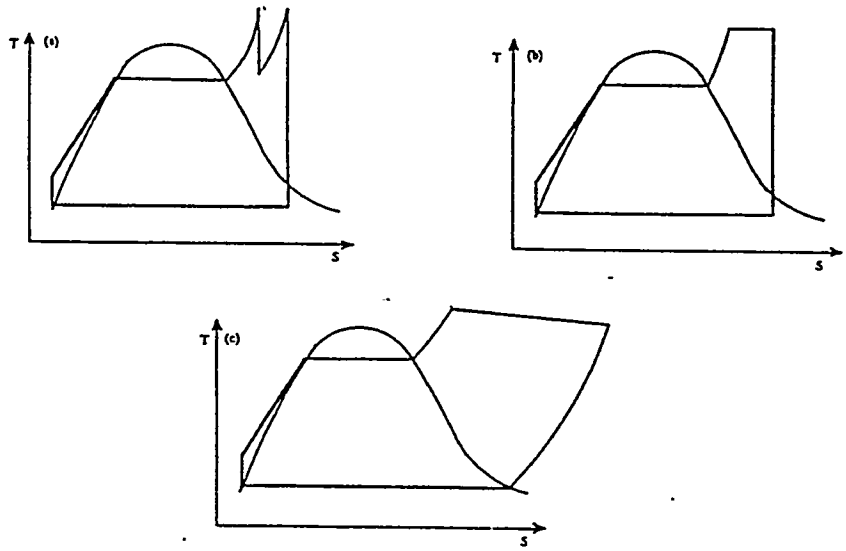

T-S Diagrams for 3 Versions of a Rankine Type Thermodynamic Cycle:

(a) A Conventional Turbine Cycle with One Reheating Stage
(b) A Combined LMMHD/Steam Turbine Cycle
(c) All LMMHD Cycle

Main Research and Development Activities performed in the Center:

1. Investigation of Physical Phenomena , mainly:
   * Two Phase Flow
   * Mixing (liquid - gas)
   * Separation (liquid - gas)
   * Liquid Metal Wetability
   * Direct Contact Boiling (Vapor Explosion)
   * MHD
   * Turbulence

2. Development of a Universal Numerical Code for the Two Phase flow data analysis, Parametric Studies, Optimization and Design of the systems.

3. Material studies, mainly corrosion in liquid lead.

4. Building and testing small and medium-scale systems using the following fluids: Mercury, Water-Air, Mercury-Nitrogen, Mercury-steam, Lead Bismuth-steam and Lead-steam.

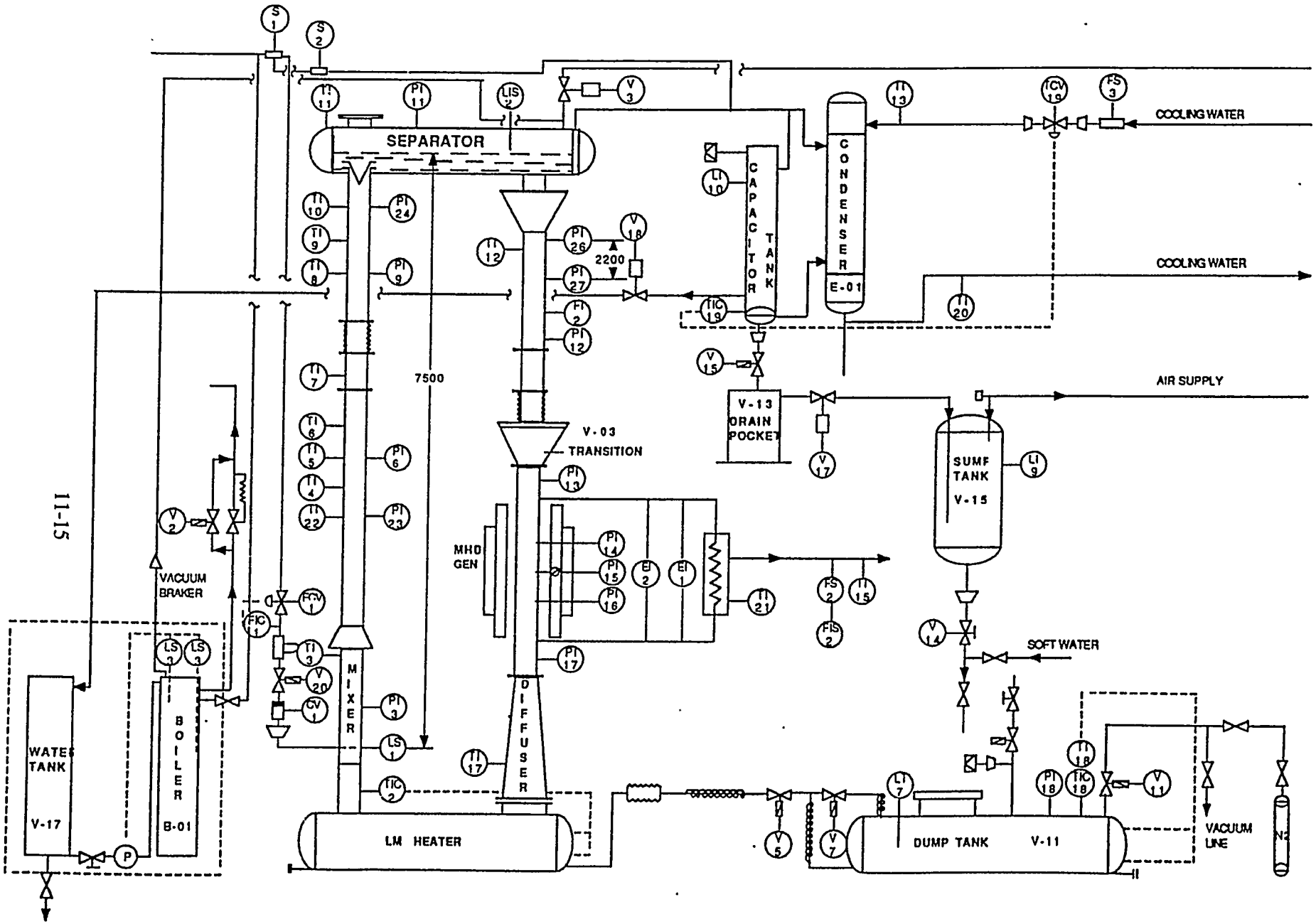

Lead/Bismuth - steam ETGAR-3 system P & ID

MERCURY-STEAM ER-4 SYSTEM P&ID

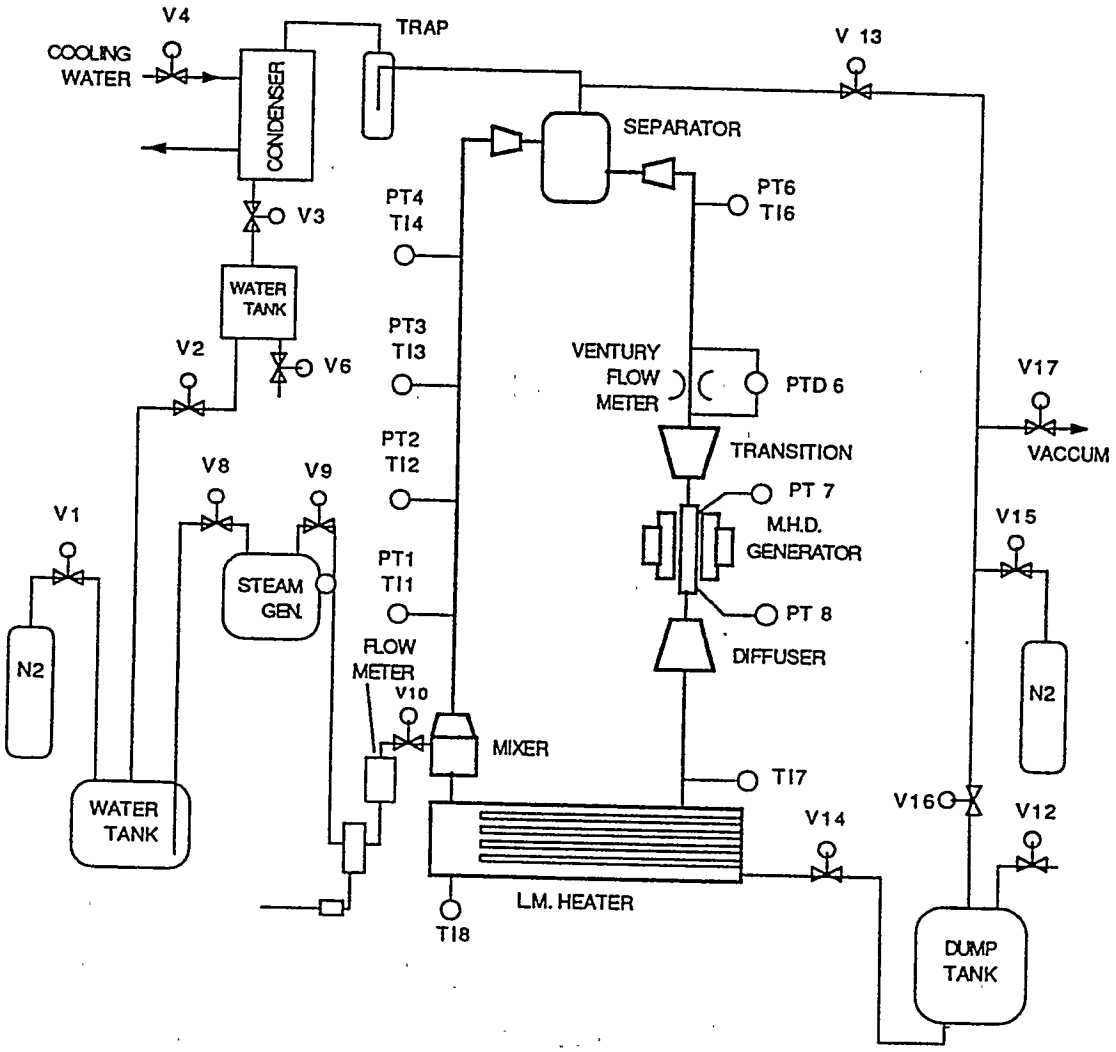

CHARACTERISTIC PARAMETERS OF THE EXPERIMENTAL SYSTEMS

ER-4 System Parameters

Liquid metal	Mercury
Volatile liquid	Steam
High temperature in cycle	431.3 K
Low temperature in cycle	338.6 K
Mixer pressure	5.34 bar
Thermal input	7.0 KW
Average void fraction in upcomer	0.3
Effective height of the system	5.0 m
Upcomer diameter	0.078 m
Downcomer diameter	0.078 m
MHD generator channel width	0.02 m
MHD generator electrode spacing	0.10 m
MHD geneator electrode length	0.35 m
Magnetic field	0-0.80 T

Etgar-3 System Parameters

Liquid metal	Lead Bismuth
Volatile liquid	Steam
High temperature in cycle	423 K
Low temperature in cycle	338 K
Mixer pressure	4.9 bar
Thermal input	97.5 KW
Average void fraction in upcomer	0.4
Effective height of the system	7.5 m
Upcomer diameter	0.203 m
Downcomer diameter	0.203 m
MHD generator channel width	0.06 m
MHD generator electrode spacing	0.15 m
MHD generator electrode length	0.525 m
Magnetic field	0-0.80 T

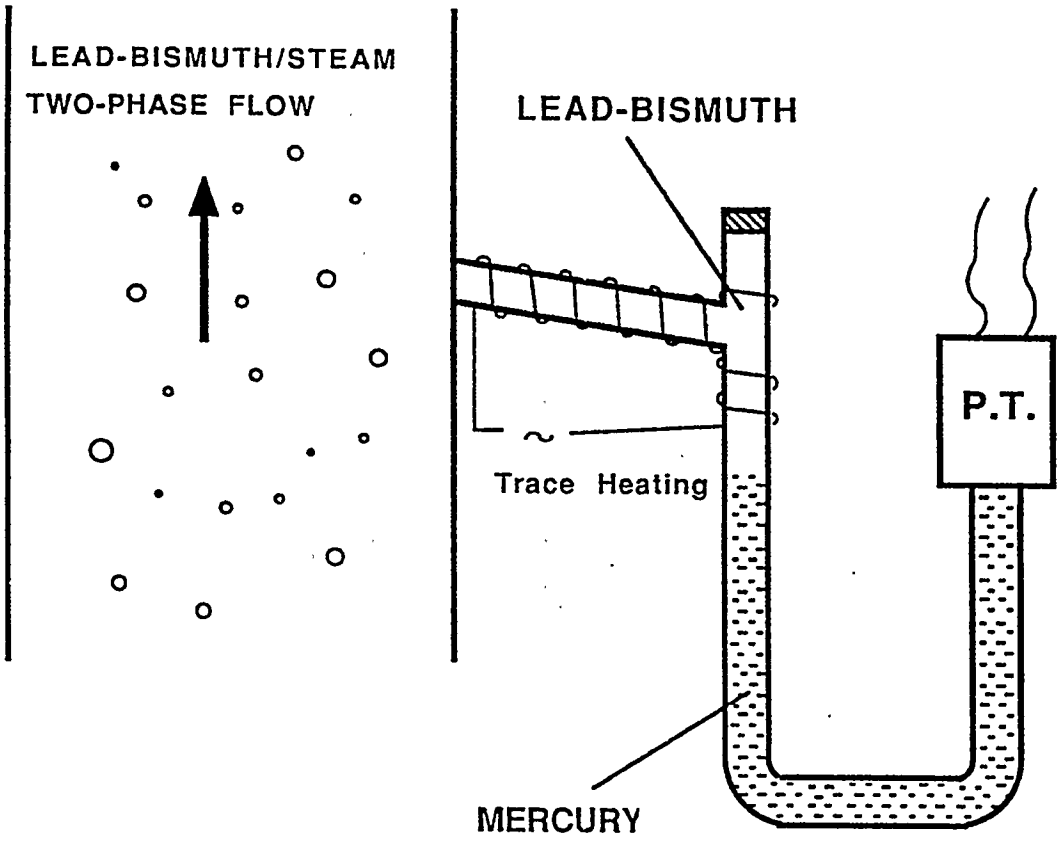

Pressure Measuring System at ETGAR 3

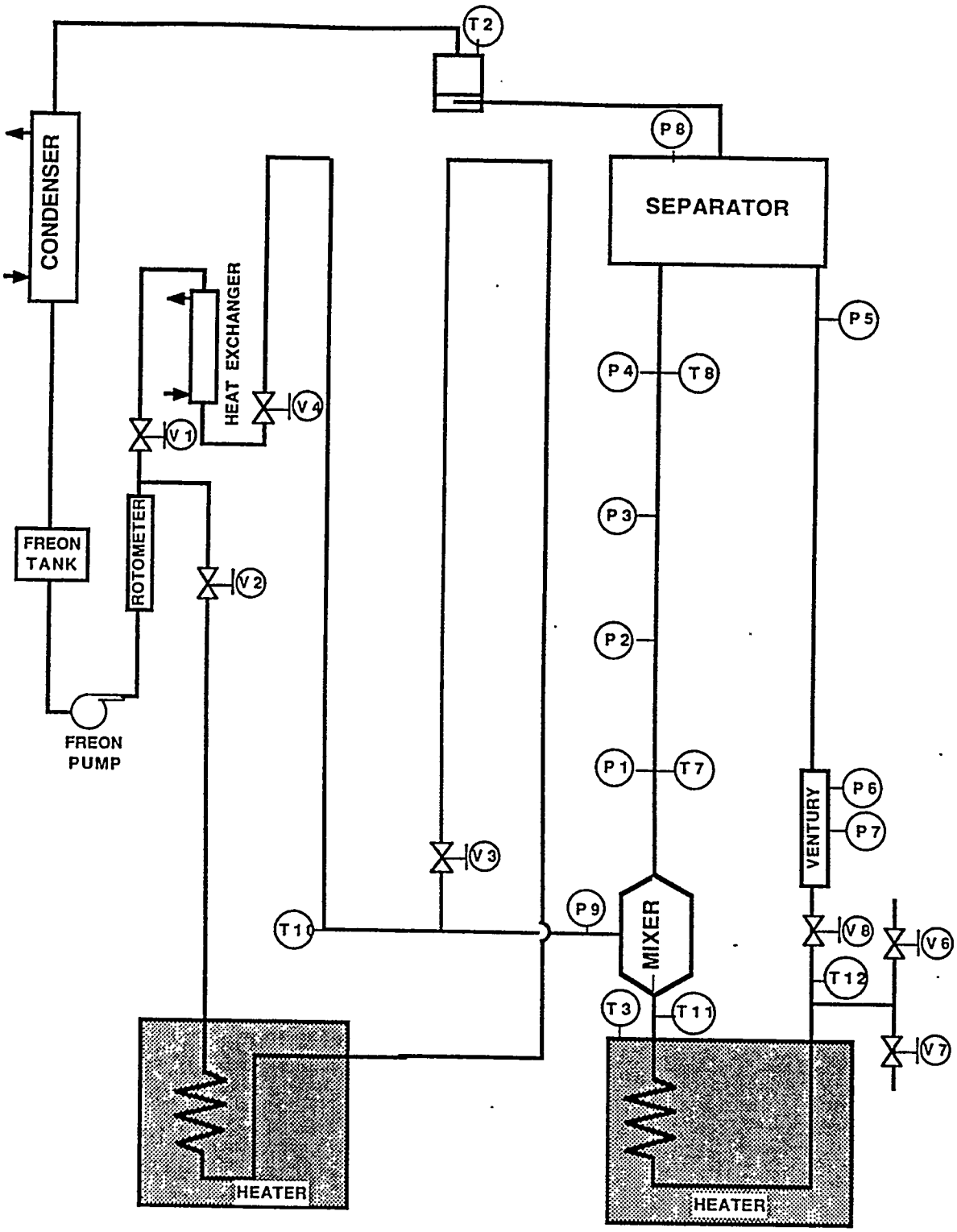

MERCURY FREON SYSTEM -R 113

Main Parameters of the Mercury Freon System

Liquid metal	Mercury
Volatile fluid	Freon
High temp. in cycle	90°C
Mixer Pressure	2.5 bar
Effective height	2 m
Upcomer diameter	20 mm

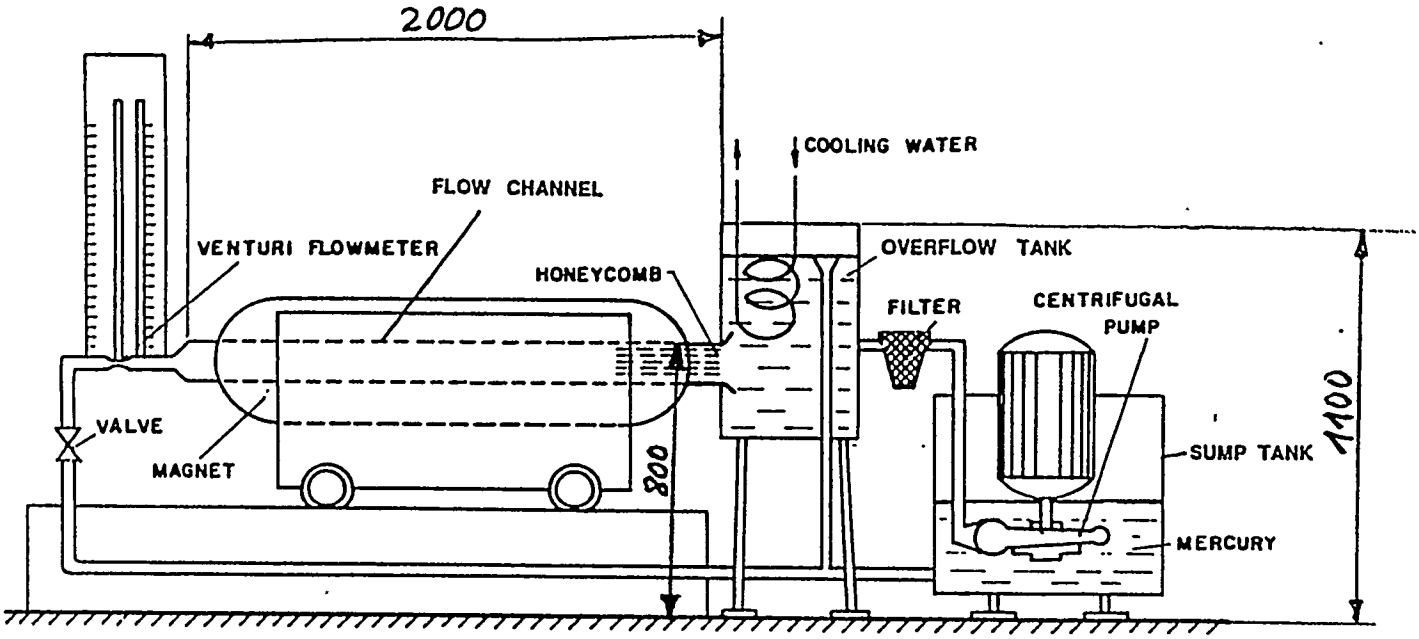

HORIZONTAL MERCURY LOOP

Main Parameters:

Liquid Metal	-	Mercury
Max. Flow Rate	-	24 liter/min.
Max Working Temp.	-	80 °C
Magnetic Field	-	0 to 1.1 Tesla
Electromagnet Pole Lenght	-	0.9 m

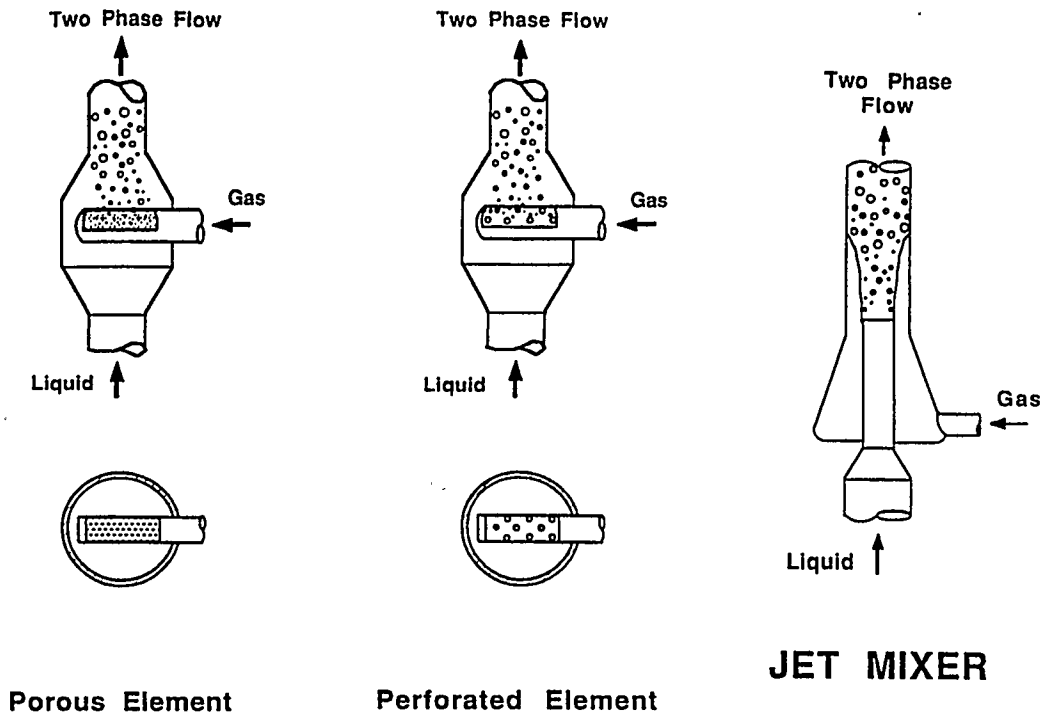

MIXERS USED

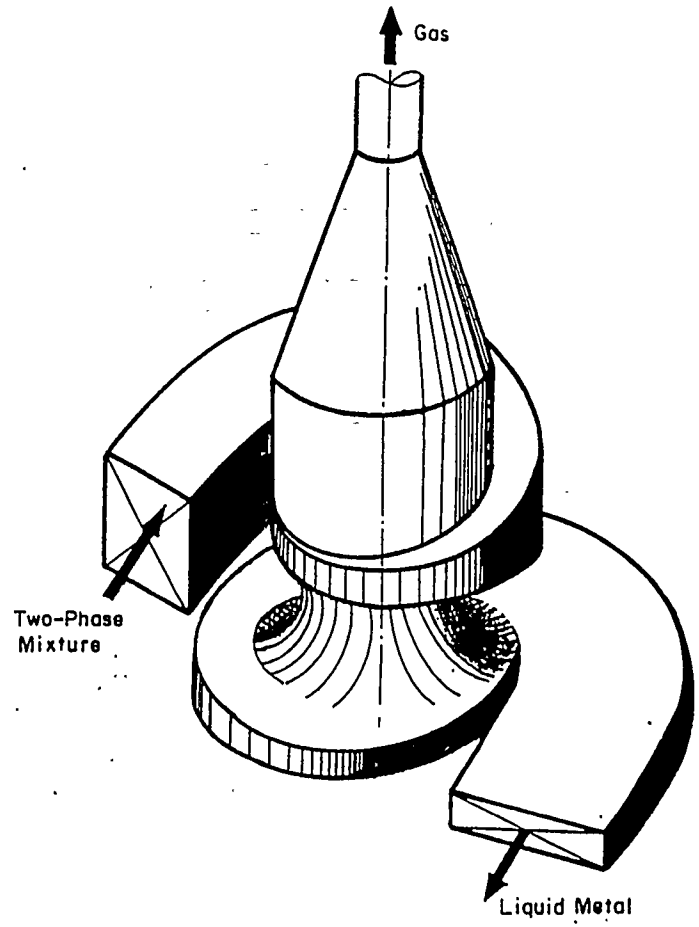

FIG. A.3. CENTRIFUGAL SEPARATOR

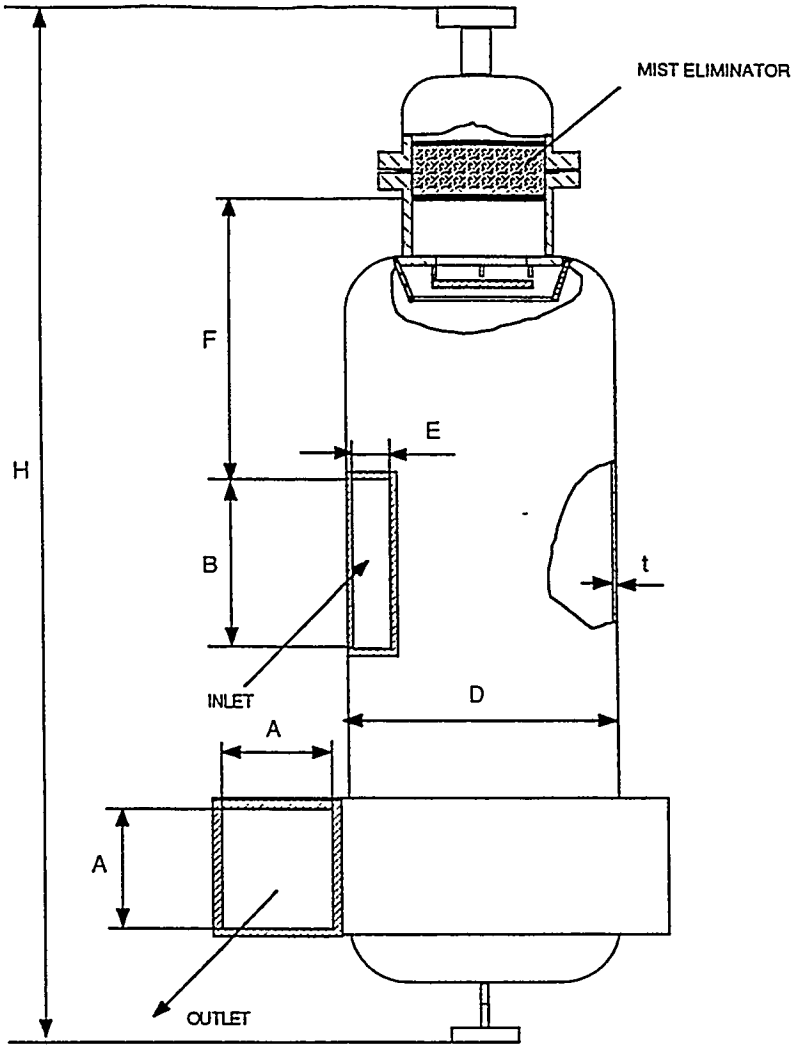

	A	B	C	D	E	F	t	H
STAGE-1	500	1000	650	900	250	500	31	3550
STAGE-2	550	1100	700	1000	300	500	18	3750
STAGE-3	550	1100	700	1000	300	500	8	3750

SEPARATOR-ETGAR 7

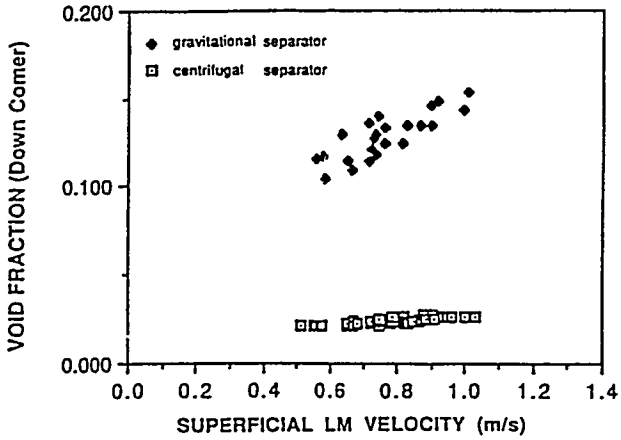

Comparison of performance between gravitational to centrifugal separator

The new void fraction empirical correlation developed at the CMHDS

$$Q_R = \frac{X\rho_L}{(1-X)\rho_G}$$ - the volumetric flow rate ratio (1)

$$Fr = \frac{V_{LO}^2}{gD}$$ - Froude number (2)

$$\mu_L/\mu_G$$ - viscosity ratio (3)

$$Re = \frac{\rho_L \cdot V_{LO} \cdot D}{\mu_L}$$ - Reynolds number (4)

$$We = \frac{V_{LO}^2 \cdot \rho_L \cdot D}{\sigma_L}$$ - Weber number (5)

The final void fraction correlation,

$$\alpha_{corr} = \left[1+0.27(Q_R)^{-0.69}(Fr)^{-0.177}\left(\frac{\mu_L}{\mu_G}\right)^{0.378}\left(\frac{Re}{We}\right)^{0.067} \right]^{-1} \quad (6)$$

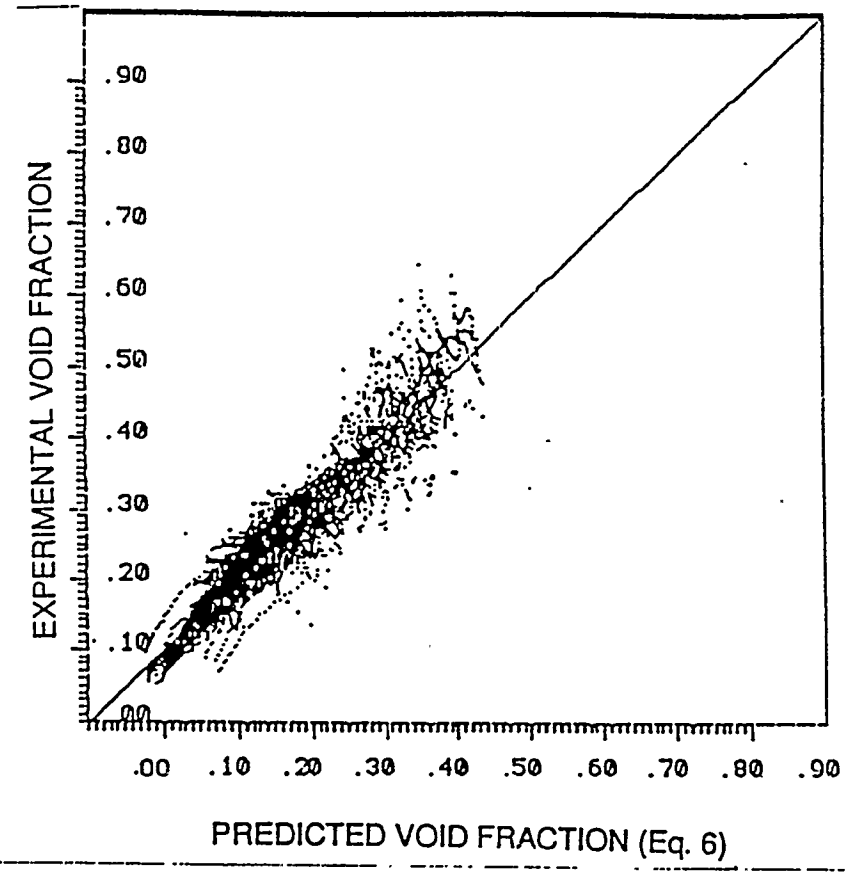

COMPARISON OF EXPERIMENTAL VOID FRACTION VALUES OF PRESENT WORK WITH VALUES CALCULATED BY THE PROPOSED CORRELATION.

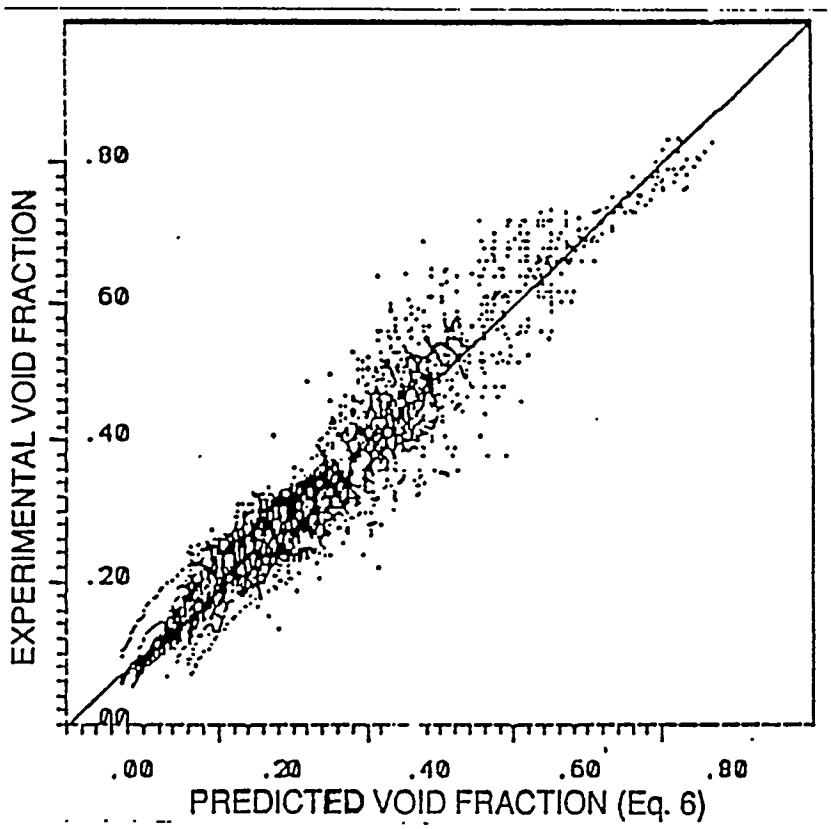

COMPARISON OF ALL DATA BANK WITH THE VALUES CALCULATED BY THE PROPOSED CORRELATION.

COMPARISON BETWEEN THE EXPERIMENTAL RESULTS AND THE PROPOSED VOID FRACTION CORRELATION

Facility and Fluids	Diameter [m]	V_{LO} [m/s]	Investigator	Number of Data Points	RMS value Proposed corr. %	RMS value of Serizawa %	RMS value of Sudo %
Water-Air + ER-4 + Etgar 3	0.044 0.078 0.203	0.273-1.6	Present work	6292	11.77	26.29	77.15
Etgar-3 Lead Bismuth -Steam	0.203	0.6-1.6	Present work	3458	10.87	22.98	33.43
ER-4 Mercury Steam	0.078	0.43-1.02	Present work	1118	14.94	32.98	173.21
Water-Air	0.044	0.273-1.5	Present work	1716	11.14	31.16	35.30
Mercury - N_2	0.0515	0.6-2.58	Unger et al. (1987)	138	17.46	16.95	39.29
Mercury - R113	0.019	0.48-0.84	Unger et al. (1987)	333	14.35	14.49	47.75
Water-Air	0.016-0.0635	0.26-0.87	Govier & L. Short (1958)	46	12.47	21.68	10.00
Water-Air	0.07	0.09-0.3	Smissaert (1963)	139	7.57	7.23	6.76
R113 - N_2	0.07	0.09-0.3	Smissaert (1963)	35	11.35	8.72	21.04
Mercury - N_2	0.0508	0.09-0.3	Smissaert (1963)	46	10.79	14.33	164.00
Total Data Bank	0.016-0.203	0.09-2.58	All	7029	11.97	27.36	77.15

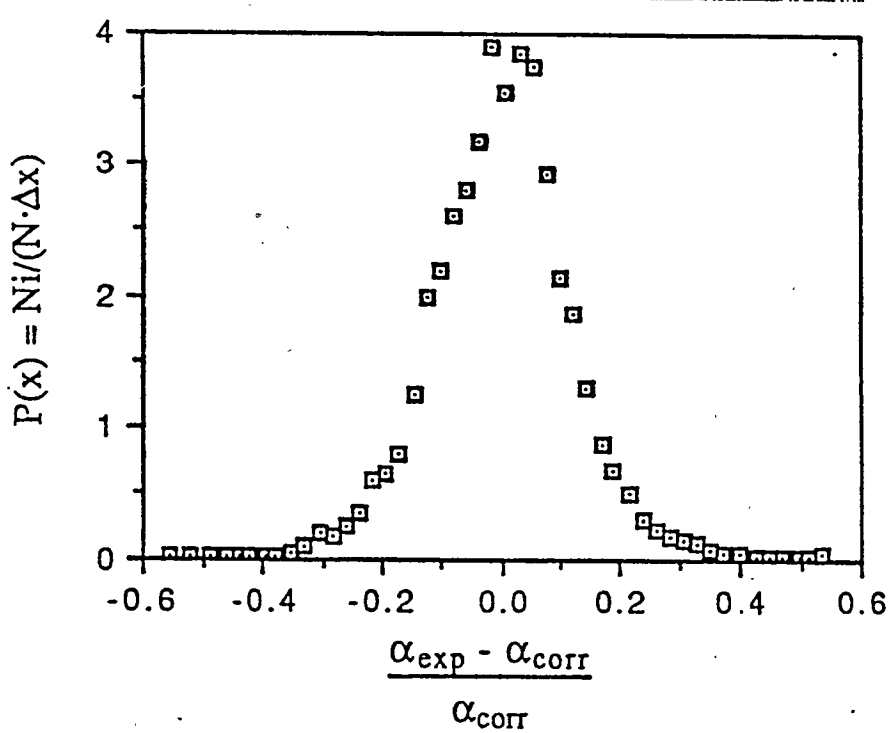

CHARACTERISTIC DEVIATION OF ALL DATA BANK FROM VALUES CALCULATED BY THE PROPOSED CORRELATION

Dynamic Surface Tension Measuring Apparatus

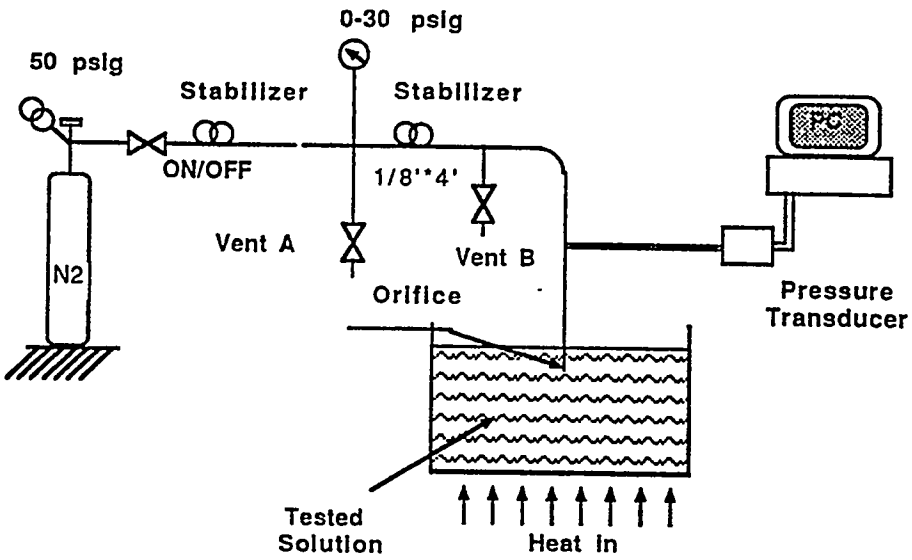

Bubble Growth and Minimum Radius (R')

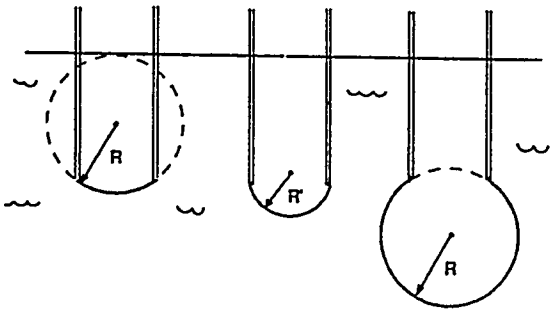

The Yaung-Laplace Equation :

$$P=P_o+P\ \frac{2\sigma}{R}$$

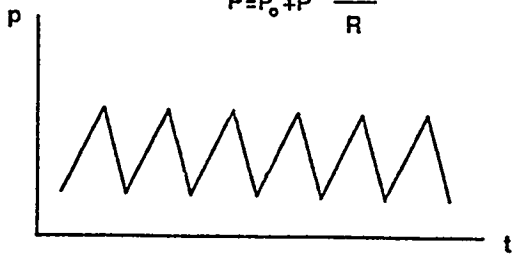

SURFACE ACTIVE ADDITIVES INFLUENCE ON THE SURFACE TENSION OF MELTED LEAD-BISMUTH

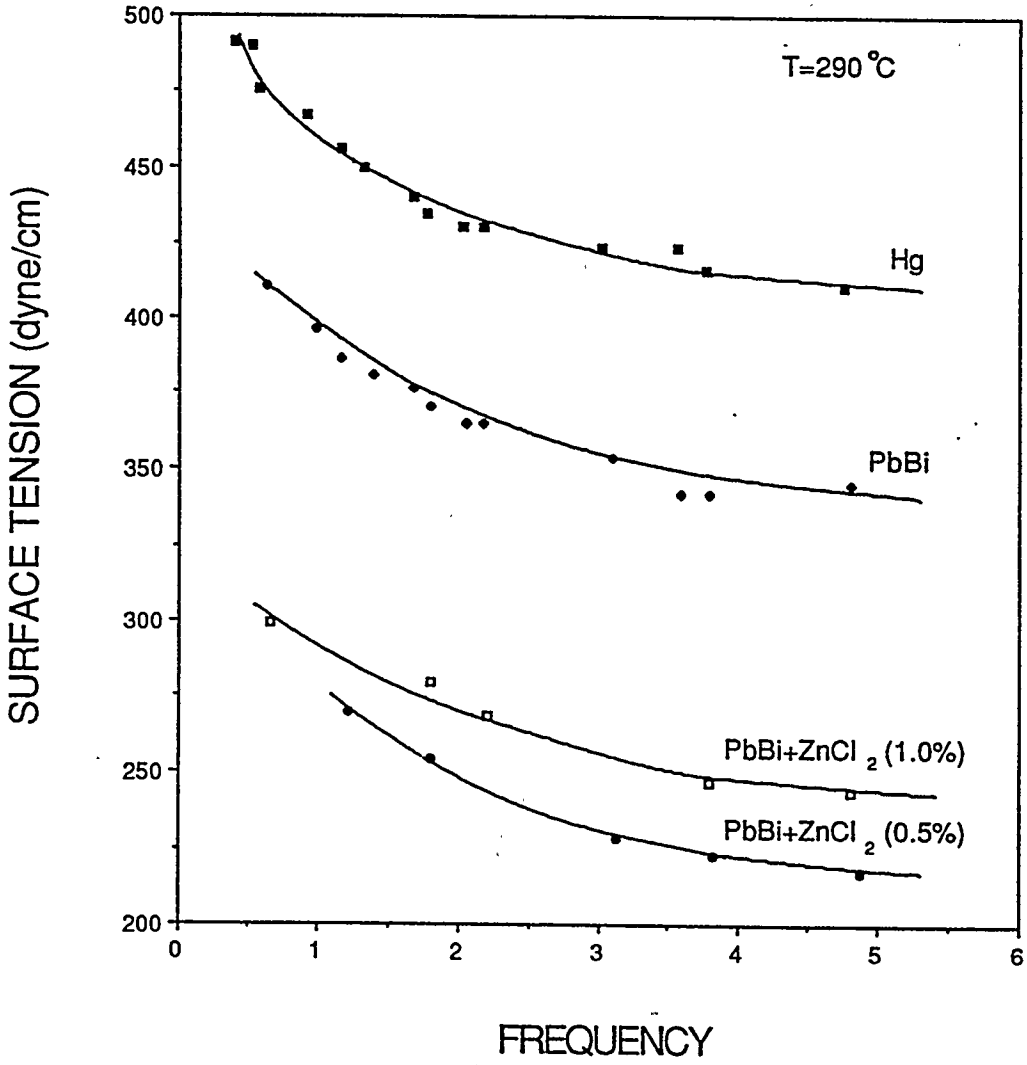

Corrosion of a structural materials in liquid lead flow

The rate of the metal dissolution

$$J_i = (0.01\, C_i/\alpha Pr^{3/4})\, a\omega\, (\nu / a^2\omega)^{1/10} \quad (g.cm^{-2}.s^{-1})$$

C_i- equilibrium solubility, $g.cm^{-3}$, $Pr = \nu/D$ (ν - is the kinematic viscosity of the liquid lead, D - diffusion coefficient of the metal (i) in liquid phase, $\alpha \approx 1$, ω - angular speed, a - the radius of the disc

Interconnection between solubility of some metals in lead at 800 K and their heat of sublimation

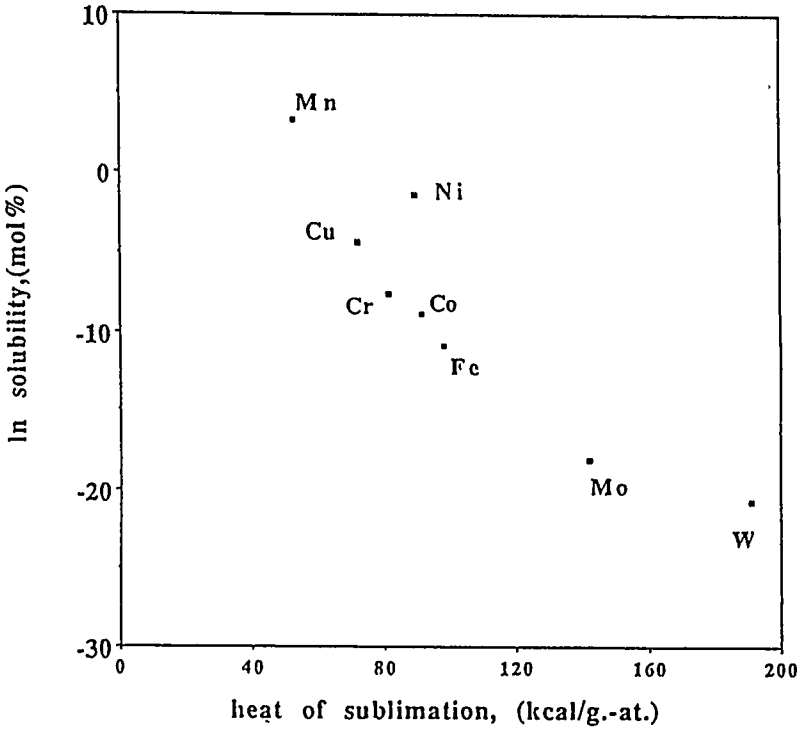

Oxygen equilibrium pressure in some metal-oxide systems

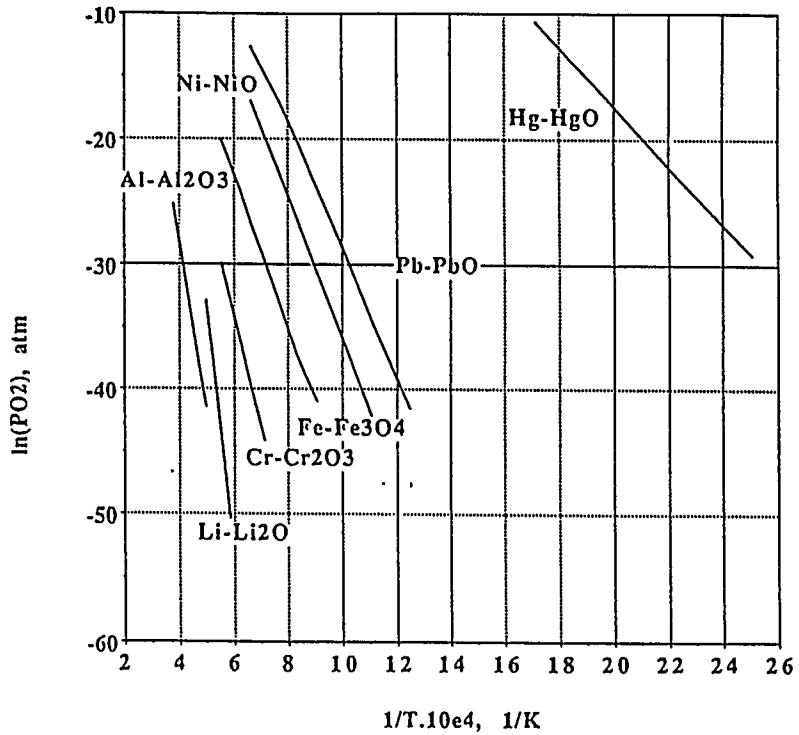

Schematic layout of the test facility

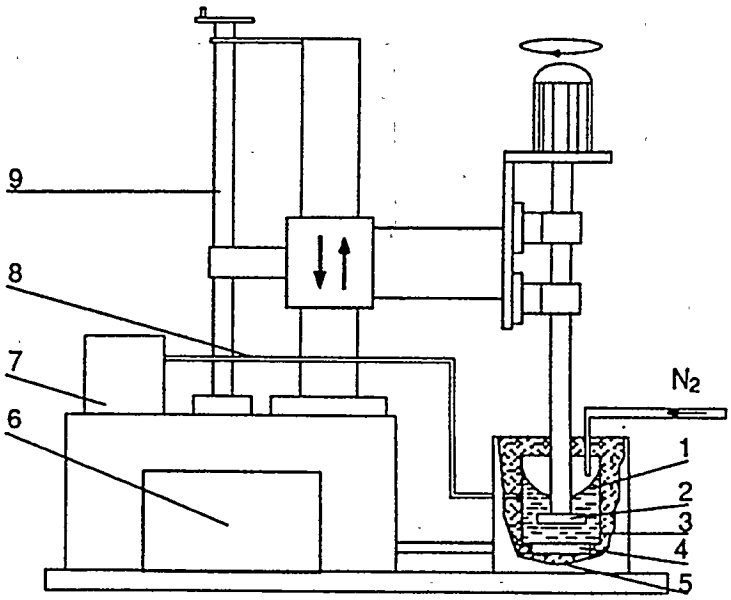

Figure 1 Schematic layout of the test facilities. 1-liquid lead, 2-sample, 3-crucible, 4-heater, 5-thermal insulation, 6-energy supply, 7-thermoregulator, 8-thermocouple, 9-screw rod.

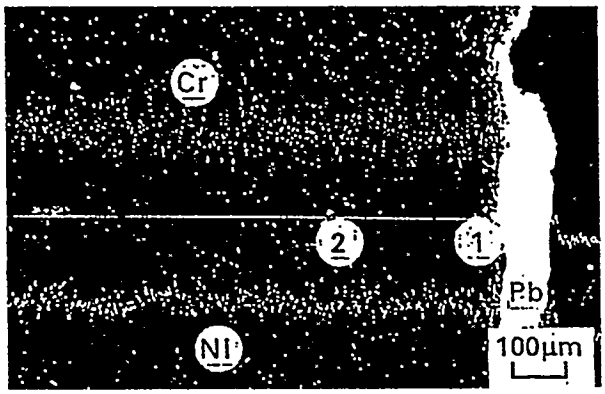

Figure 1 EPMA (wt %) of SS316 exposed to Pb at 500 °C for 800 h: cross-section with depth profiles of Ni and Cr.

Position	Fe (±2%)	Cr (±0.3%)	Ni (±0.3%)	Si (±0.3%)
1	68.5	16.9	11.0	0.7
2	70.1	17.6	10.0	0.8

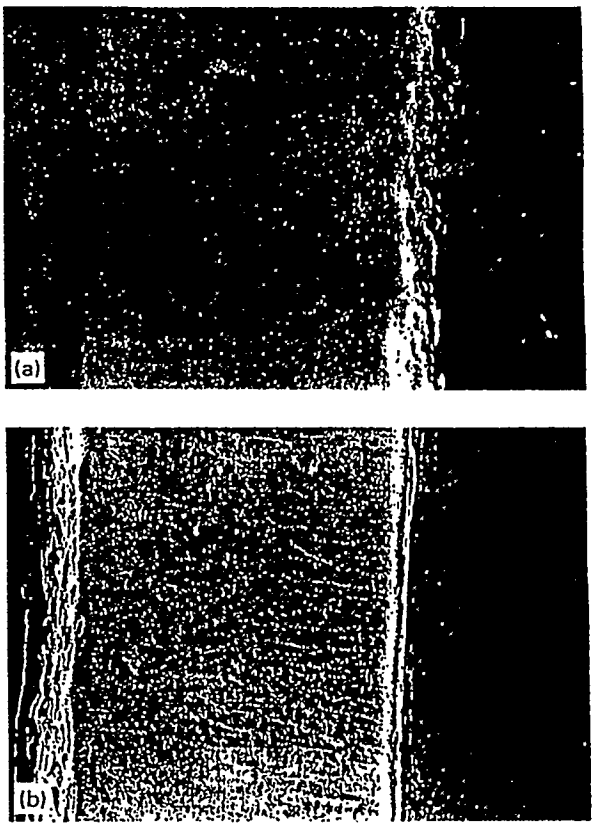

Figure 2 Microstructures of coating: before test: (a) unetched (b) after test (Murakami solution) (×350).

Steels

Ferrite-martensite ferromagnetic steels

Low nickel concentration; the steels contain: 9-12% chrome, 0-0.8% nickel (HT-9,T-91).

The rate of dissolution in circulation lead test facilities at 650° is 0.026 $g.m^{-2}hr^{-1}$, *i.e*, thickness decreasing about 90 μm at test duration 35000 hours.

Austenitic nonferromagnetic steels

These steels, *e.g.*, SS304,316,317, *etc.* **nonferromagnetic** and contain up to 18% **Cr** and 10-12% **Ni.**

At **low oxygen concentration**, *e.g.*, in **Pb-Li** eutectic, selective nickel dissolution occurs.

Consequence: porous ferritic layer formation with weak adhesion and low stability in the liquid metal flow

Even low oxygen partial pressure in the system result in oxide film formation on the surface of steels. These films completely preclude the interaction of steel with liquid phase.

Direct Contact Boiling Studies

* A tabletop experimental system for studying the microscopic phenomenon - first stage.

* A liquid metal natural circulation system (OFRA) for studying the influence of D.C.B. process on the system performance - second stage.

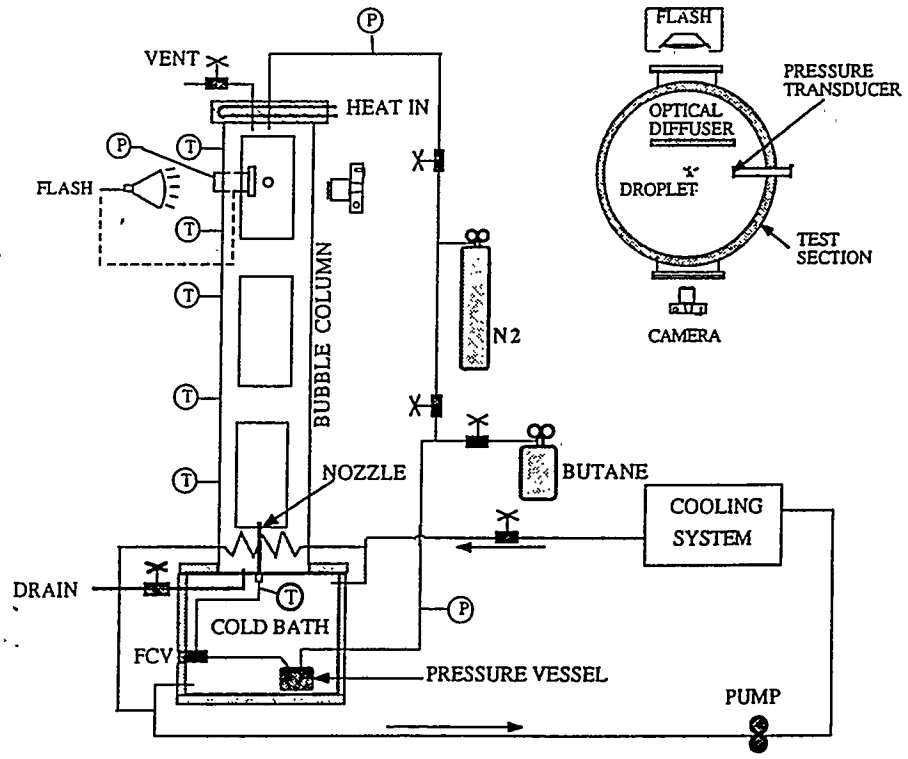

Schematic diagram of the experimental system.

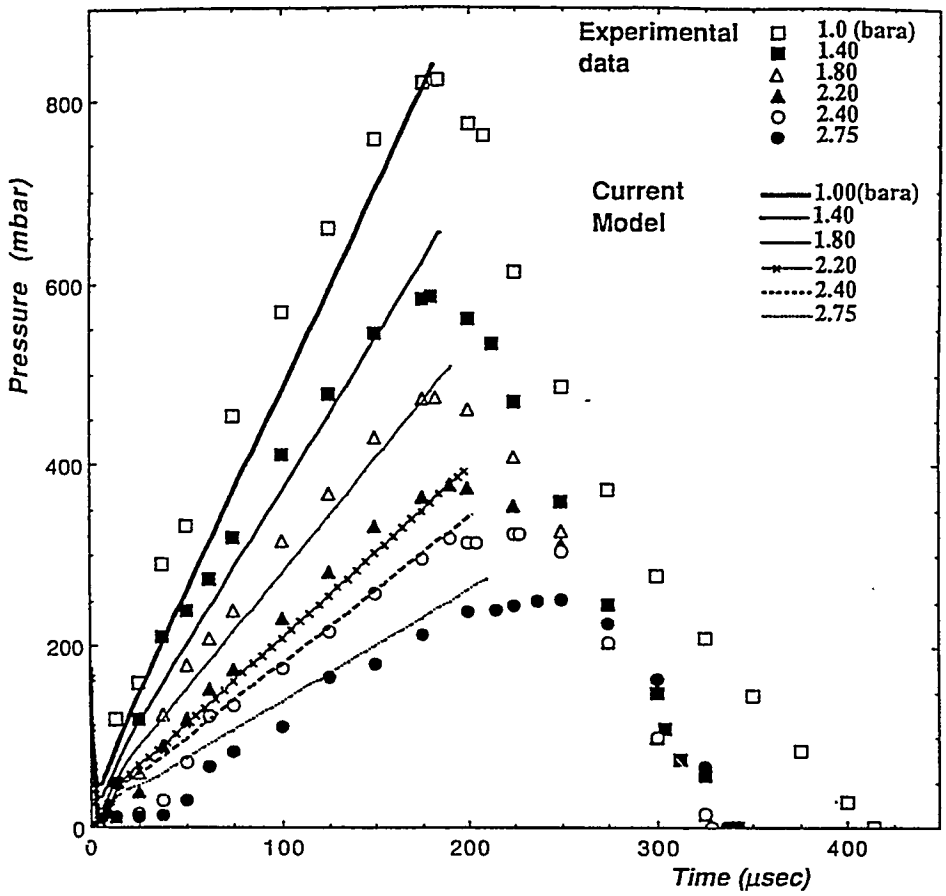

Ambient pressure effect on the bubble pressure puls.

SUMMARY

- From Phase I of the research program it can be concluded that the ambient pressure can totally suppress the explosive nature of the D.C.B. process.

- The applicability of water injection into the hot lead of a LMMHD system has yet to be verified in detail in Phase II of the program by using the "OFRA" system.

OFRA Facility - Research Targets

1. Studies of water DCHT and direct boiling phenomena in lead at temperatures up to 480°C (there is no experimental data on DCHT with water and lead in multi-bubbles bed, reported on in the literature.

2. Separation studies, mainly on carry under of vapour with LM to the downcomer and carry over of LM with vapour to the condenser.

3. Influence of different additives (surfactants, foaming materials, etc.) dissolved in the lead on the two-phase flow characteristics, mainly void fraction distribution and phase velocity ratio, flow configuration and overall system performances.

4. Studies of water reaction with molten lead over a large range of temperatures, pressures and flow rates.

5. Test of the lead reaction with the construction materials in the presence of liquid/vapor water.

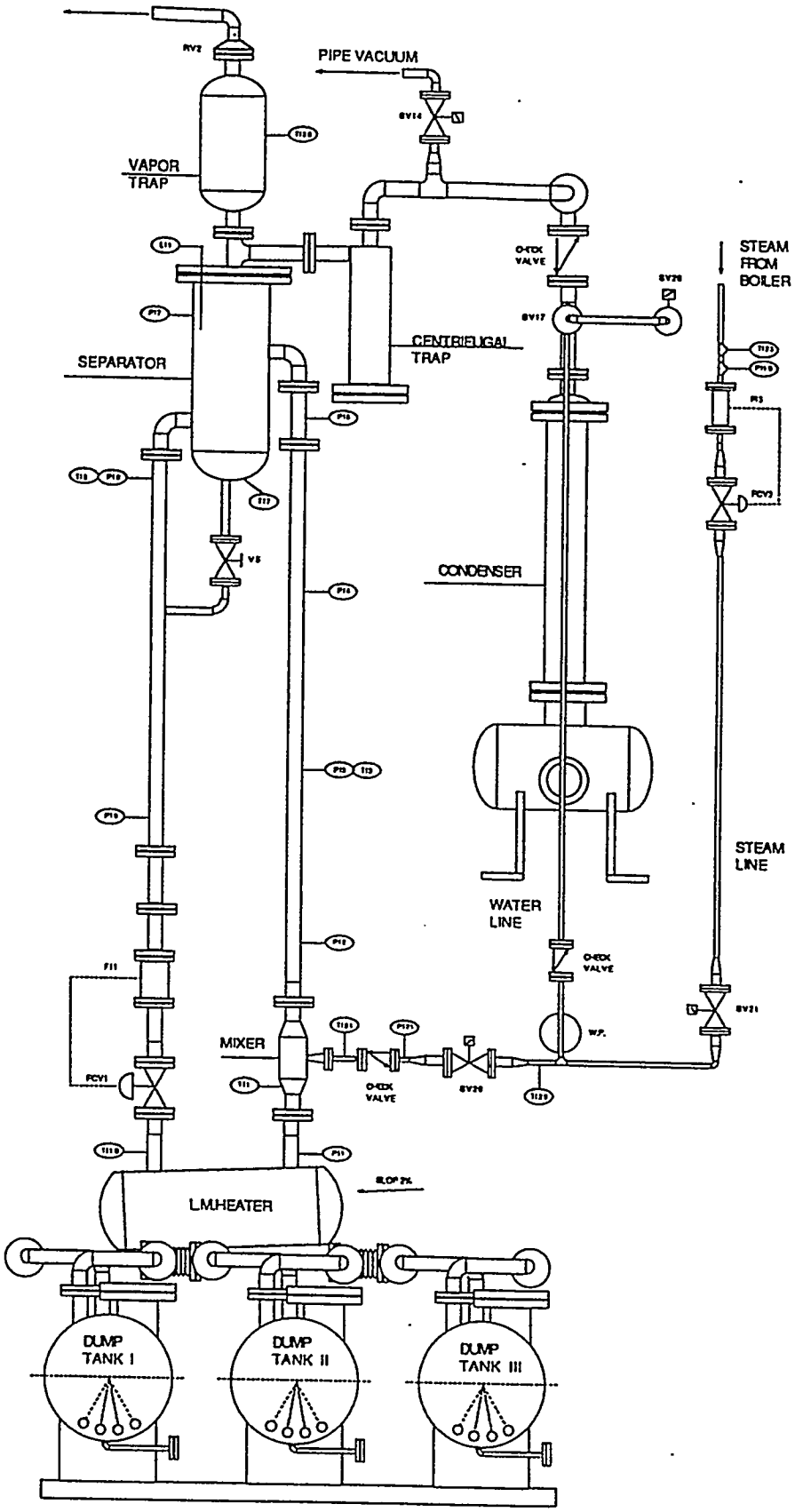

"OFRA" System Layout - Front View

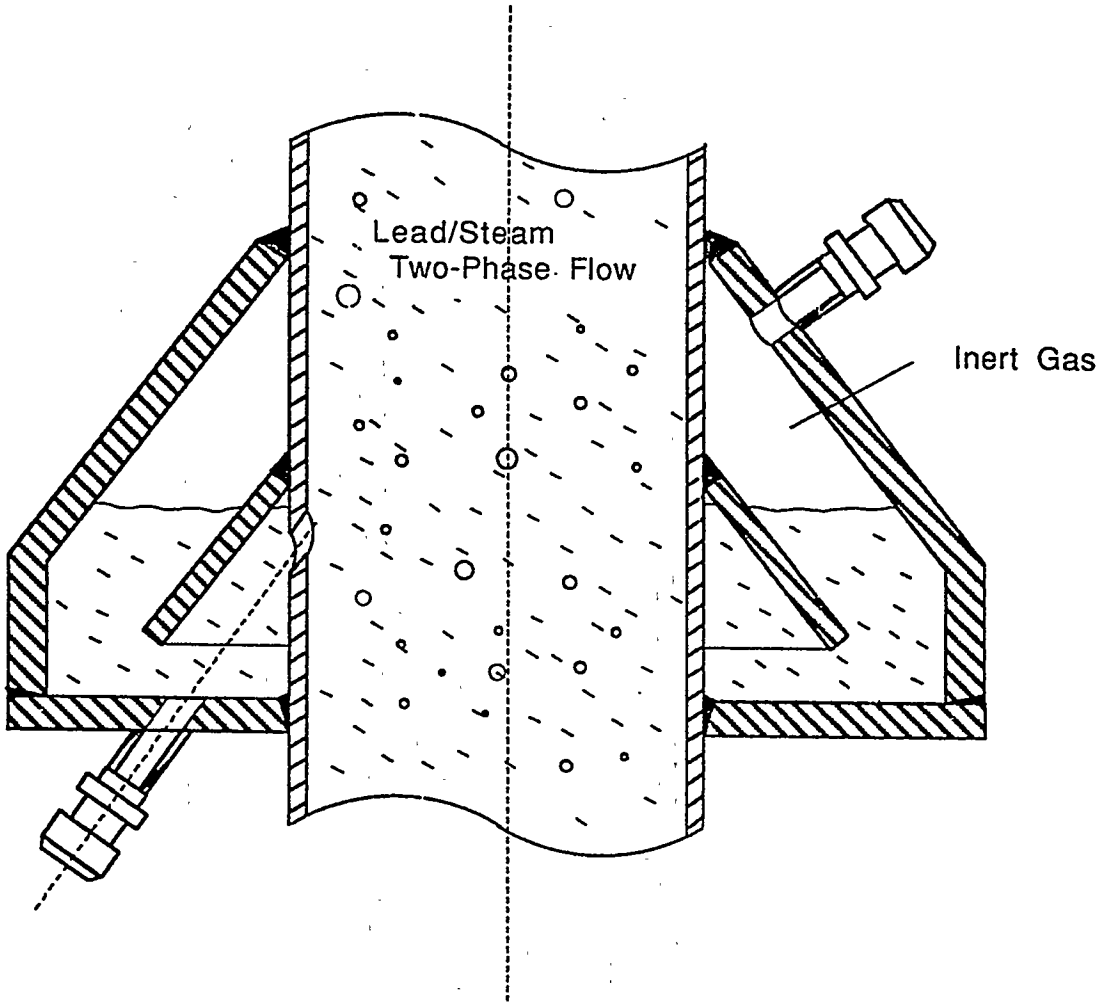

Pressure Measuring System Chamber at "Ofra"

The Experience of General Electric with Mercury for Electric Power Generation

* General electric found that at elevated temperature (400-500°C) Hg attacts the boilers steel tubes which became plugged with iron crystalline deposit
  - After more than 300 tests they found that Titanium and sodium additions improve wetting and prevent iron solution (the sodium removes oxides on steel surface and Titanium builds on surface a protective microscopic layer)
  - But, they also found that the reaction between sodium, iron oxide and oxigen led to plugging the tubes by balls of hard sodium ferrite

The solution:

magensium	at concentration of about 0.01 %
Titanium	at concentration of about 0.001 %

LM -RESEARCH OPPORTUNITIES AND ACTIVITIES AT THE LATVIAN ACADEMY OF SCIENCES

O.Lielausis
Institute of Physics of Latvian Academy of Sciences
Latvia

Abstract

In my first report (see, O.Lielausis "DESIGN ...") the experience of our Institute, regarding mercury as a very suitable material for LM-experiments was described. In the given presentation selected examples will be considered characterizing the breadth of our interests in LM applications.

So, InGaSn eutectic was used as a modeling liquid for investigation of MHD effects typical to some LM-blanket configurations. LM coatings proposed for the protection of divertor plates were considered too. Experiments were performed on a superconducting magnet providing a 5.6 T magnetic field in a 30 litters bore.

In a large vacuum chamber (12 m^3; 6.65 10^{-4} Pa) lithium cooling system for high temperature reactors was examined. Electromagnetic pumps and flowmeters able to work at lithium temperatures up to 960 °C were tested.

The experience with sodium can be characterized by a large scale stand for the calibration of flowmeters which allows to supply the produced flowmeters with a formal certificate. A second rather specific Na loop can be mentioned too, where two mounted in line electromagnetic pumps are delivering a 25 atm. pressure. The main Na loop equipped with em. pumps is based on d=10 cm tubing.

LM devices were installed in the Latvian 5000 MW nuclear research reactor IRT-5000 too. First, a equipped with conductive e.m. pumps loop, where InGaSn serves as a γ-carrier from activity generator (placed close to the core) to two outer 20 Mrad/h irradiators. Second, a LM system for rector control, where contained in InGaSn indium is used for neutron absorption and reactivity control. A closed cylindrical LM container was installed in the core instead of a traditional control rod. The container is divided in two chambers by means of elastic membranes. The one chamber contains InGaSn, the second GaSn (without In). By means of e.m. pumps the proportion between InGaSn and GaSn in the active zone can be changed ensuring a posibility to control the amount of introduced in the core absorbing material. Long term tests of the system were performed on a zero-power assembly . But for a shorter time the system was inserted in the core of the acting main reactor too and the efficiency of the control was confirmed. This type of design could be used, for example, in high seismic regions, in the absence of gravity, at non constant acceleration etc.

The room temperature non toxic alloy InGaSn is widely used in physical experiments too. With InGaSn loop a large electromagnetic (1.5 T in a 3x0.5x0.15 m^3 gap) is equipped. The total amount of InGa SN in different stands equals 180 kg. A technology for its purification is developed.

SODIUM FLOWMETER PLANT

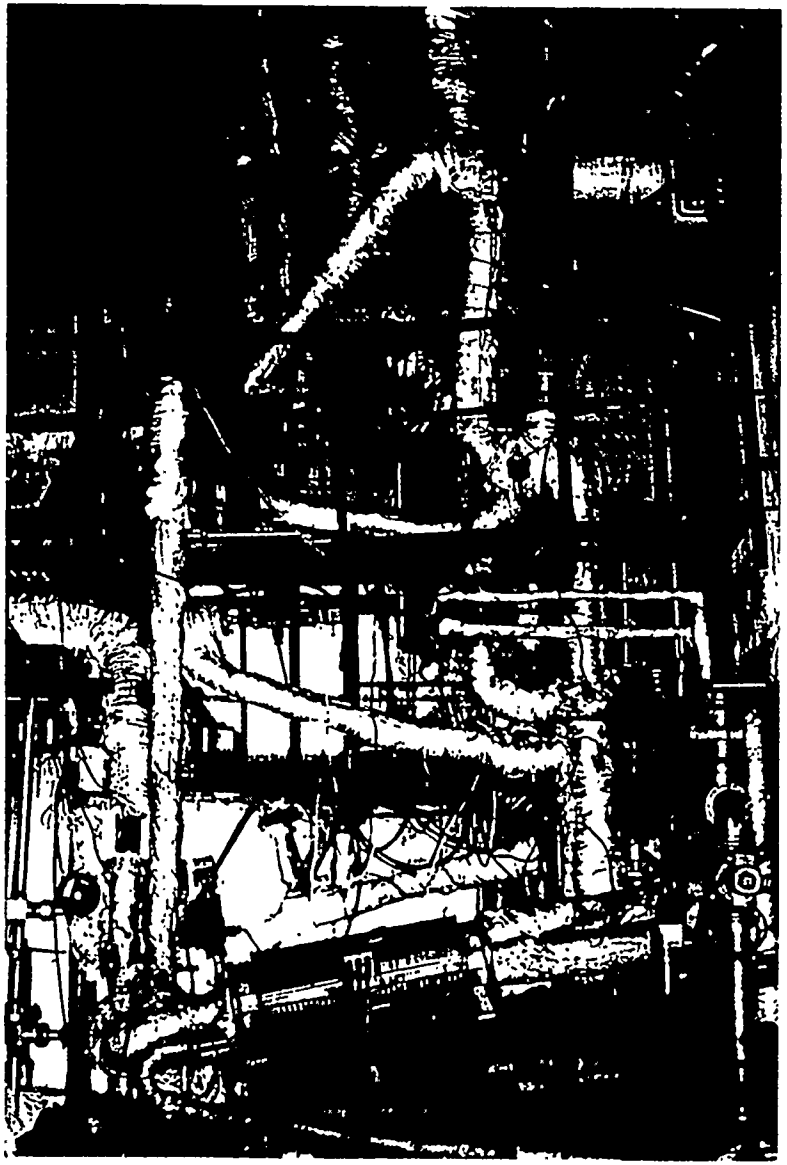

Description

The plant is designed for the graduation and testing of liquid sodium flowmeters.

The transfer cirsuit of the flow rate unit is two-staged.

The flow rate of sodium in the first stage is determined indirectly by the ratio of the volume of the gauging tank (or sodium mass) to the time of its filling. The volume of the gauging tank is graduated under normal conditions, the mass is determined by weighing under operation conditions.

The second stage permits to test flowmeters comparing their readings to standards.

Main technical characteristics

— flow rate range, kg/sec	0,2—30
— temperature range, °C	140—500
— volume of gauging tank, m^3	0,15
— volume of weighed capacity, m^3	0,1
— conditional flow diameter of main test sections, mm	70
— flow rate measurement error, %:	
— systematic component	0,3
— standard deviation	0,3

The plant has been certified by the Latvian Centre for standards and metrology

PRESSURE METERS FOR THE MEASUREMENT OF LIQUID METAL HEAT-TRANSFER AGENTS AND HIGH TEMPERATURE MEDIA

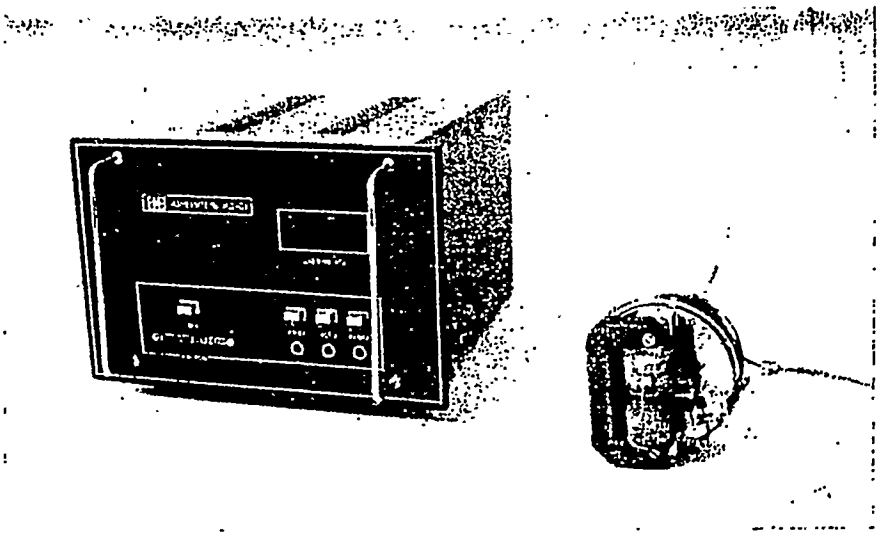

Description

The meter is designed for the measurement of liquid metal heat-transfer agents and other media at high temperatures.

The operations principle of the meter is based on the determination of the relation of difference and sum of voltage induced in two interconnected electric circuits situated in the alternating magnetic field and whose areas change mutually proportional to the pressure value as a result of linear movement of the flexible element.

The device has the following advantages:

— small temperature error;

— interchangeability of the sensor and measuring device;

— possibility to make the exit with an expanded scale relative to the operation pressure;

— standard current exit;

— four-digit digital presentation.

Main technical characteristics

— temperature of the measured media, °C	to 1600
— measured pressures, mPa	to 2,5
— basic error, not more than, %	0,3
— additional temperature error, for 10° not more, %	0,035
— non-linearity, not more than, %	0,4
— hysteresis, not more than, %	0,3
— sensor mass, kg	1—1,5
— sizea of measuring device, mm	150×180×200

ELECTROMAGNETIC CONTACTLESS FLOWMETER/DOSER FOR LIQUID METALS

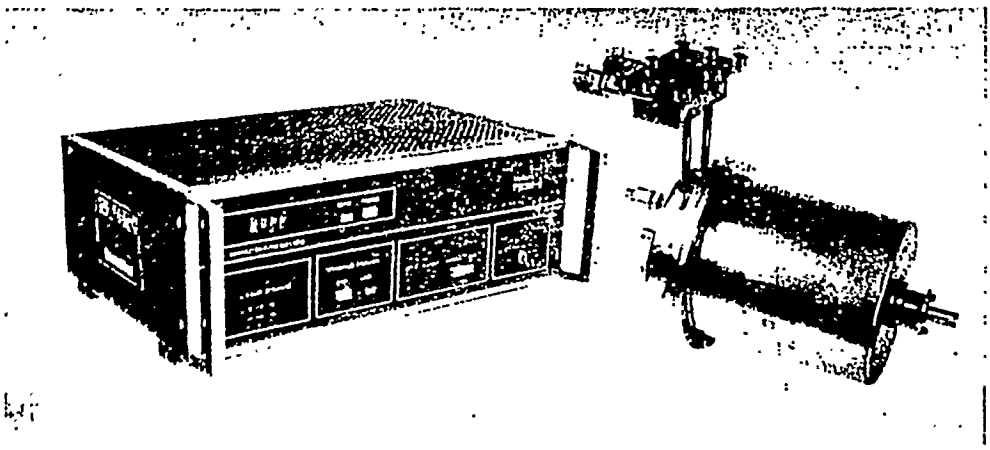

Description

The flowmeter is designed for the measuring of flow rate, volume of liquid sodium and for its dosing. Modifications of the flowmeter can be used for other media (mercury, gallium, lead and its alloys).

The operation principle of the unit is based on the determination of the ratio of velocity and vorticity components of signals of the secondary magnetic field induced in liquid metal moving in the external magnetic field.

The unit has the following advantages:

— readings are independent of the wettability degree of measuring channel walls by liquid metal and its conductivity;

— high reproducibility of readings;

— rated graduation.

Main technical characteristics

— temperature of controlled medium, °C	120—300
— flow rate measuring range, l/sec	0,1—1
— measurement range of set dose and quantity, l	10—9999
— basic relative measurement error, not more than, %	
— rated graduation	2,5
— flow graduation	1

Areas of application

The device can be used in chemical industry and nuclear power.

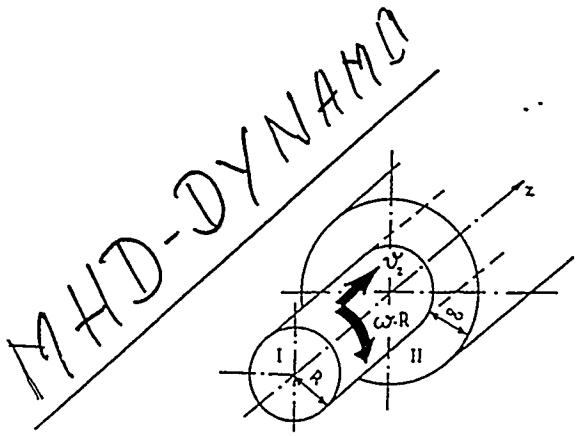

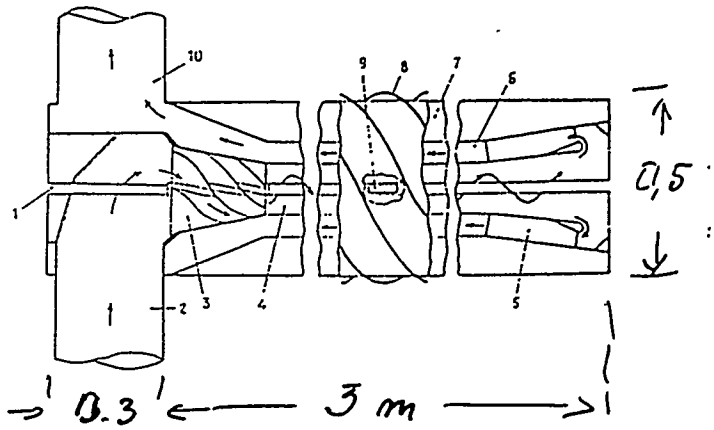

The model is all-welded from stainless steel and is filled, except for an open measuring channel 1, with liquid sodium (Fig. 9). Sodium passes through the model from entrance 2 to exit 10. In the helical labyrinth 3, the sodium stream is accelerated and made helical : axial motion + rotation round the axis. When passing through the main channel 4, the sodium rotation is maintained by inertia only. Here, both the calculation and the water test indicate less than 20 % loss of angular momentum. Rotation ends in the twelve-wall labyrinth 5 of the reverse system ; hence the flow is axial in the reverse channel 6.

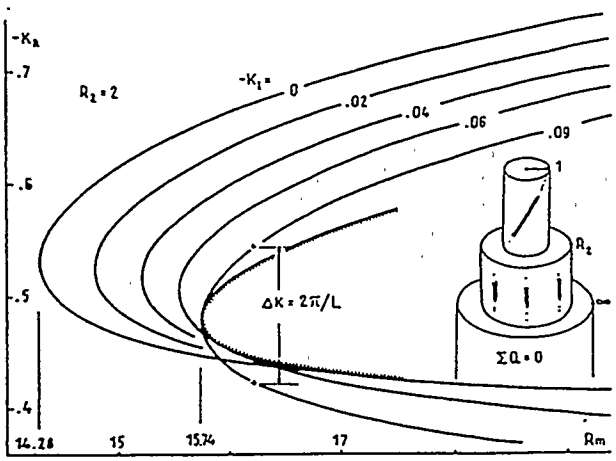

. Evolvent of k_I = const indicates an absolute generation. x = 1.

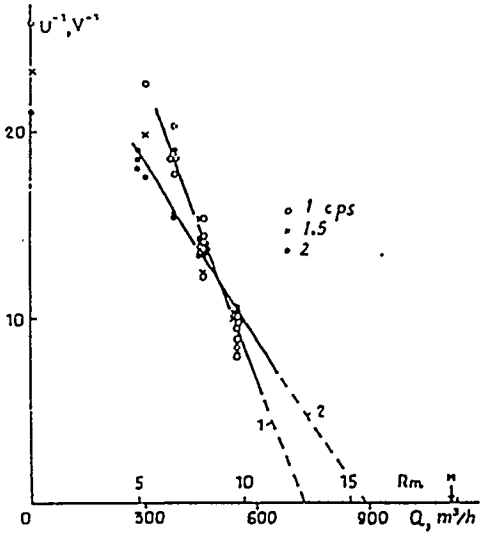

Models response to external excitation.

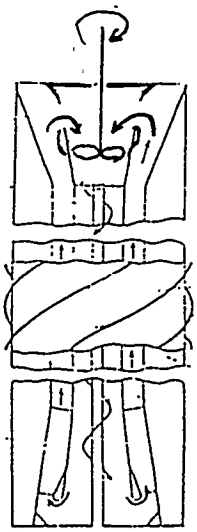

EXPERIMENTAL ALKALI METAL STAND AND FACILITIES

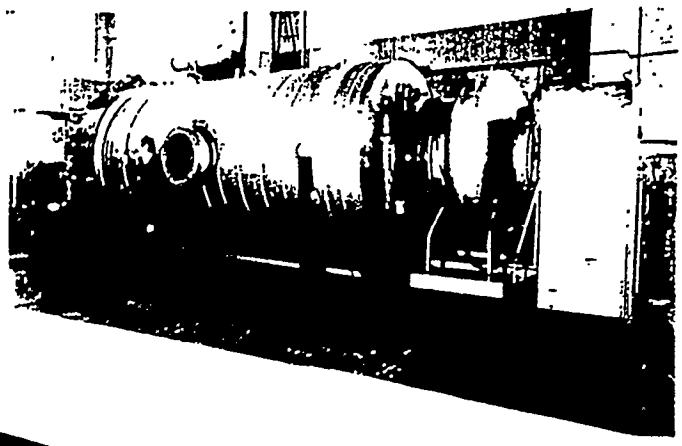

HIGH TEMPERATURE SPACE SIMULATION TEST CHAMBER

- length, mm 4000
- diameter, mm 1200
- pressure, Pa $2 \cdot 10^{3}$ -$6.65 \cdot 10^{-4}$
- dissipated power, kW 300
- medium gas (Ar, He), vacuum
- heat- transfer agent temperature, K up to 1200

(used for investigations of EMP and different MHD-devices [flowmeters, pressure meters, throttles etc.] for cooling systems of space nuclear reactors under conditions close to real)

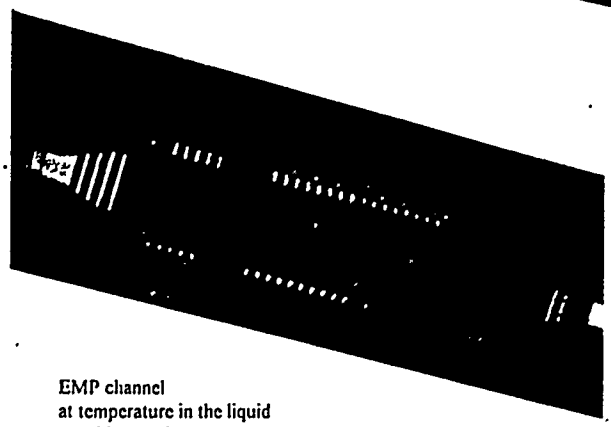

EMP channel
at temperature in the liquid
metal loop (Li) up to 1220 K.

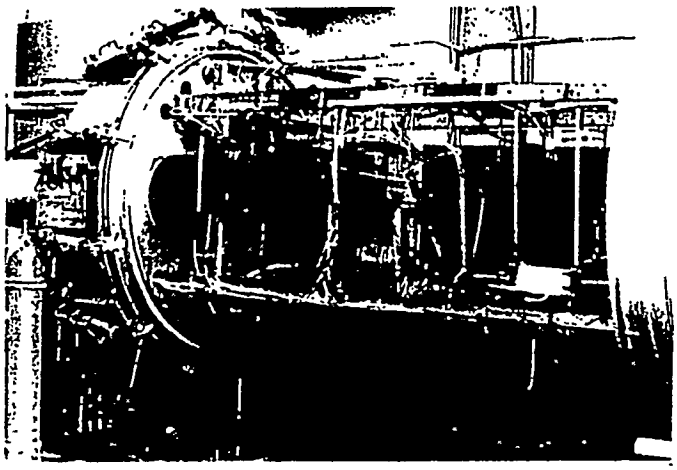

HIGH TEMPERATURE LIQUID METAL LOOP

- heat transfer agent Li
- structural material of LML Nb-Zr alloy
- investigation objects EMPs
- operating temperature, K up to 1200

EMERGENCY CASE

Leak in the channel of EMP
(liquid metal temperature in the
loop was about 1000 K)

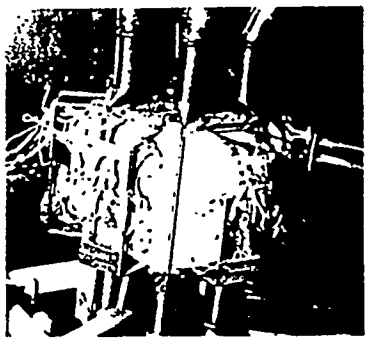

MULTICHANNEL HIGH TEMPERATURE EMP

- liquid metal Li
- number of the channels 6
- flow rate, l/s 2x6=12
- pressure in the channel, Pa $1.5 \cdot 10^{5}$

LIQUID METAL INSTALLATIONS IN THE NUCLEAR REACTOR

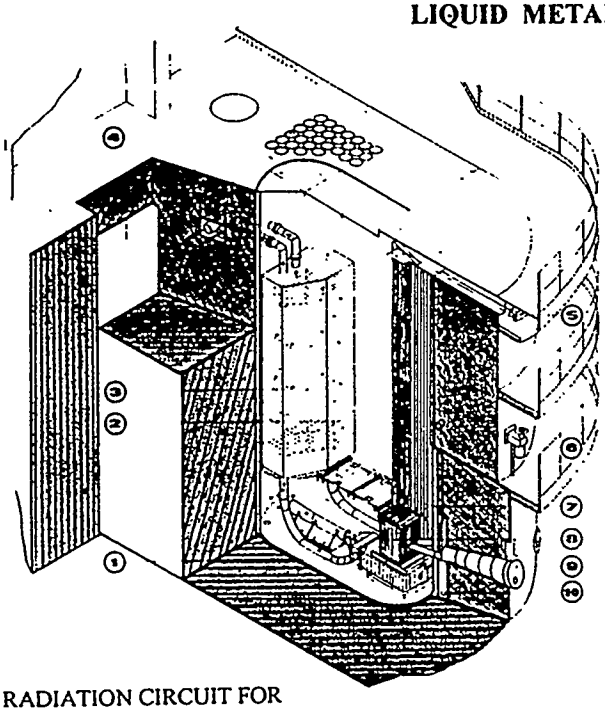

NUCLEAR RESEARCH REACTOR (ИРТ-5000)

- power, kW — 5000
- neutron flux in the core, n/cm^2.s — $5 \cdot 10^{13}$
- cooler — distillate water
- nuclear fuel — enriched ^{235}U
- neutron reflector — beryllium

1- cooling pipe-line; 2- control channels; 3- coolant delay tank; 4-dry assemblies for radioactive samples storage; 5- servodrives of control rods; 6-gate drives; 7- vertical experimental channels; 8- reactor core; 9- horizontal experimental channels; 10- heat shield

RADIATION CIRCUIT FOR NUCLEAR REACTOR

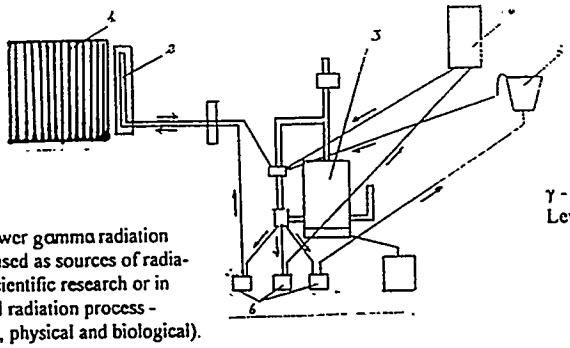

1- reactor core
2- activity generator
3- alloy (InGaSn) collector
4- irradiator -1
5- irradiator -2
6- electromagnetic pumps

γ - carrier - InGaSn
Level of γ - radiation - 20 Mrad/h

(high-power gamma radiation source, used as sources of radiation in scientific research or in industrial radiation process - chemical, physical and biological).

GENERAL VIEW

EXPERIMENTAL LIQUID METAL CONTROL SYSTEM FOR NUCLEAR REACTOR ИРТ-5000 →

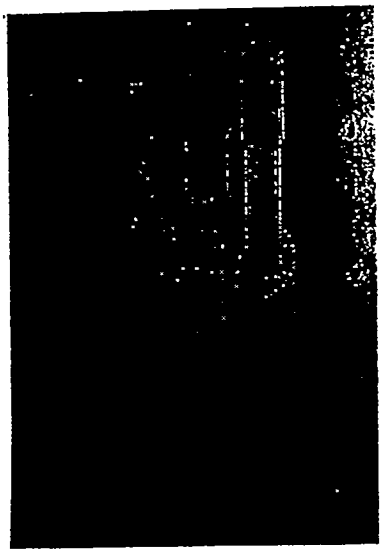

THERMOIONIC NUCLEAR REACTOR (scheme)

1- turning cylinders; 4- operation element; 5- MHD drive; 6- compensation chamber (liquid metal control systems is combined with turning cylinders)

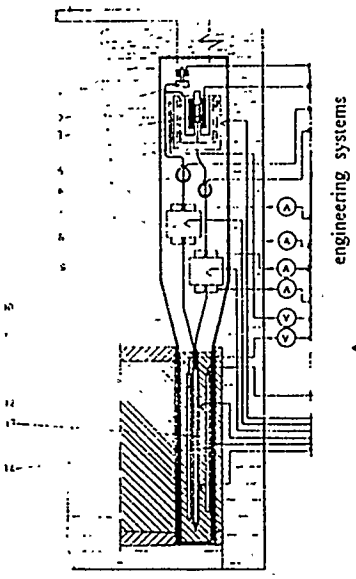

PRINCIPLE SCHEME

1, 2, 3, 6 - measuring services
5- compensation element;
7- MHD-drive; 9- protective housing;
11- reactor core; 13- operation element

- absorber — InGaSn
- replacer — GaSn
- operating temperature, K — up to 650

LIQUID METAL REACTOR CONTROL SYSTEM IN THE ZERO POWER REACTOR

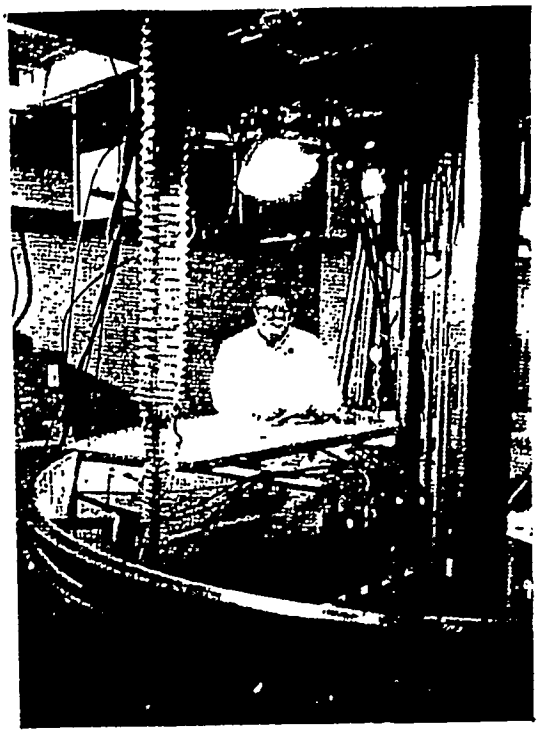

ZERO-POWER REACTOR RKS-25

- heat power, W up to 25
- neutron flux in the core, n/cm^2 s
- nuclear fuel enriched ^{235}U
- neutron reflector C, Be

(used for modeling and studying of physico-technical characteristics for reactors, for measurements of operating parameters of their elements and units; for studying and checking of control systems (including a new type liquid metal reactor control system))

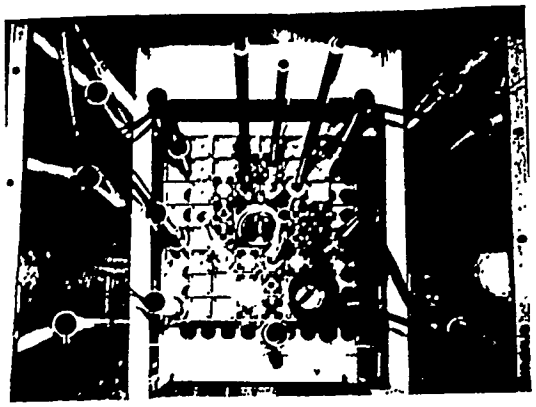

FUEL CORE OF THE RKS-25

- nuclear fuel enriched ^{235}U
- neutron reflector Be
- moderator distilled H_2O

(model of operation element of liquid metal control system inserted in the core)

PRINCIPLE SCHEME OF THE LIQUID METAL REACTOR CONTROL SYSTEM

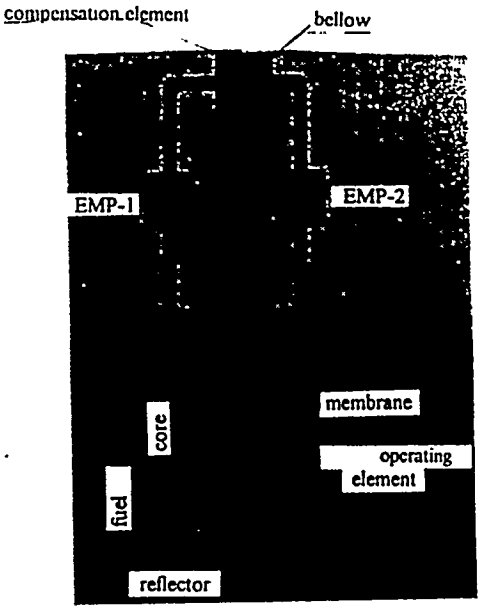

- neutron absorber InGaSn (red)
- displacer GaSn (grey)

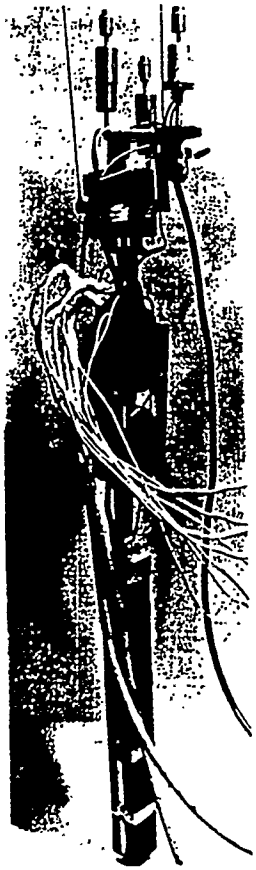

GENERAL VIEW

(liquid metal reactor control system)

LIQUID METAL CONTROL SYSTEM UNDER OPERATION IN THE NEUTRON REFLECTOR (C) OF FUEL CORE

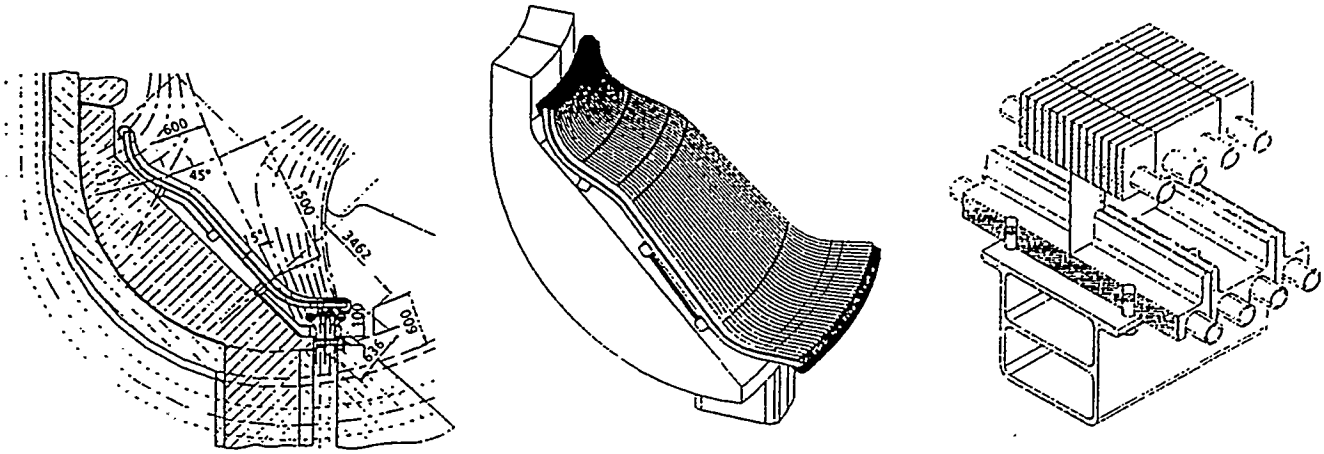

DIVERTOR PLATE DESIGN

NUCLEAR FUSION, Vol.30, No.9 (1990)

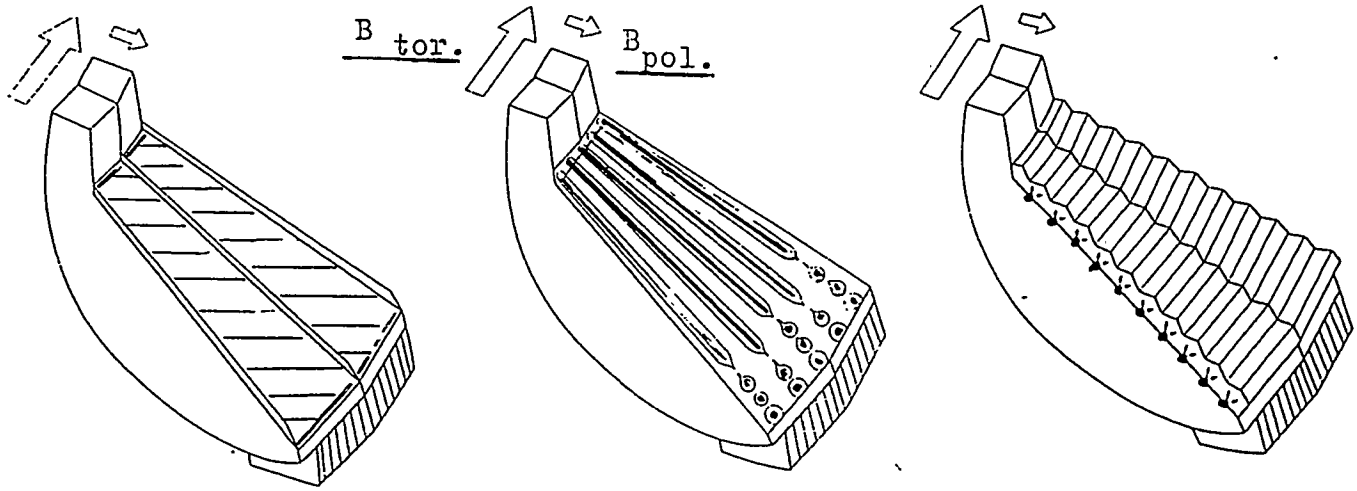

Curtain of free-flying LM jets/droplets

LM film over a conducting substrate

Light construction cooled by LM from the lower side

LM PROTECTED DIVERTOR PLATES

SUPERCONDUCTING MAGNET FOR 5.6 T FIELD IN 30 LITRE SPACE

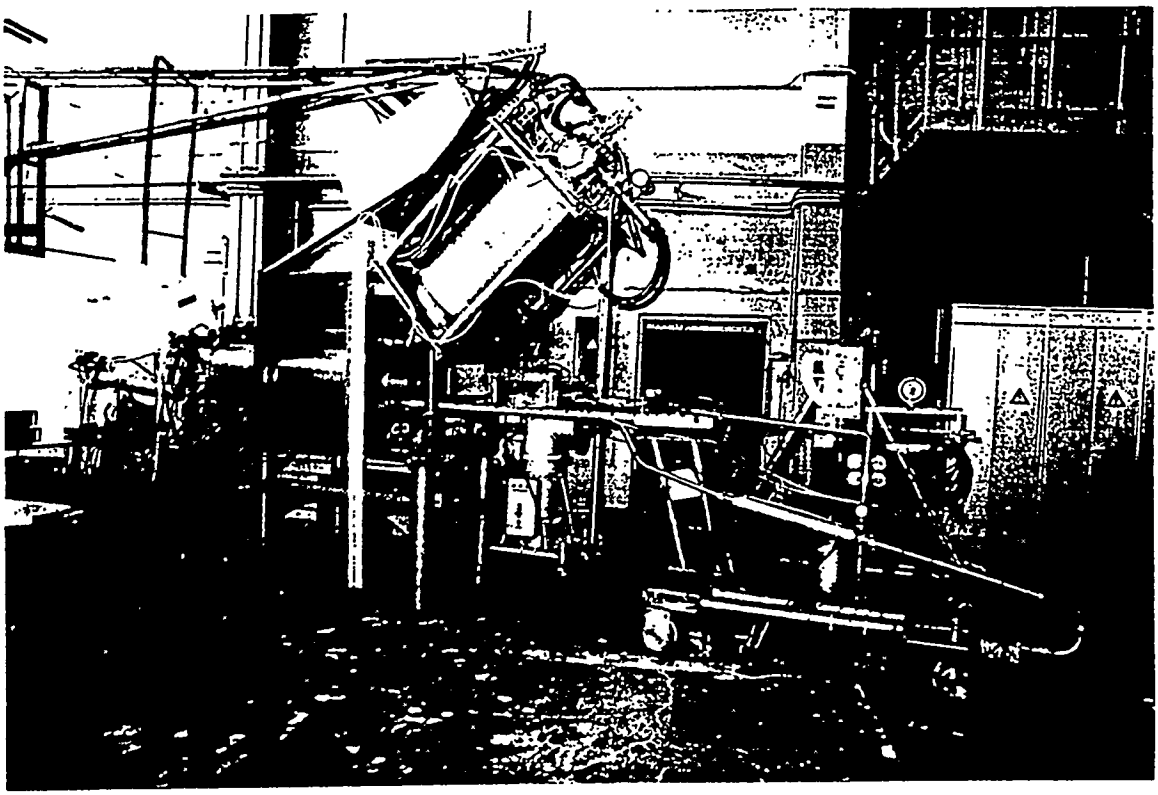

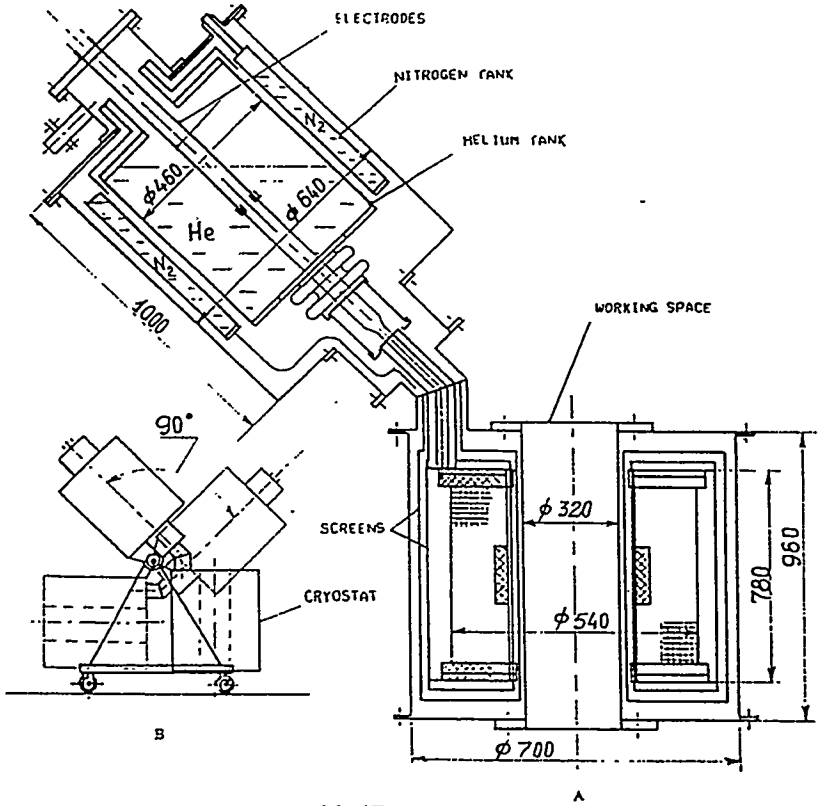

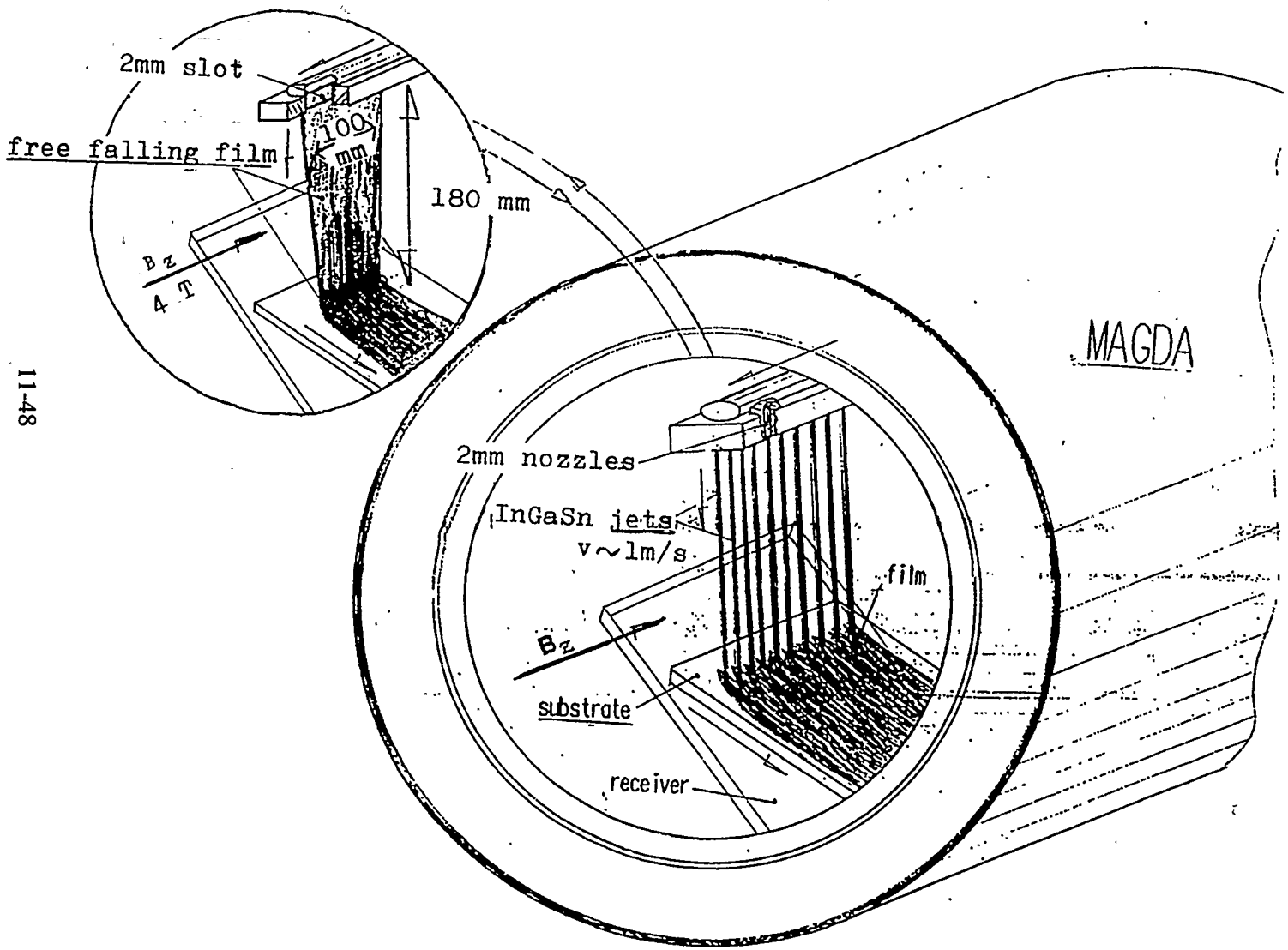
2mm slot
free falling film
100 mm
180 mm
Bz
4 T
MAGDA
2mm nozzles
InGaSn jets
v~1m/s
film
Bz
substrate
receiver

MAGNETIC FIELD DUE TO THERMOELECTRIC CURRENTS IN A FAST BREEDER REACTOR

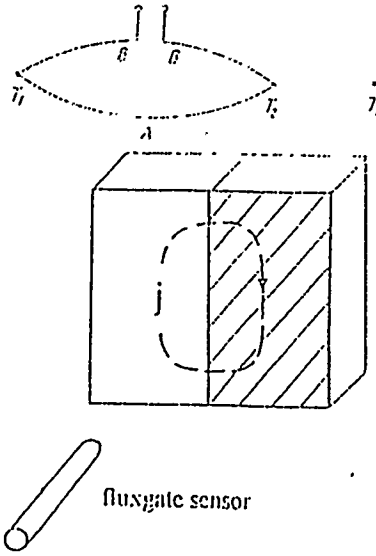

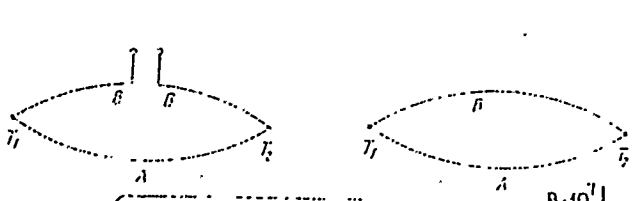

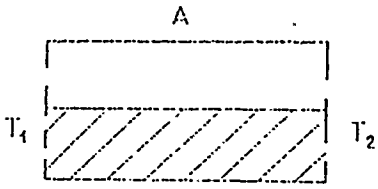

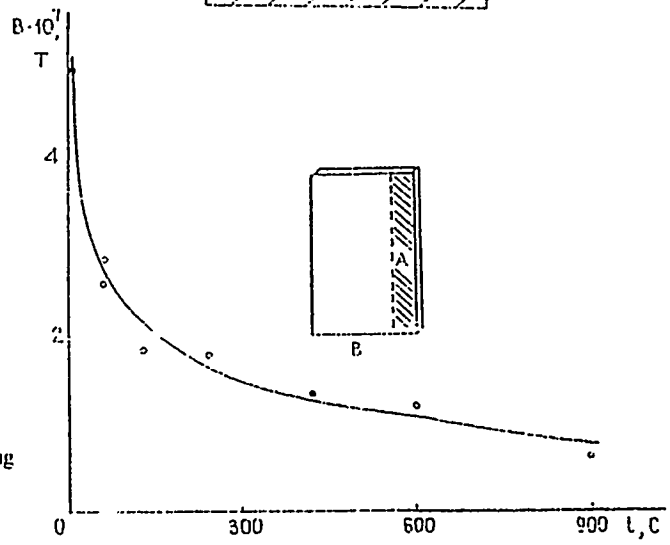

The magnetic field induction depending on Cd diffusion time in Zn

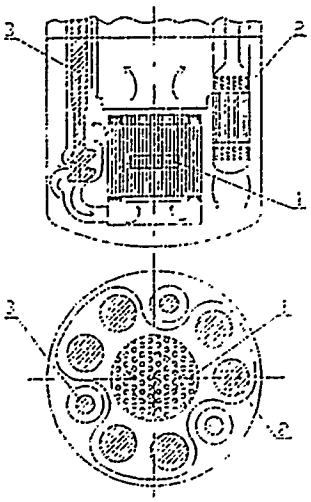

Lay-out of the thermoactive elements inside the reactor. 1 - core. 2 - heat exchangers. 3 - pumps.

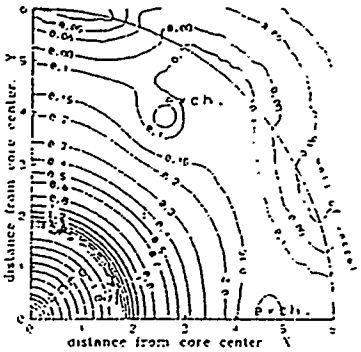

Field isolines in plane Z=0.

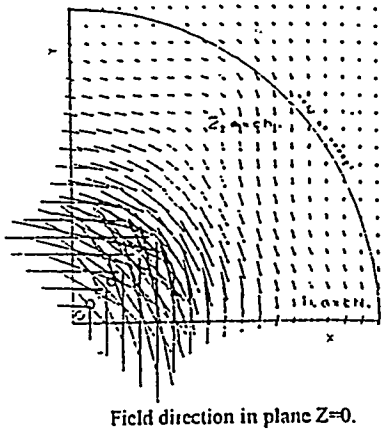

Field direction in plane Z=0.

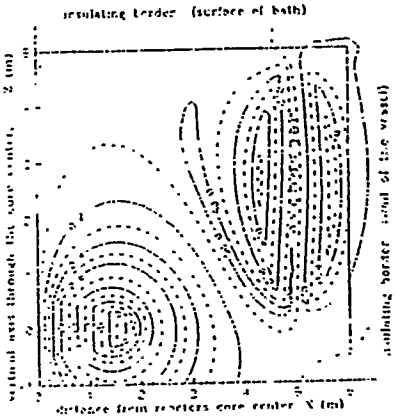

Isolines of magnetic field modulus in the vertical plane Y=0 .

Summary Session A

Different Target Materials: Corrosion and Corrosion Control

Coordinators
Y. Takeda, L. Mansur, Y. Dai, and J. DiStefano

Workshop Session on Pros and Cons for Different Target Materials/Corrosion and Corrosion Control

Y. Takeda, L. K. Mansur, Y. Dai, and J. R. DiStefano

Two of the originally planned workshop sessions, indicated by the titles on each side of the "/" in the above title were combined. The session was structured into four areas in which target material attributes were considered: nuclear properties; physical properties; compatibility; and liquid metal engineering/safety. Short presentations were either volunteered by participants or requested by the session organizers to help establish a background and stimulate discussion. G. Bauer, J. Takeda, T. Gabriel and S. Wender covered the first two areas; J. DiStefano, Y. Dai and Y. Orlov made presentations in the third area. O. Lielausis and R. Dressler spoke on the fourth area. L. K. Mansur served as moderator for the combined session.

Although there was much discussion and some difference of opinion, the overall recommendations, considering all available factors, as distilled by this session's organizers, are as follows. Choose Hg as the prime candidate target material to which most resources should be devoted. A strong alternate candidate is considered to exist in Pb-Bi eutectic. Other candidate materials such as Pb, Pb-Mg eutectic and Bi are weaker choices for various reasons, with Bi being the weakest.

(A table, listing quantitative factors where available, for the various options can be found in G. Bauer's presentation.)

Nuclear Properties

Hg appears to offer a 20-30% advantage in overall neutron production in preliminary calculations. High energy cross-sections for Hg, Pb and Bi are mainly based on nuclear models and are known to a similar level of accuracy for all three materials. Low energy cross-sections are well known for lead but relatively poorly known for the other materials. The high thermal absorption cross-section for Hg, $_a^{Hg}$ (~ 4000 $_a^{Pb}$), is a potentially significant advantage for Hg in a short pulse source. However, this may be a disadvantage for Hg in a steady-state source, or in a long pulse source. The high $_a$ of Hg eliminates the need for a separate decoupler. The distance between the target and moderator may then be reduced, leading to a higher efficiency in neutron production. Again, this is applicable only for pulsed sources.

Needs in this area are to examine available data (and possibly to make new measurements?) for Hg absorption cross-section at low energies ($kT \leq E_n$ <20 MeV), and at higher energies as available to confirm that there are no surprises that would reduce neutron production. In addition, total cross-section at high energies needs to be determined.

Low energy cross-sections will be examined at ORNL. High energy cross-sections can be determined at Los Alamos, PSI, Juelich and possibly at other laboratories. Further discussions will be needed to determine the where, how, and who of this work.

Physical Properties

Mercury is a liquid at the temperatures of interest. This leads to several consequences that are considered favorable. A liquid Hg source can operate at the lowest temperature. This, in turn, allows consideration of austenitic stainless steels as container materials, which may show better irradiation performance than ferritic/martensitic steels. At high temperatures, austenitic stainless steels would not be favored because of the probability of mass transfer of the nickel component of the alloy from hot to cold regions of

the liquid Hg system. On the negative side, Hg does have a high vapor pressure. In addition its high thermal expansion coefficient may aggravate thermal shock problems, however, this is somewhat counterbalanced by the higher thermal expansion coefficient of Hg.

Lead-Bismuth eutectic melts at a higher temperature than Hg (125 vs - 39 C). In practice, Pb-Bi eutectic systems may be operated as low as about 200 C. It has a lower vapor pressure but slightly higher corrosivity than Hg. Pb-Bi increases the possibility of requiring the use of a ferritic/martensitic steel container.

Lead-Magnesium eutectic melts at higher temperatures (250 C). It has somewhat higher corrosivity than Hg and Pb-Bi, and may require the use of a ferritic/martensitic steel container. Bismuth is not considered a viable choice.

Many needed physical properties for the liquid metal targets Hg and Pb-Bi are considered to be known. However, a number of properties for Pb-Mg are considered to be unknown. R&D work on physical properties for Hg and Pb-Bi is not considered needed at this time. One exception is that the measured thermal expansion coefficient of Pb-Bi eutectic in the liquid state is not in hand, and will need to be measured over the temperature range of interest if it is not available in the literature.

Compatibility

As the operating system temperature is increased, above 100-200 C, then Hg loses some advantage over Pb-Bi. It is known that Ni is much more soluble than Fe or Cr in these liquid metals. Most of the data available is for temperatures above ~400 C. At lower temperatures, based on this information, Ni would still show a tendency to transfer from hot to cold portions of the system, depending strongly on the T. However, this temperature gradient mass transfer may be at a low enough level for austenitic stainless steels to be viable container materials.

Needs identified in this area cover the need for specific information relating to target design conditions for

- Temperature gradient mass transfer
- Liquid metal embrittlement (a type of corrosion associated with grain boundary attack of liquid metals)
- Effects of simultaneous irradiation on corrosive behavior
- Cavitation and erosion/corrosion associated with prototype fluid flow.

Both ORNL and PSI are carrying out bench-scale programs to investigate liquid metal embrittlement and temperature gradient mass transfer. Both laboratories plan larger loop studies where more typical flow effects on corrosion can also be studied. ORNL is planning low dose irradiations of specimens in Hg, in connection with a larger irradiation program being carried out at the LAMPF. Fission reactor irradiations should also be considered as a way to obtain higher dose irradiations of specimens of container materials in Hg. A joint program was proposed among PSI, ORNL and the Institute for Nuclear Research near Moscow. INR a high energy proton accelerator is available where they would be willing to incorporate a mercury target for irradiation/corrosion/spallation product studies.

Liquid Metal Engineering/Safety

At both RIGA in Latvia and Ben Gurion University in Israel, multi-ton loops of Hg and Pb-Bi have been operated successfully for a decade. Except for short times at relatively low temperatures, these systems have operated near room temperature. However, austenitic stainless steel has been used in all these applications and has performed satisfactorily. At IPPE in Russia it was found that corrosion resistance of stainless steel was obtained by oxidation of the Cr arising from O in Pb-Bi. However, too much oxygen must be avoided to avert clogging the system. If wetting is not required, oxygen could substitute for Mg/Ti additions in Hg, which may not be practical at low temperatures.

Safety issues discussed covered the production of ^{210}Po in the Pb-Bi target and the question of public concern over the use of these heavy metals. Hg may have the worse public concern, although lead also has had some very negative press coverage in past years. These loops have operated mainly in the range of 80 to 170 C. Based on the experience cited above, the point was made that both Hg and Pb-Bi will work in the "balance of plant" outside the target region, and the task should be to focus on which liquid metal is better for the target region.

Needs identified in liquid metal engeneering centered around thermal hydraulic testing at prototype conditions

O. Lielausis offered the possibility of attaching a prototype target container configuration to an existing Hg loop at RIGA. G. Bauer and Y. Takeda plan to visit and determine whether to conduct thermal hydraulic testing there. S. Lesin suggested the possibility of fundamental studies at Ben Gurion, such as the measurement of heat trransfer coefficients of Hg and Pb-Bi as well as gas-liquid two phase flow studies including bubble generation and bubble dynamics.

Summary Session B

Heat Removal

Coordinators
T. Dury and M. Siman-Tov

* Much encouragement was received from the rich experience presented in this workshop by our guests from Obninsk, Riga and Beer-Sheva
* Additional evaluation of this information is required

3. Prediction capabilities in the CFD code

   * Bubbles behavior in mercury (if used)
   * Cross stream turbulence (ESS only)
   * Wetting/non-wetting effects

4. Cooling of Beam "Window"

   * Concentration of local heat deposition at center, especially if beam is of parabolic profile.

How can we generate the critical data, where, and by whom?

---

1. Mercury flow and heat transfer tests including wetting, non-wetting and additives issues

    * Facilities are available in Riga, Obninsk and Beer-Sheva
    * Perform full scale mercury target tests in the existing facility at Riga.
    * Perform specific tests for heat transfer, friction factor, and effects of gases and additives in the existing facility in Beer-Sheva.
    * Exchange information on past studies made at the Obninsk Institute on mercury heat transfer.

2. Mercury components and Instrumentation testing

    * Same as above plus work by Dr. Takeda from PSI

3. Flow distribution and CFD benchmarking.

    * Full scale experiments using **Water** should be performed before and simultaneously with the mercury experiments.
    * Those experiments can be done at both PSI and ORNL (existing facilities from work for the ANS project are available at ORNL for that purpose).

4. Full scale mercury target loop should be planned (later stage) for both ORNL <u>and</u> ESS. This is required for final confirmation tests and for operational experience.

5. Improved capabilities of the CFD code

   * Integrate prediction capabilities in the widely used code FLOW-3D in cooperation with the code developers (AEA Technology Engineering Software, Inc.) for:

     - bubble behavior (if used)
     - cross stream turbulence (ESS only)
     - wetting/non-wetting effects

   * Should be guided by both PSI and ORNL

6. CFD code simulation of the mercury target

   * Should be performed by both ESS (PSI) <u>and</u> ORNL as a basis for design and analysis of the various concepts considered and for planning of experiments.

ATTACHMENT

Discussion on Feasibility and Uncertainty Issues in SNS Hg Target T/H and R&D required

Categories in parentheses are as follows:

- A - Requires analysis & Engineering
- B - Requires development but "can be worked out"
- C - Requires confirmatory R&D
- D - Critical or feasibility issue (requires R&D to prove feasibility).

Proper flow distribution in target, addressing:

* Flow reversals **(B)**
* "Stagnation" points **(B)**
* "Hot spot" **(B)**
* Cross stream turbulence (ESS design only) - **(C)**
* Inclusion of non-wetting effects in CFD **(C)**

Proper Target structure cooling addressing

* Hot spots **(B)**
* "Window" cooling and deterioration **(C)**
* Outside cooling of the walls? **(B)**

CFD Code benchmarking and validation

* In water **(B)**
* In mercury **(C)**
* Analytical **(B)**
* Experimental **(B)**
* Scaling water for mercury? **(B/C)**
* Available facilities **(B)**
* Interacting streams **(C)**
* Evaporation at sharp corners (cavitation) - **(C/D)**
* Cavitation resulting from thermal shock **(C/D)**
* Bubbles behavior in CFD **(C/D)**

Mitigation of thermal shock

* He bubbles (under "static" and pulse conditions if used) - **(C/D)**
  - How to inject (back-pressure under pulse conditions)
  - How to maintain proper bubble distribution

- How to maintain proper bubble diameter
- Agglomeration, coalescence
- Experiments

* Vibration from thermal shock **(C/D)**
* Other mitigation methods (walls displacement? Cavities?) - **(C/D)**

Mercury heat transfer coefficient and friction factor
* Nominal correlations **(B)**
* Effects of non-wetting and how to investigate (different in SS than HT-9?) - **(C/D)**
* Effects of other depositions **(C)**
* Effects of gases (O2, He, etc.) - **(C)**

Uncertainty in energy deposition, shape and distribution (A)

Diagnostics and instrumentation for mercury (B)
* Visualization issue (bubbles detection and measurements)
* Other unique problems

Full scale mercury target tests for confirmation (B)
* Is it necessary?
* What scale?
* Where can or should it be done (existing facilities?)

Decay heat removal during shutdown (B)
* Natural convection cooling
* Special wall temperature gradients (cool mercury - hot wall)

Failures and Safety issues (A/B)
* Mercury pump
* Water pump
* He injection pump
* Mercury or He leaks
* Intrusion of water into Mercury system
* Others?

Non-nominal operations (A/B)
* Startup
* Transients
* Others?

Specific comments made during the discussions include:

1. As long as there is no gas in the mercury, heat transfer is not affected by whether there is wetting or not (specifically said that the Lyon-Marinelli correlation is OK without wetting, too).

2. Prof. Lielausis said that they had found that they needed good wetting for all of their electro-magnetic pumps. They used chemical and mechanical means to create good wetting, before use.

3. There was a question raised as to whether cavitation could occur as a result of the thermal shock process.

4. Concern was raised about vibrations resulting from the repeated thermal shocks.

5. Prof. Yury Orlov stated that the N_u number for mercury heat transfer was not affected much by non-wetting unless there was a good amount of gas in the mercury (see attached figure).

From Eng. Prog. [illegible] 3/28/96

Nu = f(Pe)

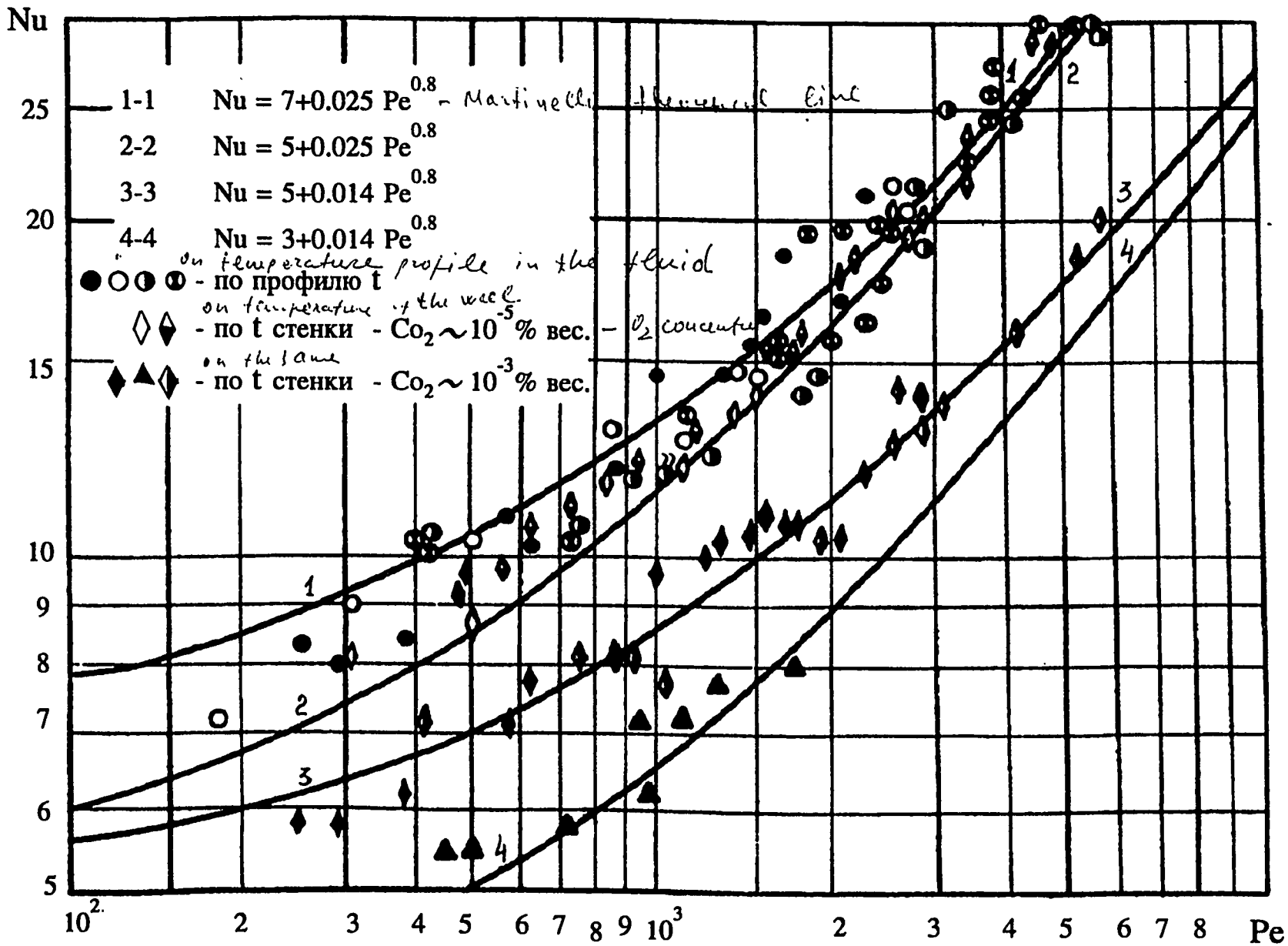

Summary Session C

Effects of Pulsed Operation

Coordinators
T. Gabriel and L. Ni

International Workshop
on the Technology and Thermal Hydraulics of Heavy Liquid Metals
Schruns, Austria, March 24-29, 1996

Working Group Summary Report on Effects of Pulsed Operation

Tony A. Gabriel, Oak Ridge National Laboratory, TN 37831-6364, USA
Liping Ni, Paul Scherrer Institute, CH-5232 Villingen-PSI, Switzerland

In a short pulsed spallation neutron source, extremely high energy ($\gtrsim$1 GeV) proton beam pulses are injected into a liquid metal target in a very short period of time (~1 μsec) at a high repetition rate (~50 Hertz). The beam energy will be deposited in the target materials (such as mercury or lead) and converted into heat. It caused a sudden temperature rise and resulting pressure wave. This pressure wave travels through the liquid, reaches the steel container wall and may possibly lead to material damage due to induced stress.

Two reports were given at this workshop on the numerical simulation of pressure waves and thermal shock in the liquid and target window. A paper by R. P. Taleyarkhan and J. Haines described the integrated ORNL's modeling of thermal shock effects in liquid and solid target designs using the CTH-code. The results indicated that it is unlikely that thermal shock becomes a serious problem for the case of a 1 MW flat beam profile. However, a systematic study will be necessary for a parabolic beam profile for all power levels, i.e., 1 to 5 MW. The presentation of K. Skala and L. Ni showed a PSI-code which models the pressure waves in the liquid and their effects on the wall stress. Results showed that the wall stress for a 5 MW ESS target will exceed the allowable stress and adding a small volume of helium bubbles, i.e., 3%, might reduce the stress level by more than two orders of magnitude.

Concerning the gas injection and the liquid metal-gas mixture, detailed worked on modeling and experiments were presented. These presentations included the influence of an external magnetic field on the mixture and bubble distributions (S. Eckert, et al.), two-component flow structure of Pb-Bi-gas (B. F. Gromov and Y. I. Orlov) and dynamic characteristics (S. Lesin, et al.). J. Carpenter presented a view in a discrete model of two-phase flow where bubble frequency might play a role in preparing for a two-phase field.

Almost all participants agreed that the shock problem due to the short pulse operation in the liquid metal target could be serious and could present a challenging problem. It was determined that the following points need to be addressed:

- equation of state for mercury
- code validation and benchmark experiments
- shock effects on the entire target system
- two phase flow by gas injection

All these investigations should be carried out in the framework of international co-operations. Two small scaled Hg pressure pulse tests are planned at ORNL to provide insight into the pressure wave propagation and thermal shock effects. One experiment will use exploding wires to generate the pulse pressure, the other the electron beam at ORELA. Also PSI, LANL, CERN (ISOLDE facility), INR and IPPE could contribute to the experimental methods for producing shock. The necessary R&D for bubble injection might be performed at PSI, RIGA, ORNL or Ben-Gurion University. All of the above experiments can possibly yield benchmarking data which is absolutely necessary for code validation.

Summary Session D

Process Technology and Effects of Spallation Products, Circuit Components

Coordinators
B. Sigg, J. Haines, R. Dressler, T. McManamy

Working Session D

- **Process technology and effects of spallation products**
- **Circuit components, maintenance, and handling**

Coordinators: B. Sigg, J. Haines, R. Dressler, T. McManamy

Working Session D included an assessment of the status of the technology and components required to: (1) remove impurities from the liquid metal (mercury or Pb-Bi) target flow loop including the effects of spallation products, (2) provide the flow parameters necessary for target operations, and (3) maintain the target system. A series of brief presentations were made to focus the discussion on these issues. The subjects of these presentations are listed below and are followed by a brief summary of each.

Spallation products and solubilities - R. Dressler

Spallation products for Pb-Bi - Y. Orlov

Clean-up/impurity removal components - B. Sigg

"Road-Map" and remote handling needs - T. McManamy

Remote handling issues and development - M. Holding

Rugard Dressler pointed out that we have already defined the spallation product distribution and the solubility of all elements in mercury. He then pointed out that we still need to understand the behavior of intermetalic compounds, H_2, carbon, O_2, and N_2 in the liquid mercury system. Dressler concluded by indicating that we need to improve the model/calculations to include the effects of the target loop structural materials.

Yuri Orlov presented an assessment of the influence of spallation products on the Pb-Bi target for SINQ. He concluded that taking into account the comparatively small amount of all spallation products and the subsequent low concentration of these elements in the coolant, the admixture generation by the proton beam will not influence the coolant properties or the coolant processing technology.

Beat Sigg presented a schematic diagram, as well as a simplified layout, for the ESS mercury target circuit identifying all major components necessary to fulfill the basic operational, safety, and availability requirements. He raised the question of whether a gas and impurity separation system was required and presented a diagram for such a system that serves as a reference approach if such equipment is found to be required.

Tom McManamy presented a "road-map" for the target R&D and design activities, emphasizing the interactions between the various elements of these two programs needed to successfully meet programmatic requirements. He identified the main target maintenance and handling issues including handling paths, shielding requirements, removal of spallation products from the mercury loop, mass transport and subsequent plugging of the heat exchanger passages, and recovery from failure modes. He also identified the reference target system layout and removal approach being developed for the SNS project.

Mike Holding identified remote handling issues that are based on his experience with the ISIS program. His major points included (1) the need to consider the remote handling and waste disposal needs in view of the many years (~20 years) of operation and final

decommissioning, (2) identifying circuit components and modifying them for remote handling, (3) defining the R&D to develop special purpose remote handling equipment where absolutely needed, (4) creating a separate remote handling cell for servicing active components and dealing with waste, (5) providing adequate space to store components during maintenance activities, (6) considering location of some components in regions that are available for hands-on maintenance (requires ~ 2 m of shielding for ISIS), and (6) the use of attachments and fittings that are made for remote handling, e.g. captive nuts and valves on each side of joints to be broken to reduce contamination releases during maintenance.

Conclusions

(a) The overall conclusion of this session was that, with the exception of

(1) spallation product related processing issues,
(2) helium injection and clean-up, and
(3) specialized remote handling equipment,

the technology for all other circuit components (excluding the target itself) exists. Operating systems at the Institute of Physics in Riga, Latvia (O. Lielausis) and at Ben-Gurion University in Beer Shiva, Israel (S. Lesin) have demonstrated that other liquid metal circuit components including pumps, heat exchangers, valves, seals, and piping are readily available and have been reliably used for many years.

(b) In the three areas listed in item (a) above, the designs and analysis are not judged to be mature enough to determine whether and what types of technology development are required. Further design and analysis of the liquid metal target system is therefore needed to define flow circuit processing and remote handling equipment requirements and thereby identify any development needs.

Summary Session E

Discussion of R&D Needs and Opportunities to Broaden the Data Base on Materials and Technology for Liquid Metal Spallation Targets

G. Bauer

International Workshop on the Technology and Thermal Hydraulics of Heavy Liquid Metals

Schruns, Austria, March 25-29, 1996

Summary on the discussions on

R&D-Needs and Opportunities to Broaden the Data Base on Materials and Technology for Liquid Metal Spallation Targets

- A Challenge for International Collaborations-

G.S. Bauer, Paul Scherrer Institut, Switzerland

Liquid metals have so far only been used to a very limited extent as spallation targets, notably at the ISOLDE-facility at CERN (Pb and La) to produce radioactive isotopes. Virtually no systematic studies have been carried out so far. The available data base is by no means sufficient to answer conclusively very important questions such as predicting reliably the service time of medium-to-high power target systems or determining precisely what technological measures are required and appropriate to maintain an optimum coolant quality, to mitigate the effects of pressure waves in short pulse sources and others. During the workshop several areas have been identified, where there exists an urgent need for improved knowledge and reliable data and opportunities have been presented to acquire such knowledge and to generate such data.

Opportunities to do such research and pertinent know-how, although scarce, are spread over institutions in several countries, and efforts to use these opportunities often require substantial resources both in man power and money. The workshop participants therefore unanimously supported the view that **a coordinated and internationally concerted effort should be undertaken to make the best possible use of existing opportunities and available resources in order to develop the knowledge and technology necessary for the deployment and safe operation of target systems suitable for pulsed spallation neutron sources in the multi-megawatt range of beam power.**

The following list summarizes needs and opportunities for such research.

A <u>The areas, where more information is needed include:</u>

A1 Reliability of predictions obtained by the use of computational fluid dynamics (CFD)-codes. Meaningful code validation experiments must be performed before these codes can be used to optimize the target configuration.

A2 Reliability of other software used to predict operational characteristics of liquid metal target systems, such as neutronics, the generation and effect of spallation products, intermetallic reactions etc.
Prototypical experimental work is required in this field.

A3 Heat transfer from solid to liquid metals and the effect of wetting and flow.
Such data may be strongly dependent on the configuration in question and must be measured for relevant geometries and materials.

A4 Experimental verification of predictions relating to pulse-generated pressure waves and their effect on the target structures.

A5 Possibility and technology of injecting gas bubbles in suitable distribution into Mercury to mitigate the effect of heat pulses and methods of measurement.

A6 Effect of gas injection on the heat transfer between solid and liquid metals under different flow configurations. It has been observed that the heat transfer between solid and liquid metals may be strongly reduced by dissolved gases in the liquid. This could affect the possibility to cool the target beam window and to remove heat from the liquid metal.

A7 Effect of irradiation on intermetallic reactions (corrosion, embrittlement, interdiffusion, wetting).

A8 Effect of strain on intermetallic reactions.

A9 Effect of simultaneous irradiation and strain on intermetallic reactions.

A10 Effect of Hydrogen and Helium production in a radiation field characteristic for spallation targets on structure materials candidates at different temperatures.

A11 Assessment of needs and methods to maintain the liquid metal quality (purity and Oxygen content, etc.) in well defined limits.

B <u>Ongoing Activities and Existing Opportunities for International Collaborations</u>

In the following mainly those installations and activities are listed, which require special equipment to make them possible or which are of sufficiently large scale to make their duplication elsewhere impossible or at least a difficult to justify expenditure. They have all been declared available for international collaborations. Smaller test rigs and equipment in use at various laboratories for supporting research have not been incorporated in the list in detail (see Fig. 1).

B1 **PSI and ISTC-supported construction of a 1 MW PbBi-pilot target for irradiation in a proton beam.**
PSI has awarded a contract to IPPE, Obninsk to study the needs for constructing a 1 MW PbBi-pilot target system to be tested in a proton beam. As a first result, IPPE has submitted a proposal to ISTC for support to design and construct such a target system. This system is planned to be tested in the LAMPF proton beam at Los Alamos. An alternative option would be testing in the proton beam of the Moscow Meson Factory at Troitsk, where the desired power density could be realized, but not the full 1 MW. When completed, the current IPPE-study will also serve as a basis for the construction of a prototype target system for SINQ.

B2 **Heat transfer, corrosion and gas separation experiments at Beer Sheva (Israel).**
The Ben Gurion University at Beer Sheva operates several liquid metal installations that have been offered to be used for collaborative test experiments, in particular in the fields of liquid metal-solid metal interaction, surface tension measurements and liquid metal-gas separation, where a large body of experience has been accumulated in the ongoing MHD-research program. These facilities are available for immediate use on the basis that any new equipment required will be provided by the user.
Local contact: S. Lesin (Beer Sheva)

B3 **Proton and neutron irradiation of test specimens at the LANSCE-facilities in Los Alamos.**
A large number of test specimens have been prepared and are due to be irradiated in a mixed proton and neutron field representative for the target region in a spallation neutron source, starting August 1996. Specimens have been provided by several different laboratories, including ORNL and PSI/KFA for the ESS-study. In addition, high pulse load experiments are being discussed.
Coordinator: W.F. Sommer (LANL).

B4 **Irradiation of test samples in the target of SINQ at PSI, Switzerland**
The SINQ-target will be a solid rod target initially. This opens up the opportunity to design and construct a certain fraction of the rods as materials test capsules in which specimens can be irradiated in the mixed proton and neutron spectrum characteristic of spallation neutron sources. The test capsules proposed would have identical outer diameter as the solid target elements and would be enclosed in a tube of the same material as the target elements are made from. Inside the tube the test specimens will be embedded between aluminum (or Zircaloy) segments in which also a dosimetry package and a thermocouple would be placed to be able to determine the irradiation conditions as precisely as possible.
After the workshop interest has been expressed in active participation in this program by representatives of LANL, ORNL, KFA, and CEA.
Operation of SINQ is expected to start towards the end of 1996 with a target not containing any test specimens. The earliest date for insertion of a target with test capsules will be mid 1997.
Coordinator Y. Dai (PSI).

B5 **Pressure pulse experiments at ISOLDE (Cern)**
ISOLDE is a radioactive beam facility at the CERN-Booster synchrotron which occasionally uses liquid Pb or La targets to generate the desired isotopes. Such targets have failed in the past due to the effect of pressure pulses, while they had survived much larger doses on the continuous beam of the previously used cyclotron. The proton pulses at the CERN-booster consist of 4 subpulses wit a total of up to 10^{13} protons per pulse. It was observed in the past, that, as the number of protons in the pulse was increased from $5x10^{12}$ to $1x10^{13}$, release of the radioactive isotopes became much more rapid but the target container was destroyed after a short period of time. This was attributed to the onset of pressure waves in the target. Although the ISOLDE-team has come up with ways to mitigate this problem by extending the proton pulses in time, interest to accomplish this by other means continues, in particular, since bubbling Helium through the system might also enhance spallation product release.
If the present activities at PSI to develop a method for controlled injection of gas bubbles into liquid metal are successful, a proposal will be made to the ISOLDE-committee to conduct such tests. ORNL has expressed interest to be partner in this activity.
Coordinators: G.S. Bauer (PSI) and J. Lettry (CERN).

B6 **High power pulse tests at the AGS-beam (BNL)**
(This opportunity is included in the present report, although it came to the author's attention only shortly after the workshop.)
The AGS at Brookhaven National Laboratory is capable of delivering proton pulses of up to 100 kJ energy content with a duration of 2.4 μs at a proton energy of 7 GeV. Although this energy is higher and the pulses are longer than envisaged for pulsed spallation neutron sources, this could provide an excellent opportunity for full-scale verification of predictions on the effect of such pulses on the container of a liquid metal target and the effectiveness of mitigation methods. The experiment can be set up in a presently unused section of the former neutrino beam line. In order to get the full

beam intensity there at the "low" energy of 7 GeV (relative to AGS's final energy of 28.5 GeV), a full aperture kicker should be developed and a section of the beam line previously dismantled will have to be rebuilt. The initial test experiments would relate to the response of the target system to individual pulses and would therefore not lead to significant activation of the system or the environment. These experiments are, nevertheless, of prime importance in validating the computer codes used to assess the loads resulting from the short power pulses. The setup might afterwards be used for further investigations relating to neutronic performance.
Discussions have been initiated between BNL, ORNL and ESS. Technically it should be possible to start experimental runs in October 1997, if the prospects for funding are clear by October 1996.
Contact : J. Axe (BNL) G. Bauer (ESS; PSI)

B7 **Dual and triple beam irradiation facilities at HMI and ORNL**
HMI (Berlin) is operating a dual and ORNL a triple beam facility which allow injection of Hydrogen and/or Helium simultaneously with the generation of dpa-damage by matrix ions (Iron in the case of steel). Although only very thin specimens can be irradiated in these facilities, they provide a convenient way to do series of experiments which can be correlated to the results of other irradiations. Both institutions have embarked on test series on materials relevant for spallation targets.
Relevant parameters:

Dual beam facility at HMI

acceleration voltage:	up to 350 kV for heavy ions (Fe^+ etc.)
	up to 70 kV for light ions (H_2^+, D_2^+, He^+..)
displacement damage rate	$5x10^{-4}$ - $5x10^{-2}$ dpa/s
Helium implantation rate	0.5 - 50 appm/s
diameter of He-beam	4 mm
temperature range	RT - 550 C (FIM-specimens)
	RT - 800 C (TEM-specimens)

Contact: E. Camus (HMI)

*Triple beam facility at ORNL**

acceleration energy	1.0 - 5.0 MeV (Van de Graff) for heavy ions (Fe^{++}, Ni^{++} etc.) (typically 2A on target)
	2.5 MeV (Van de Graff) for gaseous ions, in particular He^+ (up to 100A on targert
	0.2- 0.4 MeV (Van de Graff) for gaseous ions (H^+, He^+,O^+,N^+...) (up to 50 A on target)

homogeneous irradiation of up to 1 cm^2 achieved by beam wobbling
maximum damage depth in steel about 1m (range of heaviest particles)
Contact: L. Mansur (ORNL)

* after M.B. Lewis, W.R. Allen, R.A.Buhl, N.H.Packan, S.W. Cook and L. Mansur: Triple Ion Beam Irradiaton Facility, Nucl. Inst. Meth. in Physics Res. B 43 (1989) 243-253

B8 **Proton irradiation facility PIREX at PSI (**)**

This facility allows irradiation of thin specimens in a Helium atmosphere with protons of 590 MeV. It is currently mainly used for fusion related materials programs which includes irradiation of low activation ferritic-martensitic steels that are of interest also as container material for liquid metal spallation targets. Other irradiations can be accommodated.

Relevant parameters:

maximum current	20 μA
amount of material that can be placed in the beam	≈5 g
minimum beam cross section ($4\sigma \times 4\sigma$)	4x4 mm^2
maximum wobbling amplitude	5 mm
temperature range	30 - 350 °C.

Contact: Y. Dai, PSI

(**) see, e.g. M. Victoria and D. Gavillet: „An Overview of the PIREX Proton Irradiation Facility and its Research Program" AIP Conf. Proc 334,(1995) pp 891-902.

B9 **Heat transfer and flow experiments in a Mercury loop at Riga (Latvia)**

The Latvian Academy of Sciences operates a large liquid metal laboratory whose installations have been proposed to be used for full-scale tests on questions of flow distribution, window cooling and the effect of gas injection on these phenomena.

The main parameters for the big Mercury loop which has been proposed to be used for target testing are:

total volume	0.35 m^3
mass of Hg	4.7×10^3 kg
diameter of pipes	10 cm
outlet pressure of pump	5×10^5 N/m^2
flow rate	5×10^3 cm^3/s

The circuit could be modified to include either a full scale or a reduced scale model of the liquid metal target to be tested (Fig. 2).

Experiments could be performed relating to:

- mechanical stability and vibrations
- code validation / optimization of internal baffle structure
- heat transfer for different flow conditions
- gas injection, bubble distribution and effect on heat transfer
- gas separation from the liquid

Planning for such experiments involving ESS (PSI, KFA) and ORSNS is in progress with the goal to establish a possible work program, schedule and a cost estimate by mid 1996.

Persons involved: G.S. Bauer (PSI), J. Haines (ORNL), O. Lielausis (Riga)

B10 **Irradiation of specimens under stress in liquid metals**

The beam stop at the Moscow Meson Factory (Fig. 3) in Troitsk has been found suitable to install an irradiation facility which would allow proton irradiation of specimens in contact with liquid metal. The liquid metal container could be rotated periodically to minimize damage at the beam entry window while the specimens to be irradiated would be kept stationary to accumulate the maximum dose.

A liquid metal flow suitable to cool the window would be established which would also provide for liquid metal circulation past the specimens in order to generate a situation relevant for a flowing liquid metal target. Although the pulses are too long to generate heating rate effects, there would be

enough thermal cycling from pulse to pulse to simulate its effect, if any. Specimens under stress and unstressed specimens could be irradiated in a mixed proton-neutron field and in a pure neutron field simultaneously.
Presently the linac is capable of delivering 100 μA of 450 MeV protons. The final specifications are 600 MeV and 1 mA.
Even at the present linac rating this would be one of the most crucial tests of the whole program. Studies towards such a facility have been initiated.
Coordinators: G.S. Bauer (PSI) and S. Sidorkin (INR)

B11 **Supporting test rigs at participating laboratories**
Several test installations are available at various laboratories, which can be used for supporting research and initial trial experiments. In particular, corrosion experiments are going on at ORNL and at PSI. ORNL has a big water loop available and traditionally carries out neutron irradiation experiments in HFIR. High heating rate experiments are possible at ORELA, and pressure wave experiments are planned, using the exploding wire technique. PSI, on the other hand has an ongoing development program in liquid metal flow diagnostics and fluid mechanics and is operating several small PbBi-installations and a Na-loop.

Correlation Matrix

The following matrix shows, which of the research opportunities listed under B1-B11 can be expected to yield results relevant to the topics listed under A1-A11.
Topics in bold print are considered key issues regarding feasibility and life time of targets above 1 MW beam power.
X means principal investigation; x means supporting investigation.

Liquid metal target development correlation matrix

Topics		B1 IPPE- PbBi-pilot target	B2 Beer Sheva liquid metal installations	B3 LANSCE- radiation effects facility	B4 Irradiations in SINQ-target	B5 ISOLDE-liquid metal target	B6 AGS-100 kJ-pulses @ 7 GeV (BNL)	B7 Dual and triple beam facilities (HMI	B8 PIREX facilitx (PSI)	B9 Riga - liquid metal loop facilities	B10 INR-beam stop irradiation	B11 Local research installations at PSI
CFD.code validation	A1	x					x			X		x
Nuclear and neutronics / Metal chemistry code valid.	A2	x	X				x			x		X
Solid-liquid metal heat transfer (flow, wetting)	A3		X							X		
Verification of pressure-pulse predictions	A4					x	X					x
Injection of gas bubbles into liquid metal	A5	x	x				X			X		x
Effect of gas bubbles on heat transfer	A6		x							X		
Effect of irradiation on intermetallic reactions	A7	x									X	
Effect of temperature and strain on intermetallic reac.	A8										x	X
Combined effect of temp. and strain on interm. reac.	A9										X	
Radiation effects in spall. environment (H, He, dpa)	A10			X	X			x	x			
Liquid metal quality and technology	A11	x								X		X

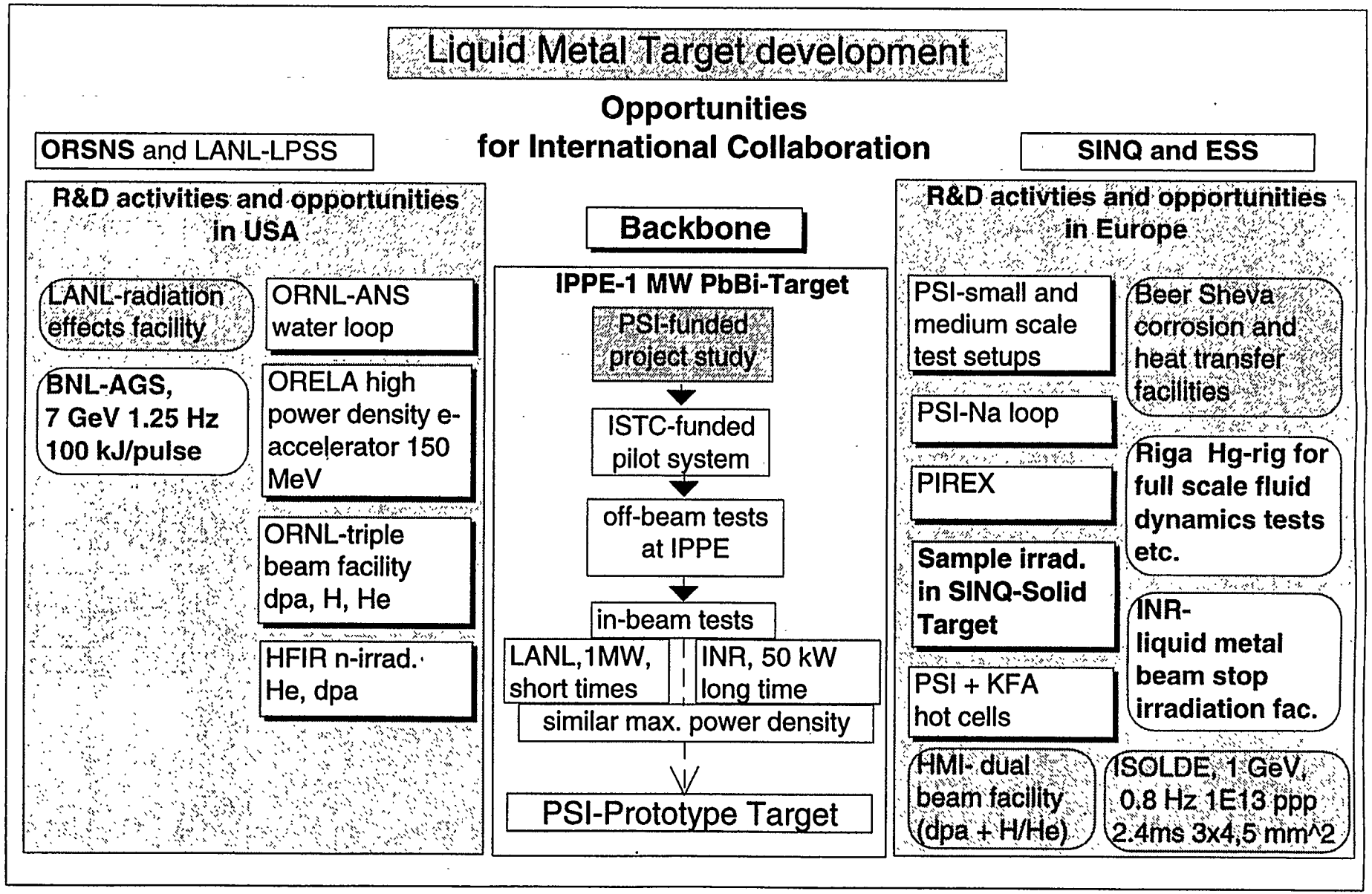

Figure 1 *Survey of opportunities for R&D-work on liquid metal target problems*

LMT-COOP.XLS

INSTALLATION OF THE TARGET IN THE Hg-LOOP

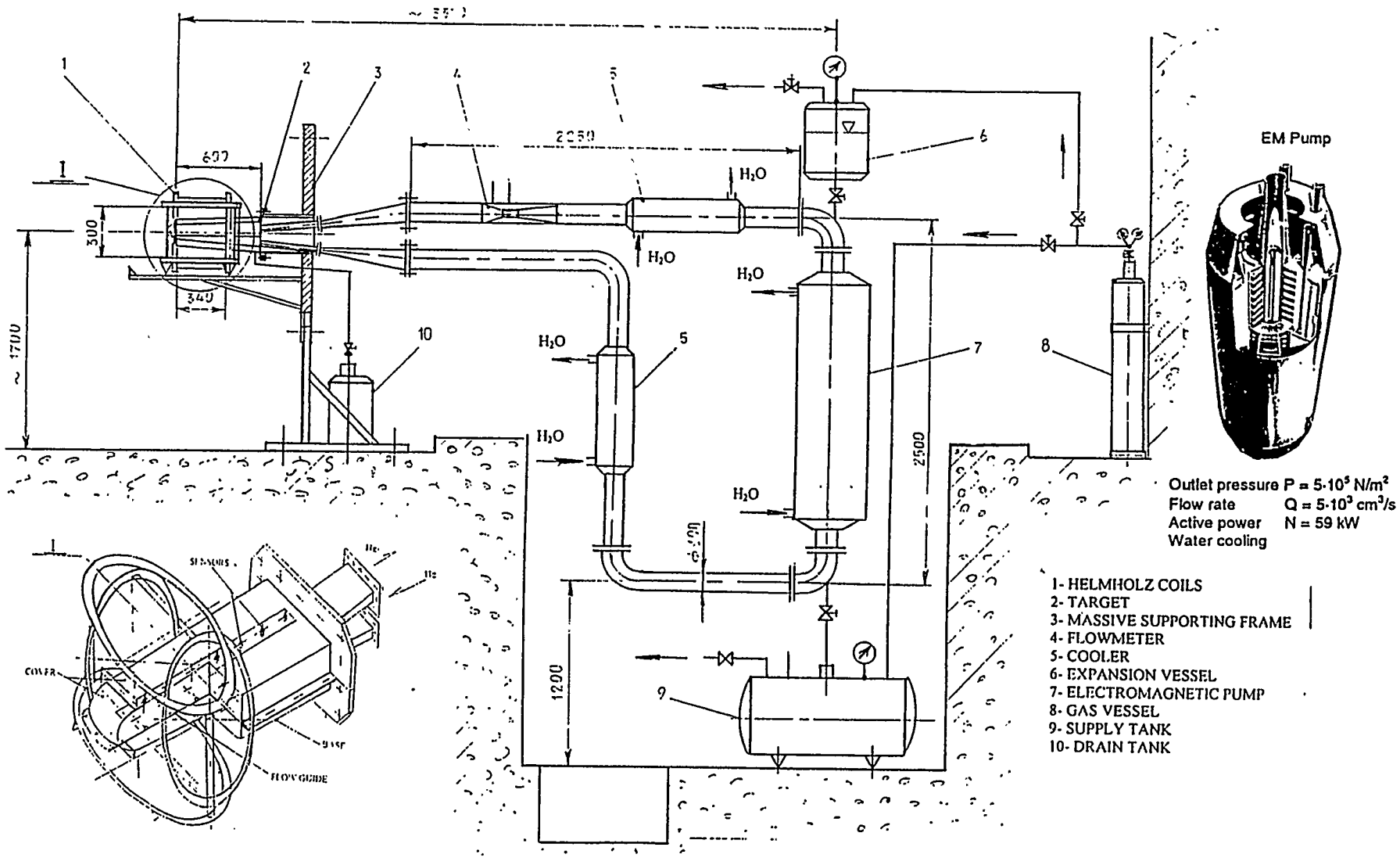

Figure 2 *Sketch of the RIGA Mercury loop with adjustments made to examine a liquid metal target*

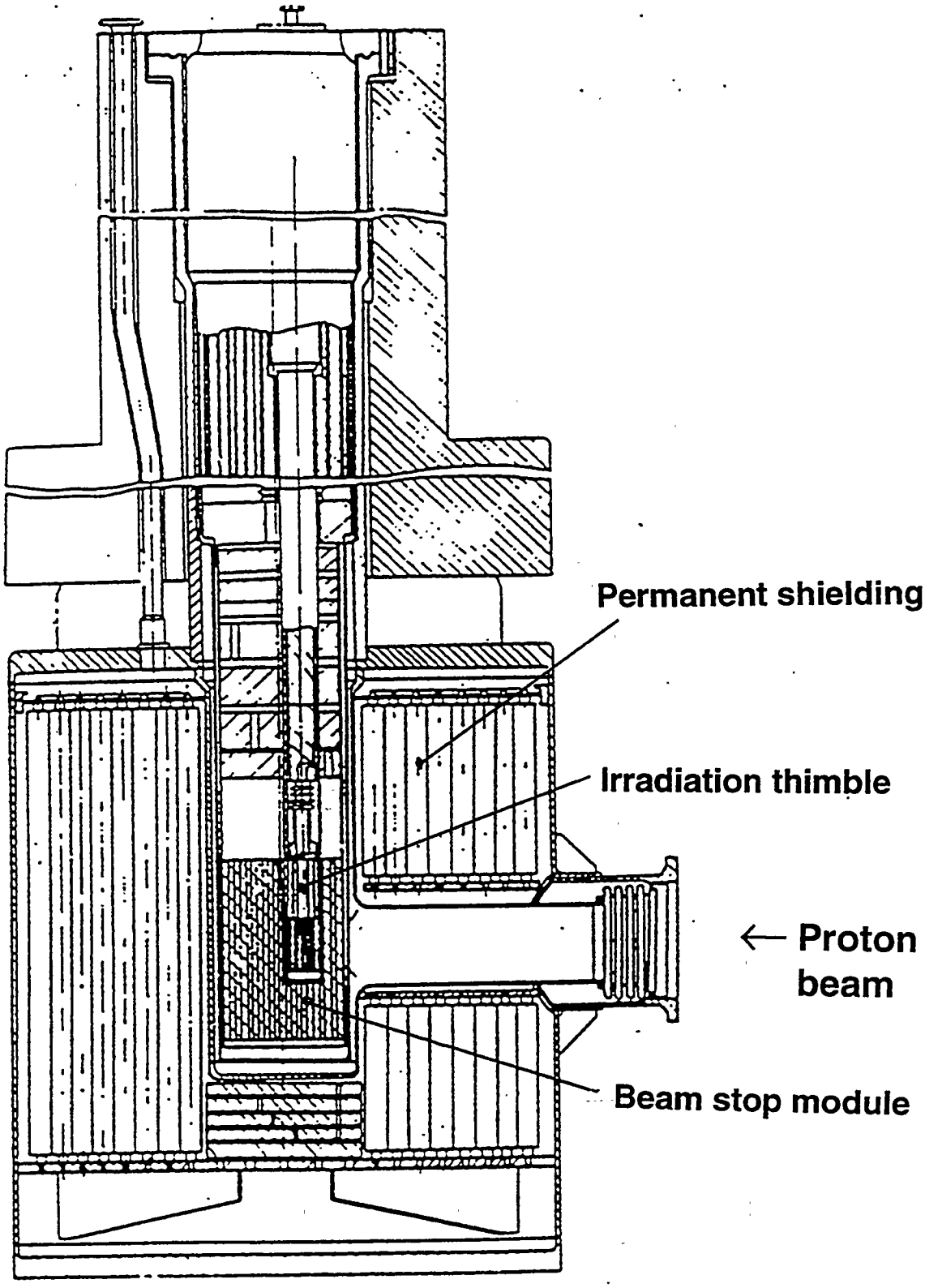

Figure 3 *Sketch of the beam stop irradiation facility at INR, Troitsk, as presently built. Test irradiations are possible in the inner thimble or by replacing the beam stop module with a liquid metal container with forcibly cooled beam window and sample inserts.*

APPENDIX A

List of Participants

List of Participants

International Workshop on the Technology and Thermal Hydraulics of Heavy Liquid Metals Schruns, March 24 - 29, 1996

Jose Alonso Lawrence Berkeley National Laboratory University of California Mail Stop 71 259 Berkeley CA 94720 USA Tel: 001 510 486 4206 Fax 001 510 486 5788 e-mail JRALONSO@LBL.GOV	Bill Appleton Oak Ridge Natl. Laboratory P.O.Box 2008 Oak Ridge, TN 37831-6240 USA Tel: 001 423 574 4321 Fax 001 423 574 0323 e-mail GXB@ORNL.GOV	**Günter Bauer** Paul Scherrer Institut WLGA/D12 5232 Villigen PSI Switzerland Tel: 0041 56 310 2524 Fax 0041 56 310 3131 e-mail BAUER@PSI.CH
Renate Bercher Paul Scherrer Institut WLGA/D12 5232 Villigen PSI Switzerland Tel: 0041 56 310 3402 Fax 0041 56 310 3131 e-mail BERCHER@PSI.CH	**Mikael Bjoernberg** University of Helsinki Department of physics 00014 University of Helsinki Finland Tel: 00358 0 1913873 Fax 00358 0 1913878 e-mail Bjornberg@phcu.helsinki.fi	**Stefano Buono** CERN 1211 Geneva 23 Switzerland Tel: 0041 22 767 9382 Fax 0041 22 767 7555 e-mail Stefano_Buono@EET.CERN.CH
John Carpenter Argonne Natl. Laboratory 9700 South Cass. Av. Argonne IL, 60439 USA Tel: 001 708 252 5519 Fax 001 708 252 4163 e-mail jmcarpenter@anl.gov	**Yong Dai** Paul Scherrer Institut OVGA/4 5232 Villigen PSI Switzerland Tel: 0041 56 310 4171 Fax 0041 56 310 2199 e-mail dai@psi.ch	**James DiStefano** Oak Ridge Natl. Laboratory P.O. Box 2009 Oak Ridge, TN 37831-6157 USA Tel: 001 423 574 4452 Fax 001 423 574 5113 e-mail DiStefanoJR@ornl.gov
Rugard Dressler Paul Scherrer Institut OFLA/103 5232 Villigen PSI Switzerland Tel: 004156 310 4698 Fax 0041 56 310 2199 e-mail DRESSLER@PSI.CH	**Paul Drumm** Rutherford Appleton Laboratory Chilton Didcot Oxon OX11 0QX UK Tel: 0044 123544 5896 Fax 0044 123544 5706 e-mail	**Trevor Dury** Paul Scherrer Institut OVGA/426 5232 Villigen PSI Switzerland Tel: 0041 56 310 2734 Fax 0041 56 310 4481 e-mail
Jean Luc Flament Centre d'etudes de Bruyeres le Chatel B.P. 12 91680 Bruyeres le Chatel France Tel: 0033 1 69265486 Fax 0033 1 69267033 e-mail Flament@bruyeres.cea.fr	**Tony Gabriel** Oak Ridge Natl. Laboratory P.O. Box 2008 Oak Ridge, TN 37831-6364 USA Tel: 001 423 574 6082 Fax 001 423 574 9619 e-mail tag@ornl.gov	**Sven Eckert** Research Center Rossendorf Inc. P.O. Box 510119 01314 Dresden Deutschland Tel: 0049 351 260 3459 Fax 0049 351 260 3484 e-mail ECKERT@FZ-ROSSENDORF.DE

List of Participants

International Workshop on the Technology and Thermal Hydraulics of Heavy Liquid Metals Schruns, March 24 - 29, 1996

Mikhail Gratchev Institut for Nuclear Research 60th Oktober Anniversary Pr. 7a 117312 Moscow Russia Tel: 007 095 3340186 Fax 007 095 3342268 e-mail GRATCHEV@AL20.INR.TROITSK.RU	**Boris Gromov** IPPE Obninsk Bondarenko Sq 1 Obninsk, 249020 Kaluga Region Russia Tel: 007 095 98283 Fax 007 095 8833112 e-mail Postbox@ippe.rssi.ru	**Bernd Guttek** Forschungszentrum Jülich Zentralabteilung Technology (ZAT) Postfach 19 13 52425 Jülich Germany Tel: 0049 2461 61 3578 Fax 0049 2461 61 6816 e-mail guttek@einstein.zat.kfa-juelich.de
John Haines Oak Ridge Natl. Laboratory P.O. Box 2009 Oak Ridge, TN 37831-8071 USA Tel: 001 615 574 0966 Fax 001 615 574 7926 e-mail hainesJR@ornl.gov	**Ryutaro Hino** JAERI Japan Tel: 0081 292 82 6424 Fax 0081 292 82 5579 e-mail	**Mike Holding** Rutherford Appleton Laboratory Chilton Didcot Oxon OX11 0QX UK Tel: Fax e-mail
Yoshiaki Kiyanagi Hokkaido University Department of Nuclear Engineering Sapporo 060 Japan Tel: 0081 11 706 6651 Fax 0081 11 706 7896 e-mail Kiyanagi@athena.hune.hokudai.ac.jp	**Shaul Lesin** Solmecs (Israel) LTD. Center for MHD Studies Ben-Gurion University of the Negev Beer Sheva 84105 Israel Tel: 00972 7 280451 Fax 00972 7 280 467 e-mail ammi@bgumail.bgu.ac.il	**Olgerts Lielausis** Institute of Physics Miera street 32 Salaspils-1 LV-2169 Latvia Tel: 00371 2944700 Fax 00371 7901214 e-mail MBROKA@SAL.LV
L.K. Mansur Oak Ridge Natl. Laboratory P.O. Box 2008, Bldg. 5500 Oak Ridge, TN 37831-6376 USA Tel: 001 423 574 4797 Fax 001 574 0641 e-mail MansurLK@ornl.gov	**T.J. McManamy** Oak Ridge Natl. Laboratory P.O. Box 2009 Oak Ridge, TN 37831-8045 USA Tel: 001 423 576 0039 Fax 001 423 576 0024 e-mail TNM@ornl.gov	**Liping Ni** Paul Scherrer Institut OTLA/103 5232 Villigen PSI Switzerland Tel: 0041 56 310 4453 Fax 0041 56 310 2549 e-mail Liping@psi.ch
Yuri Orlov IPPE Obninsk Bondarenko Sq 1 Obninsk, 249020 Kaluga Region Russia Tel: 007 095 983 25 Fax 007 095 8833112 e-mail Postbox@ippe.rssi.ru	**Dimitry Pankratov** IPPE Obninsk Bondarenko Sq 1 Obninsk, 249020 Kaluga Region Russia Tel: 007 095 984 52 Fax 007 095 8833112 e-mail Postbox@ippe.rssi.ru	**Martin Schuster** Atominstitut Schüttelstrasse 115 1020 Wien Austria Tel: 0043 1 72701 297 Fax 0043 1 7289220 e-mail Schuster@ati2.ati.ac.at

List of Participants

International Workshop on the Technology and Thermal Hydraulics of Heavy Liquid Metals Schruns, March 24 - 29, 1996

Yuri Shubin IPPE Obninsk Bondarenko Sq 1 Obninsk, 249020 Kaluga Region Russia Tel: 007 08439 98611 Fax 007 095 230 2326 e-mail shubin@cjd.obninsk.su	**Stanislav Sidorkin** Institut for Nucl. Research 60th Oktober Anniversary Pr. 7a 117312 Moscow Russia Tel: 007 095 334 0712 Fax 007 095 1352268 e-mail SIDORKIN@AL20.INR.TROITSK.RU	**Beat Sigg** ETH Zürich OVGA/415 5232 Villigen PSI Switzerland Tel: 0041 56 310 2659 Fax 0041 56 310 4481 e-mail
Moshe Siman-Tov Oak Ridge Natl. Laboratory P.O. Box 2009 Oak Ridge, TN 37831-8045 USA Tel: 001 423 574 6515 Fax 001 423 574 0740 e-mail mst@ornl.gov	**Yasushi Takeda** Paul Scherrer Institut WMHA/B22 5232 Villigen PSI Switzerland Tel: Fax e-mail Takeda@psi.ch	**John Weeks** 25 Acorn Lane Stony Brook, N.Y. 11790, USA Tel: 001 516 751 1149 Brookhaven Natl. Laboratory Guest sr. Metallurgist Upton NY 11973-5000 USA Tel: 001 516 344 2617 Fax 001 516 344 4255
Steve Wender Los Alamos Natl. Laboratory USA Tel: 001 505 667 1344 Fax 001 505 665 4121 e-mail WENDER@LANL.GOV	**Evgeni Yefimov** IPPE Obninsk Bondarenko Sq 1 Obninsk, 249020 Kaluga Region Russia Tel: 007 095 230 2326 Fax 007 095 8833112 e-mail Postbox@ippe.rssi.ru	

INTERNAL DISTRIBUTION

1. J. R. Alonso
2. B. R. Appleton
3. J. E. Cleaves
4. E. G. Cumesty-DOE/ORO
5. J. R. DiStefano
6. T. A. Gabriel
7. J. R. Haines
8. J. C. Hall-DOE/ORO
9. L. K. Mansur
10. T. J. McManamy
11. J. B. Roberto
12. M. J. Saltmarsh
13. D. L. Selby
14. M. Siman-Tov
15. J. O. Stiegler
16. A. W. Trivelpiece
17. R. I. Van Hook
18. C. D. West
19. ORNL Patent Section

20.–21. Laboratory Records Office

22. Laboratory Records (RC)

23.–24. Central Research Library Document Reference Section

25. ORNL Public Affairs Office
26. Y-12 Technical Library

EXTERNAL DISTRIBUTION

27. G. S. Bauer, Paul Scherrer Institut, WLGA/D12, 5232 Villigen PSI, Switzerland
28. R. Bercher, Pasul Scherrer Institut, WLGA/D12, 5232 Villigen PSI, Switzerland
29. M. Bjoernberg, University of Helsinki, Department of Physics, 00014 University of Helsinki, Finland
30. S. Buono, CERN, 1211 Geneva 23, Switzerland
31. J. Carpenter, Argonne National Laboratory, 9700 South Cass Avenue, Argonne, Illinois 60439
32. Y. Dai, Paul Scherrer Institut, WLGA/D12, 5232 Villigen PSI, Switzerland
33. J. F. Decker, Deputy Director, Office of Energy Research, DOE, Washington, D.C. 20585
34. P. Dehmer, Associate Director for Basic Energy Sciences, Office of Energy Research, DOE, Germantown, Maryland 20874-1290
35. R. Dressler, Paul Scherrer Institut, WLGA/D12, 5232 Villigen PSI, Switzerland
36. P. Drumm, Rutherford Appleton Laboratory, Chilton Didcot, Oxon OS11 0QX, United Kingdon
37. T. Dury, Paul Scherrer Institut, WLGA/D12, 5232 Villigen PSI, Switzerland
38. S. Eckert, Research Center Rossendort, Inc., P. O. Box 510119, 01314 Dresden, Deutschland
39. J. L. Flament, Centre d'etudes de Bruyeres le Chatel, B. P. 12, 91680 Bruyeres le Chatel, France
40. M. Gratchev, Institut for Nuclear Research, 60th Oktober Anniversary Pr. 7a, 117312 Moscow. Russia
41. B. Gromov, IPPE Obninsk, Bondarenko Sq1, Obninsk, 249020 Kaluga Region, Russia
42. B. Guttek, Forschungszentrum Jülich, Zentralabteilung Technology (ZAT), Postfach 19 13, 52425 Jülich, Germany

43. M. Holding, Rutherford Appleton Laboratory, Chilton, Didcot, Oxon, OX11 0QX, United Kingdom
44. R. O. Hultgren, Deputy Assistant Manager, Energy Research and Development, DOE-ORO, Building 4500N, MS-6269
45. Y. Kiyanagi, Hokkaido University, Department of Nuclear Engineering, Sapporo 060, Japan
46. M. Krebs, Director, Office of Energy Research, DOE, Washington, D.C. 20585
47. S. Lesin, Solmecs (Israel) LTD., Center for MHD Studies, Ben Gurion University of the Negev, Beer Sheva 84105, Israel
48. O. Lielausis, Institute of Physics, Miera Street 32. Salaspils-1:V-2169, Latvia
49. L. Ni, Paul Scherrer Institut, WLGA/D12, 5232 Villigen PSI, Switzerland
50. W. Oosterhuis, Office of Energy Research, DOE, Germantown, Maryland 20874-1290
51. Y. Orlov, IPPE Obninsk, Bondarenko Sq 1, Obninsk, 249020 Kaluga Region, Russia
52. D. Pankratov, IPPE Obninsk, Bondarenko Sq 1, Obninsk, 249020 Kaluga Region, Russia
53. M. Schuster, Atominstitut, Schuttelstrasse 115, 1020 Wien, Austria
54. Y. Shubin, IPPE Obninsk, Bondarenko Sq 1, Obninsk, 249020 Kaluga Region, Russia
55. S. Sidorkin, Institut for Nuclear Research, 60th Oktober Anniversary Pr. 7a, 117312 Moscow, Russia
56. B. Sigg, ETH Zurich, OVGA/415, 5232 Villigen PSI, Switzerland
57. Y. Takeda, Paul Scherrer Institut, WMHA/B22, 5232 Villigen PSI, Switzerland
58. I. L. Thomas, Director, Division of Materials Sciences, Office of Basic Energy Sciences, Office of Energy Research, DOE, Germantown, Maryland 20874-1290
59. J. Weeks, 25 Acorn Lane, Stony Brook, New York 11790
60. S. Wender, Los Alamos National Laboratory, MS H803, Las Alamos, New Mexico 87545
61. E. Yeflimov, IPPE Obninsk, Bondarenko Sq 1, Obninsk, 249020 Kaluga Region, Russia